Investigating the effect of *Bifidobacterium* on the host intestinal epithelium in health and disease

Lukas C. Harnisch

A thesis submitted in accordance with the requirements for the degree of Doctor of Philosophy (PhD)

Norwich Medical School, University of East Anglia

and

Quadram Institute Biosciences

2017

Abstract

Bifidobacteria are prominent members of the human gastrointestinal tract, particularly in early life. Their presence is generally linked to health, as reduced abundance of bifidobacteria is linked to a range of diseases including, Inflammatory Bowel Disease (IBD). However, how these beneficial microbes modulate host health is currently unclear. The intestinal epithelium barrier is essential for gut health, and previous studies have suggested that *Bifidobacterium breve* UCC2003 protects intestinal epithelial cells (IECs) from experimental pathological epithelial cell shedding. Thus, I hypothesised that *B. breve* directly modulates IECs, which is essential for maintaining homeostasis.

Initial studies, probing the role of the mechanosensitive ion channel Piezo1, indicated that this protein may not play a central role within the intestine (utilising zebrafish, and mouse models, and IBD patient biopsies), as had previously been described for the dermis. Furthermore, *B. breve* did not appear to modulate transcription or translation of Piezo1, suggesting other mechanisms may be involved in IEC regulation. Therefore, I next assessed the global IEC transcriptome (via RNA-seq), and determined that UCC2003 induced distinct responses in neonatal IECs including, TLR2, TLR9, IL-17C, and integrin signalling upregulation, which correlates with this microbe's ability to protect the epithelial barrier. Furthermore, analysis of the *B. breve* transcriptome *in vivo* (both in germ-free, and wild-type mice) highlighted host, and microbial community adaption responses including, bile acid resistance, iron scavenging, and differential nutrient metabolism.

In summary, *B. breve* UCC2003 induces specific modulation of the IEC transcriptome during homeostatic conditions, which reveals targets for potential disease intervention. Furthermore, distinct *B. breve* transcription profiles *in vivo*, also indicate promising microbial factors that may have host/microbiota modulatory effects, that could be targeted for development of new 'probiotics'. This work contributes novel insight into how bifidobacteria modulate intestinal responses, and supports their use for improving host health and preventing disease.

Acknowledgments

First and foremost, I would like to thank Dr Lindsay Hall. I cannot express how grateful I am for her advice, everlasting support and most certainly patience throughout the last four years. I would like to express my sincere gratitude for the opportunity to carry out research and study under her guidance. It has been an honour to be her first PhD student and I really do wholeheartedly appreciate all her time, faith, and ideas she has dedicated to me as a student and to the project. Her mentorship, knowledge, advice, empathy and support were invaluable and I would not have arrived at this point without them. With her help, I was able to grow as a scientist and as a person and her excitement and responsibility for science, research, and her group are an inspiration to me.

My thanks also go to the other members of my supervisory panel, Prof Alastair Watson and Dr Kevin Hughes, for their essential contributions to my project and studies.

Thank you in advance to my viva voce examiners Prof Dirk Haller and Prof John Wain for their time reading and discussing my thesis with me.

During my PhD, I had the opportunity to work with brilliant scientists and I would like to thank everyone in particular all past and present members of the Hall Lab for their help and the all fun we had together.

My special gratitude goes to Dr Melissa Lawson for being a friend and for being there, be it to help with a difficult protocol or for a friendly chat over a cup of tea.

Outside of the scientific setting, I am thankful to my friends (be they scientists or not) for setting me straight and giving me perspective in difficult times.

Last but not least, I am grateful to my mother and my younger sister, for all their love, for being so understanding and supporting me throughout the last four years.

This PhD has provided me with the invaluable opportunity to not only train to be a scientist but also to grow as a person. Now my responsibility is to draw from these experiences and repay this privilege by supporting others as much as possible and contributing to the research community. I will give it my best.

List of Contents

List of Figures

List of Tables

List of Abbreviations

AMP	Anti-microbial peptide
BA	Bile acid
BSH	Bile salt hydrolase
CDI	Clostridium difficile infection
cfu	Colony forming units
CRISPER	Clustered Regularly Interspaced Short Palindromic Repeats
DC	Dendritic cell
DEG	Differentially expressed gene
EPS	Exopolysaccharide
ERK	Extracellular signalling kinase
FA	Focal Adhesion
FACS	Fluorescent-activated cell sorting
FAK	Focal adhesion kinase
FISH	Fluorescent in situ hybridisation
FITC-dextran	Fluorescein isothiocyanate–dextran
GALT	Gut-associated lymphoid tissue
GF	Germ free
GH	Glycosyl hydrolase
GI	Gastro-intestinal
GSL	Genetic susceptible locus
GWAS	Genome wide association study
HLPC	High-performance liquid chromatography
HMO	Human milk oligosaccharide
HMP	Human Microbiome Project
IBD	Inflammatory Bowel Disease
IE	Intestinal epithelium
IEC	Intestinal epithelial cell
IFN	Interferon
IgA	Immunoglobulin A
IL	Interleukin
TEER	Transepithelial resistance
T-β-MA	Tauro-β-muricholic acid

KO	Knockout
LI	Large intestine
LP	Lymph follicle
LPS	Lipopolysaccharide
MAMP	Microbial-associated molecular pattern
MAPK	Mitogen-activated protein kinase
miR	micro RNA
mRNA	messenger RNA
MS	Mass spectrometry
MV	Membrane vesicle
ncRNA	non-coding RNA
NEC	Necrotising Enterocolitis
NF- κB	Nuclear factor kappa-light-chain-enhancer
NMR	nuclear factor kappa-light-chain-enhancer
DSS	Dextran sodium sulphate
NOD	nucleotide-binding oligomerization domain-like
OTU	Operational Taxonomic Unit
PCA	Principal component analysis
PCoA	Principal Coordinates Analysis
PDCD4	Programmed cell death protein 4
PP	Peyer's Patches
qPCR	quantitative PCR
RA	Rheumatoid arthritis
RegIII γ	Regenerating islet-derived protein 3 gamma
RNA-seq	RNA sequencing
rRNA	ribosomal RNA
S1P	Sphingosine-1-phosphate
SCFA	Short-chain fatty acid
SEM	Scanning electron microscopy
SF	SUbsystems Profile by databasE Reduction using FOCUS
SFB	Segmented filamentous bacteria
SI	Small intestine
siRNA	small interfering RNA
SNP	Single nucleotide polymorphism
SPF	Specific pathogen free

TGF	Transforming growth factor
T_h	T helper
TJ	Tight junction
TLR	Toll-like receptor
TNF	Tumour necrosis factor
TNF-R	Tumor necrosis factor receptor
T_{reg}	T regulatory
DC	Dendritic cell
UC	Ulcerative Colitis
WGS	Whole genome sequencing
WLI	Whole large intestine
WSI	Whole small intestine
WT	Wild type
ZO-1	Zonula occludens 1

Preface

Publications

Hughes, Kevin R., Lukas C. Harnisch, Cristina Alcon-Giner, Suparna Mitra, Chris J. Wright, Jennifer Ketskemety, Douwe van Sinderen, Alastair JM Watson, and Lindsay J. Hall. "*Bifidobacterium breve* reduces apoptotic epithelial cell shedding in an exopolysaccharide and MyD88-dependent manner." *Open biology*7, no. 1 (2017): 160155. (Contributions see Appendix 1.)

Miguel, Jennifer C., Adrienne A. Maxwell, Jonathan J. Hsieh, Lukas C. Harnisch, Denise Al Alam, D. Brent Polk, Ching-Ling Lien, Alastair JM Watson, and Mark R. Frey. "Epidermal growth factor suppresses intestinal epithelial cell shedding through a MAPK-dependent pathway." *J Cell Sci* 130, no. 1 (2017): 90-96. (Contribution see Appendix 2.)

Oral presentations

Harnisch, Lukas C., Kevin R. Hughes, Cristina Alcon-Ginger, Lindsay J. Hall, and Alastair J.M. Watson. "The role of the mechano-receptor Piezo1 in intestinal cell shedding and barrier integrity during health and disease." Gut Health and Food Safety Research in Progress, Institute of Food Research, Norwich, UK, 10th June 2014

Harnisch, Lukas C., Kevin R. Hughes, Aimee Parker, Cristina Alcon-Giner, Jennifer A.M.E. Ketskemety, Chris J. Wright, Alastair J.M. Watson and Lindsay J. Hall. "Using RNA sequencing and pathway analysis to investigate the protective effect of *Bifidobacterium breve* in intestinal inflammation and cell shedding." Annual Conference Microbiology Society, ICC Birmingham, Birmingham, UK, 25th March 2015

Harnisch, Lukas C., Kevin R. Hughes, Melissa A. Lawson, Tamas Korcsmaros, Alastair J.M. Watson, and L.J. Hall. "Probing the host health beneficial effect of Bifidobacterium using paired transcriptomics of intestinal epithelial cells and gut microbes." Gut Health and Food Safety Research in Progress, Institute of Food Research, Norwich, UK, 13th September 2016

Harnisch, Lukas C., Kevin R. Hughes, Melissa A. Lawson, Johanne Brooks Padhmanand Sudhakar, Tamas Korcsmaros, Alastair J.M. Watson, and L.J. Hall. "Investigating the effect of *Bifidobacterium breve* on intestinal health through an integrated 'omics and experimental approach." QIB Student Science Showcase, Quadram Institute Biosciences, Norwich, UK, 19th May 2017

Poster Presentations

Harnisch, Lukas C., Kevin R. Hughes, Cristina Alcon-Ginger, Lindsay J. Hall, and Alastair J.M. Watson. "Does mechano-receptive ion channel Piezo1 regulate in cell shedding in the mammalian

intestine?" Gut Health and Food Safety ISP, John Innes Conference centre, Norwich, UK, 18th March 2014

Harnisch, Lukas C., Kevin R. Hughes, Cristina Alcon-Ginger, Lindsay J. Hall, and Alastair J.M. Watson. "Does mechano-receptive ion channel Piezo1 regulate in cell shedding in the mammalian intestine?" Annual IFR Student Science Showcase, Institute of Food Research, Norwich, UK, 23rd June 2014

Harnisch, Lukas C., Kevin R. Hughes, Aimee Parker, Cristina Alcon-Giner, Jennifer A.M.E. Ketskemety, Chris J. Wright, Alastair J.M. Watson and Lindsay J. Hall. "Using RNA sequencing to investigate the protective effect of *Bifidobacterium breve* in cell shedding." Microbes in Norwich, John Innes Conference Centre, Norwich, UK, 8th January 2015

Harnisch, Lukas C., Kevin R. Hughes, Aimee Parker, Cristina Alcon-Giner, Jennifer A.M.E. Ketskemety, Chris J. Wright, Alastair J.M. Watson and Lindsay J. Hall. "Using RNA sequencing and pathway analysis to investigate the protective effect of *Bifidobacterium breve* in intestinal inflammation and cell shedding." Annual Conference Microbiology Society, ICC Birmingham, Birmingham, UK, 25th March 2015

Harnisch, Lukas C., Kevin R. Hughes, Aimee Parker, Cristina Alcon-Giner, Jennifer A.M.E. Ketskemety, Chris J. Wright, Alastair J.M. Watson and Lindsay J. Hall. "Using RNA sequencing and pathway analysis to investigate the protective effect of *Bifidobacterium breve* in intestinal inflammation and cell shedding." Institute of Food Research Science Symposium, John Innes Conference Centre, Norwich, UK, 28th April 2015.

Harnisch, Lukas C., Kevin R. Hughes, Melissa A. Lawson, Tamas Korcsmaros, Alastair J.M. Watson, and L.J. Hall. "Exploring the health beneficial effect of Bifidobacterium on intestinal epithelial cells through host and bacterial RNA sequencing." Gut Health and Food Safety Research in Progress Meeting, Institute of Food Research, Norwich, UK, 13th September 2016

Harnisch, Lukas C., Kevin R. Hughes, Melissa A. Lawson, Tamas Korcsmaros, Alastair J.M. Watson, and L.J. Hall. "Exploring the health beneficial effect of Bifidobacterium on intestinal epithelial cells through host and bacterial RNA sequencing." Annual IFR Student Science Showcase, Institute of Food Research, Norwich, UK, 16th September 2015

Harnisch, Lukas C., Kevin R. Hughes, Melissa A. Lawson, Tamas Korcsmaros, Alastair J.M. Watson, and L.J. Hall. "Probing the host health beneficial effect of Bifidobacterium using paired transcriptomics of intestinal epithelial cells and gut microbes." Exploring Human Host-Microbiome Interactions in Health and Disease, Welcome Genome Campus, Cambridge, UK, 8th September 2016

Harnisch, Lukas C., Kevin R. Hughes, Melissa A. Lawson, Tamas Korcsmaros, Alastair J.M. Watson, and L.J. Hall. "Probing the host health beneficial effect of Bifidobacterium using paired transcriptomics of intestinal epithelial cells and gut microbes." Gut Health and Food Safety Research in Progress Meeting, Institute of Food Research, Norwich, UK, 13th September 2016

Harnisch, Lukas C., Kevin R. Hughes, Melissa A. Lawson, Tamas Korcsmaros, Alastair J.M. Watson, and L.J. Hall. "Probing the host health beneficial effect of Bifidobacterium using paired transcriptomics of intestinal epithelial cells and gut microbes." Microbes in Norwich, John Innes Conference Centre, Norwich, UK, 2nd March 2017

Harnisch, Lukas C., Kevin R. Hughes, Melissa A. Lawson, Tamas Korcsmaros, Alastair J.M. Watson, and L.J. Hall. "Using integrated paired host and bacterial 'omics data to investigate the host health beneficial effect of Bifidobacterium on intestinal epithelial cells."UK Multiscale Biological Network Workshop, Earlham Institute, Norwich, UK, 23rd April 2017

Harnisch, Lukas C., Kevin R. Hughes, Melissa A. Lawson, Tamas Korcsmaros, Alastair J.M. Watson, and L.J. Hall. "Investigating the effect of Bifidobacterium on the host intestinal epithelium in health and disease." QIB Student Science Showcase, Quadram Institute Biosciences, Norwich, UK, 19th May 2017

1 General introduction

1.1 The human intestinal tract in health and homeostasis

1.1.1 Macroanatomy

The human gastrointestinal (GI) tract is an organ system forming a canal from the mouth to the anus, and is composed of the oral cavity, oesophagus, stomach, small intestine (SI, duodenum, jejunum, and ileum) and the large intestine ([LI], caecum, colon and rectum) (Figure 1-1.A). Additional organs directly associated with the GI tract include the liver, gall bladder and pancreas [1].

Research presented in this PhD thesis concentrates on the gastrointestinal (GI) tract including the small and large intestine, which directly connects to the stomach, and transports the chyme (partially digested food) towards the anus, while continuing enzymatic and mechanical digestion of food, absorbing nutrients and fluids. Each section of the GI tract has distinct physiological functions, and a specialised microscopic structure, essential for these processes (Figure 1-1.B) [2, 3]. The GI tract also harbours the intestinal microbiota (discussed in 1.3.2).

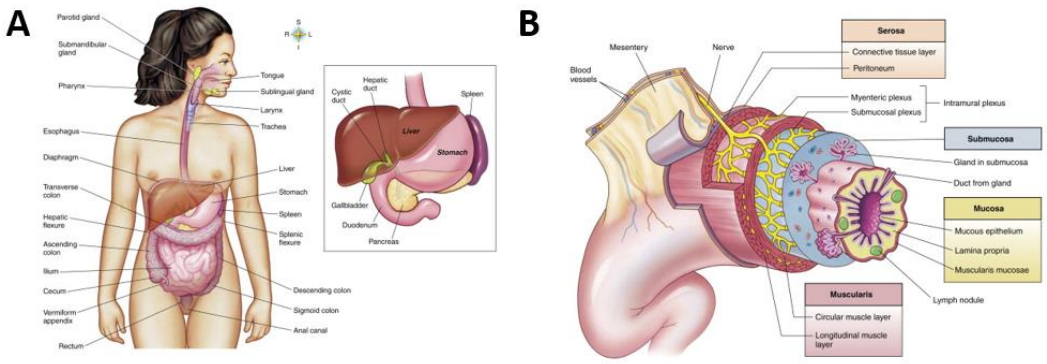

Figure 1-1 Macro- and microanatomy of the human gastrointestinal tract.

A Overview of the GI tract connecting the mouth to the anus via the oral cavity, pharynx, larynx, oesophagus, stomach, small intestine (duodenum, jejunum, ileum), large intestine (cecum, appendix, colon, rectum and anal canal), accessory organs: bile produced in the liver is stored within the gallbladder and flows into the duodenum via the major duodenal papilla, the digestive juice produced by the pancreas enters the duodenum via the ducts of Wirsung (duct of Santorini) (figure adapted from Thibodea & Patton , 2009 [2]). **B** Microanatomy of the intestinal wall, four main layers with subsections: serosa (connective

tissue, peritoneum, connects to mesentery), muscularis, submucosa, mucosa details and differences between large and small intestine highlighted in text (figure adapted from Reed & Wickam, 2007 [4])

1.1.2 Microanatomy

The overall microscopic structure of the GI tract, shared with minor differences between the small and LI, is a hollow tube with the wall made up of four layers: mucosa, submucosa, muscularis and serosa (luminal to distal) (Figure 1-1.B). The serosa is made up of connective tissue forming a bag that contains the intestine and allows for free movement. The muscularis transports intestinal contents by muscular contraction, a process called peristaltic, and is structured in circular and longitudinal layers of smooth muscle cells. Connective tissue, blood and lymph vessels, glands and the Meissner's plexus (innervating muscle fibres in muscularis) make up the submucosa, which are in direct contact with the mucosa, allowing for exchange of materials such as nutrients, fluids, electrolytes and bacterial compounds [5].

The mucosa is made up of the intestinal epithelium (IE, described in more detail in section 1.1.5), the underlying lamina propria (LP), and muscularis mucosae (luminal to distal). The separation of submucosa and mucosa is defined by the muscularis mucosa which is made up smooth muscles cells and in addition contains intestinal cells of Cajal, which control GI motility and sense extension [6]. The LP is rich in elastic fibres, which provide structural support for the epithelium during contractions of the muscle ring. Blood vessels transport nutrients absorbed from the intestinal lumen supply the IE and circulate hormones produced by intestinal endocrine cells. The LP also contains lymphatic structures which are part of the GALT (gut-associated lymphatic tissue). The GALT can contain up to 70% of all body immune cells, and is made up of isolated and aggregated lymph follicles [7, 8]. Peyer's Patches (PP) are specialised lymph nodes covered in follicle-associated epithelium which allows interaction of the host immune system with luminal antigens (Figure 1-2.A) [8, 9]. PP and their role in intestinal immunity will be expanded upon below.

The luminal surface of the mucosa is covered by a continues cell monolayer called the IE. This structure forms a selective, physical and biochemical barrier between the host and the intestinal lumen. The surface area available for contact and absorption is greatly increased by circular folds of the mucosa and formation of villi and crypts. In the small intesetin (SI) villi and crypts can be found while in the large itnestine (LI) onlt crypts

are present (Figure 1-2.) [10]. Additionally, intestinal epithelial cell membranes form microvilli towards the lumen, which increases the surface area by a further 20-fold. In total, the GI tract represents the largest surface area of the human body; > 400 m^2 (equivalent of two tennis courts). The IE in direct contact and key sight of interaction with luminal intestinal contents (including the gut microbiota), and contains a variety of specialised cell types, which will be listed below [11].

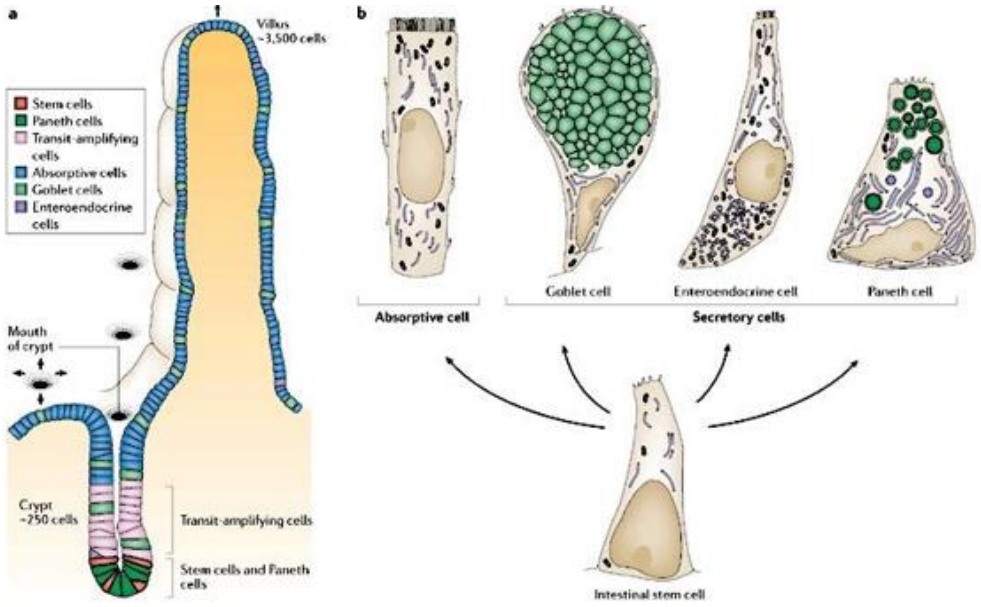

Figure 1-2 Overview of intestinal epithelial structure and cell types.

Localisation of different cell types in intestinal epithelium: stem cells – crypt base, Paneth cells – crypt base, transit amplifying cells – from end of base to neck of crypt, differentiated cells located from crypt neck to top of villus (enterocytes, goblet cells, tuft cells (not shown), enteroendocrine cells); structure similar in colon without villus, Paneth cells, differing enteroendocrine cell type; intestinal stem cells can differentiate into four cell types of the intestinal epithelium: enterocytes or absorptive cells with luminal microvilli brush boarder to increase absorption area and three secretory cell types: Goblet cells secrete mucus which is stored in apical cytoplasmic granules, enteroendocrine cells secreting various hormones stored in smaller granules, and Paneth cells secreting antimicrobial peptides again stored in apical secretory granules, (figures and legend adapted from Crosnier, Stamataki & Lewis, 2006 [10])

1.1.3 Physiological function

Historically, the main physiological function of the intestinal tract has been digestion, and nutrient absorption. Mechanical and chemical breakdown of food nutrients starts in the oral cavity and stomach, after which the chyme enters the intestine. In the SI, bile and pancreatic juice continue nutrient breakdown into amino and fatty acids, and simple sugars, which are then absorbed by the epithelium. This process is completed when the digestive mass enters the colon where water and electrolyte retention occurs during transversion, which turns the chyme into solid faeces when it reaches the anus [2, 12]. The human gut microbiota colonises the whole GI tract, but composition, bacterial load and host effects differ between sections. This will be discussed in more detail later in section 1.3.2.

1.1.3.1 The intestinal epithelium

The IE is a single layer of intestinal epithelial cells (IECs) that line the GI tract, and is the first contact point of the intestinal environment with the host. The IE provides a critical function; it forms a selective, mechanical, and biochemical barrier that controls exchange between host and lumen, including micro and macro-molecule such as nutrients, and bacteria [10]. The IE also performs immune surveillance, including initiation of immune responses to pathogenic bacterial invasion, and maintenance of homeostatic responses with respect to resident gut microbiota. This essential barrier consists of four main cell types: enterocytes, goblet cells, Paneth and stem cells (Figure 1-2.) [13] of which eneterocytes will be described in more detail as the focus of this study.

1.1.4 Intestinal epithelial cells interact with intestinal microbes

The IE is in constant contact with luminal bacteria, with these interactions essential for intestinal homeostasis, and tolerance to commensal bacteria. In the following section, the mechanisms most relavant to this study will be highlighted.

IECs are in direct contact with luminal bacteria and express receptors that allow them to sense the microbiota community, and steer the innate and adaptive immune response. This allows IECs to control homeostasis and immune tolerance in response to presence of commensal bacteria, and induce inflammatory responses in reaction to pathogens [10]. These pattern recognition receptors (PPRs) belong to the Toll-like receptors (TLRs), nucleotide-binding oligomerisation domain-like (NODs), and RIG-I-like family. The importance of this in intestinal homeostasis has been demonstrated in TLR-2, TRL-4, and adapter protein Myd88 KO mice, which all present with increased death from dextran sodium sulphate (DSS)-induced colitis [14]. To note, Inflammatory Bowel Disease (IBD) pathology can involve TLR1,2 and 6 polymorphisms, with a TLR-2 KO mouse presenting with decreased trefoil factor 3 secretion, and increased susceptibility to DSS [15].

When TLRs recognise conserved microbial molecular motifs (MAMPs), or pathogen-associated molecular patterns, they recruit signalling adapter Myd88, and TIR-domain-containing adaptor protein, which induces interferon-β, via nuclear NF-kB [16]. The importance of NF-κB signalling in IECs was demonstrated in studies with KO models of components involved in activation (NEMO NF-κB essential modulator, IKK inhibitor of NF-κB kinase), which induced increased susceptibility to DSS colitis, or resulted in spontaneous colitis [17, 18].

As the intestine is not sterile, and commensal bacteria are present, it is important that IECs can differentiate between pathogenic and symbiotic signals. Interestingly PRRs can either be present in the apical or basolateral membrane of IECs and this could help discriminate between commensal and pathogen microbial signals (pathogen – basal, commensal – luminal). It is important to note that the differentiation of commensal and pathogen signals allows IECs to process this information. As an example, signalling through surface TLR9, who recognises bacterial and viral DNA rich in unmethylated CpG-DNA, at the apical side promotes inhibition of NF-κB signalling, whereas TLR signalling from the basolateral pole promotes NF-κB activation[19, 20].

1.1.5 The intestinal epithelial barrier; the molecules involved

The selective, mechanical barrier formed by the IE is conferred by intercellular junctions between adjacent epithelial cells [21]. These complexes have both apical and basal elements. The apical part consists of adherence and tight junctions (TJ), while the basal segments include desmosomes and gap junctions. Together, these complexes are the main effectors of the mechanical barrier, with adherence junctions being responsible for cell-cell adhesion, and TJ control intercellular flux of micro- and macromolecules across the IE. TJ are made up of over 50 components including claudins and occludins, two families of membrane spanning proteins, which directly modulate movement across the epithelium [21, 22]. These two proteins are connected to intracellular acto-myosin rings, part of the cytoskeleton, through plaques formed by zone occludens 1 (ZO-1, Figure 1-3.A) [22].

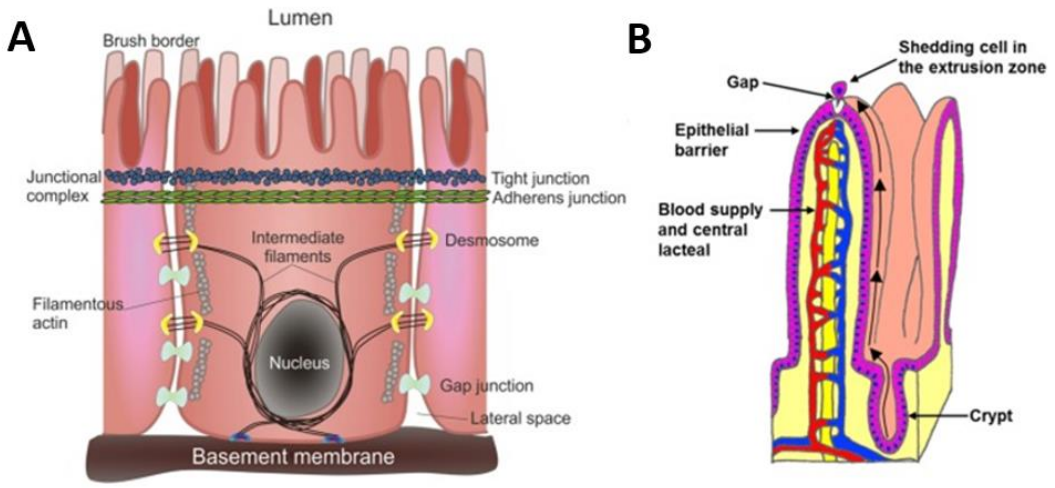

Figure 1-3 Small intestinal homeostatic epithelial cell shedding occurs predominantly at the villus tip.

A Intestinal epithelial cell junctional complexes. Individual intestinal epithelial cells joined to neighbours by continuous belt of tight junctions around the upper portion of the cell, TJs are responsible for gut/epithelial barrier function of macro and micro-molecules as well as member of the microbiota **B** Overview of small intestinal epithelium with extruded cell highlighted at tip of villus (figure and legend adapted from Wiliams *et al.*, 2015[23])

1.1.5.1 Renewal of epithelium involves cell shedding, which retains barrier function

The IE undergoes constant self-renewal due to its exposure to microbial antigens and stress factors. Cell renewal in the IE is considered the most dynamic in the human body, with a complete turnover every 2-6 days [24]. The process starts with the previously mentioned stem cell expansion, at the bottom of intestinal crypts, followed by migration of progeny cells up the crypt-villus axis [25, 26]. Factors influencing this movement includes pressure generated through stem cell expansion, and villus contraction and elongation [27]. When SI cells reach the villus tip, they are shed into the intestinal lumen via a controlled mechanism (Figure 1-3.B).

The process of cell shedding presents a considerable challenge to the host as it is essential to retain the barrier function of the IE, while continuously single cells are lost from the epithelial monolayer (approximately 1400 cells lost from single villi in 24 hours) [28]. TJ reorganisation maintains barrier function during cell shedding as during cell extrusion, a complex expansion of the intercellular junction complex ensures that the gap left by the extruded cell is sealed and the barrier maintained [29, 30].

The expansion process follows a specific pattern and is initiated by TJ reorganisation involving redistribution of ZO-1 to the basal surface of the shedding cell [31]. This is followed by movement of occludin to the basal membrane, which forms a funnel that marks the site of shedding and retains barrier function. Other junctional proteins, including claudins and E-cadherin, are recruited into the structure [32]. Members of the cytoskeleton, in particular, F-actin, myosin II, Rho-associated and myosin light chain kinases and microtubules join the shedding funnel, and allow the complex to contract [33]. This movement expels the cell from the epithelial monolayer into the lumen accompanied by contraction of the intracellular actin ring that closes the gap in the monolayer [32]. Surrounding cells move into the gap and the shedding funnel is resolved through reestablishment of the intercellular junctional complex. This whole process can be imagined as a purse string or zipper effect (Figure 1-4) [31].

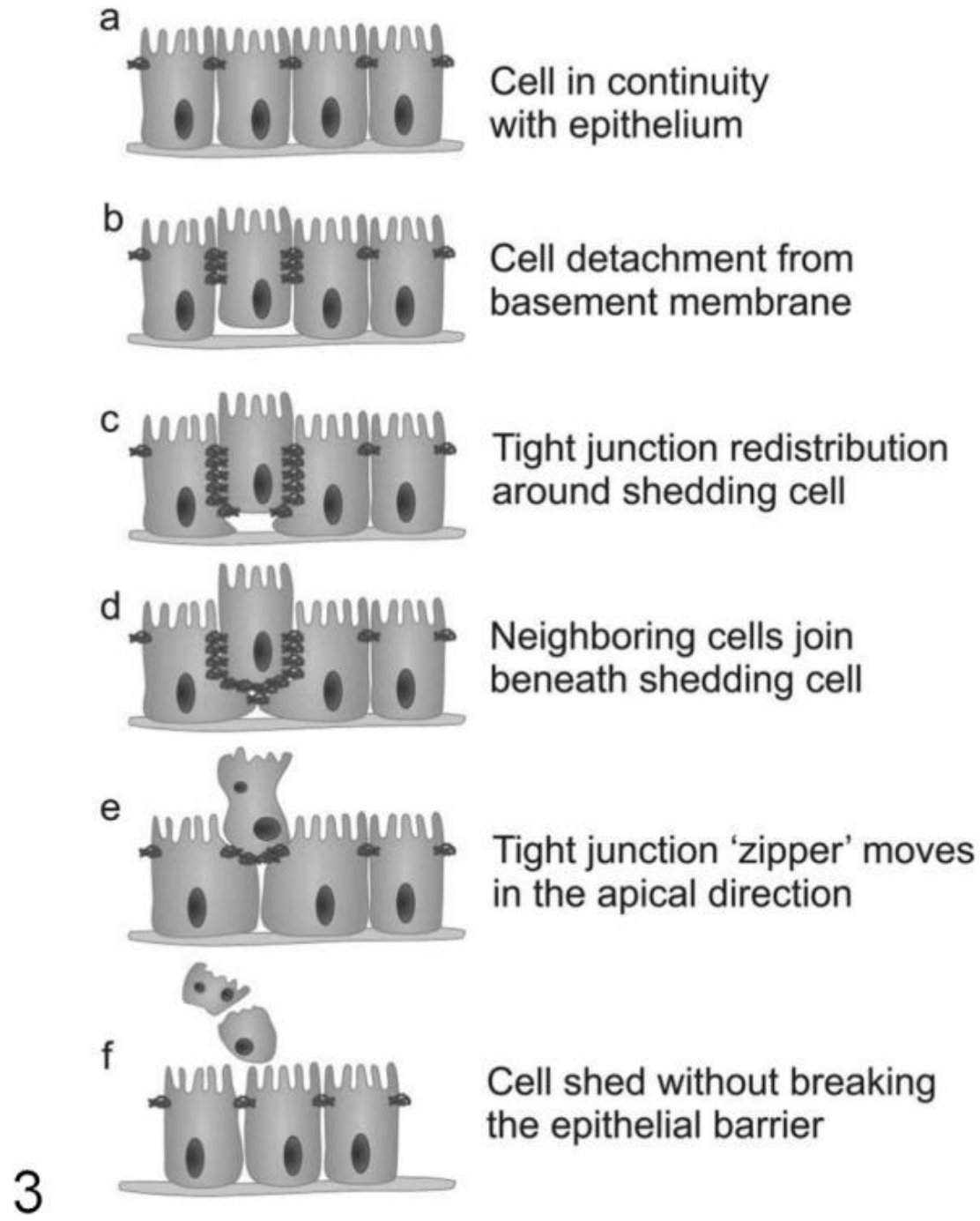

Figure 1-4 Intestinal epithelial homeostatic cell shedding retains barrier function by tight junction rearrangement.

Illustration of "zipper" or purse string effect of epithelial cell shedding. Detachment from basement membrane as initiating process still being investigated, rearrangement of tight junctions form funnel that seals gap left by shedding cell, neighbouring cells move in to close gap by advancement of lamellipodia (figure and legend adapted from Williams *et al.*, 2015 [30])

Under physiological conditions, rates of cell division and shedding are in a fine homeostatic balance to maintain equal number of IEC's and therefore an intact epithelial monolayer [25]. The underlying mechanism that balances these two processes have not yet been identified, and factors controlling cell shedding and expansion are still being investigated [34].

When enterocytes are extruded, they can be identified with markers of cell death, i.e. apoptosis, such as caspase-3 [35]. It is still unclear whether IECs undergo apoptosis while still being part of the epithelial monolayer marking them for shedding, or whether cell death is initiated after loss of contact with the epithelium through anoikis [36]. The investigation is difficult due to the temporarily and spatial closeness of these two processes. It has also been suggested that live cell shedding (followed by anoikis), and apoptotic cell shedding could exist as distinct pathways, initiated by different triggers, thus being involved in different processes, termed homeostatic and pathological shedding respectively (discussed in more detail in 4.1.1) [37]. Regulators of homoeostatic cell shedding are being heavily investigated. Recently, epithelial-associated villin has emerged as a potential regulator as it can be found in two forms within intestinal epithelial cells. In its full-length form is has an anti-apoptotic role to maintain mitochondrial integrity regulating caspase-3 and caspase-9 pathways, while cleavage induces apoptosis [34]. Cleavage of the protein occurs during migration of enterocytes along the crypt villus axis and has pro-apoptotic effect as well as causing actin formational changes, which is essential for shedding funnel formation [38]. Another specific candidate, mechano-receptive ion channel Piezo1, will be discussed and investigated further in chapter 4.

In contrast to homeostatic shedding events and levels retaining the epithelial barrier in health, pathological cell extrusion and elevated rates lead to loss of several neighbouring cells leading to a gap in the epithelial monolayer too large to be sealed by TJ expansion [39]. This results in breakdown of the IE integrity and uncontrolled exchange of matter between the host and the intestinal lumen. *In vivo* studies have shown tumour necrosis factor α (TNF-α) as an inducer of apoptosis and pathological cell shedding, leading to loss of epithelial cells at higher rates at the tip of small intestinal villi, and caused a decrease in intestinal permeability [40, 41].

Increased intestinal epithelial permeability is one of the hall marks of IBD pathology and TNF-α has been shown as a prominent cytokine in the inflammatory response of the

disease (discussed in 1.2.2) [42, 43]. These two observations logically suggest a link to TNF-α induction of pathological cell shedding and the resulting effect on epithelial barrier integrity. A study of shedding rates in IBD patients in remission by confocal endoscopy showed individuals with higher cell extrusion rates to be more likely to relapse which draws a causative link between inflammatory response and intestinal epithelial barrier impairment by increased shedding rates (Figure 1-5) [44].

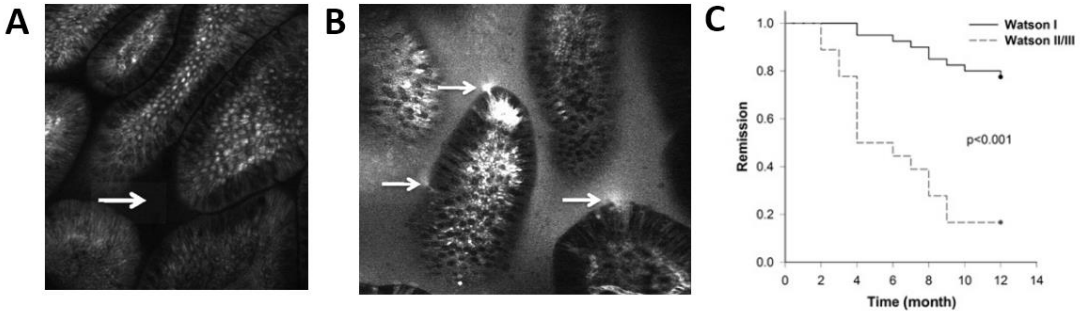

Figure 1-5 Loss of intestinal barrier function at sights of cell shedding in patients with IBD correlates with increased disease relapse.

Intestinal confocal endomicroscopy following intravenous administration of fluorescein contrast agent of **A** intact barrier function with no escape of fluorescein into gut lumen (arrow) and **B** multiple sites of efflux of fluorescein through the epithelium into gut lumen (arrows), note increased fluorescence in the gut lumen, **C** Prediction of relapse of inflammatory bowel disease (IBD) based on Watson grade of cell shedding and local barrier dysfunction shows correlation of higher relapse events in patients with increased levels of cell shedding (grade I: physiologically normal, grade II: functional defects, grade III: structural defects) (adapted from Kiesslich *et al.*, 2011 [39])

Therefore, it has been hypothesised that cell shedding, elevated by inflammation, causes barrier breakdown, which in return perpetuates the pro-inflammatory state observed in IBD, due to uncontrolled interactions of the luminal microbiota with the host immune system and results in a positive feedback loop. It remains to be determined whether the inflammatory stimuli initially cause barrier breakdown or vice versa [36].

The underlying mechanisms of pathological cell shedding (in addition to TNF-α) are still unclear and being actively investigated. A recent model showed that systemic LPS administration in mice increased apoptotic shedding. LPS activates TLR4 receptors on macrophages, which signals via Myd88 adapter protein and NF-κB in turn to increase release of TNF-α. Binding of TNF-α to tumour necrosis factor receptor 1 (TNF-R1) on

IECs induces apoptosis (Figure 1-6) [45]. This rapid model of inflammatory, elevated cell shedding in the SI has been proposed as a consistent and robust system for studying increased shedding events with respect to intestinal pathologies such as IBD, due to the similarities in observed gaps within the IE, and elevated extrusion rates induced by inflammation.

Recently, the commensal bacterium *B. breve* UCC2003, which has been shown to confer health beneficial effects for the host in several models of intestinal pathologies, offered protection from LPS induced elevated shedding (reviewed in 5.1.1) [46].

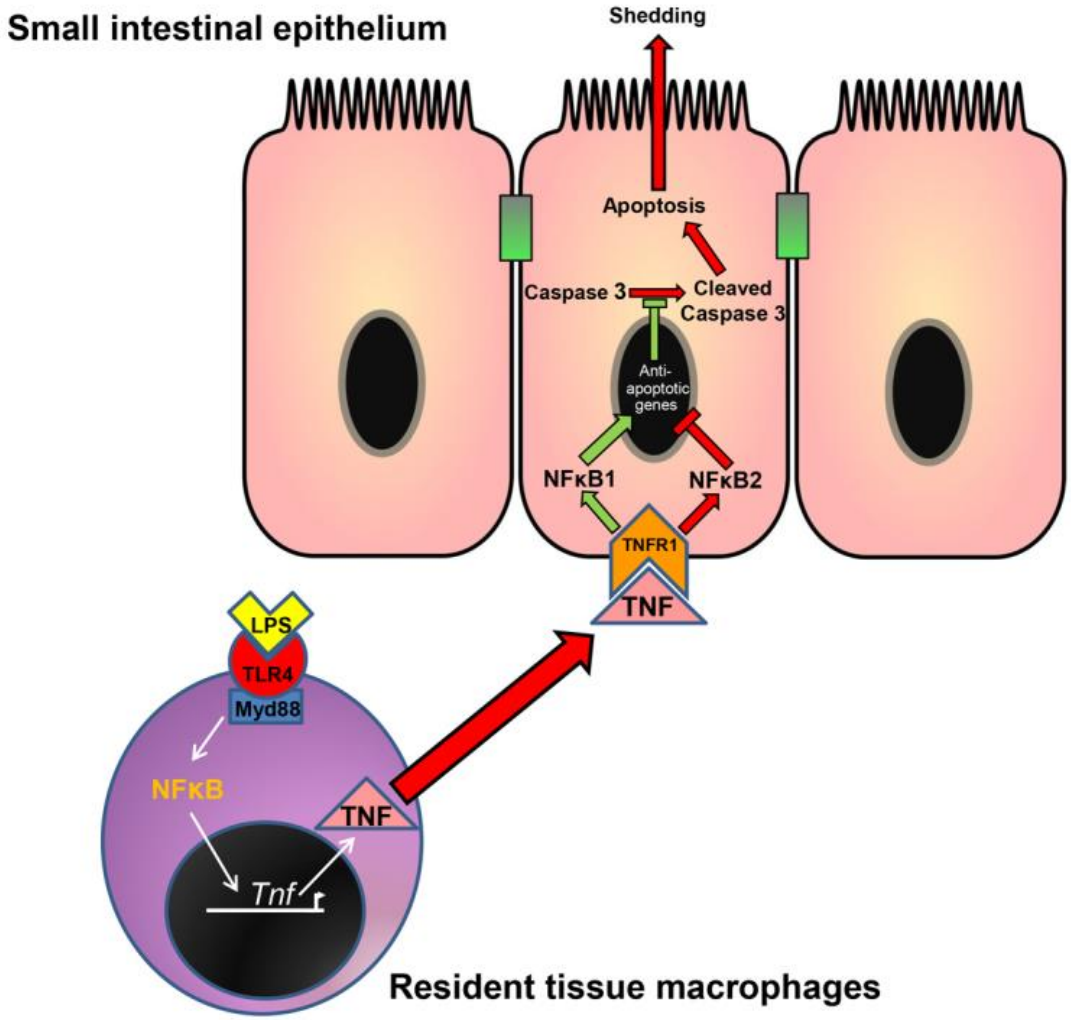

Figure 1-6 **Systemic LPS administration induces apoptotic cell shedding in small intestinal epithelial cells.**

Systemically delivered LPS is recognized by tissue resident TLR4-expressing mononuclear cells (monocytes/macrophages/dendritic cells), which produce TNF. TNF is released into the systemic circulation and binds with TNF-R1 on IECs, triggering apoptosis and shedding if NFκB2 signalling

dominates, or cell survival if NFκB1 signalling dominates (figure and legend adapted from Williams *et al.*, 2013 [45])

1.1.6 Scientific methods and models utilised to study intestinal responses

Historically, experimental investigation of human physiology has been aided by *in vitro* and *in vivo* models. The human intestinal tract is a complex system, and below I discuss the advantages and caveats of commonly applied scientific models.

1.1.6.1 *In vitro* and *ex vivo* models

In vitro models, have proved to be a useful tool for understanding intestinal responses, in part due to their simplicity and control over experimental conditions, which allows for measurements of single readouts without interfering background events.

Traditional 2D cell culture of single epithelial monolayers grown on solid supports or permeable filters have been utilised and expanded by the use of Ussing Chamber, separating basal and luminal compartment allowing for exposure of basolateral and apical side of cell monolayers to different conditions to more closely simulates *in vivo* conditions [47]. Several immortalised intestinal cell lines have been developed over the years, with Caco-2 (human colon adenocarcinoma), HT-29 (human colon adenocarcinoma) and Intestine 407 (human small intestine/HeLa) being the most commonly used ones, and therefore best characterised. [48, 49]

The development of 3D organoid cultures allows for a near physiological emulation of intestinal structure with primary cells, or stem cells self-organising into tissue structures resembling *in vivo* architecture including crypt and villi [50, 51]. However, organoid culture is still attached to significant costs, due to price of culture reagents, as well as the labour intensive nature of the work, which are factors to consider [52].

The described *in vitro* models are useful for studying various factors, but are still relatively simple models which seek to emulate the processes observed *in vivo*.

1.1.6.2 *In vivo* models

The use of laboratory mice as *in vivo* models of the IE, and its role in tissue homeostasis and host interaction with the environment, has proven significantly beneficial, due to the model's complexity and similarity to its human counterpart [53]. Other advantages include low genetic variability, due to inbred mice strains, and the possibility to generate knockout strains. For IBD, more than 74 genetically altered mouse strains have been generated. For example, IL-10, a regulatory cytokine and susceptibility gene for

IBD in adults and children, KO mice develop spontaneous colitis when conventionally raised, while being physiologically normal under GF conditions [54]. Hence, the model has been used in several studies investigating host-microbe interactions in IBD [55]. Chemically induced mouse colitis models have also been developed with DSS application in drinking water being widely used. The administration leads to colonic colitis by epithelial barrier disruption, due to loss of TJ protein ZO-1 [56, 57].

The overall intestinal tract anatomy and physiology is conserved between mouse and human. However, there are distinct difference, such as a shorter SI, but longer caecum in mice [58]. This has been attributed to differences in diet, with mice consuming a larger amount of complex carbohydrate non-digestible by the host, which requires fermentation by the gut microbiota in the caecum. Fittingly, these fermentation processes occur in humans predominantly in the colon, which is sub-compartmentalised into pouches, while the mouse LI is smooth. As the fermentation of plant derived carbohydrates is associated with short chain fatty acid (SCFA) production, which have health beneficial effects on the host, these differences in ecological niches should be taken into account when using mice in microbiota research [58].

Due to the importance of gut microbes for intestinal physiology and pathologies, it should be mentioned that the human and mouse microbiota are similar at phyla level, but 85% of genera found in mice are not present in humans. This together with implications for research will be discussed in section 6.1.2 [59].

A benefit of mouse models in microbiota research is the similarity between biological repeats due to co-housing effects, and control over diet, which generates reproducibility, which is often lacking in human samples [60]. GF mice are a powerful tool for studying interactions and effects of single or combinations of microbes on the host and even allow for colonisation so mice with human microbiota grafts. Humanised mice fed with high fat diets showed a decrease in Bacteroides/Firmicutes ratio, which emulates microbiota profiles in humans, with diets high in animal facts increasing Bacteroides abundance [61, 62].

1.2 Inflammatory Bowel Disease

Inflammatory bowel diseases are a heterogeneous, complex group of diseases involving chronic, intestinal, immune system mediated intestinal inflammation. The disease mechanisms are not completely understood, but are suggested to involve; multifactorial pathology, with dysregulated immune responses in genetically susceptible individuals to commensal intestinal bacteria, with environmental factors influencing onset and relapse of disease [63, 64]. Crucially, the IEC represents a major GI-associated cell type, with respect to disease pathophysiology, and is located at the interface between the host immune system, luminal microbes, and environmental factors (Figure 1-7).

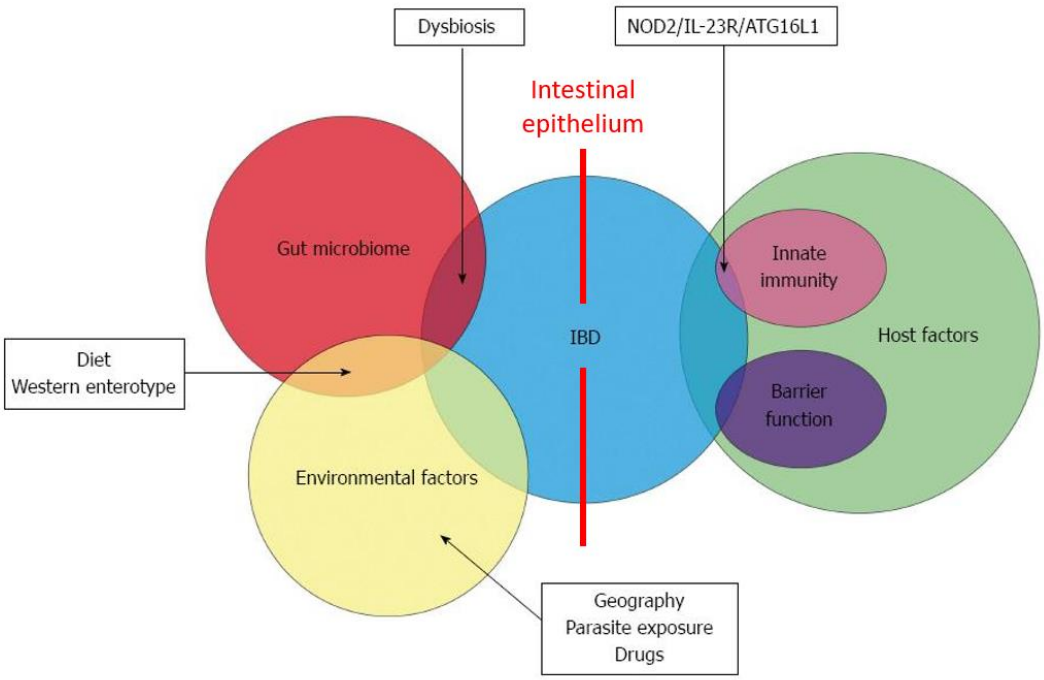

Figure 1-7 IBD pathogenesis is multifactorial with involvement of immune system and intestinal barrier in genetically predisposed individuals to gut microbes and environmental factors.

Venn diagram overlapping role of gut microbiome, host and environmental factors in the aetiopathogenesis of inflammatory bowel disease. Dysbiotic changes in gut microbiome may be influenced by diet and other environmental factors and predispose to inflammatory bowel disease (IBD). IBD patients can have genetic susceptibility factors including NOD2, ATG16L1, Interleukin

23 receptor, intestinal epithelium is located at interface between host and environment including gut microbiota (figure and legend adapted from Hold *et al.*, 2014 [63])

In the UK, more than 620,000 patients (0.5-1% of population), suffer from IBD, with a prevalence of 243 per 100,000 individuals for Ulcerative Colitis (UC), and 144 for Crohn's Disease (CD) [65-67]. IBD poses a heavy financial burden on health care systems of developed countries, with an estimated cost of at least €4.6 billion in the European Union in 2013. In the UK, treatment costs range from £1,693 to £10,760 per annum/patient, depending on disease type and severity [65, 67].

The incidence of IBD is influenced by geographical location, with the highest number of cases found in westernised countries. Notably, there is an increase in 'newly' westernised countries in Eastern Europe, and Asia, which highlights a potential link to socioeconomic development, and development of disease [66, 68].

1.2.1 IBD can be subdivided into Ulcerative colitis and Crohn's disease

IBD is an umbrella term for a diverse range of intestinal pathologies, which can be further subdivided into the two major forms UC and CD. This is an important clinical distinction, as therapy strategies between the two pathologies differ. Not all intestinal inflammation related to IBD can be definitively categorised as either UC or CD (non-classical forms), and diagnostic standards are still being improved [69].

UC is characterised by intestinal inflammation, and morphological changes limited to the colon, with the rectum being affected in many cases too. Inflammation is continuing and confined to mucosa. Patients present with bloody diarrhoea, weight loss and pain in the lower left abdomen. Figure 1-8 indicates the key pathophysiology features of UC.

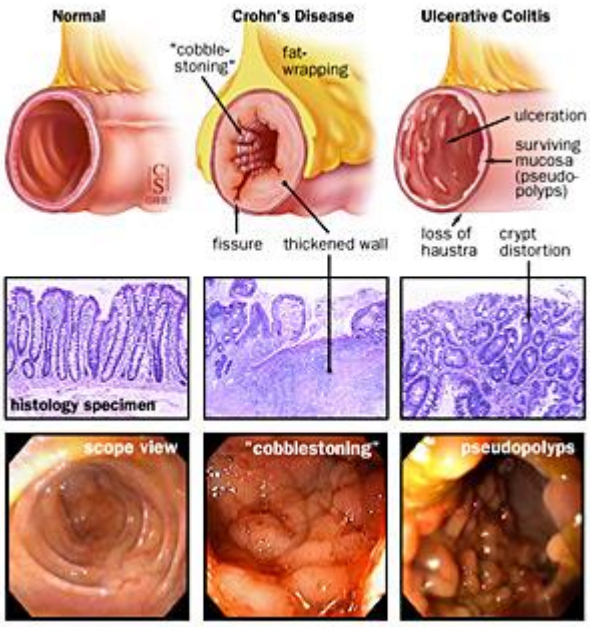

Figure 1-8 Comparison of colonic mucosa of healthy, Crohn's and ulcerative colitis patients.

Top – schematic overview, centre – histological comparison, bottom - endoscopic appearance (figure and legend adapted from John Hopkins Hospital Gastroenterology and Hepatology Division [70])

In comparison, CD-associated inflammation can affect any section of the GI tract, but is most commonly found in the distal ileum and colon. The affected areas can be discontinuous, and histologically the inflammation is transmural, and often includes the serosa. Clinical symptoms can be subtler, and are dependent on localisation of inflammation along the GI tract. Patients suffer from abdominal pain, cramps, and in certain cases also have bloody diarrhoea, which may make it difficult to differentiate from UC. Figure 1-8 displays the key intestinal pathological characteristics of CD [71].

Both diseases are chronic and can be lifelong, and drastically impact on quality of life for patients. They can also lead to life-threatening complications, including higher risk for development of colorectal cancer [72, 73]. IBD predominantly affects the GI system, but is associated with other non-intestinal manifestations including, joints, eye, and liver complications [74].

1.2.2 The aetiology of IBD

IBD is a multifactorial disease involving deregulated immune responses in genetically susceptible individuals, to the intestinal microbiota, with the intestinal barrier showing increased permeability. The pathology can be imagined as a cycle between intestinal inflammation, leading to epithelial barrier breakdown, causing further uncontrolled exposure of the host to microbial antigens, which in turn further drives inflammation [75]. It is still to be determined if the initial stimulus is generated by the immune system, or a leaky intestinal barrier [76]. However, evidence has emerged of increased permeability potentially being the initiating factor, as paracellular permeability of the IE of UC and CD patients was decreased during active and quiescent disease, compared to control (measured in biopsies in Ussing chambers culture, with FITC-dextran) [77]. Effects of low grade background inflammation in this study cannot be discounted, but further support is provided by IL-10 KO mice. This cytokine has anti-inflammatory effects and protects the IE by counteracting TNF-α and interferon γ (IFN-γ) effects [78]. KO mice develop spontaneous colitis, and increased intestinal permeability was detected early in life (starting at 2 weeks), before the on-set of inflammation (at 17 weeks) [79]. This is an interesting result particularly with paediatric IBD incidence having increased significantly over the last 15 years; in the USA at least 20% of all new cases being diagnosed in children [80, 81].

The scope of this studies lies on the pivitol role of the intestinal epithelium in human helath and disease and the following section will dicuss the IE and its barrier function in IBD as well as highlighting relevant aspects of genetics and the immune.

Environmental factors such as smoking, diet (including vitamin D), and stress are also influencing factors, but the major extrinsic factor involved in IBD pathogenesis is the microbiota, which will be covered in detail in the microbiota section (chapter 1.3.5).

1.2.3 The intestinal epithelium plays a critical role in IBD

The intestinal epithelial barrier forms a distinct border between the luminal contents of the gut, including the microbiota, and the host, and controls these interactions.

Hence, it is not surprising that it plays a pivotal role in IBD, with its breakdown contributing to the increased inflammatory response of immune cells. Several aspects of the epithelial barrier are affected in IBD, which will be described below, with a schematic overview shown in Figure 1-9.

As previously mentioned (section 1.1.5), TJs are integral to the epithelial barrier, and IBD patients present with modulated junction composition, which is linked to barrier dysfunction [82]. In CD, biopsies collected from patients with active disease, had reduced intestinal resistance, which was related to reduced and abnormal TJs. The TJ proteins occludin, claudin 5 and 8 were decreased in expression, and not integrated in the junction, while claudin 2 (forms pores within TJ allowing for ion passage) expression was increased. In addition, claudin 2 expression was inducible by TNF-α in HT-29 cells, which agrees with observations that TNF-α decreases epithelial barrier function *in vitro*, and can also induce apoptosis in IECs, as observed in a mouse model of CD [83-85]. Another pro-inflammatory cytokine involved in IBD is IFN-γ, which had previously been linked to reduced epithelial disruption, as IFN-γ KO mice had normal barrier histology, when compared to control mice [86]. A previous GWAS study linked a transcription factor of TJ proteins, hepatocyte nuclear factor 4 α (HNF4A), to UC susceptibility [87]. Correspondingly, HNF4A expression was decreased in UC and CD patients, and mice with an intestinal conditional KO, presented with increased intestinal permeability, and reduced mucus production, while also being more susceptible to DSS colitis [88].

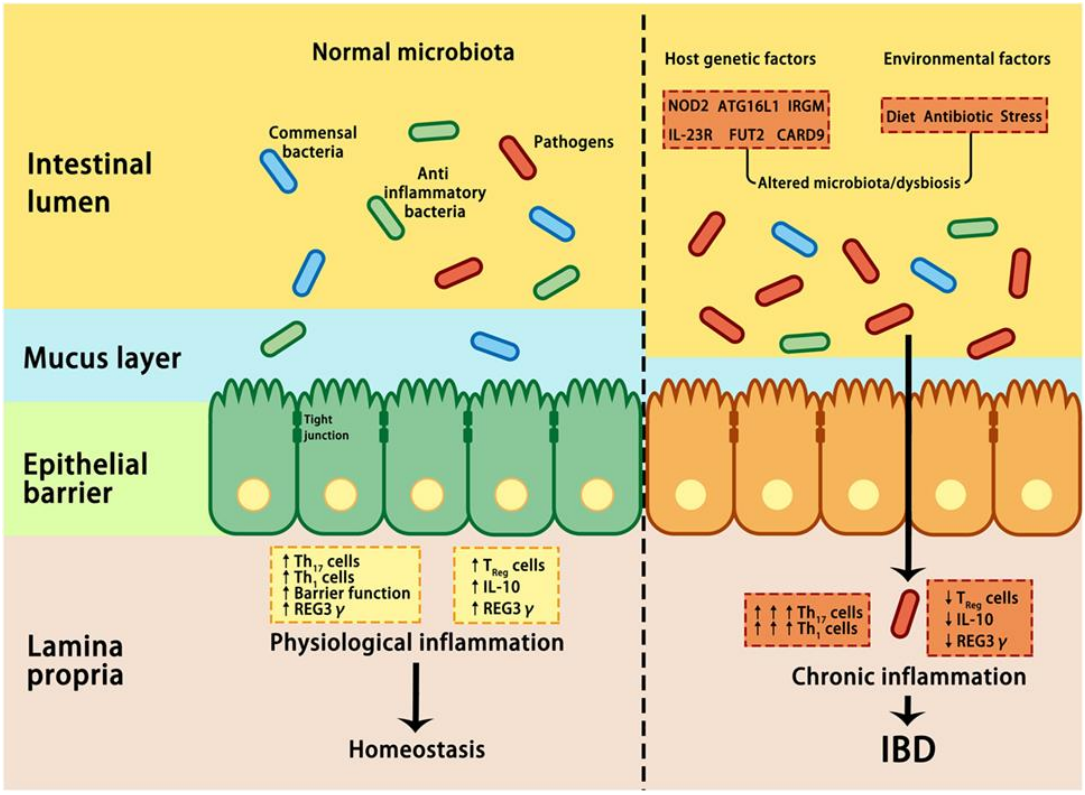

Figure 1-9 Overview over intestinal mechanisms involved in IBD pathology.

Under healthy conditions (left panel), pathogens are suppressed by beneficial commensal bacteria through the induction of antimicrobial proteins, such as IL-10 and REG3γ, thus maintaining homeostasis. In IBD (right panel), a combination of genetic factors and environmental factors (such as stress, diet, and antibiotic) lead to microbial dysbiosis, which in turn affects barrier integrity, innate, and adaptive immunity, resulting in uncontrolled chronic inflammation and hyper-activation of T helper 1 (Th1) and Th17 cells, increase in tight junction permeability, reduction in regulatory T (Treg) cells, and decrease in REG3γ and IL-10. ATG16L, autophagy-related 16-like; CARD9, caspase recruitment domain family member 9; FUT2, fucosyltransferase 2; IBD, inflammatory bowel disease; IL-10, interleukin 10; IRGM, immunity-related GTPase M; NOD2, nucleotide-binding oligomerization domain-containing protein 2; REG3γ, C-type lectin regenerating islet-derived protein 3γ (Figure and legend adapted from Zhan *et al.*, 2017 [89])

The importance of homeostatic cell shedding, and the increase in apoptotic, pathological cell shedding in IBD has been described in 1.1.5.1. Furthermore, UC patients have higher overall levels of apoptotic IECs, and numbers correlate with individuals eventually requiring surgery. In biopsies from CD patients, an increase in apoptotic IECs was localised to areas of active inflammation [90]. Notably, tumour necrosis factor-induced protein 3 (TNFAIP3), which inhibits activation of NF-κB by

TNF-α, inhibits IEC apoptosis, and previous GWAS studies have identified SNPs in this signalling molecule [91]. In *vitro*, TNFAIP3 has been shown to be critical for IEC tolerance to LPS, and *in vitro* an intestinal epithelial specific KO model showed increased susceptibility to DSS colitis and enterocytes hypersensitive to TNF-α [92, 93]. However, it is not yet known in which way the polymorphism associated with IBD affects gene function. Further support for the role of TNF-α, is provided by findings that TNF-α overexpressing mice show ileal and colonic inflammation (including villus shortening, similar to that observed in the SI of LPS challenge mice with elevated IEC apoptosis), and is comparable to CD patient histology [94]. In summary, these results agree with the hypothesis that inflammation drives IEC cell death and shedding, which in turn causes epithelial barrier breakdown, and further inflammation due to microbial exposure, thus perpetuating this vicious cycle.

Importantly, loss or impairment of epithelial integrity, is a hallmark of IBD as it directly causes the continuous exposure of microbial antigens to the mucosal immune system, and increased intestinal permeability can be used as a predictive measurement for relapse in patients with inactive disease. The role of the microbiota in IBD will be discussed in more detail in subchapter 1.3.5.

1.2.4 Scientific models of IBD

Animal models of intestinal inflammation have contributed greatly to our understanding of IBD pathogenesis, and are essential for pre-clinical drug testing.

A widely used experimental model of colitis, involves oral consumption of DSS dissolved in drinking water. This has been shown to induce both acute and chronic colitis in rodents, by inducing inflammation and recruitment of immune cells, and their subsequent activation directly through epithelial cell damage within the colon. This particular model has been found to resemble human UC in both clinical and histopathological findings. Indeed, DSS colitis is particularly useful to study innate immune mechanisms, including epithelial responses, of colitis during acute phases, whereas at later chronic stages it provides an opportunity to study the role that the adaptive immune system plays [95].

Another chemical model of colitis utilises TNBS, which is suggested to more closely recapitulate CD-associated pathology. TNBS administered (in tandem with ethanol) rectally to rats induces potent inflammatory responses, including marked epithelial destruction, which is associated with weight loss [96].

In this PhD thesis, a small intestinal model of epithelial barrier breakdown, induced by systemic LPS administration, is utilised. It induces apoptotic cell shedding, in a time, and dose dependent manner, and allows assessment of involved processes directly, and short term, without excessive off target effects. It has been described in more detail in subchapter 1.1.5.1.

Combination of transgenic mice, with microbiota modulation, can be a powerful tool to investigate microbiota involvement in IBD. Previous studies have shown that TNF overproducing mice ($TNF^{deltaARE}$) develop CD-like intestinal inflammation, with strong ileal involvement. These mice do not develop colitis or ileitis under GF conditions, with antibiotic treatment in conventionally raised mice, resulting in reduced ileum inflammation. The associated loss of antimicrobial defence mechanisms, due to failure of Paneth cells function (crytidin-2 and lysozyme), induced microbiota taxonomic and functional changes, which reproduced symptoms in GF $TNF^{deltaARE}$ mice after faecal transplantation, with no effects after transfer of faeces from healthy animals. This provides further evidence for the casual role of the microbiota in ileal CD, and the associated microbiota modulation [97].

Adoptive transfer of naive T cells ($CD4^+$ $CD45RB^{high}$), into mice deficient of T and B cells, and hence immunodeficient (SCID or RAG2 KO) induces colonic inflammation 5 to 10 weeks post administration. While transfer of mature T cells ($CD4^+$ $CD45RB^{low}$) by themselves, or in combination with naïve T cells, does not lead to colitis, due to the anti-inflammatory properties of T_{reg} cells and IL-10 [98]. Hence, it is not surprising that IL-10 deficient mice develop spontaneous colitis after weaning, which is histologically similar to human IBD. Extensive studies, indicate a multi-hit pathology during IL-10 KO colitis, as an interplay of loss of homeostasis, and suppression of innate (DC, macrophages), and adaptive immune response (T_h1/T_h17), and microbiota dysbiosis, or pathogen invasion, results in excessive pro-inflammatory cytokine production (IL-6/12/17/23, IFN- γ) [99].

1.2.5 Current treatment options for IBD

Anti-inflammatory drugs, 5-Aminosalicylates, are frequently used for treatment, and induction, or remission in UC, and may potentially prevent onset in high risk patients, however, they show very little effect in CD [100, 101]. Immunosuppressive agents can induce, and maintain remission in CD and UC [102]. Furthermore, two biologic agents have been introduced to clinical practice in the last decade, anti-TNF and anti-integrin agents [103]. Anti-TNF treatment with infliximab has revolutionised IBD treatment, and induces and maintains remission in both CD and UC [104, 105]. Anti-integrin therapy blocks activated T-cell homing to the intestine in response to inflammatory stimuli, reducing the exacerbated host response [102]. Several other new drugs are currently being developed and tested, including cytokine blockers, and inhibitors of cytokine gene expression [102]

Despite a plethora of new drugs, many patients do not respond to drug therapy (30-50% for anti-TNF therapy), and 30-40% of CD, and 20-30% of UC patients undergo surgery at some point in their life time, due to severity and progression of the diseases, with surgery associated post-operative complications [106].

Great progress has been made in IBD therapy, aided by large scale human genomic studies, complimented by mechanistic investigations, which often use IBD mouse models. Ultimately, the aim of IBD treatment is to induce remission and prevent induction in high risk individuals. There remains a large unmet need for novel therapeutics to achieve these aims. Probiotic intervention has been shown beneficial responses in IBD, and other related intestinal pathologies, which will be discussed further in general in section 1.3.5.3, as well as bifidobacteria specific in 1.4.6. Further investigation of involved mechanisms, could lead to the discovery, and identification of biomarkers and targets, for development of therapy interventions.

1.3 The intestinal microbiota and its symbiotic relationship with the human host

All surfaces of the human body, including the skin, oral cavity, and intestinal tract, are colonised by a complex microbial community called the microbiota [107]. The gut microbiota is the densest, with more than 10^{14} microorganisms, and includes bacteria, archaea, viruses, fungi and parasites. Members of the microbiota are being heavily investigated as their physiological role is essential for host health [108]. Here I will focus on the bacterial components of the microbiota.

Until the advent of next generation sequencing (NGS), the traditional method for studying the gut microbiota has been selective culturing [109]. Due to the complexity of the microbial community and their ecological niches, it has been suggested that the majority of organisms within the intestinal microbiota are un-cultivable, when comparing identified species by traditional *in vitro* growth to bioinformatic results (described below) [109, 110]. However, recent developments have increased the percentage of culturable bacterial species from intestinal samples, which has given rise to a field coined ‘culturomics’ (Lagier *et al.* [111], Lau *et al.* [112], Browne *et al.* [113]). The drawbacks of bacterial identification and isolation by culturing, are the time and labour requirements, however it is critically important to also perform phenotypic and functional analysis, particularly for development of therapeutics, hence a combined approach of sequencing identification and culturomics is warranted.

1.3.1.1 Application of next generation sequencing in microbiota studies

NGS is an umbrella term for technologies that determine the nucleotide sequence of millions of DNA or RNA fragments in parallel [114]. There are several differing technology platforms, and in general these can be separated into those that perform short or long read sequencing.

Short read length sequencing is very high throughput, cost efficient, and time requirements have improved significantly in the last years, making it a viable approach for large scale population analysis, and even clinical applications. This category includes Illumina sequencing with read lengths up to 300 bp, dependent on

the utilised platform. This technology performs sequencing by synthesis, which involves a priming adapter sequence binding to the sample DNA, and sequencing the complementary strand, nucleotide by nucleotide. The binding of fluorescent nucleotides to sample DNA allows for sequence detection, and is carried out in single base pair steps [115]. Long read length technology (utilised by Pacific Biosciences and Oxford Nanopore Technologies) is also constantly evolving, with improvements in cost and output, but has historically been applied more to *de novo* genome assembly [116, 117].

With cost of NGS decreasing, and output increasing, this has allowed the technique to be applied to the investigation of the human microbiota, which has corresponded with an explosion of research in this field.

The microbiome can be analysed/profiled in a variety of ways; metataxonomic, metagenomic, metatranscriptomics, metabolomics, and metaproteomics. Each of these techniques provides different levels of information about microbial communities, and each has certain advantages and disadvantages, and these will be discussed more fully below.

1.3.1.2 Taxonomic profiling by metagenomic 16S rRNA sequencing

To assess taxonomic composition of a microbiota sample, 16S rRNA sequencing is a powerful tool, due to its low costs, and high throughput analysis [118]. It based on sequencing of the bacterial ribosomal subunit 16S, but due to the total length of the gene (i.e. 1400 bp) being outside parameters of short read length platforms, amplicon sequencing of hypervariable regions (V1-V9) is used [118, 119]. The process involves binding of universal primers to stable regions adjacent to the hypervariable areas, amplification by PCR, followed by sequencing, and analysis; either directly (via BLAST) to reference taxa, or more commonly grouping of reads into operational taxonomic units (OTUs, based on 97% sequence identify) [120]. Importantly, the PCR amplification step can introduce bias between different taxa, which may be due to differing GC content between bacterial 16S sequences, thus affecting universal primer binding [121, 122]. Therefore, studies suggest that hypervariable region amplification should be chosen based on predicted microbiota composition, or several primer pairs used for an unbiased approached [118]. With

protocol and analysis improvements, 16S rRNA sequencing resolution has increased to genus level, and it is possible to quantify bacterial abundance relative to overall 16S rRNA transcripts [123].

Benefits of 16S metataxonomic profiling include, relatively low cost, the high throughput nature, and the identification of bacteria from theoretically single DNA copies by PCR amplification, hence increasing resolution of analysis greatly, particularly in low biomass samples. In addition, DNA can be extracted from dead cells without the need for live bacteria, in contrast to culturing, which broadens the variety of samples types capable of being studied [124-126].

1.3.1.3 Investigating the active functional profile of microbiota by metatranscriptomics and metabolomics

There has been a shift in the microbiota field from determining 'who is there' to 'what are they doing'. WGS allows the determination of potential functionality, based on genes present. This is generated by either mapping of raw reads to databases of reference genes, and their biological function, or by assembly into contigs, with the resulting predicted protein sequences being matched with similar functional databases. This has been used, for example, to assess changes occurring during IBD, with mouse models showing the acquisition of LPS secretion system during active disease [127, 128]. The fundamental limitations of this approach though are that the presence of a gene, and its associated biological function conferring functional potential, does not mean is it transcriptionally active.

This can be assessed by metatranscriptome sequencing, which analyses a snapshot of the transcriptional activity of a microbiota at a given time, via shotgun sequencing of the total RNA population [129]. Analysis of the generated data involves either mapping to reference genomes or *de novo* assembly into contigs prior to mapping [124]. The second approach is usually applied to samples, which do not have well characterised bacterial members.

The importance of analysing the transcriptional landscape is highlighted by findings from the gut microbiota, that transcription was more individualised between subjects than metagenomic functional profiles (but also less variable than taxonomy) [130]. The same publication also identified, over and underrepresentation of specific

transcripts, in relation to the abundance of their corresponding genes within the population (with 41% showing no differential regulation). Another example highlighting the importance of assessing transcription changes was observed in a gnotobiotic mouse model colonised by a model human gut microbiota. The administration of bifidobacteria and *Lactobacillus,* in fermented milk products, did not change the overall taxonomy or metagenomic composition. However, transcriptional analysis revealed an upregulation of genes related to carbohydrate metabolism, and in particular oligosaccharide fermentation *by B. animalis* subsp. *lactis* [131]. As carbohydrate metabolism is involved in bacterial cross feeding, and the resulting changes and products have been shown to affect the host (in particular butyrate production), this highlights the power of using transcriptional analysis to understand microbiome functions at a microbial community level, and how these genes may be involved in host crosstalk [132]. Furthermore, the correlation of bacterial transcription, with host effects, by dual transcriptomics (i.e. RNA sequencing, RNA-seq, of host and microbes), will further aid in understanding host-bacterial interactions. The iHMP with its paired sampling of host and microbiota aims to integrate these data [133].

Gene transcription is a proximity measurement of protein expression, but posttranscriptional modification, and translation rates can influence protein levels and functions [124]. Hence, the proteomic profile of microbiota communities is a more direct assessment of functional activity [134]. As not utilised in this study, it will not be detailed further.

Lastly, metabolomics can be used to identify and quantify metabolites, and other small molecules, in microbiota samples, and is considered a direct assessment of biological processes within a system [110, 135]. Metabolomics is based on analysis of compounds by high-performance liquid chromatography (HPLC) and mass spectrometry (MS), and/or nuclear magnetic resonance (NMR), but the heterogeneous nature of microbiome samples leads to difficulties in sample processing and analysis, due to wide range of products (e.g. carbohydrates, lipids, small molecules), and their dynamic concentration range [136]. Following data generation, pre-processing by peak picking, and deionisation, is followed by quantification of compounds through calculation of area below peaks. Metabolites

are identified by matching peak patterns to spectral databases, including machine learning for pattern recognition [137]. In IBD, metabolomics analysis showed a decrease of nicotinic acid in stool samples from CD patients [138]. Nicotinic acid is a bacterial product that signals via the same receptor as anti-inflammatory butyrate (GPR109A). Signalling through this receptor exerts anti-inflammatory effects on colonic macrophages and DCs, which in turn stimulate differentiation of T_{reg} cells, and IL-10, while colonocytes are stimulated to produce IL-18. [139].

With omics studies becoming more and more common, the next logical step is integration of different data types, to generate a holistic, dynamic network of biological function within the microbiota, and with the host [110]. Pathway analysis, based on taxonomic, genomic, transcriptional, proteomic and metabolomic databases, can aid in this process, giving deeper biological insights. This analysis could aid in hypothesis generation, associating distinct data types, and filling mechanistic gaps, as well as increase confidence in observations if several different data types arrive at the same conclusion [124]. Indeed, a recent publication utilised the previously mentioned dual RNA-seq method in a mouse colitis model, and showed a link between macrophage and granulocyte presence in the gut lumen, with bacterial upregulation of oxidative stress responses, implicating this in microbiota shifts during IBD [140]. This will be discussed further in chapter 5.

1.3.2 The human gut microbiota

The healthy adult gut is colonised with a bacterial community consisting of between 100 to 1000 unique bacterial species, with 160 commonly shared between individuals, and a total of 10^{14} microorganisms [141, 142]. The most abundant phyla are Bacteroidetes and Firmicutes, which contribute 80-90% of the total community, with the predominant classes in Firmicutes phylum being Clostridia and Bacilli, while the most abundant class in Bacteroidetes is Bacteroides [143]. In the following, I will described the overall gut microbiota composition in more detail, together with changes during the human life time, and highlight dysbiosis during IBD.

1.3.2.1 Microbiota composition in the gastrointestinal tract

In the GI tract, the composition and density of microbe colonisation increases longitudinally, and across the lumen, due to differences in the environment, and is summarised in Figure 1-10.A. In the stomach, 10^{2} microorganisms per g of content can be found, which increases in the SI, and reaches 10^{12} per g within colonic content, which is the densest ecosystem, and contributes 70% of the total number of microbes found in association with the human body [143, 144]. In the stomach, and SI, a lower pH environment, caused by gastric acid, and digestive enzymes (e.g. bile acids), and higher levels of oxygen, create a harsher environment for bacterial growth, while in the LI, which has a lower pH, an anaerobic environment, and an array of complex carbohydrates, favours dense microbiota colonisation [145].

Colonisation of microbes within the intestine cross-section differs; with complex microbial populations found in the lumen, and outer mucus layer (Figure 1-10.B). Levels in these regions are higher in the LI, due to the higher density, and thicker outer mucus layer, compared to the SI. The inner mucus layer is largely devoid of microbes [146]. Differing species can be observed by fluorescent in situ hybridisation (FISH) in the mucus layer, compared to intestinal contents, with *Bacteroides*, *Bifidobacterium*, *Streptococcus*, *Enterobacteriacae* and *Ruminococcus* preferentially found in luminal samples, while *Akkermansia* is more prevalent within intestinal mucus [147].

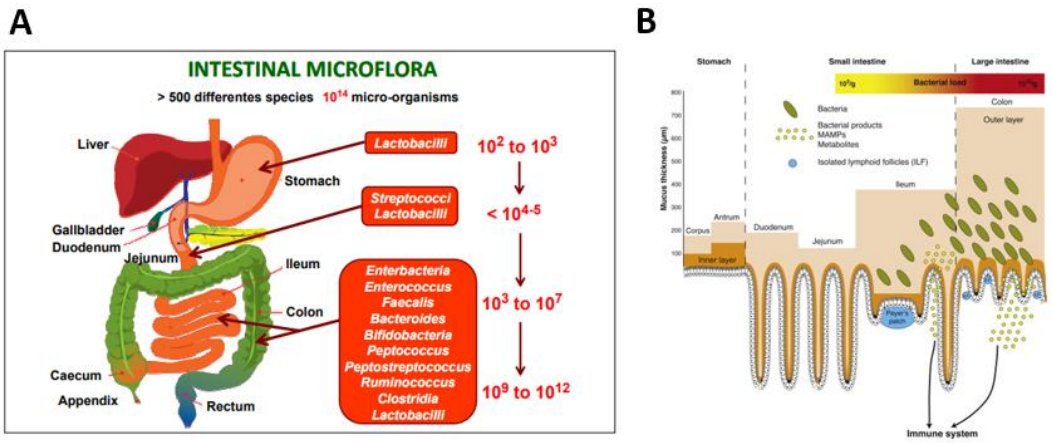

Figure 1-10 Longitudinal and transverse distribution and composition of bacteria in the gastrointestinal tract.

A Overview of composition and quantity of interinal microbiota along gastrointestinal tract. (figure and legend adapted from Konturek *et al.*, 2015 [148]). **B** Mucus layer morphology and colonisation by bacteria along intesitnal tract (figure and legend adapted from Macpherson & McCoy, 2013 [146]).

In the upper GI tract, *Lactobacillus* is the dominant genus. Within the LI, Firmicutes and Bacteroidetes are the predominant phyla, as well as Fusobacteria, Actinobacteria (which includes the beneficial member *Bifidobacterium*, which will be discussed in more detail in subsequent sections), Proteobacteria and Verrucomicrobia being represented in lower numbers (Figure 1-11.A) [147, 149]. The abundance ratio of these main components and their species composition can differ greatly across individuals. So far, the identification of "core" species in the adult intestinal microbiota has been difficult due to variation across life stages (discussed below), and between samples cohorts, especially comparing westernised and developing countries [147, 150]. Based on 16S rRNA sequencing of 17 faecal samples, and the requirement to be present in at least 50% of individuals, *Faecalibacterium prausnitzii*, *Bacteroides vulgatus*, *Roseburia intestinalis*, *Ruminoccous bromii*, *Eubacterium rectale*, *Copronacillus* sp. and *Bifidobacterium longum* was identified as potential core species [151]. Other studies identified differing shared members, and it has been hypothesised that the concept of core species is unlikely [141, 152].

In contrast to finding common taxonomic composition, the result that inter-individual taxonomic difference does not affect the functional genomic repertoire of

the gut microbiota, as observed in 18 faecal samples from monozygotic twins, is intriguing (Figure 1-11.B). The analysed microbiota shared > 90% of gene functions, suggesting core functional groups, which are involved in housekeeping processes, such as transcription and translation, and also carbohydrate metabolism of substrates found in the human GI tract (e.g. N-glycan degradation, fructose/mannose metabolism) [153]. These conserved functions are suggested to play an important role for the host, and will be discussed in detail further down below [142].

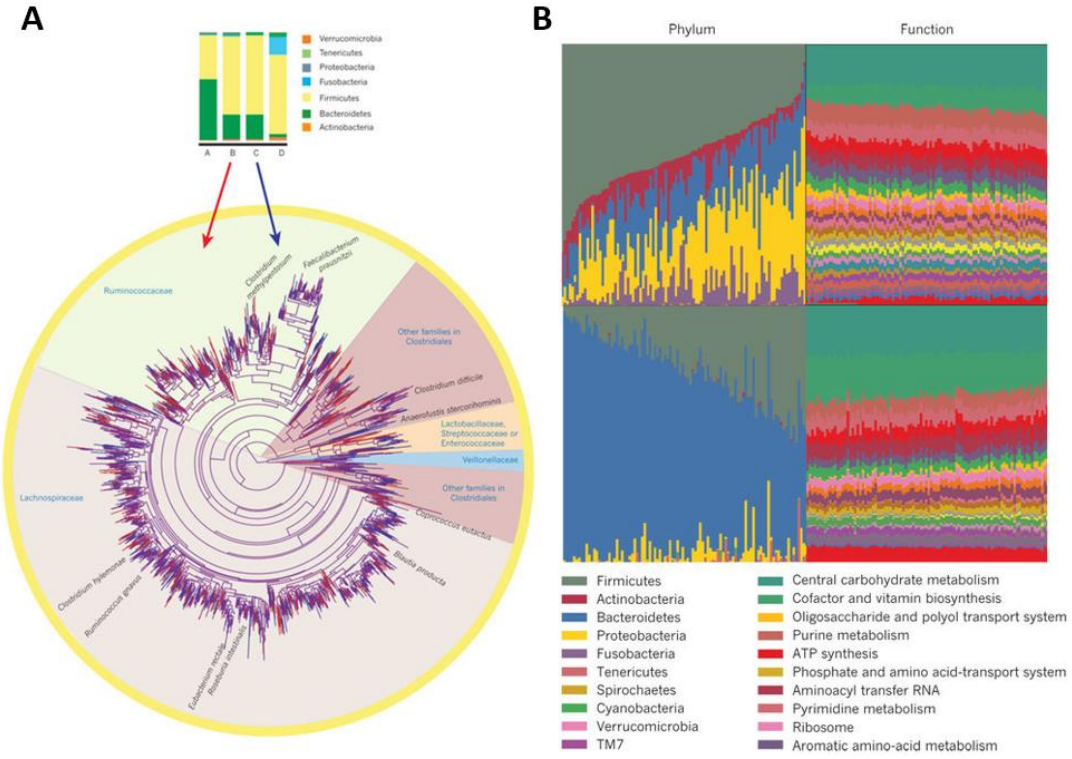

Figure 1-11 Diversity of human microbiota at different phylogenetic scales and functional redundancy of differing compositions.

A 16S rRNA sequence data of four adults from the United States, high diversity and variability among individuals, taxonomic grouping at high levels can mask this diversity is shown. Phylum level diversity can have marked variation even across healthy adults in the same population, tree depicts phylogenetic relationships between species-level phylotypes in most diverse phyla (Firmicutes) in individuals B and C, Branches specific to individual B are red; branches specific to individual C are blue; shared branches are purple. **B** Functional redundancy in microbial ecosystems may mirror that in macroecosystems, HMP data set, oral communities (top panels) and faecal communities (bottom panels) analysed using 16S rRNA, tremendous abundance diversity, shotgun metagenomics (panels

on right) have remarkably similar functional profiles. (figures and legend adapted from Lozupone *et al.*, 2012 [152])

1.3.2.2 Microbiota composition during human life time

The colonisation of the human body starts at birth, and continues throughout the life course (Figure 1-12). The development of the human gut microbiota has recently been reviewed by Thursby & Juge, 2017 [154].

Recent findings suggest that embryos *in utero* could be exposed to bacteria, as low richness, low diversity profiles were found (with Proteobacteria being the predominant member), in placenta, amniotic fluid and meconium samples from a study of 15 mother-infant pairs [155]. However, this *in utero* 'seeding' is still controversial, but represents an interesting area for further research, particularly the impact this may have on immune system development.

It is certain that the first major exposure of the human body to microbes occurs during birth [156]. Naturally born babies present with an intestinal microbiota rich in *Lactobacilli*, which is a prominent member of the vaginal microbiome, and hence birth canal [157]. In early life, the intestinal microbiota is characterised by low diversity and complexity, with Actinobacteria, Proteobacteria and Firmicutes representing the main phyla, and *B. longum*, *B breve* and *B. bifidum*, the most abundant species [156, 158, 159].

The early life microbiota is in constant flux, and diversity and richness increases over time until at 2-3 years of age an adult 'climax' community develops. Contributing factors to this change are diet, exposure to environmental microbes, and immune development [154]. The trend of increased diversity continues until adulthood, at which richness reaches its peak [142]. The adult microbiota composition (as described above) remains mostly constant from then onwards, and the described high inter-individual variability could be attributed to factors discussed below (diet, genetics, antibiotics).

Old age, defined as a decrease in physiological functions in advanced age, negatively affects gut microbiota diversity, but the specific effects are unclear [160]. It is believed that the microbiota stays temporally stable, but greater inter-individual

differences have been observed, with Bacteroides abundance ranging from 92 to 3%, and Firmicutes from 94 to 7% in a 16S rRNA study of 161 seniors [161]. Interestingly, an increase in opportunistic pathogens (*Campylobacter*, *Helicobacter*, *Fusobacterium*) has been detected in faeces of elderly individuals [162].

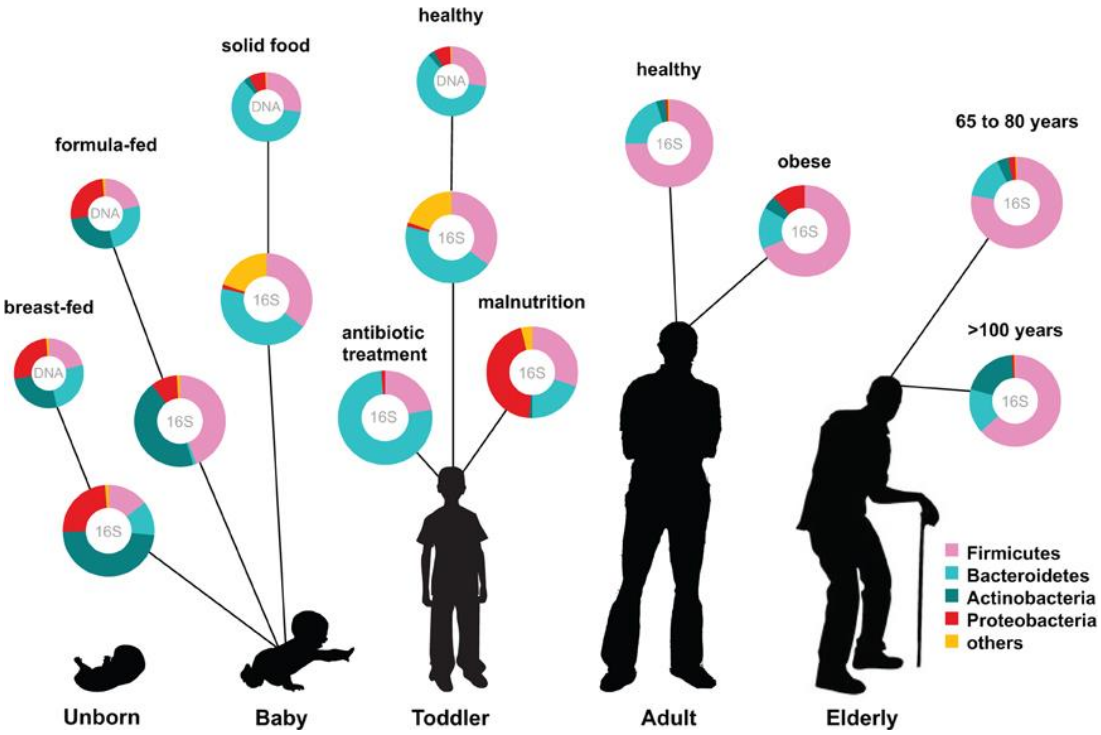

Figure 1-12 Composition of the human gut microbiota across life stages

Global overview of relative abundance of key phyla of human microbiota composition in different stages of life. Measured by either 16S RNA or metagenomic approaches (Figure and legend amended from Ottman, *et al.*, 2012 [143]).

1.3.3 Function of the gut microbiota for the host

The co-evolution of human host and gut microbiota has led to a symbiotic relationship, which under homeostatic conditions, allows the microbiota to perform beneficial functions, and in turn the host provides nutrient resources, and niches for their survival [143]. These functions are encoded in the microbiome (total genetic information of the microbiota), which is at least 100-fold larger than the human genome, and sometimes referred to as the second genome [142, 163]. At a top level, commensal bacteria participate in nutrient metabolism, immune- and intestinal barrier modulation, and colonisation resistance from pathogens (Figure 1-13) [164]. In the following sections I will give details for each functional category.

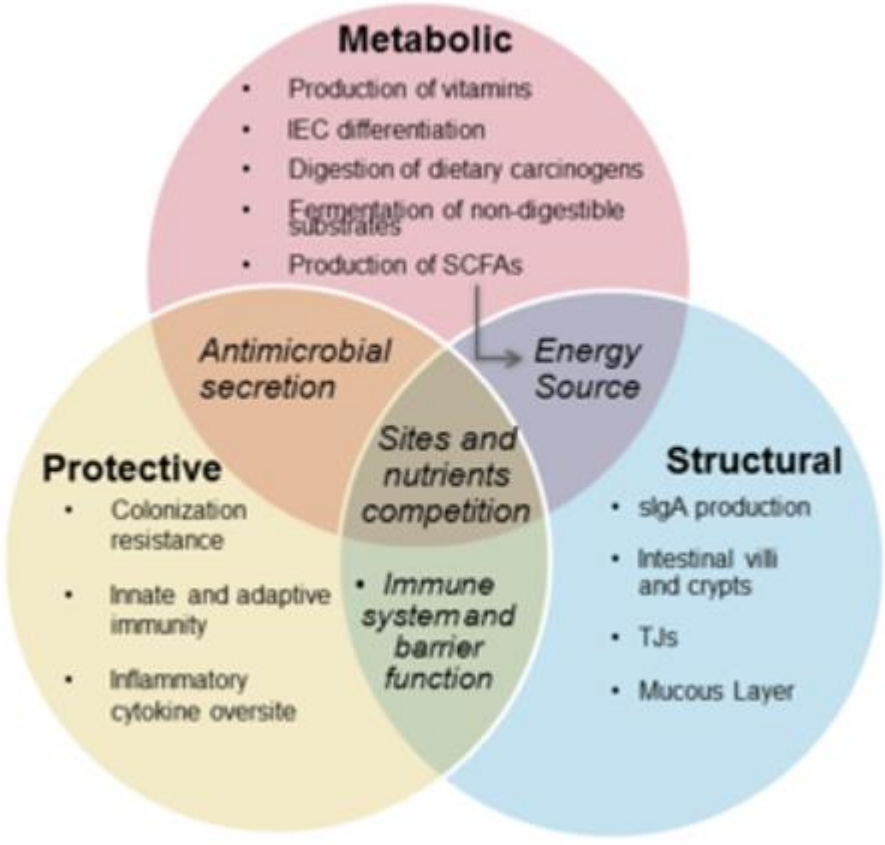

Figure 1-13 Overview of microbiota functions for the host in gastrointestinal tract

(adapted from Grenham *et al.*, 2011 [164] and Neana [165]).

1.3.3.1 Digestions of dietary components by the gut microbiota

The human gut microbiota utilises both dietary, and host derived substrates for growth and replication.

Simple carbohydrates are absorbed in the upper GI tract by the host, and the residing microbes, while non-digestible, complex carbohydrates such as resistant starches, plant cell wall polysaccharides, inulin and oligosaccharides reach the LI [166, 167]. The colonic microbiota harbours an extensive genetic repertoire for fermentation of these substrates [167]. Bifidobacteria play a significant role in this process and can cross-feed with other microbiota members, which will be discussed in more detail in section 6.1.1.

Besides bifidobacteria, *Bacteroides* are associated with plant polysaccharide degradation, with *B. ovatus*, *B. thetaiotaomicron*, and *B. uniformis* have a particularly wide substrate range, which is suggested to be responsible, at least in part, for their high abundance in the adult GI tract [168, 169]. *Bacteroides* spp., are also believed to be cellulytic, but so far only *B. cellulosilyticus* has been shown to degrade cellulose [170]. In contrast, hemi-cellulose like xylans, mannans and galactomannans can be utilised by *B. ovatus*, *B. thetaiotamicron*, and *B. xylanisovens* [171-173].

Degradation of these complex carbohydrates leads to the production of SCFAs; butyrate, propionate and acetate. They are present in a 1:1:3 ratio in the human gut, and several bacteria have been shown to produce SFCAs, with butyrate production mainly associated with Firmicutes, and propionate with Bacteroides [174, 175]. Acetate is generated by most microbes found in the intestine, including bifidobacteria [174]. SCFA production can contribute to social interactions, based on cross-feeding, which has been shown to increase e.g. butyrate levels, which will be discussed in the bifidobacteria section.

SCFAs have many health beneficial effects on the host. All three are absorbed by IECs, and acetate is gluconeogenic, while propionate is lipogenic in the liver. In this regard, acetate has been shown to reduce serum insulin levels, and supress adipocyte lipogenesis, which can reduce fatty acid flux to liver [176].

Butyrate is the best studied SCFA. It has far reaching effects; acting as an energy source for colonocytes, affecting epithelial barrier integrity (via mucus and TJ proteins), as well as modulating epithelial turnover and the immune system [154, 177].

Folate production appears to be restricted to bifidobacteria, with certain strains (e.g. *B. bifidum*, *B. longum* subsp. *infantis*) characterised as high-level producers, and others (e.g. *B. breve*, *B. longum* subsp. *longum*, *B. adolescentis*) as low level producers *in vitro* [178]. The administration of *B. adolescentis* and *B. pseudocatenulatum*, together with prebiotic oligofructose, to rats resulted in an increase in systemic and liver folate concentrations [179]. Interestingly, folate serum levels are significantly lower UC patients compared to control [180]. The intestinal effects of folate are still being investigated, however apoptosis of IECs is increased with folate deficiency, suggesting that folate is important in physiological IEC cell turnover [181].

The intestinal microbiota also participates in bile acid conjugation, and regulates production by the liver in a feedback loop, which will be described in more detail in chapter 6.

1.3.3.2 Colonisation resistance and antimicrobial production by the microbiota.

The healthy gut microbiota plays an important role in protection against pathogen infection, which has been shown in GF mice being more susceptible to *C. rodentium* infection, while the presence of a complete microbiota eradicated the pathogen within 21 days [182]. Supportive of this finding, are observations that antibiotic treatment increases susceptibility to infections in humans and mouse models, as shown with *Clostridium difficile* infection. The exposure to antibiotics reduces microbiota diversity and induces *C. difficile* overgrowth in mice [183]. Similarly, the pathogen does not colonise the human intestinal tract unless the normal microbiota has been disturbed (commonly after antibiotic treatment), and is the main cause of hospital-associated infectious diarrhoea [184].

The mechanisms by which the gut microbiota confers colonisation resistance can be subdivided into direct; i.e. competition for niches and nutrients, and anti-microbial production, and in-direct; i.e. enhancement of innate and adaptive immunity, and strengthening of the epithelial barrier.

As nutrients are limited within the intestinal tract, niche competition is fierce in individuals with a healthy, complete microbiota. Hence, it is not surprising that resident bacteria with similar metabolic requirements as invading pathogens will 'contest' their colonisation. This has been shown in a mouse model of enterohemorrhagic *E. coli*, simulated by *C. rodentium* infection. GF mice colonised by the pathogen were gavaged with an intestinal commensal *E. coli* from SPF mice causing a 200-fold reduction in *C. rodentium* faecal cfu within 3 days, and complete clearance within 14 days.

The gut microbiota modulates the host immune system, which has been shown to aid in fighting pathogen infection. Commensal microbes induce IL-22 production in innate lymphocytes, which signals to IECs, causing increased mucus production, TJ protein expression, and antimicrobial production (RegIIIγ, β-defensins) [185]. This is supported by GF mice having lower levels of IL-22, and mice genetically modified to lack IL-22 producing cells, were more susceptible to *C. rodentium* infection [186,

187]. This strongly suggests that commensal bacteria regulate IL-22 production, and via this mechanism offer protection against pathogen colonisation.

1.3.4 Interaction of the microbiota with the intestinal epithelium

The intestinal microbiota has a profound effect on the IE, as observed in GF animals, and SPF mice treated with antibiotics, as they show decreased epithelial turnover, measured by reduced crypt proliferation, and migration of enterocytes up the crypt villus axis. Interestingly, oral administration of SCFAs (i.e. acetate, propionate, butyrate) restored turnover in antibiotic treated SPF mice, suggesting these microbial products mediate this effect [188].

A summary of microbiota interact with the IE is given in Figure 1-14 and specific mechanism will be discussed below.

Butyrate can influence both IEC proliferation and apoptosis, in what has been labelled the “butyrate paradox”. Butyrate concentrations are highest in the lumen at 5 mM, with the mucus barrier causing a gradient, leading to reduced concentrations along the crypt villus axis, which reaches its lowest point (50-800 uM) at the crypt bottom [189, 190]. Butyrate influences histone acetylation in colonocytes in a dose dependent manner, with lower concentrations, as found in the crypts, being completely metabolised by the IECs, which increase acetyl-CoA a co-factor for histone acetyl transferases, causing histone acetylation. When colonocytes are exposed to higher levels (at the villus tip), not all butyrate can be metabolised, which accumulates in the nucleus where it acts as a histone deacetylase inhibitor. These two processes cause upregulation of differing gene expression profiles, and lead to a stimulation of growth in the crypts, while IECs at the tip have reduced proliferation, and undergo apoptosis [191]. This has been suggested to be protective from development of colorectal cancer.

Regarding barrier integrity, butyrate appears to potentially be the most potent of the intestinal SCFAs, as shown *in vitro*; butyrate increased barrier reestablishment following breakdown, and increased overall barrier integrity by increasing claudin-1 expression, and redistribution of ZO-1 and occludin to the TJ complex [192]. In a mouse model of hepatic ischemia, causing intestinal epithelial damage and bacterial translocation, butyrate administration maintained the epithelial barrier, and reduced

endotoxin translocation, by increasing ZO-1 expression, as well as reducing liver macrophage activation, and neutrophil infiltration, linked to a reduction in serum TNF-α and IL-6 levels [193]. These data suggest a combinatory effect of butyrate, by increasing epithelial barrier integrity, and excreting anti-inflammatory modulation, that could play an important role in host homeostasis.

Commensal bacteria also appear to facilitate epithelial repair, as shown by *L. rhamnosus* GG in a DSS mouse model. *L. rhamnosus* gavage for a single day was shown to enhance recovery from DSS damage, measured by a decrease of systemic and local inflammatory markers, and increased barrier function (FITC-dextran permeability). This effect was related to production of reactive oxygen species *in vivo*, which resulted in increased focal adhesion (FA) formation, and IEC migration (via increased focal adhesion kinase phosphorylation). FA are essential in repairing the IE, as they facilitate cell migration, thus these results suggest a health beneficial effect of *L. rhamnosus* by facilitating epithelial wound healing and restoring barrier integrity [194].

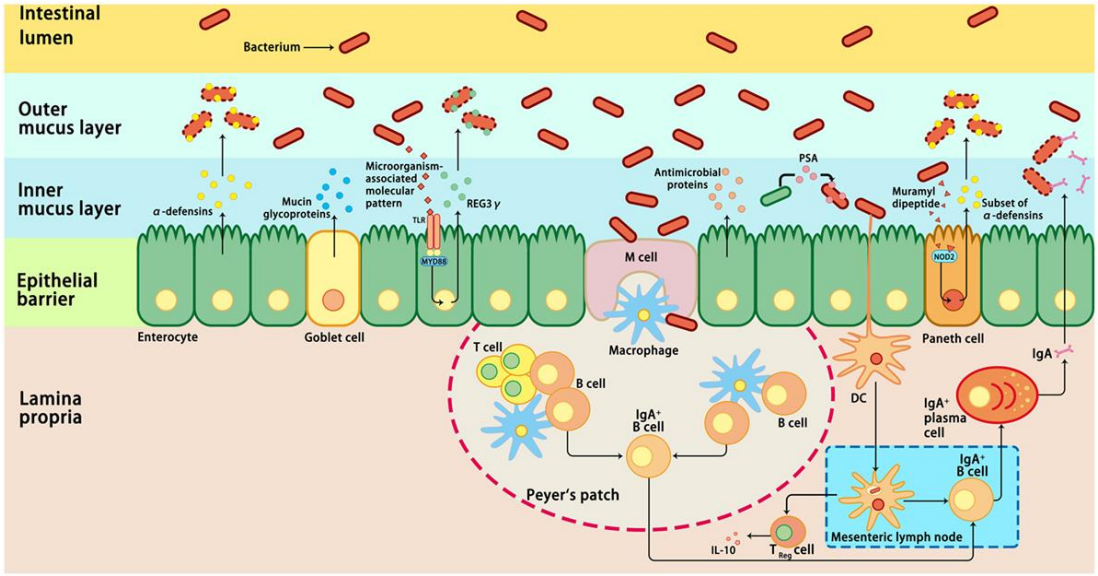

Figure 1-14 Intestinal epithelial responses to gut microbes in IBD

Several immune mechanisms work in concert to the intestinal microbiota and contribute to intestinal homeostasis. Goblet cells secret mucin glycoproteins, plasma cells secret IgA, and epithelial cells secrete antimicrobial proteins through toll-like receptors (TLRs), or nucleotide-binding oligomerization domain-containing protein 2 (NOD2)-dependent mechanisms. (figure and legend adapted from Zhang *et al.*, 2017 [89])

The mucus barrier is an important host defence mechanism. A role for the microbiota in mucus production is also suggested, as GF mice present with decreased mucus thickness, and this can be restored by administration of LPS and peptidoglycan [195, 196]. Furthermore, certain microbiota members can influence mucus production and glycosylation. *B. thetaiotaomicron* can digest host derived glycans, and when administered to GF mice increased goblet cells numbers, mucus production, and modulated glycosylation profile in the colon, 2 days following gavage [197]. Glycan modification can also confer health beneficial effects. *L. casei* and *B. thetaiotaomicron* can modify the cell-surface glycans of HT29-MTX cells *in vitro,* which blocks rotavirus infection.

The antimicrobial function of RegIIIγ has been mentioned (1.1.4), together with induction of its release from Paneth cells by the commensal *B. breve* in GF mice. This suggests a role of the microbiota in stimulating the intestinal barrier via antimicrobial secretion and is hypothesised to be depend on Myd88-dependent TLR sensing. This is supported by Myd88 IEC specific KO mice showing impaired RegIIIγ secretion [198]. Furthermore, RegIIIγ and RegIIIβ impaired mice are more susceptible to infection of several gut pathogens, including *L. monocytogenes* and *S. enterica* subsp. *enterica* [199, 200].

Lastly, strengthening of the epithelial barrier and protection from pathological IEC apoptosis via TRL2 signalling of the microbiota has previously been shown. *In vitro,* activation of TLR2 by a synthetic lipopolypeptide preserved TJ integrity and barrier function, and decreased apoptosis in Caco-2, IEC-6 and *ex vivo* murine small intestinal epithelial cells. Furthermore, *in vivo,* during DSS-induced colitis the activation of TLR2 restored TJ integrity, and reduced apoptosis in epithelial cells which resulted in reduced inflammatory responses [201]. Hence, it is suggested that the recognition of bacterial cell wall peptidoglycans by TLR2 is important for stimulation of the intestinal barrier in homeostatic settings.

1.3.5 Dysbiosis of the gut microbiota

1.3.5.1 Influencing factors potentially causing dysbiosis

The human gut microbiota can be influenced by a variety of environmental, and host derived factors. The most significant and far reaching is thought to be exposure to antibiotics. One human study observed that a seven-day course of clindamycin induced significant disturbances of the gut microbiota, with a sharp decline in *Bacteroides*, which did not recover fully during the two year observation period [202]. As discussed in the section about colonisation resistance, decreases in microbiota diversity, by antibiotic treatment, reduces colonisation resistance and increases susceptibly to various pathogens, including *C. difficile [203]*.

As the first major exposure of the human body to microbes occurs during birth, mode of delivery has a strong effect on the composition of the seeding microbiota [156]. Infants born via C-section show reduced diversity lasting for 2 years, lower abundance and diversity of *Bacteroides*, high incidence of *Staphylococcus* and *Acinetobacter*, and overall stronger similarities with the composition of the skin- and hospital-associated bacteria [204]. As the early life microbiota confers important functions for the host (immune modulation, pathogen resistance, etc.), these differences may result in negative effects for the host, such as increased risk of developing of necrotising enterocolitis (NEC) [205].

Diet can significantly shape the human gut microbiota in early life as well as in adulthood. Strong differences have been observed between breast and formula fed infants, with bifidobacteria being the predominant coloniser in response to breast feeding. Bottle feeding supports *Bacteroides* growth, with reduction of bifidobacteria abundance [206, 207]. Further studies have indicated a more complex *Bifidobacterium* microbiota is associated with breast feeding, and that specific strains (e.g. *B. longum* ssp. *infantis*) typically associates with breast feeding [208, 209]. This is particularly important as bifidobacteria have many health beneficial effects for the host, which will be covered in the next subsection.

Dietary changes in adulthood can significantly modulate the intesitnal microbiota but is not the focus of this study, hence will not be described in great detail. Diet-induced changes can be rapid, as a recent human trial showed that within five days, the intestinal bacterial composition was altered by dietary intervention, with greater effects than inter-individual differences. The effect of fibres was observed in a human study involving 14 overweight men. The diet was either high in resistant starch, or contained no starch polysaccharides, and was consumed for 3 weeks. Great inter-individual differences to diet modulation were observed, but time course analysis by 16S rRNA revealed distinct changes, which were reversed by the opposing diet regime [169].

Lastly, host genetics can shape the microbiota. This has been extensively studied in IBD, and large cohort GWAS studies showed a consistent microbial profile for certain shared SNPs, such as NOD2, across individuals [210]. Another example is a mutation in IL-10, or its receptor, which has been linked to very early onset IBD [211]. As described, IL-10 deficient mice suffer from spontaneous colitis shortly after weaning [212]. No comparison between modulation of the microbiota in IL-10 KO mice and patients carrying the SNPs have been made, but it could be hypothesised that this genetic alteration influences the profile, as the model identified intestinal microbes as the driver of colitis [99].

1.3.5.2 Diseases associated with dysbiosis

These modulating factors can alter the human microbiota, which when associated with disease, is termed dysbiosis. Many studies have observed a decrease in diversity associated with disease states, as well as shifts in overall composition, but for multifactorial pathologies no single disease-causing microbiota member has been identified.

Human studies have shown that a low diversity of the intestinal microbiota precedes asthma onset at school age [213]. Further studies showed a decrease in relative abundance of genera *Lachnospira*, *Veillonella*, *Faecalibacterium* and *Rothis* in a study of 319 infants at risk of asthma. The underlying mechanism is not yet understood, but is suggested to potentially involve invariant natural killer cells, which are elevated in the lung and the intestine in GF mice, increasing morbidity to ovalbumin driven allergic asthma, and oxazolone-induced colitis [214].

A role of the gut microbiota in obesity was first discovered when the transfer of microbiota from obese mice into GF mice resulted in a weight gain of the recipients [215]. Since then, several studies have investigated the difference between the microbiota of normal vs obese state, and have identified a decrease in *Bacteroides,* both in humans, as well as mice [59, 216]. Interestingly, diversity is decreased with weight, when comparing lean with obese twins, while weight loss increases richness [217].

Large parts of the investigations profiling microbiota dysbiosis in IBD have concentrated on analysing differences in composition, between disease samples and healthy controls. Recently, some promising functional association have emerged, and I will give an overview over both below.

In general, CD and UC microbiota profiles are lower in diversity compared to the general population, and seem to harbour distinctly different communities compared to each other [143]. Figure 1-15 shows relative abundance of statistically significant altered intestinal microbiota families in UC and CD patients, compared to controls from a recent human study, including 313 IBD patients and 512 healthy volunteers assessed by 16S rRNA sequencing [218].

In CD, a study of 6 patients and 6 controls by 16S rRNA microarray hybridisation, showed a decrease in Firmicutes, attributed to several species including *F. prausnitzii*, *R. albus*, and *B. fragilis*, while *C. difficile*, *Shigella flexneri* and *Listeria* spp. were present in higher abundance [219]. A different study of 40 twins, either concordant or discordant for CD, utilising 454 pyrotag sequencing, observed a difference between CD patients and healthy controls. Overall, colonic CD presented with increased Firmicutes abundance compared to control levels, while ileum CD had decreased abundance including *F. prausnitzii* [220].

The same twin study did not observe a clear separation in microbiota profiles between CD patients and healthy controls [220]. In contrast, phylogenetic analysis of 15 UC patients during remission and active disease, and 15 controls, found the UC microbiota to be stable and similar between patients across age, gender, and location. Diversity was reduced compared to controls, and significant decreases in abundance was observed for *Clostridium* cluster IV members, as well as butyrate and propionate producing bacteria (including *R. bromii* and *Eubacterium rectale*). Opportunistic pathogens including *Fusobacterium* spp., *Helicobacter* spp., and *Campylobacter* spp., were increased [221]. The authors hypothesised that reduced SCFAs with their anti-inflammatory and barrier strengthening effects, could be involved.

Overall, it has been suggested that IBD patients harbour reduced anti-inflammatory bacteria within the gut microbiota (e.g. *F. prausnitzii* and *B. adolescentis*), while being enriched for members with potentially pro-inflammatory properties, such as *R. gnavus* [89, 222]. However, studies have observed inconsistent results, most likely due to the diversity of the human microbiota, and the fact that IBD is a multifactorial disease, with phylogenetic differences being caused by an interplay of host genetic, microbiota and environmental factors [223, 224].

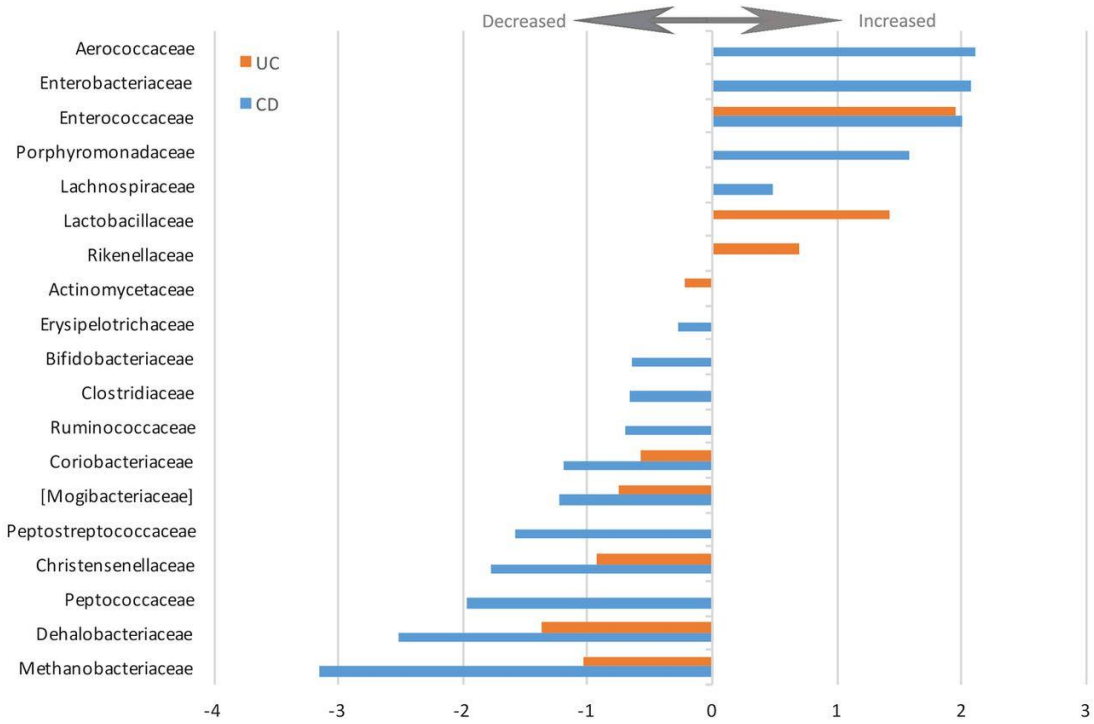

Figure 1-15 Changes to abundance of bacterial families in patients with UC and CD patients versus healthy controls.

(data shown as log2 fold change compared to healthy controls, false discovery rate<0.05, adapted from Imhann *et al.*, 2016 [218])

IBD dysbiosis is often characterised by a shift in abundance from obligate anaerobes to facultative anaerobic bacteria. As the intestinal inflammatory response in IBD produces nitric oxide and reactive oxygen species these could be utilised by facultative anaerobes such as *Enterobacteriaceae* [225]. This increase has also been observed in an immune compromised colitis mouse model, and adherent invasive *E. coli* can induce colitis in WT recipient mice [226]. Using a culture dependent approach, *E. coli* abundance was associated with the mucosa (isolation from lesions), was increased in CD patients (30%), compared to UC (6%) and healthy controls (5%) [227]. Adherent invasive *E. coli* can invade IECs, and survive in macrophages, and the preferential growth of these pro-inflammatory bacteria could potentially increase intestinal inflammation, which in turn could increase the aerobic environment further [228].

1.3.5.3 Restoring the healthy gut microbiota

With identification of microbiota dysbiosis in several human disease pathologies, modulation of the microbiota has become an interesting target for intervention and treatment.

Faecal matter transplant (FMT) is a radical approach, aiming to 're-set the system', in regard to intestinal microbiota composition. It involves transfer of a microbiota sample from a 'healthy' donor to a patient, via most commonly, enema or colonoscopy. FMT has shown very promising results for treatment of CDI with a recent metareview of 684 patients across 23 studies finding a resolution rate of 90.4% [229]. Minimal adverse effects were reported, and it was suggested as a safe and efficient alternative treatment of CDI, and is now on NHS NICE (National Institute for Health and Care excellence) guidelines in the UK [230].

Regarding treatment of IBD, a systematic review reported 18 studies with 122 patients in total (79 UC, 39 CD, 3 unclassified), and a clinical remission rate of 45%, but a low rate of randomised control trials requires further investigation [231]. As IBD is a multifactorial disease, including genetic susceptibility, these results should not detract from the potential health benefits of FMT. Further investigations should be conducted to observe effects of status of disease (active vs remission), similarity of donor and recipient microbiota profile, and differences in pathogenic factors (genetics, environment, drugs, etc.) on successfulness of FMT, as all these can potentially influence the outcome [231].

A more targeted approach for treatment of microbiota dysbiosis involves the administration of probiotics. Probiotics are defined by the World Health Organisation in 2001 as "live organisms which, when administered in adequate amounts, confer a health benefit on the host" [232]. These effects can either be direct, or by modulating the overall microbiota profile, to be more similar to a 'healthy' state.

Probiotics have historically been isolated from humans and been used successfully in treatment of different pathologies [89]. Regarding IBD, particularly *Lactobacillus* and *Bifidobacterium* species have shown health beneficial effects, with the latter being discussed further in section 1.4.6. A study using *Lactobacillus*

supplementation in UC patients undergoing ileal pouch-anal anastomosis (39 treatment vs 78 control), significantly reduced progression of UC (measured by frequency of pouchitis episodes following surgery), with cumulative risk at 3 years being 7% in treatment group, and 29% in control individuals [233]. The probiotics mechanism could involve a heat and acid stable, low molecular peptide, produced by *L. rhamnosus* GG, which induces heat shock protein 25 and 75 expression in IECs via mitogen activated protein kinases (MAPKs). This protected IECs from oxidative stress, potentially by modulating cytoskeletal integrity [234]. Oxidative stress is one of the main contributing factors in IBD, produced by macrophages and neutrophils during the inflammatory response, and induces apoptosis in IECs [235].

1.4 Bifidobacteria are an important member of the human intestinal microbiota

Bifidobacteria are one of the first colonisers of the human intestine, and persists into old age [236]. Notably, presence of bifidobacteria in the gut has been correlated with improved health, and this genus has also been used for many years as an active food ingredient, and probiotic. In the section below I will give an overview about the genus *Bifidobacterium*; including their abundance across the life course, fermentation of substrates, and colonisation factors, and relate these to modulatory effects on the wider microbiota, as well as the host (e.g. IECs) [236, 237].

1.4.1 Bifidobacteria is part of the healthy microbiota across the human life time

In section 1.3.2, the healthy human adult microbiota was described, and below I detail bifidobacterial abundance across the human life time; they are one of the earliest colonisers after birth, and they persist into old age Figure 1-16.

There is strong evidence of vertical transmission of bifidobacteria strains between mother and child. Analysis of 25 mother-infant samples by internal transcribed spacer approach (identification via sequencing of hypervariable regions), revealed seeding of the GI tract of neonates by bifidobacteria found within the GI and vaginal tract of the mother [238]. In addition, transmission was observed via breast milk of bifidobacteria strains *B. longum* spp., *B. bifidum* 1887B and *B. breve*. This transmission may explain why natural birth appears to transfer a higher level of bifidobacteria to the gut, in comparison to C-section, as exposure to GI and vaginal microbiota is substituted with exposure to the skin microbiota [157].

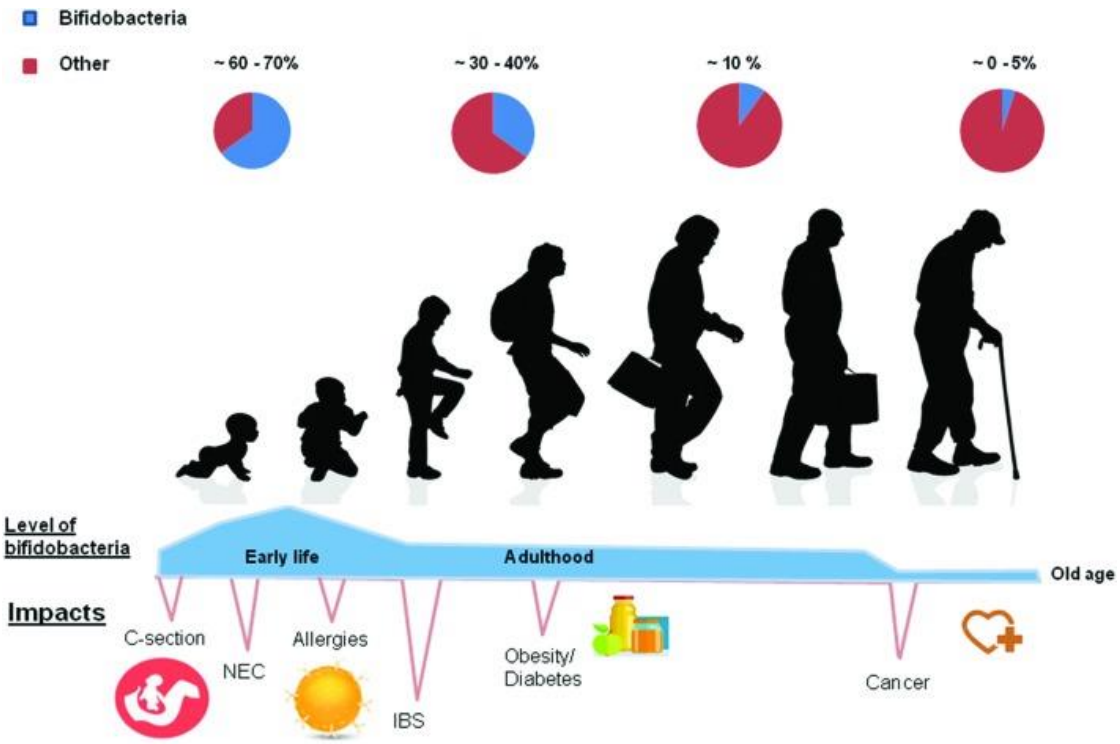

Figure 1-16 Bifidobacteria colonised human intestinal tract at birth and remain part of the microbiota until old age

Bifidobacteria colonised the intestinal tract at birth and are present at highest levels (60-70%) in early life, levels decrease in childhood and reach a plateau in adulthood at 30-40%, decreases in old age is still controversial, and dependent on geographic localisation of cohort samples, as well as use of antibiotics (Figure adapted from Arboleya *et al.*, 2016 [156])

Components in breast milk (e.g. human milk oligosaccharides, HMOs) have been shown to preferentially feed bifidobacteria (which will be discussed in more detail below), and therefore mode of feeding can also shape the infant microbiota. Interestingly, a difference in species can be found between breast and formula fed infants with *B. longum* spp. *longum* associated with formula, and *B. longum* spp. *infantis* and *B. bifidum* found more predominantly in breast fed babies [209].

At 6 months, the intestinal microbiota shifts, and diversity increases due to changes in diet (milk to solid foods), and continuing exposure to environmental bacteria. At this point in time, bifidobacteria abundance decreases to 40%, with the number further decreasing to 2-14% in adulthood [156, 239]. Due to the changing nutritional environment, there is a switch in bifidobacteria species, from the HMO degrading strains, to those capable of digesting plant-based carbohydrates. Several studies

have investigated the human adult bifidobacteria population, with slight differences in most abundance species; ranging from *B. longum* to *B. adolescentis* and *B. cetanulatum* [240].

Abundance of bifidobacteria stays stable for the remainder of adulthood, but when old age is reached, abundance appears to decrease further to 0-5% [241, 242]. Here, it should be mentioned that environmental and extrinsic factors can have a large impact on bifidobacteria intestinal abundance, with antibiotics and their high use in the elderly potentially playing a role in the observed decrease in bifidobacteria [243]. This is particularly important as higher levels of bifidobacteria have been associated with good health, while other studies did not observe a difference in frailty between elderly that had high or low bifidobacteria levels [244, 245].

Notably, many studies have determined that reduced levels of bifidobacteria, at all stages of life, correlates with various pathologies including allergy, metabolic syndrome, and chronic inflammatory conditions, and this will be discussed in more detail in section 1.4.6.

1.4.2 Genomic overview of the genus *Bifidobacterium*

Bifidobacteria were first isolated from faeces of breast fed infants in 1899, and have since then been extensively studied [246]. They are non-motile, non-spore forming, non-gas producing, anaerobic, gram positive bacteria with a Y-shape under stress free conditions (Figure 1-17) [247].

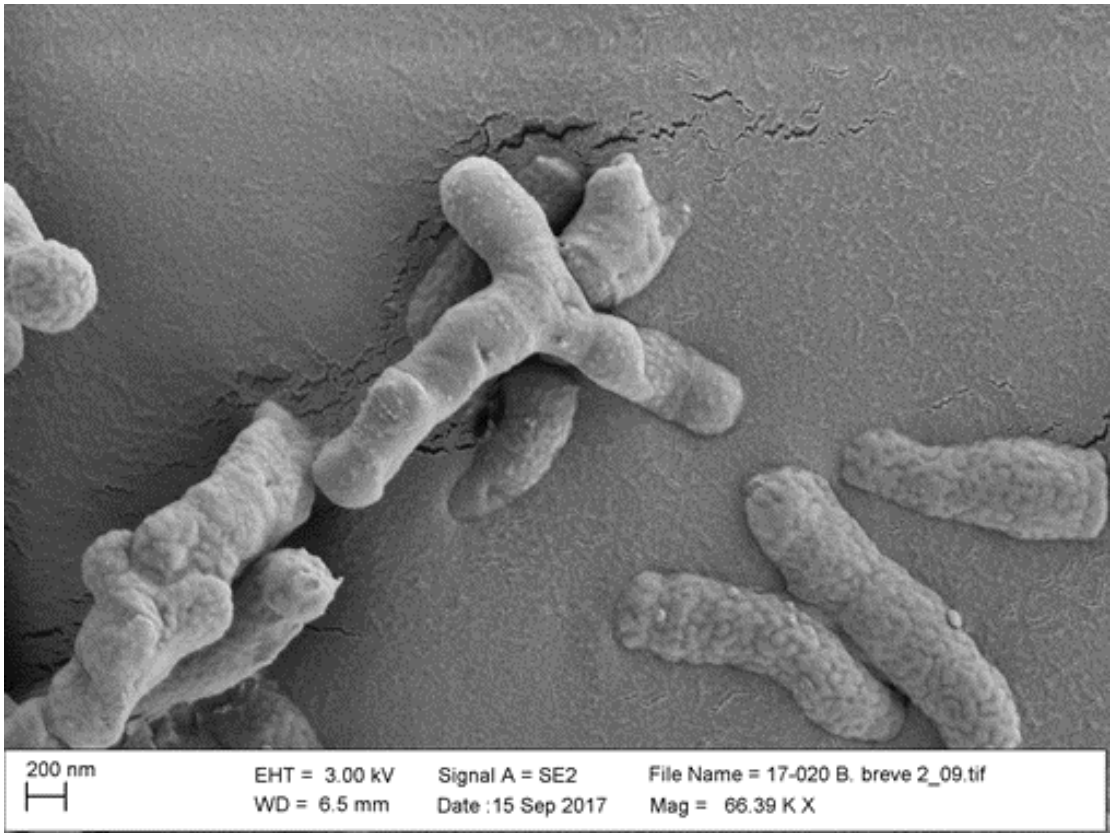

Figure 1-17 *B. breve* UCC2003 in vitro with characteristic Y-rod shape.

B. breve UCC2003 cultured in MRS and visualised by scanning electron microscopy, image courtesy of Jennifer Ketskemety and Kathryn Cross (QIB).

The first complete genome sequence of a *Bifidobacterium* spp. strain was published in 2002, and since then the total number of publicly available sequences has increased to 661 (December 2017, according to NCBI) [248]. There are 55 identified species and subspecies with an average genome size of 2.2 Mb (average gene number 1825) and a high G+C content (52.29% *B. aquikefiri* LMG28769 to 65.53% *B. choerinum* LMG 10510) [249]. Bifidobacteria can be found in ecological niches

associated with the human GI tract, including the oral cavity, SI and LI, but also the GI tract of other mammals, reptiles, insects, and in sewage [237, 250]. The composition and abundance of bifidobacteria in the human intestine has been reviewed in 1.4.1.

Analysis of bifidobacterial genomes has revealed a variety of ecological adaptations, including mechanisms for colonisation of the human GI tract, which have also been experimentally investigated, and which will be described below (1.4.3).

1.4.3 Bifidobacteria can ferment of wide range of carbohydrates, which in turn cross-feed other microbiota members

The gut microbiota utilises both diet- and host-derived sources for growth, and bifidobacteria encode a range of genomic adaptions to reside within the GI tract.

While simple sugars like lactose and sucrose are absorbed by the host in the upper part of the intestinal tract, as well as utilised by other bacteria such as lactobacilli residing in these niches, complex poly-carbohydrates, including cellulose, xylans and pectin, cannot be digested by the host due to their limited arsenal of glycosyl hydrolases (GH) [251-254]. These enzymes catalyse the breakdown of longer carbohydrates into smaller fragments [255]. Human encoded GH are not capable of digesting fructose-, glucose-, xylose-oligosaccharides, inulin or arabinoxylan, which therefore reach the LI [256]. Notably this is the main GI tract niche of *Bifidobacterium* spp, which encode transport systems and enzymes for efficient metabolism of these complex dietary substrates; 12% of the bifidobacteria genome encodes proteins involved in carbohydrate metabolism, with 5.5% of the core genome attributed to this function [257, 258]. Further specialised enzymes encoded in certain species of *Bifidobacterium* (e.g. *B. bifidum* and *B. longum* subsp *infantis),* also allow bifidobacteria to digest HMOs, which are found in breast milk [259].

Different *Bifidobacterium* strains have also been shown to cooperate, or cross-feed, via metabolism of complex carbohydrates. This includes the interaction of *B. breve* UCC2003 with *B. bifidum* PRL2010 and digestion of host mucins [260]. Indeed, 10% of all bifidobacterial GHs are secreted, which therefore make breakdown products more readily available to other bifidobacterial species and the wider

microbiota. *B. magnum* and *B. cuniculi,* which when grown together on starch, synergistically used their extracellular enzymes, and internalised the breakdown products [258]. *In vivo,* this cross-feeding behaviour was investigated by supplementing mice with four bifidobacterial strain, and results indicated that introduction of two or more strains enhanced persistence and increased the modulatory effect on the caecal microbiota. This was attributed to an increase in the glycobiome, to include digestion of plant-derived carbohydrates, and host-derived glycans [261].

Bifidobacteria can produce acetate, one of the three major SCFAs found in the GI tract, which also includes propionate and butyrate [262]. Acetate is produced as a by-product of the hexose fermentation pathway, termed the ‘‘bifid shunt’’. The key enzyme is fructose-6-phosphoketolase, which is present in all members of the family of *Bifidobacteriaceae,* and is thus considered to be a taxonomic marker for members of this group. Interestingly, supplementation of the diet with complex carbohydrates, such as prebiotic inulin-type fructans or arabionoxylan oligosaccharides, preferentially feeds bifidobacteria (i.e. is bifidogenic), and also increases butyrate producing bacteria in the gut (butyrogenic) [263]. It has been shown that prebiotic supplementation increases acetate levels, which in turn is used by butyrate producing bacteria, which increases overall concentration of butyrate in the gut. Butyrate can be used an energy source by colonocytes, and can also modulated immune responses [264]. Butyrate has been shown to decrease NF-κB activation, stimulated by TNF-α in HT-29 cells [265]. In biopsies of CD patients, butyrate decreased TNF-α production, while decreasing LPS stimulated cytokine expression in peripheral blood mononuclear cells, by decreasing NF-κB activation [266]. It has also been shown to enhance the intestinal epithelial barrier measured by TEER *in vitro,* via increased expression of claudin-1 [192]. It also has effects on the immune system with induction of T_{reg} cell differentiation [267].

1.4.4 Bifidobacteria express specific factors for GI colonisation

Bifidobacteria have evolved various adaptions to the GI environment that aid their colonisation (Figure 1-18). As previously discussed, bile acids are secreted by the host to facilitate digestion, nutrient absorption, and cholesterol homeostasis [268].

They also confer antimicrobial activity via lysis of cell membranes and DNA damage [269, 270]. To circumvent these processes bifidobacteria employ several bile resistance mechanisms which includes bile-efflux systems, and bile-salt hydrolases (BSH). Preventing intracellular accumulation of bile salts to counteract toxicity is a common trait in *Bifidobacterium* spp, and transport systems involved in bile export have been described in several species (*B. longum* 702259T, *B. longum* NCC2705, *B. breve* UCC2003) [271-274]. Functional studies have shown that mutations of the gene Bbr_0838 in *B. breve* UCC2003, a membrane bound permease, results in decreased growth in colic acid. Bile salt hydrolases offer protection via deconjugation, and have been shown to be more active in bifidobacterial species relative to other intestinal microbes including members of the *Lactobacillus* genus [274, 275]. Several strains have been shown to have BSH *in vitro* activity including *B. breve* DSM 20091 and DSM 20456 [275, 276].

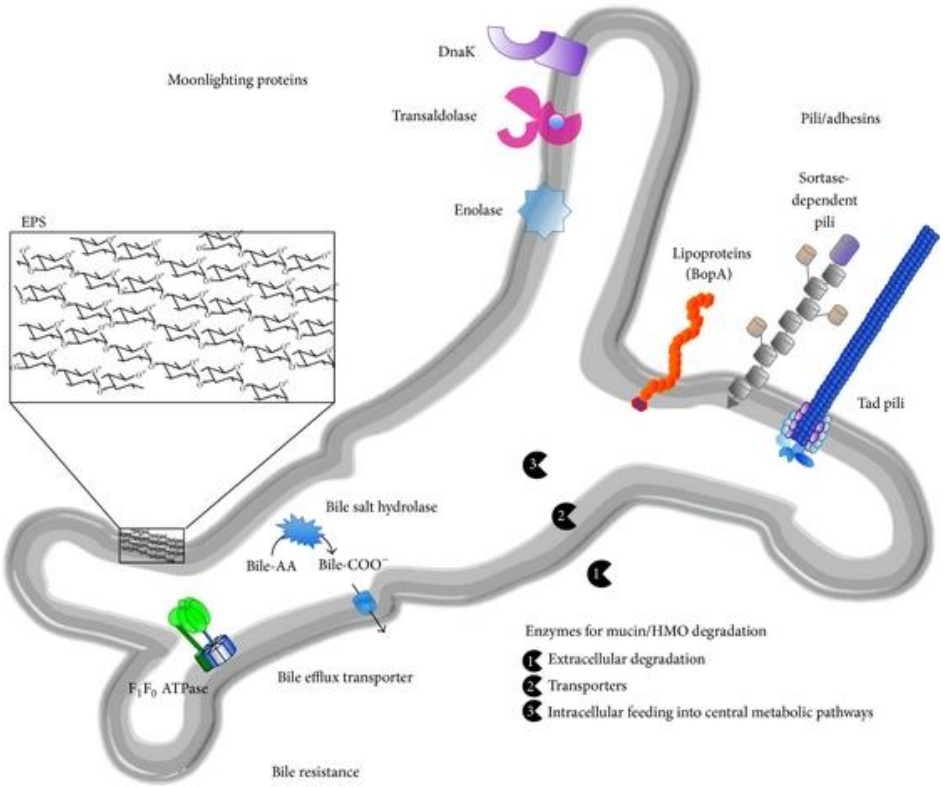

Figure 1-18 Overview of Bifidobacteria mechanisms aiding host intestinal colonisation

Several bifidobacteria components are involved in interaction with intestinal epithelium and environment, Adhesin-like factors include pili, BopA and moonlighting proteins, excreted enzymes

potentially cross feed other microbiota members with breakdown products, bile resistance by membrane transporters and hydrolases, Bile-AA (conjugated bile acids), bile-COO^- (deconjugated bile acids), Tad (tight adherence), EPS (exopolysaccharides) HMO (human milk oligosaccharides), adapted from Grimm *et al.*, 2014 [277].

Adhesion of bacteria to host structures (e.g. IECs and mucus) are a common colonisation and persistence trait, which also relates to colonisation resistance activities. The adherence to IECs by bifidobacterial strains has been studied extensively *in vitro*, for example *B. bifidum* MIMBb75 shows adherence to Caco-2 and HT-29 cell lines, whilst in the presence of fructose and mannose further increases adherence, and which is regulated via BopA lipoprotein [278]. Other factors that are important for GI colonisation include pili, and previous studies in GF mice have shown that expression of these structures are critical for efficient colonisation [279]. The EPS capsule of *B. breve* UCC2003 has also been shown to facilitate persistence, but not initial colonisation of the murine GI tract, which may also be linked to its immune-modulatory properties, which will be discussed in the next section [280].

1.4.5 Bifidobacteria confers health beneficial effects on the intestinal epithelium

The IE plays a central role on host-microbe interactions during homeostasis as well as diseases such as IBD, due to its role in barrier function and innate immunity.

Several studies have shown that bifidobacterial species can increase barrier integrity *in vitro*. Particularly, *B. bifidum* and *B. longum* were able to increase TEER as a measurement of epithelial barrier function in Caco-2 cells, in addition to preventing TNF-α induced barrier breakdown. This effect was related, at least in part, to production of acetate, as addition of this SCFA to Caco-2 cells increased TEER in TNF-α treated cells [281]. Another study utilised *B. infantis* conditioned supernatant with T84 human epithelial cells, which increased TEER, and was associated with increased expression of TJ proteins ZO-1 and occludin. Further *in vivo* studies, using the IL-10 deficient colitis model, determined that administration of conditioned media decreased intestinal leakiness in the short-term, while long term exposure

reduced inflammation and intestinal IFN-γ concentrations [282]. In another mouse model of colonic colitis, induced by DSS, a strain specific effect of *B. longum* ssp. *longum* CCDM 7952 was identified to involve an increase in intestinal epithelial barrier function (assessed by FITC-dextran permeability measurements), which was associated with retention of TJ protein expression. *In vitro* work revealed signalling that these responses were induced via TLR2 and NOD, and is in agreement with findings that TLR2 is essential to maintenance of epithelial barrier integrity via Myd88 dependent signalling cascade, with effects on TJ protein ZO-1 [201]. Further investigating the effect on IEC barrier function *in vivo*, a mouse model, inducing increased intestinal cell shedding by LPS administration, showed that *B. breve* UCC2003 reduced IEC apoptosis, which was via the bifidobacterial EPS capsule and host Myd88 (to be discussed further in chapter 4). In a NEC mouse model, *B. infantis* was shown to upregulate TJ proteins Claudin 4 and Occludin, and may link to the beneficial effects observed in infants supplemented with *Bifidobacterium* for prevention of NEC [283].

1.4.6 The role of bifidobacteria in IBD

IBD pathology is associated with disturbances in the microbiota. Importantly, several studies have identified lower bifidobacteria levels in both CD and UC patients, relative to health controls. Furthermore, epithelium-associated bifidobacteria levels were lower in active and quiescent UC, compared to control samples, while in UC patients a 30-fold decrease in bifidobacteria when compared to healthy controls was observed [284, 285].

Many studies (which have been described previously) have shown supplementation of *Bifidobacterium* strains to mouse models, or addition to *in vitro* assays, provides beneficial effects. However, there are several clinical trials that also indicate that the 're-introduction' of bifidobacteria may provide beneficial effects to IBD patients. In a study with nine UC patients and 10 healthy controls, administration of *B. longum*, isolated from the intestine of a healthy volunteer, in combination with a prebiotic, lead to reduction in mucosal TNF-α and IL-1α levels, as well as improved clinical outcomes 1 month after the feeding trial [285]. A follow up study to the one described, involved administration the *B. longum*/prebiotic mix to CD patients,

which resulted in reductions in histological inflammation, and disease activity [286]. A double-blind placebo controlled intervention study in UC patients, with administration of *B. infantis* 35624 for 6-8 weeks lead to a reduction in c-reactive protein and IL-6. Most recently, patients with mild to moderate UC were supplemented for 8 weeks with *B. longum* 536, which resulted in a significant decrease in disease activity, whereas significant reduction was not seen in the placebo group [287].

Taken together, these results together suggest that *Bifidobacterium* supplementation in IBD patients may be a suitable therapy for reducing clinical systems, and inflammatory markers. However, limitations of these studies include, small samples size, short period of probiotic supplementation, in combination with no assessment of colonisation of the administered bifidobacteria strain, as well as effects on overall microbiota profile [246].

In this chapter, I have highlighted the importance of bifidobacteria to human health, and described our current understanding on how this genus modulates immune modulation, and the IE. However, the exact mechanisms by which bifidobacteria protect the host from inflammation are still unclear and require further investigation. Due to the central role of the IE in this process, this study aims to understand the holistic effects of bifidobacteria colonisation on the IE in neonate, as well as adult stages, and to delineate how this microbiota member provides health beneficial effects for the host.

2 Overarching and specific hypotheses

2.1 Overarching hypothesis

Bifidobacterium breve UCC2003 beneficially modulates IEC responses, during both early life and adulthood, via direct mechanisms, and via modulation of the wider microbiota.

2.2 Specific hypotheses

Chapter 4 - Investigating the role of mechano-receptor Piezo1 as a regulator of mammalian intestinal epithelial cell shedding in health and disease

> **Piezo-1 regulates homeostatic and pathological mammalian epithelial cell shedding.**

Chapter 5 - *B. breve* UCC2003 induces distinct transcriptional responses in small intestinal epithelial cells of neonate mice under homeostatic condition

> **Bifidobacteria can positively influence homeostatic intestinal health by specifically modulating the transcriptome of IECs.**

Chapter 6 - *B. breve* UC2003 transcription shows distinct modulation during colonisation of gnotobiotic and conventionally raised mice, and affects wider microbiota function

> ***B. breve* transcriptional profiles differ in an *in vivo* environment, and in the presence of a diverse microbiota, which may link to modulation of wider microbiota profiles, and host IEC responses.**

3 Materials and Methods

3.1 Materials

3.1.1 General materials

All general chemicals and reagents were obtained from Fisher Scientific or Sigma-Aldrich unless otherwise indicated. Bacterial media was purchased from Oxoid. Water was deionised or where indicated ultrapure water by Mili-Q (Merck) was used.

3.1.2 Oligonucleotide primers

For quantitative PCR (qPCR) analysis of gene expression in host tissue, QuantiTect Primer Assays from Qiagen were used. A summary of primers can be found in Table 3-1.

Table 3-1 QuantiTect Primer assays used in this project

Gene	Species	Product ID	Catalog number
Piezo1	Mus musculus	Mm_Piezo1_4_SG	QT01560216
Piezo1	Homo Sapiens	Hs_PIEZO1_1_SG	QT00088403
pdcd4	Mus musculus	Hs_PDCD4_1_SG	QT00030548
Il-10	Mus musculus	Mm_Il10_1_SG	QT00106169

Analysis of micro RNA 21 (miR-21) expression in mouse tissue was performed by qPCR with TaqMan MicroRNA assays (Applied Biosciences) with primer information listed in Table 3-2.

Table 3-2 TaqMan MicroRNA primers used for miR21 qPCR

Target gene	Gene ID	Species	Mature miRNA sequence (5'-3')
miR21	miRBase ID: hsa-miR-21-5p	human, mouse	UAGCUUAUCAGACUGAUGUUGA
U6 snRNA	NCBI Accession #NR_004394	human, mouse, rat	GTGCTCGCTTCGGCAGCACATATACTAA AATTGGAACGATACAGAGAAGATTAGCATGGCCC CTGCGCAAGGATGACACGCAAATTCGTGAAGCGTTCCA TATTTT

Single stranded RNA was synthesised by Eurofins with specification shown in Table 3-3. miR sequences were obtained from NCBI (hsa-miR-21-5p ID: 406991) and scrambled controlled were designed with siRNA Wizard (v.3.1).

Table 3-3 miR mimetics used in study

miR ID	Sequence (5'-3')
hsa-miR-21-5p	uagcuuaucagacugauguuga
miR-21-scr	gcagatgctggtatttcttaaa

3.1.3 Antibodies and histological stains

Antibodies used for histology and FACS are listed in Table 3-4.

Table 3-4 Antibodies utilised for histology and FACS

Target Molecule	Host	Conjugate	Manufacturer
piezo1	rabbit	unconjugated	Novus Biologicals
caspase-3	rabbit	unconjugated	R&D Systems
CD45	goat	AlexaFluor 700	Biolegend
Rabbit IgG	goat	AlexaFluor 700	Fischer Scientific
Rabbit IgG	goat	Peroxidase	EnVision

Histological stains applied in this study are summarised in Table 3-5.

Table 3-5 List of histological stains

Stain	Target structure	Source
Haematoxin and Eosin (H&E)	acidophilic and basophilic	Sigma-Alderich
CYTOX	Nucleic acids	Thermo Fisher Scientific
DAPI	Nucleic acids	Thermo Fisher Scientific
Rhodamine Phalloidin	F-actin	Thermo Fisher Scientific
Propidium Iodide	Nucleic acids	Thermo Fisher Scientific

3.1.4 Bacterial strains

Bacterial strains utilised in this study are listed in Table 3-6. Bacteria were grown overnight in the appropriate media and growth conditions upon receipt and used to prepare stocks (15% glycerol added) followed by flash freezing and storage at -70 °C.

Table 3-6 Bacterial strains and growth conditions

Strain	Description	Media and growth conditions	Reference
Bifidobacterium breve UCC2003	nursing stool	RCM, MRS/anaerobic/37 °C	Maze et al. (2007)
Salmonella enterica subsp. enterica servora Typhimurium SL1344	heart, liver of 4 week old chickens	LB/aerobic/37 °C	ATCC-14028

3.1.5 Cell lines

Cell line IEC-6 (ATCC#CRL-1592), rat intestinal epithelial cells, was utilised for cell culture experiments. Upon on receipt of frozen stocks, the cell line was resuscitated by warming to room temperature (RT) and suspended in prewarmed Dulbecco's modified Eagle's medium (DMEM, Mediatech Inc.) with 10% foetal bovine serum and 4 mM L-glutamine. DMSO was removed by centrifugation at 100 g for 15 min and resuspended in fresh media. Cell suspension was then transferred into 25 cm^2 culture flasks (Corning) and grown to confluence at 37 °C and 5% CO_2. Following trypsination (1% in media for 10 min), cell density was adjusted to $5x10^6$ cell/ml and 5% DMSO added before flash freezing 1 ml aliquots and banking in liquid nitrogen at -190 °C. For use of cells, aliquots were resuscitated and maintained as described and used within 10 passages.

3.1.6 Zebrafish

Adult, wild type zebrafish (90-120 days) were supplied by Ching-Ling Lien at the Children's Hospital Los Angeles and maintained under standard conditions (14 h-dark/10 h-light cycle at 28.5°C). Animal use was approved and monitored by the Children's Hospital Los Angeles IACUC and designed to follow ARRIVE guidelines.

3.1.7 Mice

Conventionally raised (SPF: specific pathogen free), female C57 Bl/6 Jax mice (adult: 10-14 weeks, neonate: 2 weeks) were obtained from Charles River and housed within the Disease Modelling Unit (DMU) at the University of East Anglia (UEA) for at least 2 weeks for acclimatisation purposes prior to use.

Gnotobiotic (GF: germ free), female C57 Bl/6 Jax mice (12 weeks) were generated by the Germ Free Facility (Quadram Institute Biosciences) at the DMU and housed under sterile conditions for the duration of the experiment.

All experiments were performed under the UK Regulation of Animals (Scientific Procedures) Act of 1986. The project licence (PPL: 80/2545, PIL: I68D4DCCF)

under which these studies were carried out was approved by the UK Home Office and the UEA Ethical Review Committee.

3.2 Methods

3.2.1 Methodology involving work with bacteria

3.2.1.1 Bacterial growth conditions and gavage inoculum preparations

B. breve UCC2003 was streaked from frozen glycerol stocks onto Reinforced Clostridial Agar plates (RCA, Oxoid) and incubated in an anaerobic chamber (miniMACS, Don Whitely Scientific, 5% CO_2, 10% H_2 and 85% N_2) at 37 °C. Single colonies were picked for inoculation with prewarmed Reinforced Clostridia Medium (RCM, Oxoid).

For preparation of gavage inoculums, 5 ml of inoculated RCM was incubated overnight followed by sub-culturing into 5 ml Man Rogorosa Sharpe (RCM, Oxoid) medium. After an additional overnight incubation, another sub-culture into 40 ml RCM was performed. Inoculums were prepared from cultures by 3 rounds of centrifugation at 3220 g for 10 min followed by 3 PBS washes before dilution in sterile PBS.

For *in vivo* colonisation, the Bifidobacterial pellet was resuspended in 4 ml of PBS (adult mice) or 2 ml (neonate mice) and for *in vitro* co-culture in 4 ml of IVOC growth medium. Bacterial concentration of inoculum was enumerated by plating serial dilutions in sterile PBS on RCA plates and enumerating colonies following 2 day incubation to calculate cfu/ml.

Salmonella enterica subsp. enterica servora Typhimurium SL1344 frozen stocks were expanded on Luria broth (LB, Oxoid) agar plates and grown overnight at RT. Single colonies were used to inoculate prewarmed LB broth in conical flasks and incubated at 37 °C and 200 rpm.

3.2.1.2 Method for isolating potential vesicle from bacterial conditioned media

Overnight culture of *B. breve* UCC2003 was diluted in 2 l of prewarmed, prereduced MRS to an optical density of 0.1 at 600 nm and grown for 18 h under standard

conditions. Culture was then centrifuged at 3,000 g for 30 min at 4°C and supernatant cleared from remaining cells and debris by vacuum filtration through 0.22 µm pore-size polyethersulfone membrane bottle top filter (Sartorius). Supernatant was concentrated to 20 ml by ultrafiltration through a Vivaflow 50 filtration cassette (Satorius) with a 100 kDa molecular weight cut-off. The membrane retained any molecules above 100 kDa (including potential OMVs), whereas smaller molecules were removed together with the flow-through. Filtration was performed at speed setting 4 for 2 h and cassette and samples were placed on ice during the entire process. Afterwards, the filter was rinsed with 200 ml of ice cold PBS and ultrafiltration continued until total volume was reduced to 20 ml again. Following this, the sample was further concentrated to 10 ml using a Vivaspin 20 (Satorius) with 100 kDa molecular weight cut-off by centrifugation at 10,000 g for 30 min at 4 °C. Flow through was transferred to a ultracentrifuge tube and spun at 150,000 g for 2 h at 4 °C. Supernatant was removed and pellet resuspended in 30 µl ice cold PBS followed by sonication (10 s x 8) and a final filter-sterilisation (0.22µm). Cell lysate (5 µl) was mixed 1:2 with NuPage SDS running Buffer and heated at 70 °C for 10 min. Protein separation was performed by SDS-page gel electrophoresis by loading 10 µl of sample onto NuPage Novex Bis-Tris gel (10%) and run at 200 V for 1 h in NuPage running buffer. A negative control (10 µl sterile MRS media) was run alongside. Gel was then stored in 1% acetic acid at 4 °C until processing for protein analysis.

3.2.1.3 Proteomic analysis of isolated potential bacterial vesicles

Protein preparation was carried out together with Alfonsina D'Amato (QIB). Proteomic analysis by HPLC-MS was performed by Alfonsina D'Alomoto.

Protein bands in SDS gel were cut and stored at -80 ˚C. Samples were defrosted on ice and washed 3 times with 100 µl of 50 mM NH_4HCO_3 in acetonitrile followed by 200 µl 100% Acetonitrile for 3 min each. Afterwards, samples were incubated with 100 µl 1.5 mg/ml DTT in 50 mM NH_4HCO_3 at for 20 min at 56 ˚C followed by an Acetonitrile wash. This was repeated 3 times. Following this, liquid was aspirated and 100 µl 10 mg/ml iodacetamide in 50 mM NH_4HCO_3 added for 30 min at RT in the dark followed by 3 washes with Acetonitrile. Gel pieces were then dried down

using a Speed Vac system at the Low Drying setting (no heat) on a Speed Vac SC110 (Savant). Samples were trypsin digested by adding 1 µg trypsin in 100 µl 25 mM NH_4HCO_3 pH 8.5 at 4 ˚C for 10 min. Solution was removed and replaced with 20 µl of 25 mM AMBIC and stored over night at 4 ˚C. The following day, samples were spun down and supernatant frozen on dry ice until analysis by Orbitrap.

Prior to analysis, supernatant was defrosted and acidified by addition of 1 µl of 0.1% formic acid followed by vortexing for 20 sec and incubation at RT for 20 min. Samples were then transferred into a 0.2ml skirted 96-well PCR plate (Thermo AB-800) and placed in autosampler of Orbitrap HPLC. Samples were analysed and data saved in Orbitrap RAW data file. Data was analysed using Mascot 2.4.1.

3.2.1.4 Analysing effect of miR21 on bacterial growth kinetics

Effect of host miR21 on bacterial growth was assessed by growth kinetics. Overnight cultures of *B. breve* UCC2003 in MRS and *S.* Typhimurium 1344 in LB were set up as described (3.1.4). Growth curves were performed by inoculating 200 ml of pre-warmed, pre-reduced MRS media with *B. breve* UCC2003 overnight culture to an OD of 0.1, and incubated anaerobically at 37 ˚C. For SL 1334, overnight culture was diluted 1:100 in 100 ml fresh pre-warmed LB broth and incubated aerobically at 37 ˚C with shaking at 200 rpm.

miR21 hsa-miR- 876-5p (Sequence: GUGUUCCGACGUAUCUAUUAAU), scrabbled control (both at 1.25 uM) or PBS (control) was added to cultures at point of inoculation. At the indicated time points, 1 ml of media was removed from the culture using aseptic techniques, serial diluted, plated on the MRA (UCC2003) or LB plates (SL1344) and incubated anaerobically (UCC2003) or aerobically (SL 1344) for colony enumeration at 48 h (UCC2003) and 24 h (SL1344) post plating.

3.2.2 In vitro cell culture methods

3.2.2.1 Assessing cell shedding *in vitro* by staining shedding funnels in IEC-6 monolayers

IEC-6 cells were seeded onto chamber slides (Corning) at a density of 200,000 cells per chamber and grown under standard conditions until confluency was reached. Media was removed, chambers washed with ice cold PBS, and 200ul of 100 uM

gadolinium or PBS (control) was added. Slides were incubated for 30 min under standard conditions followed by removal of media, and fixing with 200 µl 4% neutral buffered formalin for 15 min. Cells were washed thrice with 200 µl ice cold PBS for 5 min each and stained with 20 µl (1 U) rhodamine-phalloidin in 200 µl PBS, and mounted using Prolonged Gold + DAPI (Thermo Fisher). Shedding was enumerated by counting actin rings surrounding shedding cells on a Leica DMI 6000 microscope. Data presented as events per mm^2 of a chamber.

3.2.2.2 Quantifying cell shedding via enumeration of cell in supernatant of IEC-6 monolayers

IEC-6 cells were seeded in 24-well cell culture plates (Corning) at a density of 400,000 cells per well and grown under standard conditions. When confluency was reached, media was removed, wells washed with ice cold PBS, and 100 µl of media added with 1, 10 or 100 µM gadolinium or equivalent volume of PBS in media (control). Cells were incubated for 30 min, supernatant removed into a new 24 well plate and incubated with 1 µl of 1 mg/ml DAPI at under standard conditions. After 10 min, cells were spun down at 500 g for 10 min and number of cells adhered to plate bottom counted with an Olympus BX60 microscope. Data displayed as events per mm^2 of a well.

3.2.3 Zebrafish *in vivo* methods

3.2.3.1 Assessing effect of Piezo1 inhibition by gadolinium on zebrafish intestinal cell shedding

Adult wildtype zebrafish, maintained under described conditions, were exposed to 10 and 100 uM gadolinium in water or water without inhibitor (control group), and euthanised 4 h post exposure. Midguts were collected and processed in 0.5 ml 4% neutral buffer formalin for 2 h followed by storage at -80 ˚C. Cryo-sectioning (4 um) was performed and sections mounted on Superfrost slides, stained for F-actin with rhodamine-phalloidin (1:1000, Thermo Fisher) and mounted with Vector shield with DAPI (Vectorlabs). For each fish, 30 villi were imaged using a Leica DMI 6000, and actin rings forming around shedding cells were enumerated. Data are shown as shedding events per mm of IE.

3.2.4 Mouse *in vivo* methods

3.2.4.1 Colonisation of intestinal tract with *B. breve* UCC2003 by oral gavage

Adult mice were colonised with *B. breve* UCC2003 by oral gavage with bacterial inoculations of 100 µl every 24 h for 3 consecutive days. Neonate mice received 50 µl of concentrated inoculum ensuring equal number of bacteria administered. Control mice received an oral gavage of sterile PBS. Colonisation was confirmed by collection of fresh faeces and homogenisation with 1 ml sterile PBS by shaking at 200 rpm for 15 min followed by plating of serial dilutions in sterile PBS on RCA with 50 mg l^{-1} mupirocin and counting of colonies following 2 day incubation to calculate cfu/mg of faeces.

3.2.4.2 Inducing colitis by DSS administration and assessment of severity

Mice received 1.5% DSS (TdB Consulting) ad libitum in the drinking water for 7 days inducing acute colitis, while control mice received drinking water only. Fresh DSS solution was prepared every 2 days. During DSS exposure, mice were assessed daily for disease activity index (DAI, Table 3-7) and body weight. Mice were euthanised on day 7 of DSS exposure, tissue collected, colon weight and length recorded as an assessment of severity of colitis [288].

Table 3-7 Disease Activity Index to assess severity of DSS induced colitis in mice

Characteristic	Description	Score
Stool consistency	firm - liquid	0-3
faecal bleeding	no bledding - more severe bleeding	0-3
Agility + posture	no hunched+agile - huddled+agile	0-3
Fur texture	smooth - scruffy	0-2
Anal prolapse	no prolapse - prolpase	0,1

3.2.4.3 Inducing intestinal cell shedding by LPS administration

To induce small intestinal cell shedding, a systemic LPS model was used [289]. Mice received 200 µl intraperitoneal (IP) injection of 1.25mg/kg or 10mg/kg LPS in sterile PBS. Control mice received 200 µl of sterile PBS IP. Mice were closely

monitored and reaction to LPS challenge did not exceed limits set out in UK Regulation of Animals (Scientific Procedures) Act of 1986. Mice were euthanized at 1.5 and 4 h post IP injection and tissue collected.

3.2.4.4 Collection of mouse tissue

Small and large intestinal tissue for formalin fixed paraffin embedded (FFPE) processing was collected in 5ml 10% neutral buffered formalin (NBF), fixed at RT for 24h, processed with an ASP300s tissue processor (2 h each in 70%, 80%, 90% and 100% ethanol followed by 2 consecutive baths in xylene for 2 h each and finally temporary storage in paraffin wax), and embedded in paraffin wax. For SEM, SI and LI tissue (0.6 cm in length) were collected, opened longitudinally and cut in 0.2 x 0.2 cm squares with a razor blade. Tissue was fixed in 2.5% glutaraldehyde (Agar Scientific) in 0.1M PIPES buffer (pH 7.4) overnight. Intestinal contents were squeezed into sterile tubes and stored at 4 ˚C for bacterial enumeration or into Lysing Matrix E tubes (MP Biomedicals) and snap frozen in ethanol (EtOH) cooled with dry ice for molecular analysis. For transcriptional analysis, 0.5 cm sections of SI and LI were collected in 200 µl RNAlater (Qiagen) for 24 h at 4 ˚C, removed from RNAlater, blotted dry on filter paper and stored at -80 ˚C. For protein analysis (ELISA), SI and LI tissue was snap frozen in 100% EtOH cooled with dry ice, and stored at -80 ˚C.

3.2.4.5 Isolating intestinal epithelial cells and assessing preparation purity

For SI IEC isolations, an adapted Weisser method was applied [290] [46]. Sections (10cm) of SI were collected in ice cold PBS, dissected into 0.5 cm^2 pieces and placed in 200 ml Duran bottles.

Faecal matter was washed off by inverting 10 times in 0.154M NaCl and 1mM DTT. Liquid was drained and mucus layer removed through incubation of samples in 1.5mM KCl, 96mM NaCl, 27mM Tri-sodium citrate, 8mM NaH_2PO_4 and 5.6mM Na_2HPO_4 for 15 min at 220 rpm and 37 ˚C. IECs were separated from basal membrane by incubation in 1.5mM EDTA and 0.5mM DTT for 15 min at 200 rpm and 37 °C followed by shaking vigorously 20 times. IECs were collected from solution by centrifugation at 500 g for 10 min at 4 ˚C. Supernatant was discarded and

cell pellet resuspended in 3 ml of ice cold PBS. Cell concentrations of isolated IEC samples calculated by labelling dead cell with trypan blue (Biological Industries) at a 1:1 v/v ratio and enumeration of viable cells using a haemocytometer (Hawksley) on an inverted microscope (ID03, Zeiss).

For protein extraction, volume containing $5x10^8$ cells was spun down at 500 g for 10 min at 4 ˚C and pellet resuspended in 700 µl CellLytic MT lysis buffer in Lysis Matrix E tubes, followed by 3 beat beating steps at speed setting 6 for 1 min each using a FastPrep Homogeniser (MP Bio). Samples were placed on ice between beat beating steps. Sample was cleared by centrifugation at 10,000 g for 15 min at 4 ˚C and supernatant removed into a fresh tube followed by storage at -80 ˚C. For RNA extraction, a volume containing $3x10^6$ cells was processed as described in 1.2.8.3.

Preparation purity of IEC isolations was assessed by Fluorescence-activated Cell Sorting (FACS) of collected cells and histological analysis of stripped tissue. For FACS analysis, volume of isolation containing $5x10^6$ cells were added into 5 ml FACS tubes followed by centrifugation at 510 g for 3 min at 4 ˚C and removal of supernatant. Cells were stained with CD45-A700 (1:200) in 200 µl FACS buffer (Hank's Balanced Salt Solution, 0.01 BSA, 2mM EDTA, 20mM HEPES, 0.01% NaN_3) by vortexing for 20 sec and incubation on ice for 30 min. Two washes with 2 ml FACS buffer followed and addition of 200 µl of propidium iodide (1:400) in FACS buffer. Blank samples were prepared for each isolation, substituting stains with equal volumes of FACS buffer. Samples were run on Sony FCS SH-800 and data analysed using FlowJo 7.2 (TreeStar). For histology, tissue samples were collected at end of each incubation step, FFPE processed as described in 1.2.4.4, sectioned (5 µm) and mounted on Superfrost slides. Samples were stained with Haematoxylin and Eosin (H&E) by removal of paraffin in xylene twice for 5 min, rehydration with 5 min consecutive baths in 100%, 90%, 80%, 70% EtOH followed by water, incubation with H&E stain for 4 min, differentiation with 1% acid in EtOH for 30 s, washing under running water, and bluing with 0.2% ammonia for 30 s followed by another wash under running water. Samples were dehydrated in 70%, 90% and 100% EtOH baths for 5 min each followed by 2 x 5 min xylene baths and mounting with Hydromount (National Diagnostics). Slides were imaged suing a Leica DMI 3000 B.

3.2.5 Histological methods

3.2.5.1 Scanning electron microscopy of intestinal epithelium

Scanning electron microscopy (SEM) was performed by Kathryn Cross (QIB).

Tissue was collected and fixed as described in 1.2.4.4. Fixative was washed off with 3 x 15 min baths in 0.1M PIPES buffer and tissue then dehydrated in EtOH (30, 50, 70, 80, 90, 3x 100%) for 15 min each followed by drying in a Leica EM CPD300 Critical Point Dryer using liquid carbon dioxide as transition fluid. Tissue was then mounted with quick drying conductive silver paint (Agar Scientific) on aluminium SEM stubs with intestinal epithelial layer oriented upwards. Samples were coated with gold in a high resolution sputter-coater apparatus (Agar Scientific). SEM performed on a Zeiss Supra 55 VP FEG SEM, operating at 3kV.

3.2.5.2 Visualising shedding intestinal epithelial cells by caspase-3 staining

FFPE fixed small intestinal tissue was sectioned at 5 um and mounted onto Superfrost slides. Tissue was de-paraffinised twice in Histoclear (National Diagnostics) for 5 min each, rehydrated in an ethanol series (100, 90, 80, 50% followed by water for 5 min each) and treated with 1% H_2O_2 in methanol for 12 min. Antigen retrieval was performed by boiling samples in 0.01M citrate acid buffer 9pH 6) 3 times for 10 min in a microwave (800W) and section marked of on slide with wax pen. Tissue then incubated with rabbit anti-caspase-3 antibody (1:500, R&D systems) in 1% Tris-HCl with 1% BSA for 2 h at RT. Afterwards antibody solution as flicked off and slides incubated with peroxidase conjugated goat anti-rabbit secondary antibody (EnVision DAB kit) for 30 min at RT and developed with DAB substrate for peroxidase (Vector Laboratories) for 30 s. Lastly, slides were washed in water, counterstained with Harris Haematoxylin as described in 3.2.4.5, washed in running water, dehydrated in an ethanol series (50, 80, 90, 100% for 5 min each), sealed with Safemount (VWR chemicals), and dried overnight at RT. Slides were imaged with a Leica DMI 3000 B.

Quantification of shedding events along crypt-villus axis was performed using caspase-3 stained tissue slides. Using full length, intact villi only, epithelial cells were counted from top of villus (cell position 1) towards bottom of crypt along one

side of villus (epithelial cell at base of crypt – last cell position). While counting, cell with absent caspase-3 labelling and in contact with neighbouring cell and basal membrane recorded as “normal”. Cells with positive capspase-3 labelling and loss of contact recorded as “shed”. At least 15 villi in at least 6 separate intestinal sections counted per mouse. Data recorded using WinCrypts and analysed using PRISM. Imaging was performed using an Olympus BX60 microscope.

3.2.5.3 Visualising Piezo1 within the intestine

FFPE fixed samples were sectioned de-paraffinised, rehydrated and antigen retrieval performed as stated (3.2.5.2). Tissue then incubated with rabbit anti-mouse Piezo1 (1:500, Novus Biologicals) in 1% BSA for 2 h at RT. Slides washed 3 times in PBS and incubated with goat anti-rabbit IgG antibody (1:1,000) in 1% BSA for 30 min at RT. Slides washed in PBS and mounted with Vector shield with DAPI (LifeTech) and imaged immediately using a Leica DMI 3000 B. For chromogenic staining, piezo1 antibody at 1:400 dilution was used following protocol in 1.2.4.5.

3.2.5.4 Using RNAscope technology to visualise transcripts within intestinal tissue

RNAscope was performed using a commercial kit from Advanced Cell Diagnostics as per the manufacturer’s instructions using Piezo1 and Bifidobacteria specific probes designed to bind to piezo1 RNA transcript and *B. breve* UCC2003 16S rRNA sequence respectively. Briefly, formalin fixed paraffin embedded tissue sections (5 um) were mounted on Superfrost plus slides before baking in a dry oven at 60 °C for 1 h. Slides were then deparaffinised with Xylene for 5 min and bathed in 100% ethanol for 5 min before applying Pre-treat solution 1 for 10 min at RT. Sections were washed in distilled water twice for 30 s before incubation in boiling Pretreat 2 solution for 15 min. Following 3 further washes in water for 30 s each, Pretreat 3 was applied in a humidified chamber at 40 ^{o}C for 30 min. After further 3 washes, Piezo1 specific, Bifidobacteria specific or Cyclophylin B control probe were hybridised to samples for 2 h at 40^{o}C. Following washes in wash buffer, a series of amplification probes (AMP1 to AMP6) were sequentially bound to and washed off from the slides. AMP1 to AMP4 were hybridised at 40 ˚C and AMP5 and AMP6 at

RT each for 30 min. Signal detection was achieved by adding DAB substrate to sections for 2 min followed by washing in running water. Counter stain with H&E was performed as described 3.2.4.5, tissue dehydrated and mounted for visualisation using a Leica DMI 3000 B microscope. A minimum of 12 villi per sample were observed for enumeration of Piezo1 transcripts per cell as described in 3.2.5.2. Data shown as means +/- SD of transcripts per cell along crypt-villus axis.

3.2.6 Analysis of human biopsies and *ex vivo* culture

3.2.6.1 Measuring transcription within colonic biopsies of UC patients

Study was carried out, samples collected, RNA extracted and cDNA generated by Elizabeth Thursby (QIB).

Study participants were recruited from patients undergoing colonoscopy in the gastroenterology department at the Norfolk and Norwich University Hospital (NNUH). Ethical approval was obtained through the Faculty of Medicine and Health Sciences Research Ethics Committee at the UEA (reference 2012GAST022).

Colonic biopsies were obtained from patients being assessed for a suspected flare of UC or for investigation of another possible bowel condition (found macroscopically and microscopically normal, control group). Inflammation of each patient was categorised as normal or inflamed based on grading of separate clinical samples by a histologist at the NNUH. Additional information given in Supplementary Table 1.

Pinch biopsy (5 mm) were collected from the ascending colon, immediately frozen on dry ice and stored at -80 ˚C. Frozen biopsies were placed in 200 µl RNAlater-ICE solution and stored at -20 overnight. Samples were then transferred into 350 µl RLT buffer (RNeasy Mini Kit, Qiagen) with 1% v/v β-mercaptoethanol and incubated for 5 min at RT. Tissue was disrupted using a disposable, autoclaved pellet pestle and vortexing until fully lysed. RNA was extracted following RNeasy Mini Kit ‘Purification of Total RNA from Animal Tissues’ protocol from step 5, performing steps D1-D4 in replacement of step 6, and at the end 2 elution steps with 30 µl RNase free water were carried out. Extracted RNA was banked at -80°C.

For cDNA synthesis, sample RNA was thawed on ice and RNA integrity and quantity measured using a 2100 Bioanalyzer (Agilent Technologies) according to the

manufacturer's instructions. For each reverse transcription PCR (RT-PCR), 0.5 µg RNA per sample was used. Initially, gDNA was eliminated and RT-PCR performed using the Quantitect reverse transcription kit (Qiagen), according to the manufacturer's instructions. qPCR analysis was performed as described (3.2.8.3) with QuantiTect primers assays specific for human transcripts.

3.2.6.2 Assessing transcription in colonic biopsies of UC patients

This study was carried out, and samples collected by Dr Johanna Brooks (QIB/NNUH). Co-culture was performed together with Johanna Brooks.

Study participants were recruited from patients undergoing colonoscopy in the gastroenterology department at the Norfolk and Norwich University Hospital (NNUH). Ethical approval was obtained through the Faculty of Medicine and Health Sciences Research Ethics Committee at the UEA (20162017-28HT) and NHS research and development permission was granted from the NNUH (reference 19-10-16).

Colonic biopsies were obtained from patients undergoing routine check-ups for UC monitoring, for assessed of a suspected flare of UC or for investigation of another possible bowel condition (found macroscopically and microscopically normal, control group). Inflammation of each patient was categorised as normal (control group), UC in remission (UC-R) or inflamed (UC-I) based on grading of separate clinical samples by a histologist at the NNUH.

Pinch biopsy (5 mm) were collected in quadruplets in close proximity from each other at transverse colon and stored in IVOC culture media (4.7 g/l NCTC 135 medium, 1.1 g/l sodium bicarbonate, 5 g/l D-Mannose, 10% New-born Calf Serum, 45% DMEM medium) at RT. One biopsy was frozen on dry ice and stored at -80 ˚C for baseline gene expression. RNA was extracted from frozen samples and transcriptional analysis performed as described in 3.2.8.3 using a human specific Quantitect primer assay (Qiagen).

3.2.6.3 Co-culturing *B. breve* UCC2003 with colonic UC patient biopsies in pIVOC

pIVOC was performed by cutting biopsy in half using a scalpel and sandwiching each half between two 12mm diameter Perspex disks (both with a 2 mm central aperture) on top of a cellulose nitrate filter (3 µm pore, Whatman) with the mucosal side upwards. Mounting was sealed with Histoacryl tissue glue (Braun Medical Ltd) to prevent leakage and mounted on Snapwell supports in 6 well culture plate (Croning). Basal compartment was filled with 3 ml IVOC culture media and apical compartment with 100 µl IVOC media (control) or media containing 10^7 cfu/ml *B. breve* UCC2003 and incubated at 37 °C and 5% CO_2. At 2 h, 80 µl of the apical media was removed to improve biopsy survival. Removed media was stored at -80 ˚C and 10 µl plated on RCA + 50 mg l^{-1} mupirocin for enumeration of bacteria (cfu/ml). After 8h, biopsies were removed from sandwich, washed 3 times in ice cold PBS and stored at -80 ˚C for RNA extraction (3.2.8.3)

3.2.7 Metabolomic analysis of intestinal contents

Bile acid isolation and quantification in mouse intestinal contents was performed by Mark Philo (QIB).

Intestinal content (25 mg) was added to tubes containing 6 ceramic beads, 1 ml of 70% v/v methanol and 25µl of 40 µg/ml d4-DCA and homogenised for 30 s at 3.300 g using a table shaker. Faecal slurry was then cleared by centrifugation at 800 g at 4 °C and supernatant transferred to a new tube with the addition of 25 µl of 40 µg/ml d4-CDCA. Centrifugal evaporation at 50° for 70 min was carried out until sample was almost dry and then made up to 1 ml volume with 5% v/v methanol with the addition of 25 µl of 40 µg/ml d4-CA. Reconstituted sample was passed through hydrophilic-lipophilic balance clean-up cartridge (Waters Oasis Prime HLB, 1cc, 30mg), washed with 1 ml of 5% methanol and eluted in 500 µl methanol with the addition of 25 µl of 40 µg/ml d4-GCA (primary reference internal standard) and d4-LCA. Sample was then submitted for analysis by HPLC/MS operated in multiple reaction monitoring (MRM) mode using Agilent 1260 binary HPLC coupled to an AB Sciex 4000 QTrap triple quadrupole mass spectrometer. HPLC was run using binary gradient of solvent A (Water + 5mM Ammonium Ac + 0.012% Formic acid)

and solvent B (Methanol + 5mM Ammonium Ac + 0.012% Formic acid) at a constant flow rate of 600 µl/min. Separation was made using Supelco Ascentis Express C18 150 x 4.6, 2.7µm column maintained at 40°C. Injection was made at 50% B and held for 2 min, ramped to 95% B at 20 min and held until 24 min. Column was equilibrated to initial conditions for 5 min. Mass spectrometer was operated in electrospray negative mode with capillary voltage of -4500V at 550°C. Instrument specific gas flow rates were 25ml/min curtain gas, GS1: 40 ml/min and GS2: 50 ml/min. Data was collected and quantification achieved using Analyst 1.6.2 software to integrate detected peak areas relative to the deuterated internal standards.

Metabolomic analysis of mouse intestinal contents was carried out by Gwenaelle Le Gall (QIB).

Intestinal content (25 mg) was mixed with 1 ml 5% MeOH by vortexing. Samples were then loaded onto Waters OASIS PRIME HLB 1 30mg SPE cartridges and washed with 1 ml 5% MeOH. Flow through fraction was dried using a Speedvac® centrifugal evaporator and reconstituted with 600μL NMR buffer made up of 0.1 M phosphate buffer (0.51 g Na_2HPO_4, 2.82 g K_2HPO_4, 100 mg sodium azide and 34.5 mg sodium 3-(Trimethylsilyl)-propionate-d_4 (1 mM) in 200 mL deuterium oxide). Supernatant was transferred into 5-mm NMR tube for NMR recording. High resolution ^{1}H NMR spectra were recorded on 600MHz Bruker Avance spectrometer fitted with a 5 mm TCI cryoprobe. Sample temperature was controlled at 300 K. Each spectrum consisted of 512 scans of 65,536 complex data points with a spectral width of 12.5 ppm (acquisition time 2.67 s). The “noesypr1d” pre-saturation sequence was used to suppress the residual water signal with a low-power selective irradiation at the water frequency during the recycle delay and a mixing time of 10 ms. Spectra were transformed with 0.3 Hz line broadening and zero filling, manually phased, and baseline corrected using the TOPSPIN 2.0 software. Spectra were transferred into AMIX ® software for bucketing. Metabolites were identified using Human Metabolome Database, (http://www.hmdb.ca/) and 2D-NMR methods (COSY, HSQC, and HMBC). Multivariate statistical analyses (Principal Component Analysis) were carried out using the PLS Toolbox v5.5 (Eigenvector Research Inc.) running within Matlab, v7.6 (The MathWorks Inc.). Graphs of metabolite signal intensity were plotted in Excel.

3.2.8 Molecular techniques

3.2.8.1 Analysing intestinal epithelial cell expression using qPCR arrays

Analysis of gene expression using Real-Time Ready Custom Panel 480–96 PCR arrays (Roche) was carried out by Kevin Hughes (QIB). In brief, whole small intestinal mouse tissue was collected and RNA extracted (3.2.8.3). Reverse transcription was performed, using Transcriptor First Strand cDNA Synthesis Kit (Roche) following manufacturer's instructions. qPCR was performed using LightCycler 480 Probes Master Mix and Real-rime ready Custom Panel 480–96 PCR arrays on a LightCycler II (Roche) as per manufactures instructions. CT values of target genes were normalized to expression of housekeeping genes and fold change versus control samples calculated using the $_{\Delta\Delta}$CT method.

3.2.8.2 Extracting DNA from faeces

DNA was extracted from faecal samples using with the FastDNA SPIN Kit for Soil (MP Biomedicals) following the manufacturer's instructions with elongation of bead-beading time to 3 min. In brief, a minimum of 50 mg of faeces was added to Lysis matrix E tubes prepared with 980µl Sodium Phosphate Buffer. To sample, 120 µl MT Buffer was added and sample homogenize 3 times in the FastPrep instrument for 1 min each at a speed setting of 6. In-between beat-beating, samples were placed on ice for 5 min. Tubes were centrifuge at 14,000 g for 15 min. Supernatant was transferred to a tube containing 250µl PPS. Sample was mixed by inverting 10 times and centrifugation at 14,000 g for 10 min to pellet precipitate. Supernatant was transferred to a 15 ml tube containing 1 ml of resuspended Binding Matrix and inverted for 2 min to allowed binding of DNA to Binding matrix. Following a 3 min incubation at RT to allow matrix to settle, 500µl of supernatant was removed without disturbing settled matrix. Binding Matrix was resuspended in remaining supernatant and 700µl transferred to SPIN filter. The filter was then centrifuged at 14,000 g for 1 min, catch tube emptied follow by transfer of remaining resuspended matrix to filter and an additional centrifugation at 14,000 g for 1 min. After catch tube was emptied, 500 µl SEWS-M was added and pellet resuspended. Filter was then centrifuged at 14,000 g for 1 min. Catch tube emptied again and centrifuged at 14,000 g for 1 min.

Catch tube was replaced by Eppendorf tube and sample air dried 10 min at RT followed by 5 min at 37 ˚C. Afterwards, 65 µl DES was added to the Binding Matrix, incubated at RT for 5 min, centrifuged at 14,000 g for 1 min to elute DNA into Eppendorf tube. DNA was then stored at -20˚C.

3.2.8.3 Analysing transcription in mouse tissue by qPCR

Tissue was removed from -80 ˚C on dry ice. Using a scalpel, 10 mg section were cut off and placed in 600 µl RLT buffer (RNAeasy plus mini kit, Qiagen) in Lysis Matrix E tube. Sample was homogenised using a FastPrep 24 homogeniser (MP Bio) thrice for 1 min at speed setting 6 followed by centrifugation at 10,000 g for 15 min at +4˚C. In-between beat-beating, samples were placed on ice. Supernatant was used for downstream RNA isolation.

RNA was extracted from IEC isolations by adding a volume containing $2x10^6$ cells in PBS to Qiashredder spin columns (Qiagen) followed by centrifugation at 9.300 g for 1 min. Follow-through was mixed with 600 µl RLT lysis buffer and used for subsequent RNA isolation.

Homogenised sample in RLT buffer from both tissue and IEC isolations were processed by adding 700 µl of 70% ethanol and mixing by pipetting. Into RNeasy spin column, 700 µl of sample was added and spun at 8,000 g for 15 sec. Flow through was discarded and process repeated until all of sample was filtered through column. Then 700 µl of buffer RW1 was added to column and centrifuge at 8,000 g for 30 s. Again, flow through was discarded and filter placed in a new collection tube. To the filter, 500 µl RPE was added and spun at 8,000 g for 30 s followed by discarding of flow through. An additional 500 µl RPE was pipetted into column and centrifuged at 8,000 g for 2 min. Spin column was then placed in a new collection tube and centrifuged at 8,000 g for 2 min. Columns were transferred to a RNA low-bind Eppendorf tube and 30 µl of RNase free water added to directly to the filter. After an incubation of 1 min at RT, sample was centrifuged at 8,000 g for 1 min and flow through containing RNA stored at -80 ˚C. RNA was quantified and quality controlled using a Nanodrop and Bioanalyser (Agilent Genomics).

Reverse transcription PCR (RT-PCR) was performed with the Quantitect Reverse Transcription Kit (Qiagen) following manufacturer's instructions. In brief, reagents and RNA samples were thawed on ice. RNA template (500 ng) was mixed with 2 µl of gDNA Wipeout buffer and made up to 14 µl with RNase free water on ice. Reaction was incubated at 42 ˚C for 2 min and immediately placed in ice. To sample, 14 µl reverse transcriptase and 1 µl of primer mix were added and incubated at 42 ˚C for 15 min followed by 3 min at 95. Afterwards, samples were stored at -20 until analysis by qPCR.

To analyse gene expression, qPCR of cDNA was performed using a LightCycler 480 II (Roche) with Quantifast SYBR Green PCR Kit (Qiagen) and Quantitect primer assays (Qiagen) following manufacturer's instructions. In brief, samples and reagents were thawed on ice and reaction mix (Table 3-8) set up in 384 well plates. Cycling was performed as detailed in Table 3-9. Expression levels of gene of interest were calculated using $_{\Delta\Delta}$CT method normalised against expression of housekeeper gene. Data shown as fold changes in expression compared to levels in control groups.

Table 3-8 qPCR reaction mix

Reagent	Volume (ul)
QuantiFast SYBR Green PCR Master Mix	5
QuantiTect Primer Assay	1
Template cDNA	1
Rnase free water	3

Table 3-9 PCR conditions for qPCR on cDNA generated from isolated host RNA

Time (min)	Temp (°C)	Cycles
300	95	1
10	95	35
30	60	.
hold	40	1

3.2.8.4 ELISA on Piezo1 protein in intestinal tissue

Whole tissue (10 mg) and IEC preparations (volume with $5x10^8$ cells) were homogenised in 1 ml CellLytic Cell MT lysis buffer (Sigma-Aldrich) using Lysis

Matrix E tubes and Fastprep 24 following protocol (3.2.8.3). Lysate was cleared by centrifugation and protein concentration analysed using Qubit 2.0 (Invitrogen) followed by storage at -20 ˚C.

Lysate was analysed using ELISA for mouse Piezo1 (Cusabio BioTech) following manufacturer's instructions. In brief, samples were diluted 1:1 in sample diluent and 100 µl added to wells on ELISA plate together with serial dilutions of Piezo1 standard. Plate was incubated at 37 ˚C for 2 h. Liquid was removed from wells and 100 µl of Biotin labelled Piezo1 antibody added. After incubation at 37 ˚C for 2 h, liquid was aspirated and wells washed 5 times with wash buffer followed by tapping plate dry on paper towels. To each well, 100 µl of HRP-avidin was added and incubated in the dark for 1 h at 37 ˚C. Again, plate was washed 5 times but without drying 90 µl of TMB substrate was added and incubated at 37 ˚C for 30 min in the dark. Immediately after adding 50 µl of stop solution, absorbance of wells at 450 nm was measured on a Fluostar Optima plate reader (BMG Labtech). Blank measurements were subtracted and Piezo1 protein concentration calculated using standard curve generated from absorbance of serial diluted Piezo1 standards. Data is presented as Piezo1 protein level fold changes in comparison to control mouse SI.

3.2.8.5 Measuring expression of miR21 in mouse intestinal samples

Extraction of RNA including miRNAs from mouse intestinal tissue was performed by TriZOL method [291]. Snap frozen samples stored at -80 ˚C were removed from the freezer on dry ice. Using a scalpel, 10 mg section was cut off and placed in 1 ml TRIzol (Thermo Fisher) in Lysis Matrix E Tubes and incubated at RT for 5 min. After the addition of 200 µl of chloroform, tissue was disrupted by beat beating on a FastPrep 24 for thrice 1 min at speed setting 6. Samples placed on ice between beating steps. This was followed by another incubation for 3 min at RT. Samples were then centrifuged at 12,000 g at 4 ˚C for 15 min. Aqueous phase was transferred to a fresh tube and 1 µl Glycoblue added. Mixing by inversion was performed and 500 µl isopropanol added to each tube followed by additional mixing by pipetting up and down. Samples were then incubated at -80 ˚C for 1 h and immediately without thawing centrifuged at 12,000 g for 20 min at 4 ˚C. The supernatant was removed and the pellet (RNA stained blue by Glycoblue) was washed twice with 1 ml of ice-

cold 100% EtOH and centrifuging at 7,400 g in a 4 ˚C for 5 min. EtOH was completely removed and samples air dried on bench for 30 min. Pellet was then resuspended in 25 µl nuclease-free water and RNA quantified by Nanodrop 2000 Spectrophotometer (Thermo Fisher) followed by storage at -80 ˚C.

Generation of miRNA specific cDNA by RT-PCR was carried out using miRNA 21 and endogenous control U6 snRNA specific Taqman probes and assays (Applied Biosystems) following manufacturer's instructions. In brief, Reagents and samples were defrosted on ice and reverse transcription reaction prepared on ice in PCR tubes as indicated in Table 3-10. Two RT-PCR reaction were performed for each sample with either miR21 or u6 snRNA primer added for transcript specific cDNA generation. After gently mixing by inversion, PCR was run with parameters listed in Table 3-11. on a thermocycler. PCR product was stored at -20 ˚C until use for miR expression analysis by qPCR.

Table 3-10 Reaction mix for miR specific RT-PCR reaction

RT-PCR

Reagent	Volume (ul)
100 mM dNTPs	0.15
MultiScribe Reverse Transcriptase (50 U/ul)	1
10x Reverse Transcription buffer	1.5
Rnase Inihibtor (20 U/ul)	0.19
Nuclease water	4.16
Template RNA	3 ul (>10 ng/ul)
5x RT primer (miR21 or U6 snRNA)	3

Table 3-11 miR specific RT-PCR conditions

Time (s)	Temp (°C)
30	16
30	42
300	85
hold	4

miR quantification was achieved by qPCR. cDNA and reagents were thawed on ice and reaction prepared in 384 well plates as indicated in Table 3-12. Plates were sealed and qPCR performed on a LightCycler II (Roche) with parameters listed in

Table 3-13. Expression levels of miR21 calculated using $_{\Delta\Delta}$CT method normalised against expression of U6 snRNA control. Data shown as fold changes in expression compared to levels in control groups.

Table 3-12 qPCR reaction for analysis of miR transcription by qPCR

Reagent	Volume (ul)
TaqMan Small RNA Assay (x20) (Goi or HK)	0.5
Product from RT-PCR reaction	0.67
TaqMan Universal PCR Master Mix II (2x)	5
Nuclease free water	3.83

Table 3-13 qPCR conditions using TaqMan Small RNA Assay

Time (s)	Temp (°C)	Cycles
120	50	1
600	95	2
15	95	40
60	60	.
hold	40	1

3.2.9 Sequencing and bioinformatics

3.2.9.1 Sequencing of mouse and bacterial RNA

Extracted RNA (mouse and bacterial) was quantified and quality controlled using RNA 6000 Nano kit on a 2100 Bioanalyser (Agilent). Only samples with RIN values above 8 were sequenced. RNA was transferred to 96 well plate and shipped on dry ice

RNA-seq was performed at the Welcome Trust Sanger Institute. Isolated RNA was processed by poly-A selection and/or Ribo-depletion. Sample specific information regarding library preparation and sequencing technology platforms are shown in Supplementary Table 2 and Supplementary Table 3. All samples were sequenced using non-stranded, paired end protocol.

3.2.9.2 Bioinformatic analysis of mouse RNAseq data

Analysis was performed with the support of Shabhonam Caim (QIB).

Initial processing was performed at Welcome Trust Sanger Institute as follows. Data demultiplexed and adapter removed. Raw reads quality controlled using FastQC (0.11.3, [292]) and trimmed (phred score < 30) using FASTX (0.1.5, [293]). This was followed by read alignment to mouse reference genome (NCBI *Mus musculus* GRCm38) using Tophat (2.1.1, [294]) using maximum intron size 500.000 bp and default settings. Aligned transcripts were assembled and quantified using Cufflinks (2.1.0, [294]) (applying standard parameters).

At QIB, read counts were extracted manually and differentially expressed genes (DEGs, cut-off's: q-value<0.05, log_2 fold change > +/-2.5) between sample groups calculated and visualised using DeSeq2 (3.5, [295]). DEGs were analysed using Ingenuity Pathway Analysis (Summer 2017 release, last accessed 19.12.17, Qiagen), InnateDB (last accessed: 12.12.2017, [296]) and Cytoscape (3.5.1, [297]).

3.2.9.3 Bioinformatic analysis of bacterial RNAseq

Analysis was performed with the support of Shabhonam Caim (QIB).

Initial processing including demultiplexing, adapter removal and, quality control and trimming performed at Welcome Trust Sanger Institute as described above (3.2.9.2).

At QIB, raw reads were aligned to *B. breve* UCC2003 genome (NCBI reference Sequence NC_020517.1) with Bowtie2 (2.3.2, [298]) using standard parameters and smallest intron setting (50 bp). Counts were generated with HTseq (0.8.0, [299]) using standard parameters with smallest gap skip and differential gene expression calculated and visualised with Deseq2 (setting as described in 3.2.9.2).

For metatranscriptome analysis, raw read files were analysing with SUPER-FOCUS (0.27, [300]) for microbiota taxonomic profiles and functional subset binning referencing SEED database (last accessed 14.11.2017, [301]). Taxonomic profiles were visualised with Prism as abundance of mapped reads relative to total reads. Functional profiles visualised and statistical significance analysed with Prism.

3.2.9.4 Profiling the gut microbiota using 16S rRNA sequencing

PCR amplification of 16S rRNA gene was carried out with the help of Charlotte Leclaire (QIB).

Concentration of DNA isolated from mouse faeces was quantified by Qubit (Fisher Scientific) and normalised to 5 ng/ml. DNA then used as a template for PCR amplification of V1-V2 region of the 16S rRNA gene. Primers were sourced from DNA technologies and sequences shown in Table 3-14.

Table 3-14 Primer sequence used for amplification of 16S rRNA gene

16s rRNA region	Direction	Primer sequence
V1	forward	AGMGTTYGATYMTGGCTCAG
V2	reverse	GCTGCCTCCCGTAGGAGT

To allow multiplexing of samples, primer pairs with unique barcodes were used for PCR amplification and 3 reactions were performed for each sample to ensure amplification of sufficient materials for sequencing. Samples and reagents (New England biolabs) were defrosted and kept on ice. Reaction was set up as indicated in Table 3-15 in 96 well plates on ice.

Table 3-15 PCR reaction components for 16s rRNA amplification

Reagent	Volume (ul)
Nucelase free water	15.4
5x GC buffer	5
dNTPs	0.5
5 uM forward primer	1
5 uM reverse primer	1
Polymerase	0.1
Template DNA	2

PCR conditions are listed in Table 3-16. Samples and reagents were defrosted on ice and PCR reaction set up in 96 well plates. PCR was then performed on a Thermal Cycler PCR machine (Applied Biosystems) and product stored -20 until further processing.

Table 3-16 Cycling conditions for 16s rRNA PCR

Time (s)	Temperature (°C)	Cycles
180	94	1
45	94	25
15	55	
30	72	
180	72	1
hold	4	1

Following PCR amplification, samples were cleaned up using Agencourt AMPure XP beads following manufacturer's instructions. In brief, samples in 96 well plates

and beads were brought to RT. Triplicate repeats PCR amplification reaction were combined in new 96 well plate. Beads were then vortexed for 30 sec and 75 µl added to wells and mixed by gentle pipetting. After incubation at RT for 5 min, plate was placed on magnetic stand for 2 min to trap beads. Supernatant was removed and discarded. Wells containing beads were washed twice by adding 200 µl 80% EtOH for 30 sec. Afterwards, plate was left to air dry at RT for 15 min followed by removal from magnetic stand. Following the addition of 52.5 µl of 10 mM Tris pH 8.5, samples were incubated for 2 min after which the plate was returned to the magnetic stand. Supernatant was transferred to new 96 well plate and quantified using Qubit. RT-PCR product concertation was equalised and prepared for sending on dry ice in 96 well plates. Sequencing of 16S rRNA gene libraries was carried out at Welcome Trust Sanger Institute on Illumina MiSeq platform with 300 bp paired end reads.

3.2.9.5 16S rRNA gene sequencing analysis

Analysis was performed with the support of Shabhonam Caim (QIB).

Raw data generated from sequencing of 16S RNA gene libraries were analysed using an in-house paired end protocol. Quality of raw paired reads was classified using FASTX-Toolkit (minimum quality threshold = 33, < 50% of reads per sample above threshold, 0.11.3). Quality controlled reads for each pair separately, were aligned against SILVA database (SILVA_119_SSURef_tax_silva) using BLASTN (2.2.25+; Max e-value 10^{-3}, [302]). Output files of aligned paired read sequences were annotated for taxonomic assignment using MEGAN 6 paired end protocol (threshold setting: Min Score = 50, Top Percent = 10, reads without assignment classed as "No Hit", [303]) Data was then analysed and visualised within MEGAN 6 [303].

3.2.9.6 Predicting miR21 binding sites in bacterial genomes

Analysis was performed with support by Padhmanand Sudhakar (EI).

Sequence of mature miR21 (NCBI gene ID: 406991) was used to predict potential binding site in *B. breve* UCC2003 (NCBI reference Sequence NC_020517.1) and *S.* Typhimurium SL1344 (NCBI Reference Sequence NC_016810.1) genome by

alignment using MiRbase (accessed: 12.4.2017, [304]). Entropy cut off <-16 was applied to filter results.

3.2.10 Statistical analysis

Statistical analysis performed using Prism 6, R (3.4.1), MEGAN 6 [303] and DESeq2 (3.5, [295]). Applied statistical tests within Prism include Mann-Whitney U test (comparing 2 sample groups), Kruskal-Wallis one-way test with Dunn's multiple comparison test (comparing more than 2 groups) and two ANOVA (compare difference between 2 groups with several observations). Data presented as mean +/- SD. p values < 0.05 were considered significant. Repeats per group indicated as n numbers.

4 Investigating the role of mechano-receptor Piezo1 as a regulator of mammalian intestinal epithelial cell shedding in health and disease

4.1 Introduction

The single cell layer formed by the IE is essential for health; controlling contact and exchange between the host and the luminal contents of the intestine [305, 306]. Constant renewal of the IE poses a significant challenge for maintenance of an intact barrier, as single cells are lost at the tip of intestinal villi [40, 306]. This renewal process has to be tightly controlled, as elevated shedding levels and resulting gaps are involved in intestinal disease aetiology, including IBD [305, 307]. However, the processes governing epithelial cell extrusion remain incompletely understood, and due to its integral role in human health, I sought to investigate the potential role of a newly discovered ion channel Piezo1 in this process.

4.1.1 Ion channel Piezo1 as a potential regulator of intestinal epithelial shedding and turnover by sensing cell crowding and stretching

Piezo1 belongs to a novel protein family including only one other member, Piezo2, with which it shares 47% sequence homology [308]. The proteins are over 2000 amino acids in length and predicted to from 24 to 40 transmembrane structures (Figure 4-1.A). The membrane bound ion channel can conduct K^+, Na^+ and Ca^+ and is activated by distortion of the cell membrane and converts mechanical force into biological signals, so called mechanosensation (Figure 4-1.B) [309]. This process is important in physiological nociception, in hearing, in sensing shear stress (vascular and muscular tension), as well as embryonic development. Therefore, expression levels are high in tissues constantly exposed to stretch such as lung, bladder, and skin (Figure 4-2) [308, 310].

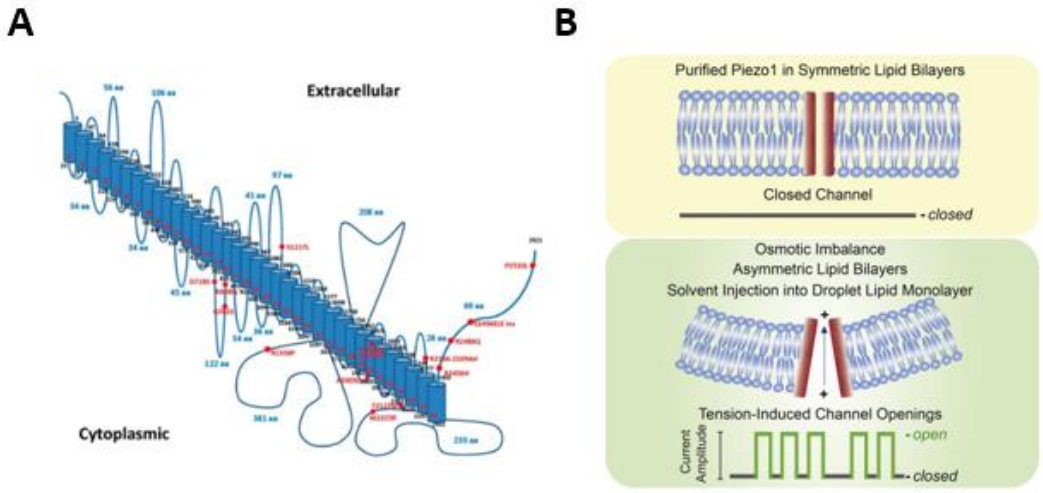

Figure 4-1 Structure and functional mechanism of membrane bound, mechanoreceptive ion channel Piezo1

A Piezo1 (Uniprot Q92508) transmembrane structure with 24-40 domains generated with Swiss-Prot tools, predicted to be one of the largest membrane spanning proteins, forms homotetramer configurations but total number of pores still unknown (figure adapted from Bagriantsev *et al.*, 2014 [309]) **B** Mechanical perturbations of the lipid bilayer alone are sufficient to activate Piezo channels, illustrating their innate ability as molecular force transducers (adapted from Seyda *et al.*, 2016 [311])

Recently, Eisenhoffer *et al.*[37], suggested that the stretch-sensitive ion channel Piezo1 is also important for sensing cell density and causing live cell extrusion in the zebrafish fin and cell culture epithelial monolayers and hypothesised its role in the intestine (Figure 4-3.A). The study presented evidence that physiological cell shedding occurs within areas of the epithelium in which cell density is highest. This was modelled using zebrafish fins, where IEC migration increases cell density at the fin tip, and Madin-Darby canine kidney (MDCK-II) monolayers grown on stretched elastic supports, where release of tension increased cell density. In both models, an increase in density caused an elevation in cell shedding, until physiological cell density was restored. By culturing extruded cells during homeostatic shedding, the authors showed that predominantly live cells were removed during this physiological cell shedding. In contrast, apoptotic stimuli (i.e. UV radiation), applied to *in vitro* cell lines, also elevated cell shedding, and was correlated to extruded cells undergoing cell death i.e. apoptosis. These data added to the body of evidence indicating the existence of two distinct pathways controlling homeostatic and injury-

induced shedding, with physiological extrusion potentially governed by cell density (Figure 4-3.B).

The authors proposed that the stretch activated channel Piezo1 may be involved in this cell shedding mechanism, and subsequently inhibited Piezo1, using gadolinium, in the zebrafish fin. Gadolinium is lanthanide frequently used as a contrast agent in magnetic resonance imaging [312, 313]. They observed decreased cell expulsion, and formation of cell masses, suggesting the ion channel as a main regulator of physiological shedding. To further probe Piezo1-induced mechanisms of cell shedding, the authors inhibited Piezo1 in MDCK-II monolayers, which were artificially stretched to induce cell crowding. Addition of gadolinium to inhibit Piezo1 reduced cell shedding, further supporting the role of Piezo1 in controlling this process.

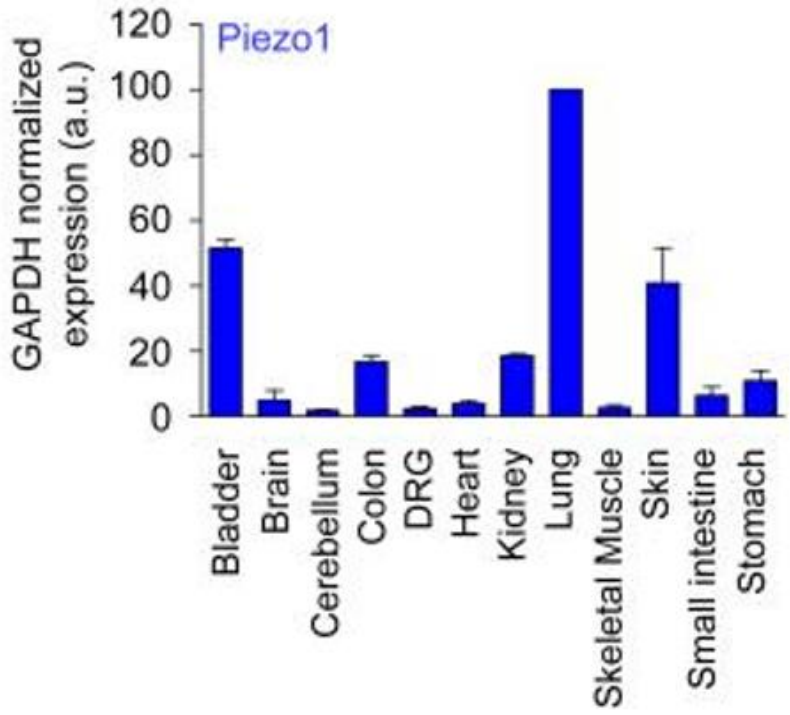

Figure 4-2 Piezo1 RNA expression levels in adult mouse tissues with differing mechanical activity

mRNA expression profiles of Piezo1 determined by qPCR from various adult mouse tissues, GAPDH used as reference gene and lung as tissue calibrator using deltadelta CT method, data shown as mean

+/- SEM of two separate experiments, DRG: dorsal root ganglion (reproduced Coste *et al.*, 2010 [308]).

Previous work by the same group had shown that shedding cells release sphingosine-1-phosphatase (S1P, a bioactive lipid), which binds to S1P receptors on surrounding cells [314]. Binding of S1P induces formation of the shedding funnel, and Rho-kinase (RHOK) mediated contraction of actin-myosin, leading to cell expulsion. S1P is released during both homeostatic and apoptotic shedding, with extrusion of dead cell being controlled by Bcl-2, a regulator of apoptosis. Building on these studies, Eisenhoffer *et al.*, determined that selective inhibition of RHOK or S1P signalling significantly decreased both homeostatic and apoptotic cell shedding, indicating that S1P signalling via RHOK is required and that Piezo1 may act upstream of S1P, however this requires further mechanist work (Figure 4-3.B).

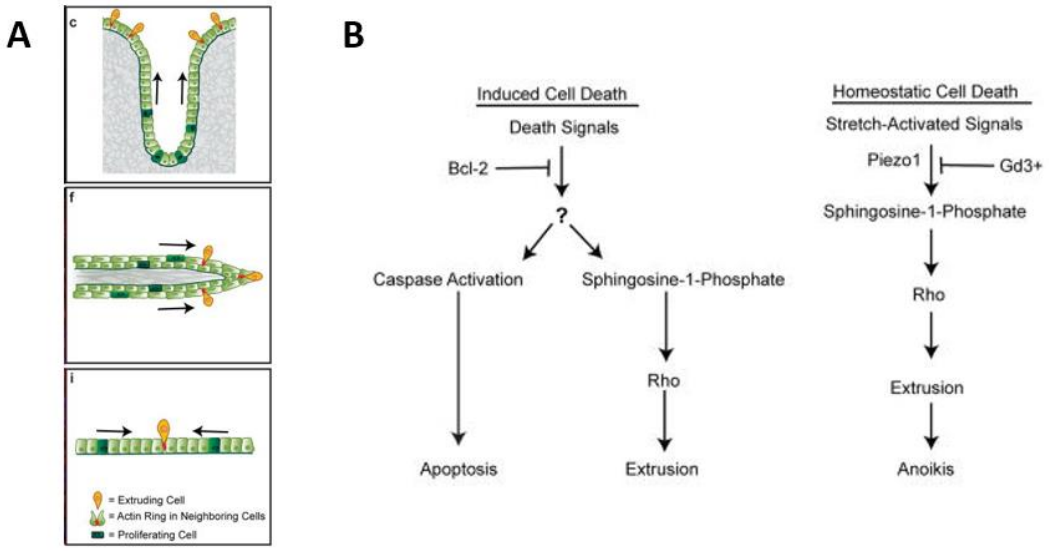

Figure 4-3 Piezo1 senses cell crowding and induces homeostatic life cell shedding

As investigated in zebrafish dermis and cell culture by Eisenhoffer *et al*, **A** Suggested role of Piezo1 in sensing cell density triggering homeostatic cell shedding in human colon epithelium, zebra fish fin tip and cell culture monolayers, cell movement pictured as black arrows, at top of colon epithelium, tip of fins and middle of monolayers, cell density is highest due to cell movement leading to shedding. Inhibition of Piezo1 using gadolinium or knockdown of the protein causes formation of cells masses in the zebrafish fin model caused by decreased cell shedding (not shown) **B** Model of induced versus homeostatic cell death (figure adapted from Eisenhoffer *et al.*, 2012 [37])

More recently, Gudipaty *et al.* [315] published a follow-on study describing the involvement of Piezo1 in controlling mitosis by sensing mechanical stretch. In MDCK-II monolayers, grown on elastic supports, stretching decreased cell density, which in turn increased stretching forces in the cell membrane, and was associated with increased cell division to return cell density to normal levels. In a pathological stretch-induced injury MDCK-II model, wounds or gaps in the epithelium were also closed through increased mitosis. Inhibition of Piezo1 with gadolinium or knock down by short interfering RNA (siRNA) was shown to inhibit this response, leading to a reduction in mitosis, and reduced wound closure, increasing the time required to return cell density to pre-stretch levels. In the zebrafish fin, knock down by CRISPR/Cas9 (Clustered Regularly Interspaced Short PalindromicRepeats/Cas 9 nuclease complex) reduced mitosis events and slowed cell turnover. Furthermore, the authors were able to correlate the cellular location of Piezo1 with function. They showed that when Piezo1 localises to the cell membrane, this correlates with sensing stretching forces, which in turn influences mitosis, whilst when located within the nuclear envelope, Piezo1 senses cell crowding, and induces live cell extrusion. The pathway through which Piezo1 links to mitosis was identified as phosphorylation of extracellular signalling kinase 1/2 (ERK1/2), by selective ERK inhibition with inhibitor U0126, and assessing the effect of stretching on mitosis. ERK activation was shown to induce activation of cycling B transcription, which in turn drives cell division.

Through these studies, the authors have proposed Piezo1 is essential for sensing cell crowding at the tip of the zebrafish fin and induction of cell extrusion to maintain homeostatic cell numbers. Although the authors did not perform any experiments using intestinal systems, they further propose that Piezo1 may also be the main regulator of homeostatic cell extrusion within the IE, however the role of Piezo1 within the intestine has yet to be determined. As Piezo1 has this potential dual role, this ion channel may link balanced cell division in intestinal crypts to cell shedding at the villus tip, and hence is an interesting candidate for further investigation (Figure 4-4). Current studies have only utilised models of the zebrafish dermis, and canine kidney epithelium as a basis to determine the role of Piezo1. However, investigating Piezo1 within the intestine is a central requirement to determine if it also has an IEC

specific role. Concurrent studies to determine involvement of Piezo1 in pathological elevated cell shedding, utilising appropriate physiologically relevant models that mimic human intestinal diseases, alongside validation in patient intestinal biopsy samples is also required. Performing these studies will further our understanding of intestinal barrier integrity in health and disease, and may provide a platform for development and design of new therapies.

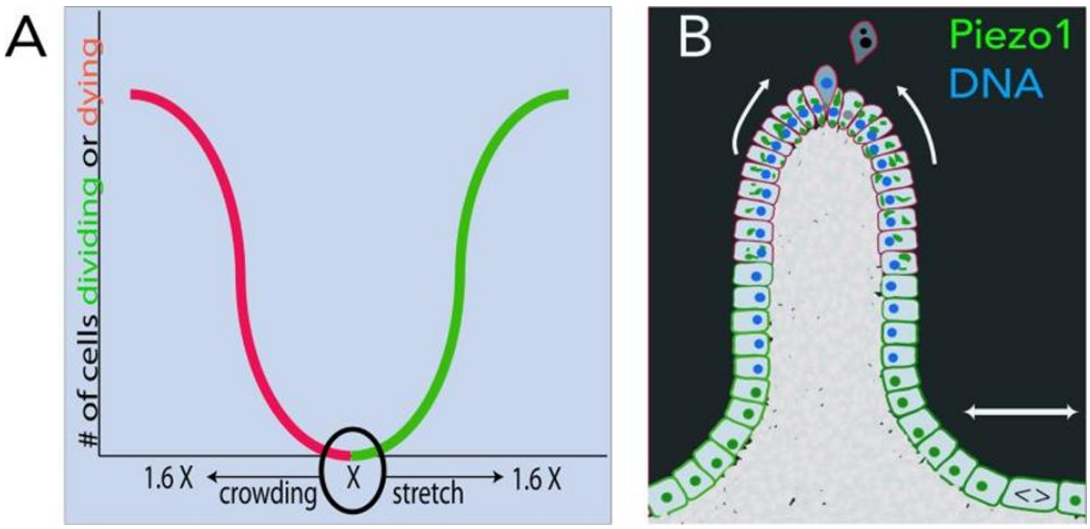

Figure 4-4 Piezo1 suggested to control intestinal epithelial homeostasis by sensing stretch in intestinal crypts and inducing mitosis while reacting to crowding at villus tip by induction of cell extrusion

A Theoretical graph of density-dependent Piezo1 function for cell division and cell death: Epithelia trend to a steady-state density, X. If density is reduced, stretching causes Piezo1 to activate cell division, if it increases, crowding causes Piezo1 to activate cells to extrude and die B Schematic showing how Piezo1 (green) localizes to plasma membrane in sub-regions of epithelia that are sparser and divide and accumulate into cytoplasmic aggregates in sub-regions that are crowded and extrude (Adapted from Gudipaty *et al.*, 2017 [315])

4.2 Hypothesis and aims

4.2.1 Hypothesis

Piezo-1 regulates homeostatic and pathological mammalian epithelial cell shedding.

4.2.2 Aims

1. Investigate effect of Piezo1 inhibition on homeostatic cell shedding in zebrafish intestinal epithelium and a mammalian intestinal epithelial cell line.
2. Assess effects of increased, pathological shedding on Piezo1 transcription and translation using an *in vivo* mouse model
3. Determine localisation of Piezo1 within mouse intestinal epithelial cells
4. Measure Piezo1 transcription in biopsies of UC patients during active disease
5. Determine role of the microbiota member *B. breve* UCC2003, on Piezo1 translation and transcription

4.3 Results

4.3.1 Inhibition of Piezo1 in zebrafish intestine and mammalian intestinal cell culture models increases homeostatic cell shedding levels.

Eisenhoffer *et al.* and Gudipaty *et al.* used zebrafish larvae fins (32 hours post fertilisation) as a model for homeostatic cell shedding, and showed reduced shedding rates when inhibiting Piezo1 using gadolinium at differing concentrations (Eisenhoffer *et al.* - 10 mM, Gudipaty *et al.* – 10 µm). As it remains unclear if Piezo1 inhibition has a similar effect on cell shedding within the intestine, I utilised the adult zebrafish mid gut (analogous to the mammalian LI) to investigate the effect of gadolinium, and thus Piezo1 inhibition, on intestinal homoeostatic cell extrusion.

Preliminary experiments (data not shown) using the same concentration of gadolinium (10 mM) as Eisenhoffer *et al.* caused exposed adult fish to die after 2 h, suggesting a lower tolerance of adult zebrafish to gadolinium than embryos, as the authors were able to collect live embryos after 28h of exposure. When exposing fish to lower concentrations of 10 µM (same concentration used as Gudipaty *et al.*) or 100 µM gadolinium, fish were alive after 4 h. Interestingly, at both concentrations of the inhibitor, an increase in cell shedding was observed within the intestine, in a dose dependent manner with a significantly elevated response ($p<0.0001$) for fish treated with 100 µM gadolinium as determined by histological analysis of F-actin formation into shedding funnels stained by phalloidin (Figure 4-5.A).

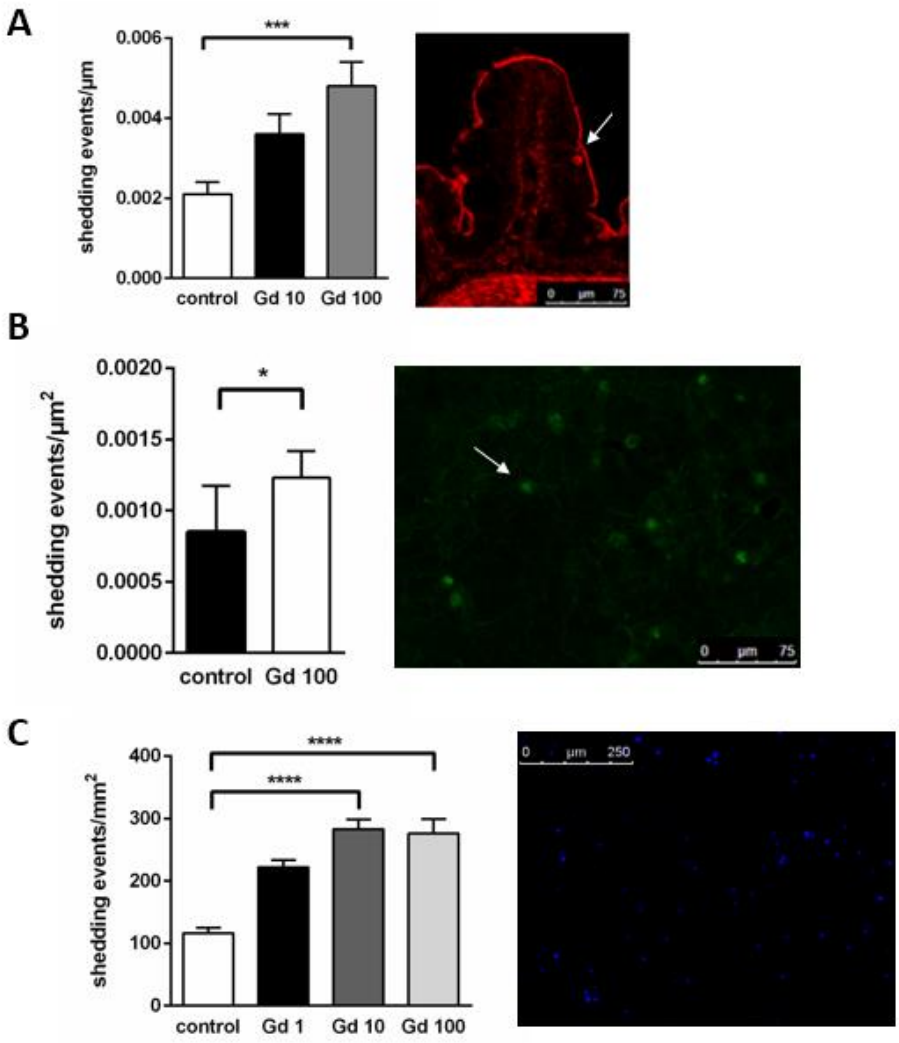

Figure 4-5 Inhibition of Piezo1 in zebrafish intestine and mammalian intestinal cell culture models increases homeostatic cell shedding events

A Zebrafish exposed to piezo1 inhibitor gadolinium at 10 and 100 µM for 4 h and intestinal cell shedding funnels enumerated by staining for F-Actin, data shown as funnels per micron of midgut epithelium, mean +/- SD (n=6), 30 villi per biological repeat counted, image shows representative zebrafish midgut villus stained with F-actin to visualize shedding funnels (white arrow). **B** Confluent IEC-6 monolayers grown on chamber slides were treated with 100 µM Gadolinium for 2 h followed by staining of F-actin to count cell ring formations around shedding events, data are shedding events per um2, mean +/- SD (n=9), three images per chamber enumerated, representative image shown with white arrow highlighting shedding funnel. **C** Cells shed into the supernatant were collected after exposure of confluent IEC-6 monolayers to 1, 10 and 100 µM gadolinium for 2h and visualized with DNA stain for quantification, data presented as shedding events per mm2 of confluent monolayer, means +/- SD (n=12), three images per well captured, representative image of shed cells collected by centrifugation and stained with DAPI shown. Statistical significance (* $p<0.05$, *** $p<0.0005$, ****

p<0.0001), data analysed with Mann Whitney U test (B) and Kruskal-Wallis and Dunn's post hoc test (B,C).

To further assess the role of Piezo1 inhibition within the intestine, I utilised the rat small intestinal epithelial cell line IEC-6. Both Eisenhoffer *et al.* and Gudipaty *et al.* utilised an *in vitro* cell line derived from canine kidney epithelium, rather than IE, and measured cell shedding by enumerating extruded cells. Cell shedding funnels can be quantified by exposing confluent IEC-6 monolayers grown on chamber slides to 100 µM gadolinium for 2 h; subsequent staining with phalloidin for F-actin can then be used as a measurement of cell extrusion. It was observed that under these homeostatic conditions, gadolinium caused a significant increase ($p<0.05$) in cell shedding as determined by funnel enumeration (Figure 4-5.B). A significant ($p<0.0001$), and dose dependent increase was also observed when quantifying the number of extruded cells in the supernatant at 2 h when exposed to 10 and 100 µM inhibitor (Figure 4-5.C).

These data indicate that Piezo1 inhibition by gadolinium, under homeostatic shedding, resulted in increased-cell extrusion, rather than a reduction as observed in the zebrafish dermis, suggesting a different role for Piezo1 within the IE of zebrafish and mammalian intestinal cell culture models.

4.3.2 Piezo1 protein levels are not influenced by experimentally-induced elevated cell shedding in mouse small intestine and large intestine.

To further investigate the function of Piezo1 in a more translationally relevant mammalian intestinal model, I focused my next studies on the mouse intestine. Previous studies indicate that *Piezo1* is highly expressed in tissues exposed to strong mechanical forces such as the bladder, lung, or endothelium [308]. Therefore, to compare expression levels in the mammalian gut, I analysed *Piezo1* transcription in the small and LI, and compared it to the lung, to analyse organs with differing levels of stretch and crowding forces (Figure 4-6). Lung tissue was observed to have significantly higher ($p<0.05$) *Piezo1* expression when compared to small intestinal samples, and there were no statistical differences between the large and SI.

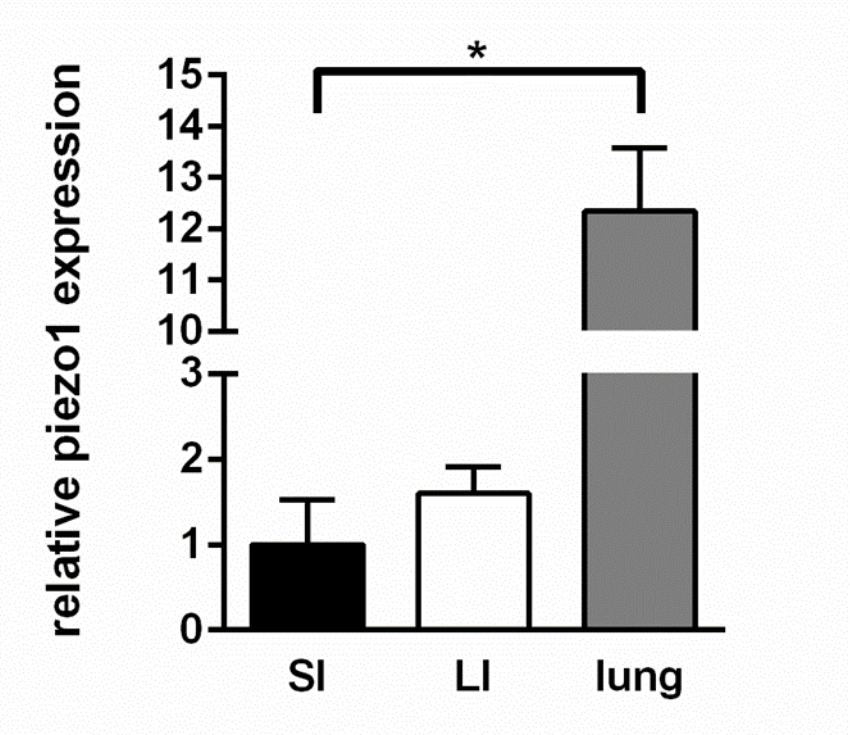

Figure 4-6 Piezo1 expression is higher in mechanically more active lung tissue compared to small and large intestine

Piezo1 expression measured under homeostatic conditions in mouse small intestine, large intestine, and lung by qPCR, mean +/- SD shown, n=3, statistical significance (*=p<0.05) analysed with Kruskal-Wallis and Dunn's post hoc test, qPCR results normalized to house keeper and relative to small intestinal expression by deltadeltaCT method.

Gadolinium is toxic to mice, causing lesions, leading to capillary embolism and liver and spleen necrosis 48 h after single intravenous injection of gadolinium III chloride [313, 316]. Hence, I was unable to utilise this Piezo1 inhibitor in my *in vivo* experiments due to animal welfare constrains, as well as potential off-target effects of toxicity on shedding. Hence, I applied an established model of pathologically elevated small intestinal cell shedding, induced by systemic administration of LPS [289] previously discussed (section 1.1.5.1). In brief, TLR4 presenting monocytes, including macrophages and dendritic cells, within intestinal tissue respond to systemic LPS and produce and release TNF-α, which in turn binds to TNF-R1 on intestinal epithelial cells. This causes cell extrusion, via apoptosis induced by capase-3 cleavage (Figure 4-7). Using this model, I aimed to determine correlations

between *Piezo1* expression and increased sensing of shedding inducing events, as well as elevated signalling responses, causing higher levels of cell extrusion.

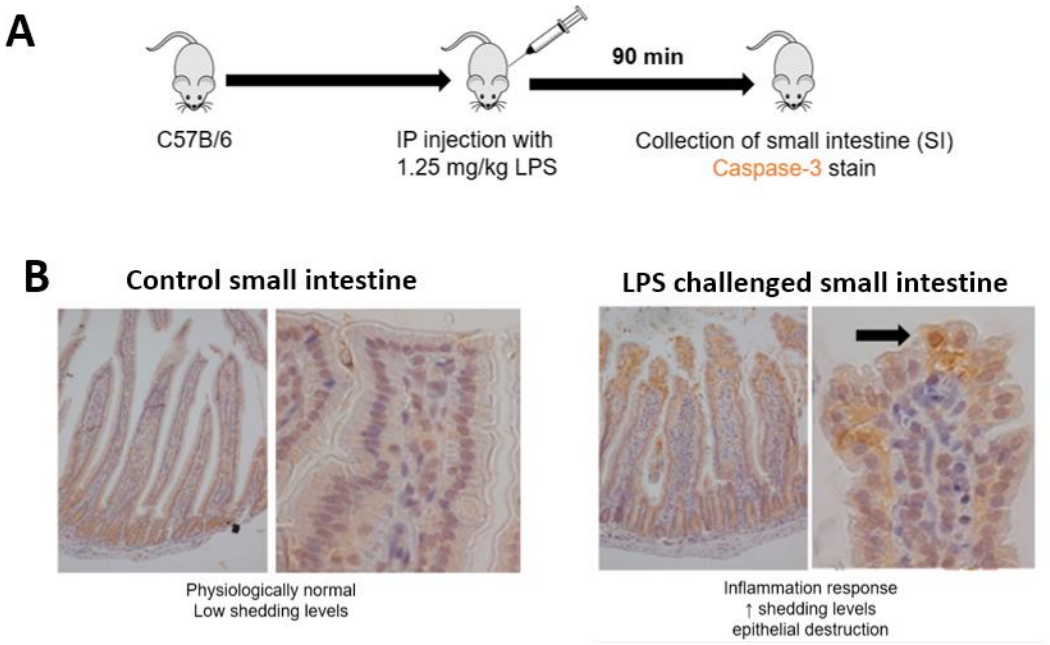

Figure 4-7 Systemic LPS administration induced small intestine apoptotic cell shedding

As shown by Williams *et al. [317]*, **A** Schematic of LPS IP induced elevated SI cell shedding model in mice, mice injected IP with PBS (control) or 1.25 and 10 mg/kg LPS, tissue collection 90 min most administration and apoptotic shedding observed by caspase-3 standing of small intestinal sections **B** Histological images of small intestine 90 min post LPS injection stained for caspase-3, LPS induces strong apoptotic response in small intestine IECs, representative images shown, apoptotic shedding events return to normal levels at 4 h post injection (not shown).

The applied model induces caspase-3 positive cell extrusion by intraperitoneal (IP) injection of LPS from the SI villus, in a dose and time dependent manner. At 90 min post injection, the strongest shedding response can be observed with shedding rates returning to physiological levels at 4 h post challenge. An injection of 10 mg/kg LPS is the highest dose possible to inject due to animal welfare constraints and induces the strongest response, whilst 1.25 mg/kg LPS is the lowest concentration at which an effect on shedding can be measured.

To compliment analysis in whole tissue samples, and to correlate Piezo1 specifically to the epithelium, I additionally isolated IECs. By applying a modified Weisser

method, the epithelial monolayer was stripped from the underlying stroma while leaving the LP intact. As systemic LPS challenge of mice causes acute inflammation, and destruction of the intestinal epithelial lining, as well as changes to the villus morphology, I tested the purity of IEC isolations using FACS staining for dead cells (PI) and a common leucocyte marker $CD45^{+}$. The analysis showed preparations to be free of contaminating leukocytes, as well as a high percentage of viable IECs (Supplementary Figure 1).

When analysing *Piezo1* expression in whole SI, expression levels were significantly elevated at 1.5 h post IP injection, when compared to the control group (PBS injected), in both 1.25mg/kg ($p<0.0001$) and 10mg/kg LPS ($p<0.005$) challenged mice. However, at 4 h post challenge, expression was no longer significant compared to control. Notably, in isolated IECs, whilst *Piezo1* expression was somewhat increased at 1.5 h post injection for both LPS concentrations, this was not statistically significant (Figure 4-8.A).

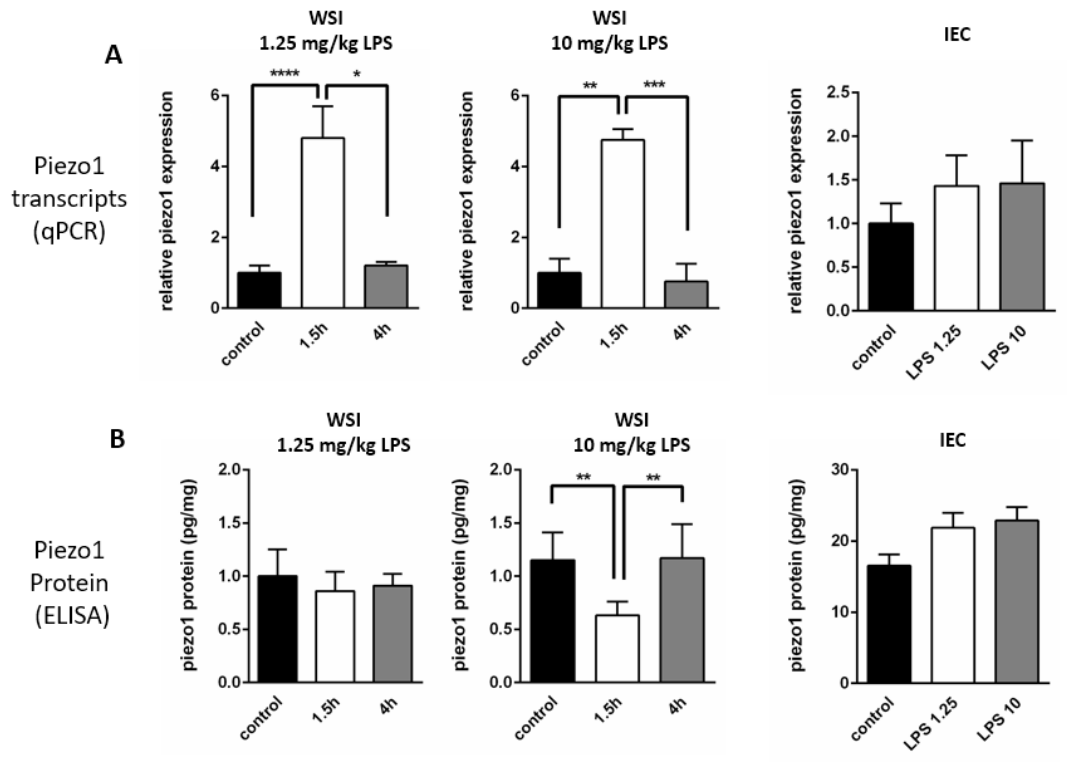

Figure 4-8 Piezo1 protein levels are not influenced by experimentally induced elevated cell shedding in mouse small intestine

A Piezo1 transcription during altered shedding rates was measured by qPCR in whole small intestine and IEC isolations comparing 1.25 and 10 mg/kg LPS administration at 1.5 and 4h post challenge (IECs collected at 1.5 h time point), qPCR results normalized to HPRT and relative to control (deltadetlaCT method), data shown as mean +/- SD, WSI n=9 IEC n=6 B Piezo1 protein content in WSI and IECs quantified by ELISA in paired samples from A, data are fractions of Piezo1 (pg) per whole SI (mg) or IEC protein (mg), statistical significance (*=p<0.05, ** p<0.005, *** p,0.0005, **** p<0.0001) analysed with Kruskal-Wallis and Dunn's post hoc test .

To validate the *Piezo1* expression data, I also measured protein levels to determine if a greater number of ion channels correlated with apoptotic shedding levels. Paired samples used for qPCR analysis were analysed for protein concentration by ELISA (Figure 4-8.B). Notably, WSI Piezo1 protein levels showed no significant difference during elevated cell shedding induced by 1.25 mg/kg LPS at 1.5 and 4 h post injection, compared to the control group. However, a significant decrease ($p<0.005$); compared to control levels, of Piezo1 protein was observed at 1.5 h post administration of 10 mg/kg LPS. Furthermore, isolated IECs showed only a slight,

but not significantly different, increase of Piezo1 protein during LPS challenge in both treatment groups.

The small and LI differ in physiology and histology, with cell shedding being investigated by application of different models. To explore the possible role of Piezo1 in colonic cell extrusion I applied a mouse model of acute colonic colitis by DSS in drinking water [288]. As expected I observed acute inflammation and hyperplasia and elevated disease activity index and colonic weight ($p<0.05$, Supplementary Figure 2). However, inflammation of the LI did not affect *Piezo1* expression, as shown by a non-significant change in transcription compared to healthy control tissue (Figure 4-9).

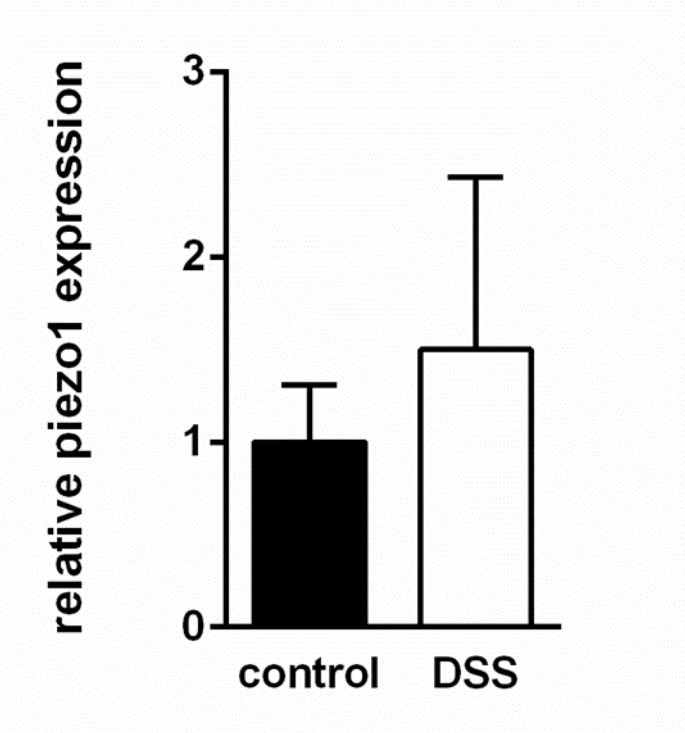

Figure 4-9 DSS induced colitis does not influence piezo1 transcription in large intestinal tissue

Large intestinal tissue analysed by qPCR for Piezo1 expression in mice with acute colonic colitis induced by administration of dextran sodium sulphate (DSS) in drinking water for 7 days, results normalized to HPRT and relative to control (deltadetlaCT method), data analysed with Mann Whitney U test, data shown as mean +/- SD, n=5.

Taken together, my results indicate that whilst Piezo1 transcription in whole SI tissue is modulated during small intestinal inflammation, this did not correlate with isolated IEC samples, or Piezo1 protein expression, indicating Piezo1 may play a somewhat different role in this system.

4.3.3 Piezo1 RNA and protein in IECs is located in the cytoplasm at the villus tip and membrane associated in the crypt.

As localisation of the protein appears to be linked to its functional effect; Gudipaty *et al.* showed Piezo1 to be localised to the cell membrane or in nuclear aggregates in zebrafish or *in vitro,* I investigated the location of *Piezo1* RNA and protein in the mammalian gut. With RNAscope, an immunofluorescent *in situ* hybridisation method allowing for visualisation of transcripts by bright field microscopy, I observed localisation of *Piezo1* within small intestinal epithelial cell crypts, with fewer to no transcripts in IECs at the top of villi (Figure 4-10.A). The intracellular position in the control group is basolateral, and interestingly *Piezo1* transcription also appeared to occur in cells present in the villus stroma. In contrast, in LPS challenged mice, greater *Piezo1* staining was observed in epithelial cells overall, with a more pronounced increase observed in crypts (as well as villus stroma). Quantification of transcripts per IEC supports this qualitative observation as transcripts were present in significantly higher numbers ($p<0.05$) overall along the crypt-villsu axis in LPS challenged SI compared to control, with greater differences towards the villus crypt (Figure 4-10.B). Intracellular localisation appears unaltered, but epithelial destruction due to LPS challenge might interfere with accurate visualisation.

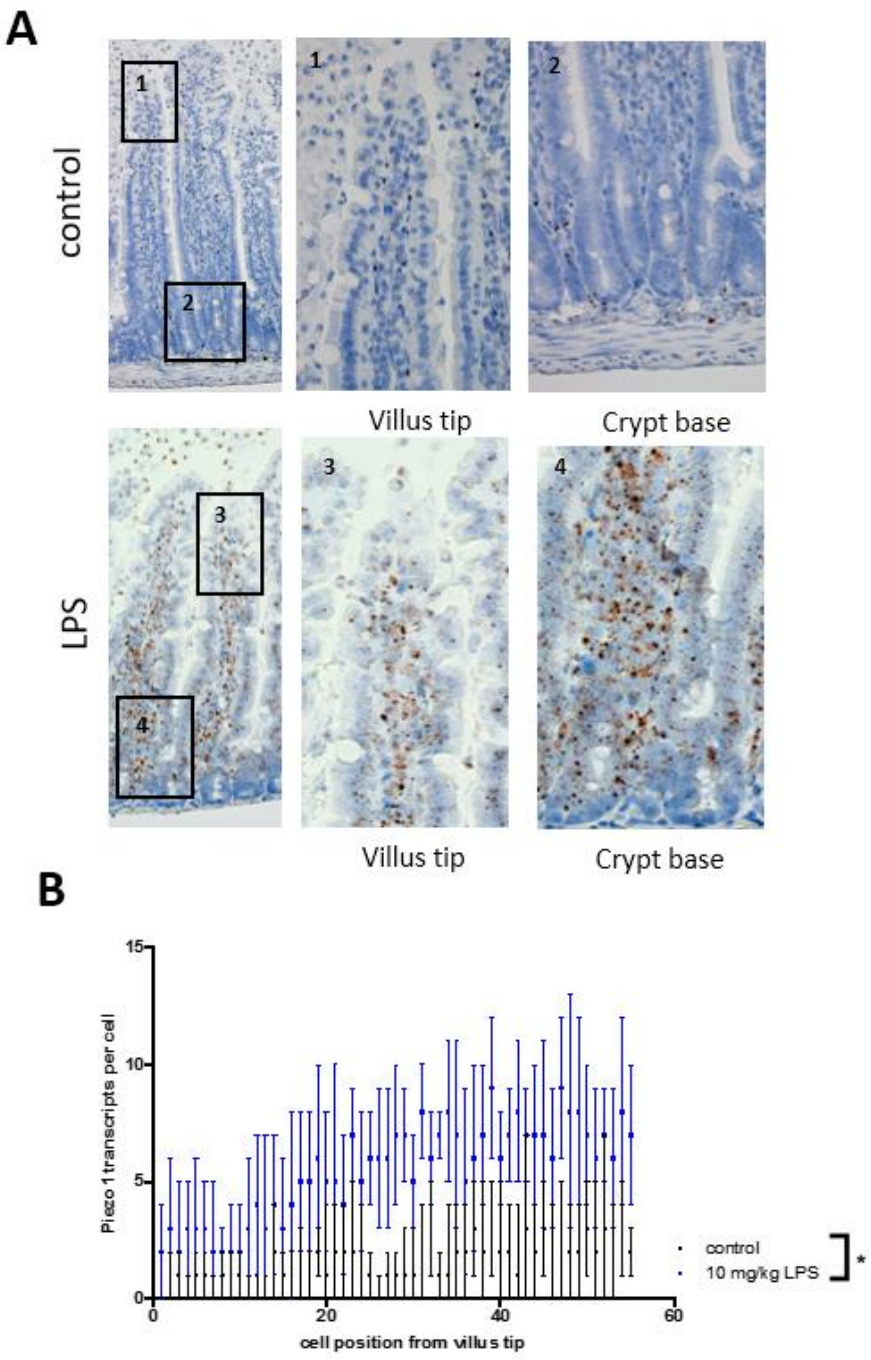

Figure 4-10 Piezo1 transcripts is increased by LPS induced cell shedding with more pronounced effects in intestinal crypts

A Piezo1 transcripts visualised by RNAscope in the small intestine under physiological conditions (control group) and during elevated cell shedding ("10 mg/kg LPS" IP injection, collection 1.5 h post), representative bright field microscopy images, brown spots: Piezo1 transcripts, counter stained with H&E **B** Quantification of Piezo1 transcripts per epithelial cell according to position on villus in

control and LPS injected groups, n=5 (12 villi per sample counted), data shown as mean +/- SD, statistical analysis by two-way ANOVA (* $p<0.05$).

To investigate the intracellular protein position of Piezo1, immunofluorescent staining of small intestinal cryosections was performed. In agreement with the transcript localisation, during homeostasis Piezo1 staining was more pronounced in the crypt compared to the villus tip (Figure 4-11). In crypt luminal cells, the protein was directly associated with the cell membrane while localised more nuclear in IECs at the villus tip with this pattern was also observed in LPS challenged mice. However, Piezo1 was not localised to the cell membrane at the villus tip IECs, but as previously indicated for RNAscope, LPS-induced epithelial destruction made accurate observations difficult.

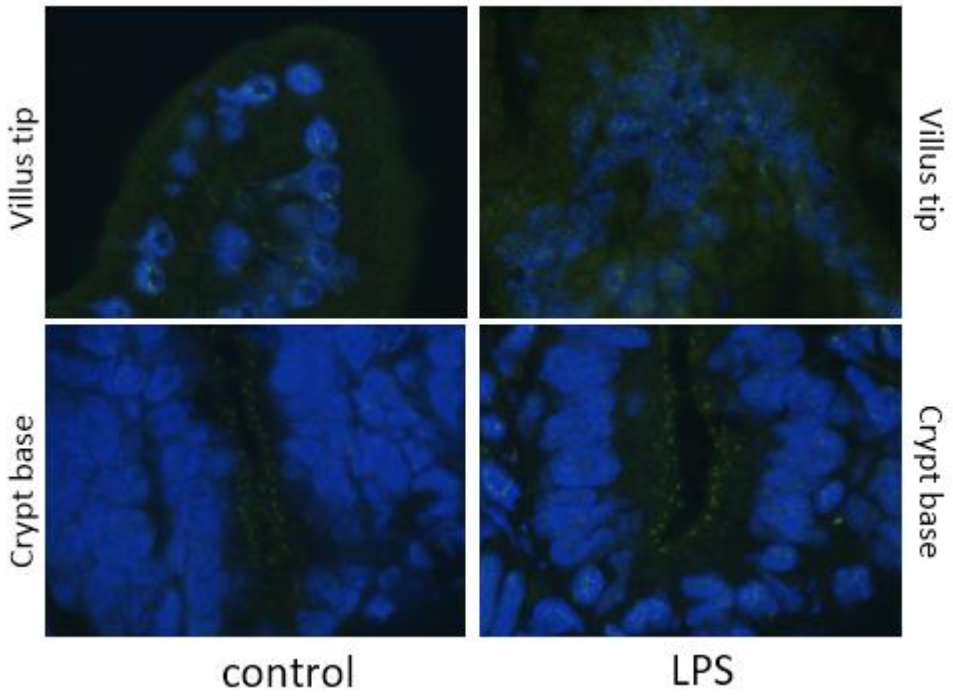

Figure 4-11 Piezo1 protein in small intestinal epithelial cells is located in the cytoplasm at the villus tip and to the luminal cell membrane in crypts

Localisation of Piezo1 protein at villus tip and crypt base in mouse small intestine in control mice (homeostasis) and LPS injected mice (increased cell shedding) visualised by IF staining. Representative images shown, green: Piezo1, blue: nuclei (DAPI), LPS administration at 10 mg/kg LPS and tissue collected at 1.5 h post injection.

In summary, this suggests cell membrane villus crypt, and cytoplasmic villus tip localisation of Piezo1 in the mouse intestine.

4.3.4 Altered mouse intestinal microbiota does not influence Piezo1 protein expression during physiological and elevated cell shedding rates.

The gut microbiota plays an essential role in regulating intestinal homeostasis, and it has been recently reported to influence IEC gene expression and function [318]. Therefore, the microbiota may be expected to play a role in Piezo1 function, with respect to epithelial physiology. Hence, I investigated this by comparing *Piezo1* transcription levels in WSI and WLI of conventionally raised and GF mice. GF mice were raised and housed in a sterile environment and gnotobiotic status verified by culture independent (faecal cytox stain, Supplementary Figure 3) and dependent methods (faecal expansion culture, Supplementary Table 4). Notably, there was no significant difference in Piezo1 expression observed in the SI and LI when GF mice and conventionally raised animals were compared (Figure 4-12), indicating that the gut microbiota does not appear to play a role in Piezo1 expression.

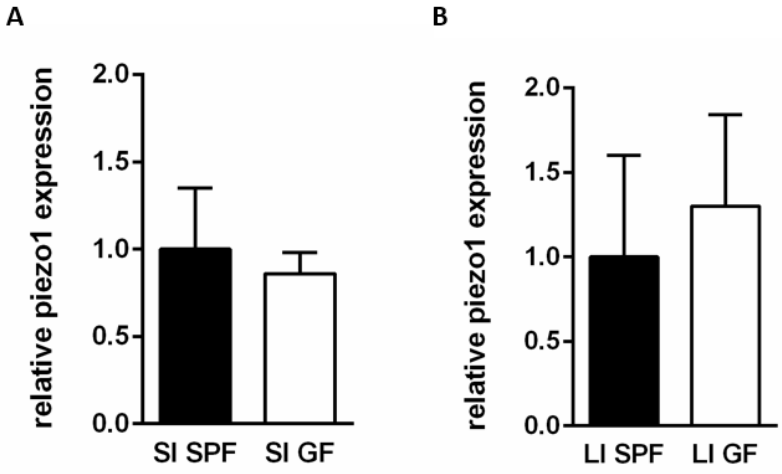

Figure 4-12 Intestinal Piezo1 expression is not influenced by microbiota colonisation status of mice

Piezo1 expression in mouse small (**A**) and large intestine (**B**) of conventionally raised (SPF) and germ free (GF) mice, quantified by qPCR, data normalized by deltadetlaCT method to housekeeper and relative to SPF group expression,), data analysed with Mann Whitney U test, data shown as mean +/- SD, n=3.

GF mice are underdeveloped in terms of epithelial and immune physiology and therefore may not represent the best model for determining impact of the microbiota in Piezo1 on cell shedding. I also determined that GF mice show a slightly decreased proliferation of intestinal epithelial cells, when compared to SPF controls, by quantification of Ki 67 positive cells (marker of proliferation), which agrees with previous studies (Supplementary Figure 4) [319, 320]. Importantly, more specific changes in microbiota composition, including reduction in overall diversity, have been correlated with pathologies. Especially gut inflammatory pathologies, including UC, are associated with a significant reduction in particular species including the microbiota member *Bifidobacterium* (reviewed in 1.4.6) [321]. Notably, administration of *Bifidobacterium longum* to patients suffering from UC has been associated with a reduction in relapse frequency [322, 323].

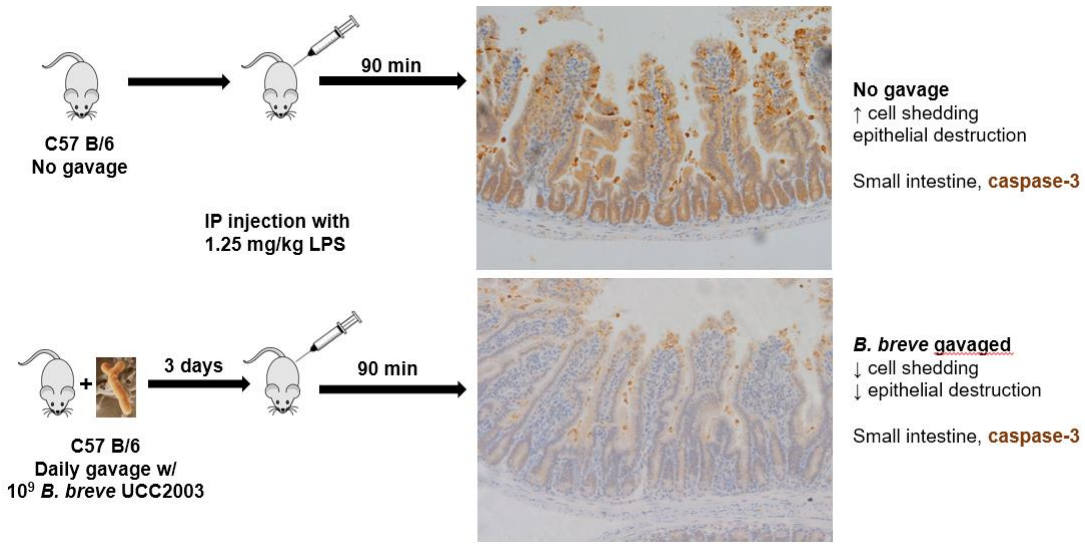

Figure 4-13 ***B. breve*** **UCC2003 colonisation protects small intestinal epithelial cells from LPS induced apoptotic cell shedding**

As shown by Hughes *et al.*, 2017 [46], schematic of protective effect of *B. breve* from LPS induced elevated SI cell shedding, mice gavaged with 109 cfu *B. breve* on three consecutive days prior to 1.25 mg/kg LPS IP injection, tissue collected 90 min post, cells being shed from small intestinal epithelium visualised with caspase-3 stain, strong reduction of shedding event in *B. breve* colonised mice, representative images shown.

Recently, it has been shown that *B. breve* UCC2003 reduces pathological intestinal epithelial cell shedding in the LPS mouse model, as utilised in my previous experiments [46]. Mice pre-colonised with *B. breve*, have reduced numbers of caspase-3 positive cells and epithelial destruction which will be further discussed in section 5.1.1 (Figure 4-13). As previously mentioned (1.1.5.1), systemic LPS administrations induces cell shedding via release of TNF-α from macrophages, which induces apoptosis in IECs via binding to TLR-4. However, the protective effect of *B. breve* appears to be independent of TNF-α production by mononuclear cells, but rather via signalling through epithelial-specific Myd88 and the bifidobacterial EPS capsule. I hypothesised that *B. breve* may impact Piezo1, which in turn could play a partial role in modulating cell shedding. Mice were gavaged with *B. breve* UCC2003 for three consecutive days leading up to LPS challenge, with colonisation levels up to 10^8 cfu/mg at time of tissue collection, while no bifidobacteria could be cultured from control group (i.e. PBS) faeces (Figure 5-4 and Figure 5-5 in chapter 5).

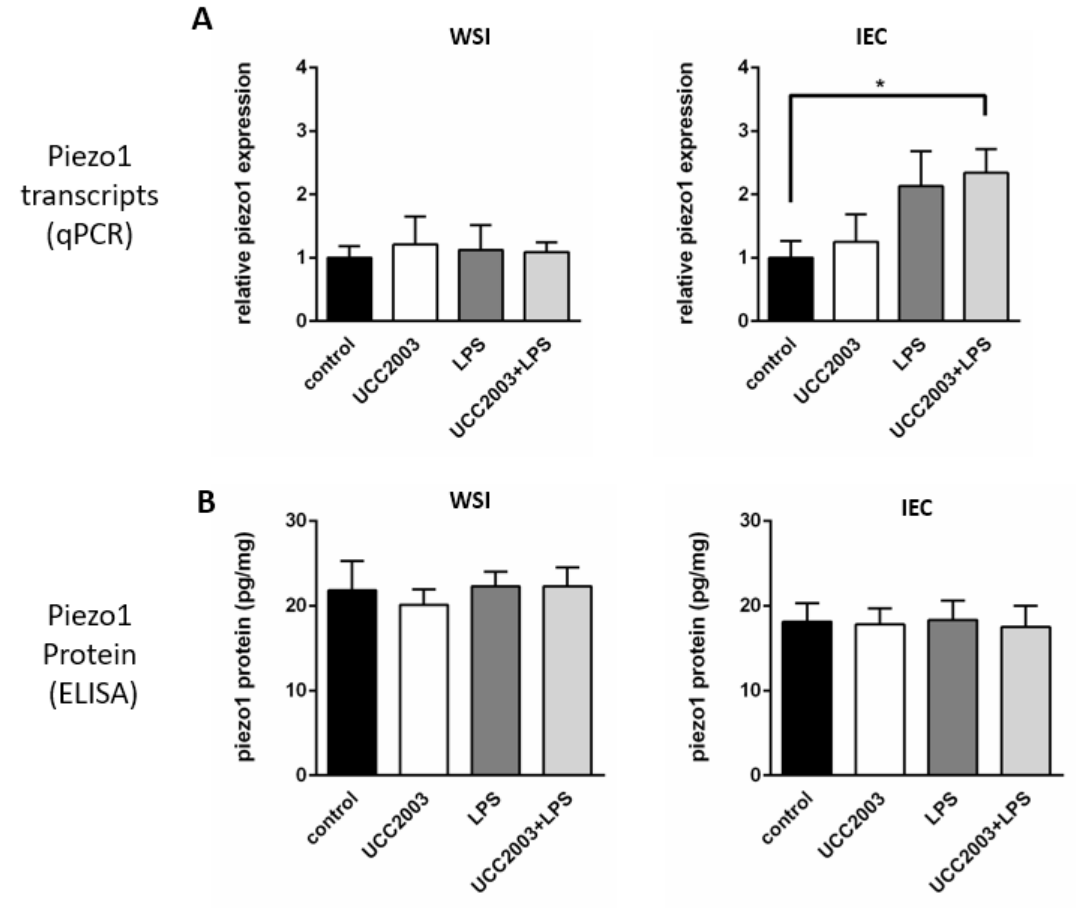

Figure 4-14 Colonisation by *B. breve* UCC2003 does not influence Piezo1 protein expression during physiological and elevated cell shedding rates

SPF mice gavaged with PBS (control) or *B. breve* UCC2003 (UCC2003 group) for 3 days prior to IP administration of LPS (UCC2003 group), tissue collected 1.5 h post administration **A** Piezo1 expression in whole small intestine (WSI) and small intestinal epithelial cell isolations (IEC) measured by qPCR, data analysed by deltadeltaCT method normalized to housekeeper and relative to control **B** Piezo1 protein quantified by ELISA in paired samples from A, data shown as fraction of Piezo1 (pg) per whole SI (mg) or IEC protein (mg), statistical significance (*=$p<0.05$) analysed with Kruskal-Wallis and Dunn's post hoc test, data shown as mean +/- SD, n=5.

When analysing intestinal *Piezo1* transcription in this model, I observed no significant differences in *B. breve* colonised mice in whole intestinal samples, when compared to control mice during homeostatic conditions at 1.5 h post challenge when the cell shedding protective effect is demonstrated. Analysing intestinal epithelial transcription, *Piezo1* expression was elevated in LPS samples compared to control tissue with a significant ($p<0.05$) in *B. breve* colonised mice. No difference

was observed between control group and *B. breve* colonisation either during homeostasis or during elevated shedding (Figure 4-14.A).

When measuring Piezo1 protein ratios, Piezo1 levels appeared unaffected by *B. breve* colonisation during homeostasis, as well as during LPS-induced elevated shedding, in both WSI and IEC isolation when compared to non-colonised mice (Figure 4-14.B). No difference between control and LPS treated samples in Piezo1 protein expression was observed.

In summary, these data indicate that the strong protective effect from pathological cell shedding by *B. breve* colonisation is not conferred by Piezo1.

4.3.5 Piezo1 expression in not altered in Ulcerative Colitis human colonic tissue.

As previously highlighted, intestinal epithelial cell shedding is important for gut homeostasis and elevated or pathological shedding plays a key role in the aetiology of intestinal pathologies such as UC [27, 32, 39]. To address the translational aspect of a potential involvement of Piezo1 in controlling intestinal shedding in human patients, I investigated transcription levels in human colonic biopsies, comparing expression rates in healthy colonic tissue, to patients suffering from acute inflamed UC (Figure 4-15.A). However, I did not observe a significant change in expression and additionally the level of inflammation did not appear to be an influencing factor, as biopsies from UC patients with mild (UC-R), versus severe inflammation (UC-I), both present with no significant changes to *Piezo1* expression (Figure 4-15.B).As mentioned above, *B. breve* provides protection from inflammation-induced cell shedding *in vivo*, and reduced levels of bifidobacteria have been observed in patients suffering from UC. Thus, I also investigated the effect of *Bifidobacterium* on *Piezo1* transcription in the human colon. Colonic biopsies from healthy volunteers and patients with mild (UC-R) and severe (UC-I) UC inflammation were co-cultured with 10^7 cfu/ml *B. breve* UCC2003 (UCC2003) or sterile media (Control) in pIVOC for 8 h followed by *Piezo1* RNA measured by qPCR (Figure 4-15.C). No significant change in transcription was observed in all three patient groups comparing expression between control and *B. breve* co-incubation.

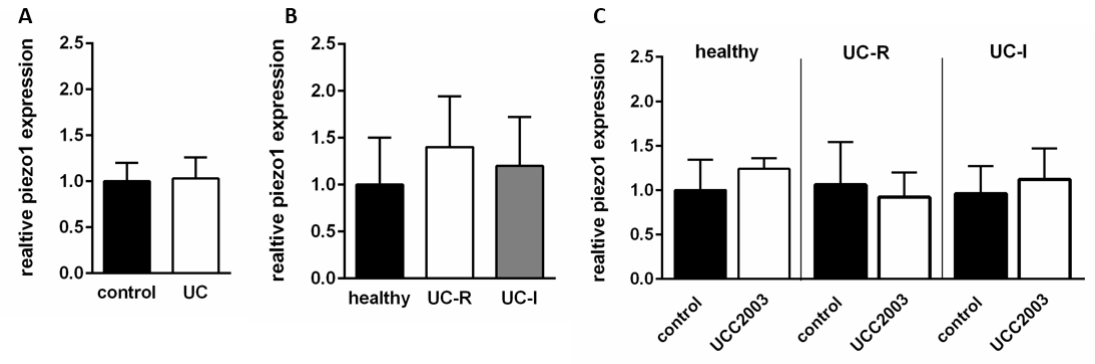

Figure 4-15 Piezo1 expression in human colonic tissue is not altered by active inflammation induced by Ulcerative Colitis

A Colonic biopsies collected from healthy volunteers (control) and patients suffering from Ulcerative Colitis with active inflammation, piezo1 transcription quantified by qPCR, n=3 **B** PIEZO1 expression in human colonic tissue of healthy volunteers and Ulcerative Colitis patients in remission (UC-R) and active inflammation (UC-I) assessed by qPCR, n=3 **C** Human biopsy samples paired with B co-incubated with apical Bifidobacterium breve UCC2003 in pIVOC (polarised in vitro organ culture) for 8 h, control group incubated with no bacteria, PIEZO1 transcription quantified by qPCR, n=3, statistical significance analysed with Mann Whitney U test (A, C) and Kruskal-Wallis and Dunn's post hoc test (B), data are mean +/- SD, qPCR results analysed by deltadeltaCT method (normalized to housekeeper, relative to control/healthy group expression).

Taking together, these results suggest that *Piezo1* expression in the human colon is not influenced by UC inflammation severity and is not directly modulated by *B. breve* UCC2003.

4.4 Discussion

The control of epithelial cell shedding from the tip of intestinal villi is essential the intestinal physiological homoeostasis [27, 31]. Dysregulation of this process can cause epithelial barrier breakdown and is involved in pathologies such as UC [307]. Hence, understanding the underlying mechanisms of cell shedding is of great importance

Recent publications by Eisenhoffer *et al.* [37] and Gudipaty *et al.* [315] have identified the mechano-sensitive Piezo1 as a main regulator of cell shedding and division. The authors used the fin of zebrafish embryos and canine kidney cell lines as study models, and were able to show that Piezo1 senses cell crowding at the tip of the fin and induces cell extrusion to maintain homeostatic cell numbers. The authors proposed the channel may also be the missing link between cell shedding and expansion, as they observed increased mitosis in areas of decreased cell density causing membrane stretch. However, these functions of Piezo1 have not been investigated within the intestine and I applied *in vivo* zebrafish and mouse models as well as *in vitro* cell culture and *ex vivo* human biopsy models to understand the role of Piezo1 in cell shedding in the mammalian IE.

Previously, the role of Piezo1 in the zebrafish fin was investigated via inhibition of the channel with gadolinium or knockdown via CRISPR, with subsequent assessment of effects on homeostatic shedding and mitosis [37, 315]. To further probe the role of Piezo1 in cell turnover in the IE, I also inhibited Peizo1 with gadolinium and assessed cell shedding in the zebrafish intestine. Surprisingly, when inhibiting Piezo1 in the zebrafish intestine, the published experimental dose of gadolinium by Eisenhoffer *et al.* led to early death in adult fish, indicating a stronger toxicological effect of the compound in adult zebrafish than in its progeny. Exposure to gadolinium, at similar concentration used by Gudipaty *et al.*, did not cause reduced cell shedding, but rather induced cell shedding in a dose dependent manner, indicating a different role for Piezo1 within the adult zebrafish intestine compared to the fin. It is possible the gadolinium has an additional toxic effect on the adult zebrafish (differing from the zebrafish larvae in effect inhibitor concentration), which may impact the apoptotic cell shedding response, which could be further investigated by applying lower concentrations and analysing changes to viability of

extruded cells [324]. With the recently described role of Piezo1 in influencing mitosis as a response to cell stretching, it may be that inhibition of the channel in the gut prevents a reduction of cell division in the intestinal crypts, and hence increases overall cell numbers within the epithelial monolayer, counterbalanced by increased shedding. A potential link between cell shedding and expansion has been heavily investigated, as reduced cell division could lead to reduced extrusion based on fewer numbers of enterocytes moving up the villus and hence reduced crowding at the tip [34]. Although stem cell expansion is the driving force of enterocyte migration towards the villus; whether rate of cell loss from the villus impacts expansion rates is still unclear [25], however ongoing studies in chronic inflammation models have indicated that SI villus damage, and cell death, does not correlate with increased crypt proliferation (Parker *et al.*, unpublished data). In contrast, acute injury of the colonic epithelium induces increased proliferation of stem cells in neighbouring crypts leading to wound closure. This process is delayed compared to the epidermis where proliferation occurs at time of injury, while in the colon expansion takes place at later phases of wound healing; highlighting the differences in homeostasis and response to injury based on tissue types [325]. Although, Piezo1 knockdown in zebrafish fins appears to reduce mitosis and extrusion, suggesting a role in dermis homeostasis, our contradictory intestinal findings, of increased shedding rates after Piezo1 inhibition, indicate that other factors may play a role in the more physiologically developed adult zebrafish intestine.

To further probe the impact of Piezo1 with respect to the IE, I also examined a mammalian cell culture system; IEC-6 monolayers, a rodent intestinal cell line, which was exposed to gadolinium at concentrations identical to the ones used by Eisenhoffer *et al.* and Gudipaty *et al.* (these authors used MDCK-II canine kidney cells). Contrary to previous studies, I observed that Piezo1 inhibition resulted in increased cell shedding during homeostatic conditions with no forces applied. However, Eisenhoffer *et al.* crowded and Gudipaty *et al.* stretched, and additionally performed a wound healing assay on the epithelium (MDCK-II cells). I sought to mimic physiological extrusion levels, rather than using external mechanical forces, and would therefore expect Piezo1 inhibition to reduce cell extrusion and division, hence causing fewer cells shed from the monolayer. These divergent observations

may correlate to the different cell lines used (intestinal vs kidney), and methods of shedding quantification as I both reproduced the method applied by Eisenhoffer *et al.* (enumerating cells extruded into supernatant), and in addition quantified formation of shedding rings within epithelial monolayers, which could be a more direct measurement of shedding events. It should also be mentioned that mechanical forces acting on the dermis, kidney and IE differ greatly [326]. The epidermis is under constant stretch and crowding, with epithelial turnover being constant due to injury and exposure to the external environment [327]. Therefore, the dermis does share some similarities with the IE (i.e. exposure to substances passing through the GI tract), however the strength of applied forces is significantly less pronounced in the IE [328, 329]. In addition, the zebrafish fin is a specific epidermis structure with its overall macroscopic structure being like the intestinal villus, but differing at the microscopic level, with the fin epithelium being layered and without directional cell movement. Regarding cell culture models, the IEC-6 cell line is widely used in investigating intestinal mechanisms, while MDCK-II cell were generated from kidney epithelial cells, which are thought to not proliferate *in vivo* unless injured [330, 331]. Further investigation, especially observing the effect of cell crowding and stretching in an intestinal cell line would offer further insights into the role of Piezo1 in IE homeostasis. This could be particularly interesting as the wound healing assay performed by Gudipaty *et al.* mimics not only cell sparsity in the intestinal crypt, inducing mitosis, but also potentially decreases cell density (causing membrane stretch), when single cells are extruded at the villus tip. Hence, Piezo1 could be involved in homeostatic cell shedding, as well as pathological extrusion (more cells lost = more membrane stretch), and may be important for epithelial repair. Furthermore, previous studies have determined that overcrowding is sensed by Piezo1, which sets in motion a downstream cascade involving S1P signalling and RHOK activation, followed by myosin contraction and cell expulsion. More recently, Gudipaty *et al.* connected Piezo1 sensing of cell density to cell division via phosphorylation of ERK1/2 leading to activation of cycling B transcription which in turn drives mitosis. However, a possible connection between cell cycle control to cell extrusion within the intestine remains to be investigated.

Whilst cell lines as model systems are useful to probe potential mammalian Piezo1 mechanisms, it is significantly worthwhile to also examine the role of Piezo1 in more complex and translationally relevant preclinical models. As an ion channel, the control of ion flux by Piezo1 across the cell membrane is essential for its physiological effect, therefore the use of gadolinium as an inhibitor in mammalian systems, including the mouse, is not possible due to its toxicity, which will be discussed in the future work section of this chapter [309, 316]. Recently, GsMTx4, another mechanosensitive ion channel selective blocker isolated from *Grammostola rosea* spider venom, has been successfully used in *ex vivo* mouse tissues and *in vivo* pig models, and thus may represent a tool for studying Piezo1 in mouse models (toxicity and dose-effect to be measured) [332, 333]. Eisenhoffer *et al.* and Gudipaty *et al.* knocked down *Piezo1* in cell culture models and zebrafish via CRISPR and with translation-blocking morpholino. However, both methods are difficult to apply consistently *in vivo* particularly when targeting the IE, due to problematic delivery orally through the stomach or the rectum, and *Piezo1* knock out mice die at mid-gestation due to defects in vascular remodelling [334]. Therefore, I decided to analyse Piezo1 transcription and translation as measurements correlated to intestinal epithelial turn over, however I acknowledge changes in levels may not be fully required for modulation of cell shedding-associated signalling events.

I chose to utilise the LPS *in vivo* model as it correlates with human UC patient pathological shedding, and it provides a rapid and increased rate of shedding, expected to mimic high epithelial cell turnover, and thus relevant for studying the role of Piezo1. Interestingly, when I profiled *Piezo1* expression in different mouse tissues (during homeostasis), there was a strong link with increased expression in organs undergoing constant mechanical movement such as the lung, whereas the small and LI had lower transcription [335]. This may be since, whilst the intestine is macroscopically exposed to peristaltic movement, and microscopically to lengthening and shortening of villi, this is relatively low mechanical induction, when compared to high mechanical forces at work within the lung [336, 337].

Notably, whilst I observed an increase in *Piezo1* expression within whole SI homogenates during LPS induced pathological cell shedding, I did not observe any significant differences in expression within the IEC compartment, suggesting that

Piezo1 may also be localised to a different intestinal cell or tissue type. Notably, *Piezo1* is highly expressed in blood vessel and lymphatic vasculature, and these structures could play a critical role in the shedding model, as inflammation is associated with increased vessel formation to allow trafficking of immune cells e.g. macrophages, which are involved with localised tissue injury and are required for TNF-α release and apoptotic cell shedding [338-340]. Therefore, these changes, correlated to elevated *Piezo1* expression, which may indirectly influence the shedding phenotype. This potential role requires further investigation in this mouse model as well as patients suffering from IBD.

As Piezo1 is a mechanosensitive ion channel protein, it is important to correlate transcription with protein. I observed increased WSI transcription during elevated shedding, which was not recapitulated by protein levels. To note, both transcription and protein levels were not statistically altered in IECs. The discrepancy between RNA and protein levels in the analysed paired samples could be due to rapid transcriptional responses, but delayed translation. It should also be mentioned that Piezo1 would not necessarily require changes in protein levels to increase signalling levels when inducing cell shedding. As an ion channel, even unchanged levels of Piezo1 could modulate and amplify signalling via ion flux across the cell membrane, and even slight alterations of ion channel numbers can potentially have great effects due to signal amplification [341]. This hypothesis would benefit from further investigation, and may be tested using GsMTx4 once this is validated in mouse models [333].

To comprehensively cover the role of Piezo1 in the gut epithelium I also examined expression within the LI using DSS to induce large intestinal colitis (a well-established model for UC [95]) and epithelial shedding, as the LPS mouse model induces cell shedding only within the SI. However, as observed in the SI, colonic inflammation and epithelial shedding did not affect *Piezo1* transcription levels further suggesting that *Piezo1* transcription does not play a role in mammalian pathological cell shedding, and other non-Piezo1 factors may be involved in this process. Interestingly, epithelial-associated villin is a potential candidate, which in its full-length form has anti-apoptotic functions, whilst cleavage induces apoptosis, followed by cell shedding. Cleavage of the protein occurs during migration of

enterocytes and binding to actin maintains mitochondria stability, which is essential for shedding funnel formation. Importantly, as the form of villin, and thus its function, is controlled by intracellular calcium concentrations, this suggest that Piezo1 is not involved in intestinal epithelial barrier homeostasis, as it appears to be calcium independent, and therefore villin may be an interesting candidate to focus on in future studies [38, 342].

Previous studies have indicated that Piezo1 is localised to the cell membrane in regions of low cell density, and in nuclear aggregates at sites of epithelial crowding. It has been hypothesised that the separate functional effects of Piezo1 on mitosis and cell shedding, and sensing of cell crowding and sparsity, is influenced by its cellular location. Translating this to the intestinal villus, cell expansion in the crypt could lead to lower cell density due to cell migration up the villus, causing Piezo1 to localise to the cell membrane, whilst at the villus tip the cell would expected to be crowded and Piezo1 would be expected to localise more within the nucleus. Indeed, IF microscopy imaging indicated that Piezo1 was localised within the cell membrane of crypt cells, and more nuclear at the villus tip, which also agrees with the observations by Gudipaty *et al.* Furthermore, the localisation of *Piezo1* transcripts presents more basolaterally, which could be explained by post translational trafficking of proteins. The increase in transcripts during elevated cell shedding, particularly in crypt cells, indicates increased cell division to replenish enterocytes lost at the villus tip. The qualitative observation of protein levels not changing during elevated cell extrusion mirrors the quantitative ELISA results, and could again be explained by delayed protein translation. Unfortunately, the LPS model does not allow for tissue collection after 4 h post injection due to ethical constraints with respect to mouse welfare. Notably, previous studies indicate that cell expansion actually increases forces in the crypt, when compared to pressure in the villus tip [343]. Furthermore, as pathological shedding rates leads to the extrusion of several cells from the villus tip, decreased cell density generates cell membrane stretch. Piezo1 has been shown to induce mitosis in response to stretch, however currently no studies have observed cell division outside of the stem cell compartment of the IE. If this was the case, there might be a potential feedback loop from the villus tip to

the crypt for induction of tissue repair after pathological cell shedding, which could be probed further to examine the role of specific Piezo1 localisation in this process.

As previously mentioned (1.3.3, 1.3.4), the gut microbiota plays an integral part in maintaining gut homoeostasis, by interacting with the host immune system and IECs; a key crosstalk interface [344-346]. Therefore, I also sought to investigate the effect of the microbiota on *Piezo1* transcription. Initially, I assessed this in GF mice as a completely 'clean' system, however, there were no differences in Piezo1 expression in either the large or SI, when compared to SPF mice, which may correlate with the reduced IE proliferation observed in these mice. Recently our lab determined that *B. breve* UCC2003 was protective in the LPS-induced cell shedding mouse model, making this microbe an ideal candidate to observe the potential role of Piezo1 in this health beneficial effect [46]. Apoptotic cell shedding levels in mice colonised with *B. breve* correlated with increasing *Piezo1* RNA levels in IECs, however this trend was not mirrored by Piezo1 protein content. As previously discussed () the ion channel might not be directly involved in cell extrusion, therefore future studies utilising Piezo1 knock out models, could investigate if *B. breve* confers its protective effect on the epithelial barrier integrity through *Piezo1,* via a yet to be identified pathway. Unfortunately, Piezo1 KO mouse models suffer from pre-weaning lethality, which does not allow us to further test the role of Piezo1 in this model [334]. Conditional KO models may be useful for future studies, but the cell type involved would need to be identified as my studies indicate epithelium-associated Piezo1 may not play a prominent role.

Thus far, the role of Piezo1 in intestinal cell shedding has been tested using mouse models of acute intestinal inflammation. However, it may be that this protein regulates extrusion within the human intestine during more chronic inflammation, thus I investigated RNA levels in the human intestine from patients suffering from UC (mild, moderate and sever disease). If Piezo1 is involved in UC pathology I would expect a strong signature, particularly in the moderate and sever disease samples, as well as the ex vivo pIVOC samples tested, however I did not observe any differences in transcription levels, supporting my mouse model findings, and further emphasising that Piezo1 may not be involved in intestinal epithelial responses to inflammation.

In summary, previous studies have utilised the zebrafish fin and canine kidney cells as models to understand the role of Piezo1 in controlling epithelial cell shedding and mitosis. These models are suitable for observing the function of Piezo1 within the dermis and the kidney epithelium, but as these tissues differ significantly in function and physiology from the IE, the key regulator position of Piezo1 in the gut, as proposed by the authors, has not been corroborated by sufficient experimental evidence. My in-depth research studies investigated Piezo1 in zebrafish, mice and human samples, and the data presented do not support a role for Piezo1 in intestinal cell shedding. More specifically, Piezo1 inhibition in the zebrafish intestine and mammalian intestine cell lines did not reduce cell shedding as expected but rather increased extrusion, strongly suggesting Piezo1 not to be involved in homeostatic cell shedding in the gut epithelium, or to have an alternate role. During mammalian, pathological cell shedding, Piezo1 protein levels were not affected by inflammation status and elevated extrusion rates in IECs in both mice and in human colonic biopsies of UC patients, suggests that differential Piezo1 translation does not play a role during inflammation-induced cell shedding. However, I did determine that in the SI Piezo1 is located to the cell membrane in crypt epithelial cells and cytoplasmically in cells at the villus tip. Although, the cellular location of Piezo1 was aligned with its proposed function of sensing cell density, my other findings did not link Piezo1 function and translation with control of epithelial turnover.

4.5 Future plans and hypothesis

4.5.1 Future work on the role of Piezo1 in intestinal cell shedding

The recently discovered dual role of Piezo1 in epithelial homeostatic turnover, suggested this protein as a promising target for further investigation within the IE. The authors of the two key publications proposed Piezo1 as a key regulator in intestinal homeostasis, but based their findings in non-relevant models for intestinal studies i.e. zebrafish dermis, kidney cells, crowding and injury, therefore there was a requirement for further tissue-specific investigations.

Based on my results, it is unlikely that Piezo1 is involved in pathological mammalian intestinal cell shedding, however the correlation of cellular localisation of the ion channel within sites of cell expansion and extrusion is interesting. The applied cell culture stretch and crowding model applied by the authors are elegant solutions to mimic homeostatic intestinal turnover *in vitro*. As previously indicated the IE is not expected to be under the same mechanical forces as observed in a zebrafish fin, nevertheless applying this model to more relevant intestinal cell lines could shed light on the involvement of Piezo1 in the processes within the gut, but studies would require the reproduction of the applied cell culture apparatus. The wound healing assay may represent an easier system to test, but these studies may only generate very preliminary data, due to the physiological differences in relation to injury and healing within the IE, when compared to the models previously used in this system.

As I did not quantify cell division rates, this would be the first potential future study to investigate the involvement of Piezo1 in modulating intestinal epithelial turnover. The ion channel could be involved in sensing cell density in the stem cell compartment and influence cell shedding in an indirect manner, based on enterocyte migration to the villus tip; homoeostasis - balanced expansion and shedding, injury - repair by increased mitosis. Analysing Piezo1 transcript and protein levels in IECs isolated from intestinal crypts, and comparing homeostatic conditions with elevated shedding rates, may answer this question. To achieve this, I would perform Weisser isolations of IECs and split the EDTA incubation into several steps, as villus IECs separate from the LP earlier than crypt IECs. Another approach would involve

measuring proliferation by staining for Ki67 positive epithelial cells during changes to cell extrusion rates induced by LPS. Unfortunately, the difficulty of not being able to specifically inhibit Piezo1 in the mouse due to gadolinium toxicity remains, and conditional KO mouse models would have to be developed. This was the reasoning for my application of the LPS model to modulate shedding rates and investigate changes to Piezo1 expression and protein levels, in a relevant *in vivo* model. Inhibition of proliferation and its effect on Piezo1 control of epithelial homeostasis would be important as reduction in epithelial turnover within the intestine would be akin to the inhibition of Piezo1 by gadolinium in the epidermis. A potential model to apply would be administration of chemotherapy drug cytosine arabinoside (ara-C) to mice, as it has shown to be successful in temporarily halting cell division in intestinal stem cells at non-toxic concentrations [25]. These studies would measure Piezo1 translation and transcription rates as a readout, however there may still be an issue of correlating protein levels to ion channel function, which can only be solved by directly measuring ion flux across cell membranes. This could be achieved by path-clamp, a technique measuring ion channel opening and closing which has been successfully used in studying neurons *in vivo* but so far, no model for the IE has been developed [347].

As mentioned, gadolinium has been shown to have serious toxic effects in mice, with a single IV injection of 7.89 µg/g (0.05 mmol/kg) resulting in liver and spleen necrosis 48 h later. Therefore, a slow perfusion has been suggested to prevent acute and severe hypertension, potentially leading to hypertension and cardiovascular collapse [313]. The drug has been successfully applied to deplete macrophages in the liver and lung, by administration of similar concentrations of 45 µg/g IP for the latter (0.9% GdCl with 5 µl/g administered IP) [348, 349]. Mice were dosed immediately after birth, and 7 days post delivery, with tissue collection on day 10 [349]. Hence the depletion effect was observed long term, most likely due to the requirement of gadolinium mineral deposit phagocytosis, leading to macrophage death [313]. Additionally, gadolinium has been applied directly to rat lung epithelium, by lavage, which resulted in a detection within the epithelial lining fluid at low levels (5 µg at 100 µg dosage) for 31 days, with a biological half-life of 136 days. It was suggested that gadolinium is absorbed and forms mineral deposits within the lung tissue with

slow metabolism. Effects on the epithelium were not investigated, but a rapid infiltration of calcium ion was detected, leading to lung toxicity in severe cases [350].

These results indicate that systemic administration of gadolinium to inhibit Piezo1 function, may not be a feasible approach, due to off target effects, such as depletion of macrophages (which are important in intestinal homeostasis), organ necrosis, with systemic effects, and Ca influx potentially affecting intestinal epithelial physiology and cytoskeletal structure. Additionally, the utilised models administered gadolinium days before tissue collection (to allow for macrophage depletion), with long-term exposure of the IE potentially preventing an accurate assessment of Piezo1 inhibition on cell shedding. This is due to shedding rates being difficult to quantify under homeostatic conditions, as very few cells are extruded without stimulation.

Therefore, a short-term gadolinium administration model, confined to the intestine, such as via an intestinal loop, may prove effective. This ligation of small and large intestinal sections has been used to study short term intestinal epithelial specific effects of otherwise toxic or harmful compounds (botulinum and *C. perfringens* toxin), with minimal systemic, and off target effects [351, 352]. Hence, gadolinium exposure of the IE within the loop system would allow for rapid and specific observation of Piezo1 inhibition effects on cell shedding in a mammalian *in vivo* system.

It should be highlighted that there is sufficient data presented by Eisenhoffer *et al.* and Gudipaty *et al.* to conclude that Piezo1 plays a central role in controlling epidermis homeostasis, as well as potentially also modulating maintenance and repair of the kidney and even lung epithelium, by sensing cell density and controlling cell extrusion and mitosis. However, with respect to its role within the intestine, my studies suggest that Piezo1 does not have a key role in tissue turnover of the epithelium. My investigation involving relevant models, including human intestinal biopsies, in both homeostatic and increased shedding did not yield supportive results for previous hypotheses regarding the role of Piezo1 in IE regulation, thus before undertaking further investigation, the success rate of future studies has to be taken into account.

4.5.2 Investigating the effect of *B. breve* on the intestinal epithelium during homeostasis and disease

Modulation of cell shedding is essential for intestinal tissue homoeostasis, due to its important role in retaining epithelial barrier function [353]. As pathological shedding induces intestinal inflammation, due to uncontrolled contact between luminal microbes with the host immune system, understanding the processes involved in cell shedding and how host and microbial factors may modulate this, gains even further importance [30, 354].

Based on the recent findings that *B. breve* UCC2003 protects the mammalian IE from pathological cell shedding, this represents an important avenue to explore, particularly with regards to development of novel therapies [46]. Probing the role of *B. breve* in epithelial crosstalk will allow me to further understand the mechanisms of cell extrusion during inflammation, as well as during homeostasis, as Bifidobacteria are resident members of the 'healthy' human gut microbiota. In addition, generated results will also increase our knowledge of the involvement of the gut microbiota and in particular Bifidobacteria in cell shedding as a physiological process, which is essential for human health.

As the investigation of a specific candidate of cell shedding, i.e. Piezo1, did not yield positive results, I decided to apply an unbiased approach (via RNA-Seq) to generate a global data set to allow a holistic analysis of the protective mechanisms of *B. breve* with respect to modulation of epithelial cell function. These studies will be presented in subsequent chapters.

5 *B. breve* UCC2003 induces distinct transcriptional responses in small intestinal epithelial cells of neonate mice under homeostatic condition

5.1 Introduction

The genus *Bifidobacterium* is an important member of the human gut microbiota throughout the life course, and various species/strains have been shown to have health beneficial effects, including immune modulation, and colonisation resistance to pathogens [156]. Importantly, gut-associated diseases such as IBD, where breakdown of the intestinal epithelial barrier is a hallmark feature, are associated with lower microbiota diversity when compared to 'healthy' controls, and specifically a lower abundance of bifidobacteria in IBD cohorts [284, 355]. Recently, a novel host beneficial effect, mediated by a specific strain of bifidobacteria has been described in an IBD experimental model. This publication by Hughes *et al.* [46], utilised a model of pathological small intestinal epithelial cell shedding, which mimics increased epithelial barrier gap formation, one of the initial stages of IBD pathogenesis. Oral administration of *B. breve* UCC2003 protected from inflammatory-induced apoptotic cell extrusion, however it is currently unclear what the exact underlying mechanisms modulating these protective effects are. Thus, this chapter describes the studies I carried out to further explore the beneficial effects of *B. breve* on the host epithelium.

5.1.1 *Bifidobacterium breve* reduces LPS induced apoptotic cell shedding in the small intestine in a EPS capsule, and Myd88-dependent manner

As previously described in Chapter 3, the applied pathological cell shedding experimental model is an apoptotic response in small intestine IECs, induced by systemic delivery of LPS. This targets tissue residing mononuclear cells, where it binds to TLR4 and induces TNF-α release. This cytokine binds to TNF-R1 on IECs, and induces NF-κB signalling leading to apoptosis, and shedding via caspase -3 cleavage [45].

Summarising the findings by Hughes *et al.* [46], (where I am second author), for the first time we showed that oral administration of *B. breve* UCC2003 reduces pathological IEC shedding in the SI, induced by LPS IP injection. This was assessed by casapase-3 staining of intestinal sections during LPS challenge in mice with and without *B. breve* colonisation (Figure 5-1.A,B), and enumeration of apoptotic cells along the crypt-villus axis, which showed a significant reduction in *B. breve* colonised mice (***Figure 5-1***.C).

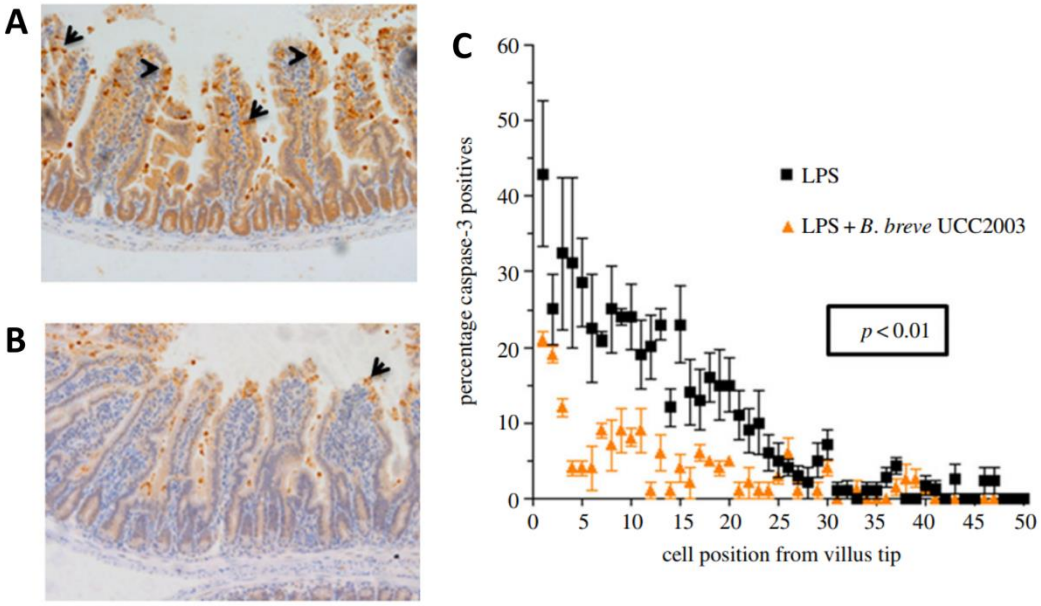

Figure 5-1 Colonisation of the mouse GI tract by *B. breve* UCC2003 decreases apoptotic IEC shedding in the small intestine induced by systemic LPS administration.

A Microscopic image of small intestine of mouse with caspase-3 positive (apoptotic) epithelial cells visualised by chromogenic staining 90 min post LPS administration, **B** Image showing small intestine of mouse colonised by *B. breve* 90 min post LPS injection with apoptotic IECs stained by caspase-3 positivity, **C** Comparison of caspase-3 positive IECs along crypt-villus axis in small intestine of mice injected with LPS with and without *B. breve* gavage, adapted from Hughes *et al.*, 2017 [46].

Notably, *B. breve* colonisation did not significantly alter protein and/or transcript levels of TNF-α in whole small intestinal tissue. Furthermore, there were no differences in F4/80^{+} macrophages within the tissue, or expression of TNF-R1 in IECs. Taken together this suggests the *B. breve*-modulatory effect is TNF-α, and

macrophage independent, and that modulation of other IEC-specific pathways downstream of this cytokine are potentially involved.

Further studies, using Myd88 KO mice, showed that this central adaptor protein was crucial to the apoptotic modulatory effects, as *B. breve* colonised mice did not show any significant reduction in caspase-3 positive IECs, when compared to PBS controls. We also observed an increase in TLR2, which is upstream of the MyD88 signalling pathway. As TLR2 may be involved, we next probed the role of the EPS capsule of *B. breve,* as previous studies indicated that *Bacillus subtilis* EPS can signal via a similar mechanism (via TLR4), and protect from intestinal inflammation caused by *C. rodentium* [356]. Importantly, a *B. breve* EPS mutant did not protect mice from pathological cell shedding, and an isogenic strain (expressing a different EPS, EPS2) also did not protect from LPS-induced IEC apoptosis, suggesting an EPS capsule dependent mechanism.

Lastly, we investigated the modulation of specific inflammatory and apoptotic signals in the whole SI of both *B. breve* EPS WT and mutant colonised mice after LPS-induced cell shedding. Interestingly, we observed increased expression of several genes involved in inflammation and apoptosis including IL-6, TNFSR15, BAD, CYCS, CASP4, FAS, TRAF5 and TNFRS9 in EPS deletion mutant colonised mice, when compared to *B. breve* WT colonised mice (Figure 5-2).

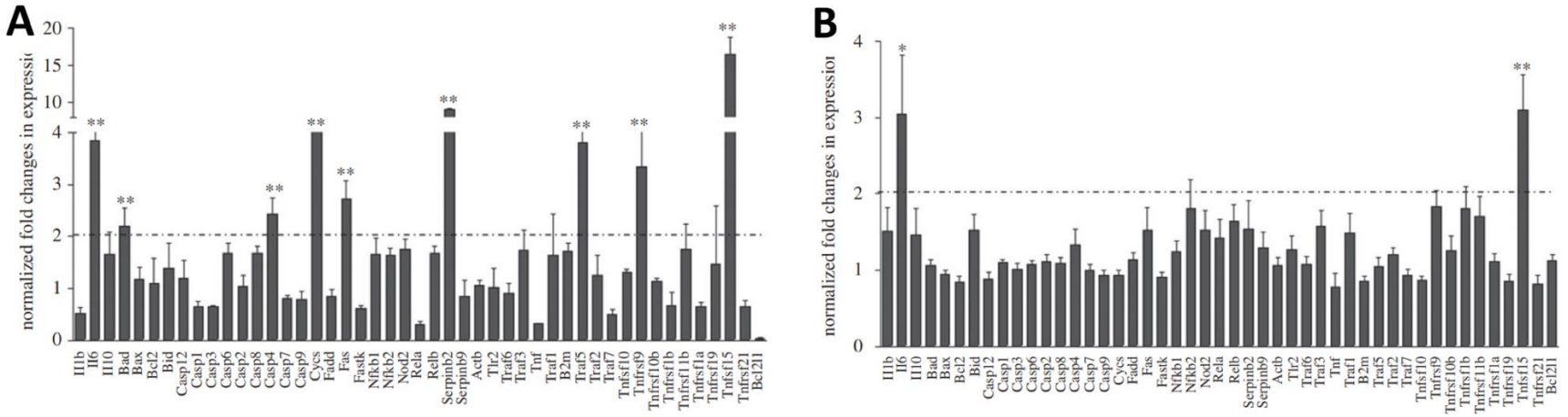

Figure 5-2 *B. breve* UCC2003 and EPS deletion mutant modulate specific inflammatory and apoptotic signalling in whole small intestine.

Transcriptional response of whole small intestine of mice colonised by **A** *B. breve* UCC2003 EPS deletion mutant and **B** *B. breve*-colonised mice for both groups 90 min post IP injected with 1.25 mg/kg LPS. Whole small intestine homogenates analysed by qPCR array for transcription of inflammatory and apoptotic markers, adapted from Hughes *et al.* 2017 [46].

In summary, this study highlights that *B. breve* induces a protective anti-apoptotic response in IECs during pathological cell shedding, in a Myd88 and EPS1 capsule dependent manner.

These data give some insights into the potential mechanisms involved in bifidobacterial-associated IEC signalling, however they do not provide a global overview of cell signalling changes. Thus, in this chapter I sought to investigate the intestinal epithelial transcriptome of IECs to capture wide-spread changes induced after *B. breve* colonisation. Importantly, our previous studies were performed in LPS-challenged mice, but this model requires pre-colonisation of the GI tract with *B. breve* UCC2003 for 3 days prior to LPS challenge. Therefore, I decided to probe the effect of *B. breve* on IEC transcription under homeostatic conditions, as it could be argued that modulation would take place during normal 'healthy' conditions. This in turn could modulate protection from disease associated stimulus, such as LPS. Furthermore, I expanded these studies to include neonatal mice at 2 weeks of age as *B. breve* is a human infant gut isolate, and the genus *Bifidobacterium* is a prominent member of the gut microbiota in early life. Thus, I hypothesised that host IEC modulation may be more prominent during earlier stages of microbial, immune and epithelial barrier development, than compared to those observed in adulthood.

Below I discuss and highlight information regarding the use of sequencing technology, and germ-free mice, as well as previously identified health beneficial effects and mechanisms of *B. breve*, which are important to this study.

5.1.2 *Bifidobacterium breve* and its role and function in the human intestinal tract

The genus *Bifidobacterium*, and its role in human health across the whole life span has been covered in the general introduction. Below I will give specific examples for the species *B. breve*, and in particular the strain *B. breve* UCC2003.

B. breve UCC2003 was first isolated from human infant faeces, and was one of the earliest *Bifidobacterium* strains to have its full genome sequenced, significantly aiding in the exploration of its health beneficial effects [279]. In addition, a transposon library has been generated for *B. breve* UCC2003 that allows for

determination of specific gene functions and complementary interaction studies [357].

B. breve UCC2003 produces a cell surface associated EPS, which is transcribed from a bidirectional gene cluster, allowing for expression of two different EPS capsules [358]. The EPS coat has been shown to promote *in vivo* persistence, while having no observable effects on initial colonisation. Through EPS, *B. breve* UCC2003 is able to stay immunologically silent by circumventing adaptive T cell responses by the host. In addition, *B. breve* UCC2003 reduces the intestinal load of the enteric pathogen *C. rodentium* by potentially forming an intestinal biofilm due to EPS capsule production. The importance of the EPS capsule in conferring the protective effect from apoptotic cell shedding in the mouse SI has been described above. The bacterium also expresses pili *in vivo*, which aids in host colonisation [279].

Host immune modulation of DCs by *B. breve* C50 has been shown to occur via TLR2 signalling, which prolongs overall survival and is effect also conferred by culture supernatant suggesting cross-talk via secreted bacterial compounds [359]. In human disease, *B. breve* M-16V has been shown to significantly reduce NEC cases in preterm infants [360]. One of the potential mechanisms involved in this NEC protective effect, as determined in a rat NEC model, may be via improved intestinal barrier integrity, by decreasing IL-16 and TNF-α expression. In the context of IBD, trials involving *B. breve* strains include a randomised control trial of patients suffering from low or mild UC that were supplemented with *B. breve* Yakult for a year, and which was associated with improvements in disease symptoms, as assessed by colonoscopy [361].

Taking this information, together with the previously observed protective effect of *B. breve* UCC2003 from apoptotic cells shedding, I decided to utilise sequencing of the IEC transcriptome in neonate and adult mice to identify *B. breve* specific gene modulation; to identify the underlying health beneficial mechanisms.

5.1.3 Utilising RNAseq to assess global transcriptional changes

The technological basis of NGS have been described in the general introduction, and in this section I will discuss utilisation of RNA-Seq for global unbiased transcriptional changes in host cells and tissues [362].

Similar to other NGS applications, RNA-Seq is high-throughput, highly sensitive, and high speed. There are still considerable costs associated with this technology, but the price is decreasing over time making this a more viable approach for different applications [363]. It can be utilised to quantify transcripts, and also as an explorative tool to investigate SNPs, and in contrast to sequencing arrays, does not require preselection of probe targets. It allows for the sequencing of the total transcriptome including messenger RNA (mRNA), and short RNAs (miRNAs, siRNAs, ncRNAs); although specific sample processing techniques have to be used to optimally perform these different studies. These include enrichment of specific RNAs such as mRNAs by polyA pulldown, as well as size selection, which can induce bias, or outright exclusion of certain RNA types [364, 365].

With RNA-Seq, as with other NGS methods, large data sets are generated that require new levels of computational processing power, skills and tools. Following the sequencing step, the raw data has to be processed for assembly of transcripts, identification of genes, precise quantification, with false positive statistical evaluation, and comparison of expression between several samples and conditions. These areas are constantly being re-worked and improved, but most developments address speed and resource management [362].

Following this, and which is essential for interpretation of the functional elements, and solving the biological interactions of identified differentially expressed genes, is pathway analysis. Databases of interactions have been generated and can be overlaid on top of transcriptional changes to allow other biologically important information to extracted from the generated data. This identification of potentially relevant transcriptional modulation would then have to be validated on the gene expression level, as well as the mechanistic.

5.1.4 The use and limitations of GF mice in microbiota research

Gnotobiotic mice are animals free of all microorganisms and can greatly aid with answering questions relating to specific phenotypes, and the potential involvement of singular bacterial species/strains [366]. Fundamentally, GF mice can be used to determine if the microbiota is a driving factor in phenotype, i.e. disease pathogenesis [367]. More recently, GF mice are also used in sophisticated mono-association studies to probe host-microbiota crosstalk, and colonisation of GF mice with a defined microbiota, consisting of selected microbes, to study bacteria-bacteria interactions, or even xenobiotic models, were for example GF mice are colonised with human microbiota, to generate a more translation model [368]. An excellent example of a successful mono-colonised study that has greatly aided our understanding of host-microbe interactions identified SFB as a key component of the intestinal microbiota that promotes the development of T_h17 cells [369].

Importantly, results generated using GF mice should be interpreted carefully as these animals have an altered physiology, including an underdeveloped immune system, deceased intestinal epithelial turnover, and differences in epithelial gene expression [370-372]. In addition, mono-colonisation may also indicate different changes as compared to those observed in the presence of a complex microbiota (i.e. in SPF mice) [369]. As indicated in the general introduction, and with respect to bifidobacteria, several studies have shown cross-feeding with other members of the gut microbiota, and therefore this should be considered when discussing GF study data. Hence the general rule is that an overall consensus should only be drawn from gnotobiotic experiments when the model has also been investigated in the presence of a complex microbiota (if possible) [373].

Difference in microbiota profiles between human and mouse, as well as between laboratory strains/colonies and conditions, should also be taken into consideration, and will be discussed in result subchapter 6.1.2.

5.2 Hypothesis

5.2.1 Hypothesis

Bifidobacteria can positively influence homeostatic intestinal health by specifically modulating the transcriptome of IECs.

5.2.2 Aims

1. Investigate impact of bifidobacteria colonisation on epithelial transcription patterns *in vivo* during healthy homeostatic conditions, and during pathological intestinal inflammation
2. Identify IEC pathways modulated by bifidobacteria

5.3 Results

5.3.1 Experimental mouse models, and design overview for investigation of small intestinal epithelial transcriptional response of mice to *B. breve* UCC2003 colonisation

We previously observed a protective anti-apoptotic effect of *B. breve* colonisation on the IE during pathological cell shedding *in vivo* [46]. Initial qPCR analysis identified apoptosis-associated genes that were downregulated during acute cell shedding in the presence of *B. breve*. I hypothesised that the protective effect conferred by *B. breve* is modulated prior to onset of pathological cell shedding, and that this critical beneficial IEC 'programming' occurs during homeostasis. The potential biological reason for this could be that *B. breve*, as a microbiota member associated with health, primes the IE to dampen down responses during inflammatory stimulus e.g. LPS, which in turn protects the IEC from damage. I therefore investigated the modulation of IEC transcription *in vivo* without LPS stimulation by RNA-seq analysis (Figure 5-3).

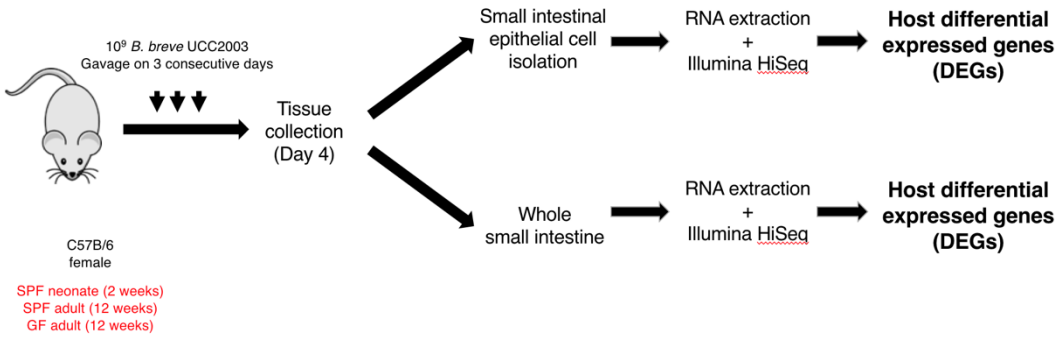

Figure 5-3 Overview of experimental design and mouse groups analysed.

C57B/6 mice were colonised by *B. breve* UCC2003 by oral gavage (10^9 cfu) daily on three consecutive days, mice groups were conventionally raised (SPF) neonate mice (2 weeks) and their mothers, conventionally raised adult mice (12 weeks) and germ free (GF) adult mice (12 weeks), tissue was collected on day 4 (24 hours post last gavage) and small intestine collected, small intestinal epithelial cells were isolated and RNA extracted from IEC isolations and whole small intestinal tissue, transcription was analysed by Illumina HiSeq and data processed for calculations of differentially expressed genes (DEGs) between control and *B. breve* UCC2003 colonised samples.

I also expanded the model from adult mice (12 weeks), to include neonatal mice (2 weeks) as *B. breve* is a prominent member of the early life gut microbiota.

To assess the modulation of IECs *in vivo*, I colonised C57 BL/6 mice with *B. breve* UCC2003 by oral gavage with 10^9 cfu on three consecutive days, based on the established model by Hughes et al [46]. Tissue collection occurred 24 h post last gavage (i.e. day 4). Neonate mice were colonised following the same protocol, with the exception that the same cfu was administered, but in a 50 µl gavage instead of 100 µl, due to the size of the neonatal stomach. Mothers were also gavaged, together with their pups, and co-housed in the same cage to include vertical transmission as neonatal mice are on a milk diet. To differentiate between the potential indirect effects on the host of *B. breve* UCC2003, via modulation of microbiota composition, and its direct effect on the IE, I utilised GF mice mono-colonised following the same gavage protocol.

5.3.2 *B. breve* UCC2003 oral gavage results in stable colonisation of conventionally raised neonate and adult mice as well as under gnotobiotic conditions, with higher levels in the large intestine compared to small intestine

Our previous work has indicated stable colonisation of *B. breve* in the GI tract; however, it is important to confirm this in my models as presence of *B. breve* would be required for downstream transcriptional responses. Therefore, I monitored colonisation via selective plating of faeces on RCA with 50 mg l^{-1} mupirocin for determination of faecal cfu counts. Control mice (and experimental group mice prior to first gavage) did not show bifidobacteria colonisation suggesting no (or below level of detection) presence of bifidobacteria in the faeces of the utilised mice (Figure 5-4.A,C,E). *B. breve* UCC2003 gavaged mice presented with stable cfu/g faeces, starting 24 hours post first administration, and for the duration of the experiment, with slightly higher levels in adult mice compared to neonates (Figure 5-4.A,C). This is in accordance with the observations made by Hughes *et al.* [46], in adult mice (10^8 cfu/g faeces). GF mice were raised and housed in a sterile environment and their gnotobiotic status verified by culture independent faecal cytox stain and culture dependent faecal expansion culture (Supplementary Figure 3 and

Supplementary Table 4). To mono-colonise mice with *B. breve* UCC2003, oral administration was performed following the protocol for SPF adult mice, and similarly stable colonisation and levels compared to conventionally raised adult was observed (Figure 5-4.E).

Bacterial load along the GI tract differs due to changes in physiological and the luminal milieu. Notably, *B. breve* was present in lower numbers (10^5 cfu/g faeces) in the SI, compared to the LI of neonate and adult SPF mice 24 h post last gavage (10^8 and 10^9 cfu/g faeces respectively, Figure 5-4.B, D). Colonisation levels were similar in the GI tract of GF mice at the same time point (Figure 5-4.F).

These data indicate a stable and high cfu intestinal colonisation of mice, which is important for profiling of paired IEC transcriptional responses in subsequent experiments.

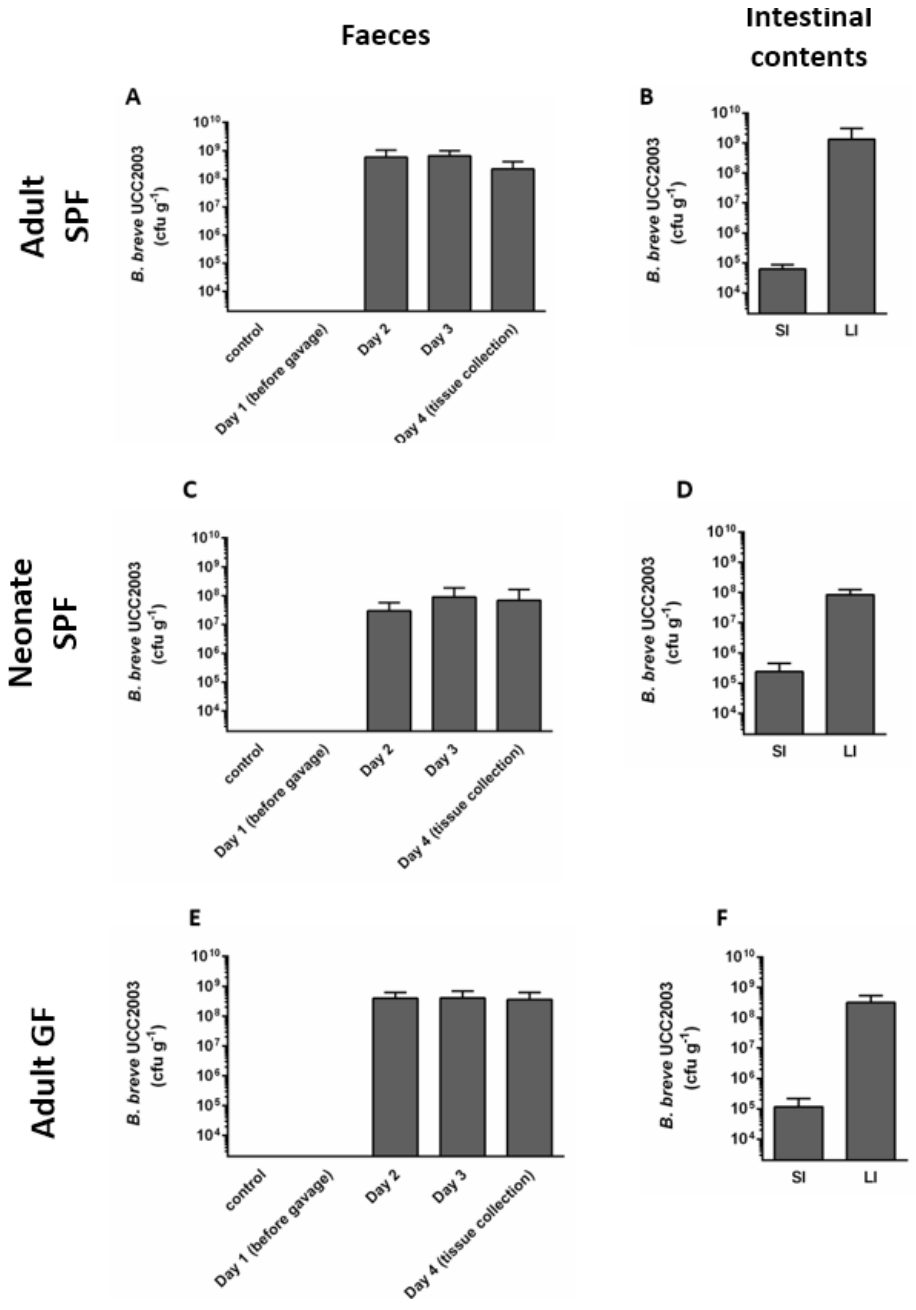

Figure 5-4 ***B. breve*** **UCC2003 stably colonises the intestine of neonate and adult conventional mice, and adult GF mice with higher levels in the large than in the small intestine.**

Bifidobacteria colonisation by oral gavage in **A** faeces and **B** intestinal contents of adult (12-14 weeks) conventionally raised mice, **C** faeces and **D** intestinal contents neonate (2 weeks) conventionally raised mice and **E** faeces and **F** intestinal content adult (12 weeks) germ free mice, oral gavage (10^9 cfu *B. breve* UCC2003) on three consecutive days, faecal samples collected on indicated days, large and small intestine content collected on day 4 (24 hours post last gavage), colonisation (cfu/g faeces) determined by homogenisation of samples in PBS, selective plating on RCA with 50 mg l^{-1} mupirocin, and counting of colonies following two day incubation, limit of

detection $2x10^3$ indicated by lowest value on y axis, data shown as mean +/- SD (A n=6, B n=5, C n=6, D n=3, E n=4, F n=6).

5.3.3 16S rRNA sequencing of mouse intestinal microbiota shows *B. breve* UCC2003 colonisation of neonate and adult conventionally raised mice by oral gavage and effect on community composition

Previous work has shown that bifidobacteria administration modulates the overall microbiota composition. Disturbances of the intestinal bacterial community is associated with disease, and in the case of IBD reduced levels of *Bifidobacterium* is associated with active disease, and reduced microbiota diversity. Importantly, these changes may have modulatory effects on the host, thus I investigated the effect of *B. breve* UCC2003 administration on the mouse gut microbiota profile via 16S rRNA sequencing.

Adult control mice showed no bifidobacteria in two out of three biological repeats, with one mouse having a very low percentage of reads (<1%) mapping (Sample contro1, Figure 5-5). In all three control mice, a similar taxonomic ratio at genus level was observed, with the most prominent genera detected being *Roseburia*, *Alobaculum*, *Blautia*, *Lactobacillus* and *Alistipes*. One sample had higher levels of *Alobaculum* and *Lactobacillus*, which correlated with a reduced presence of other taxa. The rarefaction curve of this mouse showed a much lower number of bacterial populations detected at the same read counts as the other two samples, with no plateau, suggesting a lower capture diversity at the same sequence depth, and which could explain the observed intragroup variability (Supplementary Figure 5).

B. breve UCC2003 oral gavage increased bifidobacteria abundance in the adult microbiota to 1.3 - 2.3% after four days of treatment (Figure 5-5). This was accompanied in two samples by an increase in *Lactobacillus,* and decreased abundance of *Alobacum*, *Balutia* and *Alistipes*. One sample (UCC2) differed by lower *Lactobacillus* levels, and higher *Blautia* and *Roseburia* abundance compared to other *B. breve* gavaged mice, and appeared similar to control mice composition.

Based on the 16S rRNA data, a Principal Coordinate Analysis (PCoA) was used as an exploratory data anlysis without testing null-hypothesis and shows a separation

between the control and *B. breve* gavaged adult mice, but based on the observed differences no tight clustering is present (Figure 5-6).

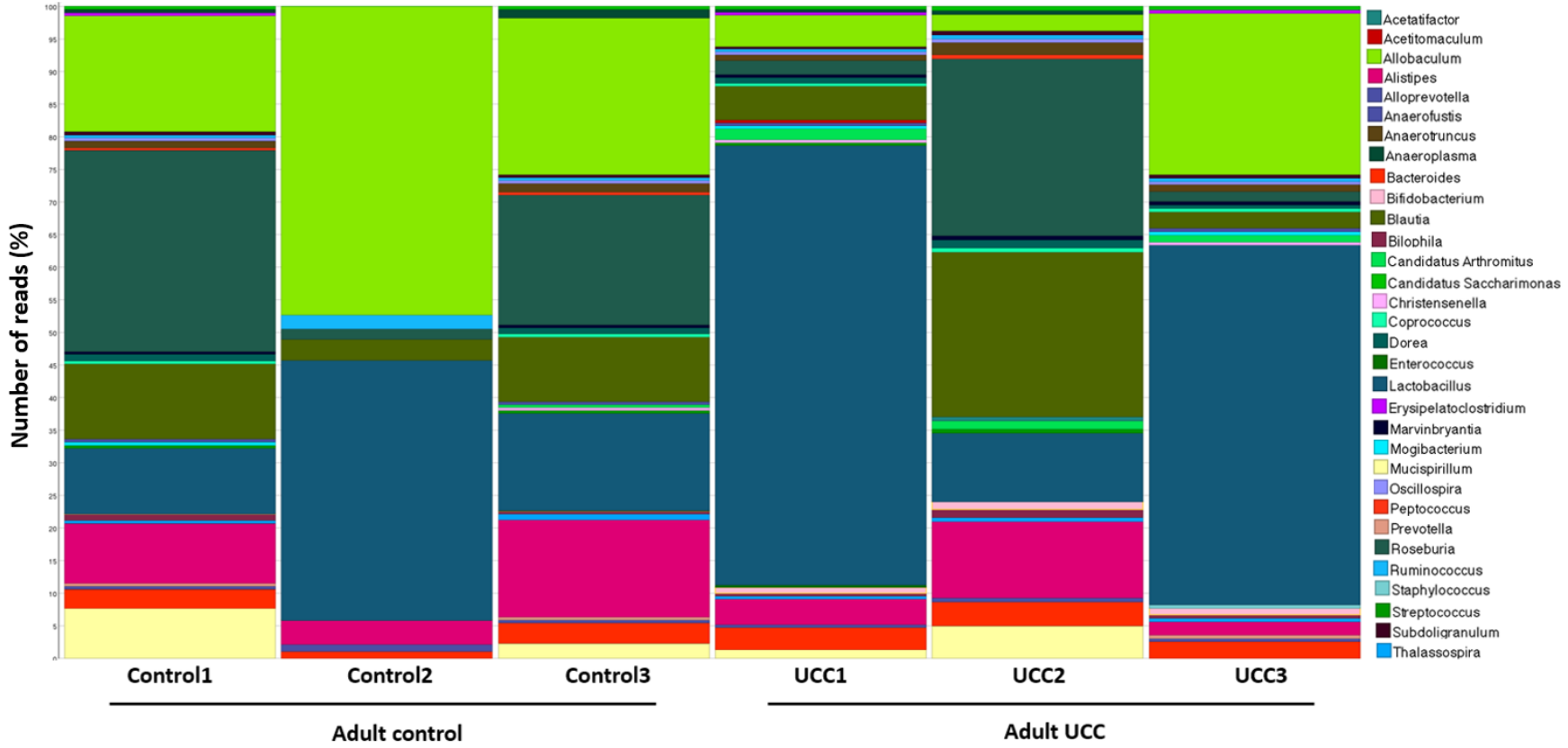

Figure 5-5 *B. breve* UCC2003 colonises the intestinal tract of adult SPF mice with effects on overall microbiota composition analysed by 16S rRNA gene sequencing.

Faecal samples collected from adult (12 weeks) conventionally raised mice colonised by *B. breve* UCC2003 by oral gavage (109 cfu for three days, sample collection 24 hours post last administration, control received PBS gavage), DNA extracted, V1-V2 of 16S rRNA gene amplified and sequenced, Reads aligned

against SILVA database and visualised in MEGAN, data shown as relative abundance normalised to percentage of reads, bar colours corresponding to genus taxa, lengths representative of relative abundance

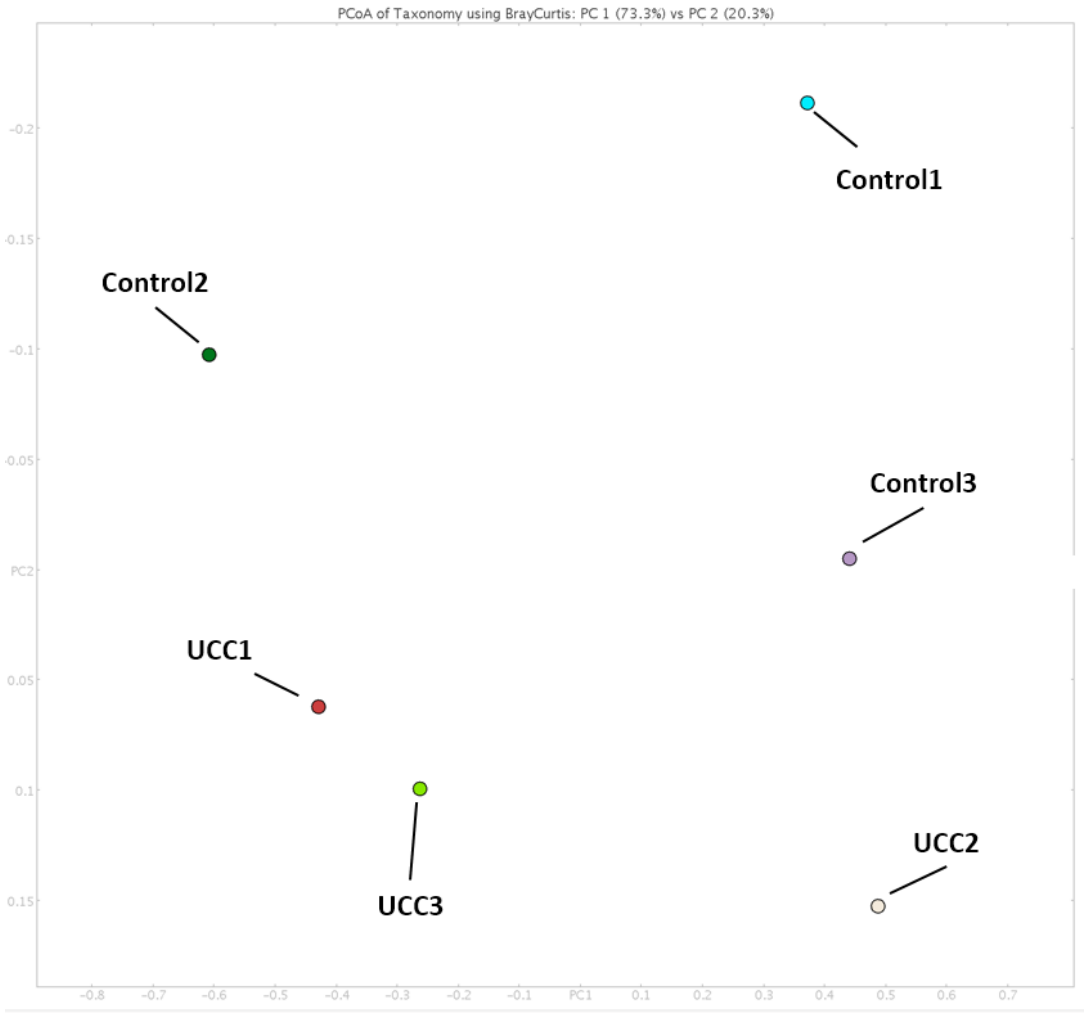

Figure 5-6 ***B. breve*** **UCC2003 gavage modulates intestinal microbiota profile of adult mice analysed by PCoA of genus level composition based on 16S rRNA sequencing.**

Faecal samples collected from adult (12 weeks) mice following oral gavage with 10^9 cfu *B. breve* UCC2003 on three consecutive days (control received PBS gavage), DNA extracted, V1-V2 of 16S rRNA gene amplified and sequenced, reads aligned against SILVA database, PCoA analysis of taxonomic assignments at genus levels performed and visualised in MEGAN.

In the intestinal microbiota of control neonate and mother mice no *Bifidobacterium* 16S rRNA reads were detected (Figure 5-7). Global composition of control mother microbiota is similar to adult mice analysed above, while neonatal controls samples had higher abundances of *Bacteroides,* and potentially *Lactobacillus,* with a decrease in *Blautia*, *Roseburia* and *Alistipes*, and overall decreased diversity. The oral gavage with *B. breve* UCC2003 increases the abundance of bifidobacteria in neonate mice to an average of 11.25% (UCC1 14%, UCC2 9%, UCC3 5%), which is accompanied by a decrease in *Blautia*, and an increase in *Bacteroides,* and potentially *Lactobacillus*.

PCoA analysis indicates a separation between the control and gavaged neonate groups with tighter clustering for the treatment samples compared to control repeats (Figure 5-8). The microbiota of mothers was distinctly different from the neonate groups, and *B. breve* administration had a lower modulatory effect on the mothers' microbiota profiles.

Lower capture diversity of two samples was detected based on rarefaction curve analysis showing much lower bacterial population quantity at similar read counts without plateau compared to experiment average leading to the exclusion of these smaples from the analysis on the basis of insufficient sequencing depth (Supplementary Figure 5).

These results support the *B. breve* colonisation data generated by plate counts with 16S rRNA sequencing presenting a higher abundance in neonates, and show a distinct modulation of the mouse microbiome by *B. breve* with effects being stronger in neonatal mice.

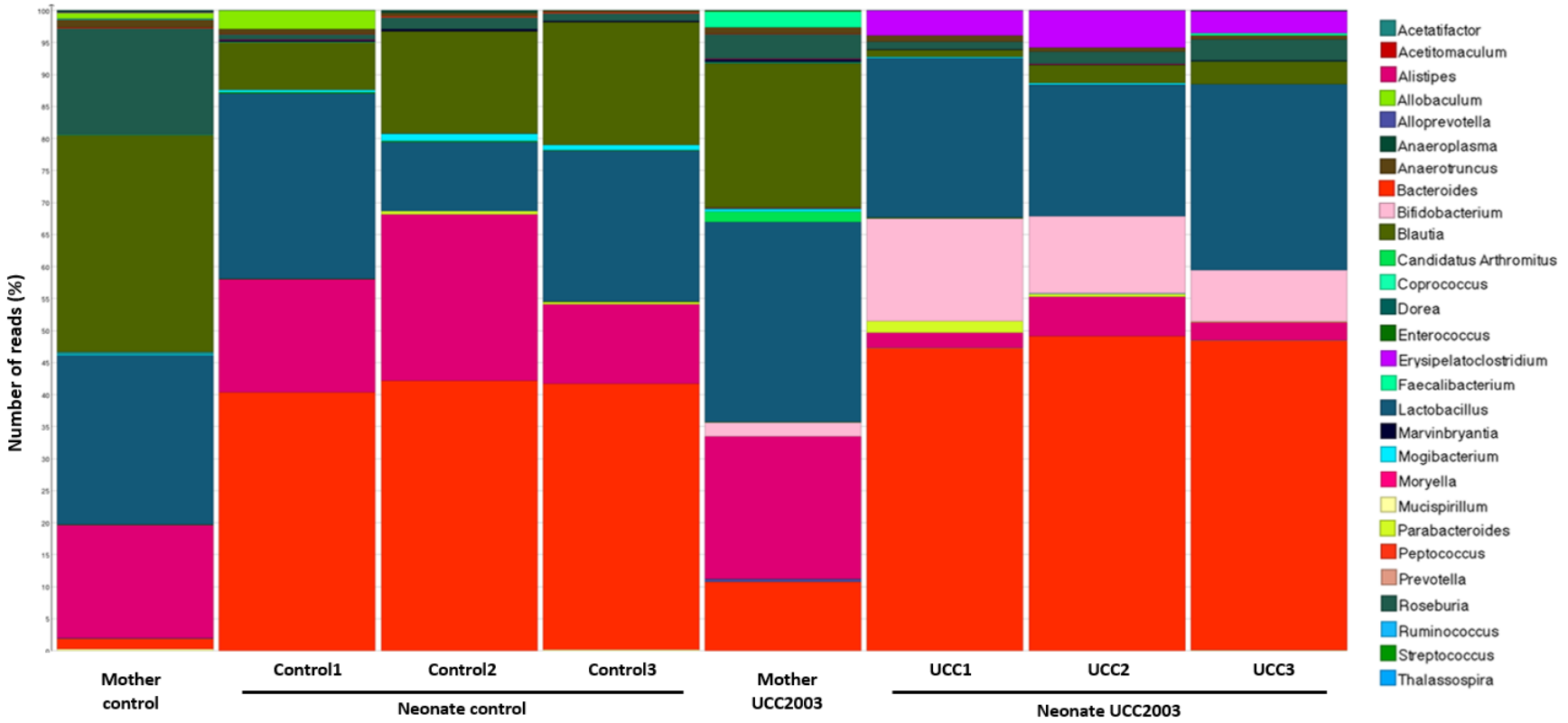

Figure 5-7 *B. breve* UCC2003 colonises the intestinal tract of neonate SPF mice and modulates microbiota profile analysed by 16S rRNA gene sequencing.

Faecal samples collected from neonate (12 weeks) conventionally raised mice and their mothers colonised by *B. breve* UCC2003 by oral gavage (10^9 cfu for three days, sample collection 24 hours post last administration, control received PBS gavage), DNA extracted, V1-V2 of 16S rRNA gene amplified and sequenced, Reads aligned against SILVA database and visualised in MEGAN, data shown as relative abundance normalised to percentage of reads, bar colours corresponding to genus taxa, lengths representative of relative abundanc

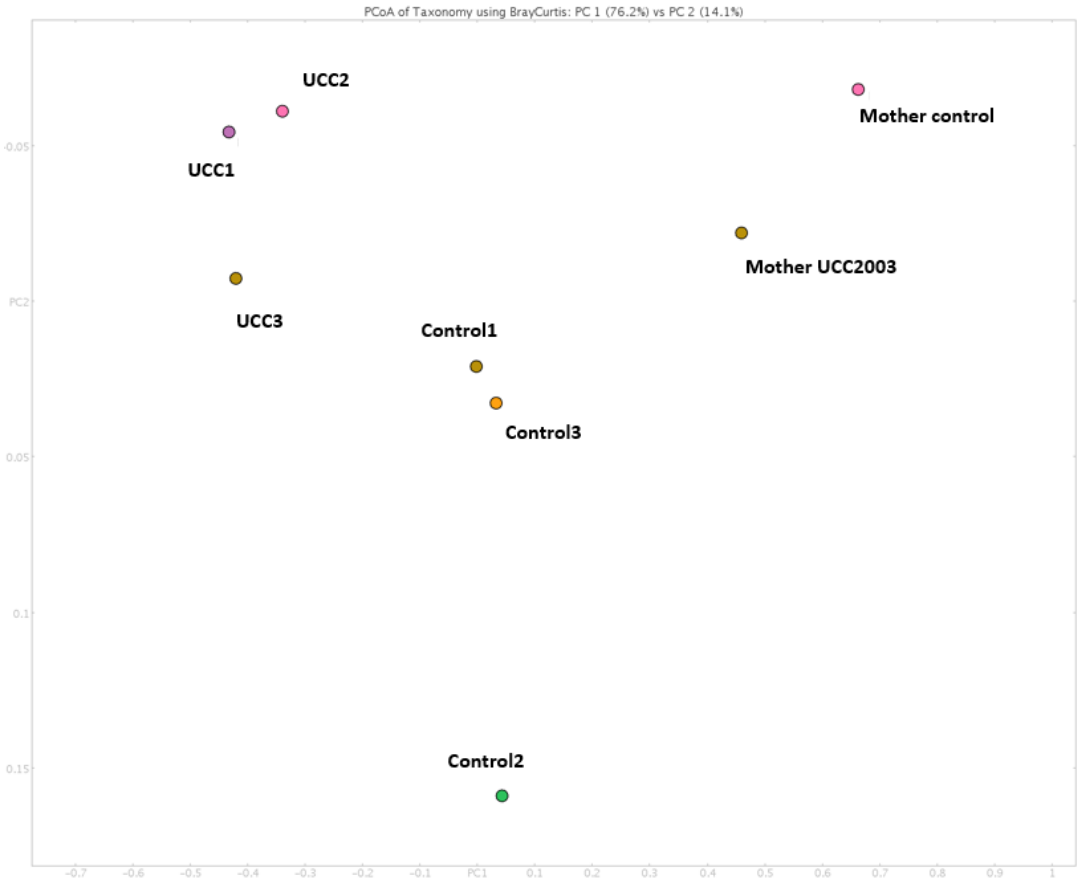

Figure 5-8 B. breve UCC2003 gavage modulates intestinal microbiota profile of neonate mice analysed by PCoA of genus level composition based on 16S rRNA sequencing.

Faecal samples collected from neonate (2 weeks) and mother mice following oral gavage with 10^9 cfu *B. breve* UCC2003 on three consecutive days (control received PBS gavage), DNA extracted, V1-V2 of 16S rRNA gene amplified and sequenced, reads aligned against SILVA database, PCoA analysis of taxonomic assignments at genus levels performed and visualised in MEGAN.

5.3.4 Localisation of *B. breve* in close proximity with the intestinal epithelium using SEM

In addition to the presence of *B. breve* in mouse faecal samples following gavage, localisation within the GI tract would be expected to be central for host modulatory effects. When present in the lumen, *B. breve* could modulate the IE via bacterial products, while localisation in close proximity to IEC could potentially allow direct cell surface interactions.

To observe the localisation of *B. breve* in realtion to the IE, SEM images were taken of the large and small intestine of gnotobiotic (Figure 5-9.A), and conventionally raised control, and gavaged mice (Figure 5-9.B). The dehydration processing step caused shrinkage, and re-localisation of the mucus layer, but was required due to alternative frozen processing retaining the mucus barrier, which would not allow visualisation of *B. breve* in close contact with the IEC. Due to the strong adhesive properties of mucus, it is unlikely that bacteria have shifted localisation post tissue collection and processing, reducing the potential of artefacts (oral communication with Kathryn Cross).

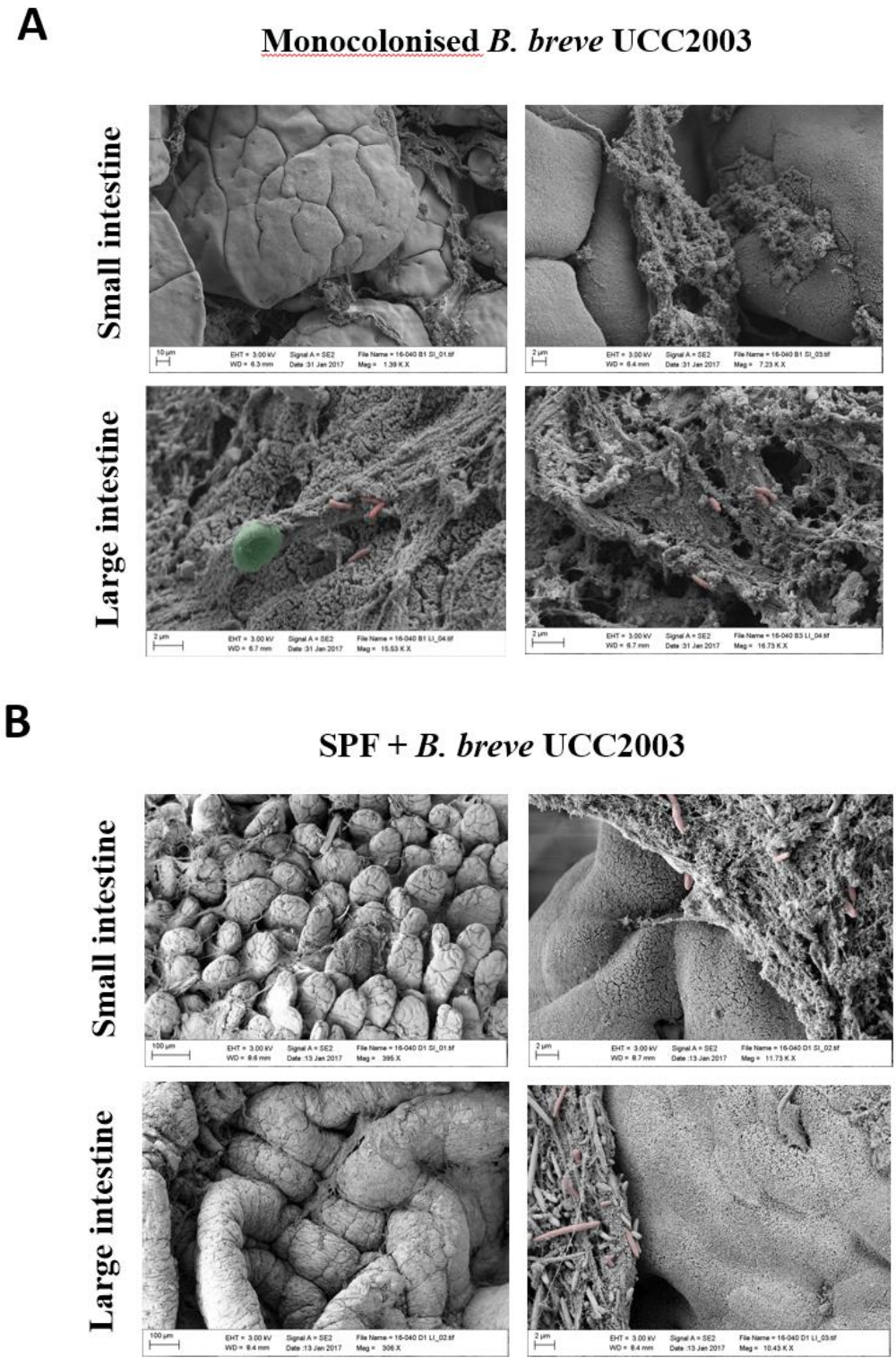

Figure 5-9 ***B. breve*** **UCC2003 resides in close proximity of the intestinal epithelium and the mucus layer shown by scanning electron microscopy.**

A Germ free (GF) and **B** conventionally raised (SPF) adult mice were gavaged on three consecutive days with 10^9 *B. breve* UCC2003, tissue collected 24 hours post last gavage, small and large intestine

fixed, dried and visualised by scanning electron microscopy (SEM), individual bacteria pseudo coloured, representative images shown.

Images taken of small intestinal mono-colonised IE did not reveal bacteria either on top of the mucus or the IE. This could be explained by the small area observed by SEM, and the fact that *B. breve* colonises the SI at lower levels. Notably, when imaging the LI, several bacteria can be seen, and are located on top of the mucus layer (and potentially within, as revealed by mucus constriction), while single bacteria are in direct contact with the epithelium (Figure 5-9.A). SEM visualisation of the small and large IE of SPF mice shows bacteria with several different morphologies; thus it is difficult to identify *B. breve* within the SPF microbiota (which would require immuno-gold labelling) (Figure 5-9.B).

In addition, I investigated the localisaiton of *B. breve* bz staining of small intestinal sections with RNAscope, an immunofluorescent *in situ* hybridisation method allowing for visualisation of transcripts by bright field microscopy, using probes designed against the *Bifidobacterium* 16S rRNA sequence. The results were inconclusive in part due to the nucleotide length of the probe required for adequate binding not allowing for sequence design specific for the *B. breve* UCC2003 species, and will require further optimisation and repetition to ensure reliability.

In summary, these studies suggest that *B. breve* UCC2003 could potentially be in close contact with the IEC. Notably, this localisation would be expected to have a direct impact on interactions with the host. Future experiments will be discussed below.

5.3.5 *B. breve* UCC2003 intestinal colonisation induces a distinct transcriptional response in neonate intestinal epithelial cells, with less pronounced effects in adult mice

Having established and validated the model of *B. breve* colonisation, I initiated holistic investigation of the effect of *B. breve* UCC2003 on IECs by RNA-Seq, as a global assessment of transcriptional changes.

As previously highlighted, *B. breve* UCC2003 appears to modulate host responses via IEC signalling. Therefore, I the processed collected SI samples for IEC isolation using a modified Weisser method, and confirmed purity of the cell preparation by

FACS of isolated cells, showing high percentage of live cell to be $CD45^-$ (marker for B, dendritic, NK cells, macrophages, and granulocytes, Supplementary Figure 1.A). In addition, histological H&E staining indicated removal of the IE, while leaving the LP intact (Supplementary Figure 1.B).

RNA was isolated from IEC preps, and whole SI from neonate and adult (control and *B. breve* UCC2003 gavaged), and GF and *B. breve* mono-colonised mice (Figure 5-3). RNA sequencing was then performed, and data analysed to calculate differences between control and *B. breve* colonised gene expression. This allowed me to identify differentially expressed gene patterns induced by *B. breve* UCC2003 colonisation in IEC and WSI tissue of neonate and adult mice, and in the presence of absence of other microbiota members.

Starting from the top down, I generated an overview of the number of host genes differentially expressed in response to *B. breve* colonisation by comparing volcano plots of DEGs in IECs and WSI, as well neonate and adult SPF mice (Figure 5-10). *B. breve* has the strongest effect on neonatal small intestinal IECs, with 14054 differentially expressed genes (DEGs, q value < 0.05) ranging from 12 $\log_2$ fold upregulation to 6 $\log_2$ downregulation. A ratio of 1:1.3 comparing down vs up regulation favours increase in expression (Figure 5-10).

In contrast to the pronounced modulation of neonate IECs, the effect of colonisation is close to 10-fold lower in IECs of adult mice, with 103 DEGs (p-value < 0.05, $\log_2$ fold change +10 to – 21, Figure 5-10). Analysis of whole SI resulted in even further reduced transcriptional regulation with 21 DEGs in neonate WSI and no clear PCA clustering observable between groups (Supplementary Figure 7). A total of 47 DEGs were identified in adult mouse WSI, with two colonised biological repeats showing similarity in expression profile while one sample (UCC3) is more similar to control gene expression (Supplementary Figure 8). This mouse had similar colonisation levels to other gavaged mice, however these were cfu's from faecal samples, and it cannot be discounted that the bacterial presence within the SI was different, and this may account for these differences.

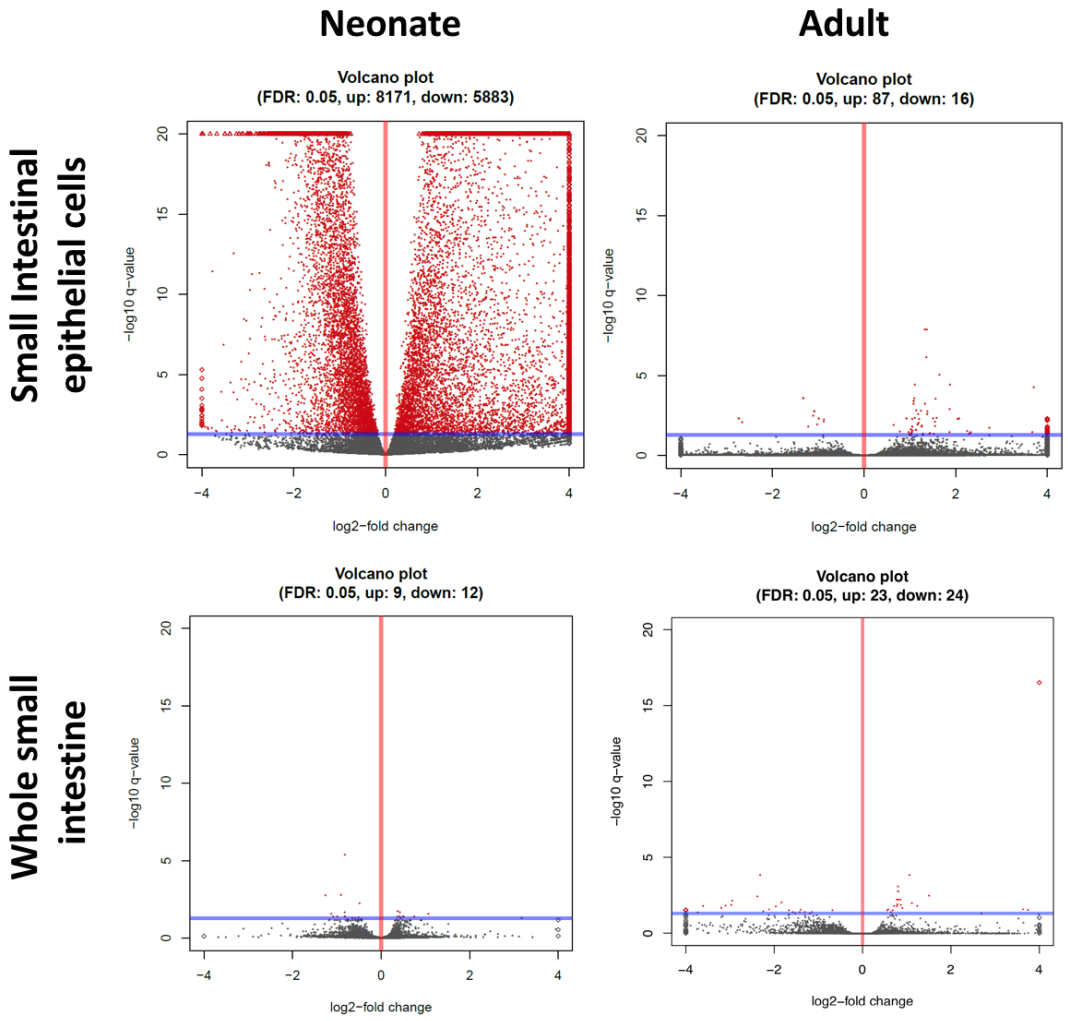

Figure 5-10 ***B. breve*** **UCC2003 intestinal colonisation induces a distinct transcriptional response in small intestinal epithelial cells of neonate mice.**

Volcano plots of neonate and adult small intestinal epithelial cells (IEC) and whole small intestine (WSI) differentially regulated genes (DEGs) compared to control (PBS gavaged), y axis shows q-value on a log10 scale, x axis presents fold change in log2, statistical significance indicated by red, blue line indicating statistical significant cut off of q-value<0.05, generated and calculated with DESe2.

Assessing transcriptional changes in mono-colonised mice compared to GF mice, indicates that *B. breve* colonisation does not significantly modulate IECs (2 DEGs, q-value < 0.05, $\log_2$ fold change below cut off of 2.5), but this could be skewed by one sample within the treatment group (UCC1) showing an expression profile different from the tight clustering of the other *B. breve* colonised samples, and is more similar to control samples based on PCA (Supplementary Figure 9), The mouse

from which this sample was collected showed similar colonisation levels compared to group average. Again, a difference in small intestinal colonisation may account for this outlier.

B. breve did induce a very strong effect on monocolonised WSI; with 10052 DEGs (q-value < 0.05, $\log_2$ fold change +29 to -17) (Supplementary Figure 10). Due to no transcriptional differential regulation of IECs the exploration of this dataset is out-with the scope of this PhD study, but these notable differences between GF and SPF IECs profiles will be explored in the discussion.

Previously we performed an investigation of potential transcriptional targets of *B. breve* UCC2003 during LPS-induced cell shedding, by analysis gene expression by qPCR array on whole SI. However, as the focus of my work is on IECs and *B. breve*, I analysed epithelial gene expression of LPS challenged mice, with and without the presence of *B. breve* UCC2003. Interestingly, no DEGs response was observed, with most of control and treatment group samples clustering closely (Supplementary Figure 11). It could be hypothesised that the strong transcriptional response induced by systemic LPS masks the homeostatic modulation of IECs by *B. breve*. As the whole IE is undergoing acute inflammation, and IECs undergo apoptosis in great numbers, this may also influence which IECs are collected from the tissue; LPS stimulated cells, both in control and *B. breve* colonised samples removed by the Weisser method, leaving non-stimulated IECs for RNA-seq analysis resulting in no DEGs. Furthermore, as the cell shedding model is so rapid (1.5h), significant modulation of transcriptional responses may not be induced in this short-time frame.

These data highlight that there are strong IEC transcriptional responses in response to *B. breve* colonisation on the transcriptome of neonate mice during intestinal 'health', but no observable differences during inflammatory cell shedding, as well as a strongly reduced effect on adult IECs, and whole small intestinal tissue of adult and neonate mice during homeostasis. This emphasises the importance of investigating the effect of *B. breve* on host IECs during homeostasis, which will be the focus of my in-depth analysis below.

5.3.5.1 Analysing neonate IEC transcriptional responses by *B. breve* reveals increased expression of TLR2, TLR9, IL17C and integrins

I used DESeq2 to quality control the dataset of *B. breve* UCC2003 induced differential gene expression in neonate IECs. Due to the overall high number of genes analysed for differential expression, and for accurate statistical determination, specifically in groups with lower n numbers in relation to genes expressed, DESeq2 applies a gene-wise dispersion estimate (by maximum likelihood estimation) to each DEG, and compares this value to the overall trend in dispersion of the sample set through processing, including shrinkage of estimated dispersion. This approach allows for the assessment of expected dispersion of the data, and identification of potential outliers, as well as the prevention of false positives. Due to biological or technical reasons, genes can fall outside of the statistical model, and the applied algorithm takes this into account when assessing general statistical certainty of the applied DEG calculation [374]. The shrinkage estimation of dispersion for the data shows a close association of genes with the line of best fit, with a small number of outliers in relation to total number of genes analysed (Figure 5-11.A).

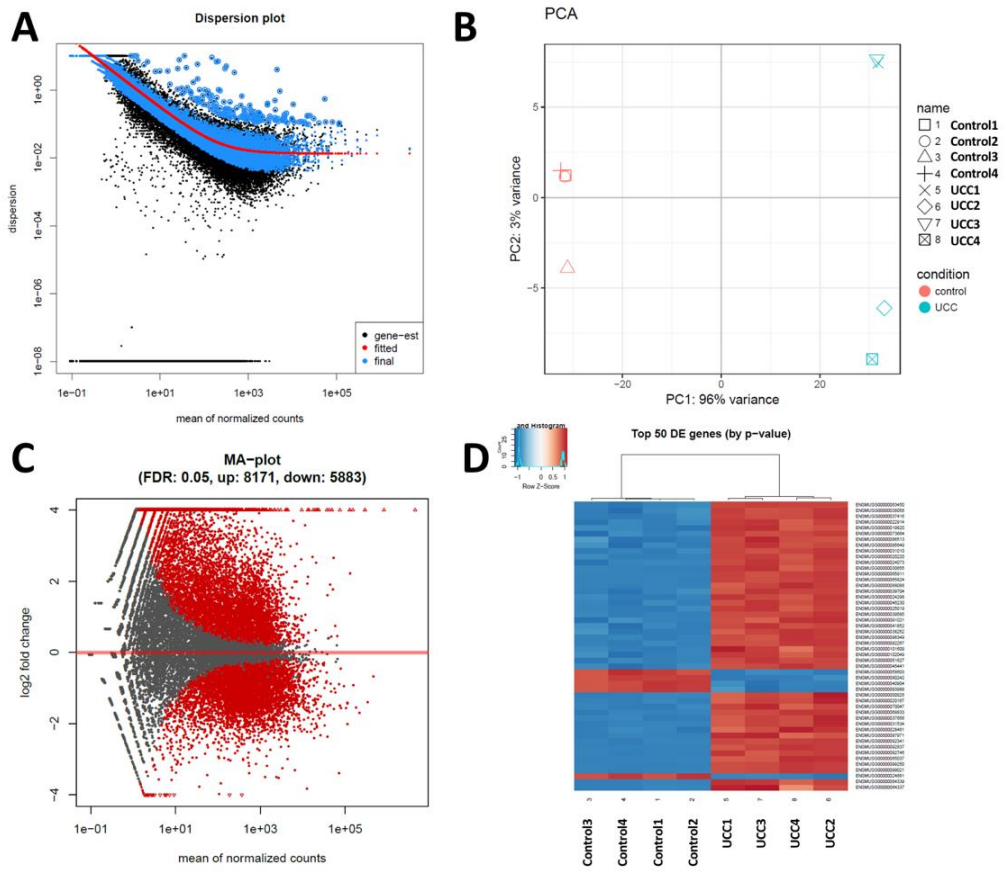

Figure 5-11 Presence of *B. breve* UCC2003 induces consistent, strong transcriptional changes in small intestine epithelial cells of neonate mice

Overview over transcriptional changes in IECs of neonate mice colonised with *B. breve* UCC2003 relative to control (PBS gavaged) **A** Shrinkage estimation of dispersion, y axis dispersion estimate, x axis mean of normalised counts, black dots individual genes, red line maximum likelihood estimation (MLE) line of best fit, black dots circled in blue – potential dispersion outliers, blue area around red line – genes used for second dispersion estimate (not outliers), **B** PCA plot of group variability **C** Bland Altman (MA) plot of transcriptional modulation by presence of *B. breve* UCC2003 relative to control, y axis log2 fold change of gene expression, x axis – mean of moralised counts, red dots – statistical sig genes (q values 0.05) **D** Hierarchical clustering of samples based on TOP 50 differentially regulated genes.

The PCA analysis (Figure 5-11.B), showed clear separation between control and treatment groups, with greater intergroup variability in the control data set. The associated Bland Altman (MA) plot gives an overview over changes in gene expression in the samples, plotted against the mean read counts, while highlighting significantly regulated genes individually (red dots, Figure 5-11.C). The dataset

shows a balanced up and down regulation with read counts correlating with fold changes. The majority of upregulated transcripts have higher read counts, while the sub-sample of downregulated genes has a similar number of higher expressed genes, but a much higher number of DEGs with strong fold changes (less with high read counts, more with average read counts). Considering the top 50 differential regulated genes (by p-value), the samples cluster hierarchically in accordance with their groups, as presented in the heat map (Figure 5-11.D). Most top differentially regulated genes in the control group are upregulated, while the opposite is the case for the *B. breve* treatment group. This suggests a dampening effect of *B. breve* colonisation on IECs, by reducing transcription of genes.

The 25 genes inversely differentially expressed between the control and UCC2003 gavaged group are based on the Ensemble gene database predicated genes 15487 and 21988, and ribosomal protein L28 (pseudogene 1), RNase K and ferritin heavy polypeptide 1 (Figure 5-11.D).

To start teasing apart the biological interactions of the substantial number of DEGs initially I investigated the genes with strongest fold changes (q value < 0.05). The top 25 up and down regulated genes are presented in Table 5-1 and Table 5-2 respectively.

Table 5-1 Transcripts showing highest upregulation in neonate IECs induced by *B. breve* UCC2003

(q value < 0.05)

Expr Log Ratio	q-value	Ensemble ID	Gene Symbol	Entrez Gene Name	Location
12.955	5.2E-35	ENSMUSG00000077714	Snord17	small nucleolar RNA, C/D box 17	
12.595	0	ENSMUSG00000099021	Rn7s1	7S RNA 1	
12.51	2.3E-33	ENSMUSG00000089617	Scarna10	small Cajal body-specific RNA 10	
12.51	2.3E-33	ENSMUSG00000099587	Gm28967	predicted gene 28967	
12.462	0	ENSMUSG00000099250	Rn7s2	7S RNA 2	
12.296	0	ENSMUSG00000092746	Rn7s6	7S RNA 6	
11.946	6.2E-30	ENSMUSG00000095260	Gm25890	predicted gene 25890	
11.938	0	ENSMUSG00000092837	Rpph1	ribonuclease P RNA component H1	
11.797	3.5E-29	ENSMUSG00000088948	Gm23262	predicted gene, 23262	
11.783	0	ENSMUSG00000065911	Gm24447	predicted gene, 24447	
11.694	1.2E-28	ENSMUSG00000096838	Gm26232	predicted gene, 26232	
11.676	0	ENSMUSG00000088088	RMRP	RNA component of mitochondrial RNA processing endoribonuclease	Cytoplasm
11.531	0	ENSMUSG00000065037	RN7SK	RNA, 7SK small nuclear	Nucleus
11.452	7.1E-53	ENSMUSG00000094306	Gm24924	predicted gene, 24924	
11.317	3E-39	ENSMUSG00000064387	Snora73a	small nucleolar RNA, H/ACA box 73a	
11.296	0	ENSMUSG00000065824	Gm26315	predicted gene, 26315	
11.187	3E-76	ENSMUSG00000064999	Gm26035	predicted gene, 26035	
11.124	6E-26	ENSMUSG00000094812	Gm22614	predicted gene, 22614	
11.115	6.7E-26	ENSMUSG00000084708	Gm22988	predicted gene, 22988	
11.01	0.00134	ENSMUSG00000098078	Gm26992	predicted gene, 26992	
10.938	5.8E-25	ENSMUSG00000071862	LRRTM2	leucine rich repeat transmembrane neuronal 2	Plasma Membrane
10.865	3.5E-71	ENSMUSG00000096659	Gm25679	predicted gene, 25679	
10.726	8E-117	ENSMUSG00000092805	Gm26461	predicted gene, 26461	
10.711	4E-236	ENSMUSG00000096349	Gm22513	predicted gene, 22513	
10.589	2.6E-23	ENSMUSG00000096954	Gdap10	ganglioside-induced differentiation-associated-protein 10	

Table 5-2 DEGs induced by *B. breve* UCC2003 in neonate IECs with strongest downregulation

(q value < 0.05)

Expr Log Ratio	q-value	Ensemble ID	Gene Symbol	Entrez Gene Name	Location
-6.333	0.00000496	ENSMUSG00000023046	IGFBP6	insulin like growth factor binding protein 6	Extracellular Space
-5.707	0.0000173	ENSMUSG00000017002	SLPI	secretory leukocyte peptidase inhibitor	Cytoplasm
-5.243	0.00131	ENSMUSG00000029675	ELN	elastin	Extracellular Space
-4.968	0.0000826	ENSMUSG00000082655	Gm7857	predicted gene 7857	
-4.906	2.24E-122	ENSMUSG00000082884	Gm13339	predicted gene 13339	
-4.683	0.00151	ENSMUSG00000085126	Gm12589	predicted gene 12589	
-4.652	6.41E-58	ENSMUSG00000064353	mt-Td	mitochondrially encoded tRNA aspartic acid	
-4.592	0.00171	ENSMUSG00000041550	SERPINA5	serpin family A member 5	Extracellular Space
-4.543	0.00178	ENSMUSG00000075122	CD80	CD80 molecule	Plasma Membrane
-4.453	0.000304	ENSMUSG00000030470	CSRP3	cysteine and glycine rich protein 3	Nucleus
-4.362	0.00369	ENSMUSG00000022598	PSCA	prostate stem cell antigen	Plasma Membrane
-4.291	0.00549	ENSMUSG00000020660	POMC	proopiomelanocortin	Extracellular Space
-4.213	0.0149	ENSMUSG00000044258	Ctla2a/Ctla2b	cytotoxic T lymphocyte-associated protein 2 alpha	Plasma Membrane
-4.142	0.000836	ENSMUSG00000066389	Rpl31-ps1	ribosomal protein L31, pseudogene 1	
-4.138	0.0013	ENSMUSG00000096974	Gm26881	predicted gene, 26881	
-4.118	0.0108	ENSMUSG00000073412	Lst1	leukocyte specific transcript 1	Cytoplasm
-4.112	0.00821	ENSMUSG00000040127	SDR9C7	short chain dehydrogenase/reductase family 9C member 7	
-4.111	0.0109	ENSMUSG00000087390	Gm7598	predicted gene 7598	
-4.011	0.00354	ENSMUSG00000081542	Gm12512	predicted gene 12512	
-4.008	0.0131	ENSMUSG00000094806	Cyp2d9 (includes others)	cytochrome P450, family 2, subfamily d, polypeptide 9	Cytoplasm
-3.975	8.8E-24	ENSMUSG00000069917	HBA1/HBA2	hemoglobin subunit alpha 2	Extracellular Space
-3.93	0.0185	ENSMUSG00000023781	HES7	hes family bHLH transcription factor 7	Nucleus
-3.874	0.0199	ENSMUSG00000060459	KNG1	kininogen 1	Extracellular Space
-3.862	0.0243	ENSMUSG00000083460	Gm12182	predicted gene 12182	
-3.82	2.59E-77	ENSMUSG00000035202	LARS2	leucyl-tRNA synthetase 2, mitochondrial	Cytoplasm

A large proportion of genes presenting with strongest upregulation in expression by *B. breve* UCC2003 are predicted genes and annotated as non-coding RNAs, but without associated function (Table 5-1). Transcripts downregulated by *B. breve* UCC2003 include CD80 (log_2 fold change -4.5, expressed in monocytes, dendritic, and B cells and essential for T cell activation), which does suggest presence of other cell types in this IEC preparation, and could be interpreted as a decreased immune cell population in the LP of *B. breve* colonised mice [375]. A decrease in cytotoxic T lymphocyte-associated protein 2 alpha (log_2 fold change -4.2, Ctla2a/Ctla2b) could further suggest a decreased pro-inflammatory immune response. These results have to be validated as the isolation method was targeted at IECs, and no definite conclusions about other cell types should be drawn from these data.

As no clear biological mechanistic modulation could be identified from analysis of genes with highest up or downregulation, I continued my search by investigating expression of three specific classes relevant in host-microbe interactions and host health (i.e. TLRs, IL's, and their receptors and caspases).

Table 5-3 *B. breve* UCC2003 modulates Toll-like receptor (TLR) expression in neonate small intestine epithelial cells.

Expr Log Ratio	q-value	Ensemble Gene ID	Gene Symbol	Entrez Gene Name	Location
2.864	0.000525	ENSMUSG00000027995	TLR2	toll like receptor 2	Plasma Membrane
0.907	1.71E-07	ENSMUSG00000031639	TLR3	toll like receptor 3	Plasma Membrane
0.767	7.52E-06	ENSMUSG00000079164	TLR5	toll like receptor 5	Plasma Membrane
3.746	0.0096	ENSMUSG00000045322	TLR9	toll like receptor 9	Plasma Membrane

Table 5-4 Small intestinal epithelial caspase expression is affected by *B. breve* colonisation of the neonate intestine

Expr Log Ratio	q-value	Ensemble Gene ID	Gene Symbol	Entrez Gene Name	Location
-0.448	0.0000345	ENSMUSG00000028914	CASP9	caspase 9	Cytoplasm
2.412	6.45E-45	ENSMUSG00000028282	CASP8AP2	caspase 8 associated protein 2	Nucleus
-1.252	6.24E-17	ENSMUSG00000027997	CASP6	caspase 6	Cytoplasm
-0.607	0.000881	ENSMUSG00000031628	CASP3	caspase 3	Cytoplasm
1.002	6.1E-11	ENSMUSG00000029863	CASP2	caspase 2	Cytoplasm
-0.748	0.0000042	ENSMUSG00000025888	CASP1	caspase 1	Cytoplasm
1.951	0.0272	ENSMUSG00000026928	CARD9	caspase recruitment domain family member 9	Cytoplasm
-1.433	1.81E-15	ENSMUSG00000037960	CARD19	caspase recruitment domain family member 19	Cytoplasm
2.029	0.0000311	ENSMUSG00000036526	CARD11	caspase recruitment domain family member 11	Cytoplasm

In Table 5-3, differential expression of TLRs by *B. breve* compared to control mice are shown. TLR 2 (which recognises Lipoteichoic acid) was strongly upregulated with a log2 fold change of +2.8. TLR9 upregulation (log2 fold change +3.7) carries out a dual role in IECs dependent on its cellular localisation [20]. Apical TLR9 activation prevents NF-κB activation and acts anti-inflammatory, while basal TLR9 ligand binding has been shown to induce IL-8 secretion, and hence drive pro-inflammatory responses. The implication of the differential regulation of these two TLRs in the host health beneficial effect of *B. breve* will also be further discussed below.

TLRs 3 and 5 show less pronounced modulation. TLR5 (log2 fold change +0.7) recognises flagellin, and IEC specific KO mice present with low grad inflammation during homeostatic conditions combined with increased susceptibility to DSS induced colitis [376]. TLR3 (log 2 fold change +0.9) surveys viral doubled stranded RNA in the intestinal lumen and its expression is significantly downregulated in IECs during active CD [377].

Investigating the effect of *B. breve* colonisation on caspase expression, revealed both up and down regulation (Table 5-4). Interestingly, caspase 3 (marker used for identification of apoptotic cell shedding in this study) is downregulated (log2 fold change -0.6), together with caspase 9, 6 and 1 (log2 fold change -0.4, -1.2, -0.7).

Interleukins (ILs) are powerful cytokines produced by immune cells and IECs, which play pivotal roles in tissue homoeostasis and disease. Table 5-5 shows all ILs and receptors differentially regulated by *B. breve* relative to control samples. Specifically, several IL17 isoform as well as IL-17 receptor classes are differentially regulated. IL-17C, which is expressed in IECs, is increased by 5.2 log2 fold (IL-17D downregulated by -2.7 log2 fold, expression undefined) (Table 5-5) [378]. IL-17 receptors are expressed in several cell types, with IL-17RC and IL-17RD present on the surface of epithelial cells. Their expression is downregulated slightly (IL-17RC, log2 fold change -0.2), as well as upregulated (IL-17RD, log2 fold change 0.9). Two other receptor classes are differentially modulated by *B. breve,* but not expressed on IECs (IL-17RB log2 fold change 2.6 T helper cells and fibroblasts, IL-17RA log2 fold change -0.3 ubiquitos) [378].

Table 5-5Interleukins and their receptor transcription in small intestinal epithelial cells is affected by *B. breve* UCC2003 colonisation.

Expr Log Ratio	q-value	Ensembl Gene ID	Gene Symbol	Entrez Gene Name	Location
-0.367	0.0179	ENSMUSG00000030748	IL4R	interleukin 4 receptor	Plasma Membrane
-1.978	0.0000493	ENSMUSG00000068758	IL3RA	interleukin 3 receptor subunit alpha	Plasma Membrane
-0.389	0.00271	ENSMUSG00000024810	IL33	interleukin 33	Extracellular Space
3.587	2.16E-15	ENSMUSG00000050377	IL31RA	interleukin 31 receptor A	Plasma Membrane
4.515	0.00846	ENSMUSG00000025383	IL23A	interleukin 23 subunit alpha	Extracellular Space
1.12	2.2E-24	ENSMUSG00000037157	IL22RA1	interleukin 22 receptor subunit alpha 1	Plasma Membrane
1.371	0.000325	ENSMUSG00000044244	IL20RB	interleukin 20 receptor subunit beta	Plasma Membrane
-1.371	0.00219	ENSMUSG00000027720	IL2	interleukin 2	Extracellular Space
0.871	0.0109	ENSMUSG00000022514	IL1RAP	interleukin 1 receptor accessory protein	Plasma Membrane
1.759	0.000000206	ENSMUSG00000070427	IL18BP	interleukin 18 binding protein	Extracellular Space
-0.719	0.00106	ENSMUSG00000039217	IL18	interleukin 18	Extracellular Space
0.935	0.00197	ENSMUSG00000040717	IL17RD	interleukin 17 receptor D	Cytoplasm
-0.273	0.0409	ENSMUSG00000030281	IL17RC	interleukin 17 receptor C	Plasma Membrane
2.06	0.000243	ENSMUSG00000015966	IL17RB	interleukin 17 receptor B	Plasma Membrane
-0.324	0.0203	ENSMUSG00000002897	IL17RA	interleukin 17 receptor A	Plasma Membrane
-2.72	2.96E-27	ENSMUSG00000050222	IL17D	interleukin 17D	Extracellular Space
5.219	0.000514	ENSMUSG00000046108	IL17C	interleukin 17C	Extracellular Space
2.602	0.0000199	ENSMUSG00000001741	IL16	interleukin 16	Extracellular Space
1.32	2.13E-08	ENSMUSG00000023206	IL15RA	interleukin 15 receptor subunit alpha	Plasma Membrane
0.664	0.00828	ENSMUSG00000031712	IL15	interleukin 15	Extracellular Space
4.814	7.38E-15	ENSMUSG00000018341	IL12RB2	interleukin 12 receptor subunit beta 2	Plasma Membrane
-0.368	0.0318	ENSMUSG00000073889	IL11RA	interleukin 11 receptor subunit alpha	Plasma Membrane
-1.101	1.52E-33	ENSMUSG00000022969	IL10RB	interleukin 10 receptor subunit beta	Plasma Membrane

5.3.5.2 Pathway analysis of genes differentially regulated by *B. breve* UCC2003 in neonate IECs shows expression upregulation of integrin, and downstream signalling components

In addition to the manual curation of the DEGs modulated by *B. breve*, I utilised downstream pathway analysis to explore wider biological functions.

As RNA-Seq gives global gene expression data, it is important to use additional pathway modelling to infer important mechanistic associations. Based on DEG lists, pathway analysis, utilising gene and protein databases greatly aids in interpretation of RNA-Seq data, as weighting of fold expression changes of specific genes are taken into account, together with the total modulation of all DEGs [379]. This allows small expression changes, such as in transcription factors, which otherwise would potentially have been overlooked to be analysed, and if present may suggest modulation of other transcripts in a wider pathway, which could have important biological function [362]. If the analysis considers direction of fold changes, this allows for an even more specific and detailed analysis. However, as with all large datasets, the number of pathways containing DEGs increases and with this the rate of false positives. This has been addressed by statistical models, but the problem remains that with RNA-Seq data identifying all true biological responses is sometimes problematic, and which is why downstream validation of targets increases the robustness of conclusions drawn.

Pathway analysis tools are under constant development, and I tested Innate DB and Cytoscape (both open source), and in addition I also used Ingenuity Pathway Analysis (IPA) by Qiagen. Based on the number of DEGs mapped to pathways, IPA had the highest resolution, and was thus taken forward for analysing the data sets (data not shown). Notably, IPA includes regular manually curated additions of experimentally validated biological interactions, together with automatic searching, while open source tools are usually reliant on only computational databases, although they have the significant added benefit of being freely available to the wider scientific community.

When analysing the IEC neonate data set pathways, the DEG cut-off was set at a relatively stringent q value < 0.05 to ensure statistical accuracy, while fold change integration barrier was kept low log2 > +/-0.8.

In the neonate dataset, integrin signalling showed very strong mapping of DEGs to this pathway (92 out of 219), a z-score of 2.157 (IPA mathematical model of correlation between predicted direction of regulation of transcripts in pathway and experimental DEG fold changes) and a p-value taking fold change direction and gene mapping to pathway into account of $2.69x10^{-5}$ (Figure 5-13, Table 5-6).

Integrin subunit α 1, 2 and 2b, 4, 6, 9, 10, E, M, V, and subunit β 6 and 7 were all increased in IECs of neonatal mice colonised by *B. breve* UCC2003. The upregulation ranged from 1 log2 fold of integrin subunit β6 to 3.8 log2 fold of subunit α10 (Table 5-6 andTable 5-7). These regulations were consistent between intergroup biological repeats, and showed relatively high mean expression counts.

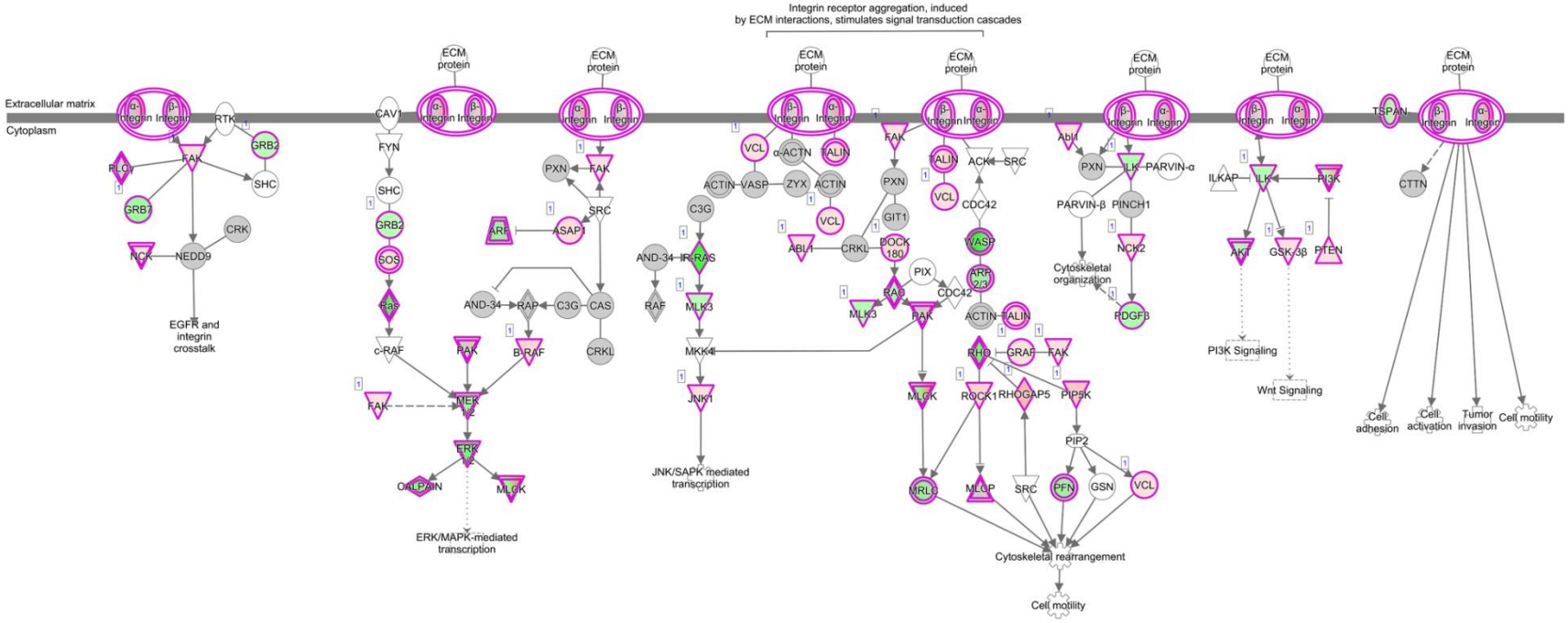

Figure 5-12 Integrin and downstream signalling component expression is upregulated by *B. breve* colonisation in neonate intestinal epithelial cells.

Pathway analysis of total differentially regulated small intestinal epithelial cell genes modulated by *B. breve* UCC2003 gavage utilising IPA shows integrin and downstream signalling, upregulation red, downregulation green, q-value <0.05, log2 fold change > 0.8.

Table 5-6 ***B. breve*** **UCC2003 intestinal colonisation of neonate mice increases expression of integrins and downstream signalling network components in IECs**

(continued next page)

Symbol	Entrez Gene Name	Ensembl	Expr Log Ratio	Expected regulation (based on pathway activation)	Location	Type(s)
ABL1	ABL proto-oncogene 1, non-receptor tyrosine kinase	ENSMUSG00000026842	0.834	Up	Nucleus	kinase
AKT1	AKT serine/threonine kinase 1	ENSMUSG00000001729	-0.886	Up	Cytoplasm	kinase
ARF1	ADP ribosylation factor 1	ENSMUSG00000048076	-0.995	Down	Cytoplasm	enzyme
ARF3	ADP ribosylation factor 3	ENSMUSG00000051853	-0.959	Down	Cytoplasm	enzyme
ARF5	ADP ribosylation factor 5	ENSMUSG00000020440	-1.356	Down	Cytoplasm	enzyme
ARHGAP5	Rho GTPase activating protein 5	ENSMUSG00000035133	2.814	Up	Cytoplasm	enzyme
ARHGAP26	Rho GTPase activating protein 26	ENSMUSG00000036452	1.058	Down	Cytoplasm	other
ARPC2	actin related protein 2/3 complex subunit 2	ENSMUSG00000006304	-0.992	Up	Cytoplasm	other
ARPC3	actin related protein 2/3 complex subunit 3	ENSMUSG00000029465	-1.313	Up	Cytoplasm	other
ARPC4	actin related protein 2/3 complex subunit 4	ENSMUSG00000079426	-1.2	Up	Cytoplasm	other
ARPC5	actin related protein 2/3 complex subunit 5	ENSMUSG00000008475	-0.842	Up	Cytoplasm	other
ARPC1A	actin related protein 2/3 complex subunit 1A	ENSMUSG00000029621	-1.062	Up	Extracellular Space	other
ASAP1	ArfGAP with SH3 domain, ankyrin repeat and PH domain 1	ENSMUSG00000022377	1.421	Up	Plasma Membrane	other
ATM	ATM serine/threonine kinase	ENSMUSG00000034218	3.713	Up	Nucleus	kinase
BRAF	B-Raf proto-oncogene, serine/threonine kinase	ENSMUSG00000002413	1.671	Up	Cytoplasm	kinase
CAPN7	calpain 7	ENSMUSG00000021893	1.018	Up	Cytoplasm	peptidase
CAPN8	calpain 8	ENSMUSG00000038599	2.238	Up	Cytoplasm	peptidase
CAPNS1	calpain small subunit 1	ENSMUSG00000001794	-1.776	Up	Cytoplasm	peptidase
DOCK1	dedicator of cytokinesis 1	ENSMUSG00000058325	1.545	Up	Cytoplasm	other
FGFR2	fibroblast growth factor receptor 2	ENSMUSG00000030849	1.473	Up	Plasma Membrane	kinase
FGFR3	fibroblast growth factor receptor 3	ENSMUSG00000054252	1.822	Up	Plasma Membrane	kinase
FNBP1	formin binding protein 1	ENSMUSG00000075415	0.93	Up	Nucleus	enzyme
FRS2	fibroblast growth factor receptor substrate 2	ENSMUSG00000020170	0.837	Up	Plasma Membrane	kinase
GRB2	growth factor receptor bound protein 2	ENSMUSG00000059923	-0.842	Up	Cytoplasm	kinase
GRB7	growth factor receptor bound protein 7	ENSMUSG00000019312	-1.176	Up	Plasma Membrane	other
GSK3B	glycogen synthase kinase 3 beta	ENSMUSG00000022812	1.156	Down	Nucleus	kinase
HRAS	HRas proto-oncogene, GTPase	ENSMUSG00000025499	-1.276	Up	Plasma Membrane	enzyme
ILK	integrin linked kinase	ENSMUSG00000030890	-0.935	Up	Plasma Membrane	kinase
IRS1	insulin receptor substrate 1	ENSMUSG00000055980	2.92	Up	Cytoplasm	enzyme
IRS2	insulin receptor substrate 2	ENSMUSG00000038894	1.847	Up	Cytoplasm	enzyme
ITGA1	integrin subunit alpha 1	ENSMUSG00000042284	2.315	Up	Plasma Membrane	other
ITGA2	integrin subunit alpha 2	ENSMUSG00000015533	2.881	Up	Plasma Membrane	transmembrane receptor
ITGA4	integrin subunit alpha 4	ENSMUSG00000027009	2.896	Up	Plasma Membrane	transmembrane receptor
ITGA6	integrin subunit alpha 6	ENSMUSG00000027111	1.29	Up	Plasma Membrane	transmembrane receptor
ITGA9	integrin subunit alpha 9	ENSMUSG00000039115	2.434	Up	Plasma Membrane	other
ITGA10	integrin subunit alpha 10	ENSMUSG00000090210	3.801	Up	Plasma Membrane	other
ITGA2B	integrin subunit alpha 2b	ENSMUSG00000034664	1.632	Up	Plasma Membrane	transmembrane receptor
ITGAE	integrin subunit alpha E	ENSMUSG00000005947	2.448	Up	Plasma Membrane	other
ITGAM	integrin subunit alpha M	ENSMUSG00000030786	1.154	Up	Plasma Membrane	transmembrane receptor
ITGAV	integrin subunit alpha V	ENSMUSG00000027087	1.532	Up	Plasma Membrane	transmembrane receptor
ITGB6	integrin subunit beta 6	ENSMUSG00000026971	1.064	Up	Plasma Membrane	other
ITGB7	integrin subunit beta 7	ENSMUSG00000001281	1.502	Up	Plasma Membrane	transmembrane receptor
KL	klotho	ENSMUSG00000058488	4.003	Up	Extracellular Space	enzyme
MAP2K2	mitogen-activated protein kinase kinase 2	ENSMUSG00000035027	-1.242	Up	Cytoplasm	kinase

Table 5-7 ***B. breve*** **UCC2003 intestinal colonisation of neonate mice increases expression of integrins and downstream signalling network components in IECs**

(continued from previous page)

Symbol	Entrez Gene Name	Ensembl	Expr Log Ratio	Expected regulation (based on pathway activation)	Location	Type(s)
MAP3K11	mitogen-activated protein kinase kinase kinase 11	ENSMUSG00000004054	-0.886	Up	Cytoplasm	kinase
MAPK3	mitogen-activated protein kinase 3	ENSMUSG00000063065	-1.809	Up	Cytoplasm	kinase
MAPK8	mitogen-activated protein kinase 8	ENSMUSG00000021936	1.018	Up	Cytoplasm	kinase
MPRIP	myosin phosphatase Rho interacting protein	ENSMUSG00000005417	1.852		Cytoplasm	other
MYL12A	myosin light chain 12A	ENSMUSG00000034868	-0.98	Up	Cytoplasm	other
MYL12B	myosin light chain 12B	ENSMUSG00000024048	-1.466	Up	Cytoplasm	other
MYLK3	myosin light chain kinase 3	ENSMUSG00000031698	-1.235	Up	Cytoplasm	kinase
NCK2	NCK adaptor protein 2	ENSMUSG00000066877	0.844	Up	Cytoplasm	kinase
PAK3	p21 (RAC1) activated kinase 3	ENSMUSG00000031284	2.687	Up	Cytoplasm	kinase
PDGFB	platelet derived growth factor subunit B	ENSMUSG00000000489	-1.028	Up	Extracellular Space	growth factor
PFN1	profilin 1	ENSMUSG00000018293	-1.317	Up	Cytoplasm	other
PFN2	profilin 2	ENSMUSG00000027805	-0.871	Up	Cytoplasm	enzyme
PIK3C2A	phosphatidylinositol-4-phosphate 3-kinase catalytic subunit type 2 alpha	ENSMUSG00000030660	1.756	Up	Cytoplasm	kinase
PIK3C2B	phosphatidylinositol-4-phosphate 3-kinase catalytic subunit type 2 beta	ENSMUSG00000026447	1.98	Up	Cytoplasm	kinase
PIK3C2G	phosphatidylinositol-4-phosphate 3-kinase catalytic subunit type 2 gamma	ENSMUSG00000030228	4.569	Up	Cytoplasm	kinase
PIK3CA	phosphatidylinositol-4,5-bisphosphate 3-kinase catalytic subunit alpha	ENSMUSG00000027665	1.409	Up	Cytoplasm	kinase
PIK3CG	phosphatidylinositol-4,5-bisphosphate 3-kinase catalytic subunit gamma	ENSMUSG00000020573	1.118	Up	Cytoplasm	kinase
PIK3R1	phosphoinositide-3-kinase regulatory subunit 1	ENSMUSG00000041417	1.59	Up	Cytoplasm	kinase
PIK3R3	phosphoinositide-3-kinase regulatory subunit 3	ENSMUSG00000028698	1.182	Up	Cytoplasm	kinase
PIK3R5	phosphoinositide-3-kinase regulatory subunit 5	ENSMUSG00000020901	1.375	Up	Cytoplasm	kinase
PIKFYVE	phosphoinositide kinase, FYVE-type zinc finger containing	ENSMUSG00000025949	2.237	Up	Cytoplasm	kinase
PLCG2	phospholipase C gamma 2	ENSMUSG00000034330	0.892	Up	Cytoplasm	enzyme
PPP1R12A	protein phosphatase 1 regulatory subunit 12A	ENSMUSG00000019907	2.276		Cytoplasm	phosphatase
Ppp1r12b	protein phosphatase 1, regulatory (inhibitor) subunit 12B	ENSMUSG00000073557	2.485		Cytoplasm	other
PTEN	phosphatase and tensin homolog	ENSMUSG00000013663	1.054	Down	Cytoplasm	phosphatase
PTK2	protein tyrosine kinase 2	ENSMUSG00000022607	0.954	Up	Cytoplasm	kinase
RAC1	ras-related C3 botulinum toxin substrate 1	ENSMUSG00000001847	-0.995	Up	Plasma Membrane	enzyme
RAC3	ras-related C3 botulinum toxin substrate 3	ENSMUSG00000018012	-0.912	Up	Cytoplasm	enzyme
RHOC	ras homolog family member C	ENSMUSG00000002233	-1.682	Up	Plasma Membrane	enzyme
RHOD	ras homolog family member D	ENSMUSG00000041845	-1.074	Up	Cytoplasm	enzyme
RHOG	ras homolog family member G	ENSMUSG00000073982	-2.262	Up	Cytoplasm	enzyme
RHOT2	ras homolog family member T2	ENSMUSG00000025733	-0.908	Up	Cytoplasm	enzyme
RHOV	ras homolog family member V	ENSMUSG00000034226	-0.939	Up	Plasma Membrane	enzyme
RND2	Rho family GTPase 2	ENSMUSG00000001313	-1.392	Up	Cytoplasm	enzyme
RND3	Rho family GTPase 3	ENSMUSG00000017144	0.961	Up	Cytoplasm	enzyme
ROCK1	Rho associated coiled-coil containing protein kinase 1	ENSMUSG00000024290	1.775	Up	Cytoplasm	kinase
RRAS	related RAS viral (r-ras) oncogene homolog	ENSMUSG00000038387	-2.432	Up	Cytoplasm	enzyme
SOS1	SOS Ras/Rac guanine nucleotide exchange factor 1	ENSMUSG00000024241	1.702	Up	Cytoplasm	other
SOS2	SOS Ras/Rho guanine nucleotide exchange factor 2	ENSMUSG00000034801	1.14	Up	Cytoplasm	other
TLN1	talin 1	ENSMUSG00000028465	1.096	Up	Plasma Membrane	other
TLN2	talin 2	ENSMUSG00000052698	2.582	Up	Nucleus	other
TLR9	toll like receptor 9	ENSMUSG00000045322	3.746	Up	Plasma Membrane	transmembrane receptor
TSPAN5	tetraspanin 5	ENSMUSG00000028152	0.995		Plasma Membrane	other
TSPAN6	tetraspanin 6	ENSMUSG00000067377	-0.957		Plasma Membrane	other
TSPAN7	tetraspanin 7	ENSMUSG00000058254	-1.134		Plasma Membrane	other
TTN	titin	ENSMUSG00000051747	6.038	Up	Cytoplasm	kinase
VCL	vinculin	ENSMUSG00000021823	0.861	Up	Plasma Membrane	enzyme
WAS	Wiskott-Aldrich syndrome	ENSMUSG00000031165	-3.696	Up	Cytoplasm	other

Within the integrin signalling pathway, I observed elevated fold changes of direct downstream adapter and signal transducers of integrins including protein tyrosine kinase 2 (log2 fold change +0.9, also known as focal adhesion kinase, FAK), Talin 1 and Talin 2 (log 2-fold change +1 and +2.5) and Vinculin (log 2 fold change +0.8). While Talin and Vinculin link integrins to the cytoskeleton, FAK signals from integrins via phosphorylation [380]. FAK KO intestinal epithelial cells undergo increased apoptosis due to loss of survival signals mediated by cell adhesion contacts *in vitro*, while upregulation protects from apoptosis via NF-κB signalling *in vitro [381-383]*. Some downstream partners show decreased transcription such as integrin linked kinase (log2 fold change -0.9).

It should be noted that not all DEGs mapped to the pathway agree with activation of signalling based on the direction of their expression modulation by *B. breve* UCC2003. For example, Ras homolog family members C, D, G, T2 and V are downregulated (log2 fold change -0.9 to -2.2) which are involved in cytoskeletal reorganisation and transcriptional regulation.

This pathways analysis indicates that *B. breve* UCC2003 upregulates IEC integrin expression and signalling in neonatal IECs. I also observed other pathways that were differentially modulated, and additionally, as is often the case with global transcriptional pathway analysis; some pathways had both up- and down-regulated genes making conclusions difficult. It should be mentioned that my applied model utilises conventionally raised mice, which have been exposed to microbial stimuli for the duration of their life span, and thus the introduction of a single commensal bacterial species to the established microbiota, which may also explain the low number of clearly induced, strong signalling pathways.

5.3.6 Small intestinal epithelial cells of adult mice show discrete transcriptional changes induced by *B. breve* compared to neonate mice

Quality control of the adult dataset by Shrinkage Estimation of Dispersion shows most genes closely associate with the line of best fit, and most genes used for second dispersion estimation (Figure 5-13.A).

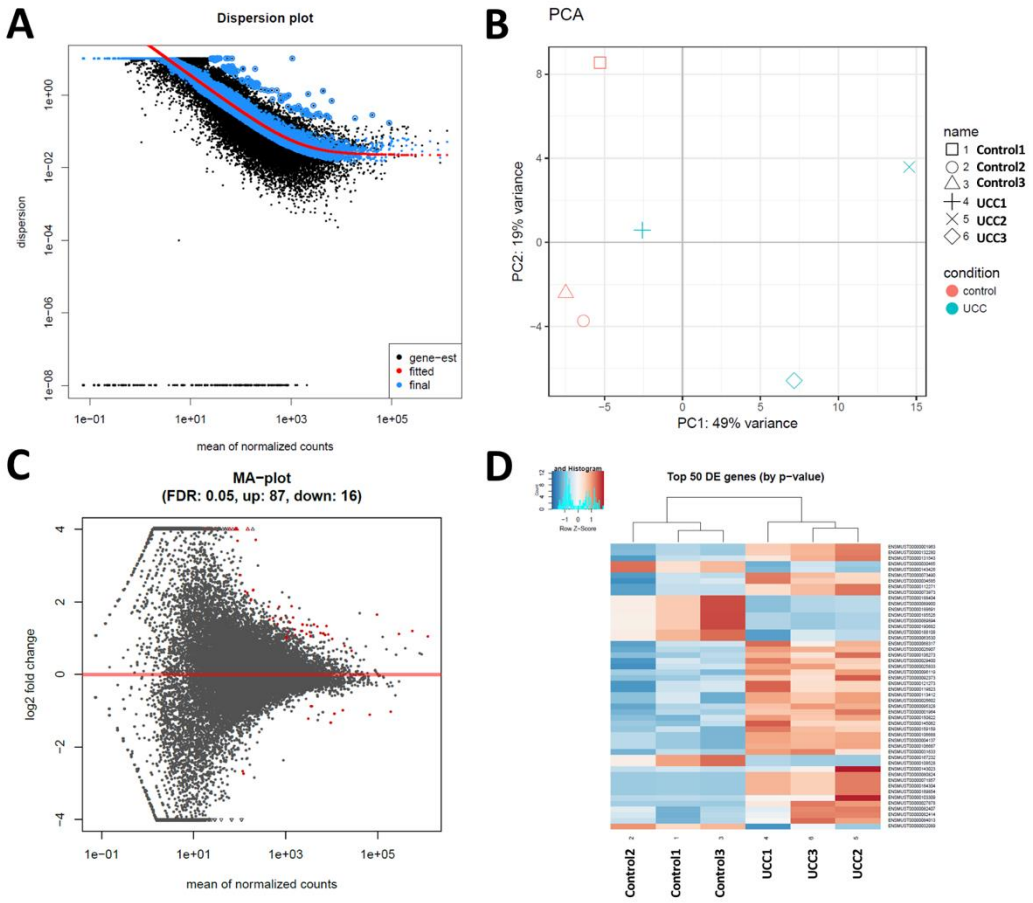

Figure 5-13 ***B. breve*** **UCC2003 colonisation of adult mice induces small changes to intestinal epithelial transcriptome**

Overview over transcriptional changes in IECs of adult mice colonised with *B. breve* UCC2003 relative to control (PBS gavaged) **A** Shrinkage estimation of dispersion, y axis dispersion estimate, x axis mean of normalised counts, black dots individual genes, red line maximum likelihood estimation (MLE) line of best fit, black dots circled in blue – potential dispersion outliers, blue area around red line – genes used for second dispersion estimate (not outliers), **B** PCA plot of group variability **C** Bland Altman (MA) plot of transcriptional modulation by presence of *B. breve* UCC2003 relative to

control, y axis log2 fold change of gene expression, x axis – mean of moralised counts, red dots – statistical sig genes (q values 0.05) **D** Hierarchical clustering of samples based on TOP 50 differentially regulated genes.

The biological repeats present with clear separation between groups based on a PCA (Figure 5-13.B), except for one sample in the *B. breve* colonised group (UCC1), which is more similar to control group gene expression, but colonisation level analysis by plate counts showed similar cfu counts compared to biological repeats. Based on the MA plot (Figure 5-13.C), 87 DEGs are upregulated, while 16 are downregulated.

The samples based on hierarchical clustering (Figure 5-13.D) associate within their groups based on analysis of the top 50 DEGs (p-value < 0.05), with this data set showing a more heterogonous gene expression between groups (compared to neonate samples).

As with the analysis of the neonate dataset, initially genes with highest fold changes were investigated to understand the biological process of B. breve UCC2003 modulation on adult IECs (Table 5-8, Table 5-9).

Table 5-8 Differentially expressed genes with strongest positive fold change induced by *B. breve* UCC2003 in adult IECs

Mapping pipeline alterations identified transcripts ID which were translated to gene IDs, duplicate transcripts with identical expression and q-values are represented by a single entry with total number of transcripts given in column "DEG transcripts", q value cut-off < 0.05.

Expr Log Ratio	DEG transcripts	q-value	Ensemble Transcript ID	Ensemble Gene ID	Gene Symbol	Entrez Gene Name	Location
8.223	1	0.0192	ENSMUST00000070639	ENSMUSG00000074417	LILRB3	leukocyte immunoglobulin like receptor B3	Plasma Membrane
8.179	1	0.00497	ENSMUST00000103309	ENSMUSG00000076508	Igkv17-127	immunoglobulin kappa variable 17-127	Other
8.011	4	0.00539	ENSMUST00000071857	ENSMUSG00000056917	SIPA1	signal-induced proliferation-associated 1	Cytoplasm
7.902	1	0.018	ENSMUST00000162110	ENSMUSG00000064202	4430402I18Rik	RIKEN cDNA 4430402I18 gene	Other
7.739	1	0.0334	ENSMUST00000035667	ENSMUSG00000041000	TRIM62	tripartite motif containing 62	Cytoplasm
7.222	3	0.00635	ENSMUST00000027878	ENSMUSG00000026586	PRRX1	paired related homeobox 1	Nucleus
7.117	4	0.0199	ENSMUST00000167317	ENSMUSG00000026358	RGS1	regulator of G protein signaling 1	Plasma Membrane
5.134	6	0.0155	ENSMUST00000145440	ENSMUSG00000026222	Sp100	nuclear antigen Sp100	Nucleus
4.771	1	0.0463	ENSMUST00000177368	ENSMUSG00000079323	Ip6k1	inositol hexaphosphate kinase 1	Cytoplasm
4.105	1	0.00497	ENSMUST00000143023	ENSMUSG00000022957	ITSN1	intersectin 1	Cytoplasm
3.705	1	0.0000562	ENSMUST00000031633	ENSMUSG00000038656	CYP3A5	cytochrome P450 family 3 subfamily A member 5	Cytoplasm
2.734	1	0.0188	ENSMUST00000079443	ENSMUSG00000035299	MID1	midline 1	Nucleus
2.328	1	0.0339	ENSMUST00000085671	ENSMUSG00000055991	ZKSCAN5	zinc finger with KRAB and SCAN domains 5	Nucleus

Table 5-9 Intestinal epithelial transcripts with strongest downregulation in adult mice induced by *B. breve* UCC2003 colonisation

Mapping pipeline alterations identified transcripts ID which were translated to gene IDs, duplicate transcripts with identical expression and q-values are represented by a single entry with total number of transcripts given in column "DEG transcripts", q-value cut-off < 0.05.

Expr Log Ratio	DEG transcripts	q-value	Ensemble Transcript ID	Ensemble Gene ID	Gene Symbol	Entrez Gene Name	Location
-2.731	3	0.00497	ENSMUST00000108528	ENSMUSG00000033847	PLA2G4C	phospholipase A2 group IVC	Plasma Membrane
-1.326	9	0.000267	ENSMUST00000089894	ENSMUSG00000055827	GSDMC	gasdermin C	Cytoplasm
-1.109	1	0.00323	ENSMUST00000032089	ENSMUSG00000030017	REG3G	regenerating family member 3 gamma	Extracellular Space
-1.021	1	0.011	ENSMUST00000096904	ENSMUSG00000071356	REG3A	regenerating family member 3 alpha	Extracellular Space
-0.876	2	0.00562	ENSMUST00000030465	ENSMUSG00000028699	TSPAN1	tetraspanin 1	Cytoplasm

The most upregulated gene is leukocyte immunoglobulin like receptor B3 (log2 fold change 8.2), which are expressed exclusively in immune cells highlighting, together with strong upregulation of immunoglobulin kappa variable (log2 fold change 8.1), a potential contamination of the IEC isolations by other cell types (Table 5-8). Nuclear antigen SP100 is part of the nuclear body that regulates gene transcription (potentially in response to leukaemia and viral infections), and a regulator of g-protein signalling 1, are both upregulated (fold2 change 8 and 7.1) [384]. However, these genes are involved in various cellular processes, and without identification of specific up or downstream interactors, no definite biological mechanism can be identified for the increased transcription levels.

The list of downregulated genes in adult IECs by *B. breve* (Table 5-9) contains 4 unique genes. Phospholipase group A2 is a digestive enzyme involved in digestion of fatty acid glycerol, while gasdermin C belongs to a family of proteins exclusively expressed in the skin and the GI tract, with its upregulation suggested in colon rectal cancer [385, 386]. RegIII-γ is an anti-microbial peptide that convers its function through cell wall destruction via binding to peptidoglycans [387].

Overall, I was not able to identify specific targets or pathways potentially involved in the protective effect of *B. breve* analysing adult IEC transcription. This potentially supports the suggestion that bifidobacteria intestinal colonisation conveys a stronger host modulatory effect in early life, due to the not yet fully trained host immune system, as well as stronger modulatory effects on microbiota composition. The mechanism for LPS induced apoptotic cells shedding observed in adult mice remains to be identified.

5.3.7 miRNA21 expression predicted to be downregulated by *B. breve* UCC2003 in neonate IECs

The utilised RNA-Seq approach involved isolation of RNA from tissues using a protocol that excludes transcripts with a length < 200 nt, which excludes small RNAs (18-24 nt) from the sequencing step. In addition, samples were processed by polyA pulldown, in addition to paired end sequencing generating reads > 200 nucleotides, which is optimised to enrich for mRNA, and generate long reads that aids assembly and gene mapping, but is not suitable for profiling of small RNAs.

More recently, it has become clear that small RNA types (18-24 nucleotides), including miRNA and siRNAs, play important biological roles. However, for such additional analysis, alongside mRNA RNA-Seq, I would have needed to perform additional sequencing runs, which was out with the scope of this PhD project.

Within my datasets I did observe a small number of mRNA read counts, but previous studies have indicated that the applied protocol does not allow for accurate quantification, as read counts do not always correlate with an actual abundance, due to the bias introduced during sample processing. Therefore, I did not take these results forward for additional analysis [388].

However, to potentially still investigate involvement of small RNAs in the observed transcriptional response to *B. breve*, I took an approach that used the DEG datasets from host mRNA to predict potential regulation of sRNAs, based on the expression of their known and predicted targets utilising IPA "upstream regulator" calculation. My analysis suggested miR21 to be downregulated, which appeared to be a promising target as it has previously been shown to be overexpressed in IECs of patients with UC, while *in vitro* overexpression decreases TEER, due to impaired TJ integrity [389].

The neonate IEC dataset was used to make this prediction and was based on 60 out of 87 DEGs that are known targets of miR21 and expressed to match with their expression response (upregulation) with the predicted decrease in miR21 expression (Supplementary Table 5). Further support for miR21 being modulated by *B. breve*

was the fact that miR21 reads counts were also present in the RNA-Seq sequencing data with a decrease in *B. breve* UCC2003 gavaged neonate IEC samples.

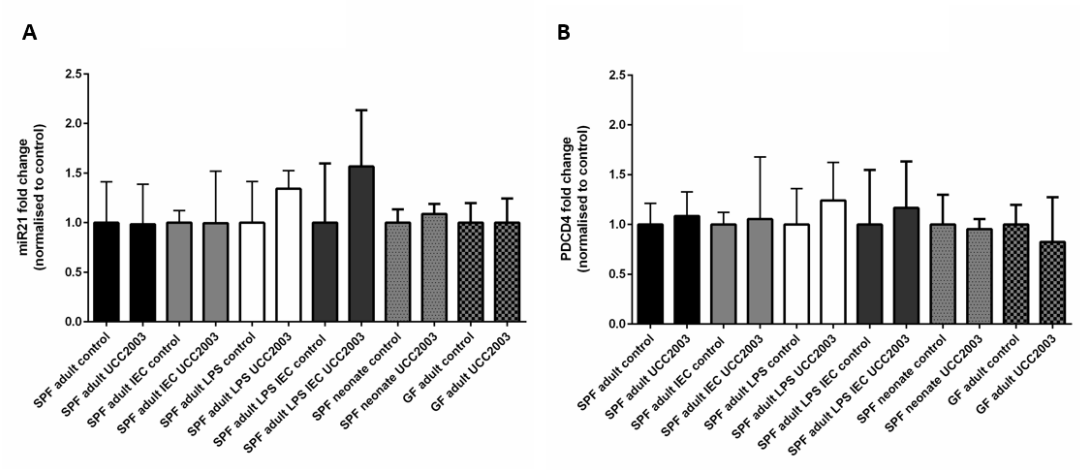

Figure 5-14 ***B. breve*** **UCC2003 colonisation does not modulate miR21 and its downstream target PDCD4 expression in whole small intestine and epithelial cells.**

(**A**) miR21and (**B)** PDCD4 expression in small intestinal tissue (whole small intestine and IECs) of conventionally (SPF) raised adult (12 weeks), neonate (2 weeks), SPF adult mice with elevated small intestine apoptotic cell shedding and germ free (GF) mice with and without *B. breve* UCC2003 colonisation, mice were colonised with *B. breve* UCC2003 by oral gavage (10^9 cfu) on three consecutive days and tissue collected on day 4, intestinal cell shedding induced by IP injection of 1.25 mg/kg LPS on day 4 and tissue collection 90 min post administration, IEC isolated from small intestinal tissue, RNA extracted from IEC isolations and whole small intestine samples, miR21 and PDCD4 expression assessed by qPCR, expression normalised to housekeeper and presented as fold change compared to age, colonisation status and treatment matched control group, data shown as mean +/- SD (SPF adult n=5, SPF neo n=5, GF adult n=6, DSS n=6).

To validate this prediction, I subsequently analysed miR21 expression changes in mouse tissue in response to *B. breve* colonisation utilising a miR specific qPCR amplification and qPCR protocol. Contradictory to what the pathway analysis had predicted, I observed that expression was not altered during homeostatic conditions in IEC and WSI of neonatal mice, as well as adult and GF mice (Figure 5-14.A). As this miRNA has been implicated to play a role in UC, I also analysed intestinal tissue from LPS challenged mice, and observed that pre-colonisation with UCC2003 induced a potential increase in miR21 expression, with a stronger response in IECs than in the WSI. A known downstream target of miR21, tumour suppressor

programmed cell death 4 (PDCD4), has previously been implicated to be protective in progression and metastasis of colon cancers [390]. A reduction in miR21 expression would theoretically increase PDCD4 expression as the miRNA targets PDCD4 transcripts for degradation [391]. However, expression of PDCD4 was not altered in any of the analysed samples (Figure 5-14.B), but it should be noted that miR21 has a large variety of targets, and the approach, inferring miRNA regulation via mRNA pathway analysis, may not cleanly dissect true biological differences, which is why further validation and investigation is required.

In addition to examining miR21 in the SI, I also analysed expression in the LI, and intriguing noted that miR21 expression was significantly downregulated in *B. breve* colonised mice in both adult and neonates. Additionally, in large intestinal samples collected from mice with DSS-induced colitis, miR21 transcription was also significantly decreased by presence of *B. breve* UCC2003. However, PDCD4 was also downregulated in these samples, and a decrease in miR21 would be expected to increase PDCD4 transcript levels due to reduced levels of degradation (Supplementary Figure 12).

To summarise, *B. breve* appears to induce distinct transcriptional responses in IECs of neonatal mice. The investigation of signalling networks suggests an upregulation of integrin signalling, as well as the induction of TLR2 and TLR9, as well as IL17C. Importantly, these targets have been shown to play critical functions within the IE, and these data highlight *B. breve*-associated beneficial traits with respect to host-microbe cross-talk.

5.4 Discussion

The integrity of the IE is essential for human health, and a break down in this barrier has been associated with uncontrolled inflammation and disease. The microbiota plays a key role in positively regulating this barrier, but currently our knowledge on how specific bacterial members modulate IEC function is unclear. Whilst previous studies, including Hughes et al, have shed light on how beneficial microbes, such as *B. breve* UCC2003 may interact with the host via specific factors, i.e. via MyD88 signalling during intestinal inflammation, it has yet to be determined, at a more global level, what genes and pathways are modulated during homeostasis. Thus, in this chapter I sought to probe *B. breve*-IEC transcriptional cross talk by performing unbiased RNA-Seq on isolated small IECs from both adult and neonatal mice, and downstream DEG and pathway analysis. The aim was to pinpoint key IEC pathways that *B. breve* may modulate to promote improved barrier integrity during homeostasis, which may allow development of improved targeted microbiota therapies for both health and disease.

An important trait for any potentially beneficial microbiota therapy, such as *B. breve*, is the ability to colonise the GI tract, and also its specific localisation within the intestine e.g. within the mucus layer, or in direct contact with IECs. Faecal and intestinal cfu's revealed that *B. breve* UCC2003 was able to colonise the murine GI tract, and therefore would be expected to interact with the host. *B. breve* may interact with the host via secretion of metabolites, as previous studies using Caco-2 cells have shown that supernatants from other bifidobacterial species were able to prevent TNF-α induced epithelial disruption, and increased wound healing, which the authors postulated was via the SCFA acetate [281]. Furthermore, the presence of *B. breve* was shown to modulate the wider microbiota, including increases in *Lactobacillus and Bacteroides*, and decreases in *Balutia* and *Alistipes* in both adult and neonatal mice, which would also be expected to modulate available metabolites for IECs (e.g. butyrate). Indeed, previous studies have highlighted the cross-feeding activities of bifidobacteria, and these microbe-microbe interactions will be probed in more detail in chapter 6 [392].

Previous studies have also indicated that a more direct interaction of *Bifidobacterium* on host cells, via contact-dependent mechanisms, may play a key role in modulating host functions. In porcine IECs, co-culture with *B. breve* MCC-117 reduced the induction of pro-inflammatory cytokines in response to challenge by *E. coli* PAMPS [393]. Furthermore, previous studies with UCC2003 have shown that surface associated molecules such as the EPS capsule, appear to be critical for persistence within the GI tract, and that EPS negative *B. breve* UCC2003 mutant failed to induce protection of IECs during LPS-induced cell shedding [358, 394].

To reach the IE, microbes must first penetrate the mucus barrier. Interestingly, previous studies have suggested certain *Bifidobacterium* species have enzymes that can digest components on the mucus layer i.e. mucins, which may facilitate their GI localisation [395]. The SEM images suggest that *B. breve* is in close proximity with the IE, and therefore it is expected that this strain may be capable of directly modulating IEC responses. However, there are some limitations of these studies, particularly the fact that the methods for tissue collection do not preserve the mucus barrier completely, which hinders visualisation of *B. breve*. This could be addressed by colonising mice with a fluorescently labelled microbe, which would allow accurate visualisation within the lumen, and additionally could be used for longitudinal imaging of colonisation via 'live' imaging [396]. This clone is present within the lab, and will be utilised in future experiments to address the question of direct interaction of *B. breve* with the IE.

After confirmation of colonisation and localisation within the GI tract, the next step was to perform global unbiased transcriptional analysis of IECs by *B. breve* UCC2003 through an RNA-Seq approach during homeostatic or 'healthy' conditions. The SI was chosen as *B. breve* had been shown by Hughes *et al.* to have a protective effect at this site from LPS-induced cell shedding, and importantly I confirmed colonisation of the SI, albeit at lower densities than observed in the colon, and observed close contact of *B. breve* with the small IECs.

My analysis indicated a strong and distinct transcriptional IEC response in neonate mice, with the effect on IECs in adult being much weaker, with 10-fold lower number of DEGs. This could be attributed to several factors. The neonatal mouse microbiota, similar to the human infant microbiota, is less complex and considered

more plastic to change, such as the introduction of a new species at very high levels by oral supplementation. This is confirmed by the high abundance of *B. breve* UCC2003 in the neonatal group microbiota 16S rRNA profiles when compared to the adult group, which may indicate a higher abundance within the microbial community is directly attributable to greater transcriptional changes. These high levels could be further supported by the fact that *B. breve* UCC2003 is a human infant isolate, and able to metabolise HMO lacto-N-tetraose and lacto-N-neo-tetratose [397]. Although, mouse breast milk has a reduced number of milk oligosaccharides, when compared to HMO diversity, this diet would still be expected to selectively support the growth and colonisation of the neonatal mouse intestinal tract [398]. However, it may not just be an 'abundance game'. Previous studies have established that the early life microbiota has a stronger effect on the host, which is based on new bacterial-host interactions in an immunologically 'naïve' host, and in later life these responses have already been primed. This is in part shown by the fact that neonatal innate immune cells, expressing TLR ligands, respond to microbial ligands distinctively differently than adult immune cells, which is characterised by reduced production of inflammatory compounds, and an increase in regulatory cytokines (i.e. IL-10) [399]. Nevertheless, I was still able to detect modulation by *B. breve* on adult IECs, which could in part be explained by the low levels of *Bifidobacterium* present in these mice, and hence the ability to induce specific pathways. As highlighted, I also probed WSI (which includes immune, and various other cells types, alongside IECs) transcriptional responses to *B. breve,* and observed low number of DEGs in both neonate and adult mice. The training of the immune system by the commensal microbiota in SPF mice could explain the low levels of DEGs observed in WSI of adult and neonate mice, which may also correlate with the strong induction of DEGs in WSI of mono-colonised mice in response to *B. breve* colonisation.

Although there was a reduced transcription response in adult IECs to *B. breve,* downregulation of RegIIIγ was observed. Mice deficient for this antimicrobial compound present with increased contact between small intestinal villus tip IEC, and luminal bacteria, due to mucus alterations, and increased immune responses to pathogen colonisation via IFN and TLR3 dependent signalling [400]. Interestingly,

previous studies in GF mice have indicated that another *B. breve* strain, *B. breve* NC29950 induced RegIIIγ, while exposure to other single commensal bacteria such as *E. coli* JM83 did not [401]. Furthermore, the induction by *B. breve* required whole cells (live and dead), as exposure of Caco-2 cells lines to culture supernatant failed to increase RegIIIγ expression. In contrast to this mono-colonisation system, *B. breve* UCC2003, as part of a complete microbiota in a conventionally raised mice, with a developed immune system, may induce downregulation of RegIIIγ to improve colonisation, and aid interaction with the host, by allowing contact with the IECs.

Examining the neonatal DEGs in more detail revealed several interesting *B. breve*-induced targets were observed; upregulation of TLR2 and TLR9, and IL17C.

TLR2, which is expressed apically, is an important receptor for Gram positive MAMPs, including lipoproteins and peptidoglycan, which is present in cell walls. Notably, our previous work reported an increase in TLR2 expression in response to UCC2003 colonisation (potentially via EPS-capsule interactions), and which was suggested to signal via MyD88. Interestingly, TLR2 (and TLR4) are expressed at low levels on IECs, and in these neonatal mice, *B. breve* may upregulate this TLR to increase signalling via surface-associated factors to promote tissue homeostasis. Indeed, previous studies have shown, that TLR2 activation via protein kinase C, caused ZO-1 translocation, and increased intestinal barrier function, and MyD88 signalling via TLR2/4 was determined to be crucial for limiting mucosal adherence and penetration of microbiota members through production of Paneth cell α-defensins and RegIIIγ [402]. Collectively, these studies suggest that TLR2 plays a key role in protection of the IE, and may be one of the key targets for *B. breve* that drives beneficial IEC responses.

Another gene target of interest that is upregulated in neonatal IECs is TLR9. TLR9 is expressed in IECs and recognises unmethylated CpG sequences in DNA, and is located at the apical and basolateral side of specialised M cells (IECs associated with PP). Notably, GF mice do not apically express TLR9, and IBD patients have downregulation of TLR9 in intestinal biopsies. The consequences of TLR9 activation differs depending on the site of binding [20]. Exposure to ligands apically prevents NF-κB activation by ubiquitination, while binding at the basolateral membrane can cause activation by chaperon degradation, leading to IL-8 secretion.

Furthermore, apical stimulation of TLR9 can inhibit inflammatory IEC responses to basolateral binding, which suggests a level of tolerance induction, and a role for TLR9 in mediating host tolerance to luminal commensal bacterial. Mice deficient in TLR9 have low IECs NF-κB thresholds, and are more susceptible to DSS colitis, and in neonatal NEC models TLR9 deficient mice also present with increased symptoms of NEC, while activation of TLR9 signalling via bacterial DNA binding reduced the severity of NEC. Finally, the authors suggest that previous studies that observed attenuation of DSS colitis and NEC by probiotic bacteria, including *B. longum*, *B. breve*, *B. infantis*, may be mediated via the TLR9 receptor signalling cascade, and further suggests the utility of *B. breve* in possibly modulating IEC functions [403].

TLR3, while showing a less pronounced upregulation, nevertheless could have a strong biological effect, as its presence in IECs is inversely correlated with susceptibility to rotavirus infection. High levels are detected in adult mice, which are resistant to infection, while adult TLR3 IEC KO mice show higher colonisation [404]. Furthermore, TLR3 expression is low in suckling neonate mice, and human infants, and expression increases during the first 3 weeks of life. Interestingly, in neonates TLR3 IEC KO did not affect or worsen susceptibility to infection suggesting an essential role of TLR3 in adults, while responses in neonates are TLR3 independent [404]. It could be hypothesised that *B. breve* is involved in the observed increase in expression as mice mature, and hence is important for the host defence against viruses.

The IL-17 cytokine family are strong inducers of inflammation, and are critical for pathogen protection. Within this family there are several isoforms (IL-17A-F), which have been shown to have distinctive roles. In response to *B. breve* colonisation, IL-17C was found to be significantly upregulated in IECs, and previous studies have indicated this isoform is important for modulating cytokine production, and stimulation of anti-microbial peptides in the GI tract. IL17C signalling, via IL-17RA/IL17RE receptor complex, reacts to pathogen colonisation by modulating innate immune response and barrier function [405]. In response to *C. rodentium* infection, IL-17C was upregulated in colonic IECs, and in synergy with IL-22, increased anti-bacterial peptides, pro-inflammatory cytokines and chemokines (e.g. TNF, IL-1β, RegIIIγ). Interestingly, *B. breve* UCC2003 has been shown to reduce *C.*

rodentium load in the GI tract, which was postulated to occur via direct colonisation resistance mechanisms (i.e. biofilm formation), but may also be linked to IL-17C modulation, and which would be of interest to pursue in future studies [358]. Studies using IL-17C KO mice, indicated greater susceptible to DSS-induced colitis, which was linked to increased IL-17A production, and reduced barrier integrity. These authors also showed that IL-17C directly regulated expression of occludin in colonic IECs, and another study using human tracheobronchial epithelial cells, indicated that IL-17 (together with IL-6) increases mucus glycoprotein genes MUC5AC and MUC5B expression, which could also be involved in enhancing barrier function [406]. These studies, together with my RNA-seq data, indicate IL17C as a promising *B. breve*-modulated target, which could be targeted to promote host defence against pathogens, and priming of the IE, via TJs, and potentially mucins.

While the observed increase in IL-23 expression in neonate IECs by *B. breve* may be associated with a negative role in intestinal inflammation and in IBD, recently IL-23 has been attributed health beneficial and protective effects, specifically in IECs [407]. IEC can produce IL-23 when stimulated by lymphotoxin beta receptor signalling, which aids in colonic wound repair, and offers protection from DSS-induced colitis [407]. This effect is IL-22 dependent, which mediates the observed increased IEC survival and mucus production. Interestingly, IL-22 receptor unit alpha expression was also upregulated in the presence of *B. breve*. Hence, it could be proposed that under homeostatic conditions, *B. breve* increases IL-23 signalling as mean of modulating intestinal homeostasis, which when an inflammatory stimulus occurs (such as LPS) this keeps the immune system response in check.

Use of pathway analysis, to expand the investigation into broader intestinal processes modulated by *B. breve*, revealed integrin signalling upregulation in neonate IECs. Integrins are a large family of transmembrane spanning proteins, which can induce cellular signalling and connect the extracellular matrix to the intracellular cytoskeleton, and are essential for intestinal epithelial barrier maintenance to macromolecules [408, 409]. Importantly, ITAG4 and ITAGV, which are upregulated in response to *B. breve* colonisation in neonate IECs, have recently been identified as IBD related SNP targets [410]. These mutations in B and T cells, resulted in increased expression, which the authors related to an increase in pro-inflammatory

responses in these immune cells, but highlighted that this hypothesis requires investigation in biological samples. Integrin signalling also play a critical role in maintenance of the epithelial barrier as previous studies have indicated with integrin αvβ6 maintaining IE integrity in T84 monolayers measured by trans epithelial resistant (ion flux) and permeability to macromolecule ovalbumin. Knockdown of this integrin increased macromolecule permeability, but not transepithelial crossing of ions [409]. In combination with cell matrix interactions and transmembrane signalling, one of the central roles of integrins is as a key regulator of cell differentiation, which has been well studied in the epidermis [411, 412]. As the IE is one of the fastest regenerating tissues of the human body, constant cell differentiation and migration is taking place. Integrins are expressed and involved in IE differentiation, but their role is this process is not well understood. Interestingly, the separation of IECs from the LP triggers anoikis (specific form of apoptosis) including signalling cascades, which are part of the integrin signalling pathway. Based on this knowledge, the effect of overexpression of integrin α5β1 in rat small intestinal cell lines RIE1 protected these cells from apoptosis when exposed to cytotoxic agents (aspirin, staurosporinem, etoposide). However, overexpression of subunit α2 did not induce protection [413].

As the integrin family is diverse in structure and composition (two subunits form one functional dimer), it could be argued that even though one major subunit (i.e. α5β1) involved in apoptosis protection is not differentially regulated, the overall increase in expression, as well as upregulation of one subunit (i.e. β6 involved in improved IE barrier function), provides strong evidence for further exploration of the involvement of these complex integrin mechanisms in *B. breve* IEC modulation and potential protection [414]. Additionally, colonisation of *B. breve* UCC2003 three days prior to tissue collection could have already induced cytoskeletal and transcriptional changes, with integrin signalling having returned to baseline levels, while cytoskeletal and protein level modulation, are retained, but not measured by RNA-seq. Furthermore, mitogen activated kinases were both up and downregulated; myosin light chains and myosin light chain kinase decreased in transcription, while myosin phosphatase Rho interacting protein showed higher mRNA levels, potentially suggesting cytoskeletal

reorganisation. It remains a possibility that changes to FA, and TJs are not only expression dependent, but also occur post translationally.

miRNAs play a critical role in global transcriptional responses and downstream functions, therefore my first validation experiment from the RNA-Seq datasets was further investigation of miR21, as overexpression of miRNA has previously been linked to both mouse and human IBD studies. Although, pathway analysis predicted downregulation of miR21 within small IECs in *B. breve* colonised mice, and downstream targets, this was not supported by further qPCR studies. Previous studies have indicated that *in vitro*, miR21 expression was increased in response to TNF-α mediated intestinal epithelial TJ breakdown [415]. In the same polarised Caco-2 cell line, miR21 expression correlated inversely with epithelial barrier permeability. Comparing between GF and conventionally raised mice, Nakata *et al.*, observed microbiota colonisation to induce miR21 expression, and regulate epithelial barrier function via upregulation of ADP ribosylation factor 4 transcription (ARF4). This small GTPase was found to be upregulated when miR21 targets programmed cell death 4 (PDCD4) and phosphate and tensin homolog PTEN were suppressed [416]. Notably, I did not observe major changes in miR21 expression in the SI induced by *B. breve* UCC2993 colonisation (except for the slight increase in in IECs and WSI during LPS induced cell shedding, but there was great intergroup variability), which may indicate *B. breve* does not have a significant role to play in miR21 regulation in the SI. However, I did observe a significant decrease in miR21 in *B. breve* UCC2003 colonised whole colonic tissue. This reduction during DSS-induced colitis suggests miR21 as a potential target for health beneficial effects specifically within the colon. However, PDCD4 (shown by Nakata *et al.* to be supressed by miR21) also showed decreased expression in the same samples. PDCD4 has been shown to have a beneficial role in colorectal cancer, while its suppression in Caco-2 cells caused a decrease in epithelial barrier function via GTPase ARF4, and its apparent downregulation by *B. breve* requires further investigation [416].

In summary, this study generated global transcriptional datasets of host responses to *B. breve* intestinal colonisation in neonatal and adult mice. A distinct response by neonate IECs was observed, with promising targets that are potentially involved in

the host health beneficial effect of *B. breve*. These targets include TLR2, TLR9, IL-17C, and integrin signalling, and which will be explored further in subsequent studies.

5.5 Future plans

The results generated so far are the first steps in understanding the host health beneficial effects of *B. breve*. Fundamental to confirm these data, is validation of the identified targets by qPCR. Following this analysis, tissue staining of TLR9, to observe its location relative to IEC baso-apical axis, would be performed. These further studies should be performed on both neonatal samples, as well as adult tissue samples, as translocation can occur within the intestinal cell membrane, which could change numbers of TLR9 receptors present at the apical surface. Previous studies have indicated expression of TLR9 in jejunal and colonic biopsies, as well as Caco-2- cell lines, and TLR9 expression within the human jejunum is promising as it suggests that human small intestinal cells could be used for *in vitro* co-culture with *B. breve*.

Integrin upregulation would also be of significant interest to pursue further as it is induced in both neonate and adult samples. Preliminary experiments would involve validation of RNA-Seq results, followed by integrin staining to assess location within the IE. Measurements of TEER, in presence and absence of *B. breve* in combination with different integrin inhibitors, would be a potential avenue to explore. An alternative approach would be the use of cell type specific integrin KO mice, which would allow for observation of *B. breve* UCC2003 modulation of integrins in a translational model.

Additional, the observed upregulation of IL-17C transcription by *B. breve* poses a promising target to investigate further, particularly with respect to its role in pathogen defence (i.e. *C. rodentium*), which also correlates with previous *B. breve* pathogen protection studies [358, 405]. Following preliminary experiments *in vitro,* observing IL-17C induction in intestinal cell lines co-cultured with *B. breve*, KO mice for IL-17C (commercially available) could be utilised for *C. rodentium* infection studies, which would allow generation of more translational results. As *B. infantis* reduces NEC incidence in neonate rats, potentially by preventing overgrowth of pathogenic or opportunistic pathogenic bacteria, and bifidobacteria being a prominent member of the “normal” infant gut microbiota, bifidobacterial-induced IL-17C could potentially confer health beneficial effects against pathogen invasion at this important age stage.[417, 418].

The downregulation of miR21 in large intestinal samples colonised by *B. breve* is an interesting observation, and although out with the focus of this investigation, is a potentially promising avenue to explore. Initially, expression of other downstream targets of miR21 could be investigated, as one important downstream target, PDCD4, was observed to be downregulated in samples with decreased miR21 expression, while an increase was expected. Recently comparing GF with conventionally raised mice, an increase in miR21 in the presence of the microbiota was observed, with accompanying decrease in PDCD4, and increase in ADP ribosylation factor 4 (ARF4), which *in vitro* has been shown to increase epithelial permeability [416]. Hence ARF4 expression would be a high priority target to investigate *in vivo*, in combination with measurements of *B. breve* UCC2003 modulation of epithelial permeability.

As mentioned above, understanding how *B. breve* modulates IEC function, either via direct interactions with the host, and/or indirect effects modulated via metabolites or bacteria-bacteria interactions is central to developing novel therapies. This requires a meta-functional analysis of the microbiota as well as *B. breve* itself. An overlay of host and bacterial functional data in form of RNA-Seq has been coined dual RNA-Seq or paired RNA-Seq and has been applied successfully in shedding light on host-microbe interactions [419]. The initial results generated using this approach will be presented in the next chapter.

6 *B. breve* UC2003 transcription shows distinct modulation during colonisation of gnotobiotic and conventionally raised mice, and affects wider microbiota function

6.1 Introduction

In the previous chapter, I have shown that *B. breve* is able to induce distinct transcriptional responses in adult and neonatal mouse IECs. This modulation could potentially play an important role in host wellbeing, and thus help define *B. breve*-associated beneficial effects that could be harnessed to promote homeostasis, and/or modulate disease pathogenesis. Probing the role of *B. breve* on host responses is key to defining pathways that are modulated by this bacterium, however to more comprehensively determine what microbial factors may modulate these host changes it is important to explore *B. breve* transcriptional responses *in vivo*, and also determine how introduction of *B. breve* into the wider microbiota may modulate the metatranscriptome, and intestinal metabolome. The aim is to identify specific changes induced by *B. breve* colonisation, and identify microbial genes/pathways that could potentially be targeted for further development of more 'personalised' probiotics.

6.1.1 Bifidobacteria metabolism: impact on the host, and wider microbiota via cross-feeding

Carbohydrates represent the main energy source within the human diet, and are essential for host and microbiota metabolism Their bio-availability depends strongly on their structure, and this influences their uptake along the GI tract. Simple carbohydrates, such as sugars (e.g. lactose and sucrose), are absorbed in the upper part of the intestinal tract by the host, and residing members of the microbiota such as *Lactobacillus* [251]. In the colon, the main site of bifidobacterial intestinal colonisation, available carbohydrates are more complex, and as such they avoid digestion and uptake by the host, and thus represent an important dietary source for microbial fermentation [420]. Plant derived complex carbohydrates include pectin, xylans, and hemicellulose, while mucins and glycosphingolipids are available host

CHs [420]. Furthermore, microbial associated carbohydrates, such as EPS capsules, also contribute to the wide variety of available carbohydrates in the gut [421].

Bifidobacteria have been shown to be able to metabolise a wide range of these carbohydrates found in the mammalian diet (defined as heterofermentative), particularly within the colon. This carbohydrate degrading ability is due to a series of carbohydrate-degrading enzymes encoded in the genome, which allow for breakdown of polymeric carbohydrates to monosaccharides; processed by fructose-6-phosphate phosphoketolase (hexose fermentation pathway). This enzyme is a key part of the "bifid" shunt, as bifidobacteria lack the ability to ferment glucose by aldolase (part of glycolysis), or glucose-6 dehydrogenase (hexose monophosphate pathway) [422]. This fermentation pathway process yields glucose, lactate and acetate, and distinguishes bifidobacteria from other gut-associated microbiota members e.g. *Lactobacillus*.

Other enzymatic pathways essential for bifidobacteria are GHs, which help cleave complexes into smaller fragments. GHs in the human genome do not process the main complex carbohydrates found in diet (e.g. fructo- and galacto-oligosacharides, inulin, etc.) [253]. However, these components can be fermented by bifidobacteria, making metabolites available to the host, and also other microbiota members lacking GHs. Analysing the overall distribution of GHs in the microbiota, bifidobacteria contain more than half, giving the genus an essential role in complex carbohydrate fermentation in the human intestine [253].

As these carbohydrates have specific growth promoting effects on bifidobacteria they have been widely used as prebiotics, defined as 'a substrate that is selectively utilised by host microorganisms conferring a health benefit' [423]. Notably, previous studies have indicated a beneficial role for prebiotic supplementation in rodent models; administration of resistant starch and fructooligosacharides to rats, increased *Bifidobacterium* and *Lactobacillus* cfu, which was correlated with increased barrier function, via MUC-2 upregulation, and an increase in the mucus barrier [424].

The fermentation of CHs is involved in cross feeding between bifidobacterial species, and other gut microbes. This involves sharing of shorter carbon chain

molecules produced by breakdown, or production of lactate and acetate, both compounds produced via bifidobacterial metabolism. This interaction has been demonstrated both for plant and host derived CH sources. For example, lactate and acetate produced by two *B. adolescentis* strains, via fermentation of either starch or fructo-oligosaccharides, was processed by *E. hallii* to butyrate, a SCFA essential for IEC metabolism [132]. Host derived CHs, such as mucins, also play a key role in intra-genus ecosystems, as *B. breve* UCC2003, whilst lacking the ability to digest mucus independently, and is able to grow by feeding on mono- saccharides, when co-cultured with *B. bifidum* PRL2010, via this strains ability to breakdown mucins.

During infancy, HMOs are a major component of the diet, and reach the colon undigested, in contrast to simple sugars, which are absorbed by the host directly. Various bifidobacteria possess the ability to metabolise HMOs, which gives them a competitive advantage, and preferentially selects these strains as early colonisers. *B. bifidum* and *B. longum subsp. infantis* possess the genetic machinery to completely process a wide variety of HMOs, while *B. breve* can only digest certain HMOs, however it does utilise downstream HMO metabolites produced by other bifidobacterial strains [259].

Iron is an essential micronutrient, which is critical for growth and persistence of bacteria within the intestine. Pathogens express iron-sequestering mechanisms to improve their colonisation success [425]. Bifidobacteria also encode iron uptake systems, and previous studies have indicated that *B. breve* UCC2003 has two putative systems; sifABCDE, which is involved in ferrous iron transport, and the bfeUO-encoded transport system, which imports both ferrous and ferric iron [426].

Vitamins can be produced and utilised by microbiota member, and are essential for overall health of the host and the wider microbiota. Folate production has been identified in several strains of *Bifidobacterium,* including *B. adolescentis* MB239 [427]. Notably, folate is linked to increased IEC turnover, with potential negative effects on colon rectal cancers, but additive folate supplementation is often suggested to patients with IBD, to reduce symptoms and relapse [428, 429].

Bifidobacteria produce a vast array of metabolites in response to dietary supplementation in the host, which are key for host wellbeing, and IEC function.

Efficient colonisation of these bacteria within the GI tract is also important for these downstream metabolic activities, and in this respect EPS capsules and pili may be expected to play a key role as discussed in section 1.4.4. Thus, this microbiota genus represents a key player to probe transcriptional changes *in vivo*, examining both intra-strain responses (i.e. *B. breve* UCC2003), and also inter-microbiota responses.

6.1.2 Differences in the microbiota between mouse models and humans

The use of mouse models to study human physiology has been discussed with regards to genetic, immunological, and intestinal epithelial differences in the general introduction. In this section, I will give a brief overview of the mouse microbiota in comparison to the human intestinal bacterial community (summarised in Figure 6-1).

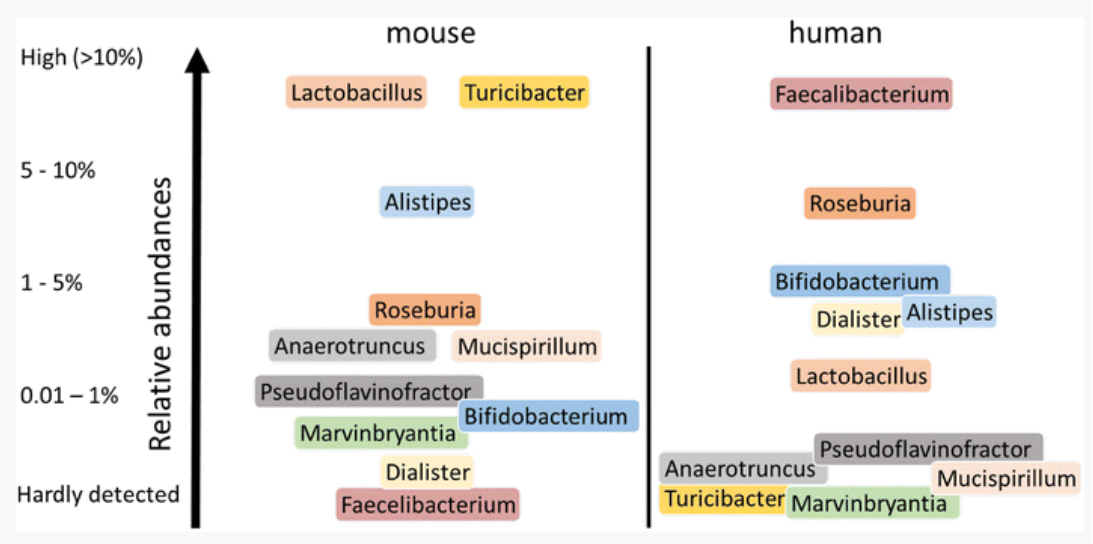

Figure 6-1 Overview over the bacterial composition and abundance of human and mouse microbiota at genus level

based on the published mouse catalogued and human microbiota studies, amended from Hugenholtz & de Vos, 2017 [430].

Human and mouse microbiota's share similarities when compared at the phyla level, with Bacteroidetes and Firmicutes being the most abundant [216]. Notably, a recent publication has generated a catalogue of mouse gut metagenomes of 184 mice,

including different strains, providers, and different mouse facilities [431]. This study is the most holistic to date, and is an excellent reference for future mouse studies. The analysis showed 541 total species in the mouse microbiota, with 26 ‘core’ species. Interestingly, the mouse microbiota shows functional similarity with the human microbiota, as 95.2% of KEGG orthologous groups are shared, but only 4% of the mouse gut bacterial genes are present in the human microbiota. Crucially, the main driver of differences in microbiota composition between mice is supplier, followed by facility. This highlights the importance of consistency when performing mouse microbiota experiments, as it has been shown that even within the same facility changes occur to the intestinal bacterial community. Hence, it has been suggested to co-house mice for as long as possible to account for inter-animal variation, and potentially retain samples or animals with the “original” microbiota composition mice for later experiments [430].

6.2 Hypothesis and aims

6.2.1 Hypothesis

B. breve transcriptional profiles differ when in an *in vivo* environment, and in the presence of a diverse microbiota, which may link to modulation of wider microbiota profiles, and host IEC responses.

6.2.2 Aims

1. Analyse the *B. breve* UCC2003 transcriptome *in vivo* (both SPF and GF models), and compare to *in vitro*
2. Assess changes to the overall microbiota metatranscriptome to identify modulation by *B. breve* UCC2003 colonisation
3. Investigate the effect of *B. breve* UCC2003 on the metabolome of the intestinal tract
4. Observe potential direct interactions between host and *B. breve* via membrane vesicles and transcriptional regulation via miRNAs studied *in vitro*

6.3 Results

6.3.1 *B. breve* UCC2003 transcription is distinctly different comparing *in vitro* with *in vivo* gnotobiotic, and conventionally raised intestinal conditions

Here, I present an investigation into the global transcriptome of *B. breve* UCC2003 *in vitro*, and *in vivo*, both in gnotobiotic and conventionally raised mice, to assess specific genes/pathways that may be involved in colonisation process, modulation of the wider microbiota, and IEC modulation (as presented in chapter 6.3).

6.3.1.1 Overview of experimental design to investigate changes to microbiota transcription, taxonomy and metabolomic profile in response to *B. breve* UCC2003 colonisation

To analyse the intestinal microbiota metatranscriptome, the colonisation model previously applied (chapter 5.3) was used. In brief, SPF and GF mice were colonised by oral gavage with 10^9 cfu on three consecutive days. Following 24 hours post the last administration, intestinal contents and faeces were collected (Figure 6-2).

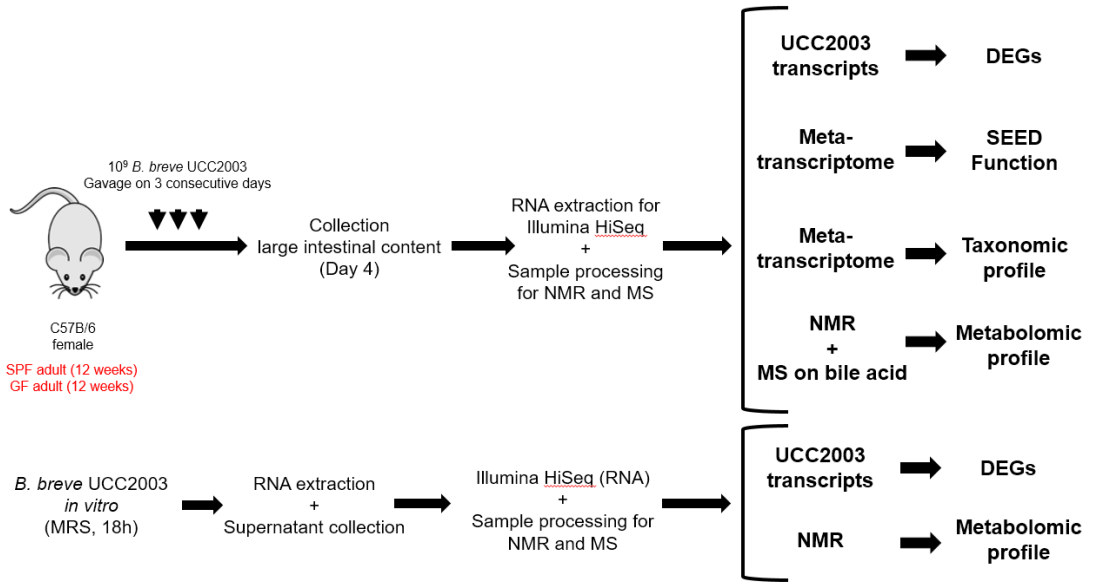

Figure 6-2 Analysing metatranscriptome and metabolome in vitro and in vivo in response to *B. breve* UCC2003 colonisation

C57B/6 adult (12 weeks) SPF and GF mice were colonised by oral gavage (10^9 cfu) with *B. breve* UCC2003 on three consecutive days, large intestinal contents were collected 24 hours post last gavage (day 4), assessment of in vivo samples by RNA extracted and sequenced using Illumina HiSeq and processed for identification of differential gene expression of UCC2003 transcripts (Bowtie2 alignment to *B. breve* UCC2003 reference genome, HTseq read counts, differential expression DeSeq2), microbial taxonomy and SEED functions of metatranscriptome (SUPER-FOCUS), metabolomic analysis of large intestinal contents by NMR and of isolated bile acid fraction by MS, assessment of *in vitro B breve* UCC2003 gene expression and metabolomic profile by culturing in MRS for 18 h, RNA extracted, transcripts sequenced and analysed following in vivo workflow, supernatant collected and analysed by NMR, in vitro samples generated by Jennifer Ketskemety, NMR performed by Gwenaelle Le Gall, bile acid fractionation and MS analysis carried out by Mark Philo.

For RNA extraction from intestinal contents, I trialled three extraction protocols. The first one was a modified RNAsnap method, which included a Percoll gradient to allow for concentration and purification of the bacterial cells prior to RNA processing [432]. The second method had been published by Illot *et al.* for extraction of transcripts from colonic contents, while the third method was a modified commercial protocol using the QiagenRNeasy RNA isolation kit, with the substitution of a beat beating step at the beginning to allow sufficient bacterial lysis [140].

With bacterial load being lower in mono-colonised, compared to SPF mice, it was essential that the utilised protocol enabled reliable extraction of high quality (RIN>8) and quantity of RNA (>1ug required for sequencing) from small samples (average pellet weight <35 mg). The modified Qiagen kit protocol was determined to be the most successful, based on these criteria, and was therefore taken forward.

RNA extraction from contents of the SI and colon of SPF and GF mice were trialled, however I did not successful obtain enough high-quality RNA from small intestinal contents of mono-colonised mice, most likely due to lower bacterial abundance (Figure 5-4 in chapter 4). Processing small intestinal samples of SPF mice did yield RNA, but of poor quality (RIN<6), potentially caused by the higher concentration of digestive enzymes leading to greater degradation. Therefore, I progressed with RNA extraction from colonic content and faeces from GF mono-colonised mice and SPF mice, and obtained reproducible and high-quality RNA suitable for downstream processing. After optimisation experiments, the large intestinal contents of mono-colonised mice had all been processed, therefore faecal samples for this group were used for sequencing. Samples were depleted of ribosomal RNA by immunoprecipitation as bacterial mRNA only makes up 1-5% of total RNA. Samples were sequenced by Illumina HiSeq 75 bp paired end protocol.

Following raw data generation, processing was performed for identification of *B. breve* UCC2003 genes, as well as overall metatranscriptome function of the total bacterial community with bioinformatic support and guidance by Shabhonam Caim (QIB).

6.3.1.2 Probing *B. breve* UCC2003 transcription for distinct patterns during *in vivo* and gnotobiotic as well as colonisation as part of a complex microbiota

To identify differential gene expression of *B. breve* UCC2003 *in vivo*, as a member of the wider microbiota community, and as a mono-coloniser, read fragments generated by RNA-seq were mapped against the *B. breve* UCC2003 genome, using Bowtie 2, followed by read count extraction with HTSeq, and differential gene expression analysis by DESeq2 (Figure 6-2) [298, 299, 374].

In addition to the described experimental groups, RNA extracted from *B. breve* UCC2003 *in vitro* (MRS media at stationary growth phase, performed by Jennifer Ketskemety, was also analysed and compared to allow comparison of *in vivo* vs. *in vivo* transcription.

Alignment of RNA fragments to reference genomes is essential for accurate gene count determination. The utilised pipeline has been successfully applied to *in vitro* samples of single bacterial species, and in this study produced adequate outputs (based on quality control) for *B. breve* UCC2003 *in vitro*, and mono-colonised samples [433]. The alignment of raw reads of metatranscriptome samples requires a different approach to ensure high quality alignment and capture resolution. In this study I utilised Bowtie 2, which has also been previously used by other groups, but there are some limitations of this approach, which will be discussed further within the discussion and future work section [434].

6.3.1.3 Comparing *B. breve* UCC2003 transcription *in vitro* and *in vivo* as part of complex microbiota, and in a gnotobiotic mouse model, reveals distinct gene expression profiles for each condition

Based on detected *B. breve* UCC2003 transcriptome, initially an overview of all three data sets was generated. The PCA plot in Figure 6-3.A shows a clear clustering of groups, suggesting a distinct gene expression profile of *B. breve* UCC2003 in different *in vitro*, and *in vivo* conditions.

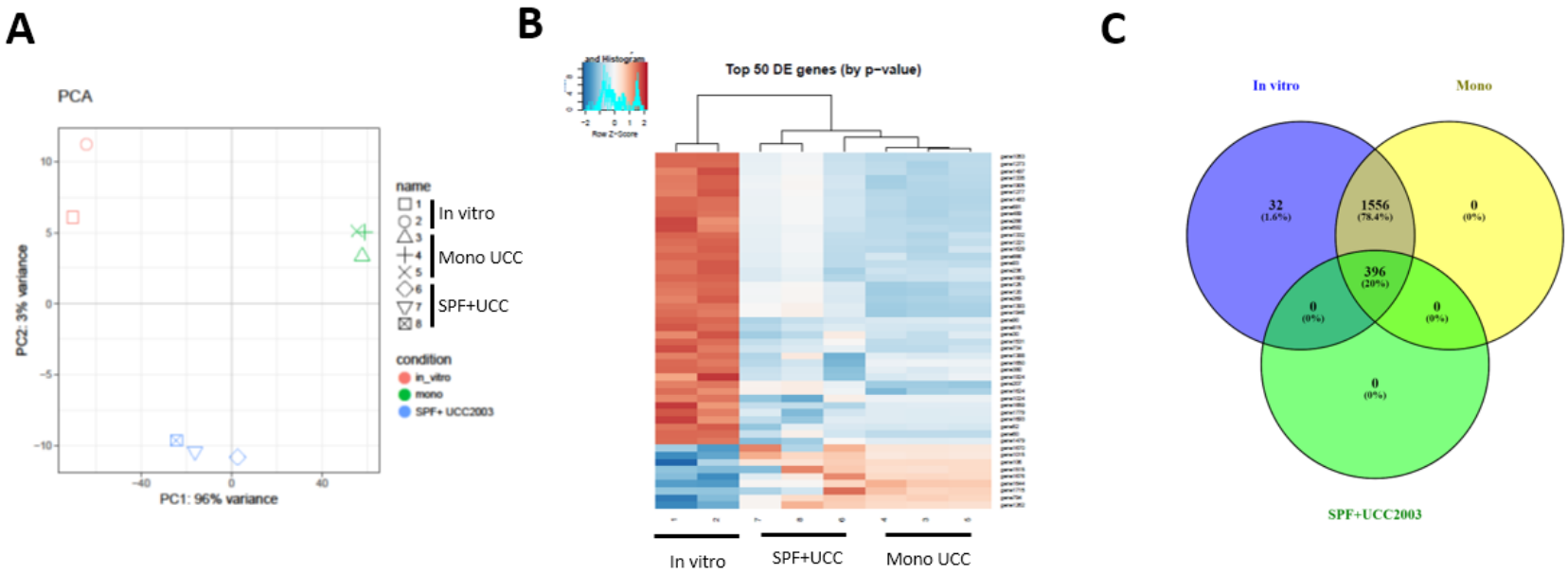

Figure 6-3 ***B. breve*** **UCC2003 RNAseq in vitro and in vivo in the intestine of GF and SPF mice reveals distinct transcriptional patterns in each condition**

In vitro – *B. breve* UCC2003 culture in MRS, Mono – GF mice colonised by *B. breve* UCC2003, SPF+UCC – conventionally raised mice colonised by *B. breve* UCC2003 **A** PCA plot of group variability, **B** Bland Altman (MA) plot, y axis log2 fold change of gene expression, x axis – mean of moralised counts, red dots – statistical sig genes (q values 0.05), **C** Overlap of unique and shared genes between sample groups.

Visualising the top 50 genes (Figure 6-3.B), based on p-value, presents hierarchical clustering of individual *in vitro* samples, separate from *in vivo* repeats, which may link to the artificial environment of culturing in MRS media, compared to the environment within the mouse intestine. A stronger intergroup similarity between mono-colonised, and samples extracted from SPF mice colonised by *B. breve* (SPF+UCC) can be observed. More than 75% of genes are strongly upregulated (red in heatmap) under *in vitro* condition, with the remaining functional units being strongly downregulated (blue). There is general consensus between direction of fold change between *in vivo* samples, with SPF+UCC repeats presenting very low expression of specific genes. To understand this, as well as clustering further, gene overlap of expressed genes between groups is shown in Figure 6-3.C. The total 1984 transcripts present in the *B. breve* UCC2003 reference genome are expressed in the sum of the data set. Mono-colonised samples share their entire expression profile with the SPF group, with 32 genes only expressed when cultured in MRS, while all 396 genes expressed by *B. breve* UCC2003 *in vivo,* as part of the wider microbiota, are also transcribed under gnotobiotic and *in vitro* conditions.

Of these uniquely expressed genes *in vitro* (Table 6-1), three were hypothetical proteins, for which no homologues sequences were found (NCBI BLAST [435], 75% coverage, 75% identity). In total, 25 of these transcripts were identified as transposases, which are located at different parts of the genome, but share sequence identity between each other. Three unique sequences were found and are indicated by letters under “Sequence Identity” in Table 1. Homology analysis of sequence C (shared between genes Bbr_0159 and Bbr_0302) did not yield similar proteins with known functions. Interestingly, transposases with sequence A (11 in total uniquely expressed under in vitro conditions) mapped with 49% identity and 90% coverage to gene BL105A_0419 in *B. longum* 105-A [436]. This transcript is labelled as a putative transposase in the organism, and suggested to be part of an EPS cluster. Two other transposases, Bbr_0433 and Bbr_463 only expressed *in vitro,* are part of the EPS cluster in *B. breve* UCC2003, with an additional 10 other transposases sharing their sequence (indicated by letter B in Table 6-1), while also unique to *in vitro* conditions, but present at other sites within the genome [280]. In addition, expression of glycosyltransferase Bbr_0438, also part of this cluster, is unique to *in*

vitro culture. Expression of all genes within the EPS cluster will be shown and discussed below. It should be mentioned though that gene Bbr_0462, a transposase in *B. breve* UCC2003 EPS cluster, shares sequence homology with the identified transposase BL105A_0419, involved in EPS production in *B. longum*, and is again is only transcribed *in vitro*.

Table 6-1 Uniquely expressed *B. breve* UCC2003 genes under in vitro conditions compared to in vivo

Gene ID (exp data)	Gene ID (ref genome)	Sequence identity	Gene description
gene1194	Bbr_1165	A	Transposase
gene1195	Bbr_1166	B	Transposase
gene1444	Bbr_1412	A	Transposase
gene1445	Bbr_1413	B	Transposase
gene154	Bbr_0152	B	Transposase
gene1545	Bbr_TRNA41		tRNA-Glu
gene1550	Bbr_1511	A	Transposase
gene1551	Bbr_1512	B	Transposase
gene1577	Bbr_1538		Hypothetical protein
gene1579	Bbr_1540	A	Transposase
gene1580	Bbr_1541	B	Transposase
gene161	Bbr_0159	C	Transposase
gene1826	Bbr_1773	B	Transposase
gene1827	Bbr_1774	A	Transposase
gene1891	Bbr_1837	B	Transposase
gene1892	Bbr_1838	A	Transposase
gene1908	Bbr_rRNA23S2		23S ribosomal RNA
gene210	Bbr_0207	A	Transposase
gene308	Bbr_0302	C	Transposase
gene445	Bbr_0433	B	Transposase
gene450	Bbr_0438		Glycosyltransferase
gene467	Bbr_0455	A	Transposase
gene468	Bbr_0456	B	Transposase
gene472	Bbr_0460		Hypothetical membrane spanning protein
gene474	Bbr_0462	B	Transposase
gene475	Bbr_0463	B	Transposase
gene598	Bbr_0586		Conserved hypothetical protein
gene704	Bbr_0690	B	Transposase
gene705	Bbr_0691	A	Transposase
gene857	Bbr_0834	A	Transposase
gene971	Bbr_0950	B	Transposase
gene972	Bbr_0951	A	Transposase

This great overlap of genes expressed between groups emphasis that the distinct transcriptional profiles observable by PCA and heatmap, are largely based on expression values. Regarding SPF+UCC samples, the very low number of genes detected could be a potential artefact of using Bowtie 2 as metatranscriptome alignment software, and will be discussed further in the future work section of this chapter.

6.3.1.4 In the intestinal tract of gnotobiotic mice, *B. breve* UCC2003 increases expression of pathways involved in HMO metabolism, and iron uptake, while decreasing EPS production compared to *in vitro* transcription

To assess genes required for *in vivo* colonisation, adaptation to the nutrients present in the intestinal tract, and potentially identify genes with host beneficial effects, I analysed DEG expression in the *B. breve* UCC2003 *in vitro* vs. the mono-colonised GF transcriptome.

Figure 6-4.A shows a PCA analysis, with both groups clustering distinctively, with stronger intergroup differences between the two *in vitro* repeats. Assessing hierarchical clustering based on top 50 differentially expressed genes (Figure 6-4.B), a clear separation between *in vitro* and mono-colonised samples is observed, with all genes upregulated *in vivo*. Calculation of DEGs shows 701 transcripts upregulated in *B. breve* when present in the intestinal tract of GF mice, while 669 are decreased in expression when compared to growth in culture (Figure 6-4.C).

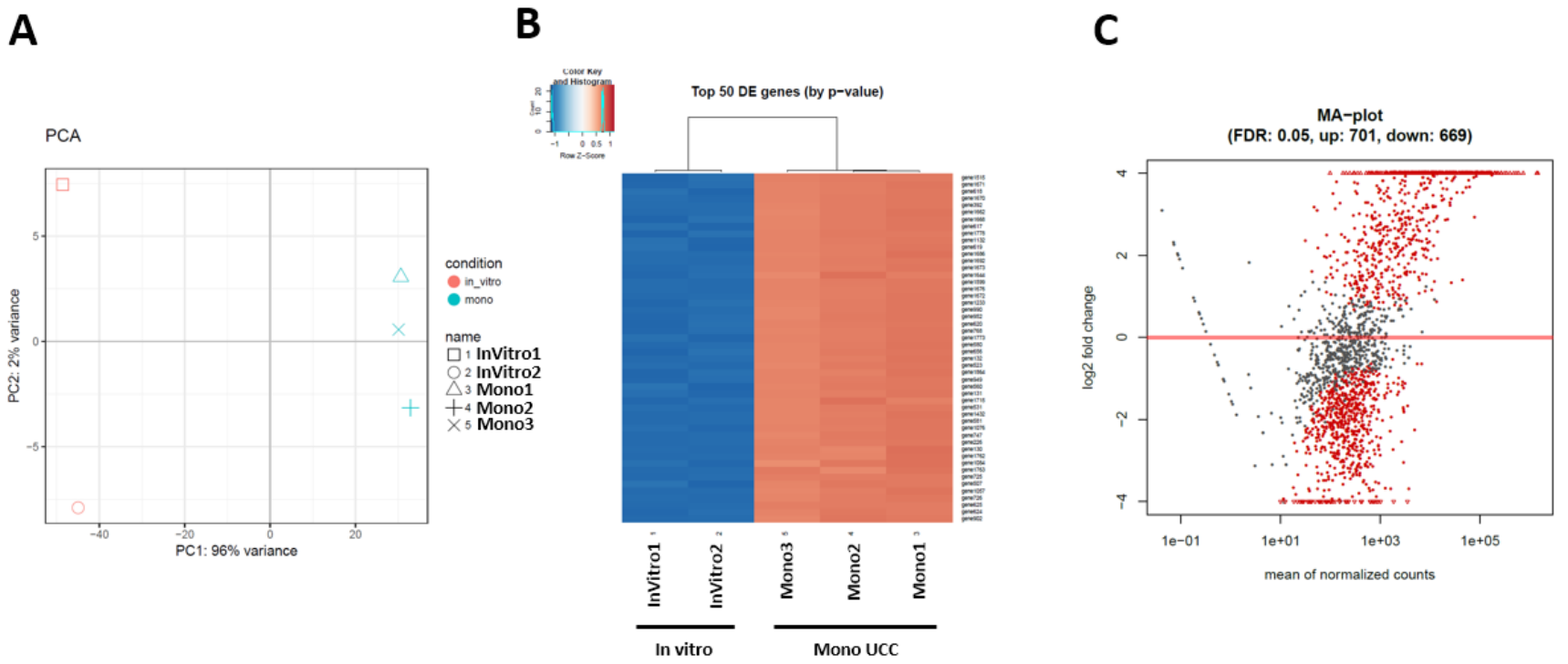

Figure 6-4 ***B. breve*** **UCC2003 colonisation of gnotobiotic mice induces distinct bacterial transcriptional responses compared to in vitro gene expression**

A PCA plot of group variability **B** hierarchical clustering of samples based on TOP 50 differentially regulated genes C Bland Altman (MA) plot, y axis log2 fold change of gene expression, x axis – mean of moralised counts, red dots – statistical sig genes (q values 0.05).

Table 6-2 presents the top 25 upregulated genes in mono-colonised samples, based on log2 fold changes. Interestingly, four genes involved in metabolism of HMOs lacto-N-tetraose (LNT) and lacto-N-neotetraose are present in this list [397]. This includes gene 1599 (Bbr_1558, NahP1) and gene1600 (Bbr_1559, nahP2), both permease proteins of ABC transporter systems, and gene1601 (Bbr_1560, nahT), a ATP binding protein of permease transporter systems. The proposed metabolomics pathway is shown in Figure 6-5, with the corresponding expression values in my dataset presented in Table 3. Out of 20 involved proteins (Table 6-3), 10 shows transcriptional upregulation, while 9 are present, but not modulated, in contrast to downregulation of gene1628 (Bbr_1586, nahK), a phosphotransferase family protein. Particularly striking is a 5-fold increase in β-galactosidase gene540 (Bbr_529, lntA), which is a key enzyme in the pathway, as it processes LNT to LNnT, making it available for the rest of the pathway.

Table 6-2 ***B. breve*** **UCC2003 top 25 upregulated DEGs under in vivo mono-colonised conditions compared to in vitro transcription**

(q-value cut-off < 0.05)

Gene ID (exp data)	Gene ID (ref)	Gene description	fold change	q-value
gene1714	Bbr_TRNA47	tRNA-Thr	11.94708032	1.00E-38
gene131	Bbr_0129	3-oxoacyl-[acyl-carrier protein] reductase	9.094254971	4.70E-246
gene1644	Bbr_1601	hypothetical protein	8.369786915	4.41E-208
gene1715	Bbr_TRNA48	tRNA-Tyr	8.358721633	8.02E-206
gene949	Bbr_0927	Branched-chain amino acid aminotransferase	8.318367964	4.10E-241
gene428	Bbr_0415	ATP-binding and permeaase modules of ABC transporter system	8.182514746	1.70E-121
gene106	Bbr_0104	Ketol-acid reductoisomerase/2-dehydropantoate 2-reductase	8.13704964	8.94E-38
gene1800	Bbr_1747	ATP-binding protein of ABC transporter system	8.102313345	2.49E-109
gene817	Bbr_TRNA25	tRNA-Arg	7.939566327	2.00E-129
gene1599	Bbr_1558	Permease protein of ABC transporter system	7.823777994	1.94E-284
gene1600	Bbr_1559	permease protein of ABC transporter system	7.660382944	9.86E-110
gene1676	Bbr_1632	30S ribosomal protein S17	7.561450235	4.17E-272
gene1015	Bbr_0994	Phosphoglycerate kinase	7.547204355	2.30E-124
gene226	Bbr_0222	Conserved hypothetical secreted protein-2C probably involved in iron uptake	7.459271134	5.15E-260
gene332	Bbr_0324	permease protein of ABC transporter system	7.457766548	1.22E-77
gene130	Bbr_0128	Nonfunctional predicted acyl-CoA reductase due to mutations	7.45567499	1.18E-203
gene338	Bbr_0330	ATP synthase epsilon chain	7.441114339	2.03E-62
gene1234	Bbr_1205	Oligopeptide-binding protein oppA	7.422715467	2.55E-49
gene560	Bbr_0549	Pyridoxine biosynthesis protein	7.335270957	2.93E-148
gene1601	Bbr_1560	ATP-binding protein of ABC transporter system	7.335030964	3.01E-116
gene1671	Bbr_1627	30S ribosomal protein S8	7.318398297	3.59E-205
gene1076	Bbr_1049	VanZ family protein	7.307016025	2.97E-213
gene618	Bbr_0605	SSU ribosomal protein S7P	7.274103892	2.26E-164
gene726	Bbr_0712	ATP-binding protein of ABC transporter system	7.216081094	1.01E-237
gene1150	Bbr_TRNA34	tRNA-Asn	7.198494069	2.18E-104

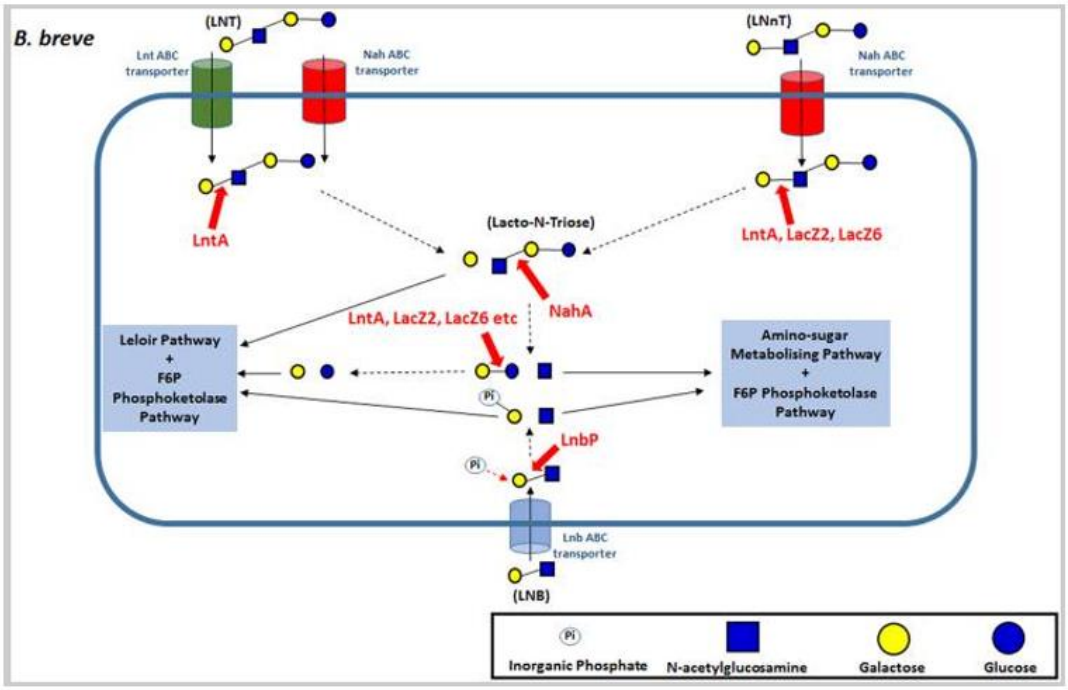

Figure 6-5 Representation of human milk oligosaccharide metabolism by *B. breve* UCC2003

Proposed by James *et al.*, overview over HMO metabolism by *B. breve* UCC2003 of lacto-N-tetraose (LNT), lacto-N-neotetraose (LNnT), and lacto-N-biose (LNB), gene names corresponding Table 3.: LntA (beta-galatosidase), LacZS (galactoside symporter), LacZ6 (beta-galactosidase), NahA (beta-N-acetylhexosaminidase), LntA (beta -galatosidase), LnbP (lacto-N-biose phorylase), (adapted from James et al, 2016).

Another candidate gene found in the top 25 upregulated transcript list (Table 6-2) is gene226 (Bbr_0222, bfeO); a conserved hypothetical secreted protein, with an iron binding domain (Table 6-4) [437]. It belongs to an iron starvation induced cluster, that has previously been shown, in *B. breve* UCC2003, to be induced by iron-starvation conditions (*in vitro*). This cluster is under the transcriptional control of interspecies signalling molecule autoinducer-2 (AI-2), which is the by-product of methylthioadenosine/S-adenosyl-homocystine nucleosidase (luxS) [438]. This gene (Bbr_0541 [gene552]), is non-significantly upregulated (2.7 log2 fold, q-value 0.08), during mono-colonisation, relative to *in vitro*.

Table 6-3 ***B. breve*** **UCC2003 genes involved in HMO metabolism are upregulated under monocolonise in vivo conditions relative to** ***in vitro***

q-value < 0.05, cluster characterised by James et al, 2016.

Gene ID (ref)	Gene Name	Gene ID (exp)	Gene description	fold change
Bbr_0526	IntR	gene537	Transcriptional regulator%2C LacI family	n.s.
Bbr_0527	IntP1	gene538	Permease protein of ABC transporter system for sugars	1.221552557
Bbr_0528	IntP2	gene539	Permease protein of ABC transporter system for sugars	n.s.
Bbr_0529	IntA	gene540	Beta-galactosidase	5.038803205
Bbr_0530	IntS	gene541	Solute-binding protein of ABC transporter system for sugars	6.106290482
Bbr_1551	lacS	gene1592	Galactoside symporter	n.s.
Bbr_1552	lacZ6	gene1593	Beta-galactosidase	n.s.
Bbr_1553	lacI	gene1594	Transcriptional regulator%2C LacI family	n.s.
Bbr_1554	nahS	gene1595	Solute-binding protein of ABC transporter system (lactose)	n.s.
Bbr_1555	nahR	gene1596	NagC/XylR-type transciptional regulator	n.s.
Bbr_1556	nahA	gene1597	Beta-N-acetylhexosaminidase	n.s.
Bbr_1558	nahP1	gene1599	Permease protein of ABC transporter system	7.823777994
Bbr_1559	nahP2	gene1600	permease protein of ABC transporter system	7.660382944
Bbr_1560	nahT	gene1601	ATP-binding protein of ABC transporter system	7.335030964
Bbr_1585	galE (lnpD)	gene1627	UDP-glucose 4-epimerase	2.404896434
Bbr_1586	nahK (lnpB)	gene1628	phosphotransferase family	-1.770120227
Bbr_1587	lndP (lnpA)	gene1629	lacto-N-biose phorylase	n.s.
Bbr_1588	galP1 (gltC)	gene1630	Permease protein of ABC transporter system for sugars	3.164447667
Bbr_1589	galP2 (gltB)	gene1631	Permease protein of ABC transporter system for sugars	5.095774409
Bbr_1590	galS (gltA)	gene1632	Solute-binding protein of ABC transporter system for sugars	6.000734115

Table 6-4 Genes involved in iron uptake differentially upregulated in *B. breve* UCC2003 during intestinal colonisation of germ free mice relative *to in vitro* conditions

q-value < 0.05, cluster characterised by Christiaen *et al.*, 2014

Gene ID (ref)	Gene ID (ref)	Gene name	Gene description	fold change
gene225	Bbr_0221	bfeU	Conserved hypothetical membrane spanning protein with iron permease FTR1 family domain	n.s.
gene226	Bbr_0222	bfeO	Conserved hypothetical secreted protein, probably involved in iron uptake	7.459271134
gene227	Bbr_0223	nfeB	Conserved hypothetical membrane spanning protein	2.748225724
gene228	Bbr_0224		Permease protein of ABC transporter system	3.532557298
gene229	Bbr_0225		Permease protein of ABC transporter system	1.899756189
gene230	Bbr_0226		ATP-binding protein of ABC transporter system	3.228281995
gene552	Bbr_0541 (Bbr_0540 in paper)	luxS	Autoinducer-2 production protein luxS (=may also have metabolic function as S-ribosylhomocysteine degradation)	(n.s.) 2.27586982385741

Table 6-5 ***B. breve*** **UCC2003 top 25 downregulated DEGs under in vivo mono-colonised conditions compared to** ***in vitro*** **transcription**

(q-value cut-off < 0.05)

Gene ID (exp)	Gene ID (ref)	Gene description	fold change	q-value
gene450	Bbr_0438	Glycosyltransferase	-9.159246497	1.32E-12
gene449	Bbr_0437	Acetyltransferase	-7.787162917	2.80E-09
gene451	Bbr_0439	Capsular polysaccharide biosynthesis protein	-7.32764294	1.05E-10
gene469	Bbr_0457	Transposase	-7.140281034	1.13E-06
gene463	Bbr_0451	Acyltransferase	-6.576437566	1.47E-08
gene448	Bbr_0436	Hypothetical membrane spanning protein	-6.550612438	1.84E-15
gene452	Bbr_0440	Polysaccharide biosynthesis protein	-6.447339023	1.93E-14
gene1624	Bbr_1582	Conserved hypothetical membrane spanning protein with PspC domain	-6.418839169	9.85E-29
gene457	Bbr_0445	Glycosyltransferase	-6.397725218	5.31E-06
gene1577	Bbr_1538	Hypothetical protein	-5.946271904	0.00120575
gene454	Bbr_0442	Capsular polysaccharide biosynthesis protein	-5.90587117	3.55E-05
gene1623	Bbr_1581	Conserved hypothetical membrane spanning protein	-5.823402817	3.12E-16
gene455	Bbr_0443	Glycosyltransferase	-5.813298305	5.65E-05
gene856	Bbr_0833	Transposase	-5.714398109	0.00846575
gene460	Bbr_0448	Glycosyltransferase	-5.700503194	1.96E-08
gene459	Bbr_0447	Conserved hypothetical protein	-5.699228169	2.68E-08
gene464	Bbr_0452	Hypothetical protein	-5.36099304	0.000329251
gene470	Bbr_0458	Hypothetical protein	-5.276064125	0.000593316
gene472	Bbr_0460	Hypothetical membrane spanning protein	-5.135797353	0.005547742
gene466	Bbr_0454	Conserved hypothetical protein	-5.09951656	0.002984992
gene206	Bbr_0203	Conserved hypothetical membrane spanning protein-2C possibly efflux system	-5.058068697	1.37E-21
gene110	Bbr_0108	Cellodextrin transport system permease protein CebG	-4.996043606	2.72E-09
gene764	Bbr_0749	Permease protein of ABC transporter system for metals	-4.960779294	4.35E-07
gene598	Bbr_0586	Conserved hypothetical protein	-4.823293331	0.012266186
gene361	Bbr_0352	Sulfatase family protein	-4.806412364	4.61E-20

Table 6-6 Gene cluster required for *B. breve* UCC2003 surface exopolysaccharide production present transcriptional downregulation under *in vivo* gnotobiotic conditions compared to in vitro

q-value < 0.05, cluster characterised by Fanning *et al.*, 2012

Gene ID (exp)	Gene ID (ref)	EPS type	Gene function	fold change
gene441	Bbr_0429		Conserved hypothetical protein	-1.481552445
gene442	Bbr_0430		UDP Galactosephosphotransferase	-3.709996569
gene443	Bbr_0431		Protein Tyrosine Phosphatase	-1.031353639
gene444	Bbr_0432		Transpoase	n.s.
gene445	Bbr_0433		Transpoase	n.s.
gene446	Bbr_0434	EPS1	Flippase (Oligosaccharide repeat unit transporter in reference)	-4.778160793
gene447	Bbr_0435	EPS1	Glycosyletransferase (Beta-1%2C6-N-acetylglucosaminyltransferase)	n.s.
gene448	Bbr_0436	EPS1	Polymerase (Hypothetical membrane spanning protein)	-6.550612438
gene449	Bbr_0437	EPS1	Acetyltransferase	-7.787162917
gene450	Bbr_0438	EPS1	Glycosyletransferase	-9.159246497
gene451	Bbr_0439	EPS1	Glycosyletransferase (Capsular polysaccharide biosynthesis protein)	-7.32764294
gene452	Bbr_0440	EPS1	Glycosyletransferase	-6.447339023
gene453	Bbr_0441	EPS1	Glycosyletransferase (Capsular polysaccharide biosynthesis protein)	n.s.
gene454	Bbr_0442	EPS2	Glycosyletransferase (Capsular polysaccharide biosynthesis protein)	-5.90587117
gene455	Bbr_0443	EPS2	Glycosyletransferase	-5.813298305
gene456	Bbr_0444	EPS2	Flippase (Membrane spanning polysaccharide biosynthesis protein)	-4.145319042
gene457	Bbr_0445	EPS2	Glycosyletransferase	-6.397725218
gene458	Bbr_0446	EPS2	Acetyltransferase (cell wall biosynthesis)	-4.404831255
gene459	Bbr_0447	EPS2	Conserved hypothetical protein	-5.699228169
gene460	Bbr_0448	EPS2	Glycosyletransferase	-5.700503194
gene461	Bbr_0449	EPS2	Conserved hypothetical protein	-2.812067092
gene462	Bbr_0450	EPS2	Polymerase (Membrane spanning protein involved in polysaccharide biosynthesis)	-2.684248729
gene463	Bbr_0451	EPS2	Acetyltransferase	-6.576437566
gene474	Bbr_0462		Transpoase	n.s.
gene475	Bbr_0463		Transpoase	n.s.
gene486	Bbr_0474		Chain length determinant (capsular polysaccharide biosynthesis/ Tyrosine-protein kinase (capsular polysaccharide biosynthesis))	-1.408254526

Table 6-5 shows the top 25 downregulated DEGs based on log2 fold$_2$ change, comparing *in vitro* conditions, with colonisation of the GF mouse gut. Of those hits, 12 belong to the bidirectional EPS-encoding gene cluster in *B. breve* UCC2003, shown in Figure 6-6 [358]. As mentioned in subchapter 1.4.4, this cluster is responsible for production of an EPS capsule that facilitates colonisation, and also provides bile, and acid resistance [439]. The gene cluster can generate two different EPS structures based on the orientation of promotor orientation. EPS polymers are produced by enzymatic chain reactions carried out by glycosyl transferases (GT) with both EPS (EPS1, EPS2) sharing one priming glycosylase (gene453/Bbr_0441 and gene454/Bbr_0442). Analysis of total DEGs revealed 20 transcripts in the pathway to be downregulated with fold changes ranging from -1 to -9, while the remaining involved genes are not statistically altered (Table 6-6). Downregulation of priming GT occurs for EPS1 (gene453/Bbr_0441), while unaltered for EPS2 (gene453/Bbr_0441).

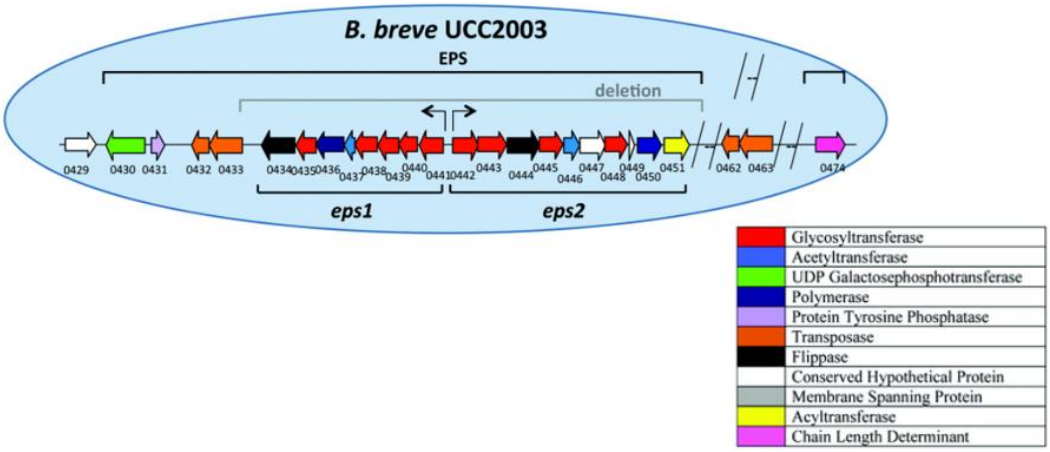

Figure 6-6 Overview over gene cluster involved in surface exopolysaccharide production in *B. breve* UCC2003

Corresponding gene expression fold changes shown in Table 6, adapted from Fanning et al, 2012

Hypothetical proteins contained within the list of downregulated DEGs under mono-colonised conditions Table 6-5, were analysed for sequence homology, and gene466 (Bbr_0454) shared 99% sequence and 100% coverage identity with insertion sequence 21 (IS21, NCBI reference sequence: WP_052814069.1), which has been

identified in eight other bifidobacterial strains [440]. Other identified IS were shown to be active during growth *in vitro,* and were suggested to cause genome reduction and rapid adaptation to new growth conditions [441]. In addition, the identical sequence overlap was found in an integrase of *B. breve* MCC114 (NCBI reference sequence KOA65106.1), further supporting the function of this transcript as a transposase.

6.3.1.5 Colonisation of intestinal tract harbouring complex microbiota induces differential expression of *B. breve* genes involved in metabolism, stress response, and transformation resistance, relative to gnotobiotic conditions

The RNA-seq analysis of the bacterial metatranscriptomic data differs significantly from single species samples as indicated above. For this analysis, I used Bowtie 2 (as the raw read aligner), due to the feasibility of implementation, and utilisation of bacterial RNA-seq in single species populations [298]. Distinct clustering can be observed for mono-colonised samples, while SPF+UCC has greater intragroup variability, based on the PCA plot (Figure 6-7.A). Hierarchical clustering, assessing expression ratios, separates samples of both groups, as shown by heatmap analysis (Figure 6-7.B). A total of 49 genes are differentially expressed, with 48 upregulated, and one downregulated (30A ribosomal protein, $\log_2$ -1.6-fold change, Figure 6-7.C). It should be noted that out of 1972 genes in the *B. breve* UCC2003 reference genome (NCBI ID 1273), 397 unique genes were mapped in SPF+UCC compared to 1953 in mono-colonised. In addition, expression counts are lower in SPF+UCC (max. 399 to 1490863), which may due to the described limitations.

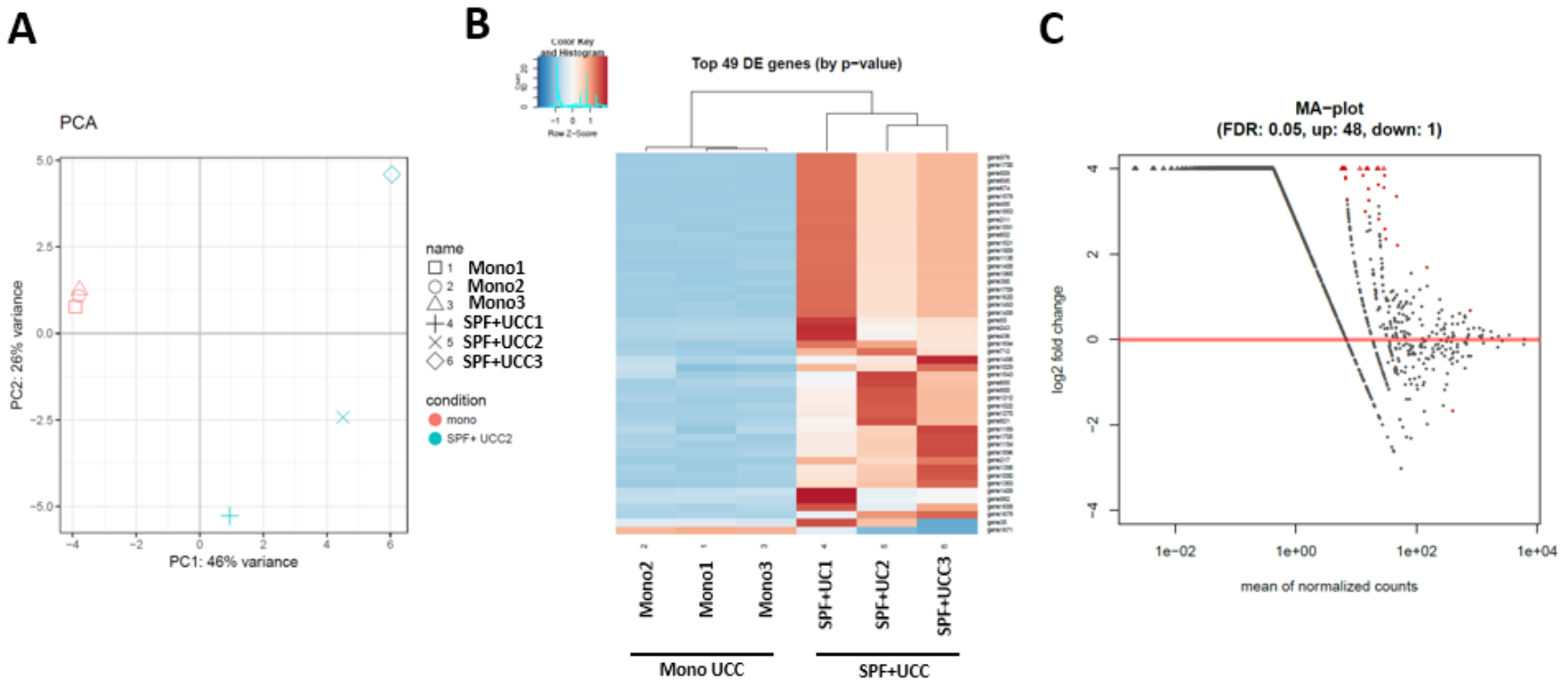

Figure 6-7 Colonising of conventionally raised mice induces upregulation of a distinct gene profile compared to gnotobiotic mice

A PCA plot of group variability **B** hierarchical clustering of samples based on TOP 49 differentially regulated genes **C** Bland Altman (MA) plot, y axis log2 fold change of gene expression, x axis – mean of moralised counts, red dots – statistical sig genes (q values 0.05)

Table 6-7 ***B. breve*** **UCC2003 top upregulated genes based on fold change comparing presence in complete microbiota with mono-colonised conditions**

(q-value cut-off < 0.05)

Gene ID (ref)	Gene ID	Gene name	fold change	q-value
Bbr_0055	gene55	Conserved hypothetical protein	8.44229807	1.74E-13
Bbr_1539	gene1578	Conserved hypothetical protein	7.713939642	8.64E-07
Bbr_0660	gene674	DNA repair protein recO	7.492089321	9.83E-06
Bbr_0681	gene695	Conserved hypothetical membrane spanning protein	7.437476028	9.71E-08
Bbr_1351	gene1383	Calcineurin-like phosphoesterase	7.075238471	7.98E-08
Bbr_0497	gene509	Conserved hypothetical protein	7.037515197	8.64E-07
Bbr_1656	gene1700	Sugar ABC transporter-2C permease protein	6.856955083	1.07E-05
Bbr_0955	gene976	Conserved hypothetical protein	6.804875894	8.64E-07
Bbr_1241	gene1270	Cell wall biosynthesis-associated protein	6.702431468	3.16E-07
Bbr_0208	gene211	Transcriptional regulator-2C TetR family	6.401113483	1.94E-06
Bbr_1800	gene1853	Conserved hypothetical membrane spanning protein	6.107085069	7.41E-06
Bbr_0483	gene495	Protease II	5.987282582	9.83E-06
Bbr_1001	gene1022	Branched chain amino acid transport system II carrier protein	5.96105715	1.07E-05
Bbr_1183	gene1212	Transcriptional regulator	5.689372859	3.04E-05
Bbr_0780	gene800	Hydrolase (HAD superfamily)	5.502679726	2.93E-05
Bbr_1111	gene1138	Conserved hypothetical secreted protein	5.408002298	0.0001361
Bbr_0214	gene217	Type II restriction-modification system restriction subunit	5.25905608	4.44E-06
Bbr_rRNA16S2	gene1909	16S ribosomal RNA	5.253670047	0.0001265
Bbr_TRNA33	gene1050	tRNA-Pro	5.042182983	0.0001594
Bbr_1487	gene1521	Conserved hypothetical protein-2C marR family	4.819467494	0.0007546
Bbr_1366	gene1398	Conserved hypothetical protein	4.778370431	0.0004648
Bbr_0590	gene602	Hypothetical protein	4.72618697	0.0019174
Bbr_1550	gene1591	Hypothetical protein	4.680628179	0.0019174
Bbr_1125	gene1154	Glycoprotease protein family	4.393638267	0.0018261
Bbr_1908	gene1965	Serine/threonine protein kinase	4.310083002	0.0034098

Table 6-7 highlights the top downregulated genes, based on log2 fold change. Hypothetical proteins were analysed by BLAST for sequence homology, with above mentioned parameters, and three hits were returned. Gene1521 (Bbr_1487) showed homology with a transcriptional regulator of the MarR family in *B. breve* ACS-071 (Ref Seq: WP_003830074.1). Genome wide studies in *B. longum* have shown bifidobacteria to harbour relatively few transcriptional regulators of this type, compared to other bacteria [248]. The exact function of the gene in *B. breve* is unknown.

The anti-restriction protein ArdA, found in the NCBI reference sequence for *B. breve* (WP_015439154.1), overlapped with upregulated hypothetical gene1578 (Bbr_1539), and could suggest an increase in transformation in the presence of other gut bacteria favouring horizontal gene transfer. Contrastingly, gene217 (Bbr_0214), a type II restriction-modification system subunit, also presents with increased expression in the presence of the wider microbiota, which could be interpreted as a defence mechanism against foreign DNA.

Hypothetical protein gene1398 (Bbr_1366) shares 100% sequence, and 99% coverage, with cell wall integrity and stress response protein 1, which was again found within the NCBI *B. breve* reference (WP_065465773.1). Studies of this protein in other microbes (e.g. *Saccharomyces cerevisiae*) have located it to the cell surface, with a function of reacting to stress, such as heat shock, or cell division, with induction of cell wall remodelling [442, 443]. Interestingly, gene1270 (Bbr_1241), a cell wall biosynthesis associated protein, is upregulated by log2 6.7-fold, which further suggests that *B. breve* UCC2003 is adapting to the presence of other gut microbiota, specifically with cell wall modulation.

Calcineurin-like phosphoesterase (Gene1383, Bbr_1351) expression is increased when *B. breve* UCC2003 is part of a complex microbiota, relative to mono-colonisation. The exact function of calcineurin-like phosphoesterase is not yet understood, but the gene has been shown to have increased expression in *B. longum* BBM68, when exposed to bile acids *in vitro.*

The Sugar ABC transporter permease (gene1700) gene was upregulated by 6.8 $\log_2$ fold in relation to mono-colonisation levels, which suggests differences in available

nutrients within the gut of GF, compared to SPF mice [444]. Other genes showing increased expression, potentially involved in adaptation to the available nutrient pool in SPF mice, are a glycoprotease (gene1154, Bbr_1125), a branched chain amino acid transport system II carrier protein (gene1022, Bbr_1001), and gene1965 (Bbr_1908), which functions as a serine/threonine protein kinase.

Lastly, gene55 (Bbr_0055), a conserved hypothetical protein, had strongest upregulation, which has previous been suggested to be non-essential, due to higher insertion frequency in this gene in a high-resolution transposon directed insertion sequencing (TraDIS) approach [357]. This highlights the potential difference in transcription encountered between *in vitro* and *in vivo* conditions.

For the previously highlighted EPS cluster genes (Figure 6-6), there were no read counts observed within the SPF+UCC sample set, while some genes transcripts involved in HMO metabolism, and iron assimilation pathways were present but with q-values < 0.05, due to intergroup variation. These findings are potentially skewed by the applied read garment mapping, and gene count quantification approach, producing lower read counts for *B. breve* UCC2003 gene expression in the metatranscriptome samples. Additional analysis will further tease apart other genes involved in the SPF environment in future studies.

6.3.2 Assessing the effect of *B. breve* colonisation on wider microbiota composition and function

The benefits of metatranscriptome sequencing of the gut microbiome include the ability to determine pan-transcriptional changes that are potentially induced by *B. breve* UCC2003 colonisation.

As touched upon earlier, the challenge of metatranscriptome data processing lies in identification of genes within the raw reads. For the gut microbiota, this includes more than 9,000,000 unique genes from 125,000 bacterial genomes, which is computationally challenging [435, 445]. For this analysis SUPER-FOCUS (SUbsystems Profile by databasE Reduction using FOCUS, SF) was utilised (Figure 6-2), which is a homolog-based approach that sorts each generated sequence into a subset (proteins families with similar function), by comparison to a pre-clustered SEED database [300, 446]. This method allows for rapid identification, without loss of sensitivity, coupled with greater functional coverage of reference databases queried. In addition, this software contains FOCUS, a profiler that constructs taxonomic compositions based on oligonucleotide sequences to reference genomes sourced from SEED servers [301, 447]. This allowed me to investigate the effect of *B. breve* UCC2003 colonisation on the gut microbiota composition.

6.3.2.1 Introduction of *B. breve* UCC2003 shifts the overall microbiota function to increased protein production, and decreased carbohydrate metabolism

The supplementation of bifidobacterial species has been shown to induce various changes in the intestinal microbiota. This may in part be due to cross-feeding mechanisms between bifidobacteria species, and other microbiota members, such as butyrate producing anaerobes (e.g. Firmicutes, Eubacteria) [132]. As these modulations are associated with health beneficial effects I analysed the effect of *B. breve* UCC2003 colonisation on the overall function of the microbiota, which will be presented below.

Analysing sample similarity, based on their SEED classification, by PCA is shown in Figure 6-8. Intergroup variability can be observed for both conventionally raised

mice, with and without *B. breve* colonisation, while the overall differences between groups, and individual samples are small, as indicated by the axis range. This agrees with previous studies supplementing mice with UCC2003, and also the small taxonomic changes investigated by 16S rRNA sequencing in this model (Figure 5-5 in Chapter 2) [46].

Figure 6-9 shows functional SEED classification on sublevel 2, of the total microbiota in groups SPF and SPF+UCC. Figure 6-9.A highlights the top 20 enriched pathways based on relative abundance. Mice supplemented with *B. breve* had significantly ($p < 0.05$) decreased abundance of the subgroup assigned to central carbohydrate metabolism, as well genes associated with lysine, threonine, methionine and cysteine metabolism, and polysaccharide production. A statistically significant increase ($p < 0.05$) was observed for protein synthesis, with a slight trend in upregulation for capsular and extracellular polysaccharides.

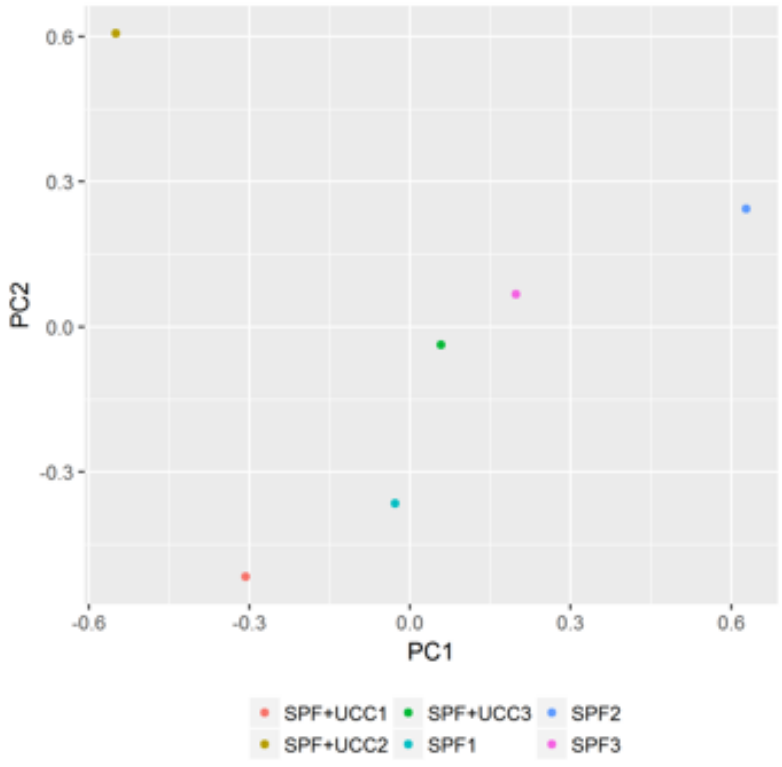

Figure 6-8 Colonisation by *B. breve* UCC2003 has small effects on the overall function profile of the intestinal microbiota with great intragroup variability

PCA plot based on SEED classification by SUPER_FOCUS of the metatranscriptome, comparison between functional profile conventionally raised mice (SPF1, SPF2, SPF3) and mice colonised by *B. breve* UCC2003 (SPF+UCC1, SPF+UCC2, SPF+UCC3)

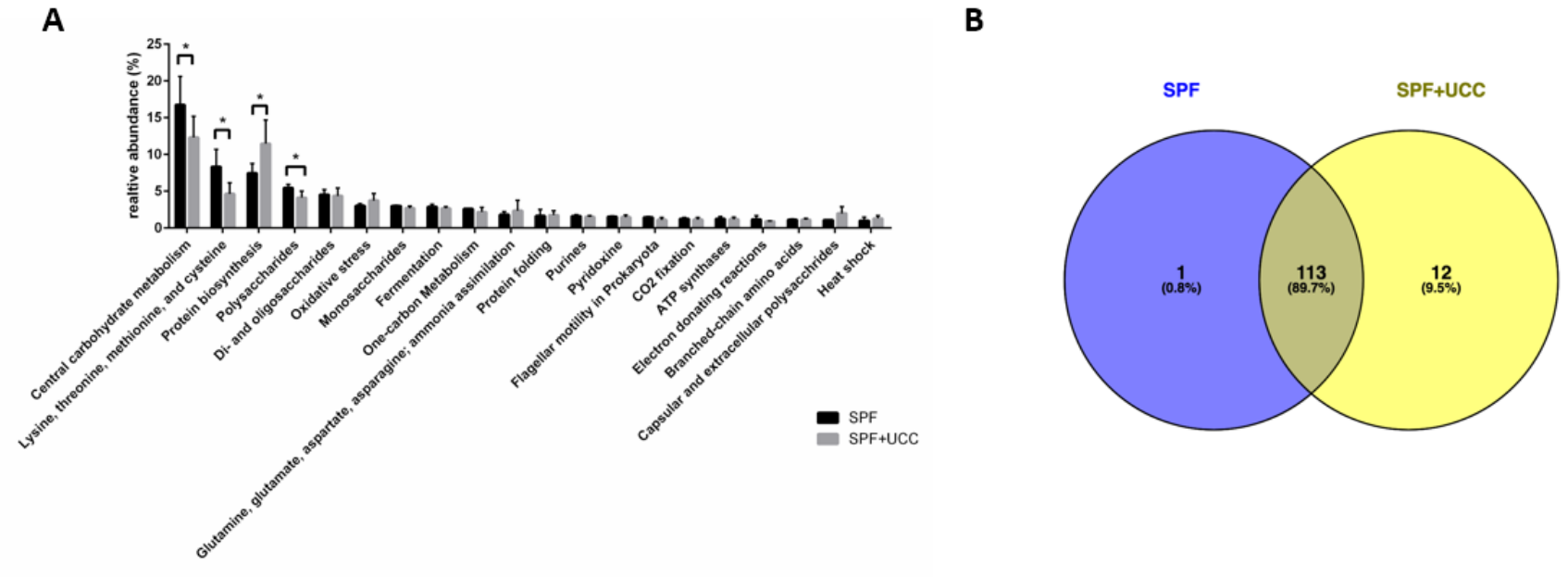

Figure 6-9 ***B. breve*** **UCC2003 colonisation induces distinct changes to overall intestinal microbiota function at high and low abundance levels**

A Top 20 sublevel 2 functional pathways identified in metatranscriptome of conventionally raised mice with (SPF+UCC) and without (SPF) *B. breve* UCC2003 colonisation based on relative abundance, n=3, statistical analysis by two-way ANOVA with Bonferroni post-test, * = p-value < 0.05 **B** Unique functional pathways identified in SPF and SPF+UCC metatranscriptome

Table 6-8 Unique SEED functions expressed in metatranscriptome of conventionally raised mice colonised by *B. breve* UCC2003 compared to control mice

based on relative abundance of sublevel 2 classifications by SUPER-FOCUS

SEED classification	relative abundance (%)
General Stress Response and Stationary Phase Response	0.000748666
Nucleotidyl-phosphate metabolic cluster	0.003282611
Protein secretion system, Type II	0.001458938
Protein secretion system, Type III	0.000121578
Regulation of virulence	0.000729469
Ribosome-related cluster	0.0000292
Sugar Phosphotransferase Systems, PTS	0.000729469
Sulfatases and sulfatase modifying factor 1 (and a hypothetical)	0.0000486
Type III secretion system, extended	0.000607891
alpha-proteobacterial cluster of hypotheticals	0.000729469
contains Thr-tRNA-syn, pyridoxine biosyn, lipid A biosyn, 3 hypos	0.0000811
heat shock, cell division, proteases, and a methyltransferase	0.0000172

Having assessed changes to functional readouts with highest enrichment, Figure 6-9.B presents overlap, and distinct differences at sublevel 2 groups, present in either SPF or SPF+UCC, to identify modulation with small overall abundance.

Interestingly, lactate racemization appears unique to SPF control mice, while *B. breve* UCC2003 induces 12 different pathways. These include; protein secretion system II and III, sugar phosphotransferase system, and sulfatases, as well as a general stress and stationary phase response pathway, and heat shock, cell division protease, and methyltransferase classes (Table 6-8) [448].

B. breve UCC203 has been shown to express a fructose phosphotransferase system, including a membrane transporter, but as this analysis is of total microbiota function, it cannot be distinguished whether *B. breve,* or another gut microbe, is responsible for the induction of this pathway in UCC2003 colonised mice. Nevertheless, this highlights a potentially unique fructose metabolic pathway associated with *B. breve* UCC2003 presence in the gut.

6.3.2.2 Colonisation by *B. breve* induces small but distinct shifts in intestinal microbiota taxonomy

In Chapter 5, I presented data that indicated that *B. breve* UCC2003 modulates the mouse intestinal microbiota (via 16S rRNA profiling, Figure 5-6 in chapter 5); with most striking differences including an increase in *Lactobacillus*, and a decrease in *Blautia* and *Alobacum*. For metatranscriptomic data, reads can be specifically assigned to unique bacterial reference genomes, allowing profiling of bacterial taxonomy. These two technologies have been compared and found to be similar in sensitivity, and ability to correctly assess community composition, with the caveat that these studies used different bioinformatic approaches [449, 450]. The FOCUS profiler, as part of SF, has been referenced by 15 primary research publications, which applied this pipeline in their analysis, and this was used to analyse the taxonomy of groups SPF and SPF+UCC, and the composition at family levels (Figure 6-10).

Both groups harbour similar abundance of *Lachnospiracea* (data set average 16%) and *Ruminococcaceae* (data set average 4%). *B. breve* UCC2003 colonisation appeared to increase *Prevotellaceae* (average abundance 6.8+ SPF to 8.7% SPF+UCC), with the gavaged group containing two samples with higher levels (SPF+UCC2, SPF+UCC3), and one (SPF+UCC1) with levels similar to control. An increase was also observed for *Spirochaetaceae* (average abundance 0.6% control to 2.8% *B. breve* colonised), and *Leptospiraceae*, with no detection in SPF to an average abundance of 1.4% in SPF+UCC (no detection in SPF+UCC3).

A decrease in abundance after *B. breve* colonisation was observed for *Eubacteriaceae* (average abundance 165 control to 8% SPF+UCC), and potentially *Clostridiaceae*, with average abundance decreasing from 10% in SPF mice to 7% in gavaged samples. Intergroup variability is high, as *Clostridiaceae* was only detected in two control samples (SPF1, SPF2), while in the gavaged group two colonised mice (SPF+UCC2, SPF+UCC3) present with low levels, but in SPF+UCC1 abundance was similar to the control group average.

Bifidobacteriaceae was detected in all three mice in SPF+UCC at an average of 0.8% relative abundance (which correlates with results from 16S metataxonomic profiling, Figure 5-5 in chapter 5), compared to no detection in SPF samples.

Results generated by selective plating of faeces showed presence of *Bifidobacterium* at 10^8 cfu/mg faeces in all SPF+UCC mice (Figure 5-4, chapter 5), while no colonies were detected from plating of control group samples, and confirms these mice were colonised with *B. breve*.

In contrast to RNA-seq, 16S rDNA sequencing amplifies the ribosomal sequences which increases detection, while RNA-seq performs unbiased replication (with the exception of ribo depletion), leading to a proportionally representation of reads from different bacterial species within the raw data. When analysing metatranscriptome taxonomy by SF, a minimum relative abundance cut-off is applied to ensure acceptable false positive rates. This minimum limit of detection could lead to low levels of *Bifidobacterium* assigned reads to be discarded, and explain the levels assigned in the taxonomic analysis.

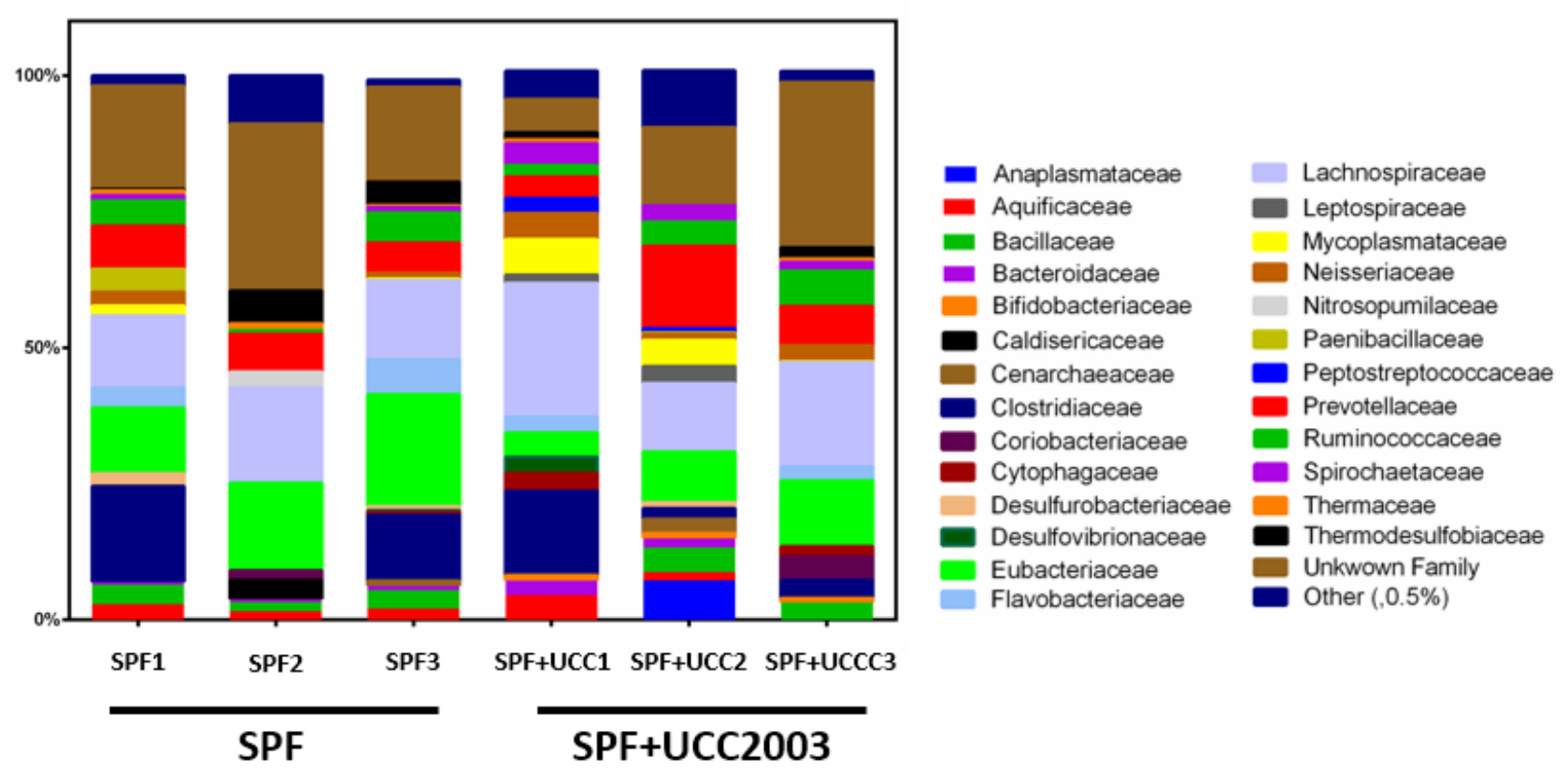

Figure 6-10 ***B. breve*** **colonisation induces small shifts in microbiota abundance at family level**

Data shown as relative abundance normalised to percentage of reads generated from meta-transcriptome, lengths representative of relative abundance, taxa with average abundance < 0.5% collated as "Other", taxonomic assignment by FASTA sequence alignment to SEED server reference genomes with FOCUS, data normalised and visualised with Prism.

6.3.3 Assessment of *B. breve* UCC2003 effect on intestinal metabolomic and bile acid profile does not reveal clear modulation in germ free and conventionally raised mice

Building on transcriptional profiling of *B. breve in vivo,* and its effect on the microbiota metatranscriptome, metabolomics analysis of intestinal contents was performed to potentially correlate transcriptional modulation, with metabolomics modulation. This was achieved by processing colonic contents for identification of bile acids (via HPLC), and other metabolites by NMR.

The PCA plots in Figure 6-11 compare similarity between GF, *B. breve* mono-colonised, conventionally raised (SPF) and SPF *B. breve* UCC2003 colonised mice, based on their metabolomic (Figure 6-11.A), and bile acid (BA, Figure 6-11.B) composition.

Metabolically, GF and *B. breve* UCC2003 mono-colonised groups cluster together (with the exception of sample GF1), and show a small, but distinct, separation (Fig11.A). Statistical analysis of individual metabolite differences recapitulates this, with Dimethylamine and Raffinose being significantly downregulated in mono-colonised samples ($p<0.05$, Figure 6-12.). Due to intergroup variability, these findings, together with other trends (shown in Figure 12 and discussed further below), will need to be investigated further, by initially increasing sample size to ensure biological significance and relevance (complete data set in Supplementary Figure 13 to Supplementary Figure 15).

Based on their metabolomic profile, SPF and SPF+UCC groups overlap (Figure 6-11.A), and no statistically significant modulation of individual compounds was identified (Supplementary Figure 16 to Supplementary Figure 18).

Investigating the BA composition in intestinal contents of these groups (Figure 6-11.B), GF and mono-colonised samples overlap when compared by PCA (Figure 6-11.B), with only Tauro-beta-muricholic acid (T-β-MA) significantly upregulated in *B. breve* colonised samples ($p<0.05$, Supplementary Figure 19). Intergroup variability is high and will require an increased number of replicates to determine biological significance.

BA profile of SPF and SPF+UCC groups overlap strongly with no clear intergroup clustering (Figure 6-11.B) and no statistically significant modulation was observed. Interestingly, T-β-MA shows a slight trend of increased concentration in *B. breve* colonised SPF mice (Supplementary Figure 20).

Figure 6-12 shows metabolites with significant differences, or non-significant trends, comparing between intestinal contents of GF and *B. breve* UCC2003 colonised samples. Butyrate, methyl- and hydroxybutyrate was detected in both groups, with a very slight increase in mono-colonised samples for butyrate. Bifidobacteria cannot produce butyrate, just like the host, and presence within the intestine is usually associated with butyrate producing bacteria. As this metabolite and its breakdown products are also detected in the GF group, and gnotobiotic status has been confirmed by culture dependent and independent methods (Supplementary Figure 3 and Supplementary Table 4), it could be hypothesised that it is present within the feed.

Significantly reduced dimethylamine (with intergroup differences between GF samples, $p<0.05$), and raffinose identified at 5.44 parts per million (ppm), was found in mono-colonised samples when compared to GF. Methylamine can be produced by gut microbes through the conversion of dietary choline [451]. Therefore, the decreased concentration in *B. breve* mono-colonised samples is surprising, as is the increased levels in choline, compared to control. Methylamines are absorbed by the intestinal mucosa, so it could be suggested that the *B. breve* is not involved in the production of this compound, and may alternatively be inducing increased absorption via the IE [452].

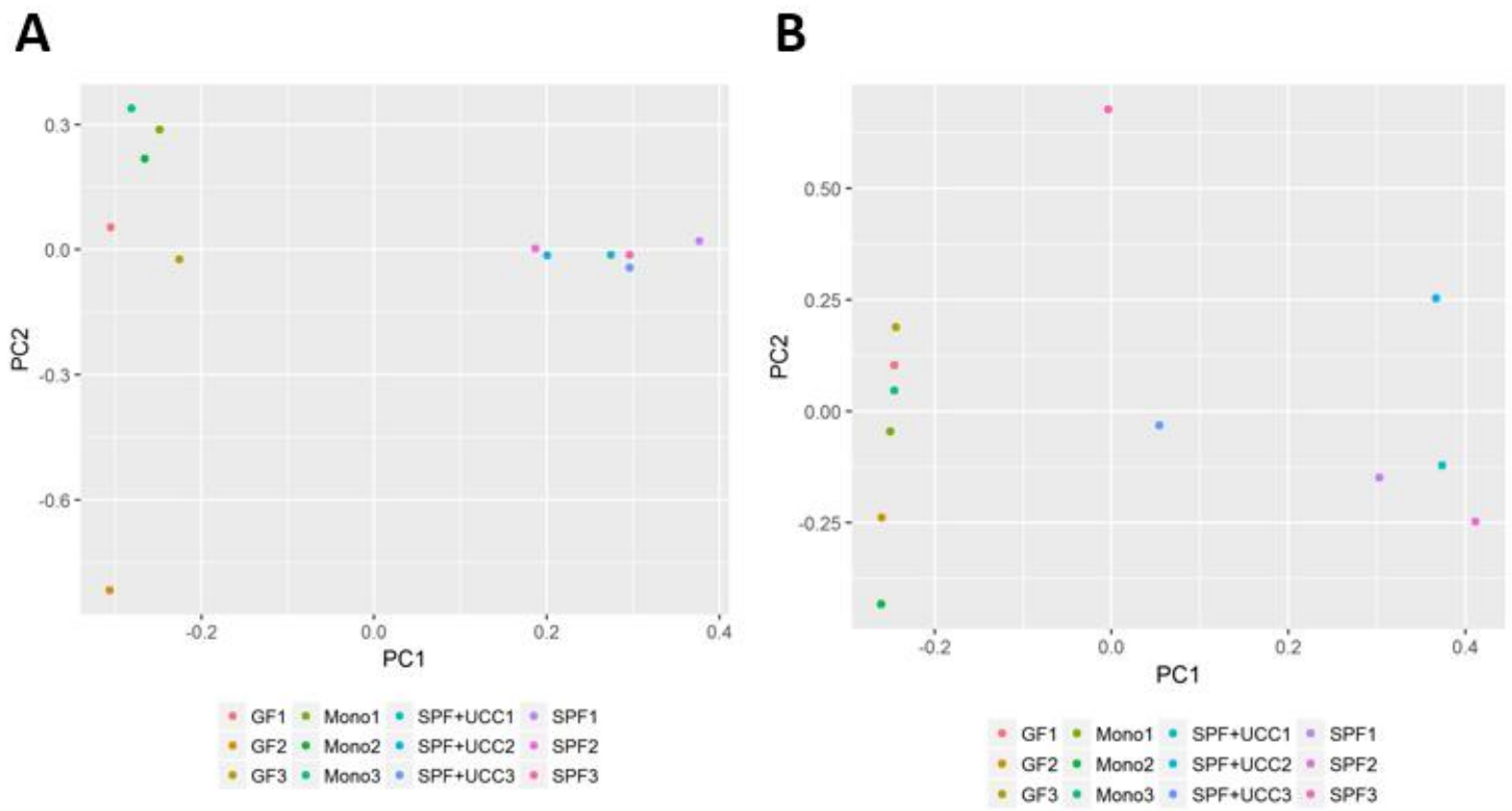

Figure 6-11 ***B. breve*** **colonisation on intestinal metabolome in GF and SPF mice**

(**A**) PCA plot of metabolomic data of germ free (GF), *B. breve* UCC2003 mono-colonised (Mono), conventionally raised (SPF) and SPF mice gavaged with *B. breve* (SPF+UCC) (**B**) PCA based on bile acid profile of GF, Mono, SPF and SPF+UCC

As previously mentioned, bifidobacteria are acetate producers, and intestinal enterocytes absorb this SCFA as a nutrient substrate. However, no significant difference was observed for acetate in GF, compared to mono-colonised mice, which may indicate that the acetate produced by *B. breve* has been absorbed by the host. However, an increase in formate concentration was detected in both the *B. breve* mono-colonised intestine, and *in vitro*, when compared to controls.

This data set was supplemented with metabolomics generated from *B. breve* UCC2003 *in vitro* cultures (stationary growth phase, performed by Jennifer Ketskemety, complete data set in Supplementary Figure 21 to Supplementary Figure 22). A statistical comparison or direct comparative visualisation to *in vivo* metabolites was not possible due to the analysis of one pooled *in vitro* sample, as well as differences in presented concentrations (*in vitro* – mM, *in vivo* – NMR insistently/mg intestinal content). Figure 6-13. shows a selection of biologically relevant metabolites comparing concentration levels in *B. breve* supernatant to non-inoculated MRS control (complete data in Supplementary 5). Strong increases in the concentration of lactate (26-fold), formate (1.29-fold), and glutamate (1.8-fold), was observed in *B. breve* cultures, while dimethylamine, choline and hydroxybuturate were detected at low levels in both conditions, but were not different between *B. breve* compared to control. A decrease in concentration was measured for lactose (-1 fold), glucose (-0.8 fold) and fructose (-0.4).

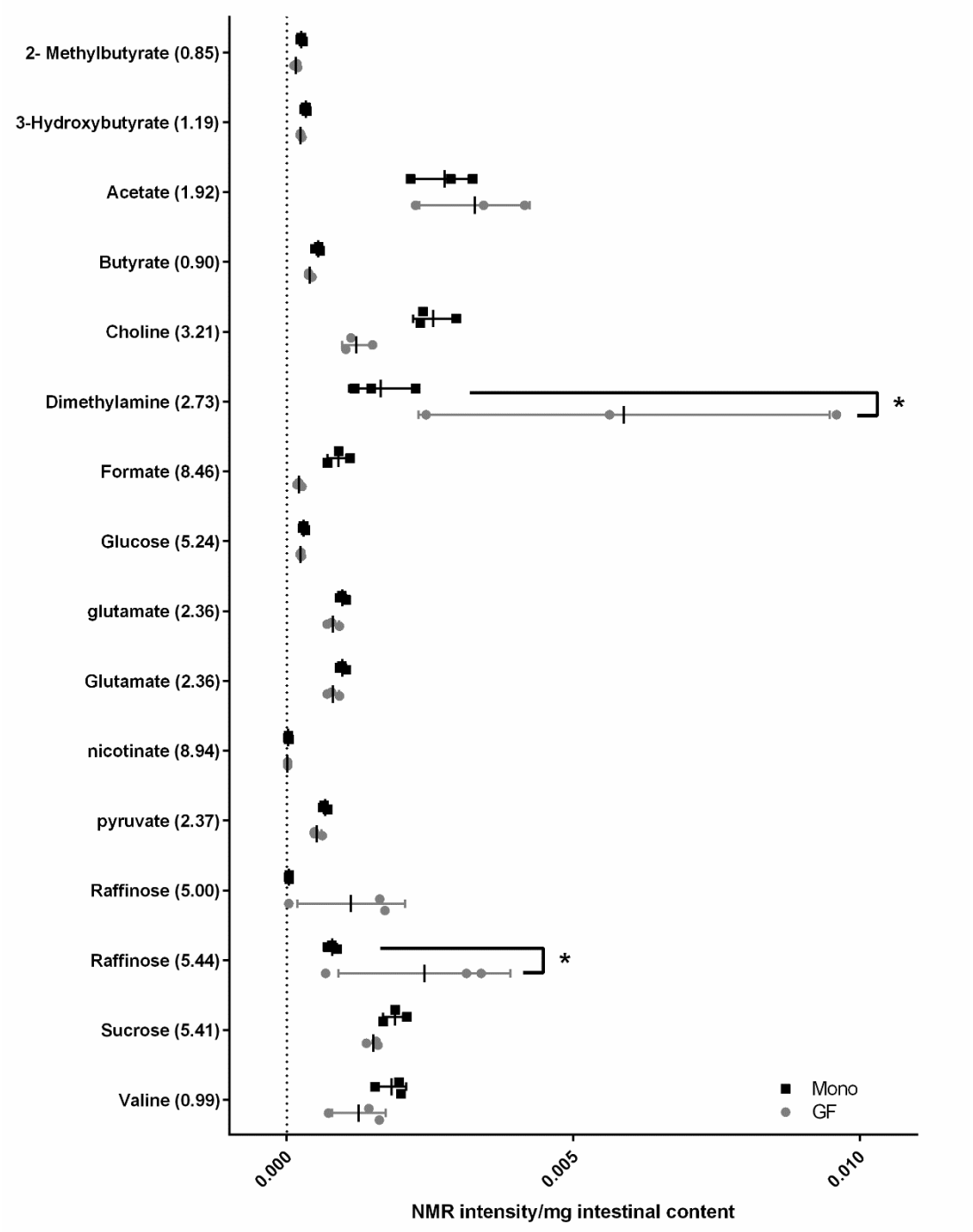

Figure 6-12 ***B. breve* UCC2003 colonisation of germ free mice does not induce a clear profile in intestinal metabolome**

Overview over metabolite concentration in large intestinal content of germ free mice (GF) and mice colonised by *B. breve* UCC2003 (Mono), Data presented as NMR intensity per mg intestinal content, individual values plotted (n=3 mice), mean and SD indicated, statistical significance analysed by Two-way ANOVA with Bonferroni post-test (* p-value < 0.05), values in metabolite name relate to peak location in parts per million (ppm) used for identification, NMR performed by Gwenaelle Le Gall.

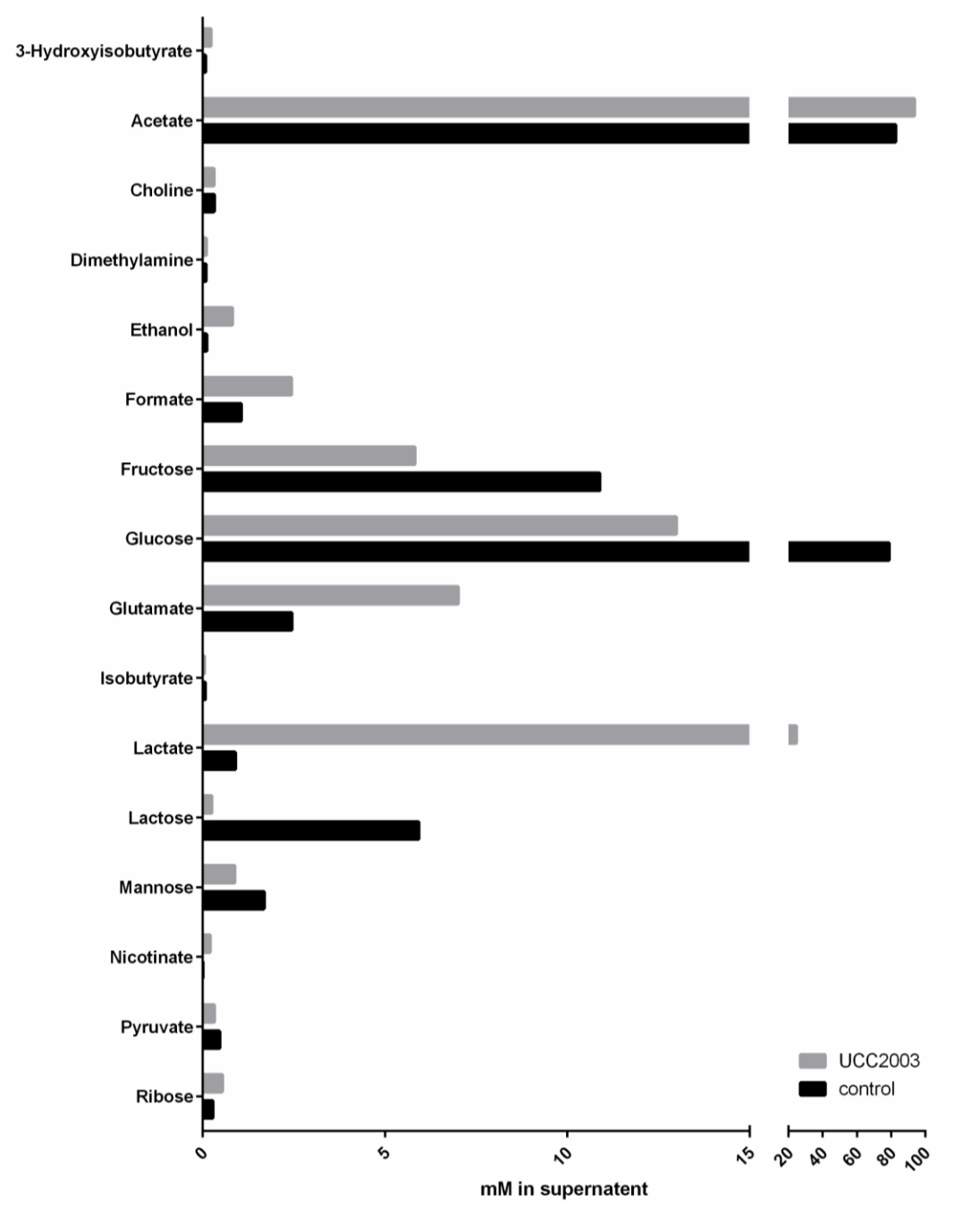

Figure 6-13 Under in vitro conditions *B. breve* UCC2003 shows clear metabolic activity including sugar consumption and lactate production

Data presented as mM concentration in supernatant, single values plotted, *B. breve* cultured in MRS and samples collected at 18 h, samples generated by Jennifer Ketskemety, NMR performed by Gwenaelle Le Gall.

6.3.4 *B. breve* may produce member vesicles, which may play a role in host interactions

As discussed above, microbial metabolites play a key role in modulating host physiology, including IECs. Much of the previous work in this area has focused on the roles of diffusible, small-molecule hormones and nutrients; however recent studies suggest that microbiota-derived metabolites may interact with the host via transport in bacterial membrane vesicles (MVs). Previous work has studied this interaction pathway in Gram positive pathogens; where, MVs are used to deliver toxins, or immune response dampening metabolites, which facilitate bacterial colonisation and invasion [453, 454]. Notably previous studies have suggested that *Bifidobacterium* species may produce MVs, in the case of *B. bifidum* LMG13195, which has the ability to induce polarisation of naïve T cells to T_{reg} cells [455].

Therefore, I hypothesised that *B. breve* UCC2003 may influent host physiology (i.e. IECs) via MVs.

6.3.4.1 Extraction method of potential *B. breve* UCC2003 membrane vesicles

Supernatant from *B. breve* UCC2003 stationary cultures was processed for MVs enrichment (with 100 kDa MW cut-off), and concentrated by ultracentrifugation following an established protocol [456]. The sample was then separated by SDS page, and mass spectrometry (MS), for qualitative assessment of proteins present (Figure 6-14).

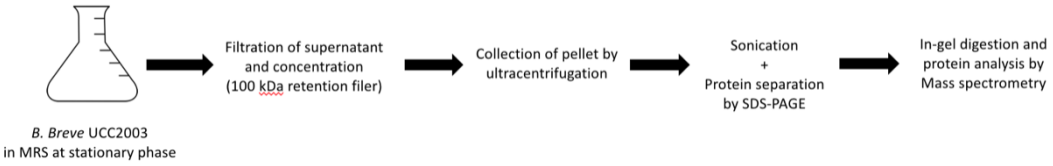

Figure 6-14 Experimental design for isolation of potential MVs from *B. breve* UCC2003 supernatant

6.3.4.2 Proteomic profile of potential *B. breve* membrane vesicle isolation could suggest host interaction potential

Amino acid sequences detected by MS were mapped against *B. breve* UCC2003 Swissprot database, and quality controlled (peptide score >2, protein match significance <0.05). A total of 625 proteins were detected with Table 6-9 presenting top 25 entries based on mascot score. Out of these, seven are involved in ABC sugar transporter systems, and nine contribute to sugar metabolism. The fact that an enolase was detected is intriguing as this putative human plasminogen receptor has been shown to locate to the cell surface of certain bifidobacterial strains, giving them the ability to bind and enzymatically process host plasminogen. This could play a role in host colonisation, and additionally facilitate host interaction, as this has been shown to allow migration across physical and molecular barriers [457].

Table 6-9 Top 25 identified proteins in potential MV isolation from *B. breve* UCC2003 from vitro culture supernatant

(based on mascot score)

Accession Numbers	Protein name	Mascot score
tr|F9Y036|F9Y036_BIFBU	Maltose/maltodextrin-binding protein	16095
tr|F9XZS9|F9XZS9_BIFBU	Solute binding protein of ABC transporter system for sugars	15378
tr|Q0R5Z4|Q0R5Z4_BIFBR	1,4-alpha-glucan branching enzyme	12007
tr|F9XYL0|F9XYL0_BIFBU	Xylulose-5-phosphate/Fructose-6-phosphate phosphoketolase	9779
tr|F9XY00|F9XY00_BIFBU	Solute-binding protein of ABC transporter system for sugars	9222
tr|F9XY86|F9XY86_BIFBU	Enolase	7320
tr|F9Y2C7|F9Y2C7_BIFBU	Solute-binding protein of ABC transporter system for sugars	6569
tr|F9Y1M2|F9Y1M2_BIFBU	Glyceraldehyde 3-phosphate dehydrogenase	4871
tr|F9Y1B7|F9Y1B7_BIFBU	ligopeptide-binding protein oppA	4745
tr|F9Y0H4|F9Y0H4_BIFBU	Penicillin binding protein	4268
tr|F9XZG5|F9XZG5_BIFBU	Phosphoenolpyruvate carboxylase	3702
tr|F9Y2B8|F9Y2B8_BIFBU	Solute binding protein of ABC transporter system	3600
tr|F9Y275|F9Y275_BIFBU	60 kDa chaperonin	3362
tr|F9Y1V3|F9Y1V3_BIFBU	Uncharacterized protein	3292
tr|Q5YBW3|Q5YBW3_BIFBR	60 kDa chaperonin	2997
tr|F9XXW6|F9XXW6_BIFBU	Solute-binding protein of ABC transporter system (Lactose)	2901
tr|F9XZU4|F9XZU4_BIFBU	Solute binding protein of ABC transporter system for sugars	2895
tr|F9Y285|F9Y285_BIFBU	Penicillin-binding protein	2875
tr|F9XZH3|F9XZH3_BIFBU	Alpha-1,4 glucan phosphorylase	2874
tr|F9XYS6|F9XYS6_BIFBU	Type I multifunctional fatty acid synthase	2847
tr|F9XYN9|F9XYN9_BIFBU	Phosphate-binding protein PstS	2835
tr|F9XY36|F9XY36_BIFBU	Glutamine synthetase	2834
tr|F9XZD0|F9XZD0_BIFBU	Beta-galactosidase	2607
tr|F9XYX5|F9XYX5_BIFBU	Glutamine-binding protein glnH	2540
tr|F9Y2R7|F9Y2R7_BIFBU	Leucine-, isoleucine-, valine-, threonine-, and alanine-binding protein	2249

6.3.5 Bacterial host interaction via short RNAs resulted in no clear identification of involved mechanisms

Additional bacterial components that could be transported in MVs, and allow interspecies crosstalk with the host and IECs, are miRNAs. A recent study *in silico* predicted that various bacterial transcripts might generate putative miRNA structures that could interact with the host genome. *In vitro,* these bacterial sequences were shown to regulate target gene expression in human embryonic kidney cells (KEK293), thus mimicking host miRNAs [458]. In another study, a *Mycobacterium marinum* nucleotide sequence was shown *in vitro,* when overexpressed during infection of HeLa cells, to be processed as a host pre-microRNA, and decrease expression of its eukaryotic gene target [459]. Furthermore, vesicles isolated from *Pseudomonas aeruginosa* contained shortRNAs, which *in vivo* reduced lung epithelial cell immune responses (decreased cytokine release and neutrophil infiltration), which facilitated colonisation [460].

6.3.5.1 No RNA detected in potential *B. breve* membrane vesicle isolations

I performed a preliminary analysis for the presence of RNAs in the isolated *B. breve* UCC2003 *in vitro* MV fraction, by detecting transcripts though Bioanalyser. No RNA was detected, with a sensitivity threshold of >5ng. Due to the short length of miRNAs, analysis by other means such as RNA-seq, miRNA targeted qPCR, or Agilent small RNA analysis kits would have to be performed. The proteomic data contained 33 entries related to RNAs processing, including ligases, methyltransferases, and polymerases, which might suggest transcript presence, but further studies would have to be performed to confirm this.

6.3.5.2 Host miR 21 has predicted binding sites within *B. breve* genome, but does not affect growth *in vitro*

Recently, it has also been determined that host transcripts (i.e. miRNAs) may modulate bacterial transcription, thus providing a two-way dialogue between microbe and host. The authors detected host miRNAs in the intestinal lumen, and observed a growth promoting effect (*in vitro)* of a specific transcript on *E. coli*. Mice

deficient in miRNAs in IECs showed abnormal gut microbiota composition, and reconstitution of these mice with faecal miRNAs restored microbiota profiles [461].

As described in chapter 5.3.7 (Supplementary Figure 12), I observed a decrease in host miR21 expression in whole large intestinal homogenates of neonate and adult mice colonised by *B. breve* UCC2003. I hypothesised that this effect could allow *B. breve* to either (i) facilitate its own colonisation (e.g. growth promoting effects), or (ii) by modulate the overall microbiota composition. In collaboration with Padhmanand Sudhakar (EI), *in silico* binding sites of miR-21-3p (NCBI gene ID 406991) were identified by miRbase in the bacterial genomes of *B. breve* UCC2003 and *S.* Typhimurium SL1344 (NCBI GenBank ID: FQ312003.1) [462]. This analysis yielded 263 miR21 targets within the *B. breve* genome, and 370 when using *S.* Typhimurium SL1344 (Supplementary Table 7 and Supplementary Table 8 respectively).

To address the first hypothesis, I performed growth kinetics of *B. breve* in the presence of miR21. No effect by the transcript was detected (Figure 6-15.A). To perform preliminary experiments on the second hypothesis, the effect of miR21 on *S.* Typhimurium SL1344 growth was assessed, but no modulation in growth was detected (Figure 6-15.B).

These generated data, including proteome of potential *B. breve* MVs, and bindings sites of host miR21 in bacterial genomes, lays the foundation for future investigations into *B. breve* host modulation via MVs, which will be outlined in the future work section.

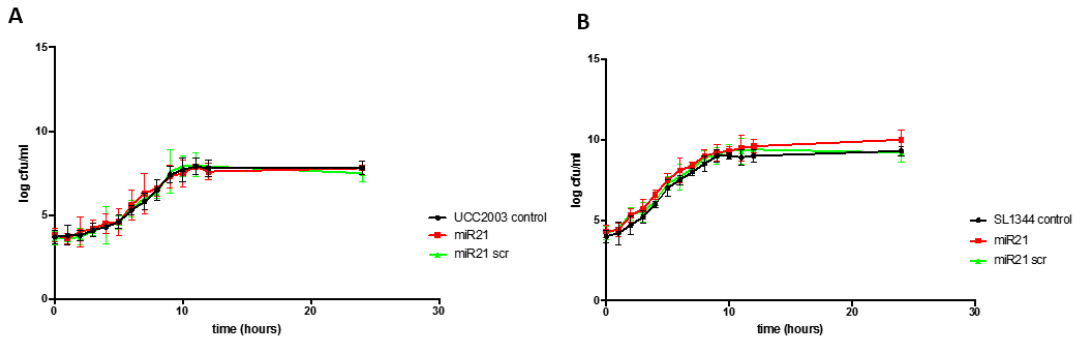

Figure 6-15 miR21does not affect growth kinetics of *B. breve* UCC2003 and *S.* Typhimurium SL1344 in vitro

Growth kinetics presented in cfu/ml over time of (**A**) *B. breve* UCC2003 and (B) *S.* Typhimurium SL1344 grown in MRS/LB with 10 µg/ml miR21, or scrambled control, data shown as mean +/- SD, limit of detection $2x10^1$ cfu/ml.

6.4 Discussion

Understanding how specific microbes, and the wider microbiota, changes at a transcriptional and metabolite level, in response to different environments (i.e. *in vitro* vs *in vivo*), is important for enhancing our understanding of what key microbial factors may promote host health, and thus aid in the design and development of new targeted therapies. In this chapter, I determined that *B. breve* UCC2003 has a distinct transcriptional profile *in vivo,* when part of the wider gut microbiota, and as a single species within the host (i.e. in gnotobiotic mice). Furthermore, *B. breve* appears to 'switch-on' specific GH, as well as iron scavenging pathways, and decreases EPS cluster gene expression in the GF gut, relative to *in vitro* levels. Assessment of the impact of *B. breve* UCC2003 colonisation on overall microbiota function indicates decreases in carbohydrate metabolism, as well as increases in overall protein synthesis. Intestinal metabolomic profiling did not suggest a clear modulation by *B. breve* UCC2003 in GF, or conventionally raised mice.

It is currently unclear what specific pathways *B. breve* UCC2003 utilises *in vivo* for metabolism of host-derived dietary components, and how this may link to colonisation of the GI tract, and modulation of the wider microbiota via cross-feeding. Notably, I identified upregulation of gene clusters previously shown to be involved in HMO utilisation in mono-colonised GF mice. HMOs in human breast milk cannot be metabolised by the infant, and are believed to directly shape the early life microbiota by acting as a prebiotic [463]. The described pathway has been characterised in *B. breve* UCC2003, but several other species, including *B. bifidum* and *B. longum* possess gene clusters with similar function [397, 464]. It is interesting to observe upregulation of key enzymes in this process when *B. breve* is present in the intestinal tract of adult mice, which feed on a chow rather than milk-based diet. Notably, HMOs have a very similar structure to host derived mucins, and previous

studies have indicated that these pathways can be utilised for both HMO and mucin degradation, which may indicate that *B. breve* is directly utilising these host-derived carbohydrates, or other similarly structured chow-based carbohydrates [395]. These findings, may lead to the identification of additional compounds able to feed bifidobacteria *in vivo,* in cases where HMO delivery via breast milk is not possible e.g. via supplementation of formulas.

Interestingly, when I compared expression profiles of mono-colonised mice to SPF mice colonised with UCC2003, there was significant upregulation of specific genes involved in metabolism, which may link to the availability of nutrients in a complex microbiota ecosystem. Within the adult microbiota, there is an intricate network of microbes that each utilise different dietary components, and in turn cross feed other microbial neighbours. I observed upregulation of an ABC sugar transporter permease in SPF mice, when compared to GF, which has been shown to facilitate transport of various oligosaccharides from simple maltose and lactose, to more complex fructo-oligosaccharides and xylose [465]. An upregulation of this permease in the presence of the wider microbiota, in comparison to gnotobiotic conditions, might be because of the availability of different sugars due to breakdown of complex carbohydrates otherwise unavailable to *B. breve* by intestinal bacteria. Indeed, other complex carbohydrate digesting bacteria, such cellulolytic *Eubacterium* spp and B*acteroides* spp may increase the availability of carbohydrates available for uptake by *B. breve,* and hence warrant an increase in specific transport systems [466]. Interestingly, metabolomics data indicated a decrease in raffinose in mono-colonised mice, in comparison to GF, and previous studies have indicated that different bifidobacterial strains show preferential utilisation for this sugar *in vitro,* over glucose [467]. Therefore, these data suggest that *B. breve* UCC2003 also prefers this sugar *in vivo*.

Regarding cross-feeding, the converse is also true, i.e. the introduction of *B. breve* into the wider microbiota would also be expected to impact overall metabolic function. As mentioned above, bifidobacteria can utilise a wide range of carbohydrate sources, with at least 10% of its genome encoding proteins related to transport and metabolism of carbohydrates, indeed this genus represents one of the most efficient microbiota members at metabolising diverse dietary components [258, 468]. This has been shown to heavily influence overall carbon source range and

availability. This effect is more pronounced in early life with bifidobacteria being one of the earliest colonisers, degrading specific HMOs, and host mucins (as discussed above), and producing breakdown products that are available to the wider microbiota (e.g. lactate and acetate). No changes were detected in either lactate or acetate comparing SPF with SPF *B. breve* colonised mice, as well as GF with *B. breve* mono-colonised mice. However, this could be due to absorption of these metabolites by IECs, which are known to act as energy sources, and also modulate anti-inflammatory effects [469]. Notably, the SCFA formate was increased in the presence of *B. breve* (*in vitro* and *in vivo*). Relatively little is known about its biological function, but a recent publication determined that overgrowth of Proteobacteria, such as *E. coli*, during intestinal inflammation, was associated with formate oxidation, and aerobic respiration [394, 470]. This was accompanied by an increase in formate concentrations in the gut, and interestingly the authors did not observe formate in GF mice, indicating it is bacterial derived. Bifidobacteria are able to also produce formate, as part of their carbohydrate metabolism, with the ratio between formate, lactate, and acetate dependent on substrate types available [471]. Generally high levels of formate production correlated with low levels of acetate and vice versa, which may indicate that *B. breve* UCC2003 is also a major formate producer, and would be of interest to follow-up in subsequent studies.

Regarding carbohydrate metabolism, I observed a decrease in overall microbiota functional abundance in this SEED class, which could suggest that the presence of *B. breve*, with its arsenal of carbohydrate digestive capabilities, allows other microbiota members to decrease their own carbohydrate breakdown systems and cross-feed in the presence *B. breve*. This could in turn allow for these members to have a more efficient metabolism, due to decreased effort in nutrient acquisition, and lead to the observed increase in protein synthesis SEED class abundance. It would be interesting to relate these functional changes to modulation of taxonomy, to investigate which specific members might cross-feed, but due to classification at family level no clear function can be associated with the modulated taxa. Taken together, it could be suggested that *B. breve* UCC2003 colonisation increases overall nutrient availability for microbiota members, causing an increase in overall metabolomic functionality. This trait could prove significant for bifidobacterial colonisation (even at low

modulation levels as observed in these data i.e. <1%), as a previous supplementation study in humans indicated that stable engraftment of *B. longum* AH1206 was associated with low abundance of resident *B. longum*, and underrepresentation of specific carbohydrate utilisation genes in the pre-treatment microbiota. This suggests that bifidobacteria may promote resource availability, which allows more efficient colonisation, which may prove central for development of long-term, and personalised microbiota reconstitution strategies [472].

Although there is a steady supply of dietary carbohydrates in the GI tract, the host directly limits the availability of certain nutrients e.g. iron, to reduce the colonisation of pathogenic microbes. To overcome this restricted availability, many microbes have evolved iron scavenging systems, including *Bifidobacterium*. Notably in GF mono-colonised mice (when compared to iron-rich *in vitro* conditions), I observed significant upregulation of an iron scavenging pathway previously shown to be under the control of auto-inducer AI-2. The transcription of the enzyme producing AI-2 as a by-product (encoded on luxS, BBr_0541, gene552) was slightly, but not statistically significantly upregulated [473]. AI-2 expression regulation has been related to population density (quorum sensing) by secretion and sensing of AI-2 in the environment [474]. It was found that conditions with high glucose and acidic pH, such as found in *in vitro* culture in MRS, has strong inhibitory effects on AI-2 activity. Hence, it is possible that *B. breve* UCC2003 does not produce AI-2 via luxS *in vitro,* due to growth conditions, while during mono-colonisation does upregulate its expression, which in turn could induce the iron scavenging pathway. Previous studies have shown that this cluster is upregulated *in vivo*; in conventionally raised Balb/C mice gavaged with *B. breve* UCC2003, relative to *in vitro* data (analysed by microarray). In the same study, using the model organism *C. elegans*, the genes bfeU and bfeB were identified to be critical for iron uptake, and GI tract colonisation, and interestingly each mutant exhibited a significantly decreased ability to confer protection to *Salmonella*-infected nematodes, as compared to the WT *B. breve* UCC2003. In my data, the corresponding gene to bfeU (gene225, BBr_0221, membrane spanning protein with iron permease) was not differentially regulated, while bfeB (gene227, Bbr_0223, hypothetical membrane spanning protein) was upregulated by 2.7 log2 fold. These data highlight the importance of iron acquisition

in gut pathogen protection, and may be important targets for subsequent colonisation resistance studies

An additional bifidobacterial component that has previous been shown to play a role in resistance to enteric infections, including the pathogen *C. rodentium* (a mouse model pathogen for human-associated Enteropathogenic *E. coli*), is the EPS capsule. Surprisingly, in mono-colonised GF mice, I observed downregulation of genes involved in EPS production in *B. breve*, relative to *in vitro*. Alongside, its potential anti-infection role, the EPS capsule has also been shown to play a role in bile and acid resistance, facilitating colonisation of the GI tract, however GF mice had high colonisation levels after gavage suggesting that EPS may not be required for optimal colonisation in the 'naïve' murine GI tract. Previous studies have indicated the GF mice have an altered pH and bile acid profile (which is directly linked to microbiota processes, and discussed in more detail below), thus may also be linked to reduced expression of EPS in these conditions; i.e. *B. breve* can downregulate EPS expression (and thus reduce its overall metabolic burden) in this environmental niche [475, 476]. Comparing this result to SPF mice, the overall microbiota functional abundance showed a significant decrease in polysaccharide production in the presence of *B. breve*, but a slight elevation of EPSs, which may indicate other microbes are inducing this expression. As the metatranscriptomics data did not map any EPS gene reads to the *B. breve* genome, we cannot determine if EPS expression is induced in this complex microbiota environment, when compared to mono-colonisation.

Within the artificial environment of *in vitro* culture, EPS expression may be high due to the largely unlimited availability of nutrients. Indeed, previous work on bifidobacterial EPS capsules has suggested that sugar precursors may be involved in modulation of expression and production; *B. longum* subsp. *longum* CRC 002 was found to have enhanced EPS production on lactose compared to glucose, which directly impacted cell wall polysaccharide biosynthesis [477]. Interestingly, and as highlighted previously (chapter 1.4.4), the EPS capsule also plays a key role in immune-modulation, serving as an immune 'silencer' to avoid recognition by the host, and thus promote long-term persistence. As GF mice have an immature immune system the downregulation of EPS gene cluster potentially links to this host

system, and it would be of significant interest to explore this further by performing additional immune assays [478].

Bifidobacteria are bile tolerant, which aids colonisation of the intestinal tract, and several factors, such as bile efflux transport systems and bile salt hydrolases, are involved in this process. Notably, calcineurin-like phosphoesterase, which convers bile resistance to *B. breve* UCC2003, is upregulated in the presence of other bacteria. While BA concentrations are higher in the ileum of GF mice compared to conventionally raised mice, the faecal excretion is 63% lower [479, 480]. Correspondingly, I observed more diverse and higher concentrations of BAs in SPF mice compared to gnotobiotic mice, suggesting the requirement of *B. breve* to increase its BA resistance mechanisms. This has been attributed to the microbiota modulating the BA pool within the LI by deconjugation, dehydrogenation and dihydroxylation, making it chemically more diverse. This metabolism of BA offers bacteria a source of carbon and nitrogen, as well as sulphur, in addition to giving bile resistance, and capabilities to grow within the presence of BAs. Indeed, gene800 (Bbr_0780), a hydrolase of the haloacid dehydrogenase super family, was upregulated, but is has not yet shown been shown if this family is involved in bile salt deconjugation. Bifidobacteria such as *B. longum* SBT2928 do harbour bile salt specific hydrolases, and can utilise these enzymes for human and animal BA modification [481]. Recently, a feedback pathway has been identified that links bile acid concentration in the intestine, to production in the liver [482]. T-β-MA is present in high concentrations in the intestine of GF mice, as is it not being deconjugated by microbes, and acts as an antagonist to farnesoid X receptor in enterocytes, which in turn reduces levels of fibroblast growth factor 15 (FGF15) release. FGF15 acts as a suppressor of T-β-MA production in the liver, closing the feedback loop. In conventionally raised mice, T-β-MA is deconjugated and hence more FGF15 is released to reduce production of the BA. However, I observed higher concentrations of T-β-MA in *B breve* mono-colonised samples, and previous publications indicate that *B. longum* can deconjugate this BA, as well as taurocholic acid. Furthermore, an publication from 1987 indicated that *B. longum* was able to process taurocholic acid, but not tauro-beta-muricholic acid [483]. As deconjugation of muricholic acid, by a complex microbiota, acts as a signalling feedback loop to

the liver to decrease bile acid production, and as no decrease in T-β-MA was observed in my samples, this might explain the higher BA concentration in SPF samples, compared to GF or mono-colonised groups.

Within the datasets, I also observed a significant number of hypothetical genes that were differentially regulated. Some shared sequence homology with other bacterial genes, while others did not. Although *Bifidobacterium* represent an important beneficial genus, mechanistic phenotypic studies into specific genes has proved difficult due to issues with molecular manipulation; particularly due to the high number of R/M systems, and the EPS capsule, which limits uptake and integration of 'foreign' DNA. These issues have somewhat limited large-scale annotation of genes to function, and thus it is not surprising I observed so many hypothetical genes in this dataset. It would be of significant interest to probe the function of these hypothetical genes, particularly the ones that are highly differentially regulated (e.g. gene55, Bbr_0055), and recently a genome wide mutagenesis library in *B. breve* UCC2003 has been generated which would allow these studies [484]. While screening of all mutants *in vivo* is not feasible (preliminary *in vitro* experiments have been performed), the generated data set could allow for better informed selection of genes for further study.

The approach used to analyse these large RNA-Seq datasets was DESeq2, which was used to detect differential gene expression between groups [374]. This software package is optimised for small samples sizes, and large dynamic range between replicates. This pipeline improves regulation analysis, via the previously mentioned shrinkage estimation (subsection 5.3.5), to ensure stable and reliable calling of differential expression, as well as accurate quantification of fold changes. It has been utilised in more than 3500 published RNA-seq studies since its release in, including several bacterial transcriptome studies (NCBI, accessed on the 24.1.2017). However, the numbers of biological repeats analysed for differential gene expression can greatly impact accuracy and precision, with lower replicates increasing false positive discovery rates [485]. The group of *B. breve* UCC2003 transcription *in vitro* contained two biological replicates, which is the suggested minimum threshold for DESeq2. Low replicate numbers have been shown to affect correct identification of differential gene expression, not only in DESeq2, but all commonly used analysis

packages [485, 486]. This is because of the requirement to account for inter-replicate variability of biological samples. To support the results presented, either sample size would have to be increased or validation by different analysis software to be performed. With regards to the metatranscriptomic datasets, there are some additional limitations of DESeq2; there is a requirement of minimum splicing distances, which in bacterial transcription discards any genes mapped to gene boundaries. As bacterial genomes lack introns, this setting causes a proportion of genes to be filtered out. In a single species sample with high expression, these changes can be disregarded as they are normalised between repeats, while in metatranscriptome samples, with typically low expression, this can significantly reduce detected gene expression. As *B. breve* colonises the adult mouse gut at low abundance, and metagenomic abundance can at least in part be correlated to metatranscriptional abundance in the gut microbiome, the limitations of this method should be considered [130]. Recently a new mapping tool, HISAT2, has been developed which allows for enumeration of mapping data based on unique reads which circumvents the Bowtie2 intron problem [487]. This tool will be applied in future analysis of the data sets to validate and ensure robust *B. breve* UCC2003 transcriptional quantification.

The potential of *B. breve* to crosstalk with the host via MV is an intriguing avenue of scientific exploration. Host modulation via MVs has been extensively studied in pathogens, but recently their role in commensal bacteria is being explored. An important finding showed extracellular vesicles from *B. breve* NutRes200 inhibited TLR2/6 induction, while enhancing TLR2/1 and TLR4 responses, and also enhancing phagocytosis by DCs *in vitro* [488]. The isolated fraction of *B. breve* culture medium could potentially include MVs, as the applied purification method enriches for molecular weight of MVs identified in *Bacteroides* spp. [489]. In addition, the generated proteomic data provides a platform for further analysis, as published proteomic analysis of MVs from *P. aeruginosa* categorised 57% of detected proteins to be cytoplasmic, 25% as extracellular, and 16% membrane bound [490]. This was performed by assignment of GO classes, which also allowed assessment of functional groups. This poses a feasible next analysis step for the

generated data, which could then form the basis for future investigations of potential bifidobacterial MVs.

The preliminary investigation of RNA presence within the potential MV isolation was based on previous studies that suggested host transcriptional regulation by bacterial non-coding RNAs. A study in *C. elegans* revealed two *E. coli* transcripts to downregulate gene expression in the host, while in *M. marinum* a short bacterial RNA was found associated with host RNA processing machinery (RISC complex) during *in vitro* cell infection, and when overexpressed resulted in host target transcriptional repression [491, 492]. Even though I was not able to detect RNA in the MV isolation, the applied method for RNA detection by Bioanalyser has a detection limit of 5 ng.

The observation that host miRNAs modulate intestinal microbiota composition, and specifically affect growth of certain species was a unique finding by Liu *et al.* [461]. However, to my knowledge no other primary research has been published on this mechanism. My preliminary growth kinetic experiments indicated that miR21 did not modulate *B. breve* or *Salmonella* growth. However, it cannot be discounted that miR21 may affect different physiological aspects of bacterial physiology, such as EPS or pili synthesis, which have implications for host bacterial interactions. To investigate this, the preliminary bindings site identification of miR21 in *B. breve* and *S.* Typhimurium genome may allow identification of specific genes that might be regulated. It should be noted that the applied method relies on sequence homology alignment, while a more precise analysis would involve bindings site prediction, taking into account secondary structure, and mismatches within mRNA seed sequences.

In summary, I have shown distinct *B. breve* transcriptional profiles *in vivo*, comparing between gnotobiotic colonisation, and presence within a complex microbiota. This includes genes involved in metabolism of differing nutrient sources, as well as bile acid resistance, and increased stress responses. In addition, relative to *in vitro* conditions, *B. breve* increases expression of iron scavenging and GH clusters, while downregulating EPS production in gnotobiotic conditions. The generated metabolomic data yielded no distinct differences due to the presence of *B. breve* in gnotobiotic and SPF mice, while overall microbiome function was

modulated by *B. breve* colonisation, with increases in protein production and decreased carbohydrate metabolism. These data provide new insights into the adaption of *B. breve* UCC2003 to each environment, and indicates key factors to be investigated further with the aim of developing new probiotics.

6.5 Future plans

The presented data implies distinct transcriptional responses of *B. breve* to differing *in vitro* and *in vivo* conditions, based on the applied bioinformatic pipeline including, Bowtie2 mapping of reads to the *B. breve* genome, followed by transcript enumeration by HTSeq and differential gene expression calculation by DESeq2 [298, 299, 374]. To improve on this approach several measures will be applied in the future.

DESeq2, as mentioned in the previous section. was optimised for small sample sizes common in next generation sequencing experiments, but an increase of biological repeats for the *in vitro* sample group (currently 2 biological replicates) will greatly improve the accuracy of DEG calculation. Similar, the comparison of *B. breve* UCC2003 transcripts between GF and SPF colonised mice can be improved upon due to the current low *B. breve* UCC2003 gene count in the SPF samples, which could interfere with the applied shrinkage estimation of gene expression dispersion and impact precision and verified calling of differential expression. This will be approached by utilising SAMSA2, a bioinformatic tool specifically designed for met-data annotation based upon MG-RAST, a public meta-data annotation service which uses DIAMOND as high throughput aligner and automated pre-processing of raw reads [493-495]. In addition, the previously mentioned difficulty in quantifying bacterial transcripts with conventionally tools (chapter 6.3.1.5), due to lack of introns in bacterial genomes, will be addressed by utilisation of HISAT2 [487]. This will allow for more accurate transcript enumeration for both the UCC2003 genome, as well as the metatranscriptome data set.

These changes will allow for increased information extraction from the metatranscriptome data, and could allow for identification of differential gene expression of other bacterial microbiota members in the presence and absence of *B. breve* UCC2003. This could lead to the identification of specific cross-feeding relationships as suggested by my presented data.

With the advent of meta-transcriptional data, instead of analysing gene expression of host and bacteria independently, “dual RNA-seq” has emerged, allowing for identification of transcriptional profiles of both from the same sample. This has been

successfully applied by Illot *et al.* to profile host responses during colitis induced by *H. hepaticus* infection, while integrating these results with changes to microbial transcription (normalised to modulation of DNA abundance changes induced by pathogen colonisation) [140]. Compared to this approach, my data would allow me for a "paired RNA-seq" analysis as host and bacterial transcripts are not identified from the same sequencing samples. This would still potentially identify overlapping responses between IEC DEGs, and bacterial DEGs, to integrate host effect with bacterial physiology.

An essential step for all next generation sequencing data is validation. Technical replication by qPCR should be the first approach with the additional benefit of potentially increasing samples size, resulting in increased certainty in the observed modulation and its biological significance. This would then be followed by probing the identified mechanism in biological systems *in vitro* or *in vivo*. Due to the difficulties in genetic manipulation of *B. breve* UCC2003, this could be circumvented by assessments of physiological changes, such as in the case of downregulation of EPS production *in vivo*, via SEM visualisation. Fortunately, the lab has access to a Transposon Directed Insertion Sequencing (TraDIS) library, which after full characterisation of the generated mutants, could allow for testing of the generated hypothesis in the different models. A potential first experiment would include the investigation of the identified HMO metabolomic cluster, showing upregulation in gnotobiotic mice, to assess its essentiality for colonisation, and going further by comparing its role in GF, and also the SPF intestine of adult and neonate mice. It could be hypothesised that this cluster is involved in processing of carbohydrates other than HMOs, as these were not present in the GF mouse. Hence an investigation into other substrates could be started *in vitro*, with a potential candidate being host derived mucus, with potential results being taken forward *in vivo*.

Lastly, future experiments regarding host bacterial crosstalk via MVs, and non-coding RNAs will also form part of potential future work, but some initial key studies need to be completed to indicate if these are worthwhile avenues to explore. In particular, to determine the production of MVs by *B. breve* UCC2003 with

certainty, SEM imagining of the supernatant isolation prior to sonication will be carried out.

7 Conclusion and perspectives

Bifidobacteria are early, and abundant, gut microbiota colonisers, that remain in the human intestinal tract throughout life [156]. The genus is generally associated with host health, and in particular lower abundance has been observed in IBD patients, with supplementation reducing incidence of relapse [284, 321]. Several studies have investigated potential health beneficial effects, including immune modulation, promoting intestinal homeostasis, and IEC specific actions, such as strengthening of TJs during homeostasis, and pathological disruption, but our understanding of the underlying mechanism is still incomplete [201, 246, 281, 282]

Therefore, I sought to determine how *B. breve* UCC2003 affects IECs, either directly, by modulating specific host functions, or in concert with the intestinal microbiota, to deliberate its health benefits.

7.1 Summary of results and future research directions

The aim of this study was to investigate the role of *B. breve*; both on the host, focussing on the ion channel Piezo1, and then more globally via the IEC transcriptome, and additionally probe *B. breve in vivo* transcription, and exploring how *B. breve* colonisation modulated the wider microbiota. The overarching goal was to identify host factors modulated by *B. breve*, and pinpoint bifidobacterial components that may regulate these effects.

Initially, using relevant mammalian intestinal *in vivo*, *in vitro*, and *ex vivo* models, I assessed the role of Piezo1 in mammalian cell shedding. However, no changes to protein levels during elevated shedding rates were observed. Additionally, no transcriptional modulation in UC patient biopsies was detected, compared to controls. This suggests that differential translation of Piezo1 does not play a role in inflammation-induced cell shedding in the mammalian intestine. However, I did observe Piezo1 cellular positions along the IE, aligning with its proposed role of sensing cell crowding at sights of cell extrusion (villus), and cell stretch at sights of division (crypt) is intriguing. This finding will be further investigated with mechanistic studies *in vivo,* as only inhibition/ depletion or activation/overexpression

can fully answer the involvement of the ion channel Piezo1 in shedding. Hence, application of the Piezo1 inhibitor gadolinium in an intestinal loop model will conclude this avenue of questioning. The generated data are a direct measurement of Piezo1 function on cell extrusion in the mammalian intestine, not only during pathological extrusion, but also in heath and homeostasis, which will significantly add to the research field and pose interestingly questions as to the requirements of this protein, in more physiologically relevant models than tested previously.

Although studies into Piezo1 did not indicate that *B. breve* colonisation altered this ion channel, my previous studies in the LPS cell shedding model indicated a direct modulatory role for *B. breve* on IECs. Thus, I utilised global RNA-seq of IECs as an unbiased approach to assess transcriptional changes induced by *B. breve* UCC2003.

I observed a strong, and distinct, profile in neonatal mice, with the effect reduced, in number of regulated genes and amplitude of regulation, in adult IECs. This is particularly interesting as early colonisation of *B. breve* has been linked to health beneficial effects, such as reduced incidence in asthma [496]. With strong immune modulatory effects on naïve hosts, and a more plastic infant microbiota, the observed stronger effects in neonates support the notion of bifidobacteria as an important early life coloniser, and could suggest that it is required for a healthy 'status quo' [154, 497].

Particularly promising targets identified in neonate IECs included; TLR2, TLR9 and IL-17C. Transcriptional upregulation of these genes could potentially improve epithelial barrier function, and induce anti-inflammatory stimuli, resulting in intestinal homeostasis. Intriguingly, these modulations occurred during homeostasis, without inflammatory insult, further supporting the pivotal role of *B. breve* in health. These findings suggest bifidobacterial effects may offer protection from disease initiation, and therefore highlight the use of this microbe as a prevention strategy. The increase in specific integrin expression, and overall integrin signalling, could be the most promising effect observed, due to their important role in intestinal epithelial integrity, barrier functions, and protection from insult [411, 413]. Future work will investigate these targets individually to observe the biological effects of their differential regulation in models of intestinal health and disease.

Analysing *B. breve* transcriptional responses *in vivo,* comparing between gnotobiotic colonisation, and in the presence of a complex microbiota, I observed a distinct profile, including upregulation of stress responses, bile acid resistance, and utilisation of different metabolism pathways. Compared to *in vitro* conditions, *B. breve* increased expression of iron scavenging, and carbohydrate metabolism clusters, while downregulating EPS production. While colonisation did not modulate the metabolome in GF and SPF mice, *B. breve* did increase overall microbiome gene expression with respect to protein production, while decreasing carbohydrate metabolism. These results indicate that *B. breve* colonisation alters both the taxonomy, and function of a complex, established community during intestinal homeostasis. This is an impressive finding, and supports the use of bifidobacteria in modulating the intestinal microbiota, with the aim to improve host health or treat disease. Exploring this effect further, by improved metatranscriptome analysis, could reveal transcriptional regulation of specific members and functions, significantly adding to our current knowledge of bifidobacteria crosstalk [258]

The *B. breve* specific upregulation of carbohydrate metabolism, and iron scavenging during monocolonisation, supports our knowledge of *in vitro* experiments and *in vivo* observations of bifidobacteria offering protection from pathogen colonisation, and as a cross feeder, through complex carbohydrate metabolism in early life and adulthood [156, 358, 498]. These *in vivo* functional observations have given insight into *B. breve* intestinal adaptation, and indicate target factors to be investigated for host and microbiota modulatory effects, with potential health beneficial effects as probiotics.

Overall, my work has generated a comprehensive overview of *B. breve* effects on the host epithelium, and intestinal microbiota transcription. These data lay the groundwork for further investigation on host-bacterial cross talk. Additional analysis of the metatranscriptome data to identify specific functional microbiota modulation by *B. breve*, as well as the integration of host and bacterial transcriptomics, will generate a holistic network furthering our understanding of microbiota intestinal epithelial interaction. Crucially, the identified bacterial and host IEC targets, are promising mechanisms to exploit for improving host health, and development of new probiotics.

7.2 Impact of findings and translational aspect of research

The intestinal epithelial barrier is crucial for health, whilst its breakdown, leading to a 'leaky' barrier, is linked to numerous diseases, therefore understanding the underlying mechanisms involved in its maintenance are essential [94].

To my knowledge, this study is the first to investigate Piezo1 as a regulator of epithelial cell shedding in the mammalian intestine, with previous studies utilising *in vitro* and zebrafish models [499]. Hence, this investigation, with the proposed additional intestinal loop study, is contributing knowledge to an important field of research for human health, which may have direct relevance for development (or not) of drugs targeting Piezo1.

Additionally, as there is a significant unmet need for new IBD treatments, which will induce, and retain remission, or even prevent onset; therapies that may induce these responses are in high demand. Bifidobacteria, which are reduced in abundance in IBD patients, and previous probiotic human trials, which suggest they may provide beneficial responses in both CD and UC patients, represent a promising cost-effective and non-toxic avenue to further explore, with the aim of improving human and intestinal health [102, 361, 500, 501].

The generated global datasets of *B. breve*-induced host, bifidobacterial, and microbiota transcription *in vivo* responses contributes substantial knowledge on host-microbe interactions to the scientific community, with future data mining, and integration of multi 'omic data, aiding in hypothesis generation and validation. Furthermore, identified host target could generate leads for drug development, while bacterial transcription patterns could aid in targeted probiotic selection and development. This could improve treatment of a wide variety of intestinal pathologies involving the IE, and inflammation, such as IBD and NEC, together with developing our understanding of how probiotics confer their effects.

Particularly modulation of IEC integrins by *B. breve*, in recent light of IBD SNP identification in these genes, and drug treatment targeting immune homing via this mechanism, offers an intriguing insight into the potential future of personalised medicine and a novel mechanism of improving epithelial integrity [102, 410].

Additionally, this study has shed light on the homeostatic modulatory effects of bifidobacteria during different life stages, including early and later life, which significantly increases the scientific knowledge of “lifelong” gut health, as a public health target. As bifidobacteria are an important member of the gut microbiota, this is a particularly important area of research [67, 236, 502].

Lastly, this study has given scientific support to the notion that specific bacteria, and their modulation of the intestinal microbiota, can affect host health. This is particularly important, as changes observed during homeostasis, when this signature is lost, could indicate heightening risk of disease development, offering biomarkers, and targets for prevention or cure. Hence, administration of beneficial or probiotic bacteria, and modulation of the microbiota, could support the healthy host state, and offer protection from disease, which could be particularly important in diseases like IBD.

Supplementary Information

Supplementary Table 1 Clinical data including assessment of inflammation severity at time of biopsy collection from Ulcerative Colitis patients and histological grading of biopsies to be used transcriptional analysis during acute inflamed colitis.

Biopsies were collected from the sigmoidal colon from patients being assessed for a suspected flare of UC or for investigation of another possible bowel condition (found macroscopically and microscopically normal). Inflammation of each patient was categorised as normal or inflamed based on grading of separate clinical samples by a histologist at the NNUH.

Tissue bank number	Age	Gender	Diagnosis/referral	History	Clinical severity	Endoscopic severity	Histology		Medication at time of endoscopy
							Overall	Sigmoid	
13TB0614	68	Female	UC	PSC (++ right colon)	Mild	Moderate in Ascending	Focally active chronic colitis	Mild	5ASA/Thiopurines
14TB0086	57	Female	UC		Quiescent	Mild in Ascending	Moderately active ulcerative colitis	Moderate	5ASA
14TB0197	51	Male	UC		Mild-Moderate	Mild-Mod Sigmoid, Mild Ascending	Active proctitis	Borderline	Steroids
14TB0617	72	Male	Gorlins syndrome	N/A	N/A	N/A	N/A	N/A	N/A
14TB0047	47	Male	Diarrhoea and bloating	N/A	N/A	N/A	N/A	N/A	N/A
14TB0168	54	Male	Anaemia	N/A	N/A	N/A	N/A	N/A	N/A

Supplementary Table 2 Summary and additional information on sequencing and immunoprecipitation of samples analysed by RNAseq

RNAseq was performed at the Welcome Trust Sanger Institute, Legend: WSI – whole small intestine, IEC – intestinal epithelial cells, LI content – large intestinal content, SPF – single pathogen free (conventionally raised), GF – germ free, adult – 12 weeks of age, neonate – 2 weeks of age, control – PBS sham gavage and/or PBS sham IP injection, + UCC2003 – oral gavage with 10^9 cfu *B. breve* UCC2003 on three consecutive days with tissue collection on day 4, LPS = IP injection of 1.25 mg/kg LPS with tissue collection 09 min post challenge.

File name	Age	Colonisation status	Tissue type	Treatment	Sequencing details	Immunopercipitation
19535 7#1	adult	SPF	WSI	control	HiSeq V4 75 bp PE	PolyA pulldown
19535 7#2	adult	SPF	WSI	control	HiSeq V4 75 bp PE	PolyA pulldown
19535 7#3	adult	SPF	WSI	control	HiSeq V4 75 bp PE	PolyA pulldown
19535 7#4	adult	SPF	WSI	+ UCC2003	HiSeq V4 75 bp PE	PolyA pulldown
19535 7#5	adult	SPF	WSI	+ UCC2003	HiSeq V4 75 bp PE	PolyA pulldown
19535 7#6	adult	SPF	WSI	+ UCC2003	HiSeq V4 75 bp PE	PolyA pulldown
19535 7#7	neonate	SPF	WSI	control	HiSeq V4 75 bp PE	PolyA pulldown
19535 7#9	neonate	SPF	WSI	control	HiSeq V4 75 bp PE	PolyA pulldown
19535 7#10	neonate	SPF	WSI	control	HiSeq V4 75 bp PE	PolyA pulldown
19535 7#11	neonate	SPF	WSI	control	HiSeq V4 75 bp PE	PolyA pulldown
19535 7#12	neonate	SPF	WSI	+ UCC2003	HiSeq V4 75 bp PE	PolyA pulldown
19535 7#13	neonate	SPF	WSI	+ UCC2003	HiSeq V4 75 bp PE	PolyA pulldown
19535 7#14	neonate	SPF	WSI	+ UCC2003	HiSeq V4 75 bp PE	PolyA pulldown
19535 7#15	neonate	SPF	WSI	+ UCC2003	HiSeq V4 75 bp PE	PolyA pulldown
19535 7#16	neonate	SPF	WSI	+ UCC2003	HiSeq V4 75 bp PE	PolyA pulldown
19535 7#17	adult	GF	WSI	control	HiSeq V4 75 bp PE	PolyA pulldown
19535 7#18	adult	GF	WSI	control	HiSeq V4 75 bp PE	PolyA pulldown
19535 7#19	adult	GF	WSI	control	HiSeq V4 75 bp PE	PolyA pulldown
19535 7#20	adult	GF	WSI	control	HiSeq V4 75 bp PE	PolyA pulldown
19535 7#21	adult	GF	WSI	+ UCC2003	HiSeq V4 75 bp PE	PolyA pulldown
19535 8#1	adult	GF	WSI	+ UCC2003	HiSeq V4 75 bp PE	PolyA pulldown
19535 8#3	adult	GF	WSI	+ UCC2003	HiSeq V4 75 bp PE	PolyA pulldown
19535 8#2	adult	GF	WSI	+ UCC2003	HiSeq V4 75 bp PE	PolyA pulldown
14256 3#1	adult	SPF	IEC	control	HiSeq V3 100bp PE	PolyA pulldown
14256 3#2	adult	SPF	IEC	control	HiSeq V3 100bp PE	PolyA pulldown
14256 3#3	adult	SPF	IEC	control	HiSeq V3 100bp PE	PolyA pulldown
14256 3#4	adult	SPF	IEC	+ UCC2003	HiSeq V3 100bp PE	PolyA pulldown
14256 4#5	adult	SPF	IEC	+ UCC2003	HiSeq V3 100bp PE	PolyA pulldown
14256 4#6	adult	SPF	IEC	+ UCC2003	HiSeq V3 100bp PE	PolyA pulldown

Supplementary Table 3 Summary and additional information on sequencing and immunoprecipitation of samples analysed by RNAseq

(continued from Supplementary Table 2)

File name	Age	Colonisation status	Tissue type	Treatment	Sequencing details	Immunopercipitation
14256 4#7	adult	SPF	IEC	LPS	HiSeq V3 100bp PE	PolyA pulldown
14256 4#8	adult	SPF	IEC	LPS	HiSeq V3 100bp PE	PolyA pulldown
14256 5#9	adult	SPF	IEC	LPS	HiSeq V3 100bp PE	PolyA pulldown
14256 5#10	adult	SPF	IEC	LPS	HiSeq V3 100bp PE	PolyA pulldown
14256 5#11	adult	SPF	IEC	LPS	HiSeq V3 100bp PE	PolyA pulldown
14256 5#12	adult	SPF	IEC	LPS + UCC2003	HiSeq V3 100bp PE	PolyA pulldown
14256 6#13	adult	SPF	IEC	LPS + UCC2003	HiSeq V3 100bp PE	PolyA pulldown
14256 6#14	adult	SPF	IEC	LPS + UCC2003	HiSeq V3 100bp PE	PolyA pulldown
14256 6#15	adult	SPF	IEC	LPS + UCC2003	HiSeq V3 100bp PE	PolyA pulldown
19535 8#4	neonate	SPF	IEC	control	HiSeq V4 75 bp PE	PolyA pulldown
19535 8#5	neonate	SPF	IEC	control	HiSeq V4 75 bp PE	PolyA pulldown
19535 8#6	neonate	SPF	IEC	control	HiSeq V4 75 bp PE	PolyA pulldown
19535 8#7	neonate	SPF	IEC	control	HiSeq V4 75 bp PE	PolyA pulldown
19535 8#9	neonate	SPF	IEC	+ UCC2003	HiSeq V4 75 bp PE	RiboZero, PolyA pulldown
19535 8#10	neonate	SPF	IEC	+ UCC2003	HiSeq V4 75 bp PE	RiboZero, PolyA pulldown
19535 8#11	neonate	SPF	IEC	+ UCC2003	HiSeq V4 75 bp PE	RiboZero, PolyA pulldown
19535 8#12	neonate	SPF	IEC	+ UCC2003	HiSeq V4 75 bp PE	RiboZero, PolyA pulldown
19535 8#14	adult	GF	IEC	control	HiSeq V4 75 bp PE	PolyA pulldown
19535 8#15	adult	GF	IEC	control	HiSeq V4 75 bp PE	PolyA pulldown
19535 8#16	adult	GF	IEC	control	HiSeq V4 75 bp PE	PolyA pulldown
19535 8#17	adult	GF	IEC	control	HiSeq V4 75 bp PE	PolyA pulldown
19535 8#18	adult	GF	IEC	+ UCC2003	HiSeq V4 75 bp PE	PolyA pulldown
19535 8#19	adult	GF	IEC	+ UCC2003	HiSeq V4 75 bp PE	PolyA pulldown
19535 8#20	adult	GF	IEC	+ UCC2003	HiSeq V4 75 bp PE	PolyA pulldown
19535 8#21	adult	GF	IEC	+ UCC2003	HiSeq V4 75 bp PE	PolyA pulldown
22045 3#1	adult	GF	Faeces	+ UCC2003	HiSeq V4 75 bp PE	RiboZero
22045 3#2	adult	GF	Faeces	+ UCC2003	HiSeq V4 75 bp PE	RiboZero
22045 3#3	adult	GF	Faeces	+ UCC2003	HiSeq V4 75 bp PE	RiboZero
22045 3#4	adult	SPF	LI content	control	HiSeq V4 75 bp PE	RiboZero
22045 3#5	adult	SPF	LI content	control	HiSeq V4 75 bp PE	RiboZero
22045 3#6	adult	SPF	LI content	control	HiSeq V4 75 bp PE	RiboZero
22045 3#7	adult	SPF	LI content	+ UCC2003	HiSeq V4 75 bp PE	RiboZero
22045 3#8	adult	SPF	LI content	+ UCC2003	HiSeq V4 75 bp PE	RiboZero
22045 3#9	adult	SPF	LI content	+ UCC2003	HiSeq V4 75 bp PE	RiboZero

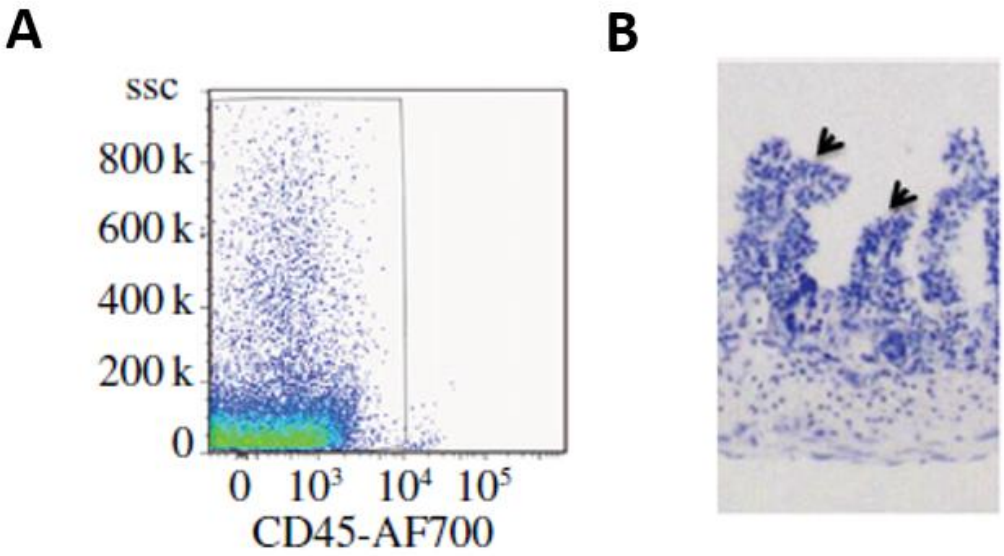

Supplementary Figure 1 Analysis of IEC isolation purity by FACS and histology pf striped tissue

A FACS of isolated IECs using PI dead/alive stain and anti-CD45 as general leucocyte marker, main live cell population CD-45 negative (gated left), representative sample shown **B** H&E stain of intestinal epithelium post IEC stripping using modified Weisser method, representative microscopic image shown, epithelial cells have been stripped off while lamina propria is intact (indicated by arrows).

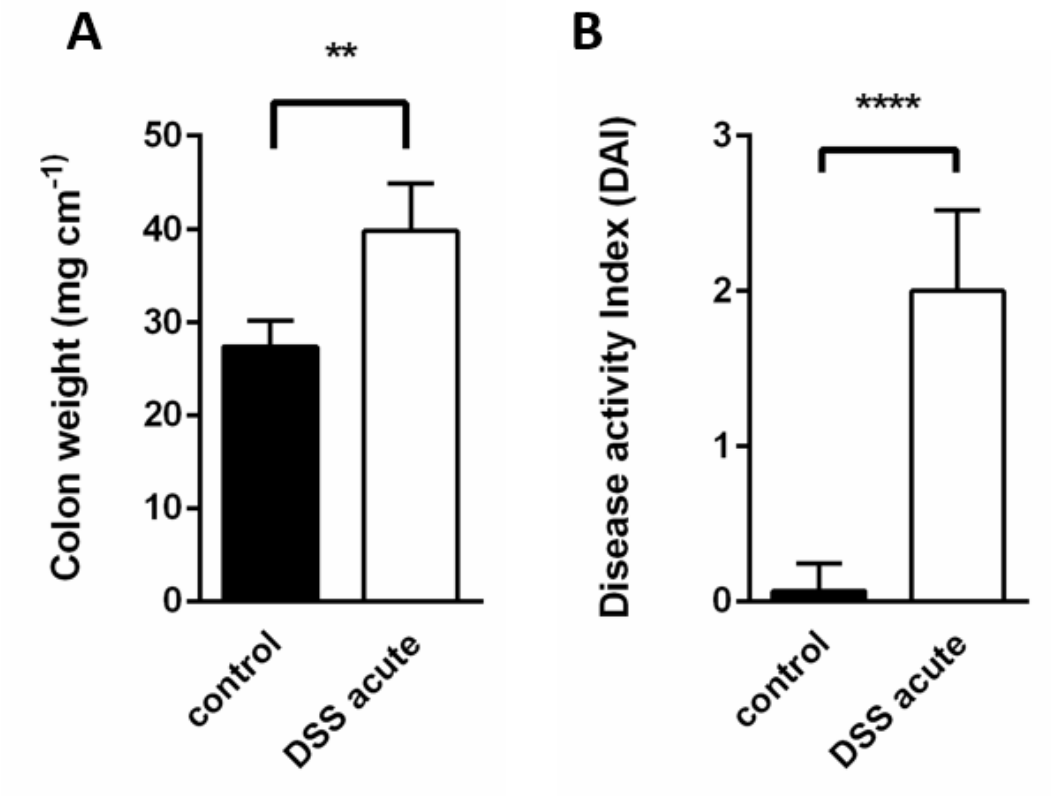

Supplementary Figure 2 Assessment of acute colonic colitis induced by DSS administration

A total colon weight normalised to length at day 7 of DSS administration in control and treatment group (DSS acute) **B** disease activity index (DAI) at day 7 of DSS administration comparing control croup to treatment group, n=5, mean +/- SD, Mann-Whitney test, ** $p<0.005$, **** $p<0.0001$.

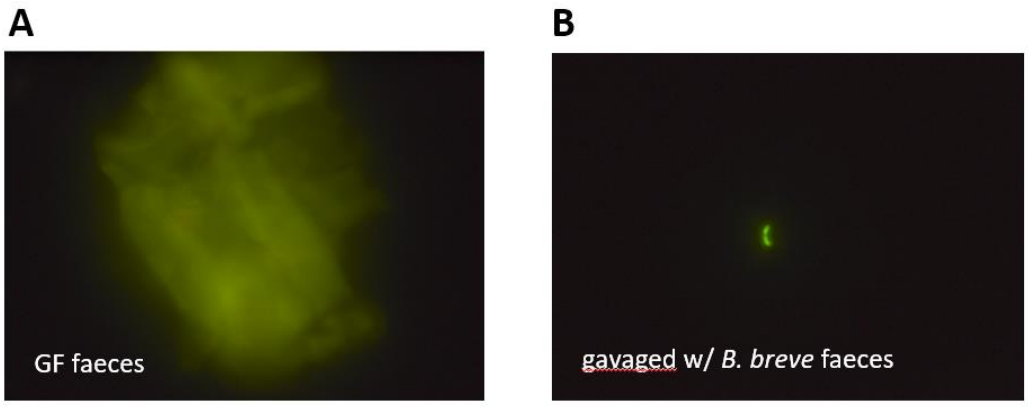

Supplementary Figure 3 Verification of germ free status of mice by culture independent faecal cytox stain

Faeces of germ free control (A) and *B. breve* UCC2003 gavaged mice (B) collected at day 4, cytox stain labelling DNA showing no microbial presence in gnotobiotic faeces while in gavaged mice bacterial presence was observed, representative images shown.

Supplementary Table 4 Supplementary Figure 4 Verification of germ free status of mice by expansion culture

Faeces collected from germ free control mice **(A)** and *B. breve* UCC2003 (**B**) at indicated days were cultured in RCM under anaerobic conditions, - indicated no observed growth, + indicates growth after 2 days, incubation under aerobic conditions did no support growth in either group (data not shown).

Day 1 (before gavage)		Day 2		Day 3		Day 4	
control	UCC2003	control	UCC2003	control	UCC2003	control	UCC2003
-	-	-	+	-	+	-	+
-	-	-	+	-	+	-	+
-	-	-	+	-	+	-	+
-	-		+	-		-	+

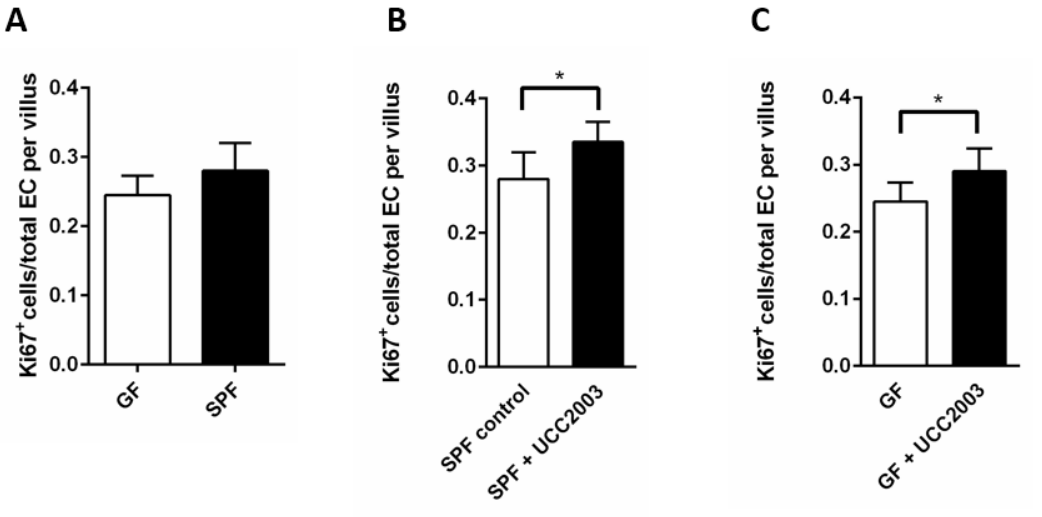

Supplementary Figure 4 Assessing IEC proliferation of GF and SPF animals and the effect of *B. breve* UCC2003 colonisation on both conditions

Comparing proliferation rates between germ free (GF) and conventionally raised mince (SPF) (**A**) and assessing the effect of *B. breve* colonisation in SPF animals (**B**) and GF conditions (**C**), Ki67 stain of SI tissue, data presented as ratio of Ki67 positive intestinal epithelial cells per total number of enterocytes per villus, n=3, 30 villi per mouse counted, Mann-Whitney test, * $p<0.05$.

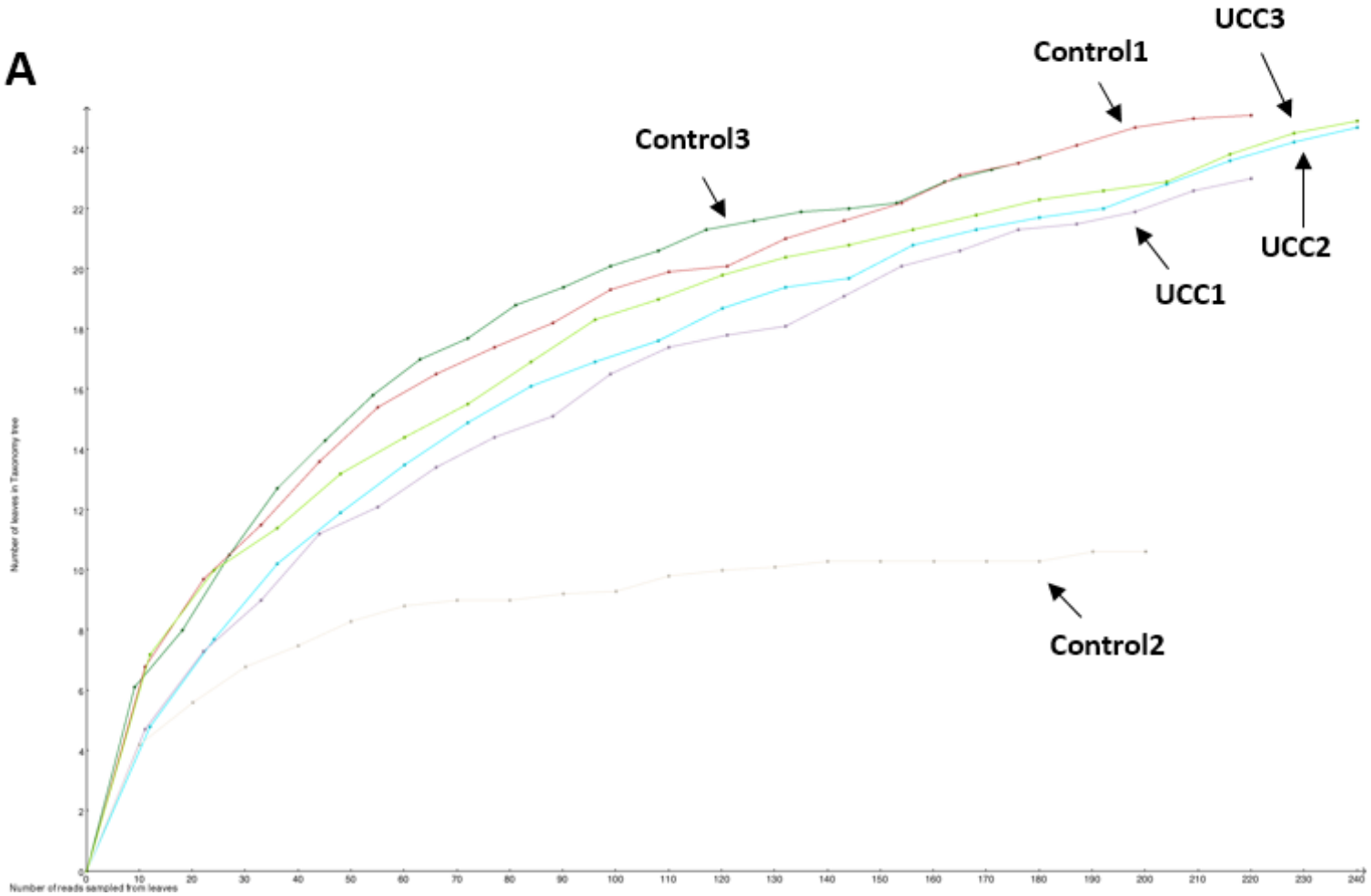

Supplementary Figure 5 Rarefaction curves of 16S rRNA gene sequencing data.

A adult group, data shown as numbers of species detected (number of leaves in taxonomic tree) plotted against number of reads sampled.

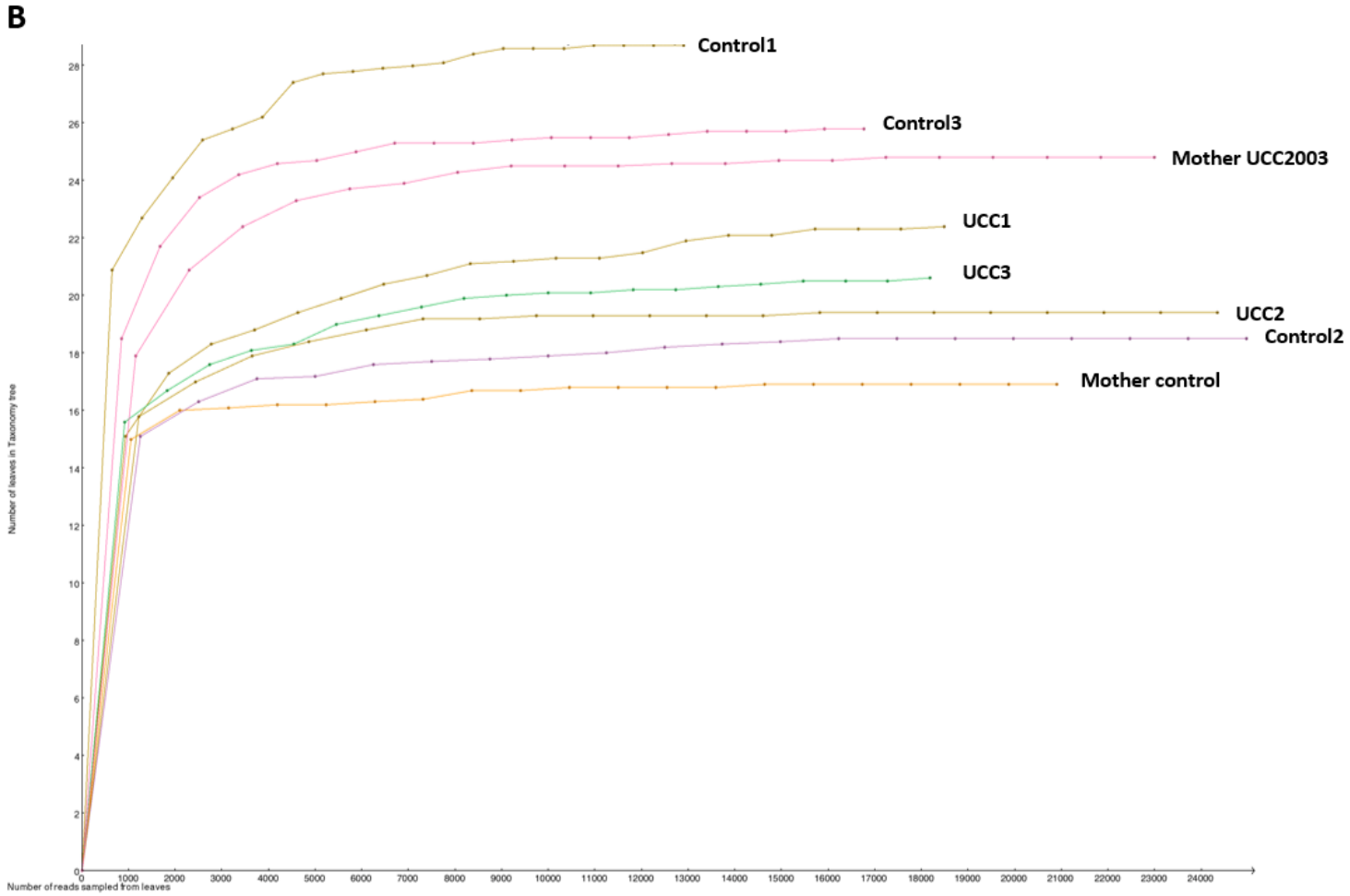

Supplementary Figure 6 Rarefaction curves of 16S rRNA gene sequencing data.

B neonate + mothers, data shown as numbers of species detected (number of leaves in taxonomic tree) plotted against number of reads sampled.

	Mother control	Control1	Control2	Control3	Mother UCC	UCC1	UCC2	UCC3
Mother control	0	0.4395915	0.51131666	0.4130482	0.25755486	0.67595756	0.6611461	0.60964924
Control1	0.4395915	0	0.21582167	0.14426556	0.32616445	0.2949264	0.2843675	0.22558546
Control2	0.51131666	0.21582167	0	0.16332108	0.3678944	0.41106272	0.34907928	0.3792385
Control3	0.4130482	0.14426556	0.16332108	0	0.319063	0.29310498	0.26868576	0.2670336
Mother UCC	0.25755486	0.32616445	0.3678944	0.319063	0	0.56195295	0.54578733	0.46961474
UCC1	0.67595756	0.2949264	0.41106272	0.29310498	0.56195295	0	0.10285021	0.10877255
UCC2	0.6611461	0.2843675	0.34907928	0.26868576	0.54578733	0.10285021	0	0.113070115
UCC3	0.60964924	0.22558546	0.3792385	0.2670336	0.46961474	0.10877255	0.113070115	0

Supplemetary

Variation between 16S rRNA gene sequencing data of neonate microbiota samples based on abundance of species at genus level

Component value as visualised in PCA plot in Figure 5.8

***B. breve* is localised in close contact with the small intestinal epithelium shown by staining of family specific 16s rRNA transcripts.**

Conventionally raised adult (12 weeks) mice were colonised with *B. breve* UCC2003 by oral gavage (10^9 cfu on three consecutive days, tissue collection on day 4), small intestinal tissue sections were processed and Bifidobacteria 16S transcripts visualised by RNAscope (brown chromogenic staining), counter stained with H&E, arrows indicate staining events, representative bright field microscopic images show (amended from Hughes *et al.*, 2017).

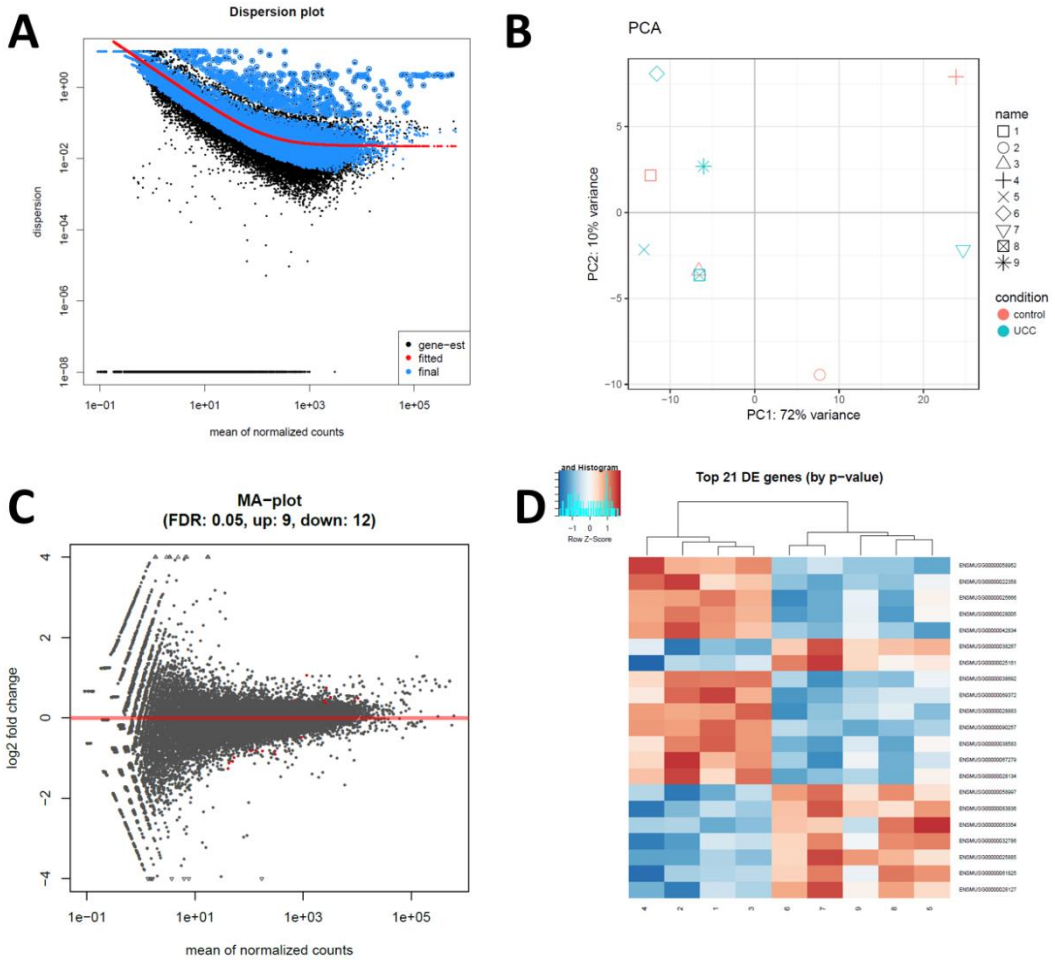

Supplementary Figure 7 DEGS induced by *B. breve* UCC2003 in neonate WSI.

Overview over transcriptional changes in whole small intestine (WSI) of neonate mice colonised with *B. breve* UCC2003 relative to control (PBS gavaged) **A** Shrinkage estimation of dispersion, y axis dispersion estimate, x axis mean of normalised counts, black dots individual genes, red line maximum likelihood estimation (MLE) line of best fit, black dots circled in blue – potential dispersion outliers, blue area around red line – genes used for second dispersion estimate (not outliers), **B** PCA plot of group variability **C** Bland Altman (MA) plot of transcriptional modulation by presence of *B. breve* UCC2003 relative to control, y axis log2 fold change of gene expression, x axis – mean of moralised counts, red dots – statistical sig genes (q values 0.05) **D** Hierarchical clustering of samples based on TOP 50 differentially regulated genes.

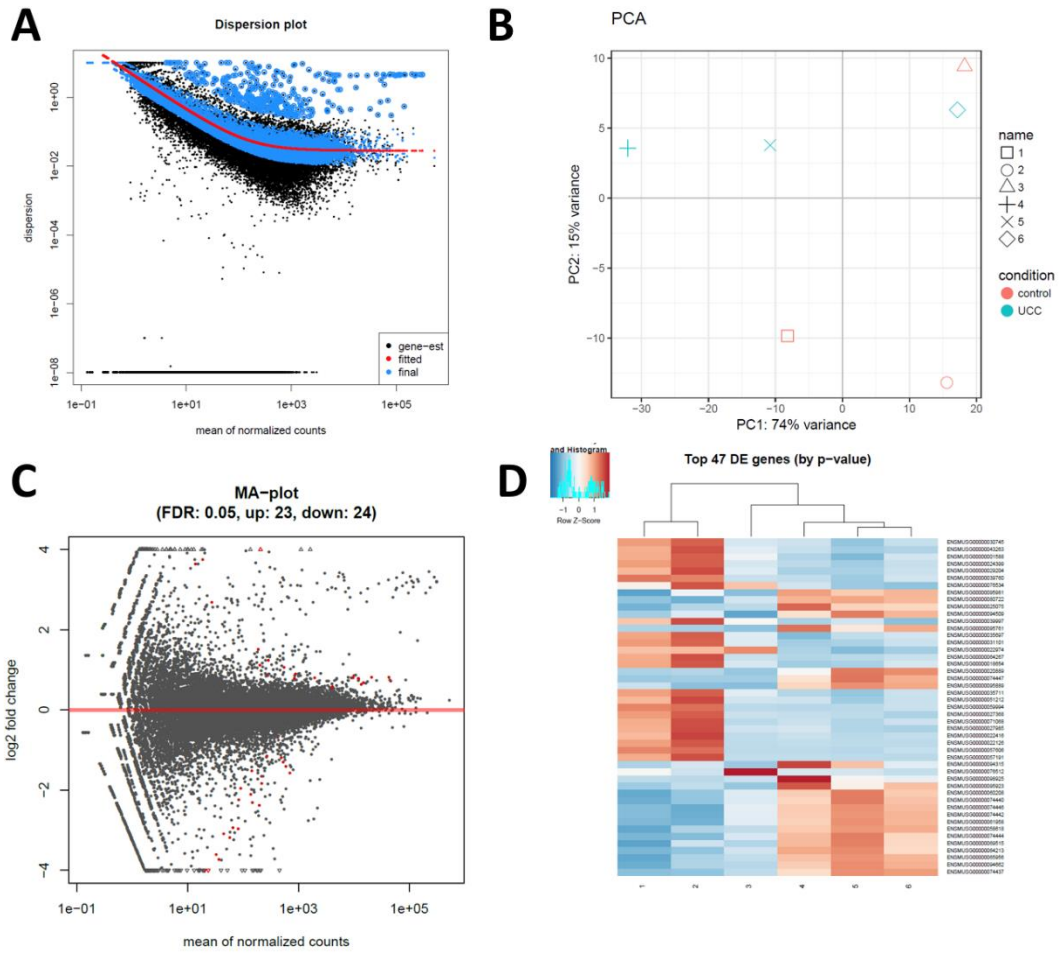

Supplementary Figure 8 DEGS induced by *B. breve* UCC2003 in adult WSI.

Overview over transcriptional changes in whole small intestine (WSI) of adult mice colonised with *B. breve* UCC2003 relative to control (PBS gavaged) **A** Shrinkage estimation of dispersion, y axis dispersion estimate, x axis mean of normalised counts, black dots individual genes, red line maximum likelihood estimation (MLE) line of best fit, black dots circled in blue – potential dispersion outliers, blue area around red line – genes used for second dispersion estimate (not outliers), **B** PCA plot of group variability **C** Bland Altman (MA) plot of transcriptional modulation by presence of *B. breve* UCC2003 relative to control, y axis log2 fold change of gene expression, x axis – mean of moralised counts, red dots – statistical sig genes (q values 0.05) **D** Hierarchical clustering of samples based on TOP 50 differentially regulated genes.

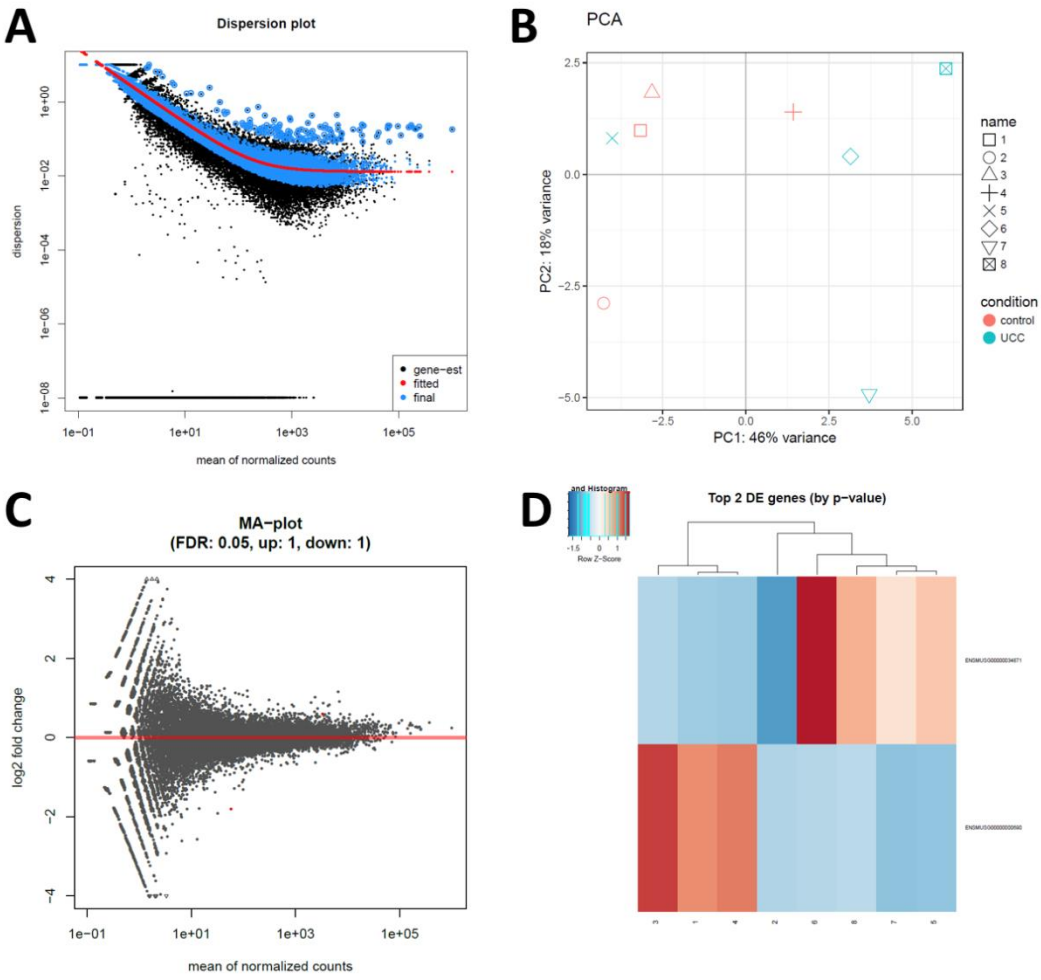

Supplementary Figure 9 DEGS induced by *B. breve* UCC2003 in GF IEC.

Overview over transcriptional changes in intestinal epithelial cells (IEC) of germ free (GF), adult mice colonised with *B. breve* UCC2003 relative to control (PBS gavaged) **A** Shrinkage estimation of dispersion, y axis dispersion estimate, x axis mean of normalised counts, black dots individual genes, red line maximum likelihood estimation (MLE) line of best fit, black dots circled in blue – potential dispersion outliers, blue area around red line – genes used for second dispersion estimate (not outliers), **B** PCA plot of group variability **C** Bland Altman (MA) plot of transcriptional modulation by presence of *B. breve* UCC2003 relative to control, y axis log2 fold change of gene expression, x axis – mean of moralised counts, red dots – statistical sig genes (q values 0.05) **D** Hierarchical clustering of samples based on TOP 50 differentially regulated genes.

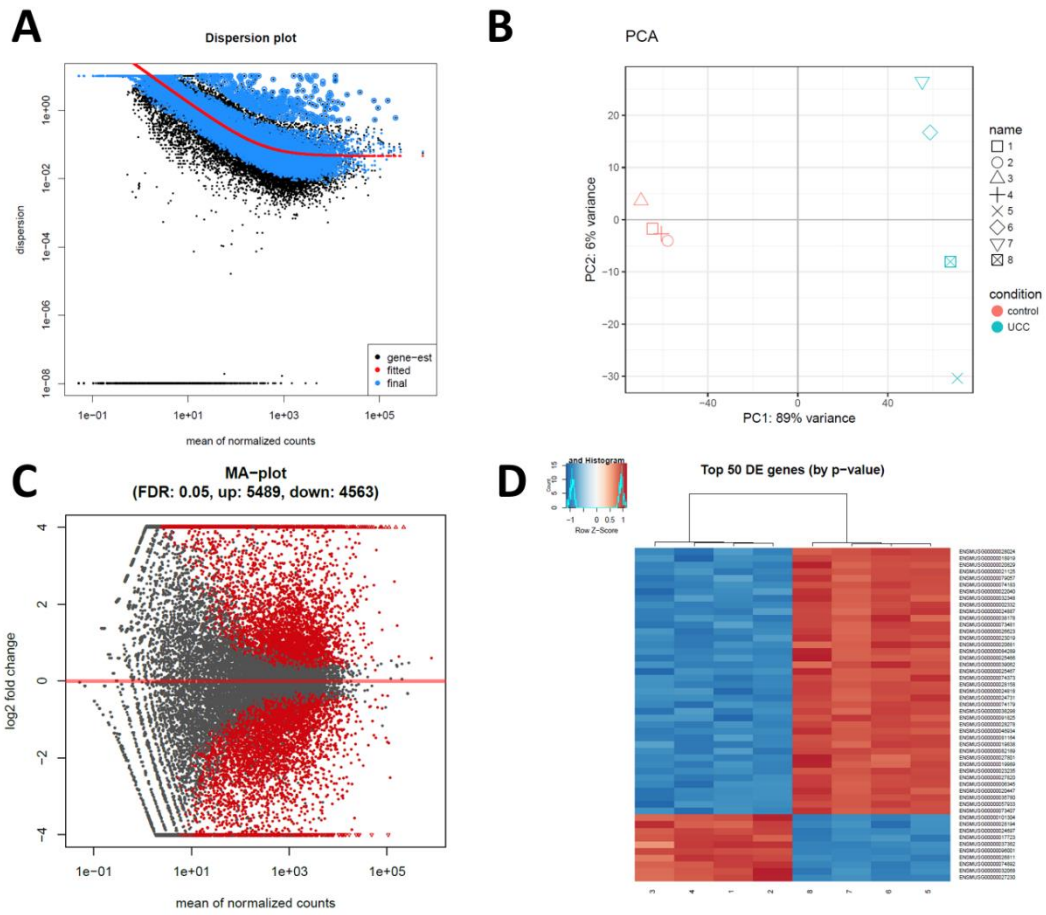

Supplementary Figure 10 DEGS induced by *B. breve* UCC2003 in GF WSI.

Overview over transcriptional changes in whole small intestine (WSI) of germ free (GF), adult mice colonised with *B. breve* UCC2003 relative to control (PBS gavaged) **A** Shrinkage estimation of dispersion, y axis dispersion estimate, x axis mean of normalised counts, black dots individual genes, red line maximum likelihood estimation (MLE) line of best fit, black dots circled in blue – potential dispersion outliers, blue area around red line – genes used for second dispersion estimate (not outliers), **B** PCA plot of group variability **C** Bland Altman (MA) plot of transcriptional modulation by presence of *B. breve* UCC2003 relative to control, y axis log2 fold change of gene expression, x axis – mean of moralised counts, red dots – statistical sig genes (q values 0.05) **D** Hierarchical clustering of samples based on TOP 50 differentially regulated genes.

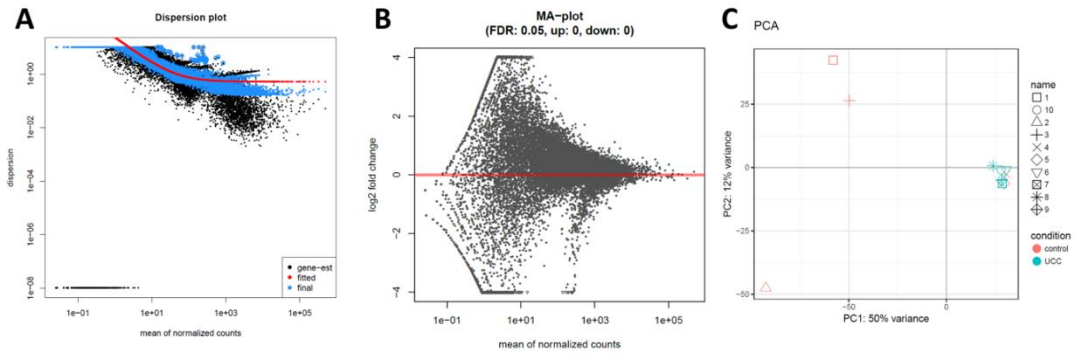

Supplementary Figure 11 DEGS induced by *B. breve* UCC2003 in adult IECs stimulated by systemic LPS.

Overview over transcriptional changes in intestinal epithelial cells (IEC) of adult mice colonised with *B. breve* UCC2003 relative to control (PBS gavaged) at 90 min post 1.25 mg/kg LPS IP injection inducing SI apoptotic IEC shedding with *B. breve* colonisation conferring protection from the LPS effect, **A** Shrinkage estimation of dispersion, y axis dispersion estimate, x axis mean of normalised counts, black dots individual genes, red line maximum likelihood estimation (MLE) line of best fit, black dots circled in blue – potential dispersion outliers, blue area around red line – genes used for second dispersion estimate (not outliers), **B** PCA plot of group variability **C** Bland Altman (MA) plot of transcriptional modulation by presence of *B. breve* UCC2003 relative to control, y axis log2 fold change of gene expression, x axis – mean of moralised counts, red dots – statistical sig genes (q values 0.05) **D** Hierarchical clustering of samples based on TOP 50 differentially regulated genes.

Supplementary Table 5 DEGs in neonate IECs induced by *B. breve* UCC2003 colonisation that are known targets of miR21 with their predicted regulation by miR21 and their fold change expression in the data set (q value < 0.05)

Ensmble Gene ID	Genes Symbol	Gene Name	Expr Log Ratio	Effect of miR21 on target gene (based on literature)	Predicted miR21 modulation in expr data (based on regulation direction of traget genes)
ENSMUSG00000032400	ZWILCH	zwilch kinetochore protein	2.928	Downregulates (1)	Inhibited
ENSMUSG00000021115	VRK1	vaccinia related kinase 1	1.087	Downregulates (1)	Inhibited
ENSMUSG00000018548	TRIM37	tripartite motif containing 37	1.149	Downregulates (1)	Inhibited
ENSMUSG00000070914	TOP2A	DNA topoisomerase II alpha	2.979	Downregulates (1)	Inhibited
ENSMUSG00000002489	TIAM1	T-cell lymphoma invasion and metastasis 1	3.401	Downregulates (9)	Inhibited
ENSMUSG00000037313	TACC3	transforming acidic coiled coil containing protein 3	1.104	Downregulates (1)	Inhibited
ENSMUSG00000028312	SMC2	structural maintenance of chromosomes 2	2.487	Downregulates (1)	Inhibited
ENSMUSG00000025880	SMAD7	SMAD family member 7	0.97	Downregulates (13)	Inhibited
ENSMUSG00000034248	SLC25A37	solute carrier family 25 member 37	1.424	Downregulates (1)	Inhibited
ENSMUSG00000030346	RAD51AP1	RAD51 associated protein 1	2.169	Downregulates (1)	Inhibited
ENSMUSG00000023015	RACGAP1	Rac GTPase activating protein 1	1.622	Downregulates (1)	Inhibited
ENSMUSG00000013663	PTEN	phosphatase and tensin homolog	1.054	Downregulates (36)	Inhibited
ENSMUSG00000038943	PRC1	protein regulator of cytokinesis 1	1.778	Downregulates (1)	Inhibited
ENSMUSG00000020463	PPP4R3B	protein phosphatase 4 regulatory subunit 3B	1.366	Downregulates (1)	Inhibited
ENSMUSG00000022383	PPARA	peroxisome proliferator activated receptor alpha	1.593	Downregulates (4)	Inhibited
ENSMUSG00000031538	PLAT	plasminogen activator, tissue type	3.358	Downregulates (1)	Inhibited
ENSMUSG00000028957	PER3	period circadian regulator 3	2.925	Downregulates (1)	Inhibited
ENSMUSG00000055866	PER2	period circadian regulator 2	1.218	Downregulates (1)	Inhibited
ENSMUSG00000022033	PBK	PDZ binding kinase	0.856	Downregulates (1)	Inhibited
ENSMUSG00000027306	NUSAP1	nucleolar and spindle associated protein 1	1.45	Downregulates (1)	Inhibited
ENSMUSG00000026434	NUCKS1	nuclear casein kinase and cyclin dependent kinase substrate 1	1.612	Downregulates (1)	Inhibited
ENSMUSG00000026643	NMT2	N-myristoyltransferase 2	1.117	Downregulates (1)	Inhibited
ENSMUSG00000074151	NLRC5	NLR family CARD domain containing 5	2.329	Downregulates (1)	Inhibited
ENSMUSG00000038252	NCAPD2	non-SMC condensin I complex subunit D2	4.506	Downregulates (1)	Inhibited
ENSMUSG00000024151	MSH2	mutS homolog 2	1.085	Downregulates (14)	Inhibited
ENSMUSG00000031004	MKI67	marker of proliferation Ki-67	4.086	Downregulates (1)	Inhibited
ENSMUSG00000065455	mir-21	microRNA 21	2.092	Upregulates (4)	Inhibited
ENSMUSG00000029414	KNTC1	kinetochore associated 1	3.721	Downregulates (1)	Inhibited
ENSMUSG00000024301	KIFC1	kinesin family member C1	2.522	Downregulates (1)	Inhibited
ENSMUSG00000006740	KIF5B	kinesin family member 5B	1.196	Downregulates (1)	Inhibited
ENSMUSG00000034311	KIF4A	kinesin family member 4A	2.033	Downregulates (1)	Inhibited
ENSMUSG00000032254	KIF23	kinesin family member 23	2.735	Downregulates (1)	Inhibited
ENSMUSG00000027276	JAG1	jagged 1	1.833	Downregulates (2)	Inhibited
ENSMUSG00000091191	IRF1	interferon regulatory factor 1	0.811	Downregulates (1)	Inhibited
ENSMUSG00000042590	IPO11	importin 11	1.34	Downregulates (1)	Inhibited
ENSMUSG00000018341	IL12RB2	interleukin 12 receptor subunit beta 2	4.814	Downregulates (1)	Inhibited
ENSMUSG00000078606	Gvin1 (includes others)	GTPase, very large interferon inducible pseudogene 1	4.928	Downregulates (1)	Inhibited
ENSMUSG00000022385	GTSE1	G2 and S phase expressed 1	1.765	Downregulates (1)	Inhibited
ENSMUSG00000020740	GGA3	golgi associated, gamma adaptin ear containing, ARF binding protein 3	0.98	Downregulates (1)	Inhibited
ENSMUSG00000034438	Gbp8	guanylate-binding protein 8	2.835	Downregulates (1)	Inhibited
ENSMUSG00000040253	GBP7	guanylate binding protein 7	0.906	Downregulates (1)	Inhibited
ENSMUSG00000029298	GBP6	guanylate binding protein family member 6	3.184	Downregulates (2)	Inhibited
ENSMUSG00000053332	GAS5	growth arrest specific 5 (non-protein coding)	2.239	Downregulates (1)	Inhibited
ENSMUSG00000028034	FUBP1	far upstream element binding protein 1	1.549	Downregulates (1)	Inhibited
ENSMUSG00000039521	FOXP3	forkhead box P3	1.137	Upregulates (1)	Inhibited
ENSMUSG00000005371	FBXO11	F-box protein 11	0.956	Downregulates (18)	Inhibited
ENSMUSG00000029675	ELN	elastin	-5.243	Upregulates (3)	Inhibited
ENSMUSG00000030068	EIF4E3	eukaryotic translation initiation factor 4E family member 3	4.738	Downregulates (2)	Inhibited
ENSMUSG00000027699	ECT2	epithelial cell transforming 2	1.569	Downregulates (1)	Inhibited
ENSMUSG00000037544	DLGAP5	DLG associated protein 5	2.121	Downregulates (1)	Inhibited
ENSMUSG00000030641	DDIAS	DNA damage induced apoptosis suppressor	2.166	Downregulates (1)	Inhibited
ENSMUSG00000072521	CREBBP	CREB binding protein	2.536	Downregulates (1)	Inhibited
ENSMUSG00000040549	CKAP5	cytoskeleton associated protein 5	1.827	Downregulates (1)	Inhibited
ENSMUSG00000040274	CDK6	cyclin dependent kinase 6	2.802	Downregulates (2)	Inhibited
ENSMUSG00000048574	CCNB1	cyclin B1	1.988	Downregulates (1)	Inhibited
ENSMUSG00000027715	CCNA2	cyclin A2	0.936	Downregulates (1)	Inhibited
ENSMUSG00000057329	BCL2	BCL2, apoptosis regulator	2.082	Downregulates (3)	Inhibited
ENSMUSG00000022360	ATAD2	ATPase family, AAA domain containing 2	2.583	Downregulates (1)	Inhibited
ENSMUSG00000033952	ASPM	abnormal spindle microtubule assembly	4.168	Downregulates (1)	Inhibited
ENSMUSG00000036777	ANLN	anillin actin binding protein	3.296	Downregulates (1)	Inhibited
ENSMUSG00000027078	UBE2L6	ubiquitin conjugating enzyme E2 L6	1.59	Downregulates (1)	Activated
ENSMUSG00000058317	UBE2E2	ubiquitin conjugating enzyme E2 E2	-1.236	Downregulates (1)	Activated
ENSMUSG00000016308	UBE2A	ubiquitin conjugating enzyme E2 A	1.556	Downregulates (1)	Activated
ENSMUSG00000037278	TMEM97	transmembrane protein 97	-0.953	Downregulates (1)	Activated
ENSMUSG00000027995	TLR2	toll-like receptor 2	2.864	Upregulates (1)	Activated
ENSMUSG00000002603	TGFB1	transforming growth factor beta 1	0.888	Downregulates (1)	Activated
ENSMUSG00000026222	Sp100	SP100 nuclear antigen	-0.956	Downregulates (1)	Activated
ENSMUSG00000072941	SOD3	superoxide dismutase 3	1.649	Downregulates (1)	Activated
ENSMUSG00000021540	SMAD5	SMAD family member 5	0.828	Upregulates (1)	Activated
ENSMUSG00000017002	SLPI	secretory leukocyte peptidase inhibitor	5.707	Downregulates (1)	Activated
ENSMUSG00000072620	Slfn2	schlafen 2	-1.112	Downregulates (1)	Activated
ENSMUSG00000020089	PPA1	pyrophosphatase (inorganic) 1	-1.01	Downregulates (1)	Activated
ENSMUSG00000033020	POLR2F	RNA polymerase II subunit F	-1.847	Downregulates (1)	Activated
ENSMUSG00000011752	PGAM1	phosphoglycerate mutase 1	-1.064	Downregulates (1)	Activated
ENSMUSG00000037601	NME1	NME/NM23 nucleoside diphosphate kinase 1	1.104	Downregulates (1)	Activated
ENSMUSG00000078920	Ifi47	interferon gamma inducible protein 47	-1.055	Downregulates (1)	Activated
ENSMUSG00000037405	ICAM1	intercellular adhesion molecule 1	1.384	Downregulates (1)	Activated
ENSMUSG00000017830	DHX58	DExH-box helicase 58	-0.906	Downregulates (1)	Activated
ENSMUSG00000034855	CXCL10	C-X-C motif chemokine ligand 10	2.168	Downregulates (1)	Activated
ENSMUSG00000026043	COL3A1	collagen type III alpha 1 chain	0.915	Upregulates (3)	Activated
ENSMUSG00000001506	COL1A1	collagen type I alpha 1 chain	1.567	Upregulates (4)	Activated
ENSMUSG00000022037	CLU	clusterin	0.95	Downregulates (2)	Activated
ENSMUSG00000030654	ARL6IP1	ADP-ribosylation factor-like GTPase 6 interacting protein 1	-0.955	Downregulates (1)	Activated
ENSMUSG00000021322	AOAH	acyloxyacyl hydrolase	1.01	Downregulates (1)	Activated
ENSMUSG00000023067	CDKN1A	cyclin dependent kinase inhibitor 1A	-1.514	Regulates (2)	Affected
ENSMUSG00000021611	TERT	telomerase reverse transcriptase	1.012	Regulates (1)	Affected
ENSMUSG00000022615	TYMP	thymidine phosphorylase	-0.827	Regulates (1)	Affected

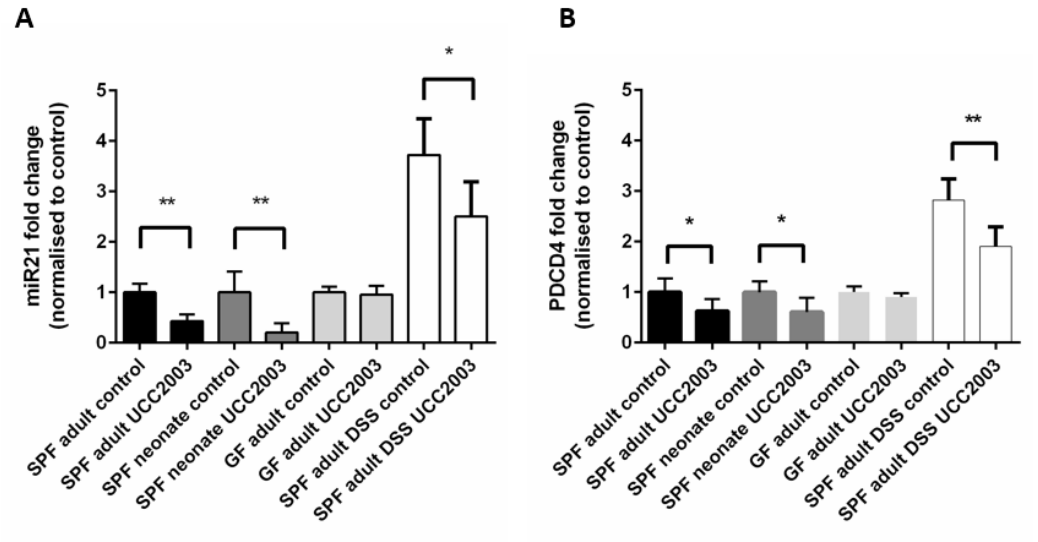

Supplementary Figure 12 *B. breve* UCC2003 colonisation decreases miR21 and its downstream target PDCD4 expression in the large intestine of conventionally raised adult and neonate mice as well as during DSS induced colitis.

A miR21 and **B** PCDC4 expression in large intestine of conventionally (SPF) raised adult (12 weeks), neonate (2 weeks), SPF adult mice with acute colonic colitis (DSS) and GF mice with and without *B. breve* UCC2003 colonisation, mice were colonised with *B. breve* UCC2003 by oral gavage (10^9 cfu) on three consecutive days and tissue collected on day 4 (days 7 for DSS groups), acute colonic colitis was induced by administration of 1.5% DSS in drinking water until tissue collection at day 7, miR2 and PDCD4 expression assessed by qPCR, expression normalised to housekeeper and presented as fold change compared to age, colonisation status and treatment matched control group (with the exception of DSS samples normalised to SPF adult), data shown as mean +/- SD (SPF adult n=5, SPF neo n=5, GF adult n=6, DSS n=6), statistical significance * = $p<0.01$, ** $p<0.05$ (Mann-Whitney U test).

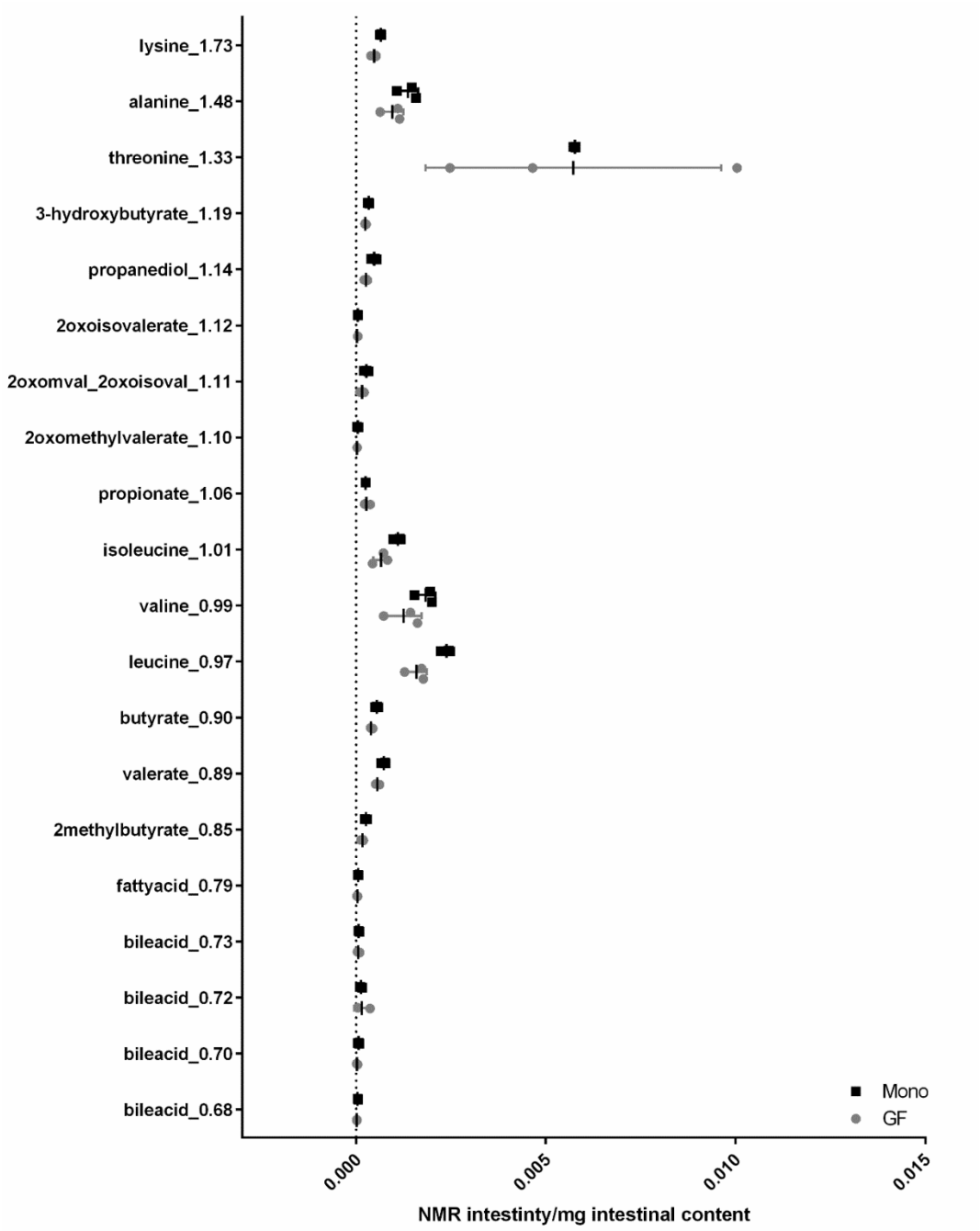

Supplementary Figure 13 Overview over metabolite concentration in large intestinal content of germ free mice (GF) and mice colonised by *B. breve* UCC2003 (Mono)

Data presented as NMR intensity per mg intestinal content, individual values plotted (n=3 mice), mean and SD indicated by lines, statistical significance analysed by Two-way ANOVA with Bonferroni post-test (* p-value < 0.05), values in metabolite name relate to peak location in parts per million (ppm) used for identification.

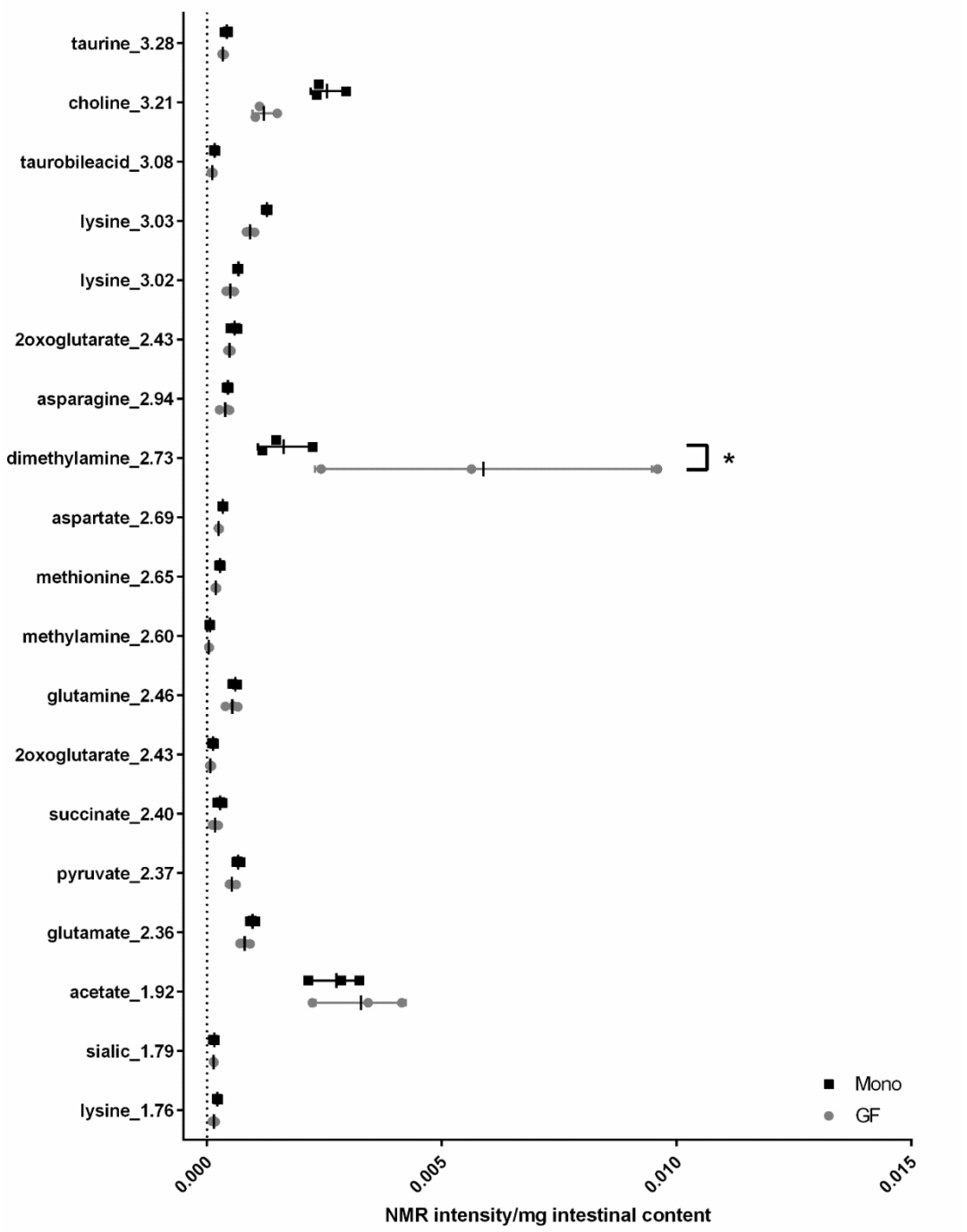

Supplementary Figure 14 Overview over metabolite concentration in large intestinal content of germ free mice (GF) and mice colonised by *B. breve* UCC2003 (Mono)

Data presented as NMR intensity per mg intestinal content, individual values plotted (n=3 mice), mean and SD indicated by lines, statistical significance analysed by Two-way ANOVA with Bonferroni post-test (* p-value < 0.05), values in metabolite name relate to peak location in parts per million (ppm) used for identification.

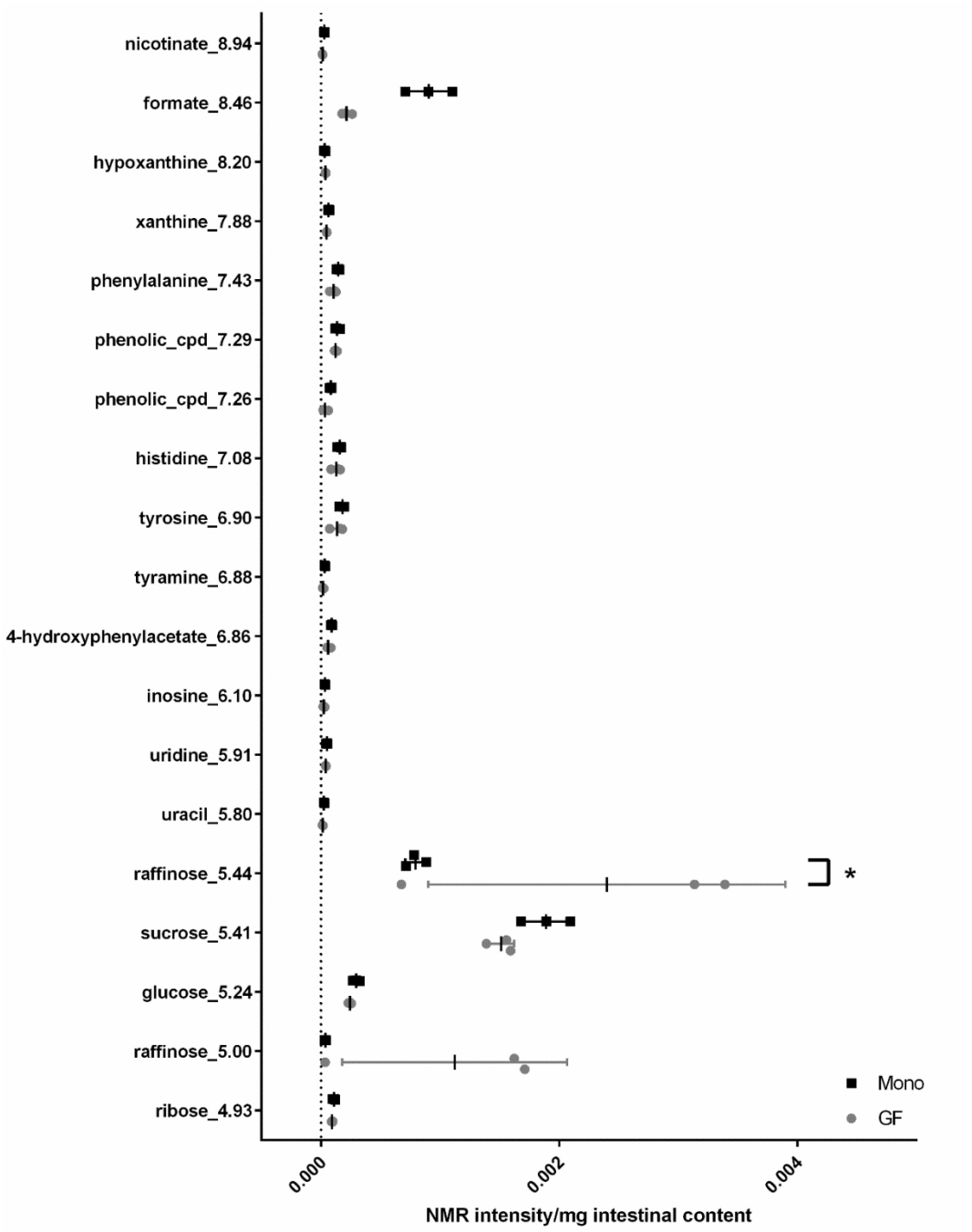

Supplementary Figure 15 Overview over metabolite concentration in large intestinal content of germ free mice (GF) and mice colonised by *B. breve* UCC2003 (Mono)

Data presented as NMR intensity per mg intestinal content, individual values plotted (n=3 mice), mean and SD indicated by lines, statistical significance analysed by Two-way ANOVA with Bonferroni post-test (* p-value < 0.05), values in metabolite name relate to peak location in parts per million (ppm) used for identification.

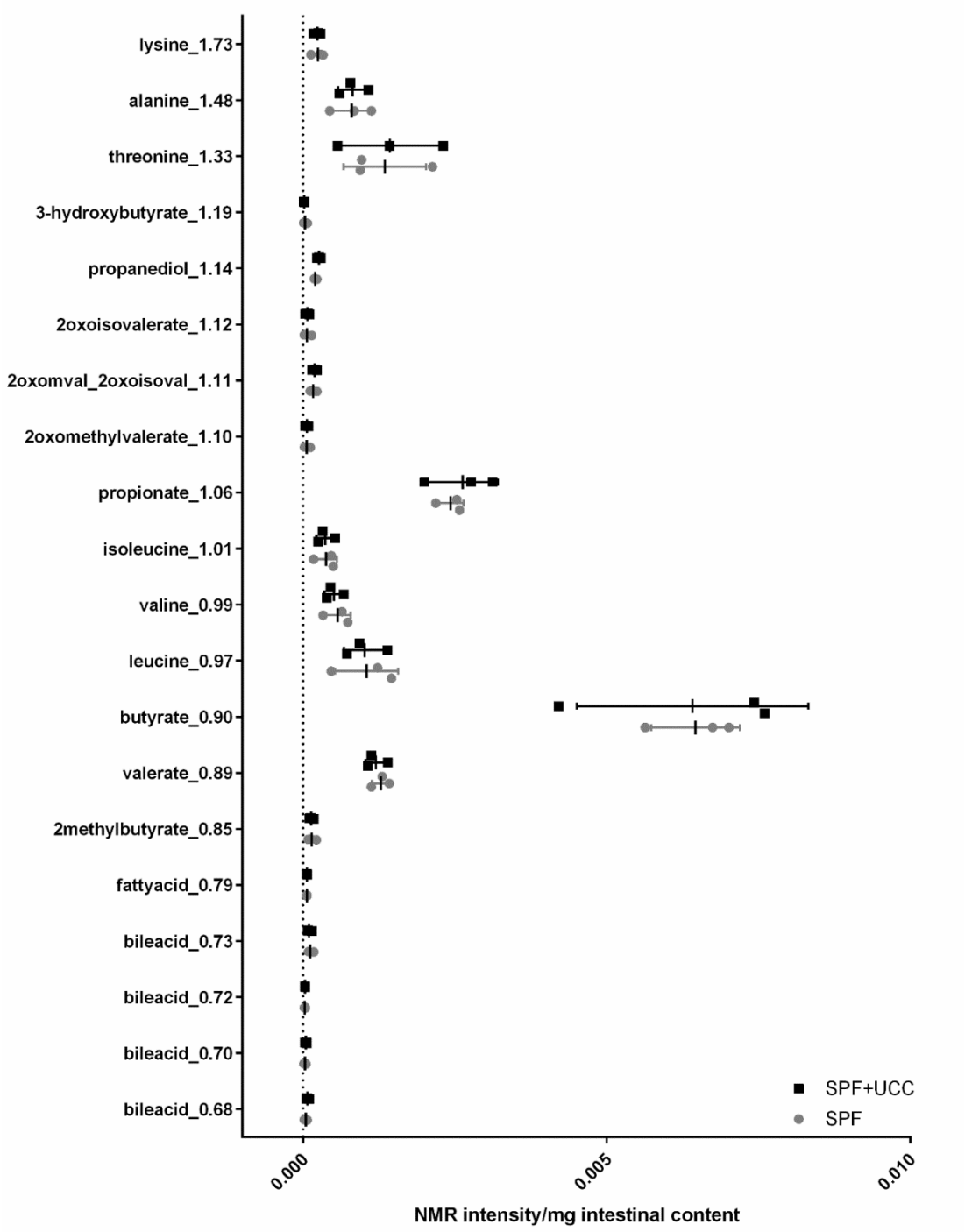

Supplementary Figure 16 Overview over metabolite concentration in large intestinal content of conventionally raised mice with (SPF+UCC) and without (SPF) *B. breve* UCC2003 colonisation

Data presented as NMR intensity per mg intestinal content, individual values plotted (n=3 mice), mean and SD indicated by lines, statistical significance analysed by Two-way ANOVA with Bonferroni post-test (* p-value < 0.05), values in metabolite name relate to peak location in parts per million (ppm) used for identification.

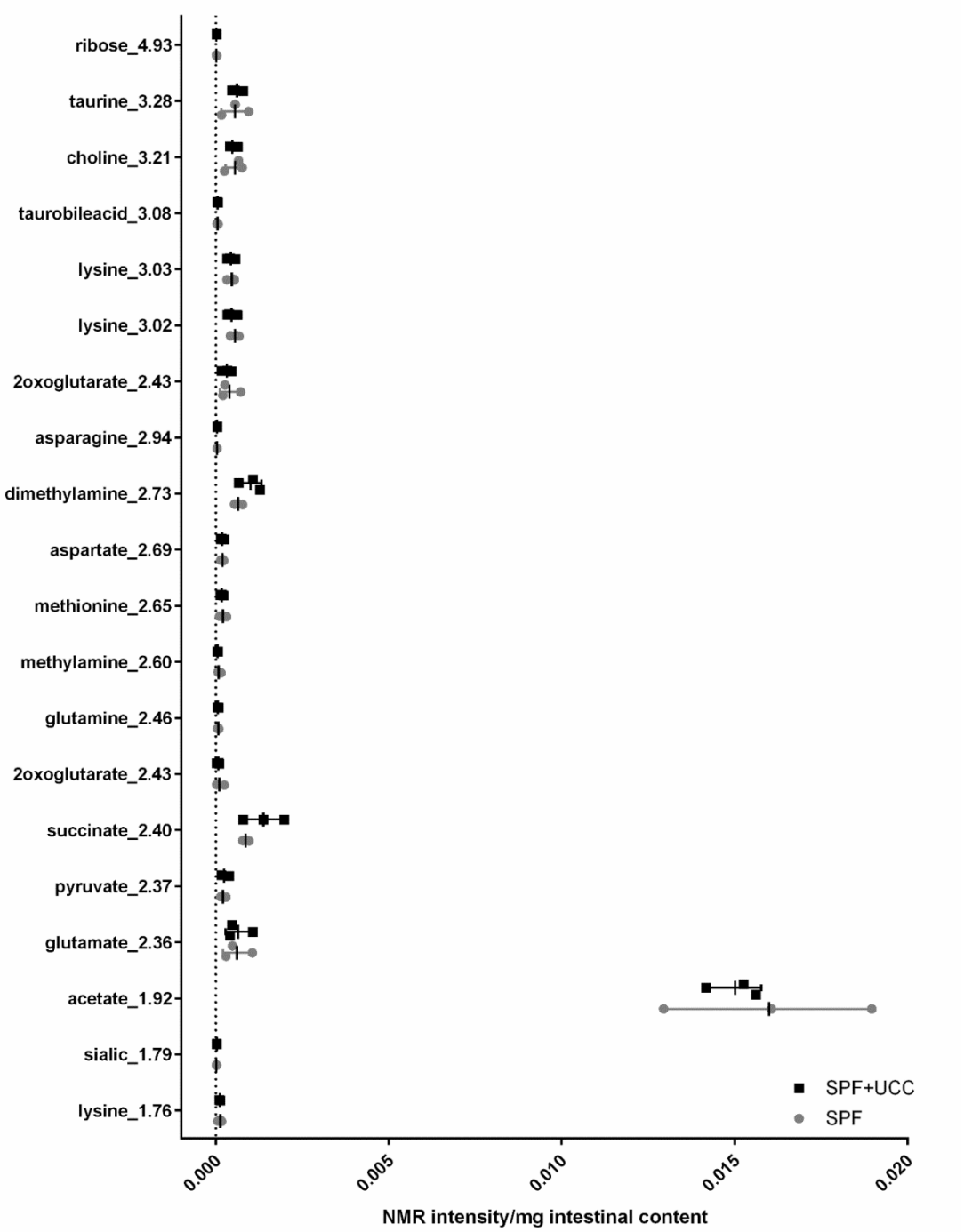

Supplementary Figure 17 Overview over metabolite concentration in large intestinal content of conventionally raised mice with (SPF+UCC) and without (SPF) *B. breve* UCC2003 colonisation

Data presented as NMR intensity per mg intestinal content, individual values plotted (n=3 mice), mean and SD indicated by lines, statistical significance analysed by Two-way ANOVA with Bonferroni post-test (* p-value < 0.05), values in metabolite name relate to peak location in parts per million (ppm) used for identification

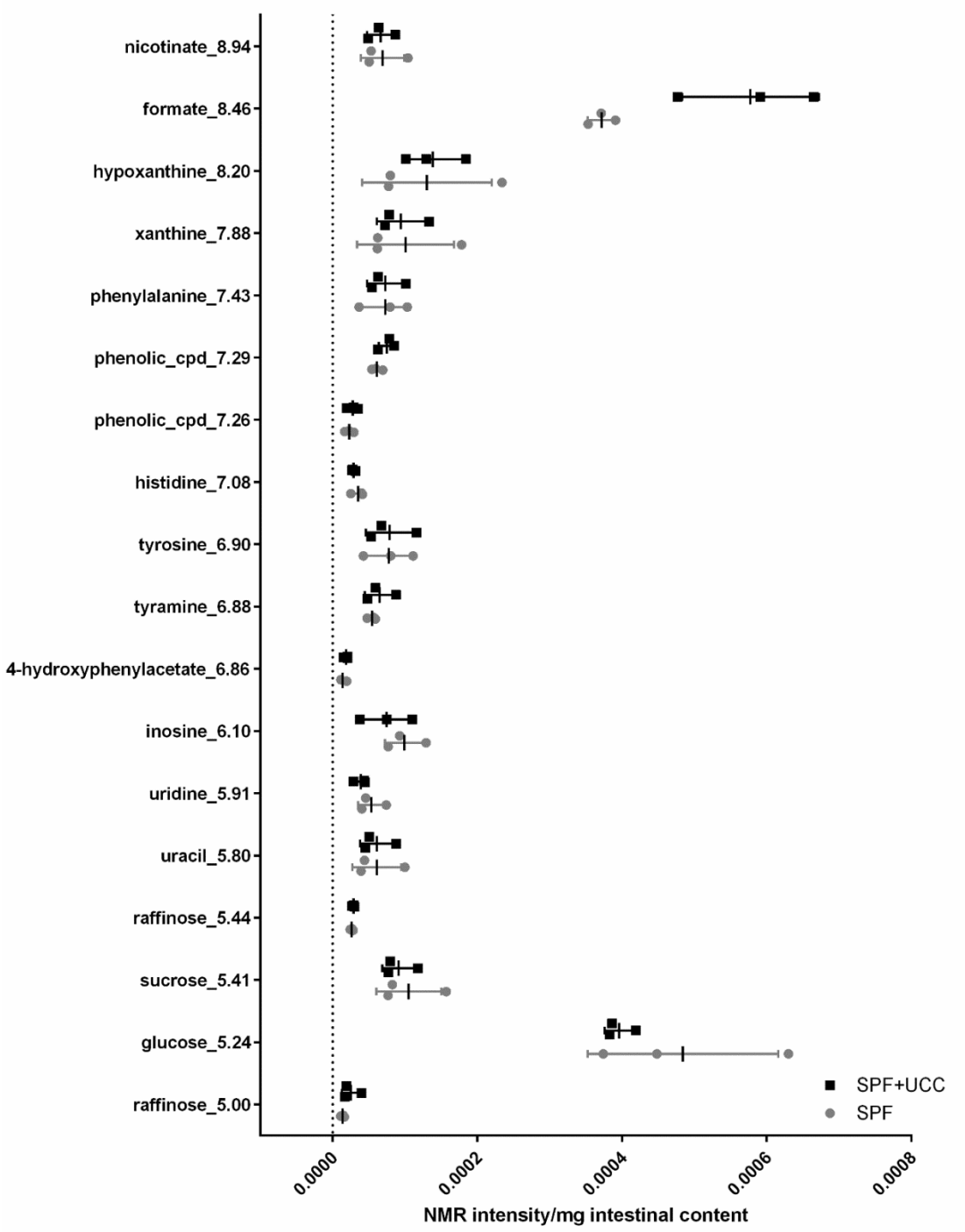

Supplementary Figure 18 Overview over metabolite concentration in large intestinal content of conventionally raised mice with (SPF+UCC) and without (SPF) *B. breve* UCC2003 colonisation

Data presented as NMR intensity per mg intestinal content, individual values plotted (n=3 mice), mean and SD indicated by lines, statistical significance analysed by Two-way ANOVA with Bonferroni post-test (* p-value < 0.05), values in metabolite name relate to peak location in parts per million (ppm) used for identification

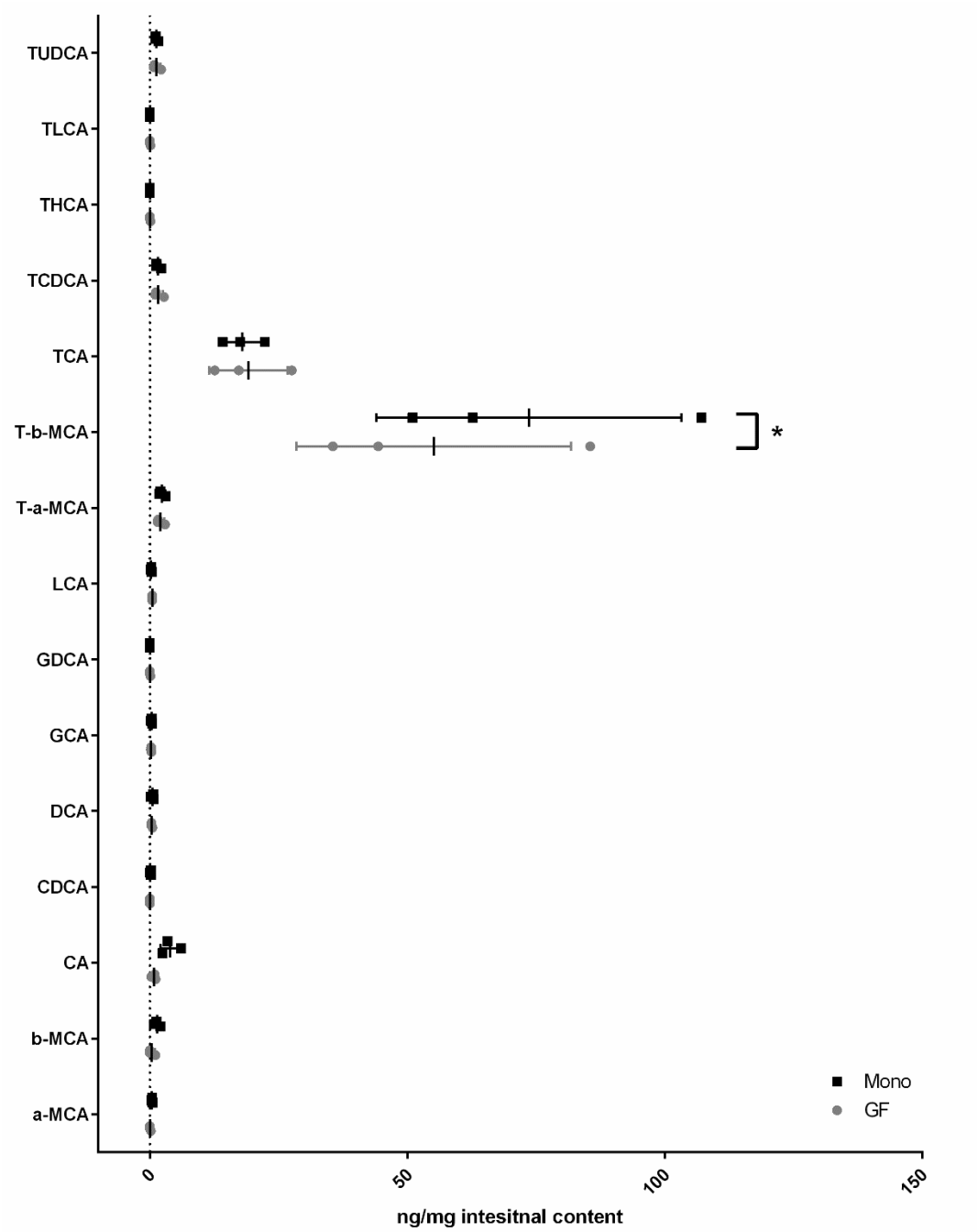

Supplementary Figure 19 Overview over bile acid concentrations in large intestinal content of germ free mice (GF) and mice colonised by *B. breve* UCC2003 (Mono)

Data presented as ng of bile acid per mg intestinal content, individual values plotted (n=3 mice), mean and SD indicated by lines, statistical significance analysed by Two-way ANOVA with Bonferroni post-test (* p-value < 0.05), bile acid identifiers given in Supplementary Table 6.

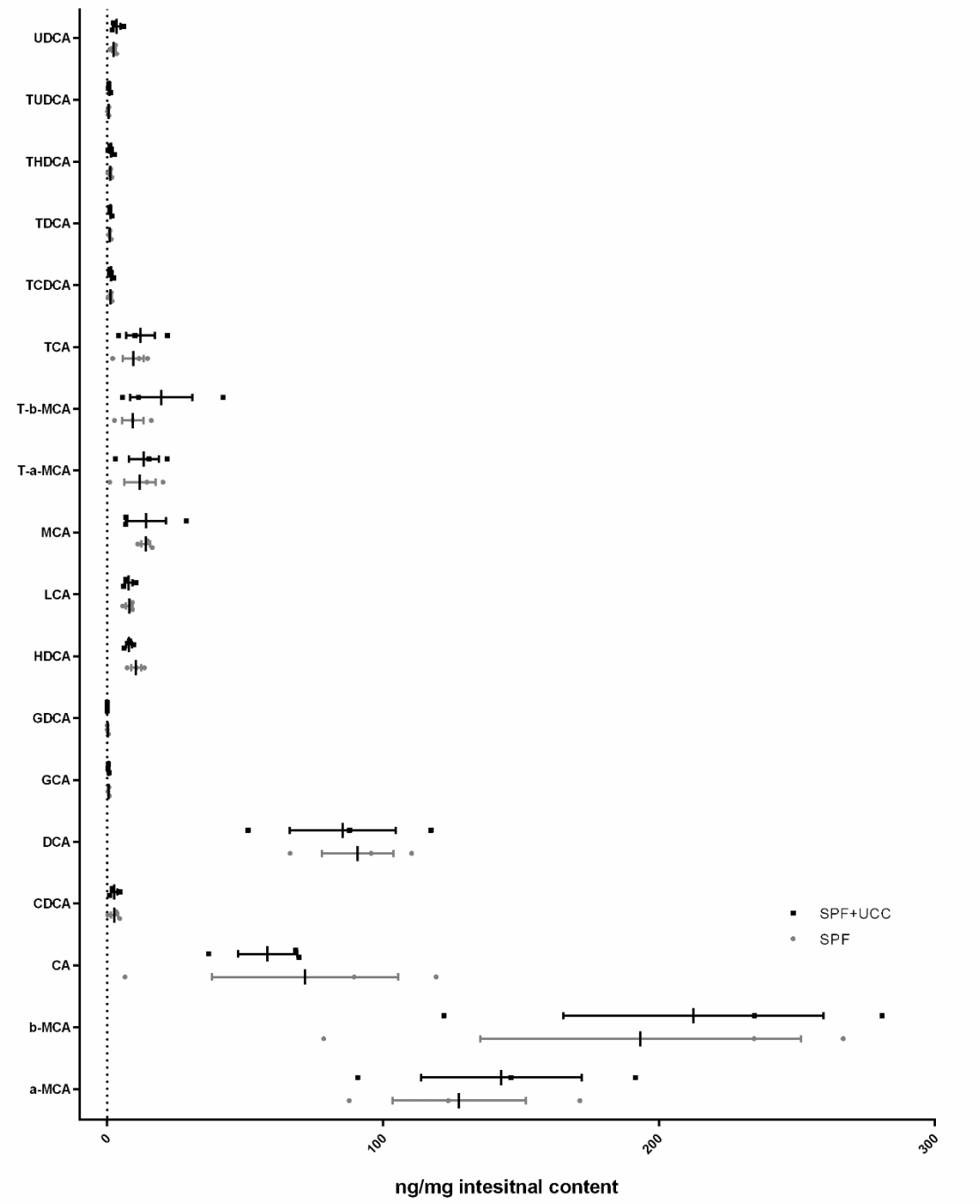

Supplementary Figure 20 Overview over bile acid concentration in large intestinal content of conventionally raised mice with (SPF+UCC) and without (SPF) *B. breve* UCC2003 colonisation

Data presented as ng of bile acid per mg intestinal content, individual values plotted (n=3 mice), mean and SD indicated by lines, statistical significance analysed by Two-way ANOVA with Bonferroni post-test (* p-value < 0.05), bile acid identifiers given in Supplementary Table 6.

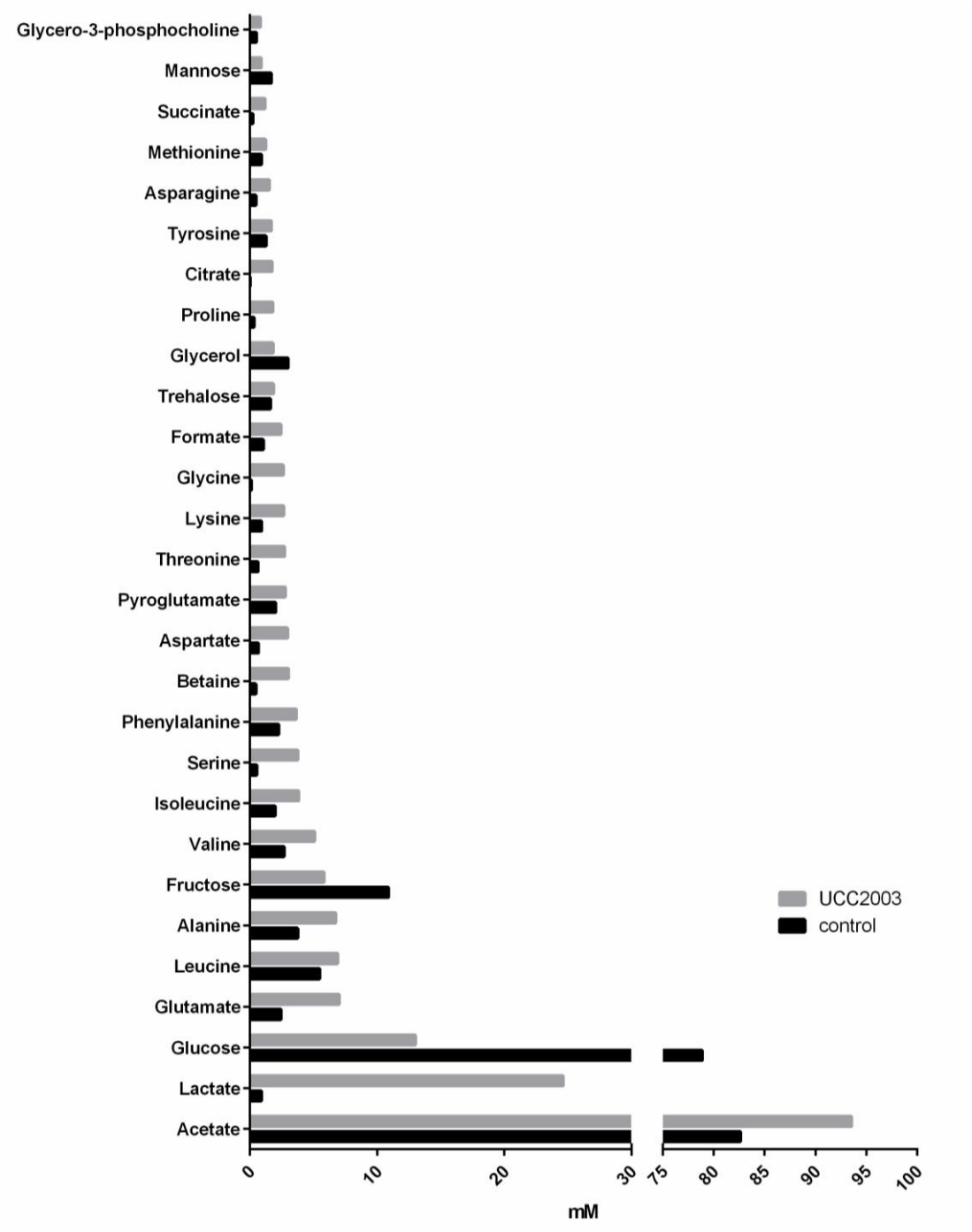

Supplementary Figure 21 Overview over metabolite concentration in supernatant of *B. breve* UCC2003 in vitro culture during stationary growth (UCC) compared to media control (control)

Data presented as mM concentration in supernatant, single values plotted, *B. breve* grown in MRS and samples collected at 18 h, Samples generated by Jennifer Ketskemety, NMR performed by Gwenaelle Le Gall.

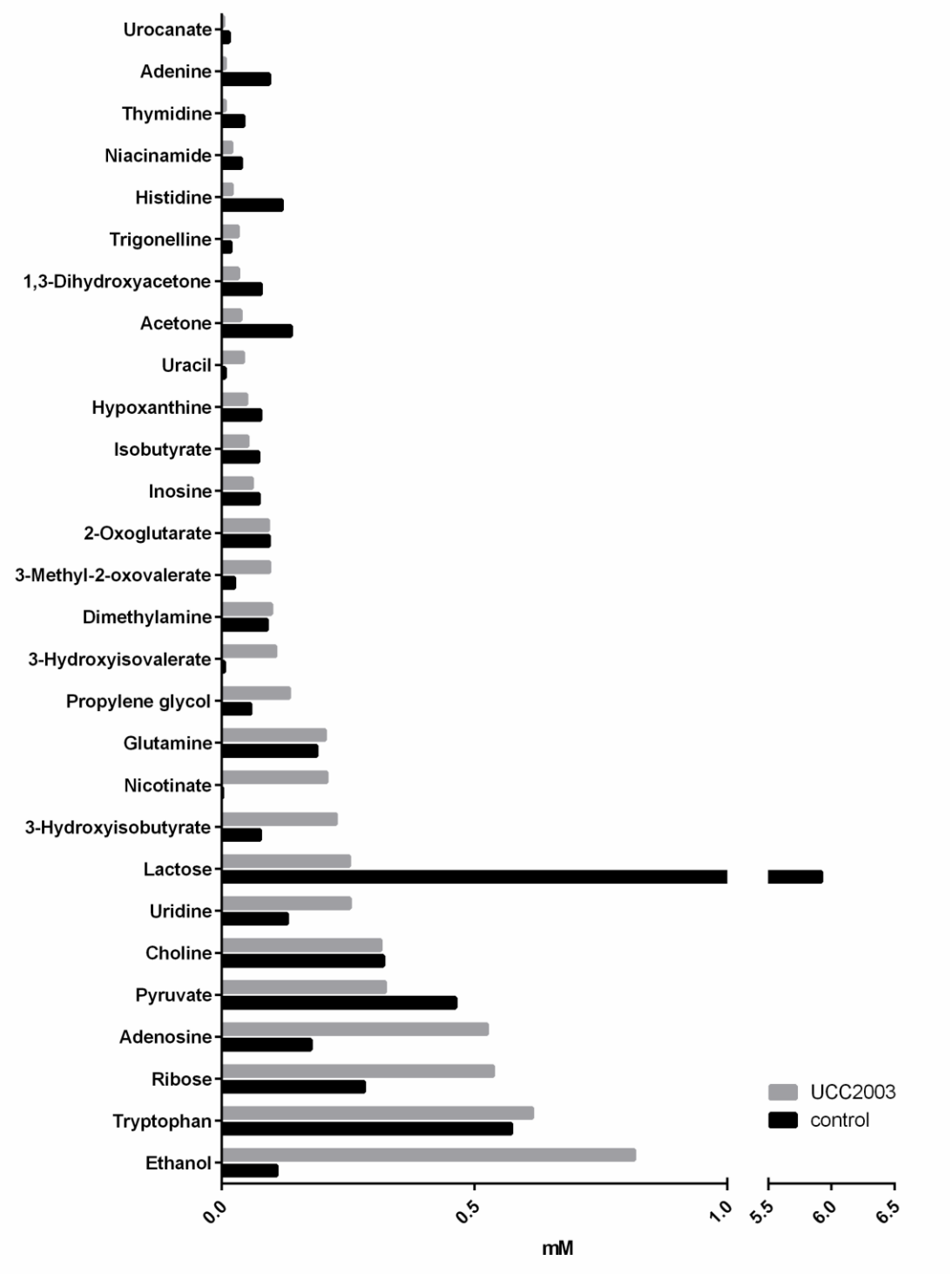

Supplementary Figure 22 Overview over metabolite concentration in supernatant of *B. breve* UCC2003 in vitro culture during stationary growth (UCC) compared to media control (control)

Data presented as mM concentration in supernatant, single values plotted, *B. breve* grown in MRS and samples collected at 18 h, Samples generated by Jennifer Ketskemety, NMR performed by Gwenaelle Le Gall.

Supplementary Table 6 Bile acid names and their corresponding abbreviations.

Bile acid name	Abbreviation
Chenodeoxycholic acid	CDCA
Deoxycholic acid	DCA
Dehydrocholic acid	DHCA
Glycocholic acid	GCA
Glycochenodeoxycholic acid	GCDCA
Glycodeoxycholic acid	GDCA
Lithocholic acid	LCA
Taurocholic acid	TCA
Taurochenodeoxycholic acid	TCDCA
Taurodeoxycholic acid	TDCA
Ursodeoxycholic acid	UDCA
Taurolithocholic acid	TLCA
α-Muricholic acid	a-MCA
β -Muricholic acid	b-MCA
Cholic acid	CA
Glycolithocholic acid	GLCA
Hyodeoxycholic acid	HDCA
Muricholic acid	MCA
Tauro-α-Muricholic acid	T-a-MCA
Tauro- β -Muricholic acid	T-b-MCA
Glycohyocholic acid	GHCA
Glycoursodeoxycholic acid	GUDCA
Taurohyocholic acid	THCA
Taurohyodeocycholic acid	THDCA
Tauroursodeoxycholic acid	TUDCA
Glycohyodeoxycholic acid	GHDCA
Taurodehydrocholic acid	TDHCA
DEOXYCHOLIC ACID -D4	d4-DCA
LITHOCHOLIC ACID -D4	d4-LCA
CHOLIC ACID-D4	d4-CA
GLYCOCHOLIC ACID -D4	d4-GCA
CHENODEOXYCHOLIC ACID -D4	d4-CDCA
GLYCOCHENODEOXYCHOLIC ACID – D4	D4-GCDCA

Supplementary Table 7 Predicated top 25 miR21 binding sites in *B. breve* UCC2003 genome (entropy cut-off < -16)

Entropy	Start position	End position	length of allignment
-34.5	1398323	1398346	21
-29.53	1317659	1317681	20
-29.4	2204	2226	20
-28.99	1887858	1887879	19
-28.82	1050561	1050582	18
-28.48	1326755	1326776	19
-27.72	2042274	2042295	17
-27.69	1751803	1751828	23
-27.64	60570	60591	18
-27.54	198841	198861	16
-27.49	778770	778790	12
-27.25	103344	103365	19
-27.23	923217	923238	14
-27.2	1948113	1948136	21
-27.09	1731095	1731114	18
-26.79	1322661	1322682	16
-26.54	1267061	1267080	17
-26.49	2247621	2247642	19
-26.29	2388612	2388635	21
-26.28	1362668	1362687	18
-26.08	150240	150265	22
-26.05	1903619	1903640	20

Supplementary Table 8 Predicated top 25 miR21 binding sites in S. Typhimurium SL1344 genome (entropy cut-off -16)

Entropy	Start position	End position	length of allignment
-32.05	693235	693257	20
-30.98	2490703	2490724	19
-30.59	4404814	4404835	19
-30.29	2346913	2346934	16
-30.29	4035438	4035459	16
-29.33	3699641	3699660	18
-29.29	2771412	2771434	20
-29.08	4619125	4619145	14
-28.88	2362590	2362617	24
-28.67	4734299	4734323	22
-28.56	4201391	4201414	21
-28.52	3672739	3672758	18
-28.36	4214358	4214376	18
-28.29	754414	754433	18
-28.28	3511852	3511875	21
-28.27	1048713	1048733	11
-27.68	229019	229042	21
-27.65	1936299	1936320	16
-27.59	3417763	3417784	16
-27.59	1952047	1952070	21
-27.46	4114970	4114994	21
-27.33	953266	953287	12
-27.3	3924877	3924898	19
-26.99	1397840	1397867	25
-26.95	706447	706465	18

References

1. Johnson, L., *Gastrointestinal Physiology*. Vol. 8th. 2017: Elsevier.
2. Reed, K.K. and R. Wickham, *Review of the gastrointestinal tract: from macro to micro.* Semin Oncol Nurs, 2009. **25**(1): p. 3-14.
3. Johnson, L., *Gastrointestinal Physiology* Vol. 7th. 2017: Elsevier.
4. Gary A. Thibodeau, K.T.P., *Anatomy & physiology*. Vol. 6th. 2007: Elsevier.
5. Hall, J., *Guyton and Hall Textbook of Medical Physiology*. Vol. 13th. 2017: Elsevier.
6. Ward, S.M. and K.M. Sanders, *Physiology and pathophysiology of the interstitial cell of Cajal: from bench to bedside. I. Functional development and plasticity of interstitial cells of Cajal networks.* Am J Physiol Gastrointest Liver Physiol, 2001. **281**(3): p. G602-11.
7. Jung, C., J.-P. Hugot, and F. Barreau, *Peyer's patches: the immune sensors of the intestine.* International journal of inflammation, 2010. **2010**.
8. Koboziev, I., F. Karlsson, and M.B. Grisham, *Gut-associated lymphoid tissue, T cell trafficking, and chronic intestinal inflammation.* Ann N Y Acad Sci, 2010. **1207 Suppl 1**: p. E86-93.
9. Neutra, M.R., N.J. Mantis, and J.P. Kraehenbuhl, *Collaboration of epithelial cells with organized mucosal lymphoid tissues.* Nat Immunol, 2001. **2**(11): p. 1004-9.
10. Peterson, L.W. and D. Artis, *Intestinal epithelial cells: regulators of barrier function and immune homeostasis.* Nat Rev Immunol, 2014. **14**(3): p. 141-53.
11. Jiri Mestecky, W.S., Michael W. Russell, Hilde Cheroutre, Bart N. Lambrecht and Brian L Kelsall *Mucosal Immunology*. 2015.
12. McCance, K.L. and S.E. Huether, *Pathophysiology : the biologic basis for disease in adults and children*. Vol. 5th. 2006: Elsevier
13. Crosnier, C., D. Stamataki, and J. Lewis, *Organizing cell renewal in the intestine: stem cells, signals and combinatorial control.* Nature Reviews Genetics, 2006. **7**: p. 349.
14. Wu, H.-J. and E. Wu, *The role of gut microbiota in immune homeostasis and autoimmunity.* Gut microbes, 2012. **3**(1): p. 4-14.
15. Podolsky, D.K., et al., *Colitis-associated variant of TLR2 causes impaired mucosal repair because of TFF3 deficiency.* Gastroenterology, 2009. **137**(1): p. 209-220.
16. Cavalcante-Silva, L.H., et al., *Obesity-driven gut microbiota inflammatory pathways to metabolic syndrome.* Frontiers in physiology, 2015. **6**.
17. Nenci, A., et al., *Epithelial NEMO links innate immunity to chronic intestinal inflammation.* Nature, 2007. **446**(7135): p. 557-561.
18. Greten, F.R., et al., *IKKβ links inflammation and tumorigenesis in a mouse model of colitis-associated cancer.* Cell, 2004. **118**(3): p. 285-296.
19. Coban, C., et al., *Immunogenicity of whole-parasite vaccines against Plasmodium falciparum involves malarial hemozoin and host TLR9.* Cell host & microbe, 2010. **7**(1): p. 50-61.
20. Lee, J., et al., *Maintenance of colonic homeostasis by distinctive apical TLR9 signalling in intestinal epithelial cells.* Nature cell biology, 2006. **8**(12): p. 1327-1337.
21. Odenwald, M.A. and J.R. Turner, *The intestinal epithelial barrier: a therapeutic target?* Nature reviews Gastroenterology & hepatology, 2016.
22. Zihni, C., et al., *Tight junctions: from simple barriers to multifunctional molecular gates.* Nature reviews Molecular cell biology, 2016. **17**(9): p. 564-580.
23. Williams, J., et al., *Epithelial cell shedding and barrier function: a matter of life and death at the small intestinal villus tip.* Veterinary pathology, 2015. **52**(3): p. 445-455.
24. Mayhew, T.M., et al., *Epithelial integrity, cell death and cell loss in mammalian small intestine.* Histol Histopathol, 1999. **14**(1): p. 257-67.
25. Parker, A., et al., *Cell proliferation within small intestinal crypts is the principal driving force for cell migration on villi.* The FASEB Journal, 2017. **31**(2): p. 636-649.
26. Patterson, A.M. and A.J. Watson, *Deciphering the Complex Signaling Systems That Regulate Intestinal Epithelial Cell Death Processes and Shedding.* Frontiers in immunology, 2017. **8**: p. 841.
27. Watson, A.J.M., et al., *Mechanisms of Epithelial Cell Shedding in the Mammalian Intestine and Maintenance of Barrier Function.* Molecular Structure and Function of the Tight Junction: from Basic Mechanisms to Clinical Manifestations, 2009. **1165**: p. 135-142.

28. Potten, C.S., *A comprehensive study of the radiobiological response of the murine (BDF1) small intestine.* International journal of radiation biology, 1990. **58**(6): p. 925-973.
29. Madara, J.L., *Maintenance of the macromolecular barrier at cell extrusion sites in intestinal epithelium: physiological rearrangement of tight junctions.* The Journal of membrane biology, 1990. **116**(2): p. 177-184.
30. Williams, J.M., et al., *Epithelial Cell Shedding and Barrier Function: A Matter of Life and Death at the Small Intestinal Villus Tip.* Veterinary Pathology, 2015. **52**(3): p. 445-455.
31. Guan, Y., et al., *Redistribution of the tight junction protein ZO-1 during physiological shedding of mouse intestinal epithelial cells.* American Journal of Physiology-Cell Physiology, 2011. **300**(6): p. C1404-C1414.
32. Marchiando, A.M., et al., *The Epithelial Barrier Is Maintained by In Vivo Tight Junction Expansion During Pathologic Intestinal Epithelial Shedding.* Gastroenterology, 2011. **140**(4): p. 1208-+.
33. Miguel, J.C., et al., *Epidermal growth factor suppresses intestinal epithelial cell shedding through a MAPK-dependent pathway.* J Cell Sci, 2017. **130**(1): p. 90-96.
34. Patterson, A.M. and A.J.M. Watson, *Deciphering the Complex Signaling Systems That Regulate Intestinal Epithelial Cell Death Processes and Shedding.* Frontiers in Immunology, 2017. **8**: p. 841.
35. Marchiando, A.M., et al., *The epithelial barrier is maintained by in vivo tight junction expansion during pathologic intestinal epithelial shedding.* Gastroenterology, 2011. **140**(4): p. 1208-1218. e2.
36. Watson, A.J.M., L.J. Hall, and K.R. Hughes, *Cell shedding: old questions answered.* Gastroenterology, 2012. **143**(5): p. 1389-91.
37. Eisenhoffer, G.T., et al., *Crowding induces live cell extrusion to maintain homeostatic cell numbers in epithelia.* Nature, 2012. **484**(7395): p. 546-9.
38. Wang, Y., et al., *Both the anti-and pro-apoptotic functions of villin regulate cell turnover and intestinal homeostasis.* Scientific reports, 2016. **6**.
39. Kiesslich, R., et al., *Local barrier dysfunction identified by confocal laser endomicroscopy predicts relapse in inflammatory bowel disease.* Gut, 2011: p. gutjnl-2011-300695.
40. Kiesslich, R., et al., *Identification of epithelial gaps in human small and large intestine by confocal endomicroscopy.* Gastroenterology, 2007. **133**(6): p. 1769-1778.
41. Piguet, P.F., et al., *TNF-induced enterocyte apoptosis in mice is mediated by the TNF receptor 1 and does not require p53.* European journal of immunology, 1998. **28**(11): p. 3499-3505.
42. Antoni, L., et al., *Intestinal barrier in inflammatory bowel disease.* World journal of gastroenterology: WJG, 2014. **20**(5): p. 1165.
43. Neurath, M.F., *Cytokines in inflammatory bowel disease.* Nature Reviews Immunology, 2014. **14**(5): p. 329-342.
44. Kiesslich, R., et al., *Local barrier dysfunction identified by confocal laser endomicroscopy predicts relapse in inflammatory bowel disease.* Gut, 2012. **61**(8): p. 1146-1153.
45. Williams, J.M., et al., *A mouse model of pathological small intestinal epithelial cell apoptosis and shedding induced by systemic administration of lipopolysaccharide.* Disease models & mechanisms, 2013. **6**(6): p. 1388-99.
46. Hughes, K.R., et al., *Bifidobacterium breve reduces apoptotic epithelial cell shedding in an exopolysaccharide and MyD88-dependent manner.* Open Biol, 2017. **7**(1).
47. Clarke, L.L., *A guide to Ussing chamber studies of mouse intestine.* American Journal of Physiology-Gastrointestinal and Liver Physiology, 2009. **296**(6): p. G1151-G1166.
48. Le Ferrec, E., et al., *In vitro models of the intestinal barrier.* Atla, 2001. **29**: p. 649-668.
49. McKay, D., D. Philpott, and M. Perdue, *In vitro models in inflammatory bowel disease research—a critical review.* Alimentary pharmacology & therapeutics, 1997. **11**(s3): p. 70-80.
50. Fatehullah, A., S.H. Tan, and N. Barker, *Organoids as an in vitro model of human development and disease.* Nature cell biology, 2016. **18**(3): p. 246-254.
51. Finkbeiner, S.R., et al., *Generation of tissue-engineered small intestine using embryonic stem cell-derived human intestinal organoids.* Biology open, 2015. **4**(11): p. 1462-1472.
52. Miyoshi, H. and T.S. Stappenbeck, *In vitro expansion and genetic modification of gastrointestinal stem cells in spheroid culture.* Nature protocols, 2013. **8**(12): p. 2471-2482.
53. Gkouskou, K., et al., *The gut microbiota in mouse models of inflammatory bowel disease.* Frontiers in Cellular and Infection Microbiology, 2014. **4**(28).

54. Kühn, R., et al., *Interleukin-10-deficient mice develop chronic enterocolitis.* Cell, 1993. **75**(2): p. 263-274.
55. Matharu, K.S., et al., *Toll-like receptor 4-mediated regulation of spontaneous Helicobacter-dependent colitis in IL-10–deficient mice.* Gastroenterology, 2009. **137**(4): p. 1380-1390. e3.
56. Hoentjen, F., et al., *Antibiotics with a selective aerobic or anaerobic spectrum have different therapeutic activities in various regions of the colon in interleukin 10 gene deficient mice.* Gut, 2003. **52**(12): p. 1721-1727.
57. Laroui, H., et al., *Dextran sodium sulfate (DSS) induces colitis in mice by forming nano-lipocomplexes with medium-chain-length fatty acids in the colon.* PloS one, 2012. **7**(3): p. e32084.
58. Treuting, P.M. and S.M. Dintzis, *Comparative anatomy and histology: a mouse and human atlas (expert consult)*. 2011: Academic Press.
59. Ley, R.E., et al., *Obesity alters gut microbial ecology.* Proceedings of the National Academy of Sciences of the United States of America, 2005. **102**(31): p. 11070-11075.
60. Justice, M.J. and P. Dhillon, *Using the mouse to model human disease: increasing validity and reproducibility*. 2016, The Company of Biologists Ltd.
61. Zhang, C., et al., *Structural resilience of the gut microbiota in adult mice under high-fat dietary perturbations.* The ISME journal, 2012. **6**(10): p. 1848-1857.
62. Wu, G.D., et al., *Linking long-term dietary patterns with gut microbial enterotypes.* Science, 2011. **334**(6052): p. 105-108.
63. Hold, G.L., et al., *Role of the gut microbiota in inflammatory bowel disease pathogenesis: what have we learnt in the past 10 years?* World journal of gastroenterology: WJG, 2014. **20**(5): p. 1192.
64. Sartor, R.B., *Mechanisms of disease: pathogenesis of Crohn's disease and ulcerative colitis.* Nature clinical practice Gastroenterology & hepatology, 2006. **3**(7): p. 390-407.
65. Ghosh, N. and P. Premchand, *A UK cost of care model for inflammatory bowel disease.* Frontline Gastroenterology, 2015. **6**(3): p. 169-174.
66. Molodecky, N.A., et al., *Increasing Incidence and Prevalence of the Inflammatory Bowel Diseases With Time, Based on Systematic Review.* Gastroenterology, 2012. **142**(1): p. 46-54.e42.
67. Burisch, J., et al., *The burden of inflammatory bowel disease in Europe.* Journal of Crohn's and Colitis, 2013. **7**(4): p. 322-337.
68. Kaplan, G.G., *The global burden of IBD: from 2015 to 2025.* Nature Reviews Gastroenterology & Hepatology, 2015. **12**(12): p. 720-727.
69. Tontini, G.E., et al., *Differential diagnosis in inflammatory bowel disease colitis: state of the art and future perspectives.* World Journal of Gastroenterology: WJG, 2015. **21**(1): p. 21.
70. Gastroenterology and Hepatology Division, J.H.H., East Baltimore City, Maryland. *Ulcerative Colitis: Introduction*. [cited 2017 5.12.]; Available from: https://www.jhmicall.org/GDL_Disease.aspx?CurrentUDV=31&GDL_Disease_ID=2A4995B2-DFA5-4954-B770-F1F5BAFED033&GDL_DC_ID=D03119D7-57A3-4890-A717-CF1E7426C8BA.
71. Fakhoury, M., et al., *Inflammatory bowel disease: clinical aspects and treatments.* Journal of inflammation research, 2014. **7**: p. 113.
72. Stewenius, J., et al., *Incidence of colorectal cancer and all cause mortality in non-selected patients with ulcerative colitis and indeterminate colitis in Malmö, Sweden.* International journal of colorectal disease, 1995. **10**(2): p. 117-122.
73. Jess, T., et al., *Increased risk of intestinal cancer in Crohn's disease: a meta-analysis of population-based cohort studies.* The American journal of gastroenterology, 2005. **100**(12): p. 2724-2729.
74. Hendrickson, B.A., R. Gokhale, and J.H. Cho, *Clinical aspects and pathophysiology of inflammatory bowel disease.* Clinical microbiology reviews, 2002. **15**(1): p. 79-94.
75. Michielan, A. and R. D'Incà, *Intestinal permeability in inflammatory bowel disease: pathogenesis, clinical evaluation, and therapy of leaky gut.* Mediators of inflammation, 2015. **2015**.
76. Khor, B., A. Gardet, and R.J. Xavier, *Genetics and pathogenesis of inflammatory bowel disease.* Nature, 2011. **474**(7351): p. 307-317.
77. Vivinus-Nébot, M., et al., *Functional bowel symptoms in quiescent inflammatory bowel diseases: role of epithelial barrier disruption and low-grade inflammation.* Gut, 2014. **63**(5): p. 744-752.

78. Lee, S.H., *Intestinal permeability regulation by tight junction: implication on inflammatory bowel diseases.* Intestinal research, 2015. **13**(1): p. 11-18.
79. Arrieta, M.-C., et al., *Reducing small intestinal permeability attenuates colitis in the IL10 gene-deficient mouse.* Gut, 2009. **58**(1): p. 41-48.
80. Benchimol, E.I., et al., *Trends in Epidemiology of Pediatric Inflammatory Bowel Disease in Canada: Distributed Network Analysis of Multiple Population-Based Provincial Health Administrative Databases.* The American Journal of Gastroenterology, 2017.
81. Glick, S.R. and R.S. Carvalho, *Inflammatory Bowel Disease.* Pediatrics in Review, 2011. **32**(1): p. 14-25.
82. Coskun, M., *Intestinal epithelium in inflammatory bowel disease.* Frontiers in medicine, 2014. **1**.
83. Zeissig, S., et al., *Changes in expression and distribution of claudin 2, 5 and 8 lead to discontinuous tight junctions and barrier dysfunction in active Crohn's disease.* Gut, 2007. **56**(1): p. 61-72.
84. Cui, W., et al., *Tumor necrosis factor alpha increases epithelial barrier permeability by disrupting tight junctions in Caco-2 cells.* Brazilian Journal of Medical and Biological Research, 2010. **43**(4): p. 330-337.
85. Marini, M., et al., *TNF-αneutralization ameliorates the severity of murine Crohn's-like ileitis by abrogation of intestinal epithelial cell apoptosis.* Proceedings of the National Academy of Sciences, 2003. **100**(14): p. 8366-8371.
86. Ito, R., et al., *Interferon-gamma is causatively involved in experimental inflammatory bowel disease in mice.* Clinical & Experimental Immunology, 2006. **146**(2): p. 330-338.
87. Barrett, J.C., et al., *Genome-wide association study of ulcerative colitis identifies three new susceptibility loci, including the HNF4A region.* Nature genetics, 2009. **41**(12): p. 1330-1334.
88. Ahn, S.H., et al., *Hepatocyte nuclear factor 4α in the intestinal epithelial cells protects against inflammatory bowel disease.* Inflammatory bowel diseases, 2008. **14**(7): p. 908-920.
89. Zhang, M., et al., *Interactions between Intestinal Microbiota and Host Immune Response in Inflammatory Bowel Disease.* Frontiers in Immunology, 2017. **8**(942).
90. Di Sabatino, A., et al., *Increased enterocyte apoptosis in inflamed areas of Crohn's disease.* Diseases of the colon & rectum, 2003. **46**(11): p. 1498-1507.
91. Catrysse, L., et al., *A20 in inflammation and autoimmunity.* Trends in immunology, 2014. **35**(1): p. 22-31.
92. Wang, J., et al., *Ubiquitin-editing enzyme A20 promotes tolerance to lipopolysaccharide in enterocytes.* The Journal of Immunology, 2009. **183**(2): p. 1384-1392.
93. Vereecke, L., et al., *Enterocyte-specific A20 deficiency sensitizes to tumor necrosis factor–induced toxicity and experimental colitis.* Journal of Experimental Medicine, 2010: p. jem. 20092474.
94. Blander, J.M., *Death in the intestinal epithelium—basic biology and implications for inflammatory bowel disease.* The FEBS journal, 2016. **283**(14): p. 2720-2730.
95. Chassaing, B., et al., *Dextran sulfate sodium (DSS)-induced colitis in mice.* Curr Protoc Immunol, 2014. **104**: p. Unit 15.25.
96. Antoniou, E., et al., *The TNBS-induced colitis animal model: An overview.* Annals of Medicine and Surgery, 2016. **11**: p. 9-15.
97. Schaubeck, M., et al., *Dysbiotic gut microbiota causes transmissible Crohn9s disease-like ileitis independent of failure in antimicrobial defence.* Gut, 2015: p. gutjnl-2015-309333.
98. Kiesler, P., I.J. Fuss, and W. Strober, *Experimental Models of Inflammatory Bowel Diseases.* Cellular and Molecular Gastroenterology and Hepatology, 2015. **1**(2): p. 154-170.
99. Keubler, L.M., et al., *A Multihit Model: Colitis Lessons from the Interleukin-10–deficient Mouse.* Inflammatory bowel diseases, 2015. **21**(8): p. 1967.
100. Allgayer, H., *Review article: mechanisms of action of mesalazine in preventing colorectal carcinoma in inflammatory bowel disease.* Aliment Pharmacol Ther, 2003. **18 Suppl 2**: p. 10-4.
101. Velayos, F.S., J.P. Terdiman, and J.M. Walsh, *Effect of 5-aminosalicylate use on colorectal cancer and dysplasia risk: a systematic review and metaanalysis of observational studies.* Am J Gastroenterol, 2005. **100**(6): p. 1345-53.
102. Neurath, M.F., *Current and emerging therapeutic targets for IBD.* Nature Reviews Gastroenterology &Amp; Hepatology, 2017. **14**: p. 269.

103. Danese, S., L. Vuitton, and L. Peyrin-Biroulet, *Biologic agents for IBD: practical insights.* Nature Reviews Gastroenterology &Amp; Hepatology, 2015. **12**: p. 537.
104. Schnitzler, F., et al., *Mucosal healing predicts long-term outcome of maintenance therapy with infliximab in Crohn's disease.* Inflamm Bowel Dis, 2009. **15**(9): p. 1295-301.
105. Colombel, J.F., et al., *Early mucosal healing with infliximab is associated with improved long-term clinical outcomes in ulcerative colitis.* Gastroenterology, 2011. **141**(4): p. 1194-201.
106. Ferrari, L., M.K. Krane, and A. Fichera, *Inflammatory bowel disease surgery in the biologic era.* World Journal of Gastrointestinal Surgery, 2016. **8**(5): p. 363-370.
107. Hattori, M. and T.D. Taylor, *The human intestinal microbiome: a new frontier of human biology.* DNA research, 2009. **16**(1): p. 1-12.
108. Savage, D.C., *Microbial ecology of the gastrointestinal tract.* Annual Reviews in Microbiology, 1977. **31**(1): p. 107-133.
109. Hayashi, H., M. Sakamoto, and Y. Benno, *Phylogenetic analysis of the human gut microbiota using 16S rDNA clone libraries and strictly anaerobic culture-based methods.* Microbiology and immunology, 2002. **46**(8): p. 535-548.
110. Aguiar-Pulido, V., et al., *Metagenomics, metatranscriptomics, and metabolomics approaches for microbiome analysis.* Evolutionary bioinformatics online, 2016. **12**(Suppl 1): p. 5.
111. Lagier, J.C., et al., *Microbial culturomics: paradigm shift in the human gut microbiome study.* Clinical Microbiology and Infection, 2012. **18**(12): p. 1185-1193.
112. Lau, J.T., et al., *Capturing the diversity of the human gut microbiota through culture-enriched molecular profiling.* Genome Medicine, 2016. **8**(1): p. 72.
113. Browne, H.P., et al., *Culturing of 'unculturable'human microbiota reveals novel taxa and extensive sporulation.* Nature, 2016. **533**(7604): p. 543-546.
114. Behjati, S. and P.S. Tarpey, *What is next generation sequencing?* Archives of Disease in Childhood-Education and Practice, 2013. **98**(6): p. 236-238.
115. Guo, J., et al., *Four-color DNA sequencing with 3'-O-modified nucleotide reversible terminators and chemically cleavable fluorescent dideoxynucleotides.* Proceedings of the National Academy of Sciences, 2008. **105**(27): p. 9145-9150.
116. Ip, C.L., et al., *MinION Analysis and Reference Consortium: Phase 1 data release and analysis.* F1000Research, 2015. **4**.
117. Goodwin, S., J.D. McPherson, and W.R. McCombie, *Coming of age: ten years of next-generation sequencing technologies.* Nature Reviews Genetics, 2016. **17**(6): p. 333-351.
118. Alcon-Giner, C., et al., *Optimisation of 16S rRNA gut microbiota profiling of extremely low birth weight infants.* BMC Genomics, 2017. **18**(1): p. 841.
119. Nguyen, N.-P., et al., *A perspective on 16S rRNA operational taxonomic unit clustering using sequence similarity.* npj Biofilms and Microbiomes, 2016. **2**: p. 16004.
120. Eren, A.M., et al., *Oligotyping: differentiating between closely related microbial taxa using 16S rRNA gene data.* Methods in Ecology and Evolution, 2013. **4**(12): p. 1111-1119.
121. Bazinet, A.L. and M.P. Cummings, *A comparative evaluation of sequence classification programs.* BMC bioinformatics, 2012. **13**(1): p. 92.
122. Laursen, M.F., M.D. Dalgaard, and M.I. Bahl, *Genomic GC-Content Affects the Accuracy of 16S rRNA Gene Sequencing Based Microbial Profiling due to PCR Bias.* Frontiers in microbiology, 2017. **8**: p. 1934.
123. Mizrahi-Man, O., E.R. Davenport, and Y. Gilad, *Taxonomic classification of bacterial 16S rRNA genes using short sequencing reads: evaluation of effective study designs.* PloS one, 2013. **8**(1): p. e53608.
124. Franzosa, E.A., et al., *Sequencing and beyond: integrating molecular'omics' for microbial community profiling.* Nature Reviews Microbiology, 2015. **13**(6): p. 360-372.
125. Sabat, A.J., et al., *Targeted next-generation sequencing of the 16S-23S rRNA region for culture-independent bacterial identification-increased discrimination of closely related species.* Scientific reports, 2017. **7**(1): p. 3434.
126. Li, R., et al., *Comparison of DNA-, PMA-, and RNA-based 16S rRNA Illumina sequencing for detection of live bacteria in water.* Scientific reports, 2017. **7**: p. 5752.
127. Knight, R., et al., *Unlocking the potential of metagenomics through replicated experimental design.* Nature biotechnology, 2012. **30**(6): p. 513-520.
128. Sharpton, T., et al., *Development of Inflammatory Bowel Disease Is Linked to a Longitudinal Restructuring of the Gut Metagenome in Mice.* MSystems, 2017. **2**(5): p. e00036-17.

129. Moran, M.A., *Metatranscriptomics: Eavesdropping on Complex Microbial Communities-Large-scale sequencing of mRNAs retrieved from natural communities provides insights into microbial activities and how they are regulated.* Microbe, 2009. **4**(7): p. 329.
130. Franzosa, E.A., et al., *Relating the metatranscriptome and metagenome of the human gut.* Proceedings of the National Academy of Sciences, 2014. **111**(22): p. E2329-E2338.
131. McNulty, N.P., et al., *The impact of a consortium of fermented milk strains on the gut microbiome of gnotobiotic mice and monozygotic twins.* Science translational medicine, 2011. **3**(106): p. 106ra106-106ra106.
132. Belenguer, A., et al., *Two routes of metabolic cross-feeding between Bifidobacterium adolescentis and butyrate-producing anaerobes from the human gut.* Applied and environmental microbiology, 2006. **72**(5): p. 3593-3599.
133. Duran-Pinedo, A.E. and J. Frias-Lopez, *Beyond microbial community composition: functional activities of the oral microbiome in health and disease.* Microbes and infection, 2015. **17**(7): p. 505-516.
134. Altelaar, A.M., J. Munoz, and A.J. Heck, *Next-generation proteomics: towards an integrative view of proteome dynamics.* Nature Reviews Genetics, 2013. **14**(1): p. 35-48.
135. Bernini, P., et al., *Individual human phenotypes in metabolic space and time.* Journal of proteome research, 2009. **8**(9): p. 4264-4271.
136. Turnbaugh, P.J. and J.I. Gordon, *An invitation to the marriage of metagenomics and metabolomics.* Cell, 2008. **134**(5): p. 708-713.
137. Smolinska, A., et al., *NMR and pattern recognition methods in metabolomics: from data acquisition to biomarker discovery: a review.* Analytica chimica acta, 2012. **750**: p. 82-97.
138. Santoru, M.L., et al., *Cross sectional evaluation of the gut-microbiome metabolome axis in an Italian cohort of IBD patients.* Scientific reports, 2017. **7**: p. 9523.
139. Singh, N., et al., *Activation of Gpr109a, receptor for niacin and the commensal metabolite butyrate, suppresses colonic inflammation and carcinogenesis.* Immunity, 2014. **40**(1): p. 128-139.
140. Ilott, N.E., et al., *Defining the microbial transcriptional response to colitis through integrated host and microbiome profiling.* The ISME journal, 2016.
141. Qin, J., et al., *A human gut microbial gene catalogue established by metagenomic sequencing.* nature, 2010. **464**(7285): p. 59-65.
142. The Human Microbiome Project, C., *Structure, function and diversity of the healthy human microbiome.* Nature, 2012. **486**: p. 207.
143. Ottman, N., et al., *The function of our microbiota: who is out there and what do they do?* Frontiers in Cellular and Infection Microbiology, 2012. **2**(104).
144. Jandhyala, S.M., et al., *Role of the normal gut microbiota.* World journal of gastroenterology: WJG, 2015. **21**(29): p. 8787.
145. Donaldson, G.P., S.M. Lee, and S.K. Mazmanian, *Gut biogeography of the bacterial microbiota.* Nature Reviews Microbiology, 2016. **14**(1): p. 20-32.
146. Macpherson, A.J. and K.D. McCoy, *Stratification and compartmentalisation of immunoglobulin responses to commensal intestinal microbes.* Seminars in Immunology, 2013. **25**(5): p. 358-363.
147. Eckburg, P.B., et al., *Diversity of the human intestinal microbial flora.* science, 2005. **308**(5728): p. 1635-1638.
148. Konturek, P.C., et al., *Emerging role of fecal microbiota therapy in the treatment of gastrointestinal and extra-gastrointestinal diseases.* J Physiol Pharmacol, 2015. **66**(4): p. 483-91.
149. Hollister, E.B., C. Gao, and J. Versalovic, *Compositional and functional features of the gastrointestinal microbiome and their effects on human health.* Gastroenterology, 2014. **146**(6): p. 1449-1458.
150. Yatsunenko, T., et al., *Human gut microbiome viewed across age and geography.* Nature, 2012. **486**(7402): p. 222-227.
151. Tap, J., et al., *Towards the human intestinal microbiota phylogenetic core.* Environmental microbiology, 2009. **11**(10): p. 2574-2584.
152. Lozupone, C.A., et al., *Diversity, stability and resilience of the human gut microbiota.* Nature, 2012. **489**: p. 220.
153. Turnbaugh, P.J., et al., *A core gut microbiome in obese and lean twins.* Nature, 2008. **457**: p. 480.

154. Thursby, E. and N. Juge, *Introduction to the human gut microbiota.* Biochemical Journal, 2017. **474**(11): p. 1823-1836.
155. Collado, M.C., et al., *Human gut colonisation may be initiated in utero by distinct microbial communities in the placenta and amniotic fluid.* Scientific reports, 2016. **6**: p. 23129.
156. Arboleya, S., et al., *Gut bifidobacteria populations in human health and aging.* Frontiers in microbiology, 2016. **7**.
157. Dominguez-Bello, M.G., et al., *Delivery mode shapes the acquisition and structure of the initial microbiota across multiple body habitats in newborns.* Proceedings of the National Academy of Sciences, 2010. **107**(26): p. 11971-11975.
158. Koenig, J.E., et al., *Succession of microbial consortia in the developing infant gut microbiome.* Proceedings of the National Academy of Sciences, 2011. **108**(Supplement 1): p. 4578-4585.
159. Turroni, F., et al., *Diversity of bifidobacteria within the infant gut microbiota.* PloS one, 2012. **7**(5): p. e36957.
160. Imahori, K., *How I understand aging.* Nutrition reviews, 1992. **50**(12): p. 351-352.
161. Claesson, M.J., et al., *Composition, variability, and temporal stability of the intestinal microbiota of the elderly.* Proceedings of the National Academy of Sciences, 2011. **108**(Supplement 1): p. 4586-4591.
162. Biagi, E., et al., *Through ageing, and beyond: gut microbiota and inflammatory status in seniors and centenarians.* PloS one, 2010. **5**(5): p. e10667.
163. Weinstock, G.M., *Genomic approaches to studying the human microbiota.* Nature, 2012. **489**(7415): p. 250-256.
164. Grenham, S., et al., *Brain–gut–microbe communication in health and disease.* Frontiers in physiology, 2011. **2**.
165. Neana, F. *The leaky gut syndrome*. [cited 2017 16.12.]; Available from: https://www.slideshare.net/fathineana/the-leaky-gut-syndrome.
166. Zoetendal, E.G., et al., *The human small intestinal microbiota is driven by rapid uptake and conversion of simple carbohydrates.* The Isme Journal, 2012. **6**: p. 1415.
167. Flint, H.J., et al., *Microbial degradation of complex carbohydrates in the gut.* Gut microbes, 2012. **3**(4): p. 289-306.
168. Wedekind, K., H. Mansfield, and L. Montgomery, *Enumeration and isolation of cellulolytic and hemicellulolytic bacteria from human feces.* Applied and environmental microbiology, 1988. **54**(6): p. 1530-1535.
169. Walker, A.W., et al., *Dominant and diet-responsive groups of bacteria within the human colonic microbiota.* The ISME journal, 2011. **5**(2): p. 220-230.
170. Robert, C., et al., *Bacteroides cellulosilyticus sp. nov., a cellulolytic bacterium from the human gut microbial community.* International journal of systematic and evolutionary microbiology, 2007. **57**(7): p. 1516-1520.
171. Gherardini, F.C. and A.A. Salyers, *Purification and characterization of a cell-associated, soluble mannanase from Bacteroides ovatus.* Journal of bacteriology, 1987. **169**(5): p. 2038-2043.
172. McCarthy, R., S. Kotarski, and A. Salyers, *Location and characteristics of enzymes involved in the breakdown of polygalacturonic acid by Bacteroides thetaiotaomicron.* Journal of bacteriology, 1985. **161**(2): p. 493-499.
173. Mirande, C., et al., *Dietary fibre degradation and fermentation by two xylanolytic bacteria Bacteroides xylanisolvens XB1AT and Roseburia intestinalis XB6B4 from the human intestine.* Journal of applied microbiology, 2010. **109**(2): p. 451-460.
174. Louis, P. and H.J. Flint, *Formation of propionate and butyrate by the human colonic microbiota.* Environmental microbiology, 2017. **19**(1): p. 29-41.
175. Macfarlane, G., G. Gibson, and J. Cummings, *Comparison of fermentation reactions in different regions of the human colon.* Journal of applied microbiology, 1992. **72**(1): p. 57-64.
176. Crouse, J.R., et al., *Role of acetate in the reduction of plasma free fatty acids produced by ethanol in man.* Journal of lipid research, 1968. **9**(4): p. 509-512.
177. Corrêa-Oliveira, R., et al., *Regulation of immune cell function by short-chain fatty acids.* Clinical & translational immunology, 2016. **5**(4): p. e73.
178. Pompei, A., et al., *Folate production by bifidobacteria as a potential probiotic property.* Applied and environmental microbiology, 2007. **73**(1): p. 179-185.
179. Pompei, A., et al., *Administration of folate-producing bifidobacteria enhances folate status in Wistar rats.* J Nutr, 2007. **137**(12): p. 2742-6.

180. Pan, Y., et al., *Associations between Folate and Vitamin B12 Levels and Inflammatory Bowel Disease: A Meta-Analysis.* Nutrients, 2017. **9**(4): p. 382.
181. Novakovic, P., et al., *Effects of folate deficiency on gene expression in the apoptosis and cancer pathways in colon cancer cells.* Carcinogenesis, 2006. **27**(5): p. 916-924.
182. Kamada, N., et al., *Regulated virulence controls the ability of a pathogen to compete with the gut microbiota.* Science, 2012. **336**(6086): p. 1325-1329.
183. Lawley, T.D., et al., *Antibiotic treatment of Clostridium difficile carrier mice triggers a supershedder state, spore-mediated transmission, and severe disease in immunocompromised hosts.* Infection and immunity, 2009. **77**(9): p. 3661-3669.
184. Rupnik, M., M.H. Wilcox, and D.N. Gerding, *Clostridium difficile infection: new developments in epidemiology and pathogenesis.* Nature Reviews Microbiology, 2009. **7**(7): p. 526-536.
185. Schreiber, F., J.M. Arasteh, and T.D. Lawley, *Pathogen Resistance Mediated by IL-22 Signaling at the Epithelial–Microbiota Interface.* Journal of Molecular Biology, 2015. **427**(23): p. 3676-3682.
186. Shaw, M.H., et al., *Microbiota-induced IL-1β, but not IL-6, is critical for the development of steady-state TH17 cells in the intestine.* Journal of Experimental Medicine, 2012. **209**(2): p. 251-258.
187. Satoh-Takayama, N., et al., *Microbial Flora Drives Interleukin 22 Production in Intestinal NKp46+ Cells that Provide Innate Mucosal Immune Defense.* Immunity, 2008. **29**(6): p. 958-970.
188. Park, J.-h., et al., *Promotion of intestinal epithelial cell turnover by commensal bacteria: role of short-chain fatty acids.* PloS one, 2016. **11**(5): p. e0156334.
189. Hamer, H.M., et al., *The role of butyrate on colonic function.* Alimentary pharmacology & therapeutics, 2008. **27**(2): p. 104-119.
190. Corfe, B.M., *Hypothesis: butyrate is not an HDAC inhibitor, but a product inhibitor of deacetylation.* Molecular bioSystems, 2012. **8**(6): p. 1609-1612.
191. Donohoe, D.R., et al., *The Warburg effect dictates the mechanism of butyrate-mediated histone acetylation and cell proliferation.* Mol Cell, 2012. **48**(4): p. 612-26.
192. Wang, H.-B., et al., *Butyrate enhances intestinal epithelial barrier function via up-regulation of tight junction protein Claudin-1 transcription.* Digestive diseases and sciences, 2012. **57**(12): p. 3126-3135.
193. Liu, B., et al., *Butyrate protects rat liver against total hepatic ischemia reperfusion injury with bowel congestion.* PloS one, 2014. **9**(8): p. e106184.
194. Swanson, P.A., et al., *Enteric commensal bacteria potentiate epithelial restitution via reactive oxygen species-mediated inactivation of focal adhesion kinase phosphatases.* Proceedings of the National Academy of Sciences, 2011. **108**(21): p. 8803-8808.
195. Petersson, J., et al., *Importance and regulation of the colonic mucus barrier in a mouse model of colitis.* American Journal of Physiology-Gastrointestinal and Liver Physiology, 2010. **300**(2): p. G327-G333.
196. Kamada, N., et al., *Role of the gut microbiota in immunity and inflammatory disease.* Nature Reviews Immunology, 2013. **13**(5): p. 321-335.
197. Wrzosek, L., et al., *Bacteroides thetaiotaomicron and Faecalibacterium prausnitziiinfluence the production of mucus glycans and the development of goblet cells in the colonic epithelium of a gnotobiotic model rodent.* BMC biology, 2013. **11**(1): p. 61.
198. Frantz, A., et al., *Targeted deletion of MyD88 in intestinal epithelial cells results in compromised antibacterial immunity associated with downregulation of polymeric immunoglobulin receptor, mucin-2, and antibacterial peptides.* Mucosal immunology, 2012. **5**(5): p. 501-512.
199. Brandl, K., et al., *MyD88-mediated signals induce the bactericidal lectin RegIIIγ and protect mice against intestinal Listeria monocytogenes infection.* Journal of Experimental Medicine, 2007. **204**(8): p. 1891-1900.
200. van Ampting, M.T., et al., *Intestinally secreted C-type lectin Reg3b attenuates salmonellosis but not listeriosis in mice.* Infection and immunity, 2012. **80**(3): p. 1115-1120.
201. Cario, E., G. Gerken, and D.K. Podolsky, *Toll-Like Receptor 2 Controls Mucosal Inflammation by Regulating Epithelial Barrier Function.* Gastroenterology, 2007. **132**(4): p. 1359-1374.
202. Jernberg, C., et al., *Long-term ecological impacts of antibiotic administration on the human intestinal microbiota.* The ISME journal, 2007. **1**(1): p. 56-66.

203. Schubert, A.M., H. Sinani, and P.D. Schloss, *Antibiotic-induced alterations of the murine gut microbiota and subsequent effects on colonization resistance against Clostridium difficile.* MBio, 2015. **6**(4): p. e00974-15.
204. Jakobsson, H.E., et al., *Decreased gut microbiota diversity, delayed Bacteroidetes colonisation and reduced Th1 responses in infants delivered by caesarean section.* Gut, 2014. **63**(4): p. 559-566.
205. Wang, Y., et al., *16S rRNA gene-based analysis of fecal microbiota from preterm infants with and without necrotizing enterocolitis.* The ISME journal, 2009. **3**(8): p. 944-954.
206. Harmsen, H.J., et al., *Analysis of intestinal flora development in breast-fed and formula-fed infants by using molecular identification and detection methods.* J Pediatr Gastroenterol Nutr, 2000. **30**(1): p. 61-7.
207. Bezirtzoglou, E., A. Tsiotsias, and G.W. Welling, *Microbiota profile in feces of breast-and formula-fed newborns by using fluorescence in situ hybridization (FISH).* Anaerobe, 2011. **17**(6): p. 478-482.
208. Roger, L.C., et al., *Examination of faecal Bifidobacterium populations in breast-and formula-fed infants during the first 18 months of life.* Microbiology, 2010. **156**(11): p. 3329-3341.
209. Guaraldi, F. and G. Salvatori, *Effect of breast and formula feeding on gut microbiota shaping in newborns.* Frontiers in cellular and infection microbiology, 2012. **2**.
210. Knights, D., et al., *Complex host genetics influence the microbiome in inflammatory bowel disease.* Genome medicine, 2014. **6**(12): p. 107.
211. Zhu, L., et al., *IL-10 and IL-10 Receptor Mutations in Very Early Onset Inflammatory Bowel Disease.* Gastroenterology Research, 2017. **10**(2): p. 65.
212. Steidler, L., et al., *Treatment of murine colitis by Lactococcus lactis secreting interleukin-10.* Science, 2000. **289**(5483): p. 1352-1355.
213. Abrahamsson, T., et al., *Low gut microbiota diversity in early infancy precedes asthma at school age.* Clinical & Experimental Allergy, 2014. **44**(6): p. 842-850.
214. Olszak, T., et al., *Microbial exposure during early life has persistent effects on natural killer T cell function.* Science, 2012. **336**(6080): p. 489-493.
215. Turnbaugh, P.J., et al., *An obesity-associated gut microbiome with increased capacity for energy harvest.* nature, 2006. **444**(7122): p. 1027-131.
216. Ley, R.E., et al., *Microbial ecology: human gut microbes associated with obesity.* Nature, 2006. **444**(7122): p. 1022-1023.
217. Turnbaugh, P.J., et al., *A core gut microbiome in obese and lean twins.* nature, 2009. **457**(7228): p. 480-484.
218. Imhann, F., et al., *Interplay of host genetics and gut microbiota underlying the onset and clinical presentation of inflammatory bowel disease.* Gut, 2016: p. gutjnl-2016-312135.
219. Kang, S., et al., *Dysbiosis of fecal microbiota in Crohn's disease patients as revealed by a custom phylogenetic microarray.* Inflamm Bowel Dis, 2010. **16**(12): p. 2034-42.
220. Willing, B.P., et al., *A Pyrosequencing Study in Twins Shows That Gastrointestinal Microbial Profiles Vary With Inflammatory Bowel Disease Phenotypes.* Gastroenterology, 2010. **139**(6): p. 1844-1854.e1.
221. Rajilic-Stojanovic, M., et al., *Phylogenetic analysis of dysbiosis in ulcerative colitis during remission.* Inflammatory bowel diseases, 2013. **19**(3): p. 481-488.
222. Pitcher, M., E. Beatty, and J. Cummings, *The contribution of sulphate reducing bacteria and 5-aminosalicylic acid to faecal sulphide in patients with ulcerative colitis.* Gut, 2000. **46**(1): p. 64-72.
223. Joossens, M., et al., *Dysbiosis of the faecal microbiota in patients with Crohn's disease and their unaffected relatives.* Gut, 2011: p. gut. 2010.223263.
224. Frank, D.N., et al., *Molecular-phylogenetic characterization of microbial community imbalances in human inflammatory bowel diseases.* Proceedings of the National Academy of Sciences, 2007. **104**(34): p. 13780-13785.
225. Winter, S.E., C.A. Lopez, and A.J. Bäumler, *The dynamics of gut-associated microbial communities during inflammation.* EMBO reports, 2013. **14**(4): p. 319-327.
226. Garrett, W.S., et al., *Communicable Ulcerative Colitis Induced by T-bet Deficiency in the Innate Immune System.* Cell, 2007. **131**(1): p. 33-45.
227. Darfeuille-Michaud, A., et al., *High prevalence of adherent-invasive Escherichia coli associated with ileal mucosa in Crohn's disease.* Gastroenterology, 2004. **127**(2): p. 412-421.

228. Ni, J., et al., *Gut microbiota and IBD: causation or correlation?* Nature Reviews Gastroenterology & Hepatology, 2017.
229. Dowle, C., *Faecal microbiota transplantation: a review of FMT as an alternative treatment for Clostridium difficile infection.* Bioscience Horizons: The International Journal of Student Research, 2016. **9**: p. hzw007.
230. *Faecal microbiota transplant for recurrent Clostridium difficile infection | Guidance and guidelines | NICE.* 2017.
231. Colman, R.J. and D.T. Rubin, *Fecal microbiota transplantation as therapy for inflammatory bowel disease: A systematic review and meta-analysis.* Journal of Crohn's and Colitis, 2014. **8**(12): p. 1569-1581.
232. Hotel, A.C.P. and A. Cordoba, *Health and nutritional properties of probiotics in food including powder milk with live lactic acid bacteria.* Prevention, 2001. **5**(1).
233. Gosselink, M.P., et al., *Delay of the first onset of pouchitis by oral intake of the probiotic strain Lactobacillus rhamnosus GG.* Diseases of the colon & rectum, 2004. **47**(6): p. 876-884.
234. Tao, Y., et al., *Soluble factors from Lactobacillus GG activate MAPKs and induce cytoprotective heat shock proteins in intestinal epithelial cells.* American Journal of Physiology-Cell Physiology, 2006. **290**(4): p. C1018-C1030.
235. Balmus, I.M., et al., *The implications of oxidative stress and antioxidant therapies in Inflammatory Bowel Disease: Clinical aspects and animal models.* Saudi journal of gastroenterology: official journal of the Saudi Gastroenterology Association, 2016. **22**(1): p. 3.
236. Leahy, S., et al., *Getting better with bifidobacteria.* Journal of Applied Microbiology, 2005. **98**(6): p. 1303-1315.
237. Nuriel-Ohayon, M., H. Neuman, and O. Koren, *Microbial changes during pregnancy, birth, and infancy.* Frontiers in microbiology, 2016. **7**.
238. Duranti, S., et al., *Maternal inheritance of bifidobacterial communities and bifidophages in infants through vertical transmission.* Microbiome, 2017. **5**(1): p. 66.
239. Odamaki, T., et al., *Age-related changes in gut microbiota composition from newborn to centenarian: a cross-sectional study.* BMC microbiology, 2016. **16**(1): p. 90.
240. Gavini, F., et al., *Differences in the distribution of bifidobacterial and enterobacterial species in human faecal microflora of three different (children, adults, elderly) age groups.* Microbial Ecology in Health and Disease, 2001. **13**(1): p. 40-45.
241. Biagi, E., et al., *Ageing of the human metaorganism: the microbial counterpart.* Age, 2012. **34**(1): p. 247-267.
242. Hopkins, M., R. Sharp, and G. Macfarlane, *Age and disease related changes in intestinal bacterial populations assessed by cell culture, 16S rRNA abundance, and community cellular fatty acid profiles.* Gut, 2001. **48**(2): p. 198-205.
243. Woodmansey, E.J., et al., *Comparison of compositions and metabolic activities of fecal microbiotas in young adults and in antibiotic-treated and non-antibiotic-treated elderly subjects.* Applied and environmental microbiology, 2004. **70**(10): p. 6113-6122.
244. Wang, F., et al., *Qualitative and semiquantitative analysis of fecal Bifidobacterium species in centenarians living in Bama, Guangxi, China.* Current microbiology, 2015. **71**(1): p. 143-149.
245. van Tongeren, S.P., et al., *Fecal microbiota composition and frailty.* Applied and environmental microbiology, 2005. **71**(10): p. 6438-6442.
246. O'Neill, I., Z. Schofield, and L.J. Hall, *Exploring the role of the microbiota member Bifidobacterium in modulating immune-linked diseases.* Emerging Topics in Life Sciences, 2017. **1**(4): p. 333-349.
247. Scardovi, V., *Genus bifidobacterium.* Bergey's manual of systemic bacteriology, 1986. **2**: p. 1418-1434.
248. Schell, M.A., et al., *The genome sequence of Bifidobacterium longum reflects its adaptation to the human gastrointestinal tract.* Proceedings of the National Academy of Sciences, 2002. **99**(22): p. 14422-14427.
249. Lugli, G.A., et al., *Comparative genomic and phylogenomic analyses of the Bifidobacteriaceae family.* BMC Genomics, 2017. **18**(1): p. 568.
250. Corby-Harris, V., P. Maes, and K.E. Anderson, *The bacterial communities associated with honey bee (Apis mellifera) foragers.* PloS one, 2014. **9**(4): p. e95056.

251. Vaughan, E.E., et al., *Diversity, vitality and activities of intestinal lactic acid bacteria and bifidobacteria assessed by molecular approaches.* FEMS Microbiology Reviews, 2005. **29**(3): p. 477-490.
252. O'Callaghan, A. and D. van Sinderen, *Bifidobacteria and their role as members of the human gut microbiota.* Frontiers in microbiology, 2016. **7**.
253. El Kaoutari, A., et al., *The abundance and variety of carbohydrate-active enzymes in the human gut microbiota.* Nature reviews Microbiology, 2013. **11**(7): p. 497-504.
254. Korakli, M., M. Gänzle, and R. Vogel, *Metabolism by bifidobacteria and lactic acid bacteria of polysaccharides from wheat and rye, and exopolysaccharides produced by Lactobacillus sanfranciscensis.* Journal of applied microbiology, 2002. **92**(5): p. 958-965.
255. Breton, C., et al., *Structures and mechanisms of glycosyltransferases.* Glycobiology, 2006. **16**(2): p. 29R-37R.
256. Guarner, F. and J.-R. Malagelada, *Gut flora in health and disease.* The Lancet, 2003. **361**(9356): p. 512-519.
257. Milani, C., et al., *Genomic encyclopedia of type strains of the genus Bifidobacterium.* Applied and environmental microbiology, 2014. **80**(20): p. 6290-6302.
258. Milani, C., et al., *Bifidobacteria exhibit social behavior through carbohydrate resource sharing in the gut.* Scientific reports, 2015. **5**: p. 15782.
259. Duranti, S., et al., *Insights from genomes of representatives of the human gut commensal Bifidobacterium bifidum.* Environmental microbiology, 2015. **17**(7): p. 2515-2531.
260. Egan, M., et al., *Cross-feeding by Bifidobacterium breve UCC2003 during co-cultivation with Bifidobacterium bifidum PRL2010 in a mucin-based medium.* BMC Microbiology, 2014. **14**: p. 282.
261. Ferrario, C., et al., *How to feed the mammalian gut microbiota: bacterial and metabolic modulation by dietary fibers.* Frontiers in Microbiology, 2017. **8**: p. 1749.
262. Fukuda, S., et al., *Bifidobacteria can protect from enteropathogenic infection through production of acetate.* Nature, 2011. **469**(7331): p. 543-547.
263. Falony, G., et al., *In vitro kinetics of prebiotic inulin-type fructan fermentation by butyrate-producing colon bacteria: implementation of online gas chromatography for quantitative analysis of carbon dioxide and hydrogen gas production.* Applied and environmental microbiology, 2009. **75**(18): p. 5884-5892.
264. Bergman, E., *Energy contributions of volatile fatty acids from the gastrointestinal tract in various species.* Physiological reviews, 1990. **70**(2): p. 567-590.
265. Kane, P. and E. Kane, *Methods and compositions for treating symptomes of diseases related to imbalance of essential fatty acids*. 2006, Google Patents.
266. Segain, J.P., et al., *Butyrate inhibits inflammatory responses through NFkappaB inhibition: implications for Crohn's disease.* Gut, 2000. **47**(3): p. 397-403.
267. Furusawa, Y., et al., *Commensal microbe-derived butyrate induces the differentiation of colonic regulatory T cells.* Nature, 2013. **504**(7480): p. 446-450.
268. Hylemon, P.B., et al., *Bile acids as regulatory molecules.* Journal of lipid research, 2009. **50**(8): p. 1509-1520.
269. De Boever, P., et al., *Protective effect of the bile salt hydrolase-active Lactobacillus reuteri against bile salt cytotoxicity.* Applied microbiology and biotechnology, 2000. **53**(6): p. 709-714.
270. Bernstein, H., et al., *Activation of the promoters of genes associated with DNA damage, oxidative stress, ER stress and protein malfolding by the bile salt, deoxycholate.* Toxicology letters, 1999. **108**(1): p. 37-46.
271. Piddock, L.J., *Multidrug-resistance efflux pumps? not just for resistance.* Nature Reviews Microbiology, 2006. **4**(8): p. 629-636.
272. Price, C.E., et al., *The Bifidobacterium longum NCIMB 702259T ctr gene codes for a novel cholate transporter.* Applied and environmental microbiology, 2006. **72**(1): p. 923-926.
273. Gueimonde, M., et al., *Bile-inducible efflux transporter from Bifidobacterium longum NCC2705, conferring bile resistance.* Applied and environmental microbiology, 2009. **75**(10): p. 3153-3160.
274. Ruiz, L., et al., *A bile-inducible membrane protein mediates bifidobacterial bile resistance.* Microbial biotechnology, 2012. **5**(4): p. 523-535.
275. Jarocki, P., et al., *A new insight into the physiological role of bile salt hydrolase among intestinal bacteria from the genus Bifidobacterium.* PloS one, 2014. **9**(12): p. e114379.

276. Begley, M., C. Hill, and C.G. Gahan, *Bile salt hydrolase activity in probiotics.* Applied and environmental microbiology, 2006. **72**(3): p. 1729-1738.
277. Grimm, V., C. Westermann, and C.U. Riedel, *Bifidobacteria-host interactions—an update on colonisation factors.* BioMed research international, 2014. **2014**.
278. Guglielmetti, S., et al., *Study of the adhesion of Bifidobacterium bifidum MIMBb75 to human intestinal cell lines.* Current microbiology, 2009. **59**(2): p. 167-172.
279. Motherway, M.O.C., et al., *Functional genome analysis of Bifidobacterium breve UCC2003 reveals type IVb tight adherence (Tad) pili as an essential and conserved host-colonization factor.* Proceedings of the National Academy of Sciences, 2011. **108**(27): p. 11217-11222.
280. Fanning, S., et al., *Bifidobacterial surface-exopolysaccharide facilitates commensal-host interaction through immune modulation and pathogen protection.* Proceedings of the National Academy of Sciences, 2012. **109**(6): p. 2108-2113.
281. Hsieh, C., et al., *Strengthening of the intestinal epithelial tight junction by Bifidobacterium bifidum. Physiol Rep 3: e12327*. 2015.
282. Ewaschuk, J.B., et al., *Secreted bioactive factors from Bifidobacterium infantis enhance epithelial cell barrier function.* American Journal of Physiology-Gastrointestinal and Liver Physiology, 2008. **295**(5): p. G1025-G1034.
283. Bergmann, K.R., et al., *Bifidobacteria Stabilize Claudins at Tight Junctions and Prevent Intestinal Barrier Dysfunction in Mouse Necrotizing Enterocolitis.* The American Journal of Pathology, 2013. **182**(5): p. 1595-1606.
284. Mylonaki, M., et al., *Molecular characterization of rectal mucosa-associated bacterial flora in inflammatory bowel disease.* Inflammatory bowel diseases, 2005. **11**(5): p. 481-487.
285. Macfarlane, S., et al., *Mucosal bacteria in ulcerative colitis.* British Journal of Nutrition, 2005. **93**(S1): p. S67-S72.
286. Steed, H., et al., *Clinical trial: the microbiological and immunological effects of synbiotic consumption–a randomized double-blind placebo-controlled study in active Crohn's disease.* Alimentary pharmacology & therapeutics, 2010. **32**(7): p. 872-883.
287. Tamaki, H., et al., *Efficacy of probiotic treatment with Bifidobacterium longum 536 for induction of remission in active ulcerative colitis: A randomized, double-blinded, placebo-controlled multicenter trial.* Dig Endosc, 2016. **28**(1): p. 67-74.
288. Hall, L.J., et al., *Natural killer cells protect mice from DSS-induced colitis by regulating neutrophil function via the NKG2A receptor.* Mucosal Immunology, 2013. **6**(5): p. 1016-1026.
289. Hall, et al., *A mouse model of pathological small intestinal epithelial cell apoptosis and shedding induced by systemic administration of lipopolysaccharide.* 2013.
290. *SHIP-Deficient Mice Develop Spontaneous Intestinal Inflammation and Arginase-Dependent Fibrosis - ScienceDirect.* 2017.
291. Rio, D.C., et al., *Purification of RNA using TRIzol (TRI reagent).* Cold Spring Harb Protoc, 2010. **2010**(6): p. pdb.prot5439.
292. Andrews, S., *FastQC: a quality control tool for high throughput sequence data*. 2010.
293. Gordon, A. and G. Hannon, *Fastx-toolkit. FASTQ/A short-reads pre-processing tools.* Unpublished Available online at: http://hannonlab. cshl. edu/fastx_toolkit, 2010.
294. Pachter, C.T., et al., *Differential gene and transcript expression analysis of RNA-seq experiments with TopHat and Cufflinks.* Nature Protocols, 2012. **7**: p. 562-578.
295. Anders, M.I.L., H. Wolfgang, and Simon, *Moderated estimation of fold change and dispersion for RNA-seq data with DESeq2.* Genome Biology, 2014. **15**(12): p. 550.
296. Breuer, K., et al., *InnateDB: systems biology of innate immunity and beyond—recent updates and continuing curation*, in *Nucleic Acids Res*. 2013. p. D1228-33.
297. Shannon, P., et al., *Cytoscape: a software environment for integrated models of biomolecular interaction networks.* Genome Res, 2003. **13**(11): p. 2498-504.
298. Langmead, B. and S.L. Salzberg, *Fast gapped-read alignment with Bowtie 2.* Nature methods, 2012. **9**(4): p. 357-359.
299. Anders, S., P.T. Pyl, and W. Huber, *HTSeq—a Python framework to work with high-throughput sequencing data.* Bioinformatics, 2015. **31**(2): p. 166-169.
300. Silva, G.G.Z., et al., *SUPER-FOCUS: a tool for agile functional analysis of shotgun metagenomic data.* Bioinformatics, 2015. **32**(3): p. 354-361.
301. Aziz, R.K., et al., *SEED servers: high-performance access to the SEED genomes, annotations, and metabolic models.* PloS one, 2012. **7**(10): p. e48053.

302. Quast, C., et al., *The SILVA ribosomal RNA gene database project: improved data processing and web-based tools.* Nucleic Acids Research, 2017. **41**(D1).
303. Huson, D.H., et al., *Integrative analysis of environmental sequences using MEGAN4.* Genome Res, 2011. **21**(9): p. 1552-60.
304. Kozomara, A., et al., *miRBase: integrating microRNA annotation and deep-sequencing data.* Nucleic Acids Research, 2017. **39**(suppl_1).
305. Rescigno, M., et al., *Dendritic cells express tight junction proteins and penetrate gut epithelial monolayers to sample bacteria.* Nat Immunol, 2001. **2**(4): p. 361-7.
306. Artis, D., *Epithelial-cell recognition of commensal bacteria and maintenance of immune homeostasis in the gut.* Nat Rev Immunol, 2008. **8**(6): p. 411-20.
307. Duckworth, C.A. and A.J. Watson, *Analysis of epithelial cell shedding and gaps in the intestinal epithelium.* Permeability Barrier: Methods and Protocols, 2011: p. 105-114.
308. Coste, B., et al., *Piezo1 and Piezo2 are essential components of distinct mechanically activated cation channels.* Science, 2010. **330**(6000): p. 55-60.
309. Bagriantsev, S.N., E.O. Gracheva, and P.G. Gallagher, *Piezo proteins: regulators of mechanosensation and other cellular processes.* Journal of biological Chemistry, 2014. **289**(46): p. 31673-31681.
310. Gottlieb, P.A. and F. Sachs, *Piezo1: properties of a cation selective mechanical channel.* Channels (Austin), 2012. **6**(4): p. 214-9.
311. Syeda, R., et al., *Piezo1 Channels Are Inherently Mechanosensitive.* Cell Reports, 2016. **17**(7): p. 1739-1746.
312. Raymond, K.N. and V.C. Pierre, *Next generation, high relaxivity gadolinium MRI agents.* Bioconjugate chemistry, 2005. **16**(1): p. 3-8.
313. Adding, L.C., G.L. Bannenberg, and L.E. Gustafsson, *Basic experimental studies and clinical aspects of gadolinium salts and chelates.* Cardiovascular Therapeutics, 2001. **19**(1): p. 41-56.
314. Andrade, D. and J. Rosenblatt, *Apoptotic regulation of epithelial cellular extrusion.* Apoptosis, 2011. **16**(5): p. 491-501.
315. Gudipaty, S., et al., *Mechanical stretch triggers rapid epithelial cell division through Piezo1.* Nature, 2017. **543**(7643): p. 118-121.
316. Spencer, A., S. Wilson, and E. Harpur, *Gadolinium chloride toxicity in the mouse*. Hum Exp Toxicol, 1998. **17**(11): p. 633-7.
317. Williams, J.M., et al., *A mouse model of pathological small intestinal epithelial cell apoptosis and shedding induced by systemic administration of lipopolysaccharide.* Disease models & mechanisms, 2013. **6**(6): p. 1388-1399.
318. Reikvam, D.H., et al., *Depletion of murine intestinal microbiota: effects on gut mucosa and epithelial gene expression.* PloS one, 2011. **6**(3): p. e17996.
319. Zhan, Y., et al., *Gut microbiota protects against gastrointestinal tumorigenesis caused by epithelial injury.* Cancer research, 2013. **73**(24): p. 7199-7210.
320. Cherbuy, C., et al., *Microbiota matures colonic epithelium through a coordinated induction of cell cycle-related proteins in gnotobiotic rat.* American Journal of Physiology-Gastrointestinal and Liver Physiology, 2010. **299**(2): p. G348-G357.
321. Macfarlane, S., et al., *Chemotaxonomic analysis of bacterial populations colonizing the rectal mucosa in patients with ulcerative colitis.* Clinical Infectious Diseases, 2004. **38**(12): p. 1690-1699.
322. Fujimori, S., et al., *A randomized controlled trial on the efficacy of synbiotic versus probiotic or prebiotic treatment to improve the quality of life in patients with ulcerative colitis.* Nutrition, 2009. **25**(5): p. 520-5.
323. Furrie, E., et al., *Toll-like receptors-2,-3 and-4 expression patterns on human colon and their regulation by mucosal-associated bacteria.* Immunology, 2005. **115**(4): p. 565-574.
324. Bretaud, S., S. Lee, and S. Guo, *Sensitivity of zebrafish to environmental toxins implicated in Parkinson's disease.* Neurotoxicology and teratology, 2004. **26**(6): p. 857-864.
325. Seno, H., et al., *Efficient colonic mucosal wound repair requires Trem2 signaling.* Proceedings of the National Academy of Sciences, 2009. **106**(1): p. 256-261.
326. Gayer, C.P. and M.D. Basson, *The effects of mechanical forces on intestinal physiology and pathology.* Cell Signal, 2009. **21**(8): p. 1237-44.
327. Evans, N.D., et al., *Epithelial mechanobiology, skin wound healing, and the stem cell niche.* Journal of the mechanical behavior of biomedical materials, 2013. **28**: p. 397-409.

328. Richardson, R., et al., *Adult Zebrafish as a Model System for Cutaneous Wound-Healing Research.* Journal of Investigative Dermatology, 2013. **133**(6): p. 1655-1665.
329. Li, Q. and J. Uitto, *Zebrafish as a Model System to Study Skin Biology and Pathology.* Journal of Investigative Dermatology, 2014. **134**(6): p. 1-6.
330. Ren, H.J., et al., *Normal mouse intestinal epithelial cells as a model for the in vitro invasion of Trichinella spiralis infective larvae.* PLoS One, 2011. **6**(10): p. e27010.
331. Dukes, J.D., P. Whitley, and A.D. Chalmers, *The MDCK variety pack: choosing the right strain.* BMC Cell Biology, 2011. **12**(1): p. 43.
332. Bowman, C.L., et al., *Mechanosensitive Ion Channels and the Peptide Inhibitor GsMTx-4: History, Properties, Mechanisms and Pharmacology.* Toxicon : official journal of the International Society on Toxinology, 2007. **49**(2): p. 249-270.
333. Bae, C., F. Sachs, and P.A. Gottlieb, *The mechanosensitive ion channel Piezo1 is inhibited by the peptide GsMTx4.* Biochemistry, 2011. **50**(29): p. 6295-300.
334. Ranade, S.S., et al., *Piezo1, a mechanically activated ion channel, is required for vascular development in mice.* Proceedings of the National Academy of Sciences, 2014. **111**(28): p. 10347-10352.
335. Kamba, M., et al., *Comparison of the mechanical destructive force in the small intestine of dog and human.* International journal of pharmaceutics, 2002. **237**(1): p. 139-149.
336. Suki, B., et al., *Biomechanics of the lung parenchyma: critical roles of collagen and mechanical forces.* Journal of applied physiology, 2005. **98**(5): p. 1892-1899.
337. Pathak, M.M., et al., *Stretch-activated ion channel Piezo1 directs lineage choice in human neural stem cells.* Proceedings of the National Academy of Sciences, 2014. **111**(45): p. 16148-16153.
338. Li, J., et al., *Piezo1 integration of vascular architecture with physiological force.* Nature, 2014. **515**(7526): p. 279-282.
339. Martins, J.R., et al., *Piezo1-dependent regulation of urinary osmolarity.* Pflügers Archiv-European Journal of Physiology, 2016. **468**(7): p. 1197-1206.
340. Faucherre, A., et al., *Piezo1 plays a role in erythrocyte volume homeostasis.* Haematologica, 2013: p. haematol. 2013.086090.
341. Lewis, A.H., et al., *Transduction of Repetitive Mechanical Stimuli by Piezo1 and Piezo2 Ion Channels.* Cell Reports. **19**(12): p. 2572-2585.
342. Wang, Y., et al., *A novel role for villin in intestinal epithelial cell survival and homeostasis.* Journal of Biological Chemistry, 2008. **283**(14): p. 9454-9464.
343. Gayer, C.P. and M.D. Basson, *The effects of mechanical forces on intestinal physiology and pathology.* Cellular signalling, 2009. **21**(8): p. 1237-1244.
344. Kelly, Caleb J., et al., *Crosstalk between Microbiota-Derived Short-Chain Fatty Acids and Intestinal Epithelial HIF Augments Tissue Barrier Function.* Cell Host & Microbe, 2015. **17**(5): p. 662-671.
345. Sommer, F. and F. Backhed, *The gut microbiota engages different signaling pathways to induce Duox2 expression in the ileum and colon epithelium.* Mucosal Immunol, 2015. **8**(2): p. 372-379.
346. Armbruster, N.S., E.F. Stange, and J. Wehkamp, *In the Wnt of Paneth Cells: Immune-Epithelial Crosstalk in Small Intestinal Crohn's Disease.* Frontiers in Immunology, 2017. **8**(1204).
347. Stava, E., et al., *Mechanical actuation of ion channels using a piezoelectric planar patch clamp system.* Lab Chip, 2012. **12**(1): p. 80-7.
348. Hardonk, M., et al., *Heterogeneity of rat liver and spleen macrophages in gadolinium chloride-induced elimination and repopulation.* Journal of Leukocyte Biology, 1992. **52**(3): p. 296-302.
349. Jankov, R.P., et al., *Gadolinium Chloride Inhibits Pulmonary Macrophage Influx and Prevents O2-Induced Pulmonary Hypertension in the Neonatal Rat.* Pediatric Research, 2001. **50**: p. 172.
350. Yoneda, S., et al., *Effects of gadolinium chloride on the rat lung following intratracheal instillation.* Toxicological Sciences, 1995. **28**(1): p. 65-70.
351. Caserta, J.A., et al., *Development and application of a mouse intestinal loop model to study the in vivo action of Clostridium perfringens enterotoxin.* Infect Immun, 2011. **79**(8): p. 3020-7.
352. Matsumura, T., et al., *Botulinum toxin A complex exploits intestinal M cells to enter the host and exert neurotoxicity.* Nature Communications, 2015. **6**: p. 6255.

353. Pastorelli, L., et al., *Central Role of the Gut Epithelial Barrier in the Pathogenesis of Chronic Intestinal Inflammation: Lessons Learned from Animal Models and Human Genetics.* Frontiers in Immunology, 2013. **4**: p. 280.
354. Kell, D.B. and E. Pretorius, *On the translocation of bacteria and their lipopolysaccharides between blood and peripheral locations in chronic, inflammatory diseases: the central roles of LPS and LPS-induced cell death.* Integrative Biology, 2015. **7**(11): p. 1339-1377.
355. Macfarlane, S., et al., *Chemotaxonomic analysis of bacterial populations colonizing the rectal mucosa in patients with ulcerative colitis.* Clin Infect Dis, 2004. **38**(12): p. 1690-9.
356. Jones, S.E., et al., *Protection from intestinal inflammation by bacterial exopolysaccharides.* J Immunol, 2014. **192**(10): p. 4813-20.
357. Ruiz, L., et al., *Transposon mutagenesis in Bifidobacterium breve: construction and characterization of a Tn5 transposon mutant library for Bifidobacterium breve UCC2003.* PLoS One, 2013. **8**(5): p. e64699.
358. Fanning, S., L.J. Hall, and D. van Sinderen, *Bifidobacterium breve UCC2003 surface exopolysaccharide production is a beneficial trait mediating commensal-host interaction through immune modulation and pathogen protection.* Gut microbes, 2012. **3**(5): p. 420-5.
359. Hoarau, C., et al., *Supernatant of Bifidobacterium breve induces dendritic cell maturation, activation, and survival through a Toll-like receptor 2 pathway.* Journal of Allergy and Clinical Immunology, 2006. **117**(3): p. 696-702.
360. Patole, S.K., et al., *Benefits of Bifidobacterium breve M-16V supplementation in preterm neonates-a retrospective cohort study.* PloS one, 2016. **11**(3): p. e0150775.
361. Ishikawa, H., et al., *Randomized controlled trial of the effect of bifidobacteria-fermented milk on ulcerative colitis.* Journal of the American College of Nutrition, 2003. **22**(1): p. 56-63.
362. Han, Y., et al., *Advanced applications of RNA sequencing and challenges.* Bioinformatics and biology insights, 2015. **9**(Suppl 1): p. 29.
363. Wang, Z., M. Gerstein, and M. Snyder, *RNA-Seq: a revolutionary tool for transcriptomics.* Nature reviews genetics, 2009. **10**(1): p. 57-63.
364. Hangauer, M.J., I.W. Vaughn, and M.T. McManus, *Pervasive transcription of the human genome produces thousands of previously unidentified long intergenic noncoding RNAs.* PLoS genetics, 2013. **9**(6): p. e1003569.
365. Yang, L., et al., *Genomewide characterization of non-polyadenylated RNAs.* Genome biology, 2011. **12**(2): p. R16.
366. Ericsson, A.C. and C.L. Franklin, *Manipulating the gut microbiota: methods and challenges.* ILAR journal, 2015. **56**(2): p. 205-217.
367. Yi, P. and L. Li, *The germfree murine animal: an important animal model for research on the relationship between gut microbiota and the host.* Vet Microbiol, 2012. **157**(1-2): p. 1-7.
368. Wikoff, W.R., et al., *Metabolomics analysis reveals large effects of gut microflora on mammalian blood metabolites.* Proceedings of the national academy of sciences, 2009. **106**(10): p. 3698-3703.
369. Gaboriau-Routhiau, V., et al., *The key role of segmented filamentous bacteria in the coordinated maturation of gut helper T cell responses.* Immunity, 2009. **31**(4): p. 677-689.
370. Atarashi, K., et al., *Induction of colonic regulatory T cells by indigenous Clostridium species.* Science, 2011. **331**(6015): p. 337-341.
371. Chowdhury, S.R., et al., *Transcriptome profiling of the small intestinal epithelium in germfree versus conventional piglets.* BMC genomics, 2007. **8**(1): p. 215.
372. Hooper, L.V., et al., *Molecular analysis of commensal host-microbial relationships in the intestine.* Science, 2001. **291**(5505): p. 881-884.
373. Fritz, J.V., et al., *From meta-omics to causality: experimental models for human microbiome research.* Microbiome, 2013. **1**(1): p. 14.
374. Love, M.I., S. Anders, and W. Huber, *Moderated estimation of fold change and dispersion for RNA-seq data with DESeq2.* Genome biology, 2014. **15**(12): p. 550.
375. Peach, R.J., et al., *Both extracellular immunoglobin-like domains of CD80 contain residues critical for binding T cell surface receptors CTLA-4 and CD28.* Journal of Biological Chemistry, 1995. **270**(36): p. 21181-21187.
376. Zhang, B., et al., *Prevention and cure of rotavirus infection via TLR5/NLRC4–mediated production of IL-22 and IL-18.* Science, 2014. **346**(6211): p. 861-865.

377. Cario, E. and D.K. Podolsky, *Differential alteration in intestinal epithelial cell expression of toll-like receptor 3 (TLR3) and TLR4 in inflammatory bowel disease.* Infection and immunity, 2000. **68**(12): p. 7010-7017.
378. Pappu, R., V. Ramirez-Carrozzi, and A. Sambandam, *The interleukin-17 cytokine family: critical players in host defence and inflammatory diseases.* Immunology, 2011. **134**(1): p. 8-16.
379. Khatri, P., M. Sirota, and A.J. Butte, *Ten years of pathway analysis: current approaches and outstanding challenges.* PLoS computational biology, 2012. **8**(2): p. e1002375.
380. Critchley, D., *Cytoskeletal proteins talin and vinculin in integrin-mediated adhesion*. 2004, Portland Press Limited.
381. Zhang, H.M., et al., *Induced focal adhesion kinase expression suppresses apoptosis by activating NF-κB signaling in intestinal epithelial cells.* American Journal of Physiology-Cell Physiology, 2006. **290**(5): p. C1310-C1320.
382. Bouchard, V., et al., *Fak/Src signaling in human intestinal epithelial cell survival and anoikis: Differentiation state-specific uncoupling with the PI3-K/Akt-1 and MEK/Erk pathways.* Journal of cellular physiology, 2007. **212**(3): p. 717-728.
383. Dufour, G., et al., *Human intestinal epithelial cell survival and anoikis differentiation state-distinct regulation and roles of protein kinase B/Akt isoforms.* Journal of Biological Chemistry, 2004. **279**(42): p. 44113-44122.
384. Bloch, D.B., et al., *Sp110 localizes to the PML-Sp100 nuclear body and may function as a nuclear hormone receptor transcriptional coactivator.* Molecular and cellular biology, 2000. **20**(16): p. 6138-6146.
385. Tamura, M., et al., *Members of a novel gene family, Gsdm, are expressed exclusively in the epithelium of the skin and gastrointestinal tract in a highly tissue-specific manner.* Genomics, 2007. **89**(5): p. 618-629.
386. Miguchi, M., et al., *Gasdermin C is upregulated by inactivation of transforming growth factor β receptor type II in the presence of mutated apc, promoting colorectal cancer proliferation.* PloS one, 2016. **11**(11): p. e0166422.
387. Lehotzky, R.E., et al., *Molecular basis for peptidoglycan recognition by a bactericidal lectin.* Proceedings of the National Academy of Sciences, 2010. **107**(17): p. 7722-7727.
388. Kawaji, H. and Y. Hayashizaki, *Exploration of small RNAs.* PLoS genetics, 2008. **4**(1): p. e22.
389. Yang, Y., et al., *Overexpression of miR-21 in patients with ulcerative colitis impairs intestinal epithelial barrier function through targeting the Rho GTPase RhoB.* Biochemical and Biophysical Research Communications, 2013. **434**(4): p. 746-752.
390. Wang, Q., Z. Sun, and H. Yang, *Downregulation of tumor suppressor Pdcd4 promotes invasion and activates both β-catenin/Tcf and AP-1-dependent transcription in colon carcinoma cells.* Oncogene, 2008. **27**(11): p. 1527-1535.
391. Xia, X., et al., *Prognostic role of microRNA-21 in colorectal cancer: a meta-analysis.* PloS one, 2013. **8**(11): p. e80426.
392. Turroni, F., et al., *Glycan Utilization and Cross-Feeding Activities by Bifidobacteria.* Trends in Microbiology, 2017.
393. MURATA, K., et al., *Bifidobacterium breve MCC-117 induces tolerance in porcine intestinal epithelial cells: study of the mechanisms involved in the immunoregulatory effect.* Bioscience of microbiota, food and health, 2014. **33**(1): p. 1-10.
394. Hughes, E.R., et al., *Microbial Respiration and Formate Oxidation as Metabolic Signatures of Inflammation-Associated Dysbiosis.* Cell Host & Microbe, 2017. **21**(2): p. 208-219.
395. Tailford, L.E., et al., *Mucin glycan foraging in the human gut microbiome.* Frontiers in Genetics, 2015. **6**(81).
396. Cronin, M., et al., *High resolution in vivo bioluminescent imaging for the study of bacterial tumour targeting.* PloS one, 2012. **7**(1): p. e30940.
397. James, K., et al., *Bifidobacterium breve UCC2003 metabolises the human milk oligosaccharides lacto-N-tetraose and lacto-N-neo-tetraose through overlapping, yet distinct pathways.* Scientific reports, 2016. **6**: p. 38560.
398. Fuhrer, A., et al., *Milk sialyllactose influences colitis in mice through selective intestinal bacterial colonization.* The Journal of Experimental Medicine, 2010. **207**(13): p. 2843-2854.
399. Kollmann, T.R., et al., *Innate immune function by Toll-like receptors: distinct responses in newborns and the elderly.* Immunity, 2012. **37**(5): p. 771-783.

400. Loonen, L.M., et al., *REG3γ-deficient mice have altered mucus distribution and increased mucosal inflammatory responses to the microbiota and enteric pathogens in the ileum.* Mucosal immunology, 2014. **7**(4): p. 939-947.
401. Natividad, J.M., et al., *Differential induction of antimicrobial REGIII by the intestinal microbiota and Bifidobacterium breve NCC2950.* Applied and environmental microbiology, 2013. **79**(24): p. 7745-7754.
402. Bevins, C.L. and N.H. Salzman, *Paneth cells, antimicrobial peptides and maintenance of intestinal homeostasis.* Nature Reviews Microbiology, 2011. **9**: p. 356.
403. Kamdar, K., V. Nguyen, and R.W. DePaolo, *Toll-like receptor signaling and regulation of intestinal immunity.* Virulence, 2013. **4**(3): p. 207-212.
404. Pott, J., et al., *Age-dependent TLR3 expression of the intestinal epithelium contributes to rotavirus susceptibility.* PLoS Pathog, 2012. **8**(5): p. e1002670.
405. Song, X., et al., *IL-17RE is the functional receptor for IL-17C and mediates mucosal immunity to infection with intestinal pathogens.* Nature immunology, 2011. **12**(12): p. 1151-1158.
406. Chen, Y., et al., *Stimulation of airway mucin gene expression by interleukin (IL)-17 through IL-6 paracrine/autocrine loop.* Journal of Biological Chemistry, 2003. **278**(19): p. 17036-17043.
407. Macho-Fernandez, E., et al., *Lymphotoxin beta receptor signaling limits mucosal damage through driving IL-23 production by epithelial cells.* Mucosal immunology, 2015. **8**(2): p. 403-413.
408. Campbell, I.D. and M.J. Humphries, *Integrin structure, activation, and interactions.* Cold Spring Harbor perspectives in biology, 2011. **3**(3): p. a004994.
409. Yu, Y., et al., *Alphavbeta6 is required in maintaining the intestinal epithelial barrier function.* Cell biology international, 2014. **38**(6): p. 777-781.
410. de Lange, K.M., et al., *Genome-wide association study implicates immune activation of multiple integrin genes in inflammatory bowel disease.* Nature genetics, 2017. **49**(2): p. 256-261.
411. Aplin, A., et al., *Signal transduction and signal modulation by cell adhesion receptors: the role of integrins, cadherins, immunoglobulin-cell adhesion molecules, and selectins.* Pharmacological reviews, 1998. **50**(2): p. 197-264.
412. Watt, F.M., *Epidermal stem cells: markers, patterning and the control of stem cell fate.* Philosophical Transactions of the Royal Society of London B: Biological Sciences, 1998. **353**(1370): p. 831-837.
413. Lee, J.W. and R. Juliano, *α5β1 Integrin Protects Intestinal Epithelial Cells from Apoptosis through a Phosphatidylinositol 3-Kinase and Protein Kinase B–dependent Pathway.* Molecular Biology of the Cell, 2000. **11**(6): p. 1973-1987.
414. Gribar, S.C., et al., *Reciprocal expression and signaling of TLR4 and TLR9 in the pathogenesis and treatment of necrotizing enterocolitis.* The Journal of Immunology, 2009. **182**(1): p. 636-646.
415. Zhang, L., et al., *MicroRNA-21 regulates intestinal epithelial tight junction permeability.* Cell biochemistry and function, 2015. **33**(4): p. 235-240.
416. Nakata, K., et al., *Commensal microbiota-induced microRNA modulates intestinal epithelial permeability through the small GTPase ARF4.* Journal of Biological Chemistry, 2017. **292**(37): p. 15426-15433.
417. Caplan, M.S., et al., *Bifidobacterial supplementation reduces the incidence of necrotizing enterocolitis in a neonatal rat model.* Gastroenterology, 1999. **117**(3): p. 577-83.
418. Niño, D.F., C.P. Sodhi, and D.J. Hackam, *Necrotizing enterocolitis: new insights into pathogenesis and mechanisms.* Nature reviews. Gastroenterology & hepatology, 2016. **13**(10): p. 590-600.
419. Das, A., et al., *Dual RNA sequencing reveals the expression of unique transcriptomic signatures in lipopolysaccharide-induced BV-2 microglial cells.* PloS one, 2015. **10**(3): p. e0121117.
420. Pokusaeva, K., G.F. Fitzgerald, and D. van Sinderen, *Carbohydrate metabolism in Bifidobacteria.* Genes & nutrition, 2011. **6**(3): p. 285-306.
421. Rios-Covian, D., et al., *Bacteroides fragilis metabolises exopolysaccharides produced by bifidobacteria.* BMC Microbiology, 2016. **16**(1): p. 150.
422. De Vries, W. and A. Stouthamer, *Pathway of glucose fermentation in relation to the taxonomy of bifidobacteria.* Journal of bacteriology, 1967. **93**(2): p. 574-576.

423. Gibson, G.R., et al., *Expert consensus document: The International Scientific Association for Probiotics and Prebiotics (ISAPP) consensus statement on the definition and scope of prebiotics.* Nature Reviews Gastroenterology &Amp; Hepatology, 2017. **14**: p. 491.
424. de Souza Aquino, J., et al., *Models to Evaluate the Prebiotic Potential of Foods*, in *Functional Food-Improve Health through Adequate Food*. 2017, InTech.
425. Cassat, J.E. and E.P. Skaar, *Iron in infection and immunity.* Cell host & microbe, 2013. **13**(5): p. 509-519.
426. Lanigan, N., et al., *Genome-Wide Search for Genes Required for Bifidobacterial Growth under Iron-Limitation.* Frontiers in Microbiology, 2017. **8**: p. 964.
427. Amaretti, A., et al., *Fermentation of xylo-oligosaccharides by Bifidobacterium adolescentis DSMZ 18350: kinetics, metabolism, and β-xylosidase activities.* Applied microbiology and biotechnology, 2013. **97**(7): p. 3109-3117.
428. Pellis, L., et al., *High folic acid increases cell turnover and lowers differentiation and iron content in human HT29 colon cancer cells.* British journal of nutrition, 2008. **99**(4): p. 703-708.
429. Biasco, G., et al., *Folic acid supplementation and cell kinetics of rectal mucosa in patients with ulcerative colitis.* Cancer Epidemiology and Prevention Biomarkers, 1997. **6**(6): p. 469-471.
430. Hugenholtz, F. and W.M. de Vos, *Mouse models for human intestinal microbiota research: a critical evaluation.* Cellular and Molecular Life Sciences, 2017: p. 1-12.
431. Xiao, L., et al., *A catalog of the mouse gut metagenome.* Nat Biotechnol, 2015. **33**(10): p. 1103-8.
432. Stead, M.B., et al., *RNA snap™: a rapid, quantitative and inexpensive, method for isolating total RNA from bacteria.* Nucleic acids research, 2012. **40**(20): p. e156-e156.
433. McClure, R., et al., *Computational analysis of bacterial RNA-Seq data.* Nucleic acids research, 2013. **41**(14): p. e140-e140.
434. Creecy, J.P. and T. Conway, *Quantitative bacterial transcriptomics with RNA-seq.* Current opinion in microbiology, 2015. **23**: p. 133-140.
435. *Database Resources of the National Center for Biotechnology Information.* Nucleic Acids Res, 2017. **45**(D1): p. D12-d17.
436. Tahoun, A., et al., *Capsular polysaccharide inhibits adhesion of Bifidobacterium longum 105-A to enterocyte-like Caco-2 cells and phagocytosis by macrophages.* Gut pathogens, 2017. **9**(1): p. 27.
437. Christiaen, S.E., et al., *Autoinducer-2 plays a crucial role in gut colonization and probiotic functionality of Bifidobacterium breve UCC2003.* PLoS One, 2014. **9**(5): p. e98111.
438. Cronin, M., et al., *Identification of iron-regulated genes of Bifidobacterium breve UCC2003 as a basis for controlled gene expression.* Bioengineered, 2012. **3**(3): p. 159-169.
439. Ruiz, L., A. Margolles, and B. Sánchez, *Bile resistance mechanisms in Lactobacillus and Bifidobacterium.* Frontiers in microbiology, 2013. **4**.
440. Lee, J.-H. and D.J. O'Sullivan, *Genomic insights into bifidobacteria.* Microbiology and Molecular Biology Reviews, 2010. **74**(3): p. 378-416.
441. Lee, J.-H., et al., *Comparative genomic analysis of the gut bacterium Bifidobacterium longum reveals loci susceptible to deletion during pure culture growth.* BMC genomics, 2008. **9**(1): p. 247.
442. Philip, B. and D.E. Levin, *Wsc1 and Mid2 are cell surface sensors for cell wall integrity signaling that act through Rom2, a guanine nucleotide exchange factor for Rho1.* Molecular and cellular biology, 2001. **21**(1): p. 271-280.
443. Verna, J., et al., *A family of genes required for maintenance of cell wall integrity and for the stress response in Saccharomyces cerevisiae.* Proc Natl Acad Sci U S A, 1997. **94**(25): p. 13804-9.
444. Wei, X., et al., *Fructose Uptake in Bifidobacterium longum NCC2705 Is Mediated by an ATP-binding Cassette Transporter.* The Journal of Biological Chemistry, 2012. **287**(1): p. 357-367.
445. Yang, X., et al., *More than 9,000,000 unique genes in human gut bacterial community: estimating gene numbers inside a human body.* PLoS One, 2009. **4**(6): p. e6074.
446. Overbeek, R., et al., *The subsystems approach to genome annotation and its use in the project to annotate 1000 genomes.* Nucleic acids research, 2005. **33**(17): p. 5691-5702.
447. Silva, G.G.Z., et al., *FOCUS: an alignment-free model to identify organisms in metagenomes using non-negative least squares.* PeerJ, 2014. **2**: p. e425.

448. Mazé, A., et al., *Identification and Characterization of a Fructose Phosphotransferase System in Bifidobacterium breve UCC2003*, in *Appl Environ Microbiol*. 2007. p. 545-53.
449. Razzauti, M., et al., *A comparison between transcriptome sequencing and 16S metagenomics for detection of bacterial pathogens in wildlife.* PLoS neglected tropical diseases, 2015. **9**(8): p. e0003929.
450. Leimena, M.M., et al., *A comprehensive metatranscriptome analysis pipeline and its validation using human small intestine microbiota datasets.* BMC genomics, 2013. **14**(1): p. 530.
451. Blusztajn, S.H.Z., J.S. Wishnok, and K. J, *Formation of methylamines from ingested choline and lecithin.* 1983.
452. Carding, S., et al., *Dysbiosis of the gut microbiota in disease.* Microbial ecology in health and disease, 2015. **26**(1): p. 26191.
453. Kesty, N.C., et al., *Enterotoxigenic Escherichia coli vesicles target toxin delivery into mammalian cells.* The EMBO journal, 2004. **23**(23): p. 4538-4549.
454. Duncan, L., et al., *Loss of lipopolysaccharide receptor CD14 from the surface of human macrophage-like cells mediated by Porphyromonas gingivalis outer membrane vesicles.* Microbial pathogenesis, 2004. **36**(6): p. 319-325.
455. López, P., et al., *Treg-inducing membrane vesicles from Bifidobacterium bifidum LMG13195 as potential adjuvants in immunotherapy.* Vaccine, 2012. **30**(5): p. 825-829.
456. Stentz, R., et al., *Cephalosporinases associated with outer membrane vesicles released by Bacteroides spp. protect gut pathogens and commensals against β-lactam antibiotics.* Journal of Antimicrobial Chemotherapy, 2015. **70**(3): p. 701-709.
457. Amblee, V. and C.J. Jeffery, *Physical features of intracellular proteins that moonlight on the cell surface.* PLoS One, 2015. **10**(6): p. e0130575.
458. Shmaryahu, A., M. Carrasco, and P.D. Valenzuela, *Prediction of bacterial microRNAs and possible targets in human cell transcriptome.* Journal of Microbiology, 2014. **52**(6): p. 482-489.
459. Duval, M., P. Cossart, and A. Lebreton. *Mammalian microRNAs and long noncoding RNAs in the host-bacterial pathogen crosstalk*. in *Seminars in cell & developmental biology*. 2017. Elsevier.
460. Koeppen, K., et al., *A novel mechanism of host-pathogen interaction through sRNA in bacterial outer membrane vesicles.* PLoS pathogens, 2016. **12**(6): p. e1005672.
461. Liu, S., et al., *The host shapes the gut microbiota via fecal microRNA.* Cell host & microbe, 2016. **19**(1): p. 32-43.
462. Griffiths-Jones, S., et al., *miRBase: microRNA sequences, targets and gene nomenclature.* Nucleic acids research, 2006. **34**(suppl_1): p. D140-D144.
463. Solís, G., et al., *Establishment and development of lactic acid bacteria and bifidobacteria microbiota in breast-milk and the infant gut.* Anaerobe, 2010. **16**(3): p. 307-310.
464. Kitaoka, M., *Bifidobacterial enzymes involved in the metabolism of human milk oligosaccharides.* Advances in Nutrition: An International Review Journal, 2012. **3**(3): p. 422S-429S.
465. González, R., et al., *Differential transcriptional response of Bifidobacterium longum to human milk, formula milk, and galactooligosaccharide.* Applied and environmental microbiology, 2008. **74**(15): p. 4686-4694.
466. Chassard, C., et al., *The cellulose-degrading microbial community of the human gut varies according to the presence or absence of methanogens.* FEMS microbiology ecology, 2010. **74**(1): p. 205-213.
467. Trojanova, I., et al., *Different utilization of glucose and raffinose in Bifidobacterium breve and Bifidobacterium animalis.* Folia Microbiol (Praha), 2006. **51**(4): p. 320-4.
468. McLaughlin, H.P., et al., *Carbohydrate catabolic diversity of bifidobacteria and lactobacilli of human origin.* International journal of food microbiology, 2015. **203**: p. 109-121.
469. Kahlert, S., et al., *Physiological concentration of exogenous lactate reduces antimycin a triggered oxidative stress in intestinal epithelial cell line IPEC-1 and IPEC-J2 in vitro.* PloS one, 2016. **11**(4): p. e0153135.
470. Morrison, D.J. and T. Preston, *Formation of short chain fatty acids by the gut microbiota and their impact on human metabolism.* Gut Microbes, 2016. **7**(3): p. 189-200.
471. Palframan, R.J., G.R. Gibson, and R.A. Rastall, *Carbohydrate preferences of Bifidobacterium species isolated from the human gut.* Curr Issues Intest Microbiol, 2003. **4**(2): p. 71-5.

472. Maldonado-Gómez, María X., et al., *Stable Engraftment of Bifidobacterium longum AH1206 in the Human Gut Depends on Individualized Features of the Resident Microbiome.* Cell Host & Microbe. **20**(4): p. 515-526.
473. Parveen, N. and K.A. Cornell, *Methylthioadenosine/S-adenosylhomocysteine nucleosidase, a critical enzyme for bacterial metabolism.* Molecular microbiology, 2011. **79**(1): p. 7-20.
474. Sun, Z., et al., *Bifidobacteria exhibit LuxS-dependent autoinducer 2 activity and biofilm formation.* PLoS One, 2014. **9**(2): p. e88260.
475. Ward, F. and M. Coates, *Gastrointestinal pH measurement in rats: influence of the microbial flora, diet and fasting.* Laboratory animals, 1987. **21**(3): p. 216-222.
476. Selwyn, F. and C.D. Klaassen, *Characterization of bile acid homeostasis in germ-free mice.* The FASEB Journal, 2012. **26**(1 Supplement): p. 1155.1-1155.1.
477. Audy, J., et al., *Sugar source modulates exopolysaccharide biosynthesis in Bifidobacterium longum subsp. longum CRC 002.* Microbiology, 2010. **156**(3): p. 653-664.
478. Arrieta, M.-C. and B.B. Finlay, *The commensal microbiota drives immune homeostasis.* Frontiers in immunology, 2012. **3**.
479. An, H., et al., *Integrated transcriptomic and proteomic analysis of the bile stress response in a centenarian-originated probiotic Bifidobacterium longum BBMN68.* Molecular & Cellular Proteomics, 2014. **13**(10): p. 2558-2572.
480. Selwyn, F.P., et al., *Importance of large intestine in regulating bile acids and glucagon-like peptide-1 in germ-free mice.* Drug Metabolism and Disposition, 2015. **43**(10): p. 1544-1556.
481. Tanaka, H., et al., *Bile salt hydrolase of Bifidobacterium longum—biochemical and genetic characterization.* Applied and environmental microbiology, 2000. **66**(6): p. 2502-2512.
482. Sayin, Sama I., et al., *Gut Microbiota Regulates Bile Acid Metabolism by Reducing the Levels of Tauro-beta-muricholic Acid, a Naturally Occurring FXR Antagonist.* Cell Metabolism, 2013. **17**(2): p. 225-235.
483. Chikai, T., H. Nakao, and K. Uchida, *Deconjugation of bile acids by human intestinal bacteria implanted in germ-free rats.* Lipids, 1987. **22**(9): p. 669-671.
484. Ruiz, L., et al., *The essential genomic landscape of the commensal Bifidobacterium breve UCC2003.* Scientific Reports, 2017. **7**: p. 5648.
485. Schurch, N.J., et al., *How many biological replicates are needed in an RNA-seq experiment and which differential expression tool should you use?* Rna, 2016. **22**(6): p. 839-851.
486. Seyednasrollah, F., A. Laiho, and L.L. Elo, *Comparison of software packages for detecting differential expression in RNA-seq studies.* Briefings in bioinformatics, 2013. **16**(1): p. 59-70.
487. Kim, D., B. Langmead, and S.L. Salzberg, *HISAT: a fast spliced aligner with low memory requirements.* Nature Methods, 2015. **12**: p. 357.
488. van Bergenhenegouwen, J., et al., *Extracellular vesicles modulate host-microbe responses by altering TLR2 activity and phagocytosis.* PLoS One, 2014. **9**(2): p. e89121.
489. Stentz, R., et al., *Cephalosporinases associated with outer membrane vesicles released by Bacteroides spp. protect gut pathogens and commensals against β-lactam antibiotics.* Journal of Antimicrobial Chemotherapy, 2014. **70**(3): p. 701-709.
490. Choi, D.S., et al., *Proteomic analysis of outer membrane vesicles derived from Pseudomonas aeruginosa.* Proteomics, 2011. **11**(16): p. 3424-3429.
491. Liu, H., et al., *Escherichia coli noncoding RNAs can affect gene expression and physiology of Caenorhabditis elegans.* Nature communications, 2012. **3**: p. 1073.
492. Furuse, Y., et al., *Search for microRNAs expressed by intracellular bacterial pathogens in infected mammalian cells.* PloS one, 2014. **9**(9): p. e106434.
493. Westreich, S.T., et al., *SAMSA2: A standalone metatranscriptome analysis pipeline.* bioRxiv, 2017.
494. Meyer, F., et al., *The metagenomics RAST server–a public resource for the automatic phylogenetic and functional analysis of metagenomes.* BMC bioinformatics, 2008. **9**(1): p. 386.
495. Buchfink, B., C. Xie, and D.H. Huson, *Fast and sensitive protein alignment using DIAMOND.* Nature methods, 2015. **12**(1): p. 59-60.
496. Petursdottir, D.H., et al., *Early-life human microbiota associated with childhood allergy promotes the T helper 17 axis in mice.* Frontiers in Immunology, 2017. **8**: p. 1699.
497. Ruiz, L., et al., *BIFIDOBACTERIA AND THEIR MOLECULAR COMMUNICATION WITH THE IMMUNE SYSTEM.* Frontiers in Microbiology, 2017. **8**: p. 2345.

498. Rivière, A., et al., *Bifidobacteria and Butyrate-Producing Colon Bacteria: Importance and Strategies for Their Stimulation in the Human Gut.* Frontiers in Microbiology, 2016. **7**(979).
499. Gudipaty, S.A., et al., *Mechanical stretch triggers rapid epithelial cell division through Piezo1*. Nature, 2017. **543**(7643): p. 118-121.
500. Saez-Lara, M.J., et al., *The role of probiotic lactic acid bacteria and bifidobacteria in the prevention and treatment of inflammatory bowel disease and other related diseases: a systematic review of randomized human clinical trials.* BioMed research international, 2015. **2015**.
501. Duranti, S., et al., *Elucidating the gut microbiome of ulcerative colitis: bifidobacteria as novel microbial biomarkers.* FEMS Microbiology Ecology, 2016. **92**(12): p. fiw191-fiw191.
502. *Inflammatory bowel disease | Guidance and guidelines | NICE*. 2017; Available from: https://www.nice.org.uk/guidance/qs81/chapter/introduction.

Appendix

Appendix 1.

Hughes, Kevin R., Lukas C. Harnisch, Cristina Alcon-Giner, Suparna Mitra, Chris J. Wright, Jennifer Ketskemety, Douwe van Sinderen, Alastair JM Watson, and Lindsay J. Hall. "*Bifidobacterium breve* reduces apoptotic epithelial cell shedding in an exopolysaccharide and MyD88-dependent manner." *Open biology*7, no. 1 (2017): 160155.

- Contribution by Lukas Harnisch to:
- Figure 3. – D), E), F), G), H), I), J), and K)
- Supplementary Figure 3.

OPEN BIOLOGY

rsob.royalsocietypublishing.org

Research

Cite this article: Hughes KR, Harnisch LC, Alcon-Giner C, Mitra S, Wright CJ, Ketskemety J, van Sinderen D, Watson AJM, Hall LJ. 2017 *Bifidobacterium breve* reduces apoptotic epithelial cell shedding in an exopolysaccharide and MyD88-dependent manner. *Open Biol.* **7**: 160155.
http://dx.doi.org/10.1098/rsob.160155

Received: 26 May 2016
Accepted: 15 December 2016

Subject Area:
microbiology/immunology/molecular biology

Keywords:
Bifidobacterium, epithelial cell shedding, inflammatory bowel disease, exopolysaccharide

Authors for correspondence:
K. R. Hughes
e-mail: kevinhughes79@gmail.com
A. J. M. Watson
e-mail: alastair.watson@uea.ac.uk
L. J. Hall
e-mail: lindsay.hall@ifr.ac.uk

Electronic supplementary material is available online at https://dx.doi.org/10.6084/m9.figshare.c.3655565.

THE ROYAL SOCIETY PUBLISHING

Bifidobacterium breve reduces apoptotic epithelial cell shedding in an exopolysaccharide and MyD88-dependent manner

K. R. Hughes[1,2], L. C. Harnisch[1,2], C. Alcon-Giner[1], S. Mitra[1], C. J. Wright[1,2], J. Ketskemety[1], D. van Sinderen[3,4], A. J. M. Watson[1,2] and L. J. Hall[1]

[1]The Gut Health and Food Safety Programme, Institute of Food Research, Norwich Research Park, Colney, Norwich NR4 7UA, UK
[2]Norwich Medical School, University of East Anglia, Norwich Research Park, Norwich NR4 7UQ, UK
[3]APC Microbiome Institute, and [4]School of Microbiology, University College Cork, Cork, Ireland

DvS, 0000-0003-1823-7957; AJMW, 0000-0003-3326-0426; LJH, 0000-0001-8938-5709

Certain members of the microbiota genus *Bifidobacterium* are known to positively influence host well-being. Importantly, reduced bifidobacterial levels are associated with inflammatory bowel disease (IBD) patients, who also have impaired epithelial barrier function, including elevated rates of apoptotic extrusion of small intestinal epithelial cells (IECs) from villi—a process termed 'cell shedding'. Using a mouse model of pathological cell shedding, we show that mice receiving *Bifidobacterium breve* UCC2003 exhibit significantly reduced rates of small IEC shedding. Bifidobacterial-induced protection appears to be mediated by a specific bifidobacterial surface exopolysaccharide and interactions with host MyD88 resulting in downregulation of intrinsic and extrinsic apoptotic responses to protect epithelial cells under highly inflammatory conditions. Our results reveal an important and previously undescribed role for *B. breve*, in positively modulating epithelial cell shedding outcomes via bacterial- and host-dependent factors, supporting the notion that manipulation of the microbiota affects intestinal disease outcomes.

1. Introduction

Bifidobacteria represent one of the first colonizers of the infant gut and are prominent members of the adult gut microbiota [1,2]. They have been linked to a number of health-promoting activities, including the promotion of anti-tumour immunity [3], modulation of antimicrobial activities against pathogenic bacteria [4] and protection against relapse of ulcerative colitis [5,6]. Despite these purported benefits, the molecular mechanisms underlying these protective effects by bifidobacteria remain largely unknown, although recently components of their surface, including the exopolysaccharide (EPS), have been shown to play a significant role in modulating protective effects [7]. It is critical to obtain detailed insights into the mode of action by which microbiota members sustain and improve host health, as this will be central to future disease treatment/prevention strategies.

There is a growing body of evidence suggesting that the microbiota influences intestinal epithelial cell (IEC) function, including gene expression, cell division and energy balance [8–11]. These symbiotic bacterial/host relationships have co-evolved to the extent that the microbiota is indispensable for the maintenance of gut homeostasis [12]. Importantly, microbial dysbiosis, as indicated by a reduction in overall diversity, including specific reductions in *Bifidobacterium*, has been linked to inflammatory bowel disease (IBD) [13–15], underlining the critical importance of host/microbe interactions in maintaining a steady state within the intestine.

The epithelium of the small intestine represents the first line of defence against entry of bacteria into host tissues. Cell division in the crypt, under physiological conditions, is counterbalanced by cell shedding from the villi to maintain homeostasis and integrity of the crypt/villus axis. When the epithelial cell is shed, a discontinuity in the villus epithelial monolayer is created, which potentially compromises the epithelial barrier. In health, epithelial barrier function is maintained [16], owing to a dramatic redistribution of apical junction complex proteins, including zonula occludin 1 (ZO-1), occludin 1 and E-cadherin, which form a funnel that surrounds the shedding cell and plugs the resulting gap until the movement of neighbouring epithelial cells restores epithelial continuity [17–19].

TNF-α is a key cytokine in IBD. We and others have shown that TNF-α induces apoptosis of villus tip epithelial cells causing excessive shedding, leading to breakdown of the epithelial barrier and microulceration [16,20]. Delayed repair of epithelial defects caused by excessive cell shedding contributes to the development of macroscopic ulceration [21]. Our studies with confocal endomicroscopy of patients with IBD in clinical remission have demonstrated that those patients with high rates of cell shedding are more likely to relapse than those with low shedding rates, demonstrating a causative link between barrier function and the inflammatory response [21].

Given reports of beneficial effects of certain members of the gut microbiota in IBD and potential roles of microbial dysbiosis in these diseases, we hypothesized that certain health-promoting microbiota members, including *Bifidobacterium*, may play a role in protecting against the cell shedding response by modulating IEC function. To determine the contribution of bifidobacteria in cell shedding, we employed a well characterized *in vivo* mouse model in which pathological cell shedding is induced by intraperitoneal (IP) administration of lipopolysaccharide (LPS), driving mononuclear cell expression of TNF-α and subsequent caspase-3-positive shedding cells [22]. Our results suggest a particular bifidobacterial strain (i.e. human isolate *B. breve* UCC2003) positively modulates the small intestinal cell shedding response via host MyD88- and bacterial EPS-dependent interactions which serve to significantly reduce apoptotic signalling in the epithelial compartment. These data identify a previously unknown mechanism by which *Bifidobacterium* protects its host against pathological cell shedding. These findings may thus have important implications for the future design of therapeutic strategies in the context of intestinal diseases.

2. Material and methods

2.1. Animals

C57 BL/6 Jax mice (6–10 weeks) were obtained from Charles River. Vil-cre MyD88 transgenic mice (i.e. Cre recombinase expression causes truncation and resulting non-function of the MyD88 protein in IECs) were obtained from the Wellcome Trust Sanger Institute (kind gift from S. Clare).

2.2. Bacterial culture and inoculations

Bifidobacterium breve strains UCC2003, UCC2003del and UCC2003inv were used for animal inoculations. These strains and corresponding culturing conditions have been previously described in detail [7]. In brief, colonies were established from frozen glycerol stocks onto reinforced clostridial agar (RCA) plates before being subcultured into reinforced clostridial medium and subsequently Man Rogosa Sharpe medium (Oxoid, Hampshire) under anaerobic conditions. Bacteria were then purified by centrifugation and washed in PBS containing L-cysteine before being reconstituted in sterile PBS at a final concentration of approximately 1×10^{10} bacteria ml^{-1}. 0.1 ml of inoculum was then administered to mice by oral gavage in 3 × 24 h doses followed by plating of faecal pellets on RCA containing 50 mg l^{-1} mupirocin to confirm stable colonization. Control mice received oral gavage of PBS only.

2.3. Lipopolysaccharide injections and tissue collections

Twenty-four hours after the last doses of *B. breve* or PBS control, mice received an IP injection of 1.25 mg kg^{-1} LPS from *Escherichia coli* 0111:B4 (Sigma) or sterile saline (control) and mice were sacrificed 1.5 h post-challenge with LPS. Proximal small intestine was collected in 10% neutral buffered formalin saline (Sigma) and fixed for 24 h followed by paraffin embedding. Samples of proximal small intestine were also collected into RNA Later (Qiagen) for transcriptome analysis or frozen on dry ice for subsequent ELISA analysis. In some cases, proximal small intestine was also collected into Hanks buffered saline solution (HBSS) for isolation of IECs.

2.4. Immunohistochemistry

Sections (5 µm) of paraffin-embedded small intestinal tissue were sectioned and used for immunohistochemistry. Following de-parafinization and rehydration, tissue sections were treated with 1% hydrogen peroxide in methanol to block endogenous peroxidases. Subsequently, slides were treated using heat-induced antigen retrieval in 0.01 M citrate acid buffer (pH 6) followed by incubation with a rabbit polyclonal anti-active caspase-3 (CC3) antibody (AF835: R&D Systems). Visualization of caspase-3 positivity was via a peroxidase-labelled anti-rabbit EnVision secondary antibody (Dako) and 3,3′-diaminobenzidine followed by counterstaining with haematoxylin. For macrophage staining, an antibody against F4/80 antigen (ab6640: Abcam) was employed using biotinylated anti-rat (BA-9401) and avidin–biotin reagent (PK-6100; Vector Laboratories).

2.5. Quantification of caspase-3 positivity

IECs were counted on a cell positional basis from villus tip (cell position (CP) 1) down towards the crypts under 400× magnification. Twenty well-orientated hemi-villi were counted per mouse and analysed using the Score, WinCrypts [23] and PRISM analysis software. IECs were defined as 'normal' in cases where staining for active caspase-3 was absent. Immunolabelled cells with either unaltered or shedding morphology were treated as caspase-3 positive. Imaging was performed with an Olympus BX60 microscope and C10plus digital camera.

2.6. RNA isolation and real-time polymerase chain reaction

Samples fixed in RNAlater solution were processed through RNeasy plus mini spin columns to isolate total RNA (Qiagen).

In brief, samples were homogenized using a rotor stator hand held homogenizer in buffer RLT before processing through a QIAshredder column and subsequently RNeasy mini-spin columns. Purified RNA was eluted into RNAase free water. Reverse transcription was performed using the Quantitect reverse transcription kit (Qiagen) and cDNA used for real-time (RT-)PCR analysis. For RT-PCR, transcripts were amplified using Quantifast SYBR green mastermix (Qiagen) and Quantitect primer assays for TNF-α, TNF-R1 and F4/80 (EMR1). Expression of the housekeeping gene hypoxanthine–guanine phosphoribosyltransferase (HPRT) 5′-GACCAGTCAACAG GGGACAT-3′ (sense) and 5′-AGGTTTCTACCAGTTCCAGC-3′ (antisense) [24] was also determined. Cycling was performed on a Roche LightCycler 480 using the following conditions: 95°C, 5 min then 40 cycles of 95°C, 10 s; 60°C, 35 s. Relative quantification of levels of transcript expression was calculated using the Pfaffl method [25] by comparing cycle threshold (CT) value of each target gene to the CT value of housekeeper. Data are presented as a 'fold change' in expression (normalized against control untreated mice per cells).

2.7. Isolation of intestinal epithelial cells and FACS analysis

IECs were isolated using a modification of the Weiser methodology [26]. In brief, whole small intestine was collected in ice-cold HBSS before being chopped into 0.5 cm^2 pieces and washed in a solution containing 0.154 M NaCl and 1 mM DTT, and subsequently a solution containing 1.5 mM KCl, 96 mM NaCl, 27 mM tri-sodium citrate, 8 mM NaH_2PO_4 and 5.6 mM Na_2HPO_4, pH 7.3. IECs were then isolated by incubation in PBS containing 1.5 mM EDTA and 0.5 mM DTT, shaking at 200 r.p.m. and at 37°C. Purity of epithelial preparations was confirmed by histological analysis of stripped intestinal mucosa and by FACS analysis of isolated cells. For FACS analysis, 5×10^6 cells were stained with anti-mouse CD45-A700 (Biolegend) on ice for 30 min. After two washes in HBSS containing 0.01 BSA, 2 mM EDTA, 20 mM HEPES and 0.01% NaN_3, propidium iodide was added (Biolegend) and samples analysed on a Sony FCS SH-800 flow cytometer. Data were analysed using FlowJo (TreeStar).

2.8. ELISA

Frozen proximal small intestinal samples were homogenized in extraction buffer containing protease inhibitors (Roche), cleared by centrifugation and analysed using a commercial ELISA kit for TNF-α (eBioscience) as per manufacturer's protocol. Measurement of TNF-α immunoreactivity was at 450 nm, using a Fluostar Optima plate reader (BMG Labtech).

2.9. SDS–PAGE and Western blotting

Isolated IECs were lysed in CelLytic MT reagent (Sigma) before centrifugation at 10 000 rpm for 10 min to pellet cellular debris. Supernatants were mixed with 2 × Laemmli sample buffer before being separated by sodium dodecyl sulfate (SDS)–PAGE with 3–14% acrylamide gel and transferred to Hybond-P PVDF membrane (GE Healthcare, Buckinghamshire, UK) and blocking with 5% Marvel milk in with tris(hydroxymethyl)aminomethane (Tris). (Tris)-buffered saline containing Tween 20 (TTBS) immunostaining was performed with 1/1000 anti-TNF-R1 antibody (Abcam) and 1/5000 goat anti-Rabbit IgG HRP conjugate (Millipore) on a reduced gel. Macrophage expression was analysed similarly using antibody against F4/80 antigen (Abcam) at 1 : 1000 and goat anti-rat IgG-HRP (SantaCruz, at 1 : 3000), on a non-reduced gel. Washes were in TTBS. For detection, Immobilon Western chemiluminescent HRP substrate (Millipore) was applied to the membrane as recommended by the manufacturer and signal was detected, using a FluorChem E imaging system (Protein Simple). Band densities were quantified using Fiji [27].

2.10. Polymerase chain reaction array analysis

Real-rime ready Custom Panel 480–96+ PCR arrays were obtained (Roche) and quantitative PCR analysis performed. RNA was extracted from whole small intestinal tissue preserved in RNAlater reagent (Sigma), using RNeasy plus mini kits (Qiagen). Reverse transcription was performed, using Transcriptor First Strand cDNA Synthesis Kit followed by analysis of targets using LightCycler 480 Probes Master on a LightCycler 480 platform (all Roche). Standard protocols as per manufacturer recommendations were followed. CT values of target genes were normalized to expression of the housekeeping gene HPRT and fold change versus control samples calculated using the delta/delta CT method [25].

2.11. Statistical analysis

Experimental results were plotted and analysed for statistical significance with Prism v. 5 software (GraphPad Software). A p-value of less than 0.05 was used as significant in all cases.

3. Results

3.1. Lipopolysaccharide induces cell shedding from small intestinal villi in a dose-dependent manner

Caspase-3 is activated in IECs during their extrusion from the tips of small intestinal villi [18,28]. Similar to previous reports, we found that control C57 BL/6 mice receiving IP PBS injection showed low levels of cell shedding as evidenced by low level expression of cleaved caspase-3 (CC3) in the epithelial cell layer (figure 1*a*). Recent studies have demonstrated that following IP injection of mice with LPS isolated from *Escherichia coli* 0111:B4, a potent cell shedding response is induced, similar to that observed in relapsing IBD patients [22]. In agreement with these studies, we found a significant increase in CC3-mediated cell shedding at 1.5 h post-injection of 1.25 mg kg^{-1} LPS, not only at the villus tip, but also along the shoulders and sides of the villus (figure 1*b*). Effects of LPS on the cell shedding response were found to be dose-dependent, in agreement with previous observations [22] (data not shown).

3.2. *Bifidobacterium breve* modulates lipopolysaccharide-induced cell shedding

Various members of the microbiota are known to promote a healthy gut [29], although the precise mechanisms behind this remain incompletely understood. We reasoned that because the integrity of the intestinal epithelium is intrinsically

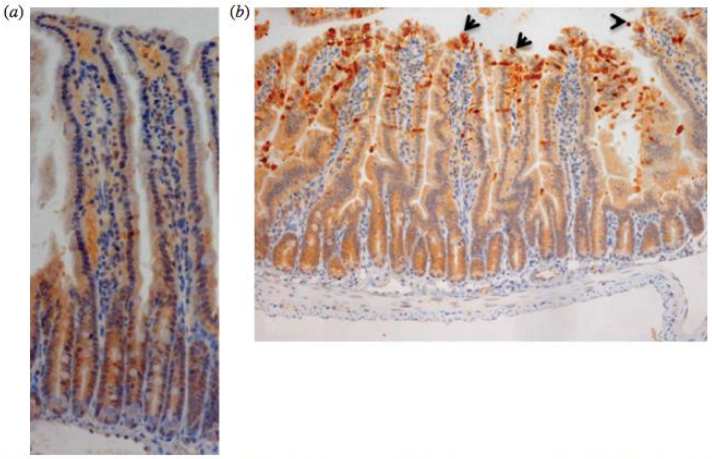

Figure 1. LPS challenge induces cell shedding from small intestinal villi. C57 BL/6 mice were administered either (*a*) PBS (control) or (*b*) LPS by IP injection and proximal small intestines removed after 1.5 h. Processed tissue was sectioned and stained by immunohistochemistry for CC3 (i.e. brown cells indicate shedding event), also highlighted by arrows. A representative picture for each group is shown (12 mice per group, two independent experiments).

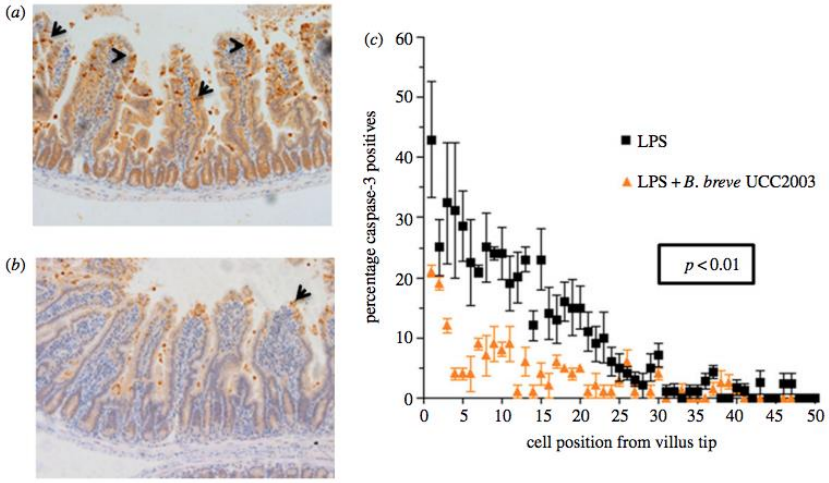

Figure 2. *Bifidobacterium breve* UCC2003 protects against LPS-induced cell shedding. C57 BL/6 mice received three daily oral gavage doses of (*a*) PBS or (*b*) approximately 1×10^9 *B. breve* UCC2003 followed by IP challenge with LPS 24 h later. Representative images are shown. Formalin-fixed, paraffin-embedded intestinal sections were sectioned and stained with anti-CC3 and (*c*) quantified using the WinCrypts and Score programs, 20 well-orientated hemi-villi were counted per mouse. Data are mean $\pm$ s.d., $n = 12$ (two independent experiments) analysed with a Mann–Whitney *U*-test.

linked to the well-being of the host and because the microbiota is expected to impact on epithelial cross-talk, such health-promoting species might play a role in regulating cell shedding. To test this, groups of C57 BL/6 mice were initially dosed with vehicle control (PBS) or with 1×10^9 *B. breve* UCC2003 (isolated from a healthy infant) in 3×24 h doses orally to establish stable colonization [7]. Colonization was confirmed by faecal CFU counts on day 4 (electronic supplementary material, figure S1). Mice were then administered LPS to induce pathological cell shedding, followed by sacrifice at 1.5 h. Following dosing with *B. breve* UCC2003 and induction of cell shedding with LPS, mice showed a marked reduction in the levels of CC3-positive shedding cells compared with LPS-treated control mice receiving PBS gavage (figure 2*a*,*b*). Cell count analysis confirmed significant reduction ($p < 0.01$) in cell shedding at the majority of positions along the length of the villus in *B. breve* UCC2003-treated mice (figure 2*c*). Thus, *B. breve* appears to modulate epithelial integrity/survival during periods of inflammatory insult.

Previous studies have indicated that bifidobacteria may modulate the composition of other microbiota members, and within the context of IBD, studies have linked

microbiota disturbances with active disease. Thus, to determine if bifidobacterial colonization impacts the gut microbiota, we analysed the community composition using a 16S rRNA-based sequencing approach. We found minor changes to the community structure in *B. breve* UCC2003 versus control treated mice (C57 BL/6), but overall, no notable differences (but expected increase in Actinobacteria in the *B. breve* UCC2003 group) in microbiota class abundance between the treatment groups (electronic supplementary material, figure S2). Bifidobacterial colonization takes place along the gastrointestinal (GI) tract including the small/large intestine and caecum. RNAscope analysis showed that *B. breve* UCC2003 was found in intimate contact with the IECs of the small intestine in colonized C57 BL/6 mice (electronic supplementary material, figure S3). Together, these data suggest that colonization with *B. breve* does not produce significant shifts in the overall gut microbiota community structure and that the observed protective effects after colonization are more likely to be related to direct effects of *B. breve*, possibly through interactions with the IECs.

3.3. The mechanism of protection against lipopolysaccharide-induced cell shedding is TNF-α independent

LPS-induced cell shedding is caused by the release of TNF-α from lamina propria tissue-resident macrophages, which binds to TNF-receptor 1 (TNF-R1), on IECs [22], thereby driving the apoptotic response. Conditioning of macrophage responses by the microbiota has been reported previously [30] and, consistent with these data, bacteria such as *B. breve* have been described to possess immunomodulatory properties [31]. Thus, to determine whether the cell shedding outcome, as modulated by *B. breve*, was caused by reduced expression of TNF-α from macrophages, we isolated RNA and protein from whole small intestine of control and *B. breve* UCC2003-treated C57 BL/6 mice following LPS-mediated induction of cell shedding. As shown in figure 3*a*, no significant difference ($p > 0.05$) in levels of TNF-α protein was observed between groups, and this was confirmed at the transcriptional level (data not shown). We also found no significant changes ($p > 0.05$) in expression of TNF-α in the plasma of *B. breve* UCC2003-treated versus control mice following LPS-induced cell shedding (figure 3*b*), nor any significant difference ($p > 0.05$) in the numbers/levels of F4/80$^+$ macrophages infiltrating the small intestine (figure 3*c–f*). Together, these data suggest that modulation of the reduced cell shedding response is independent of TNF-α induction. Because the microbiota may be able to interact directly with IECs, we postulated that *B. breve* modulates a signalling pathway downstream of the TNF-α ligand. To test whether expression of TNF-R1 was altered in the epithelium following dosing with *B. breve* UCC2003, IECs were isolated from whole small intestinal tissue using a modified Weiser methodology [32], after which purity of the IEC population was confirmed by histological analysis of stripped intestinal tissue and FACS analysis (figure 3*g*,*h*). Subsequent quantitative RT-PCR and western blot analysis of isolated IEC populations showed no significant changes ($p > 0.05$) to expression of the TNF-R1 transcript or protein following exposure to *B. breve* UCC2003 (figure 3*i–k*), suggesting that there is no impairment of signalling at the level of the receptor.

3.4. Functional epithelial MyD88 signalling is required for *Bifidobacterium breve*-mediated protection against cell shedding

IECs sample microbe-associated molecular patterns (MAMPS) of the intestinal luminal contents using a variety of receptors including members of the nucleotide-binding oligomerization domain (NOD) family, the C-type lectin receptor (CLR) family and the Toll-like receptor (TLR) superfamily. MyD88 is a critical adaptor protein in signalling downstream of the majority of the TLR family members [33]. We thus used epithelial-specific (Vil-Cre) MyD88 knockout mice to determine whether *B. breve* elicits its protective effects via epithelial TLR signalling pathways.

C57 BL/6 MyD88$^{-/-}$ villin-cre mice (i.e. IEC MyD88 KO mice) colonized with *B. breve* UCC2003, showed similar rates ($p > 0.05$) of LPS-induced cell shedding to PBS gavaged IEC MyD88$^{-/-}$ mice. In comparison, control mice (i.e. C57 BL/6 MyD88$^{+/+}$ villin-cre) showed the expected protection ($p < 0.01$) against cell shedding in the presence of *B. breve* UCC2003 (figure 4*a–d*). Furthermore, RT-PCR analysis of IEC homogenates showed increased expression ($p < 0.001$) of TLR2 in *B. breve* UCC2003-colonized mice when compared with control mice (i.e. PBS, figure 4*e*). Taken together, these data indicate that functional MyD88 signalling, potentially via TLR2 is required for modulating the protective effect of *B. breve* against cell shedding outcomes.

3.5. *Bifidobacterium breve* exopolysaccharide plays a role in modulating protection against lipopolysaccharide-induced cell shedding

Recently, a number of functions modulated by bifidobacteria have been shown to be mediated through surface-associated EPS including resistance to gut infection [7]. Interestingly, the *eps* gene clusters represent a relatively conserved feature of bifidobacterial genomes, including those of the species *B. breve* [34]. In order to investigate the role of EPS in modulating the response against cell shedding, we used a deletion mutant (*B. breve* UCC2003-EPSdel) that expresses neither EPS1 nor EPS2 [7]. Mice were stably colonized by dosing with *B. breve* EPS-positive or EPS-negative strains followed by challenge with LPS (electronic supplementary material, figure S1). Strikingly, when colonized with the *B. breve* UCC2003-EPSdel, no significant protection ($p > 0.05$) against cell shedding was observed in control (i.e. PBS) versus colonized mice (figure 5*a*,*b*).

Bifidobacterium breve UCC2003 controls EPS biosynthesis via a bidirectional gene cluster which results in expression of either EPS1 (*B. breve* UCC2003) or EPS2 (*B. breve* UCC2003-EPSInv) [7]. Thus, to gain further insights into the role of a different EPS in the protective cell shedding response, we undertook studies using *B. breve* UCC2003-EPSInv. Colonization with EPS2 expressing *B. breve* (i.e. *B. breve* UCC2003-EPSInv) also failed to show any significant protection ($p > 0.05$) against LPS-induced cell shedding, suggesting considerable variation in the protective response dependent upon EPS genetic and chemical structure and organization (figure 5*c*,*d*). All strains are directly compared in electronic supplementary material, figure S4.

Together, these studies emphasize the striking strain variant specificity that is observed with regard to the individual

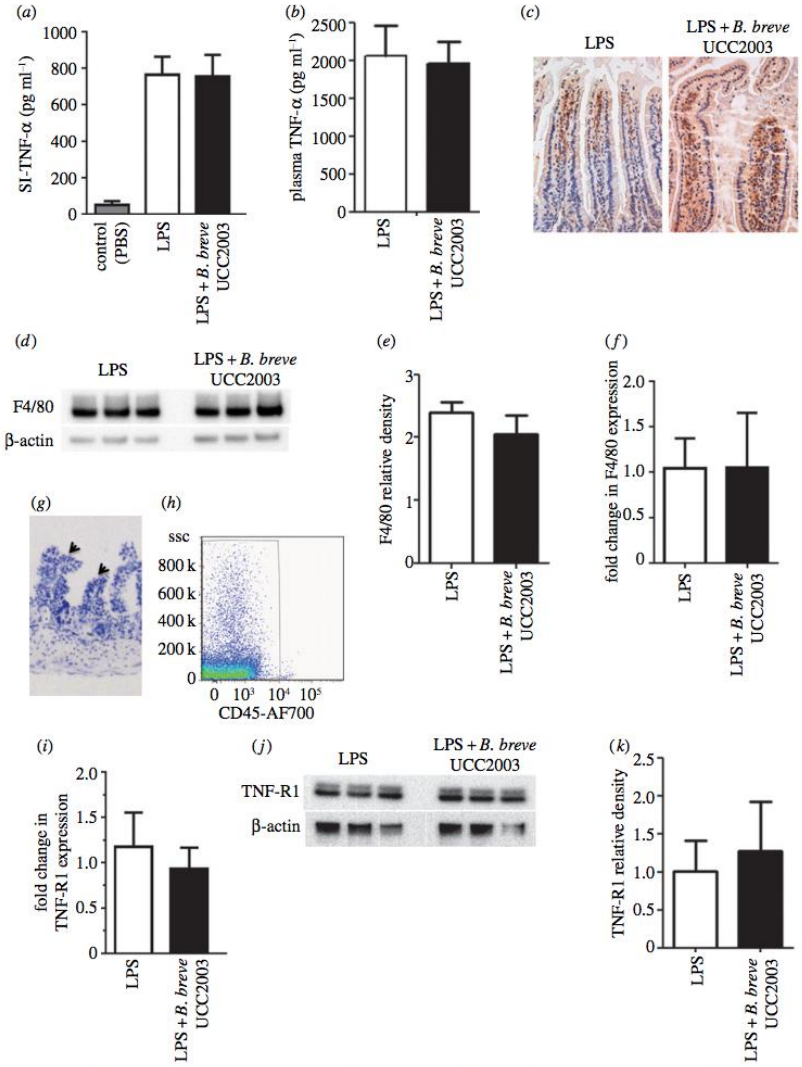

Figure 3. The cytoprotective effect of *B. breve* is not mediated by the TNF-α signalling pathway. C57 BL/6 mice were gavaged with PBS or *B. breve* and challenged with PBS or LPS for 1.5 h. Columns show TNF-α levels (via ELISA) in (*a*) whole small intestine intestinal homogenates or (*b*) plasma ± s.d. (*c*) Representative immunohistochemical staining for F4/80^{+} macrophages (brown cells) in control or *B. breve*-colonized mice. (*d*) Western blot analysis (F4/80 or housekeeping β-actin) of whole small intestinal homogenates, with (*e*) columns show relative density of F4/80 from (from *d*) whole intestinal homogenates. (*f*) Columns show F4/80 expression via RT-PCR ± SD. (*g*) Representative histology image of epithelial cell stripping protocol (modified Weiser method) leaving lamina propria intact (as indicated by arrows) and (*h*) FACS analysis for purity (anti-CD45). (*i*) Columns shown TNF-R1 expression via RT-PCR ± SD and (*j*) western blotting for protein expression in isolated intestinal epithelial cells, with (*k*) columns showing relative density of TNF-R1 (from (*j*)). $n = 9$ mice per group, representative of three experiments analysed with ANOVA Kruskal–Wallis test with Dunn's multiple comparison test (*a*), and with Mann–Whitney *U*-test (*b,e,f,i,k*).

protective effects of these bacteria following LPS-induced cell shedding. This is probably regulated by the specific molecules produced by each strain, including the EPS. This highlights the critical need to fully genetically characterize 'probiotic' strains of bacteria to enable a detailed dissection of their functional effects *in vivo* for optimal translation to human patients.

3.6. *Bifidobacterium breve* exopolysaccharide attenuates inflammatory and apoptosis signalling

In order to gain further insights into the changes taking place in the small intestine following colonization with *B. breve* UCC2003 and the influence of EPS, whole small intestinal

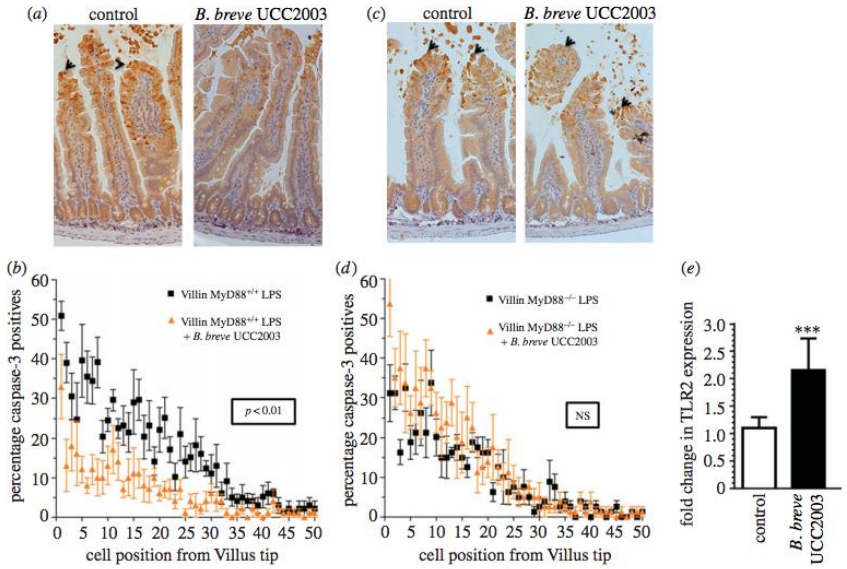

Figure 4. The cytoprotective effect of *B. breve* is MyD88 dependent. (*a,b*) IEC MyD88$^{+/+}$ mice and (*c,d*) IEC MyD88$^{-/-}$ mice were gavaged with PBS (control) or *B. breve* UCC2003 and challenged with LPS. Paraffin-embedded intestinal sections were stained with anti-CC3 and quantified using the WinCrypts and Score programs. (*e*) Columns shown TLR2 expression via RT-PCR. Data are mean ± s.d., $n = 12$ (two independent experiments) analysed with Mann–Whitney *U*-test.

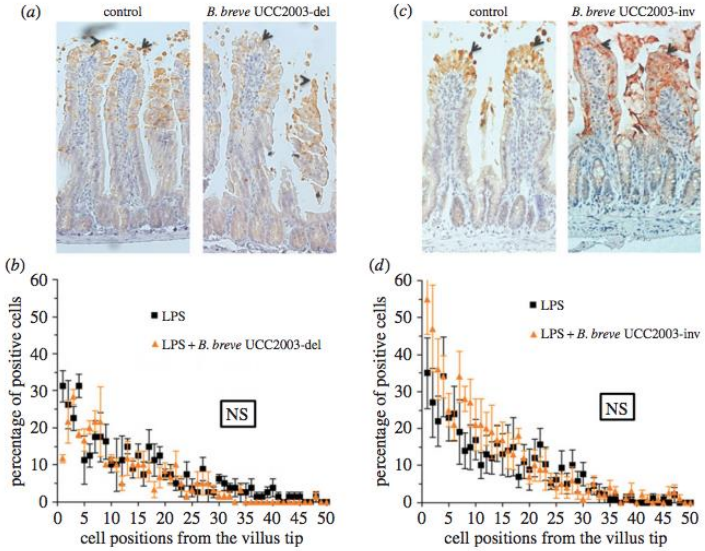

Figure 5. *Bifidobacterium breve* EPS plays a role in modulating the cytoprotective effect. C57 BL/6 mice were gavaged with either *B. breve* UCC2003 or (*a,b*) *B. breve* UCC2003del (i.e. EPS-negative) or (*c,d*) *B. breve* UCC2003inv (i.e. EPS2). Formalin-fixed, paraffin-embedded intestinal sections were stained with anti-CC3 and quantified using the WinCrypts and Score programs. Data are mean ± s.d., $n = 12$ (two independent experiments) analysed with Mann–Whitney *U*-test.

samples from control (i.e. PBS) and colonized (EPS-positive *B. breve* UCC2003 and EPS-negative *B. breve* UCC2003-del) mice following challenge with LPS were analysed using a custom RT-PCR array (figure 6: 49/84 targets are shown; full set of data is displayed in electronic supplementary material, figure S5) to look for transcriptional changes to key inflammatory transcripts and those involved in the apoptotic cascade. Interestingly, small intestinal samples from *B. breve* UCC2003-EPSdel-colonized mice (figure 6*a*; electronic supplementary material, figure S5*a,b*) showed

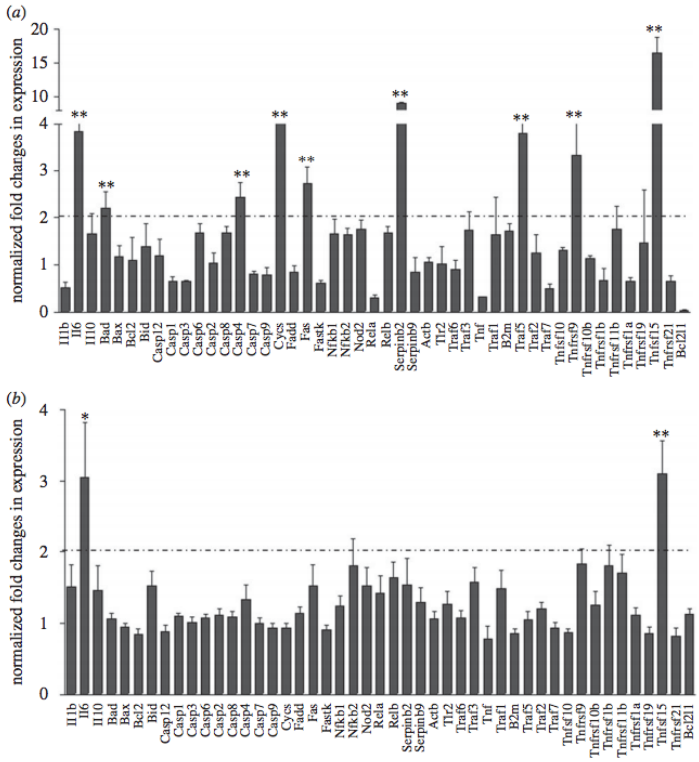

Figure 6. *Bifidobacterium breve* EPS attenuates inflammatory and apoptosis signalling. Whole small intestinal homogenates from LPS-challenged (*a*) *B. breve* UCC2003-EPSdel and (*b*) *B. breve*-colonized mice compared with control (i.e. PBS) were analysed using a custom RT-PCR array. Data are mean ± SD, $n = 6$ (two independent experiments), $*p < 0.05$ and $**p < 0.01$ and analysed with Mann–Whitney *U* test.

significant increases (more than twofold and $p < 0.01$) in IL-6 and Tnfrs15 when compared with control and LPS-challenged mice. Moreover, numerous other apoptotic and inflammatory genes were significantly upregulated (more than twofold, $p < 0.01$) including Bad, Cycs (cytochrome *c*, Somatic), casp4, Fas, Traf5 and Tnfrs9. In contrast, in EPS-positive-colonized mice (i.e. *B. breve* UCC2003), our analysis showed only subtle changes to the expression of the majority of the targets when compared with PBS-treated control mice challenged with LPS (figure 6*b*; electronic supplementary material, figure S5c,*d*). In addition, while significant elevation (more than twofold and $p < 0.05$) in IL-6 and Tnfrs15 was observed following colonization with *B. breve* UCC2003, Tnfrs15 expression was markedly decreased versus *B. breve* UCC2003-EPSdel-colonized mice (threefold versus 16-fold increase). These data suggest that signalling via EPS may downregulate inflammatory and apoptotic networks, which would otherwise lead to elevated cell shedding.

4. Discussion

We report that colonization of mice with *B. breve* significantly reduces pathological/apoptotic epithelial cell shedding, through a previously unknown mechanism involving bifidobacterial EPS-MyD88 signalling.

The gut microbiota appears central to maintaining epithelial barrier integrity and, importantly, disturbances in the microbiota appear pivotal in IBD pathogenesis. Indeed, IBD patients (paediatric and adult cohorts) have been shown to possess a reduced overall microbiota diversity and reductions in specific genera including *Clostridium*, *Bacteroides*, *Faecalibacterium* and (of particular interest here) *Bifidobacterium* [6,15,35]. Previous clinical trials have shown that administration of bifidobacterial strains can reduce the incidence of relapse in patients suffering from IBD [36]. Following LPS-induced cell shedding, we observed that *a priori* administration of *B. breve* UCC2003 (which is a human-isolated strain, thus more translationally relevant) conferred a significant level of protection, which manifested as significantly reduced caspase-3 positivity within the villus epithelium (figure 2*a–c*). Previous studies have highlighted that bifidobacterial supplementation may also modulate the wider microbiota in mouse models [37]. However, our data indicate that while there are modest differences between PBS and *B. breve*-colonized mice (as indicated by taxa abundance), there are no notable differences (with high variability between animals), suggesting limited effects on overall microbiota profiles (electronic supplementary material, figure S2).

These data therefore suggests a more direct link between bifidobacteria and maintenance of epithelial integrity in the prevention of intestinal inflammation.

Previous studies have indicated that *Bifidobacterium* predominantly colonizes the colon of infants and adults, as determined from faecal or mucosal scrapings, or biopsy samples [38,39]; however, in this work (using a murine model), we have described SI-specific responses. From a translational perspective, in humans, these protective cell shedding responses may result from bifidobacteria cross-talk in the lower SI. Although difficult to measure in humans, previous studies have indicated *Bifidobacterium* colonization in the lower SI (i.e. the ileum, as we observe in our model). Notably, select studies using ileostomy effluents and illeum biopsies have indicated bifidobacteria (specifically *B. animalis* subsp. *lactis* and *B. breve*, respectively) are present in this area of the infant and adult GI tract [40,41]. Therefore, in the human context, we may observe direct SI signalling via resident bifidobacteria and/or remote SI feedback signalling from colonic bifidobacteria epithelium cross-talk, which could be tested in future clinical intervention studies.

As previously mentioned, studies have shown that this experimental model of LPS-induced cell shedding is driven by an induction in expression of TNF-α from the intestinal mucosa [22,42]. One of the key functions of the gut microbiota is induction of tolerogenic or anti-inflammatory immune responses and thus we hypothesized that bifidobacteria may reduce cell shedding as a direct result of inhibiting TNF-α and macrophages—a potential source of TNF. However, we were unable to detect any changes in levels of TNF-α expression or macrophage infiltration from *B. breve* UCC2003-treated or control (i.e. PBS) mice (figure 3*a–f*), suggesting that the protection conferred by *Bifidobacterium* strains is TNF-α independent. Previous studies have indicated that colonization of *B. breve* UCC2003 during homeostatic conditions does not induce differences in splenic TNF-α-positive macrophage numbers when compared with non-colonized controls [7]. Coupled with the lack of change in expression in TNF-R1 following colonization (figure 3*i–k*), it appears that macrophages, TNF-α production and TNF-R1 signalling are not involved in modulating this protective response and suggests that *B. breve* UCC2003 acts preferentially from the luminal side through interactions with IECs. We cannot exclude the potential for EPS to block signalling via TNF-R1. However, TNF-R1 expression appears to be restricted to the basolateral surface of epithelial cells and thus *B. breve* would not be expected to have direct access to this cellular compartment for direct inhibition via binding [43]. Furthermore, quantification of downstream effectors (electronic supplementary material, figure S5) including FADD, TRAF2 and caspase 2 and 8 does not significantly differ between *B. breve* UCC2003 and *B. breve* UCC2003-del-colonized mice, which suggests EPS does not play a key role via TNF-R1.

To delineate these protective luminal bifidobacterial–epithelial interactions, we used epithelial-specific MyD88 KO mice; MyD88 is a key adaptor protein downstream of microbe-TLR signalling. Notably, mice carrying truncated epithelial MyD88 (i.e. C57 BL/6 MyD88$^{-/-}$ villin-cre) showed no protection against cell shedding after colonization of *B. breve* UCC2003 (figure 4*c*,*d*); this was in stark contrast to MyD88-positive control animals, which again showed significant protection against LPS-induced cell shedding (figure 4*a*,*b*). Furthermore, we observed significant increases in IEC TLR2 expression in *B. breve* UCC2003-colonized mice (figure 4*e*). Interestingly, previous work has indicated that TLR2 may enhance ZO-1 associated intestinal epithelial barrier integrity [44], and other studies indicate that mice deficient in MyD88 signalling have increased susceptibility to intestinal inflammation [12]. In a UV model of apoptosis, MyD88 signalling appears to reduce caspase-3 and in turn increase cell survival, and more recently *B. bifidum* has been shown to reduce apoptosis *in vitro* (necrotizing enterocolitis IEC-6 cell model), as also indicated by reduced CC3-positive cells [45]. Thus, our data, in tandem with these studies, indicate that *B. breve* UCC2003 may regulate epithelial integrity in response to LPS-induced cell shedding (as marked by caspase-3) via these central MyD88 signalling mechanisms, potentially downstream of TLR2.

Having determined the importance of host adaptor MyD88, we next sought to determine if there was a specific bifidobacterial molecule central to the observed protective response. Because we have previously shown that surface EPS of *B. breve* UCC2003 can regulate the host response [7], we investigated the ability of an EPS mutant *B. breve* UCC2003-EPSdel (complete deletion of *eps* biosynthetic cluster) to modulate LPS-induced cell shedding. Notably, mice receiving *B. breve* UCC2003-EPSdel showed no significant protection against cell shedding when compared with EPS-positive (i.e. *B. breve* UCC2003) colonized mice (figure 5*a*,*b*), suggesting an important role for this EPS in microbe–host cross-talk. Importantly, EPS structures can be recognized via TLR2 (and signal via MyD88), and previous work with the polysaccharide A (PSA) capsule of *Bacteroides fragilis* highlights that PSA can modulate dendritic cell and T regulatory cell function via TLR2 signalling [46,47]. Additionally, previous work has highlighted that a strain of *B. breve* (Yakult strain) can also induce IL-10 producing T regulatory cells via TLR2; however they did not determine if this was via an EPS-specific mechanisms [48]. Furthermore, recent studies using *Bacillus subtilis* have demonstrated that the EPS capsule of this bacterium is able to protect against intestinal inflammation in a murine model of colitis (in this instance via TLR4), providing further support for the likely role of bifidobacterial EPS in the effects observed in these studies [49]. Notably, the probiotic genus *Lactobacillus* also produces distinct EPSs, which are structurally similar to those observed in bifidobacteria [50]. Recently, within an *in vitro* system (HT29-19A epithelial cell line), the EPS from *Lactobacillus acidophilus* 5e2 was shown to increase IL-8 expression and also TLR2 expression (we also observe that *B. breve* UCC2003 induces IEC TLR2 expression), and additionally upregulation of TLR2 was found to potentially 'sensitize' epithelial cells to subsequent stimulation with peptidoglycan (a TLR2 agonist) [51]. Furthermore, the authors also observed a modest increase in TLR4 expression after addition of EPS, but did not detect any significant modulation of IL-8 responses after priming with EPS and subsequent addition of LPS, which may indicate less of a role for EPS–TLR4 interactions [51]. From a more systemic perspective, in the instance that *Lactobacillus* or indeed *B. breve* UCC2003 potentially translocate across the epithelial barrier, it could by hypothesized they directly influence macrophage function. Previous studies have shown that *L. casei* Shirota can dampen down inflammatory macrophage responses, and *L. rhamnosus* EPS has also been shown to modulate macrophage function *in vitro*, but on this occasion induced proinflammatory responses [52,53]. Ideally, we would test our *B. breve* strains in TLR2 and/or TLR4 KO animals; unfortunately, previous work has shown that these mice do not respond to LPS and

thus would not have a cell shedding response, making these further studies not possible. However, in studies using RNAscope, we found significant numbers of *B. breve* UCC2003 associated with the villi in colonized mice (electronic supplementary material, figure S3), suggesting that direct signalling interactions between the bacteria (possibly via EPS and TLRs, and *B. breve* UCC2003 colonization increases TLR2 expression) and IECs may play an important role in modulating this response. These data, alongside our findings, suggest that *B. breve* EPS may regulate cell shedding by acting as TLR ligands via MyD88, leading to protective epithelial responses.

To probe these EPS–epithelial interactions further, we took advantage of the bidirectional *eps* gene cluster in *B. breve* UCC2003, which can express two genetically and importantly chemically distinct surfaces EPSs [7]. All previous studies used EPS1 (i.e. with *B. breve* UCC2003), but we also determined responses following EPS2 (i.e. *B. breve* UCC2003-EPSInv) colonization. Strikingly, and contrary to our expectations, we found that this isogenic strain was unable to confer protection against LPS-induced cell shedding (figure 5*c*,*d*). Importantly, EPSs are composed of repeating mono- or oligosaccharides linked by various glycosidic linkages, and the three-dimensional structures and other physiochemical features of EPSs can vary widely [54]. The variability in chemical composition of these two *B. breve* EPSs (previous work suggests the EPSs may include glucose, galactose and/or the *N*-acetylated versions of these two sugars in different ratios or composition [7]) could, in part, explain the different modulatory properties of this molecule in relation to receptor-ligand binding, and further highlights the issues with significant strain (or in this case isogenic), variation in effects on host responses. Importantly, these different EPS-epithelium protective responses do not appear to be linked to colonization ability as all strains colonized mice at similar levels (electronic supplementary material, figure S1). Previous limited studies have indicated that specific chemical structures of EPSs such as PSA of *B. fragilis* (comprised an unusual repeating tetrasaccharide moiety, free carboxyl, phosphate and amino groups, that contribute to its zwitterionic nature) are important for function [46]. Additionally, *in vitro* studies on *L. reuteri* strains (DSM 17938 and L26 Biocenol) indicate both EPSs are high-molecular-weight D-glucan polysaccharides with differing spatial conformations, which may relate to induction of different cytokine responses. However, the direct chemical structures involved in this modulation have yet to be defined [55]. Future challenges will include studies to fully chemically characterize the different strains of 'probiotic' bacteria, as evidently significant differences in response to small strain variations (including variations in EPS expression and structure and also other MAMPS) may impact beneficial host responses [56,57].

We have previously shown that EPS-positive *B. breve* UCC2003 does not induce inflammatory host responses after colonization, which we hypothesize is to the advantage of the bacterium and host for maintaining efficient symbiosis and homeostasis [7]. Interestingly, when we probed the downstream signalling transcriptional events after colonization and LPS challenge, we determined that presence of EPS1 (i.e. *B. breve* UCC2003) appeared to attenuate apoptosis-induced signalling activation, in stark contrast to mice colonized with the *B. breve* UCC2003-EPSdel strain, which had significantly elevated apoptotic gene expression (figure 6; electronic supplementary material, figure S5). Importantly, previous work has demonstrated that activation of MyD88 can downregulate several of these genes including Fas (CD95) [58]. Fas is a cell surface receptor and member of the TNF superfamily, and when bound by its ligand induces apoptosis through the assembly of a multiprotein complex called DISC, which in turn activates caspase 8 (i.e. extrinsic apoptosis pathway) [59]. Further evidence of an EPS-specific mechanism attenuating epithelial apoptosis comes from the observation that Bad, Cycs, casp4, Traf5 and Tnfr9 are upregulated in the intestinal mucosa of mice colonized by *B. breve* UCC2003-del compared with *B. breve* UCC2003-colonized mice. Bad is a pro-apoptotic (BH3-only) member of the bcl-2 family that antagonizes the anti-apoptosis proteins bcl-2, bcl-xl and bcl-2, allowing activation of bax/bak oligomers and release of cytochrome *c* from the mitochondria. Within the same pathway, Cycs encodes the haem protein cytochrome *c*, which forms a multiprotein complex called the apoptosome, which activates a cascade of caspases which cause apoptotic cell death [60]. Traf5 is a scaffold protein that forms a multiprotein complex with TRAF2, RIP1 and the TNF receptor, and can potentially mediate the activation of apoptosis and NF-κB [61]. We have previously shown that NF-κB1 inhibits LPS-induced apoptotic cell shedding, whereas NF-κB2 stimulates apoptotic cell shedding [22]. TNFRF9 (CD137) is expressed on T cells and has been reported to enhance their cytolytic activity [62]. These data strongly suggest that, mechanistically, *B. breve* UCC2003, via EPS, may block intrinsic and extrinsic apoptosis signalling (via activation of MyD88) during inflammation to protect epithelial cells under highly apoptotic conditions.

In summary, we have demonstrated that certain bifidobacteria (i.e. *B. breve* UCC2003) are able to protect against pathologic cell shedding induced by IP injection of LPS, and that this protection appears to be independent of TNF-α production by resident tissue macrophages. Using wild-type and mutant *B. breve*, we have demonstrated that a specific EPS is able to confer this protection and, using knockout mice, have shown that this protection appears contingent on functional (MyD88) signalling downstream of the epithelial TLR family members and modulation of pro-apoptotic gene pathways. Understanding how health-promoting species of bacteria such as the *Bifidobacterium* genus interact with the intestinal epithelium and how these species confer their protective effects may drive progress towards understanding how pathologic cell shedding in IBD patients is linked to changes in the intestinal microbiota and how intervention strategies could positively impact disease progression. Future human studies could be considered to address issues of microbial dysbiosis, the relationship to the cell shedding response, to what extent microbial dysbiosis is linked to periods of remission and relapse in such patients, and how bifidobacterial supplementation could be used to reduce relapse in IBD patients.

Ethics. All experiments were performed under the UK Regulation of Animals (Scientific Procedures) Act of 1986. The project licence (PPL 80/2545) under which these studies were carried out was approved by the UK Home Office and the UEA Ethical Review Committee. Mice were sacrificed by CO_2 and cervical dislocation.

Data accessibility. The datasets supporting this article have been uploaded as part of the electronic supplementary material.

Authors' contributions. K.R.H, A.J.M.W. and L.J.H., designed research; K.R.H., C.A.G., L.C.H., S.M., C.J.W. and J.K.F. performed research; D.v.S contributed new reagents/analytic tools; K.R.H, D.v.S, A.J.M.W. and L.J.H. analysed data; and K.R.H, D.v.S, A.J.M.W and L.J.H. wrote the paper.

Competing interests. We declare we have no competing interests.

Funding. This work was supported via a Wellcome Trust New Investigator award to L.J.H. (100974/Z/13/Z), a Wellcome Trust grant awarded to A.J.M.W. (WT0087768MA), support of the Biotechnology and Biological Sciences Research Council (BBSRC) Institute Strategic Programme grant for Gut Health and Food Safety BB/J004529/1 (L.J.H. and A.J.M.W.), and Science Foundation Ireland through the Irish Government's National Development Plan (grant number SFI/12/RC/2273, D.v.S.).

References

1. Ventura M, Turroni F, Lugli GA, van Sinderen D. 2014 Bifidobacteria and humans: our special friends, from ecological to genomics perspectives. *J. Sci. Food Agric.* **94**, 163–168. (doi:10.1002/jsfa.6356)
2. Turnbaugh PJ, Gordon JI. 2009 The core gut microbiome, energy balance and obesity. *J. Physiol.* **587**, 4153–4158. (doi:10.1113/jphysiol.2009.174136)
3. Sivan A *et al.* 2015 Commensal *Bifidobacterium* promotes antitumor immunity and facilitates anti-PD-L1 efficacy. *Science* **350**, 1084–1089. (doi:10.1126/science.aac4255)
4. Fukuda S *et al.* 2011 Bifidobacteria can protect from enteropathogenic infection through production of acetate. *Nature* **469**, 543–547. (doi:10.1038/nature09646)
5. Ishikawa H, Akedo I, Umesaki Y, Tanaka R, Imaoka A, Otani T. 2003 Randomized controlled trial of the effect of bifidobacteria-fermented milk on ulcerative colitis. *J. Am. Coll. Nutr.* **22**, 56–63. (doi:10.1080/07315724.2003.10719276)
6. Maukonen J, Kolho KL, Paasela M, Honkanen J, Klemetti P, Vaarala O, Saarela M. 2015 Altered fecal microbiota in paediatric inflammatory bowel disease. *J. Crohns Colitis* **9**, 1088–1095. (doi:10.1093/ecco-jcc/jjv147)
7. Fanning S *et al.* 2012 Bifidobacterial surface-exopolysaccharide facilitates commensal-host interaction through immune modulation and pathogen protection. *Proc. Natl Acad. Sci. USA* **109**, 2108–2113. (doi:10.1073/pnas.1115621109)
8. Backhed F, Manchester JK, Semenkovich CF, Gordon JI. 2007 Mechanisms underlying the resistance to diet-induced obesity in germ-free mice. *Proc. Natl Acad. Sci. USA* **104**, 979–984. (doi:10.1073/pnas.0605374104)
9. McDermott AJ, Huffnagle GB. 2014 The microbiome and regulation of mucosal immunity. *Immunology* **142**, 24–31. (doi:10.1111/imm.12231)
10. Peterson LW, Artis D. 2014 Intestinal epithelial cells: regulators of barrier function and immune homeostasis. *Nat. Rev. Immunol.* **14**, 141–153. (doi:10.1038/nri3608)
11. Sommer F, Nookaew I, Sommer N, Fogelstrand P, Backhed F. 2015 Site-specific programming of the host epithelial transcriptome by the gut microbiota. *Genome Biol.* **16**, 62. (doi:10.1186/s13059-015-0614-4)
12. Rakoff-Nahoum S, Paglino J, Eslami-Varzaneh F, Edberg S, Medzhitov R. 2004 Recognition of commensal microflora by toll-like receptors is required for intestinal homeostasis. *Cell* **118**, 229–241. (doi:10.1016/j.cell.2004.07.002)
13. Tamboli CP, Neut C, Desreumaux P, Colombel JF. 2004 Dysbiosis in inflammatory bowel disease. *Gut* **53**, 1–4. (doi:10.1136/gut.53.1.1)
14. Sokol H *et al.* 2008 *Faecalibacterium prausnitzii* is an anti-inflammatory commensal bacterium identified by gut microbiota analysis of Crohn disease patients. *Proc. Natl Acad. Sci. USA* **105**, 16 731–16 736. (doi:10.1073/pnas.0804812105)
15. Duranti S *et al.* 2016 Elucidating the gut microbiome of ulcerative colitis: bifidobacteria as novel microbial biomarkers. *FEMS Microbiol. Ecol.* **92**, fiw191. (doi:10.1093/femsec/fiw191)
16. Guan Y, Watson AJ, Marchiando AM, Bradford E, Shen L, Turner JR, Montrose MH. 2011 Redistribution of the tight junction protein ZO-1 during physiological shedding of mouse intestinal epithelial cells. *Am. J. Physiol. Cell Physiol.* **300**, C1404–C1414. (doi:10.1152/ajpcell.00270.2010)
17. Potten CS, Loeffler M. 1990 Stem cells: attributes, cycles, spirals, pitfalls and uncertainties. Lessons for and from the crypt. *Development* **110**, 1001–1020.
18. Bullen TF, Forrest S, Campbell F, Dodson AR, Hershman MJ, Pritchard DM, Turner JR, Montrose MH, Watson AJ. 2006 Characterization of epithelial cell shedding from human small intestine. *Lab Invest.* **86**, 1052–1063. (doi:10.1038/labinvest.3700464)
19. Watson AJ, Hughes KR. 2012 TNF-α-induced intestinal epithelial cell shedding: implications for intestinal barrier function. *Ann. N.Y. Acad. Sci.* **1258**, 1–8. (doi:10.1111/j.1749-6632.2012.06523.x)
20. Kiesslich R *et al.* 2007 Identification of epithelial gaps in human small and large intestine by confocal endomicroscopy. *Gastroenterology* **133**, 1769–1778. (doi:10.1053/j.gastro.2007.09.011)
21. Kiesslich R *et al.* 2012 Local barrier dysfunction identified by confocal laser endomicroscopy predicts relapse in inflammatory bowel disease. *Gut* **61**, 1146–1153. (doi:10.1136/gutjnl-2011-300695)
22. Williams JM *et al.* 2013 A mouse model of pathological small intestinal epithelial cell apoptosis and shedding induced by systemic administration of lipopolysaccharide. *Dis. Model. Mech.* **6**, 1388–1399. (doi:10.1242/dmm.013284)
23. Potten CS, Owen G, Booth D. 2002 Intestinal stem cells protect their genome by selective segregation of template DNA strands. *J. Cell Sci.* **115**, 2381–2388.
24. McKaig BC, Hughes K, Tighe PJ, Mahida YR. 2002 Differential expression of TGF-beta isoforms by normal and inflammatory bowel disease intestinal myofibroblasts. *Am. J. Physiol. Cell Physiol.* **282**, C172–C182. (doi:10.1152/ajpcell.00048.2001)
25. Pfaffl MW. 2001 A new mathematical model for relative quantification in real-time RT-PCR. *Nucleic Acids Res.* **29**, e45. (doi:10.1093/nar/29.9.e45)
26. McLarren KW, Cole AE, Weisser SB, Voglmaier NS, Conlin VS, Jacobson K, Popescu O, Boucher JL, Sly LM. 2011 SHIP-deficient mice develop spontaneous intestinal inflammation and arginase-dependent fibrosis. *Am. J. Pathol.* **179**, 180–188. (doi:10.1016/j.ajpath.2011.03.018)
27. Schindelin J *et al.* 2012 Fiji: an open-source platform for biological-image analysis. *Nat. Methods* **9**, 676–682. (doi:10.1038/nmeth.2019)
28. Watson AJ, Chu S, Sieck L, Gerasimenko O, Bullen T, Campbell F, McKenna M, Rose T, Montrose MH. 2005 Epithelial barrier function *in vivo* is sustained despite gaps in epithelial layers. *Gastroenterology* **129**, 902–912. (doi:10.1053/j.gastro.2005.06.015)
29. Manichanh C, Borruel N, Casellas F, Guarner F. 2012 The gut microbiota in IBD. *Nat. Rev. Gastroenterol. Hepatol.* **9**, 599–608. (doi:10.1038/nrgastro.2012.152)
30. Wu MH, Pan TM, Wu YJ, Chang SJ, Chang MS, Hu CY. 2010 Exopolysaccharide activities from probiotic bifidobacterium: immunomodulatory effects (on J774A.1 macrophages) and antimicrobial properties. *Int. J. Food Microbiol.* **144**, 104–110. (doi:10.1016/j.ijfoodmicro.2010.09.003)
31. Fanning S, Hall LJ, van Sinderen D. 2012 *Bifidobacterium breve* UCC2003 surface exopolysaccharide production is a beneficial trait mediating commensal–host interaction through immune modulation and pathogen protection. *Gut Microbes* **3**, 420–425. (doi:10.4161/gmic.20630)
32. Weiser MM. 1973 Intestinal epithelial cell surface membrane glycoprotein synthesis. I. An indicator of cellular differentiation. *J. Biol. Chem.* **248**, 2536–2541.
33. Corr SC *et al.* 2014 MyD88 adaptor-like (Mal) functions in the epithelial barrier and contributes to intestinal integrity via protein kinase C. *Mucosal Immunol.* **7**, 57–67. (doi:10.1038/mi.2013.24)
34. Bottacini F *et al.* 2014 Comparative genomics of the *Bifidobacterium breve* taxon. *BMC Genomics* **15**, 170. (doi:10.1186/1471-2164-15-170)
35. Gevers D *et al.* 2014 The treatment-naive microbiome in new-onset Crohn's disease. *Cell Host Microbe.* **15**, 382–392. (doi:10.1016/j.chom.2014.02.005)
36. Saez-Lara MJ, Gomez-Llorente C, Plaza-Diaz J, Gil A. 2015 The role of probiotic lactic acid bacteria and bifidobacteria in the prevention and treatment of inflammatory bowel disease and other related diseas.es: a systematic review of randomized human clinical trials. *Biomed. Res Int.* **2015**, 505878. (doi:10.1155/2015/505878)

Supplementary Methods & Figures for manuscript:

"*Bifidobacterium breve* reduces apoptotic epithelial cell shedding in an exopolysaccharide and MyD88-dependent manner"

K.R. Hughes, L.C. Harnisch, C. Alcon-Giner, S. Mitra, C.J. Wright, J. Ketskemety, D. van Sinderen, A.J.M Watson and L.J. Hall

Supplementary Materials and Methods

RNAscope

RNAscope was performed using a commercial kit (RNAscope FFPE reagent kit) from Advanced Cell Diagnostics (California, USA) as per the manufacturer's instructions. Briefly, 5 µm formalin fixed paraffin embedded small intestinal tissue was mounted on Superfrost plus slides (ThermoFisher) before baking in a dry oven at 60°C for 1 h. Slides were then deparaffinised with Xylene and 100% ethanol before applying Pre-treat solution 1 for 10 minutes at room temperature. Slides were then washed in distilled water before incubating in boiling Pre-treat 2 solution for 15 minutes. Following further washes, Pre-treat solution 3 was applied in a humidified chamber at 40°C for 30 minutes. After further washes, *B. breve* UCC2003 specific probe (probe name: B-Bifido-16SrRNA) or Cyclophylin B control probe was hybridised to the slides for 2 h at 40°C. Following washing in wash buffer, a series of amplification probes (AMP1 to AMP6) were sequentially bound and washed to/from the slides before signal detection using DAB substrate as per the manufacturer's recommendations. Slides were then counterstained with haematoxylin, dehydrated and mounted for visualisation.

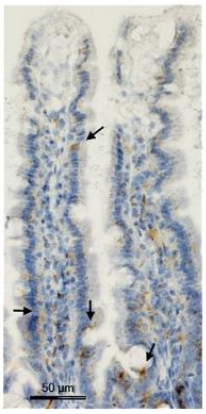

Supplementary Figure 3: *B. breve* UCC2003 resides in close contact with the small intestinal epithelium.

Representative RNAscope staining for *B. breve* (*B. breve* specific probe) brown cells and arrows) in the small intestine of *B. breve* colonised mice (after 3 x 24 h doses at ~1 x 10^9).

Appendix 2.

Miguel, Jennifer C., Adrienne A. Maxwell, Jonathan J. Hsieh, Lukas C. Harnisch, Denise Al Alam, D. Brent Polk, Ching-Ling Lien, Alastair JM Watson, and Mark R. Frey. "Epidermal growth factor suppresses intestinal epithelial cell shedding through a MAPK-dependent pathway." J Cell Sci 130, no. 1 (2017): 90-96.

Contribution by Lukas C. Harnisch to:

- Figure 2. - A), B), and C)
- Figure 3. – A), B), and C)

© 2017. Published by The Company of Biologists Ltd | Journal of Cell Science (2017) 130, 90-96 doi:10.1242/jcs.182584

SPECIAL ISSUE: 3D CELL BIOLOGY

SHORT REPORT

Epidermal growth factor suppresses intestinal epithelial cell shedding through a MAPK-dependent pathway

Jennifer C. Miguel[1,*], Adrienne A. Maxwell[1,*], Jonathan J. Hsieh[1], Lukas C. Harnisch[2], Denise Al Alam[3], D. Brent Polk[1,4], Ching-Ling Lien[3,4], Alastair J. M. Watson[2,‡] and Mark R. Frey[1,4,‡]

ABSTRACT

Cell shedding from the intestinal villus is a key element of tissue turnover that is essential to maintain health and homeostasis. However, the signals regulating this process are not well understood. We asked whether shedding is controlled by epidermal growth factor receptor (EGFR), an important driver of intestinal growth and differentiation. In 3D ileal enteroid culture and cell culture models (MDCK, IEC-6 and IPEC-J2 cells), extrusion events were suppressed by EGF, as determined by direct counting of released cells or rhodamine-phalloidin labeling of condensed actin rings. Blockade of the MEK–ERK pathway, but not other downstream pathways such as phosphoinositide 3-kinase (PI3K) or protein kinase C (PKC), reversed EGF inhibition of shedding. These effects were not due to a change in cell viability. Furthermore, EGF-driven MAPK signaling inhibited both caspase-independent and -dependent shedding pathways. Similar results were found *in vivo*, in a novel zebrafish model for intestinal epithelial shedding. Taken together, the data show that EGF suppresses cell shedding in the intestinal epithelium through a selective MAPK-dependent pathway affecting multiple extrusion mechanisms. EGFR signaling might be a therapeutic target for disorders featuring excessive cell turnover, such as inflammatory bowel diseases.

KEY WORDS: Intestinal epithelium, Inflammatory bowel disease, Epidermal growth factor receptor, EGFR, MAP kinases, MAPKs, Epithelial cell, Cell shedding

INTRODUCTION

The intestinal epithelium, a monolayer of polarized cells separating the organism from luminal gut contents, is the most rapidly renewing tissue in adult mammals (Sancho et al., 2004). Routine turnover of this tissue without loss of the barrier requires coordination between stem cell proliferation and shedding (also called extrusion) of mature cells from the upper villus or colonic surface mucosa. Accelerated shedding, which can lead to infection and exacerbated immune responses (Hausmann, 2010; Knodler et al., 2010), is associated with inflammatory bowel diseases (IBD; Kiesslich et al., 2012; Liu et al., 2011) and endotoxemia (Assimakopoulos et al., 2012). This 'pathological' shedding can be induced by proinflammatory cytokines (Marchiando et al., 2011) or lipopolysaccharide (Williams et al., 2013). However, little is known about regulation of constitutive physiological shedding, and especially about signals that repress it. Understanding the mechanisms controlling normal physiological cell extrusion could identify targets for correcting pathological shedding in diseases such as IBD.

Physiological cell shedding occurs through at least two mechanisms. *In situ* apoptosis of a damaged cell can trigger extrusion (Andrade and Rosenblatt, 2011; Bullen et al., 2006; Marchiando et al., 2011). Alternatively, acute crowding promotes shedding of live cells through a sphingosine-1-phosphate- and Rho-kinase-dependent mechanism (Eisenhoffer et al., 2012), with apoptosis occurring after loss of attachment rather than as a cause. In either case, the process involves Rho-driven myosin ring formation and contraction by neighboring cells (Eisenhoffer et al., 2012) and remodeling of tight junctions (Guan et al., 2011; Marchiando et al., 2011). These mechanisms are conserved in several epithelial cell types (Madara, 1990; Rosenblatt et al., 2001) and presumably across most vertebrates.

Endogenous regulators of constitutive shedding, especially factors that restrain it, are not well understood. In this study, we tested whether epidermal growth factor (EGF) receptor (EGFR) is involved in this process. EGFR is a receptor tyrosine kinase that controls intestinal cell growth, repair and migration (Frey et al., 2006; Polk, 1998). The overlap in the mechanical forces and cytoskeletal alterations in cell migration and cell extrusion suggest a possible role for EGFR in shedding; furthermore, as EGF is an epithelial cell mitogen (Sheng et al., 2006), EGFR activation might be expected to induce crowding and thus increase shedding. We used coordinated *in vitro* (3D enteroids and cultured IEC-6, MDCK and IPEC-J2 cells) and *in vivo* (adult zebrafish gut) models to study the role of EGFR in constitutive non-pathological shedding. Our results show that, surprisingly, EGFR suppresses cell extrusion through a MAPK-dependent mechanism.

RESULTS AND DISCUSSION

EGF suppresses cell shedding *in vitro*

To model intestinal turnover, we first generated ileal epithelial enteroids (Sato et al., 2011a) from mice expressing the Lifeact–EGFP cytoskeleton-labeling construct (Riedl et al., 2010). Shedding events in these enteroids (Fig. 1A) show the characteristic early saccular and funnel morphologies described *in vivo* (Marchiando et al., 2011) and can be viewed in real time (Movie 1, the box encloses an event). Shed cells per unit distance of epithelial perimeter can be counted over time. Cultures treated with EGF showed a 40% decrease in shedding per unit distance versus control (Fig. 1A).

Similar results were observed in cell culture. MDCK cells on Transwell inserts were treated with EGF (10 ng/ml) or EGFR

[†]Department of Pediatrics, University of Southern California Keck School of Medicine and The Saban Research Institute at Children's Hospital Los Angeles, Los Angeles, CA 90027, USA. [2]Department of Medicine, Norwich Medical School, University of East Anglia, Norwich Research Park, Norwich NR4 7UQ, UK. [3]Department of Surgery, University of Southern California Keck School of Medicine and The Saban Research Institute at Children's Hospital Los Angeles, Los Angeles, CA 90027, USA. [4]Department of Biochemistry and Molecular Biology, University of Southern California Keck School of Medicine, Los Angeles, CA 90089, USA.
*These authors contributed equally to this work

[‡]Authors for correspondence (mfrey@chla.usc.edu; alastair.watson@uea.ac.uk)

Received 2 November 2015; Accepted 18 March 2016

Journal of Cell Science

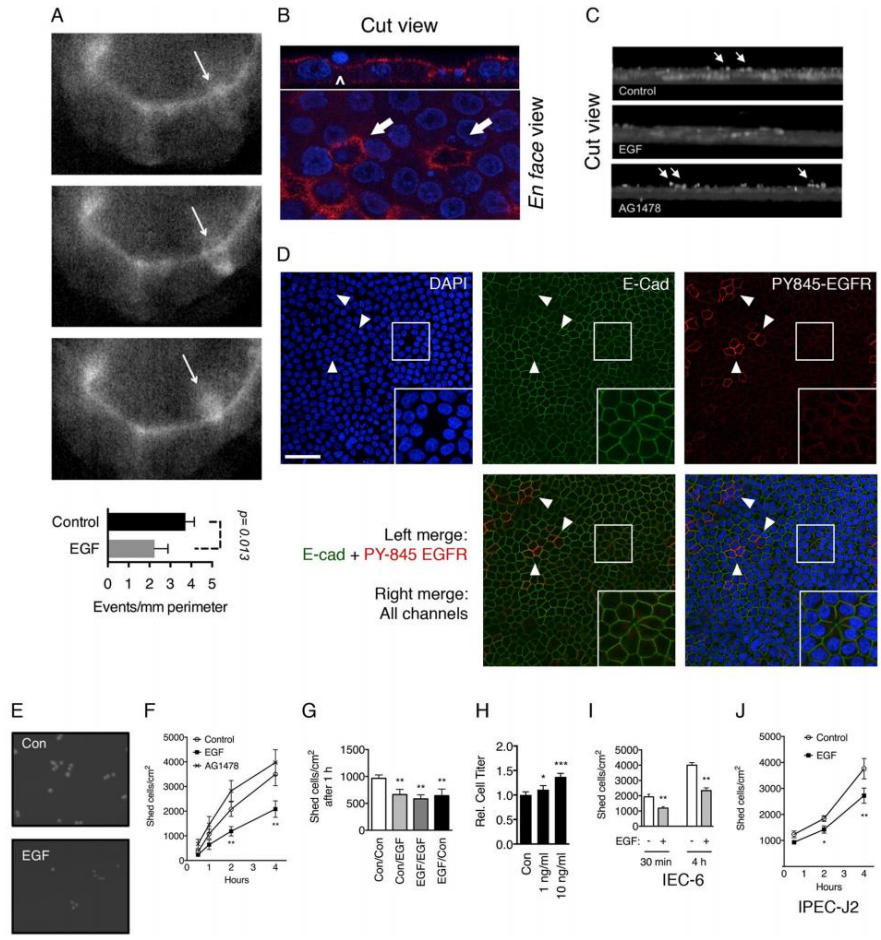

Fig. 1. EGF suppresses cell shedding *in vitro*. (A) Ileal enteroids isolated from Lifeact–EGFP-expressing mice were starved of growth factors for 24 h, then treated with vehicle (PBS) or 10 ng/ml EGF and live-imaged for 24 h. Characteristic morphological stages of apical cell shedding (arrows) and the number of events per µm of the epithelial perimeter per 24 h are shown. (B,C) MDCK cells were treated with vehicle (Control), EGF (10 ng/ml) or EGFR inhibitor AG1478 (150 nM) for 4 h, fixed and stained with Rhodamine–phalloidin (red) and DAPI (blue). See text for quantification. (B) Example image showing cell 'rosettes' (arrows) indicating shedding events. Arrowhead in top panel, nucleus from shedding cell. *n*=6 independent experiments. (C) Orthogonal projections of confocal *z*-stacks; arrows, shedding nuclei above the monolayer. *n*=6. (D) MDCK cells stained with anti-E-cadherin, anti-PY-845-EGFR and DAPI. Cell rosettes are sites of shedding. An example is shown in the magnification boxes. Arrowheads, cells positive for PY-845-EGFR. Scale bar: 50 µm. (E,F) MDCK (*n*=8) cells were labeled with DAPI and treated with vehicle, EGF or AG1478; shed cells were collected and counted; representative images in D. (G) MDCK cultures were exposed to EGF for 4 h, EGF was washed out, and then cells were cultured either with or without EGF and shed cells were counted at 4 h. (H) Relative cell numbers after 48 h in control and EGF-treated cultures, determined by resazurin reduction assay (*n*=4). (I) IEC-6 and (J) IPEC-J2 cells were cultured with or without EGF and shed cells at 30 min or 4 h were counted (*n*=4). Quantitative results are mean±s.e.m. **P*<0.05 vs control; ***P*<0.01 vs control ; ****P*<0.001 vs control (one-way ANOVA with Tukey's post-test analysis).

inhibitor (AG1478, 150 nM) for 4 h and stained with Rhodamine–phalloidin. EGF reduced the number of shedding events (0.55 versus 3.0 per field in control; $P<0.01$), identified as a cell surrounded by a condensed actin ring or funnel with neighboring cells assembled in the characteristic 'rosette' pattern [(Rosenblatt et al., 2001) and Fig. 1B]. By counting the number of nuclei

displaced above the plane of the monolayer in orthogonal projection (Fig. 1C), we also observed that EGF reduced and AG1478 induced shedding (4.5 or 19.8 displaced nuclei per field versus 12.5 in control; $P<0.01$). Interestingly, phosphorylated (activated) EGFR in unstimulated MDCK monolayers was only found in cells distant to a shedding event (Fig. 1D), consistent with the notion that EGFR activation restrains shedding.

To develop a convenient model for mechanistic studies, we live-labeled cells with DAPI (Daniel and DeCoster, 2004), washed away debris and cultured in fresh medium for up to 4 h. Over time, extruded cells were collected and counted by fluorescence microscopy (example images, Fig. 1E). Results from this method were consistent with enteroids and Transwell cultures; EGF reduced shedding, whereas AG1478 caused a consistent but nonsignificant trend towards more cell extrusion (Fig. 1F). Suppression appears to be an early event in the shedding process, as an EGF pulse followed by wash-out and chase did not provoke a synchronized wave of shedding (Fig. 1G). Thus, EGF is likely blocking the onset of the process rather than arresting it midway. Consistent with decreased extrusion and the known mitogenic effects of EGF, 48 h exposure (Fig. 1H) resulted in increased cell density, although the effects of suppressed shedding and increased proliferation cannot be separated over this longer period. *In vivo*, increased mucosal area as a response to EGF (Berlanga-Acosta et al., 2001) likely relieves the compressive pressure of the resulting increased cellularity. EGF also reduced shedding of IEC-6 rat intestinal and IPEC-J2 pig jejunal epithelial cells (Fig. 1I,J). Overall, these results show that EGFR-mediated suppression of cell extrusion is conserved in cell culture models.

MEK–ERK signaling is required for EGFR suppression of shedding

To examine the molecular mechanisms of this effect, we used inhibitors to signaling intermediates which might impact caspase or Rho-kinase activity. Labeled cells were treated with EGF with or without inhibitors to MEK1 and MEK2 (MEK1/2, also known as MAP2K1 and MAP2K2, respectively; 5 µM U0126), protein kinase C (PKC; 1 µM BisI) or phosphoinositide 3-kinase (PI3K; 5 µM LY294002), and shed cells were collected and counted. MEK–ERK inhibition reversed the suppression of shedding mediated by EGF in both MDCK and IEC-6 cells (Fig. 2A–C). In contrast, neither PKC nor PI3K inhibition had any effect. Consistent with a role for MAPK signaling, constitutively shed cells showed low basal ERK1 and ERK2 (ERK1/2, also known as MAPK3 and MAPK1, respectively) activation versus attached cells (Fig. 2D,E). Furthermore, treatment with neuregulin-1β (NRG1β) or fibroblast growth factor 10 (FGF10), both of which stimulate ERK1/2 (Frey et al., 2010; Yamada et al., 2016), suppressed shedding (Fig. 2F,G). Taken together, these data suggest a model in which overall MAPK activation, which can be stimulated by multiple growth factors, regulates shedding. Although off-target effects of U0126 are a possibility, identical results were obtained with a second inhibitor

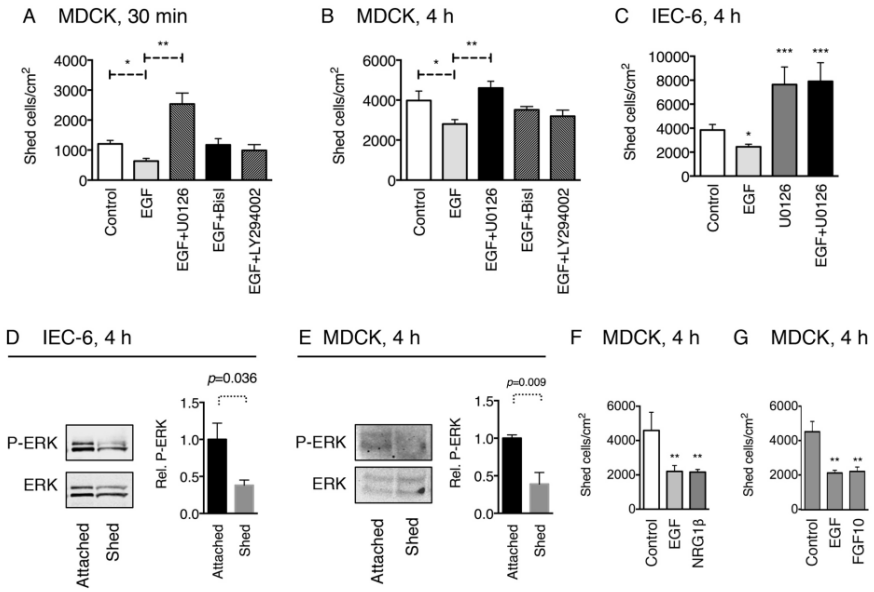

Fig. 2. MEK1/2 activity is required for EGF suppression of epithelial cell shedding *in vitro*. (A,B) MDCK (n=6) and (C) IEC-6 (n=5) cells were labeled and then treated with vehicle (Control) or EGF, with or without 5 µM U0126 (a MEK1/2 inhibitor), 5 µM LY294002 (a PI3K inhibitor) or 1 µM BisI (a PKC inhibitor) for 30 min or 4 h. Shed cells were collected and counted. (D,E) Attached and shed cells from control cultures (no EGF) collected over 4 h were subjected to western blotting for phosphorylated ERK (P-ERK) (n=4). (F,G) MDCK cells (n=4) were treated with 10 ng/ml NRG1β or 2.5 ng/ml FGF10 and shed cells were counted.. *P<0.05; **P<0.01; ***P<0.001 (one-way ANOVA with Tukey's post-test analysis).

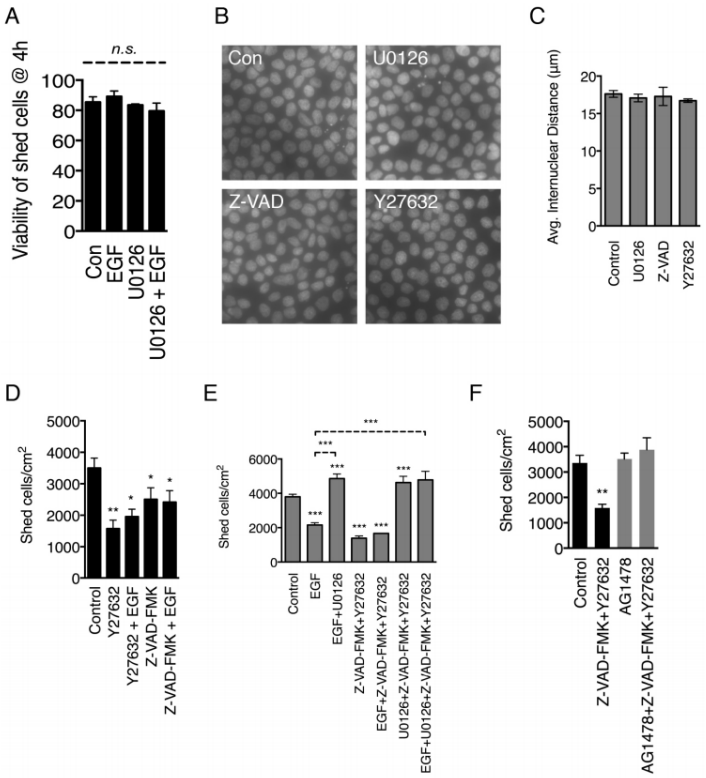

Fig. 3. MEK inhibition reverses suppression of cell shedding by EGF, caspase inhibitor or Rho-kinase inhibitor. (A) Shed MDCK cells in vehicle (Control), EGF- and U0126-treated cultures were collected after 4 h, and viability was assessed by Trypan Blue exclusion (n=4). (B) MDCK cells were treated as indicated for 4 h and DAPI-stained to show density. (C) Delaunay analysis of mean internuclear distance on cultures. (D) MDCK cells (n=6) were labeled then treated with vehicle, EGF, Z-VAD-FMK (caspase inhibitor; 1 µM) or Y27632 (Rho-kinase inhibitor; 20 µM) for 4 h; shed cells were collected and counted. *P<0.05 versus control (one-way ANOVA with Tukey's post-test analysis). (E,F) MDCK (n=5) cells were labeled then treated as indicated for 4 h. Shed cells were collected and counted. Quantitative results are mean±s.e.m. ***P<0.001 vs control; *** brackets, P<0.001 between columns indicated (one-way ANOVA with Tukey's post-test analysis).

(PD98059, data not shown) and the apparent increase in shedding beyond baseline in the presence of inhibitor is likely due to loss of the basal MAPK activity in untreated cells.

EGFR regulates both caspase- and Rho-dependent shedding

Physiological shedding from epithelial monolayers includes both apoptotic cells (caspase-dependent mechanism) and Rho-kinase driven extrusion of live cells (Eisenhoffer et al., 2012; Marchiando et al., 2011). Trypan Blue staining of shed MDCK cells at 4 h showed no difference in cell viability with EGF or U0126 (Fig. 3A; control 85.3±3.6% viable; EGF 89.2±1.0%; U0126 83.4±1.3%; U0126+EGF 79.5±9.2%; mean±s.e.m., P=0.31, ANOVA), suggesting that the effects of EGF and MAPK are not simply due to blocking cell death. To further explore which pathways are impacted, we performed shedding experiments using caspase (Z-VAD-FMK, 1 µM) or Rho-kinase (Y27632, 20 µM) inhibitors in the presence or absence of EGF and/or U0126. None of the inhibitors affected the bulk density of cultures in the short term (Fig. 3B,C), showing that shedding changes are not simply due to altered cell numbers. Both caspase and Rho-kinase inhibitors reduced MDCK shedding, as expected (Fig. 3D,E). However, EGF did not augment this reduction. These results suggest that EGFR is blocking both the apoptotic caspase and the Rho-kinase-dependent myosin contraction shedding pathways. Interestingly, MEK inhibition stimulated shedding even at baseline or in the presence of caspase plus Rho-kinase inhibitors (Fig. 3E), suggesting that EGF→MEK→ERK signaling blocks shedding downstream of both of these pathways. Similarly, the EGFR inhibitor AG1478 reversed suppression of baseline shedding by Z-VAD-FMK+Y27632 (Fig. 3F). As MEK→ERK signals are known to contribute to tight junction maintenance in the intestine (Kinugasa et al., 2000), it is possible that an initial step in the mechanical shedding process requires loss of MAPK activity in the target cell to dissolve cell–cell junctions.

EGFR suppresses constitutive intestinal epithelial cell shedding *in vivo* in zebrafish through the MEK–ERK pathway

To test our findings *in vivo*, we established the adult zebrafish intestine as a shedding model. On Rhodamine–phalloidin-stained sections of adult zebrafish midgut, all stages of the shedding process – including actin 'funnels' characteristic of cytoskeletal rearrangements in epithelial cells preparing to undergo extrusion – are clearly visible (Fig. 4A). We injected adult fish intraperitoneally with 20 µl vehicle (0.01% DMSO), EGF (1 µg/ml; final 60 µg/kg) or AG1478 (200 nM; final 388 µg/kg). After 4 h, intestines were collected and stained with Rhodamine–phalloidin to detect F-actin-

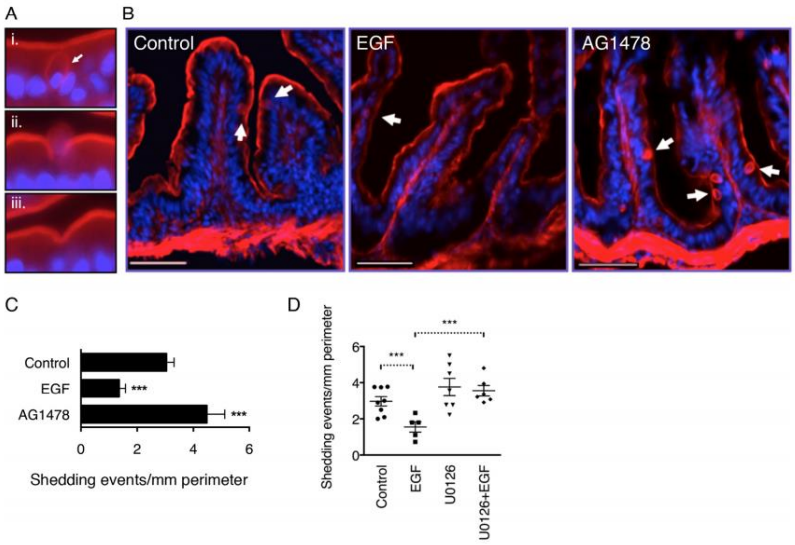

Fig. 4. EGF inhibits cell shedding in zebrafish intestine via MAPK signaling. (A) Zebrafish midgut tissue was fixed and stained with Rhodamine–phalloidin (red, F-actin) and DAPI (blue, nuclei). Examples of (i) early, (ii) late and (iii) completion of shedding process shown. Arrow, example saccular stage event. (B) Fish were treated intraperitoneally with vehicle (Control), EGF or AG1478 for 4 h. Early-stage shedding funnels (arrows) per mm of tissue perimeter were counted (C). Scale bars: 50 µm. ***P<0.001 vs control, n=5 per condition. (D) Fish were treated intraperitoneally with vehicle (Control), EGF or U0126 for 4 h. Tissue was fixed, stained and shedding funnels counted; n=6–8 per condition as shown. Quantitative results are mean±s.e.m. ***P<0.001 (one-way ANOVA with Tukey's post-test analysis).

rich shedding funnels. EGF suppressed and AG1478 induced shedding compared to control (1.7 or 4.3 shedding events/mm tissue perimeter versus 2.5 in control; P<0.05, Fig. 4B,C). Comparing the location of shedding events, we found that a greater proportion of events in AG1478-treated fish were in the lower half of the villus folds or in the inter-fold region (61.4±10.2% in AG1478 versus 45.1±12.1% in control; mean±s.e.m.) suggesting altered localization with EGFR blockade. As the MEK–ERK MAPK cascade was essential for EGF-mediated suppression of cell shedding *in vitro* (Fig. 2), we tested the effect of this pathway in zebrafish using the pharmacological MEK inhibitor U0126 (10 µM; final 228 µg/kg). Similar to our *in vitro* results, MEK inhibition abrogated EGF-induced reduction in detectable shedding events on intestinal villus folds of the fish (Fig. 4D).

Taken together, these data indicate that EGFR suppresses constitutive intestinal epithelial cell shedding and position EGFR ligands as a suite of soluble factors potentially used by the tissue to regulate its own turnover. The relevant physiological ligands for controlling shedding have not yet been defined, but as discussed above, any ligand that stimulates MAPK is potentially important. Endogenous EGF from salivary and Brunner's glands is present in the intestinal lumen (Playford and Wright, 1996; Scheving et al., 1989; Thompson et al., 1994), but its availability to EGFR on the basolateral membranes of enterocytes (Playford et al., 1996) might be limited and thus, for example, TGF-α released from basolateral surfaces (Dempsey et al., 2003) might be more relevant under homeostatic conditions. Ligands are also produced by subepithelial myofibroblasts (Shao and Sheng, 2010) and Paneth cells (Poulsen et al., 1986; Sato et al., 2011b), possibly creating growth factor gradients along the crypt–villus axis. This could explain why extrusion is normally restricted to the upper villi. Consistent with this notion, weaning pigs exhibit increased intestinal epithelial turnover (Skrzypek et al., 2005) coincident with a loss of EGFR expression on the villi (Schweiger et al., 2003). Studies in *Drosophila* gut indicate that intestinal stem cells and enterocytes communicate to coordinate generation of new cells with loss of old ones (O'Brien et al., 2011) and that EGF plays an important role in maintaining the intestinal stem cell compartment (Xu et al., 2011). Thus, EGFR ligand gradients within the epithelium could provide a mechanism for coordination between stem cells and the shedding zone.

In summary, we have shown that EGF helps regulate epithelial homeostasis by suppression of constitutive cell extrusion through a MEK–ERK signaling mechanism. Ongoing work is focused on understanding the fundamental cellular mechanisms targeted by this signaling pathway, and on determining whether EGFR also regulates pathologic cell shedding under inflammatory conditions. Several investigators have reported reduced EGFR ligand expression in IBD (Alexander et al., 1995; Hormi et al., 2000). Furthermore, cytokines involved in Crohn's disease, which promote shedding and the formation of epithelial gaps in the mouse small intestine (Marchiando et al., 2011, 2010), can also inhibit EGFR activation in intestinal epithelial cells *in vitro* (Kaiser and Polk, 1997; McElroy et al., 2008) and *in vivo* (Feng and Teitelbaum, 2012). Thus, understanding the mechanism regulating constitutive shedding might lead to insight into pathological processes as well.